

Durham E-Theses

Enantioselective Synthesis and Application of N-stereogenic Ammonium Cations

BEGG, CALLUM,SCOTT

How to cite:

BEGG, CALLUM,SCOTT (2024) *Enantioselective Synthesis and Application of N-stereogenic Ammonium Cations*, Durham theses, Durham University. Available at Durham E-Theses Online:
<http://etheses.dur.ac.uk/15479/>

Use policy

The full-text may be used and/or reproduced, and given to third parties in any format or medium, without prior permission or charge, for personal research or study, educational, or not-for-profit purposes provided that:

- a full bibliographic reference is made to the original source
- a [link](#) is made to the metadata record in Durham E-Theses
- the full-text is not changed in any way

The full-text must not be sold in any format or medium without the formal permission of the copyright holders.

Please consult the [full Durham E-Theses policy](#) for further details.

Enantioselective Synthesis and Application of *N*-stereogenic Ammonium Cations



Callum S. Begg, MSci
University of Durham
Department of Chemistry
Grey College

A thesis presented in fulfilment of the requirements
for the degree of *Doctor of Philosophy*

December 2023

Every crystal is a message written in the language of symmetry.

(anon)

Enantioselective Synthesis and Application of *N*-stereogenic Ammonium Cations

Callum S. Begg

Submitted for the degree of Doctor of Philosophy

Primary supervisor: Dr Matthew O. Kitching

Abstract

Enantioselective synthesis is vital in the construction of many biologically and commercially relevant molecules. Despite having potentially wide-ranging applications, routes to synthesise enriched heteroatomic stereocentres have received less consideration than carbon-based analogues. The use of nitrogen as a stereocentre is commonly neglected due to its ability to readily pyramidally invert at room temperature, enabled by quantum tunnelling. In 1899, Pope and Peachy achieved the first successful resolution of a quaternary ammonium salt, establishing a conformationally and configurationally stable nitrogen stereocentre.¹ However despite this, a general enantioselective methodology to access these stereogenic elements remained elusive until recently.²

Novel work by our group pioneered the enantioselective synthesis of *N*-stereocentres as the sole stereogenic element in a molecule. This methodology was made possible through the integration of a supramolecular recognition event and *in situ* racemisation within a crystallisation-induced asymmetric transformation (CIAT). The supramolecular recognition was facilitated by 1,1'-bi-2-naphthol (BINOL), which played a crucial role in orchestrating the molecular interactions and directing the desired stereochemical outcome.

To better explore the utility of the CIAT and increase both the scope and application of this methodology, initially the the supramolecular recognition phenomenon is investigated on a diverse library of achiral ammonium salts. The salts form ternary complexes with BINOL, which serve as supramolecular recognition units in solution. These recognition units assemble into a dynamic and flexible hydrogen-bonded network of (*R*)-BINOLs and counterions. Subsequently, this network is abstracted into

the solid phase, manifesting as a crystalline helical host that encapsulates ammonium cations. These hosts create discrete isostructures, adapting to offer a suitable multipoint recognition environment for the cation to which they are presented. Remarkably, quaternary ammonium cation complexes access a lower energy solid-state compared to their less substituted counterparts, resulting in their selective abstraction from solution, even under aqueous conditions. This discovery challenges selectivity based on hydrogen bonding ability and cation- π interaction strength, marking a potential paradigm shift in the field through use of the solid state.

Due to the significance of the crystalline state to a CIAT-like methodology any manipulation of its morphology has pronounced effects on the products synthesised. As such, it was established that consideration of both solvent selection and the enantiopurity of the chiral resolving agent is imperative to precisely control the solid-state end-point of the recognition process.

Leveraging an improved understanding of solid-state recognition phenomenon, this study integrates knowledge into the enantioselective methodology, shedding light on the influence of isostructure selection on enantiopurity. Furthermore, empirical observations on ammonium salt-BINOL complexes reveal that positioning steric bulk in close proximity to the stereocentre and minimising functionality on substituent groups are important factors in enhancing enantioselectivity. Analysis of the thermodynamic parameters dictating enantiomer selection in microcrystalline solids illuminates how the stereoselectivity is dictated through multiple mechanisms based on diastereomeric interactions in the solid-state. The study also reports a chiral High-Performance Liquid Chromatography (HPLC) methodology to determine the enrichment levels of the newly synthesised ammonium salts. Finally, a newly synthesised ammonium salt (*N*-allyl, *N*-methyl, *N*-phenylacetyl anilinium bromide) was successfully applied to direct the stereochemistry of a substituted atropisomeric scaffold, showcasing its potential as valuable tool for precise control over molecular chirality in complex chemical structures.

Declaration

I declare that;

This submission is entirely my own work and is based on research carried out within the Kitching group at Durham University. I confirm that I have read and understood the Department and University regulations on plagiarism. No part of this thesis has been submitted elsewhere for any other degree or qualification. Each contribution to, and quotation in this submission which is taken from the work or works of other people, has been cited correctly.

Signed:



Callum S. Begg

Copyright © 2023 by CALLUM S. BEGG.

The copyright of this thesis rests with the author. No quotations from it should be published without the author's prior written consent and information derived from it should be acknowledged.

Acknowledgements

I extend my sincere gratitude to my colleagues at Durham University and beyond for their invaluable input and advice during my PhD. While there are too many individuals to name, I am immensely thankful to all those who contributed to this work.

Foremost, I would like to express my deepest appreciation to my supervisor, Dr. Matthew O. Kitching. His guidance and wealth of knowledge have been instrumental and I am truly grateful for the priceless advice he has provided.

Special thanks go to the members of the Kitching group, past and present, for their support over the years. To those who I have worked directly alongside, your efforts have significantly contributed to the progression of the work in this thesis.

I also acknowledge the work of the analytical services within the Durham Chemistry Department, particularly Dr. Dmitry S. Yufit and Dr. Toby J. Blundell for sharing their expertise in crystallography with me. I extend my best wishes to Dr. Dmitry S. Yufit on his well-deserved retirement.

Lastly, I would like to express my gratitude to friends and family for their unwavering support throughout this journey.

Contents

Abstract	iv
Declaration	vii
Acknowledgements	ix
Abbreviations	xv
1 Introduction	1
1.1 Chirality	1
1.2 Nitrogen stereocentres	4
1.2.1 Aziridines and strained ring systems	6
1.2.2 <i>N</i> -oxides	10
1.2.3 History of nitrogen stereogenicity	12
1.3 Resolution of nitrogen stereocentres	15
1.3.1 Crystallisation	15
1.3.2 Enzymatic resolution	18
1.3.3 Ammonium cation-BINOL resolution	18
1.3.4 Conglomerate crystallisation of ammonium salts	19
1.4 Quaternary ammonium cations	21
1.4.1 Alkylation and dealkylation	21
1.4.2 Diastereoselective alkylation	22
1.4.3 Transfer of <i>N</i> -stereochemical information	24
1.5 Ammonium cation recognition	27
1.5.1 Supramolecular recognition units	27
1.5.2 Neurotransmitters	28
1.6 Bioactive nitrogen stereocentres	31
1.7 Enantioselective preparation of <i>N</i> -stereocentres	33
1.8 Aims and objectives	34
2 Recognition of achiral ammonium salts	35
2.1 Ammonium cation recognition	36
2.1.1 Quaternary ammonium cation selectivity in biology	37
2.1.2 Supramolecular quaternary ammonium cation selectivity	37
2.2 Achiral ammonium salt ternary complexes with (<i>R</i>)-BINOL	40
2.3 Crystallographic analysis	43
2.3.1 Encapsulation by a hydrogen bonded network	43
2.3.2 Precipitated material versus crystallised material	45
2.4 Isostructure analysis	46

CONTENTS

2.4.1	COMPACT matrix	47
2.4.2	Isostructure characterisation	48
2.4.3	Composite Hirshfeld fingerprint plot analysis	49
2.5	Quaternary ammonium salt selectivity	52
2.5.1	<i>In silico</i> calculations	53
2.6	Aqueous ammonium salt extraction and competition	55
2.7	Chapter 2 summary	57
3	Polymorphic and pseudopolymorphic ternary complexes	59
3.1	Ethanol versus chloroform	62
3.1.1	Changes in selectivity of quaternary ammonium salts	67
3.2	Racemic versus enantiopure BINOL	68
3.2.1	Changes in substitutional selectivity	69
3.3	Chapter 3 summary	71
4	Enantioselective synthesis of <i>N</i>-methyl anilinium salts	73
4.1	Crystallisation induced asymmetric transformation	73
4.2	Tertiary aniline synthesis	75
4.3	Racemic ammonium salt synthesis	78
4.4	Chiral ammonium salt ternary complexes with BINOL	80
4.5	Enantioenrichment determination	88
4.5.1	Chiral HPLC	88
4.5.2	BINPHAT	89
4.6	Chiral ternary complexes crystallographic analysis	90
4.7	Crystallisation variables	95
4.7.1	Enantioenrichment	95
4.7.2	Precipitation	97
4.8	Derivatisation of chiral ammonium cations	99
4.8.1	Further chiral ammonium salts application trials	100
4.9	Resolution of substituted BINOLs	101
4.10	Chapter 4 summary	104
5	Solid state enantioselectivity of ternary complexes	105
5.1	Mismatched diastereomeric pairs	106
5.2	Long range order	112
5.3	Disordered cations	113
5.4	Isostructural basis set	114
5.5	Chapter 5 summary	117
6	Chiral crystallographic phenomena	119
6.1	Spontaneous resolution	122
6.1.1	Quaternary ammonium salt conglomerates	126

6.2	Z' >1 conglomerate search	129
6.2.1	What does Z' mean?	131
6.2.2	Conglomerates with Z' >1	132
6.2.3	Kryptoracemates	134
6.2.4	Solid solutions of enantiomers	139
6.2.5	Quasiracemates	144
6.3	Chapter 6 summary	145
7	Additional projects	147
7.1	Chiral protonated ammonium cation complexes	147
7.2	Amine catalysed Suzuki-Miyaura coupling	148
7.3	EthR booster drug development	150
7.4	Tetrahalopyridyl crystallinity	152
8	Future work	157
8.1	Application of enantioenriched ammonium salts	158
8.2	Enantioselective synthesis of other scaffolds	158
8.3	Expansion to additional heteroatoms	159
8.4	High throughput crystallography	159
9	Experimental	161
9.1	Experimental specifications	161
9.2	Tertiary aniline synthesis	166
9.2.1	General procedure for reductive amination: A	166
9.2.2	General procedure for reductive amination: B	174
9.2.3	General procedure for reductive amination: C	176
9.2.4	General procedure for reductive amination: D	178
9.2.5	General procedure for oxidation of primary alcohols	182
9.2.6	General procedure for amide coupling	185
9.2.7	General procedure for amide reduction	187
9.3	Racemic and achiral ammonium salt synthesis	189
9.3.1	General procedure for alkylation	189
9.4	Protonated ammonium salt synthesis	212
9.4.1	General procedure for preparation of protonated ammonium salts	212
9.5	Recognition of ammonium salts	219
9.5.1	General procedure for recognition of ammonium salts	219
9.6	Aqueous ammonium cation recognition	273
9.7	Selective recognition experiments	274
9.7.1	General procedure for selective complexation experiments	274
9.7.2	Ammonium cation replacement experiment	282
9.7.3	Selective recognition from biology	283
9.7.4	Selective complexation experiments in CHCl ₃	286

CONTENTS

9.7.5	Selective complexation experiments with <i>rac</i> -BINOL	289
9.8	CIAT of ammonium salts	296
9.8.1	General procedure for CIAT of ammonium cations	296
9.9	Isolation of enantioenriched ammonium salt	336
9.10	Synthesis of substituted BINOLs	338
9.10.1	General procedure for the synthesis of substituted BINOLs	338
9.10.2	Resolution of 6,6'-dibromo, 1,1'-bi-2-naphthol	341
9.11	Mismatched diastereomeric complexes	344
9.11.1	General procedure for mismatched complex synthesis	344
9.12	Chiral tertiary ammonium salt complexes	351
9.12.1	General procedure tertiary ammonium salt complex synthesis	351
9.13	Enantioenrichment determination	357
9.13.1	Racemic ammonium salt HPLC traces	357
9.13.2	(<i>R</i>)-BINOL and (<i>S</i>)-BINOL complex HPLC traces	362
9.13.3	Liberated salts HPLC traces	371
9.13.4	Substituted BINOL HPLC traces	372
9.14	Chiral shift NMR spectroscopy	374
9.14.1	Procedure for the synthesis of [(Δ , <i>R</i>)-BINPHAT][NH ₂ Me ₂ ⁺]	374
9.14.2	Counterion exchange for chiral shift NMR experiments	377
9.14.3	¹ H NMR spectra of ammonium cations · [(Δ , <i>R</i>)-BINPHAT]	378
	Appendix	409
A	Crystallographic data	409
B	CSD searches	515
B.1	Refcodes of conglomerates with $Z' > 1$	515
B.2	Refcodes of kryptoracemates	516
B.3	Refcodes of solid solutions of enantiomers	518

Abbreviations

α	optical rotation
δ	chemical shift
λ	wavelength
Ac	acetate
ACh	acetylcholine
AChase	acetylcholinesterase
AIDS	Acquired Immunodeficiency Syndrome
Bn	benzyl
BINOL	1,1'-bi-2-naphthol
BINAP	2,2'-Bis(diphenylphosphino)-1,1'-binaphthalene
BINPHAT	1,1'-binaphthalene-2,2'-diolato-(bis(tetrachloro-1,2-benzenediolato)phosphate(V)
BORBIN	bis-(1,1'-binaphthalene-2,2'-dioxy)-borate
CIAT	crystallisation induced asymmetric transformation
CIDR	crystallisation induced dynamic resolution
CIDT	crystallisation induced dynamic transformation
COF	covalent organic framework
CPME	cyclopentyl methyl ether
DABCO	1,4-diazabicyclo[2.2.2]octane
DBTA	dibenzoyltartaric acid
DCE	1,2-dichloroethane
DKR	dynamic kinetic resolution
DMAP	4-(dimethylamino)pyridine
EC ₅₀	half maximal effective concentration
ee	enantiomeric excess
er	enantiomeric ratio
equiv	equivalents
Et	ethyl
ETH	ethionamide
GoF	Goodness-of-Fit
GABA	gamma-aminobutyric acid
HOF	hydrogen bonded organic framework

CONTENTS

hrs	hours
HPLC	high performance liquid chromatography
IC ₅₀	half maximal inhibitory concentration
IUCr	International Union of Crystallography
M	metal
Me	methyl
MNTX	methylnaltrexone
MOF	metal organic framework
PDB	Protein Data Bank
Ph	phenyl
pin	pinacol
PTC	phase transfer catalysis
rt	room temperature
R _t	retention time
^t Bu	<i>tert</i> -butyl
SAM	<i>S</i> -adenosylmethionine
SCXRD	single crystal X-ray diffraction
TB	tuberculosis
TBAI	tetrabutylammonium iodide
TEA	triethylamine
TFA	trifluoroacetic acid
TCP	tetrachloropyridine
TFP	tetrafluoropyridine
THF	tetrahydrofuran
THP	tetrahalopyridine
TOF	time of flight
TQD	triple quadrupole detector
TRISPHAT	tris(tetrachloro-1,2-benzenediolato)phosphate
X	halogen
XRD	X-ray diffraction
Z	number of molecular formula units in the unit cell
Z'	number of molecular formula units in the asymmetric unit

Chapter 1

Introduction

1.1 Chirality

The term chirality, first introduced by Lord Kelvin in 1893 during a Robert Boyle lecture, pertains to a phenomenon inherent to certain rigid entities. Specifically, chirality describes the geometric attribute of an object to possess non-superposability upon its mirror image.³ This characteristic underpins the fundamental notion that such objects exist as distinct left- and right-handed variants, a property with profound implications across the spectrum of scientific disciplines. The term chirality has since become an indispensable cornerstone of synthetic chemistry.

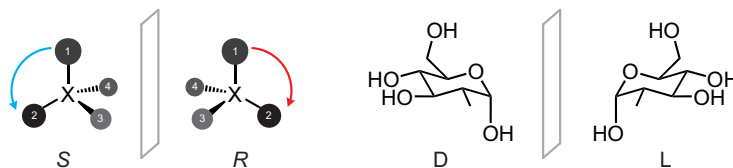
Before being coined chirality, Louis Pasteur termed the occurrence as 'dissymmetry' when he first encountered the phenomenon while investigating tartaric acid salts.⁴ Pasteur observed crystallisation of the sodium ammonium salt of paratartaric acid ((±)-tartaric acid) into a mixture of hemihedral and enantiomorphous crystals, whose optical activity measured in solution was equal in magnitude but opposite in direction. He concluded that (±)-tartaric acid was structurally dissymmetric. Subsequent research in this field unveiled helical or tetrahedral atomic configurations as plausible explanations for the phenomenon of dissymmetry.^{5,6}

Despite Le Bel and van't Hoff communicating potential explanations for dissymmetry in 1874, leading to the derivation of the Le Bel-van't Hoff rule,⁷ the term "chirality" remained predominantly associated with physics until its formal integration into the field of chemistry by Mislow in 1962.⁸ The current definition of chirality, which concerns structural dissymmetry, emerged as a result of this pioneering work by Mislow and Prelog.^{9,10} It is now understood that many molecules possess the attribute of chirality with the specific chirality exhibited contingent upon the geometric configuration and orientation of these molecules (see Figure 1.1.).

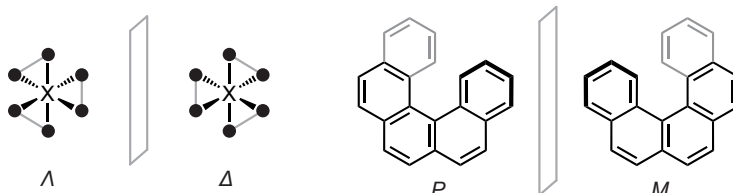
1.1. CHIRALITY

Molecular Chirality

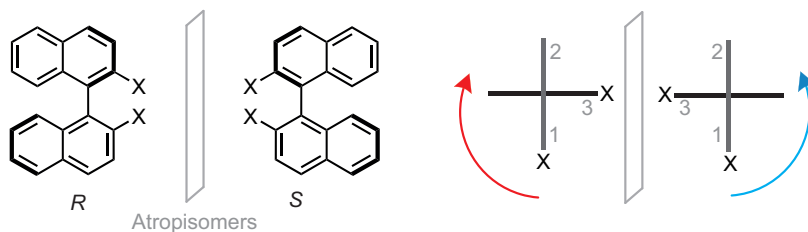
Point



Helical



Axial



Topological

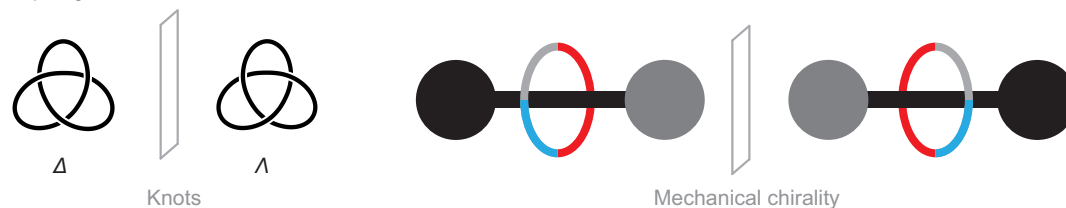


Figure 1.1: The different types of molecular chirality.

The manipulation of molecular chirality poses a significant challenge for synthetic chemists.¹¹ In the early 1900s numerous attempts, with varying levels of success, were made to create optically active compounds from achiral substrates by utilising enzymes or moulds.¹² Later successful non-enzymatic approaches began to emerge. In 1913 Bredig and Fiske detailed the first well established, non-enzymatic enantioselective synthesis by reporting the synthesis of mandelonitrile with approximately 8% enantiomeric excess (ee) from benzaldehyde and HCN, employing quinine or quinine as chiral catalysts.¹³ Subsequent research involved the development of catalytic chiral metal complexes. A fundamental development in 1956 demonstrated that the adsorption of palladium chloride onto silk fibroin fibres could be utilised for synthesising chiral amines and amino acids, marking the inaugural utilisation of this methodology.¹⁴ More recently, Knowles, Sharpless and Noyori achieved pioneering develop-

ments in enantioselective hydrogenation and oxidation reactions, meriting them the Nobel Prize in Chemistry in 2001.¹⁵ Knowles' primary objective was to establish a scalable, enantioselective catalytic synthesis, with the aim of producing the rare amino acid *L*-DOPA,¹⁶ recognised for its therapeutic value in the treatment Parkinson's disease. In 1968, Knowles reported a chiral phosphine ligand, a rhodium PAMP catalytic complex,¹⁷ later evolving it into a DiPAMP ligand.¹⁸ Subsequently, Noyori contributed to the field by devising $\text{RuCl}_2 \cdot (R)\text{-BINAP}$, a superior and more versatile enantioselective catalyst.^{19,20} Building upon these seminal achievements, many diverse variations of enantioselective catalytic syntheses have since found application in an abundance of important industrial processes.

Carbon, owing to it being the most common stereogenic atomic centre and its ubiquity in Nature, has been most extensively studied in the field of enantioselective synthesis.²¹ Presently, there is a growing interest in exploring the stereogenic potential of heteroatoms such as boron,²² nitrogen,¹ silicon,²³ phosphorus,^{24,25} sulfur,²⁶ and oxygen,²⁷ due to their capacity to also act as stereogenic elements. Given its prevalence as the second most frequently encountered stereocentre in Nature and the evident utility of heteroatoms in enantioselective syntheses, nitrogen stereocentres stand out as an obvious choice for organic chemists seeking a tool to impart and control stereochemistry in syntheses.²⁸

1.2 Nitrogen stereocentres

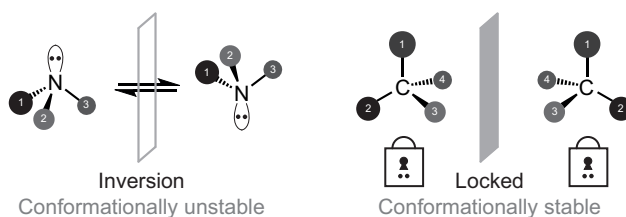


Figure 1.2: Rapid pyramidal inversion of amines in contrast to conformationally and configurationally locked quaternary carbon stereocentres.

The potential for nitrogen to act as a stereocentre is often overlooked due to its propensity for rapid pyramidal inversion and frequent quantum tunneling at room temperature (see Figure 1.2.).²⁹ Where quaternary carbon stereocentres are locked, the conformational instability of amines limits the prospect of enantioenriching molecules which contain nitrogen as the sole stereogenic element. Nonetheless, it remains possible to resolve and isolate certain enantiomers whose chirality originates from a stereogenic nitrogen by locking the lone pair in a stable conformation and configuration.

There are numerous examples reported which lock the stereochemistry of a nitrogen stereocentre. These methods include: the use of *N*-bridgeheads;³⁰ strained systems;^{31,32} coordination to metals;^{33,34} the formation of *N*-oxides;³⁵ and the synthesis of quaternary ammonium salts (see Figure 1.3.).³⁶ However, the development of resolution techniques in this context has been relatively restricted and until recently no general methodology existed to enantioselectively prepare a nitrogen stereocentre as the sole stereogenic element.^{2,37}

Bridgeheads serve as effective tools to prevent inversion of the nitrogen lone pair by making such inversion impossible without disrupting the integrity of the ring. This effect is exemplified in the *Cinchona* alkaloid family, where the *N*-bridgehead is configurationally locked, rendering the nitrogen atom stereogenic. This property, coupled with the presence of four additional carbon stereocentres, makes these compounds highly suited for precise control of chirality in synthetic processes. Notably, compounds such as quinine and quinidine, members of the *Cinchona* alkaloid family, have been employed as ligands in enantioselective synthesis, particularly in the dihydroxylation

of alkenes.³⁸

Coordination to a metal centre or a Lewis acid offers another method to immobilise the configuration of an amine. The formation of a dative bond traps the amine lone pair, establishing configurational stability at the *N*-stereocentre. In this context, the presence of the nitrogen stereocentre may introduce chirotopicity about the metal centre, enabling the chiral metal complex to convey stereochemical information during synthetic processes.³⁹

Simple alkylations to produce quaternary ammonium salts also produce nitrogen stereocentres which are conformationally and configurationally stable. This method is the most common and the simplest way to prevent lone pair inversion, due to the ease of alkylating nucleophilic nitrogen with a range of electrophiles.⁴⁰

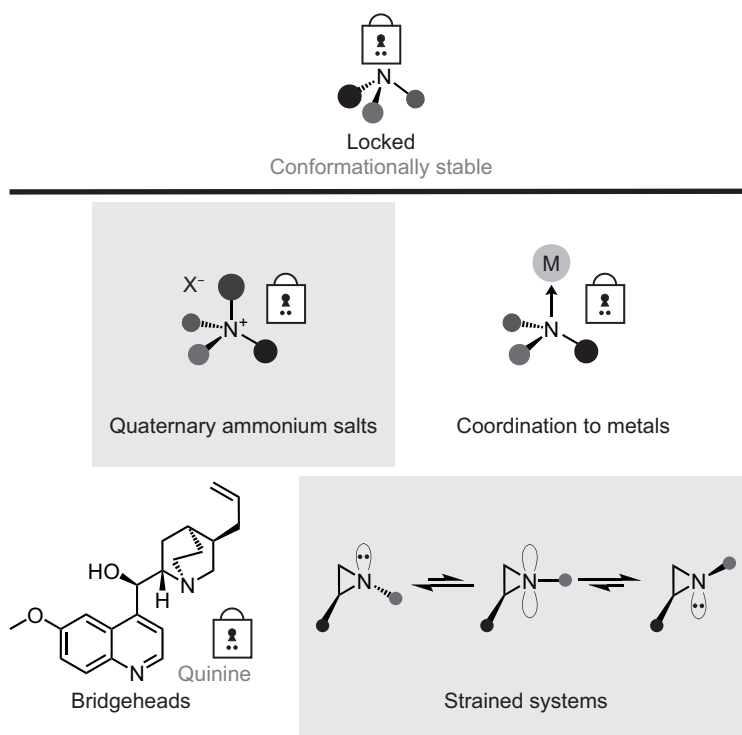


Figure 1.3: Methods to lock the *N*-lone pair into a stable conformation and configuration.

1.2.1 Aziridines and strained ring systems

Due to their ring strain, aziridines are highly activated for ring-opening reactions under mild conditions and serve as valuable synthons in organic synthesis. Gabriel's early work in 1888^{41,42} and Wenker's well-known synthesis in 1937⁴³ marked the inception of aziridine synthesis. Prior to 1891, literature reviews did not evidence stereoselective aziridine synthesis nor subsequent isolation of the nitrogen stereocentre; however, ensuing examples have emerged, facilitated by the application of chiral ligands and auxiliaries and by the functionalisation of amino acids and sugar derivatives.^{44,45}

Aziridines, owing to their substantial ring strain, exhibit a significantly reduced rate of pyramidal inversion at nitrogen, enabling the isolation of these compounds as single enantiomers.⁴⁴ The constrained C-N bond angle within the aziridine ring (60°) deviate significantly from the optimal bond angle for sp^3 hybridised centres (109.5°). During the inversion process, the bond angle of the nitrogen sp^2 intermediate exhibits an even greater deviation from the optimal trigonal planar geometry, further destabilising the transition state relative to the ground state (see Figure 1.3.). Consequently, highly strained rings exhibit heightened levels of conformational and configurational stability in contrast to their more flexible ring counterparts and acyclic amines. This stability arises from the necessity to traverse a high-energy intermediate state for inversion to take place. The elevated energy barrier to inversion enhances the effectiveness of aziridines in stereoselective processes by enabling their synthesis with precise enantiocontrol, thus facilitating subsequent regio- and stereoselective ring-opening reactions.

The energetic barrier to pyramidal inversion of nitrogen centres substituted within saturated ring systems can be rationalised by considering the same principles explaining the retarded rate of inversion observed in aziridines.²⁹ The deviation from optimal bond angle in the ground state versus the deviation from optimum bond angle in the transition state must be reasoned alongside the relative torsional strains imparted onto the system via passing through a trigonal planar intermediate. In the context of ring systems, the presence of a ring typically augments the barrier to nitrogen inversion in comparison to analogous acyclic counterparts. If n equals the number of members in a

saturated ring system containing a nitrogen centre, then the relative inversion barriers of these species follows: $n = 3 \gg 6 > 4 > 5 > 7$ (see Figure 1.4.).^{46–50}

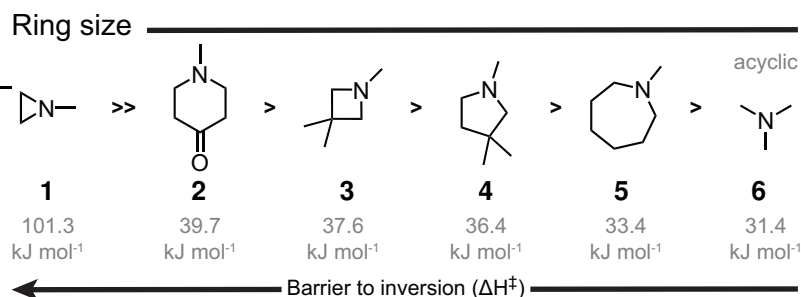


Figure 1.4: Energy barriers to inversion (ΔH^\ddagger / kJ mol^{-1}) of various cyclic amines with different ring sizes.

Pyramidal inversion proceeds through a planar transition state, where the lone pair of the tertiary amine resides in a p orbital. In the tetrahedral ground state, the lone pair adopts an sp^3 hybridisation with greater relative s character compared to the transition state. Pi (π) electron donation towards the nitrogen atom destabilises the trigonal planar transition state due to electron donation into the already occupied p orbital. In contrast, because the lone pair occupies an sp^3 orbital in the ground state, it is less destabilised than the transition state by π electron donation. Consequently, resonance from electron-donating groups toward the nitrogen centre generally increases the barrier to inversion. Conversely, π electron-withdrawing groups have the effect of reducing the barrier to inversion (see Figure 1.5.).²⁹

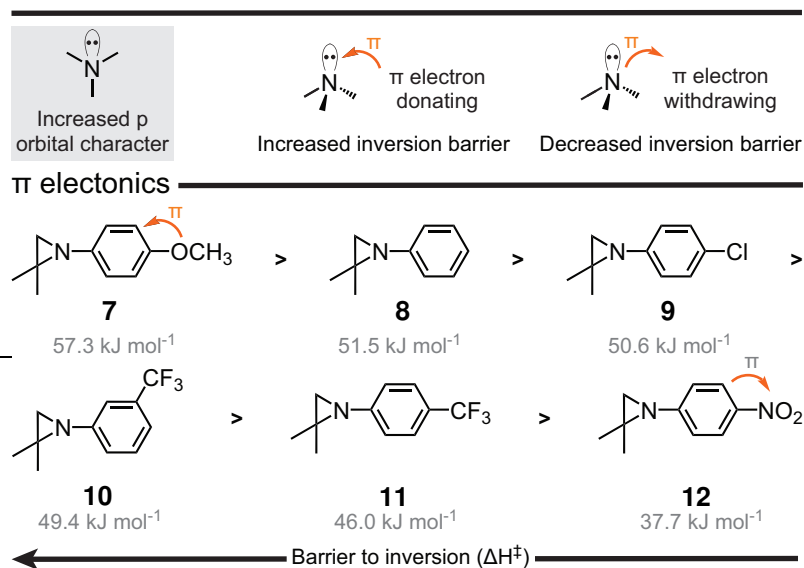


Figure 1.5: Energy barriers to inversion (ΔH^\ddagger / kJ mol^{-1}) of various cyclic amines with different substituent electronics.

1.2. NITROGEN STEREOCENTRES

Sigma (σ) electron-withdrawing groups, typically characterised by electronegative atoms, exert a dual influence on the barrier to inversion through two divergent mechanisms. Firstly, they elevate the s-character of the nitrogen lone pair, thereby reducing its ability for the sp^3 to p transition, essential for pyramidal inversion. In contrast, the repulsion between lone pairs on electronegative atoms and the lone pair of electrons on a tertiary amine destabilises the ground state, thus reducing the barrier to pyramidal inversion. In most cases, the former inductive effect prevails in significance, with inductive electron-withdrawing functionalities commonly elevating the barrier to inversion in tertiary amines (see Figure 1.6.).^{47,51–55}

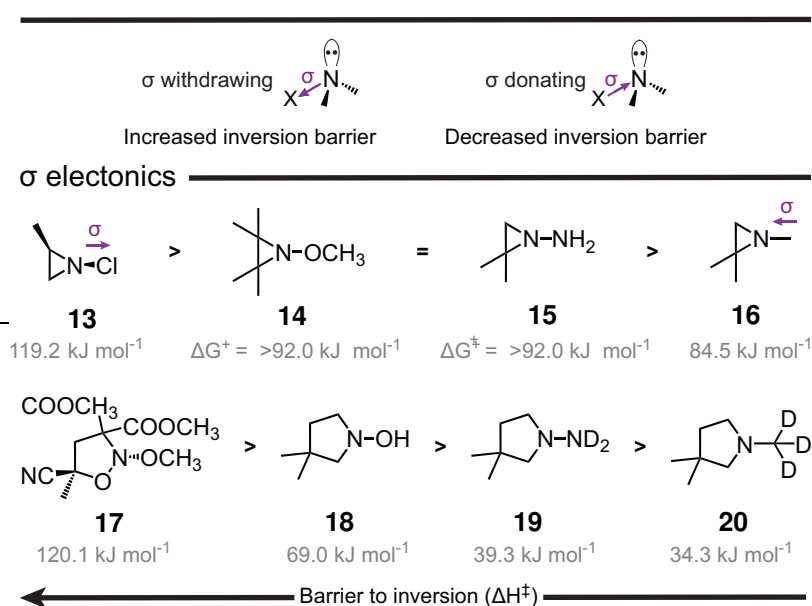


Figure 1.6: Energy barriers to inversion (ΔH^\ddagger / kJ mol⁻¹) of various cyclic amines with different substituent σ electronics.

The introduction of steric bulk in the vicinity of the inversion centre results in a reduction of the energy barrier for the pyramidal inversion process by causing greater destabilisation of the tetrahedral ground state compared to the trigonal planar transition state. This phenomenon arises from the fact that during the transition state, the substituent groups are held farther apart than in the ground state, thereby magnifying the destabilising steric effect in the ground state. Furthermore, the impact of sterics varies depending on the proximity of the substituents to the inverting centre, with bulkier groups positioned α to the nitrogen atom exerting a more pronounced influence than those positioned β to it (see Figure 1.7.).^{46,47,49,56,57}

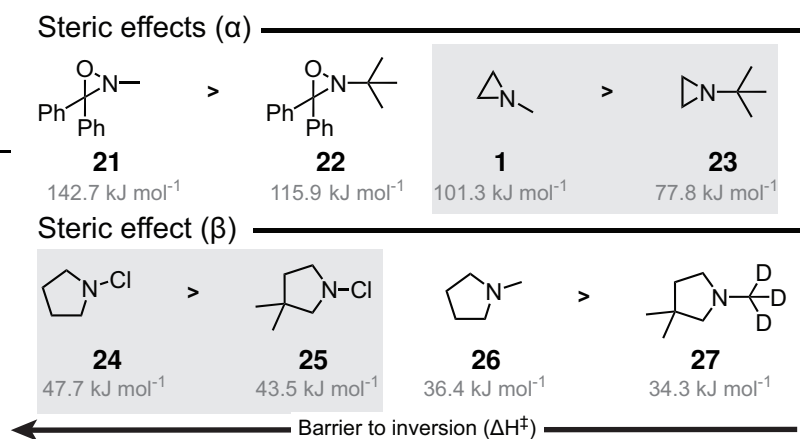


Figure 1.7: Energy barriers to inversion (ΔH^\ddagger / kJ mol⁻¹) of various cyclic amines with different steric substituents.

Understanding the relative energetic barriers associated with amine pyramidal inversion is crucial for establishing nitrogenous stereogenicity. In certain instances, tertiary amines can be isolated with well-defined stereochemistry, a concept proven in the case of aziridines.^{54,56} When considered, the factors governing pyramidal inversion can be harnessed to access other classes of compounds enriched with nitrogen stereocentres. An illustrative instance is the 5-membered ring system, *N*-methoxy-3,3-di-methoxycarbonyl-5-cyan-1,2-oxazolidine (**17**), which can be synthesised as two distinct and separable diastereomers that remain unaffected by pyramidal inversion at room temperature, thus enabling their isolation.⁵⁵

1.2.2 *N*-oxides

Tertiary amine oxides are species in which a sp^3 hybridised nitrogen atom, originating from a tertiary amine, forms a dative bond with an oxygen atom (see Figure 1.8.). Pinner and Wolfenstein first reported their synthesis in 1892,⁵⁸ and their structural confirmation through X-ray crystallography was subsequently achieved by Lister and Sutton in 1939.⁵⁹ Due to the tetrahedral geometry about the nitrogen centre, tertiary amine oxides can feature stereogenic nitrogen when all substituent groups bound to the nitrogen atom are different.⁶⁰

The most common way to prepare *N*-oxides is from direct oxidation of the corresponding tertiary amine using reagents such as: hydrogen peroxide,⁶¹ alkyl hydroperoxides,⁶² peracids,^{63,64} molecular oxygen,⁶⁵ and oxaziridines,⁶⁶ with oxidation using *m*-CPBA, a peroxycarboxylic acid, being utilised as the primary method in recent years.⁶³ The reverse-Cope cyclisation, can also be used as an alternative strategy for amine *N*-oxide synthesis and was first delineated by Cope and Le Bel in 1960.⁶⁷ Furthermore, the alkylation of hydroxylamines with alkyl halides, initially documented by Dunstan and Goulding in 1899, remains a noteworthy technique for the generation of tertiary amine *N*-oxides.⁶⁸

The first resolution of an *N*-oxide was achieved by Meisenheimer in 1908, via fractional crystallisation of *N*-ethyl, *N*-methyl, aniline *N*-oxide with 3-bromocamphor-8-sulfonic acid, yielding an isolable diastereomer of **28** ($[\alpha]_D = +67^\circ$).⁶⁹ Subsequent isolation of the *N*-oxide HCl salt (**29**) showed optical activity owing to the *N*-stereogenicity of the moiety ($[\alpha]_D = +17^\circ$). Drabowicz *et al.* later conducted NMR investigations on **29**, employing thiophosphoric acids as chiral resolving agents, to confirm the chirotopicity of the system through revealing distinct shifts for diastereotopic *N*-CH₃ protons.⁷⁰ Numerous methodologies have since emerged for the resolution and synthesis of *N*-oxides, such as the use of enantiopure BINOL by Toda *et al.* to resolve a range of *N*-oxides related to those initially studied by Meisenheimer.⁷¹

In addition to resolution, oxidation of tertiary amines can proceed diastereoselectively to produce the desired sense of the *N*-stereocentre in an *N*-oxide. For exam-

ple, oxidation of *N*-benzyl proline derivatives can be employed to yield *syn* *N*-oxide products due to forming an intramolecular hydrogen bond between O- and NH on the amide. This hydrogen bond is a crucial requirement for the observed stereoselectivity.^{72,73} The resulting products have found use in many versatile transformations such as, Meisenheimer rearrangements,^{74,75} Cope rearrangements, Polonovski reactions, co-ordination to metal complexes and as catalysts.^{62,76}

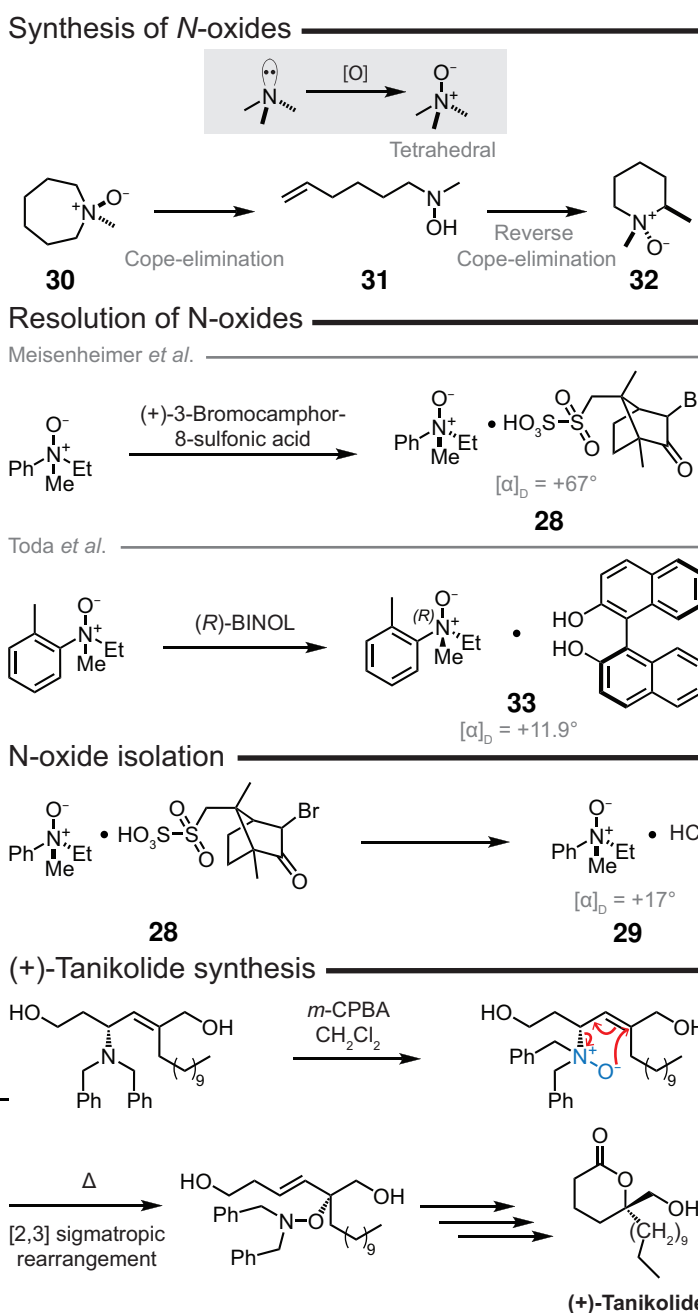


Figure 1.8: Synthesis, resolution and rearrangements of *N*-oxides.

1.2.3 History of nitrogen stereogenicity

In 1891, Le Bel proposed the existence of stereogenic nitrogen after reporting the optical activation of *N*-methyl, *N*-ethyl, *N*-propyl, *N*-isobutyl ammonium chloride **34** by *Penicillium glaucum* ($[\alpha]_D = -0.30$, see Figure 1.9.).⁷⁷ Le Bel suggested that the nominal enantioenrichment observed in solution resulted from an excess of one pentavalent nitrogen stereocentre relative to its enantiomer. However, Marckwald and von Droste-Huelshoff's attempts to replicate Le Bel's findings were unsuccessful, leading them to question Le Bel's conclusions.⁷⁸ Le Bel, in turn, argued that their findings and observed lack of enantioenrichment could be attributed to the order of alkylation of the nitrogen centre.⁷⁹ However, this assumption by Le Bel was subsequently disproven by Pope and Read in 1912.⁸⁰ They not only confirmed that the order of alkylation did not yield different salts but also established that the observed optical rotation was attributable to an impurity introduced by the microorganism, rather than the presence of a stereochemically enriched nitrogen stereocentre.

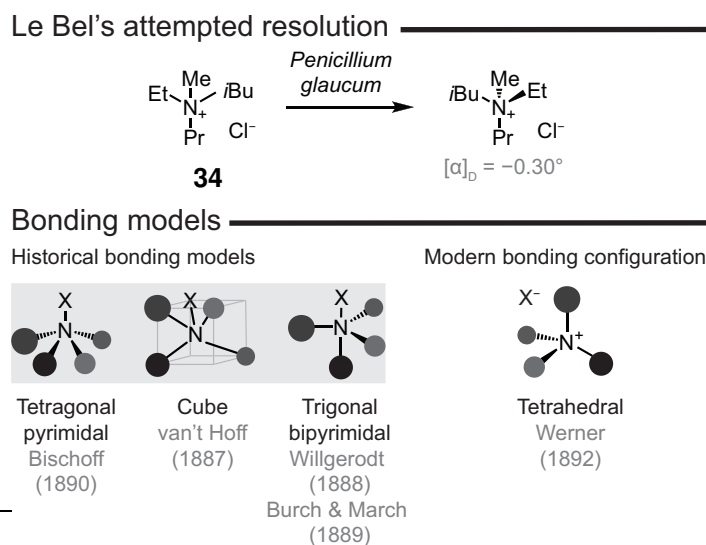


Figure 1.9: Le Bel's attempted resolution of **34** by *Penicillium glaucum* and the different bonding models proposed about a nitrogen centre.

Le Bel's belief that the order of alkylation impacted the products molecular structure can be attributed to the prevailing model of ammonium salt bonding during his time (see Figure 1.9.). During that era, the accepted model depicted ammonium cations as pentavalent, with the counterion directly bound to the nitrogen centre.⁸¹ This pentavalent model was described in various geometric forms, including tetragonal pyramidal

(as proposed by Bischoff in 1890), trigonal bipyramidal (suggested by Willgerodt in 1888 and by Burch and March in 1889), or even cube-shaped (as presented by van't Hoff in 1887).⁸²

Further investigations into Le Bel's salt (**34**) involved efforts to resolve tetraalkylammonium hydroxides using optically active acids, as exemplified by Edgar Wedekind.³⁶ Despite Wedekind's unsuccessful attempts to resolve benzylphenylallylmethylammonium hydroxide with tartaric and camphoric acid, his research proved valuable in revealing discrepancies with the accepted pentavalent bonding model.⁸³ Within his reports, Wedekind documented instances in which the order of reagent addition led to the formation of the same compound, demonstrating that the structure could not adhere to a pentavalent configuration. Notably, by employing a unique order of addition, in which methylation occurred in the final alkylation step, Wedekind somewhat surprisingly isolated trimethylanilinium bromide (see Figure 1.10.). Building upon these insights, Wedekind and Jones concluded that the ammonium salt must possess the capacity to dissociate when subjected to heating in solution.⁸⁴ Furthermore, they discerned that various alkyl groups exhibited differing degrees of readiness to dissociate, with allyl and benzyl functionalities proving more susceptible than the methyl functionality. This observation partly accounted for the shortcomings in Wedekind's earlier resolution endeavours. The presence of hydroxide counterions in aqueous solutions introduced instability onto the ammonium salts causing dissociation to tertiary amines and alcohols, consequently impeding the resolution process.

Pope and Peachy adapted Wedekind's approach, exploiting the greater stability of an ammonium salt containing an iodide counterion compared to a hydroxide anion in aprotic solvents, to prepare enantioenriched benzylphenylallylmethylammonium iodide through crystallisation with enantiomerically pure silver camphorsulfonate (**36**).¹ This milestone marked the inaugural instance of a resolved tetraalkylammonium salt and demonstrated that optically active nitrogen-containing molecules could owe their optical activity to a stereogenic centre other than carbon. Werner's assertion that the stereogenicity of nitrogen could be explained in the same manner as that of carbon prompted a shift from the previously accepted pentavalent bonding models to the tetrahedral model for ammonium bonding, which is now widely recognised in synthetic

chemistry.

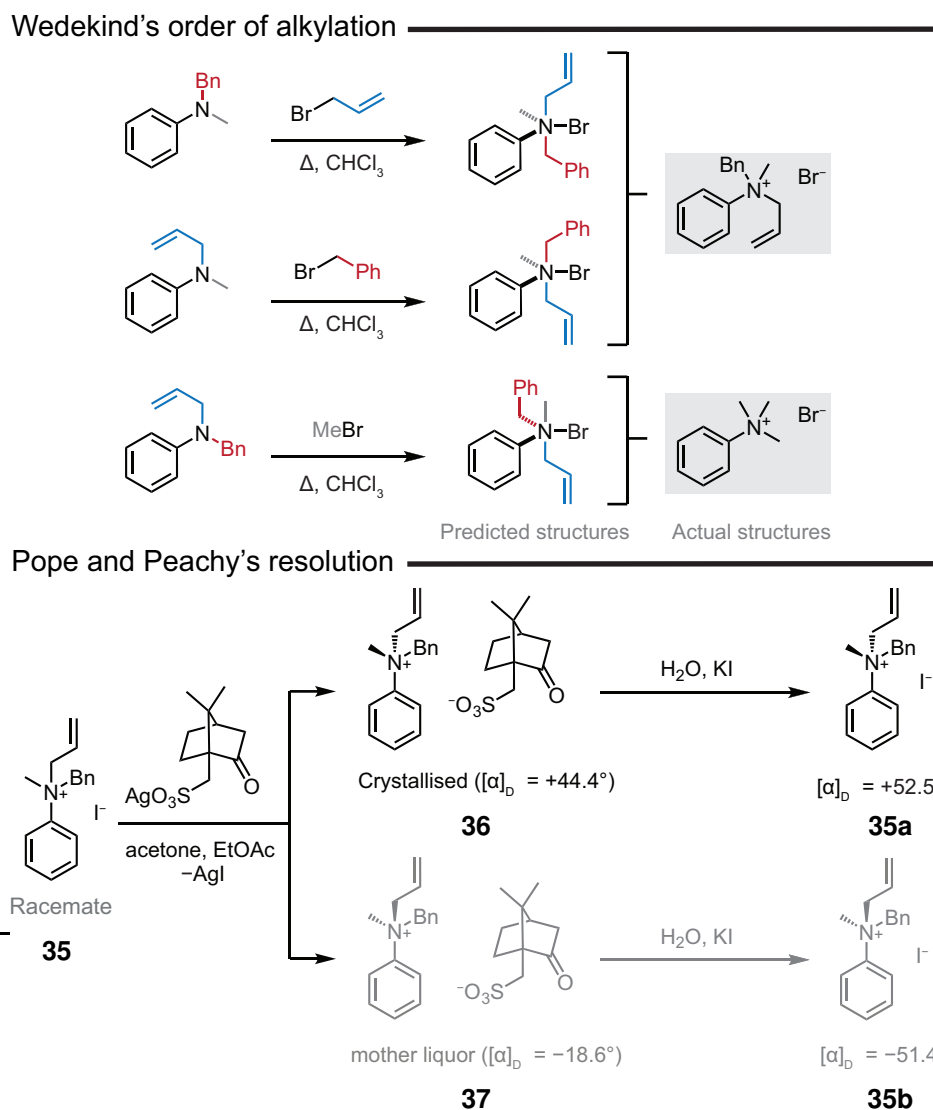


Figure 1.10: Wedekind's order of alkylation experiments and Pope and Peachy's resolution of **35** with silver camphorsulfonate.

1.3 Resolution of nitrogen stereocentres

The most common way to synthesise enantiopure compounds is via the resolution of racemates.^{85,86} However, for chiral compounds containing a nitrogen stereocentre this has been a challenge due to the following reasons: enantiomers have identical physical properties; ammonium salts are hard to isolate owing to their inherent hygroscopicity; and the stereocentre has the capacity to undergo spontaneous rearrangements at room temperature.⁸⁷ Fortunately, advancements in organic chemistry have led to the development of methods that address these challenges, enabling the isolation of enantiopure compounds containing nitrogen stereocentres. Here, crystallisation is focused on as a key resolution technique.

1.3.1 Crystallisation

Crystallisation stands as the primary technique employed by synthetic chemists for the resolution of enantiomers. This process encompasses various methodologies, including preferential crystallisation, diastereoisomeric crystallisation and catalytic kinetic resolution.⁸⁸

Preferential crystallisation involves the sequential and alternating crystallisation of both enantiomers as conglomerates from a racemic mixture.⁸⁹ Diastereomeric crystallisation, which employs a stoichiometric amount of resolving agent, and catalytic kinetic resolution, utilising a sub-stoichiometric amount of resolving agent, facilitates the separation of enantiomers by capitalising on the energy disparity between the two possible diastereomeric salts formed (enantiomers-enantiopure agent).^{90,91} These techniques rely on the different chemical properties exhibited by diastereomers when a chiral resolving agent is introduced to a racemic solution, a phenomenon exploited in the first successful isolation of an optically active quaternary ammonium salt by Pope and Peachy.¹

1.3. RESOLUTION OF NITROGEN STEREOCENTRES

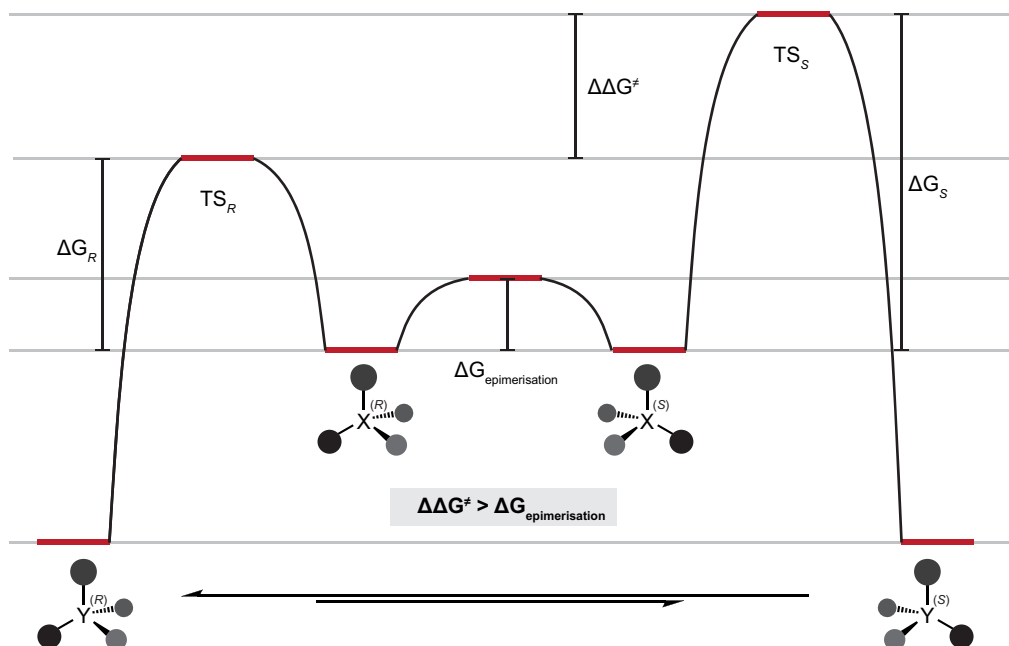


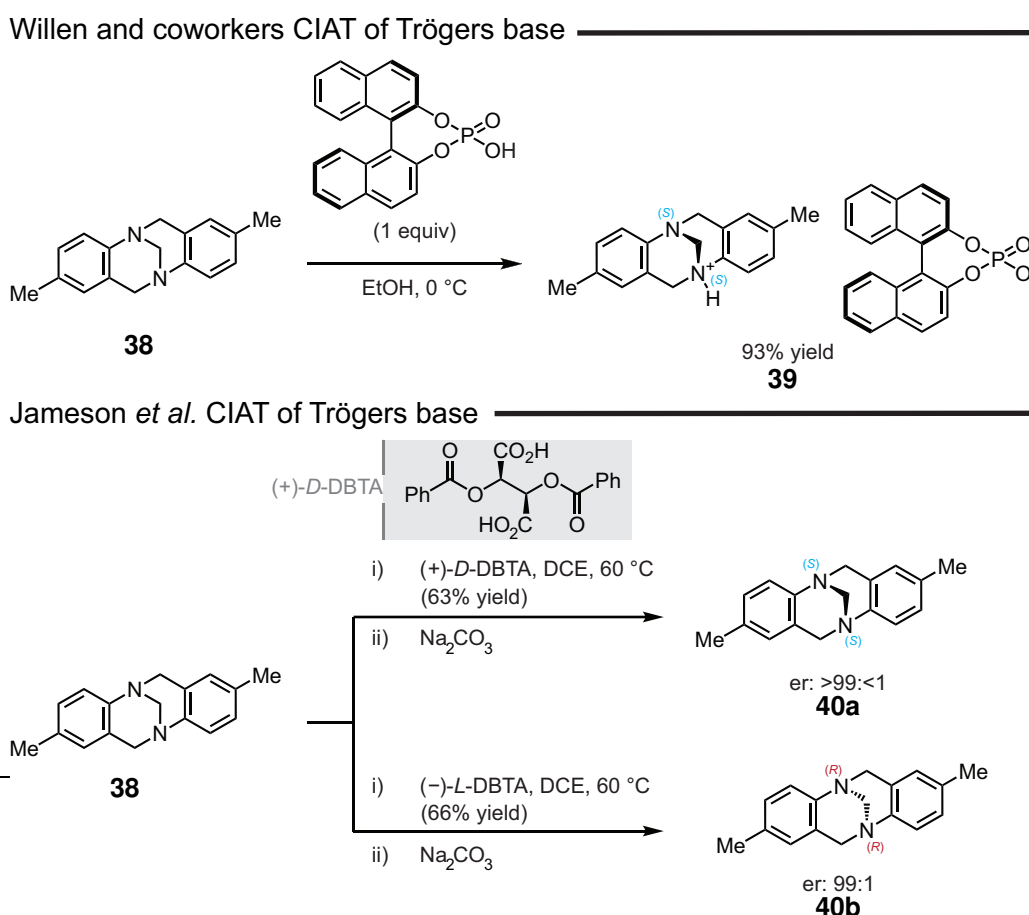
Figure 1.11: Energy level diagram for a typical dynamic kinetic resolution process. Y refers to product and X refers to starting material (reactant). In this instance the *R* enantiomer would be the major product.

The key drawback of a crystallographic kinetic resolution is that the maximum theoretical yield of the process is limited to 50%, since half of the material remains within the mother liquor in the form of the undesired enantiomer.⁹² Moreover, the method necessitates multiple recrystallisations and ion exchanges, which increases the workload for experimentalists. A more efficient methodology, termed dynamic kinetic resolution (DKR), offers the distinct advantage of potentially attaining a 100% yield without compromising the high enantiomeric purity characteristic of a kinetic resolution.⁸⁵ Centred on the Curtin-Hammett principle, DKR capitalises on the fact that in certain systems the activation energy to the reaction of either enantiomer with an enantiopure agent is higher than the energy barrier to racemisation, leading to *in situ* racemisation.⁹³ Consequently, this results in a preferential reaction pathway for the desired enantiomer, as it passes a lower energy transition state (see Figure 1.11.).

Crystallisation-induced asymmetric transformation (CIAT) has found utility in the resolution of chiral ammonium cations, exemplified by the case of Tröger's base (**38**).⁹⁴ Wilen *et al.* co-crystallised a 1:1 mixture of (*R*)-1,1'-binaphthalene-2,2'-diyl hydrogen phosphate with Tröger's base. In the presence of an acid, Tröger's base undergoes racemisation via the formation of a chiral iminium intermediate. Notably, due to the

1.3. RESOLUTION OF NITROGEN STEREOCENTRES

chiral nature of the acid employed, the preferential formation of one of the intermediate diastereomers is favoured over the other, leading to crystallisation of the desired enantiomer from the solution. The key resolution step occurs via crystallisation to give a more thermodynamically stable diastereomeric product (see Figure 1.12.). Subsequently, Jameson *et al.* further refined this methodology, employing enantiopure *O,O'*-dibenzoyltartaric acid (DBTA) to facilitate the CIAT of Tröger's base derivatives (see Figure 1.12.).⁹⁵ This approach mirrors that elucidated by Wilen *et al.* however, Jameson *et al.* extended this process to encompass various substituted derivatives, additionally quantifying the enantioenrichment through the utilisation of chiral high-performance liquid chromatography (HPLC).



1.3.2 Enzymatic resolution

Expanding the spectrum of resolution techniques for Tröger's base derivatives, Kamiyama devised an enzymatic kinetic resolution approach.⁹¹ In this method, treatment with *Candida antarctica* lipase, in the presence of isoprenyl acetate, induced a selective acylation of **41**, primarily favouring the alcohol of the (*S,S*) enantiomer, ultimately yielding **42** in conjunction with the residual, unreacted material, **43** (see Figure 1.13.). This enzymatic kinetic resolution showcased remarkable selectivity, allowing for efficient separation of products when conducted at a preparative scale. Following separation, the products were hydrolysed to remove the acetate group and to afford further functionalisation opportunities.

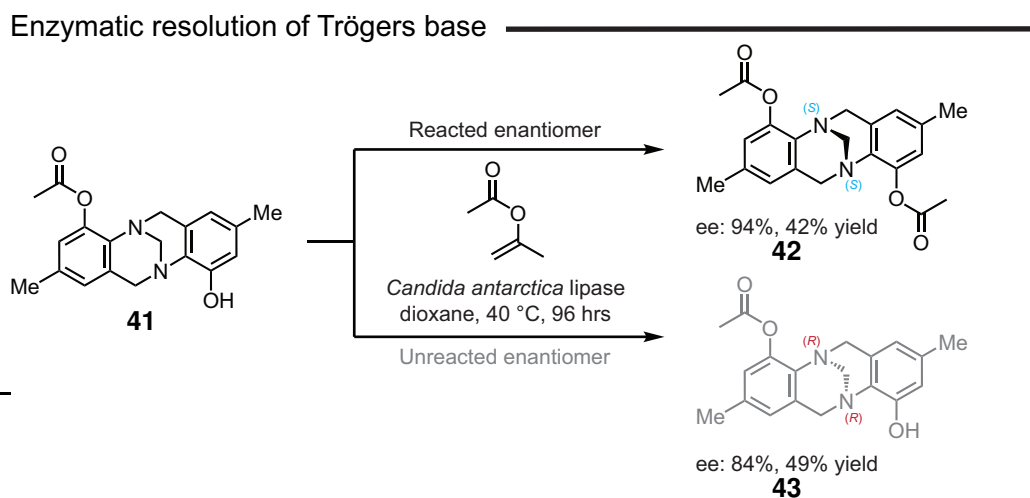
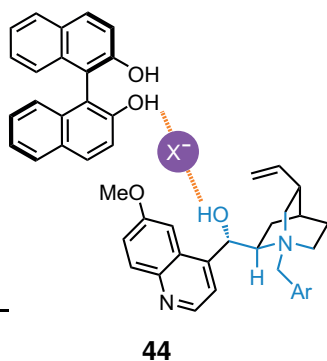


Figure 1.13: Enzymatic resolution of Tröger's base derivatives.

1.3.3 Ammonium cation-BINOL resolution



Molecular complexation between an enantiopure quaternary cinchonium salt and 1,1'-bi-2-naphthol (BINOL) is a well-established technique for the resolution of BINOL enantiomers.^{96,97} The formation of a ternary complex, comprising alkaloid, counterion and BINOL, is facilitated by the presence of hydroxyl groups on both the ammonium resolving agent and the racemic BINOL. These

hydroxyl moieties permit hydrogen bonding contacts to form, ultimately culminating in

the formation of inclusion crystals. Here, the presence of an enantiopure host dictates the diastereo- and enantioselective adductive crystallisation.

This same relationship has also been shown to work in reverse, to recognise and resolve racemic *N*-benzyl ammonium salts using enantiopure (*R*)-BINOL.^{98,99} Because β -hydroxyalkylammonium bromides mimic the structure of Cinchona alkaloids, Tayama and Tanaka were able to develop the first efficient optical resolution of the salts using (*R*)-BINOL (see Figure 1.14.).¹⁰⁰ In a subsequent study, Pan *et al.* advanced this methodology by subjecting a mixture of β -hydroxyalkylammonium bromide epimers to (*R*)-BINOL, achieving significant levels of enrichments (up to 99:1 dr), heightened from the nearly racemic mixture isolated via alkylation alone (53:47 dr).¹⁰¹

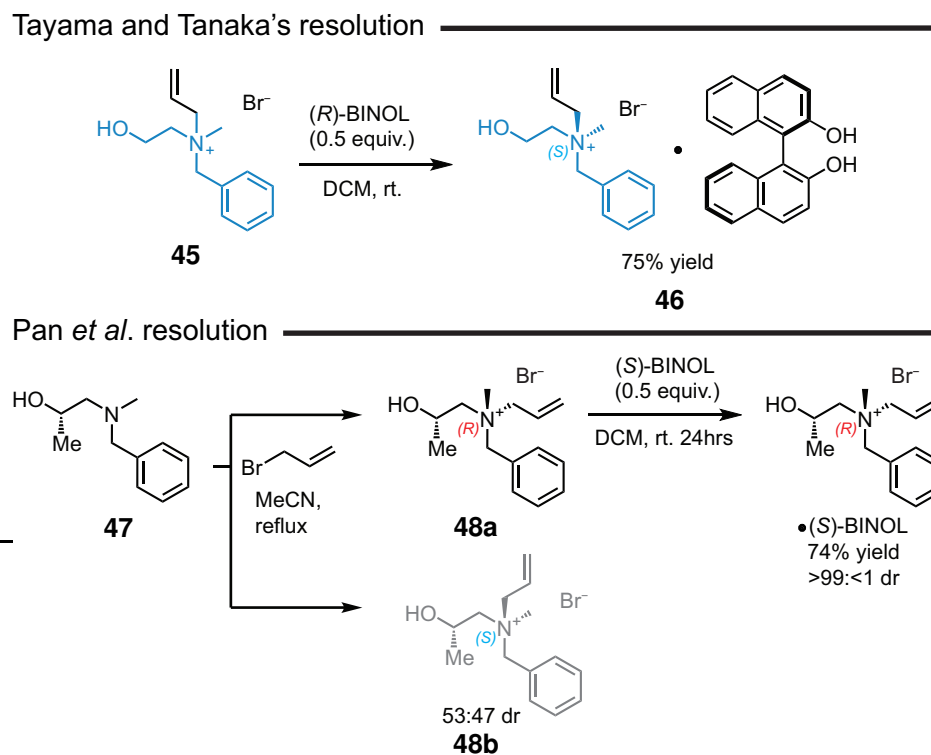


Figure 1.14: Tayama and Tanaka's resolution of **45** using (*R*)-BINOL and Pan *et al.* resolution of epimers employing (*S*)-BINOL.

1.3.4 Conglomerate crystallisation of ammonium salts

The inception of our understanding of chirality can be traced back to Louis Pasteur,⁴ who achieved the first successful resolution through conglomerate crystallisation of sodium ammonium tartrate. Conglomerate crystallisation of racemates is a phe-

1.3. RESOLUTION OF NITROGEN STEREOCENTRES

nomenon characterised by the spontaneous formation of discrete enantiopure crystals from a racemic material. It is estimated that only a modest proportion, approximately 5–10%, of all racemates undergo this form of spontaneous resolution.^{102–104} The identification of conglomerates poses a notable challenge due to the substantial amount of experimental evidence required to prove their distinct crystallisation behaviour. This can further be complicated by polymorphism where specific crystallisation conditions are required to form enantiopure crystals rather than racemic crystals.¹⁰⁵ Given the scarcity of reported conglomerates in the existing literature and our inability to predict this behaviour, it is unclear which and how many ammonium salts have the potential to be resolved directly by conglomerate crystallisation.

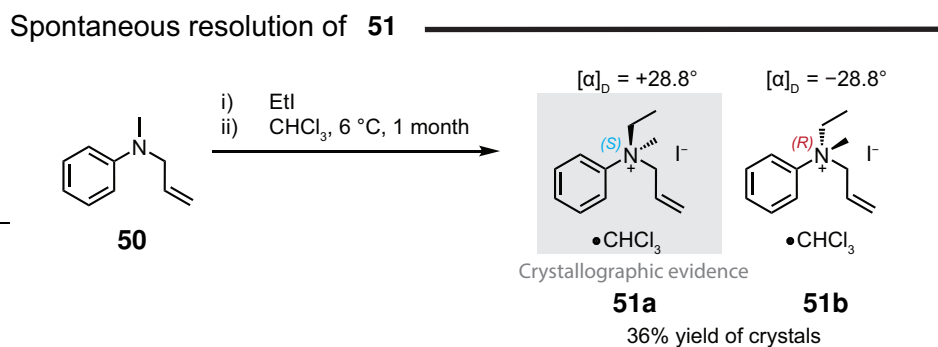


Figure 1.15: Kostyanovsky *et al.* conglomerate crystallisation.

In 1954, Havinga reported the first conglomerate crystallisation involving a stereogenic nitrogen.¹⁰⁶ Havinga's work purported the spontaneous resolution of *N*-methyl, *N*-ethyl, *N*-allyl anilinium iodide (**51**) in chloroform. However, the credibility of the result was called into question due to the peculiar optical rotations obtained and the reported yields. Consequently, Kostyanovsky *et al.* conducted a thorough reinvestigation into the claims.¹⁰⁷ In 2001, they verified the potential for spontaneous resolution of molecules with a nitrogen stereocentre through conglomerate crystallisation by successfully achieving spontaneous resolution of **51** (see Figure 1.15.). This validation was supported by SCXRD data (**51a**, (*S*)-configuration, CHCl₃ solvate, space group: *P*2₁2₁2₁), confirming enantioenrichment of the Wedekind–Fock–Havinga salt through conglomerate crystallisation.

1.4 Quaternary ammonium cations

Due to their unique properties, quaternary ammonium cations serve versatile applications as reagents,¹⁰⁸ phase-transfer catalysts,¹⁰⁹ ionic liquids,¹¹⁰ electrolytes,¹¹¹ surfactants,¹¹² antistatic agents,¹¹³ structural directing agents (e.g. Zeolites),¹¹⁴ and as herbicides and antimicrobials.^{115,116} The demonstrable utility of these cations is illustrated by their annual global production surpassing 500,000 tons. However, despite the evident demand for molecules possessing this functionality, a general methodology for the enantioselective synthesis of quaternary ammonium stereocentres has only recently been developed.²

1.4.1 Alkylation and dealkylation

The original technique for directly alkylating primary and secondary amines to generate quaternary ammonium cations was developed by Hofmann in 1850.¹¹⁷ Whilst this can prove an effective route to more highly substituted amines and ammonium cations, the well-known problem with this methodology is that it offers limited control to the ratio of substituents in quaternary ammonium salts compared to other methodologies. To enhance the selectivity of attached groups, racemic quaternary salts can also be synthesised from tertiary amines by employing various alkylating agents (see Figure 1.16.). This approach, known as quaternisation, was established by Menshutkin in 1890 and remains a popular synthetic approach to produce quaternary ammonium salts.^{118,119}

The reverse Menshutkin reaction of quaternary ammonium cations can be induced through the use of high temperatures in neutral or acidic environments.¹²⁰ This forces the equilibrium towards the tertiary amine and alkylating agent, leading to dealkylation of the ammonium centre. Notably, the observed trend of decreasing stability of $R_4N^+X^-$ compared to $R_3N + RX$ in the molten ammonium salt corresponds to the increasing X^- nucleophilicity, although it is important to note that this order can be significantly influenced by the specific medium in which the salt is solvated.¹²¹ Additionally, strong nucleophiles can facilitate dealkylation of quaternary ammonium centres through S_N2 reactions.¹²² Dealkylation can also occur through β -elimination, known as

1.4. QUATERNARY AMMONIUM CATIONS

the Hofmann elimination.^{117,123} This reaction, involving quaternary ammonium hydroxides, results in the production of the respective amine and alkene. In the presence of only methyl substituents, the reaction yields the amine along with methanol or dimethyl ether.

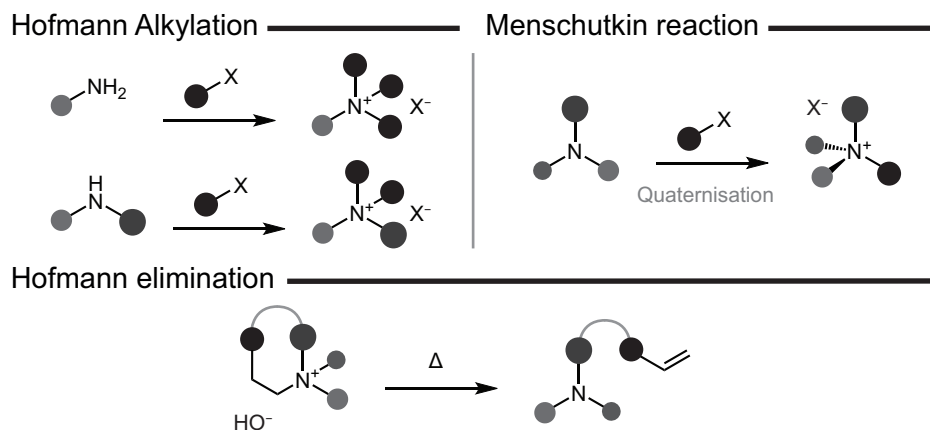


Figure 1.16: Alkylation and dealkylation of ammonium cations.

1.4.2 Diastereoselective alkylation

Diastereoselective alkylations represent the most dependable approach for establishing the stereogenicity at a *N*-stereocentre. These reactions rely upon the chirotopic environment surrounding the prochiral amine, which serves as a conduit for transferring stereochemical information from an adjacent stereocentre to the newly synthesised ammonium centre. Zones *et al.* successfully synthesised camphidine-based ammonium salts in a diastereoselective manner for applications as structure-directing agents in zeolite synthesis.¹¹⁴ Depending on the order of alkylation, **52** can be diastereoselectively synthesised as both enantioenriched *R* and *S* nitrogen epimers. The synthesis of compound **52a** from **53** demonstrated high efficiency, yielding exclusively the *R* ammonium stereocentre. Conversely, when the order of alkylation steps was reversed, compound **52b** emerged as the predominant product, albeit with a diastereomeric ratio (dr) of 75:25 (see Figure 1.17.).

Zones's diastereoselective quaternisation

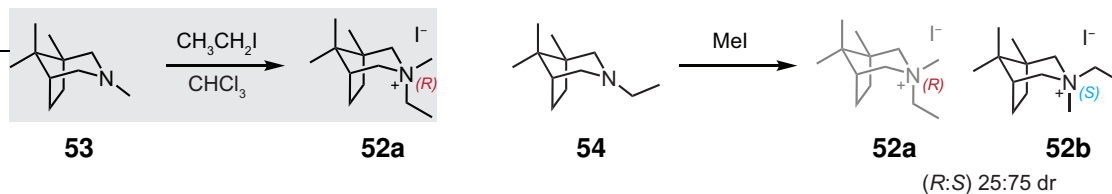
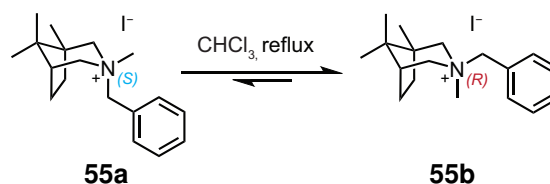


Figure 1.17: Diastereoselective alkylations to produce stereogenic nitrogen centres.

Studies have also demonstrated that refluxing tropane alkaloids, such as **55a** (see Figure 1.18.), leads to isomerisation, resulting in the formation of the thermodynamically stable diastereomer **55b**, which bears the larger benzyl substituent in the equatorial position.¹²⁴

Dynamic isomerisation of camphidine



Diastereoselective alkylation of proline derivative

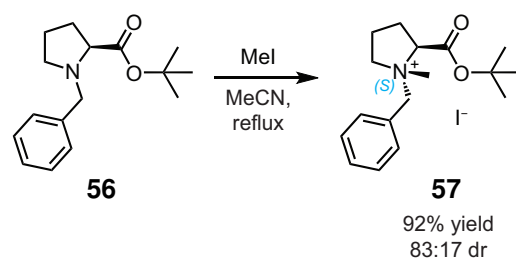


Figure 1.18: Diastereoselective alkylations to produce stereogenic nitrogen centres.

Tayama *et al.* synthesised enantioenriched quaternary ammonium salts of proline via diastereoselective alkylation of the amine (see Figure 1.18.). Following alkylation of **56** with methyl iodide, **57** was obtained in high yield. The initially modest dr of 87:13 could be significantly enhanced to 99:1 dr through recrystallisation.^{98,125,126}

1.4.3 Transfer of *N*-stereochemical information

Using diastereoselectively synthesised proline-based ammonium salts, Tayama *et al.* demonstrated that a [1,2]-Stevens rearrangement and [2,3]-Sommelet-Hauser rearrangement could be utilised to transfer stereochemical information from a nitrogen stereocentre onto an adjacent carbon atom (see Figure 1.19.).^{126,127} Both transformations were reported in good yield and displayed exceptional enantioselectivity (>90% ee). Upon treatment with CsOH, the [1,2]-Stevens rearrangement was promoted (**58**), whilst utilising ^tBuOK (on a different derivative) at -40 °C favoured the [2,3]-Sommelet-Hauser rearrangement product (**59**, see Figure 1.19.). A similar transfer of stereochemical information was also shown by West and Glaeske when using a temporary cyclic stereogenic nitrogen.¹²⁸ They reported selective [1,2]- or [2,3]-shifts depending on substituent groups present.

Steven's versus Sommelet-Hauser rearrangement

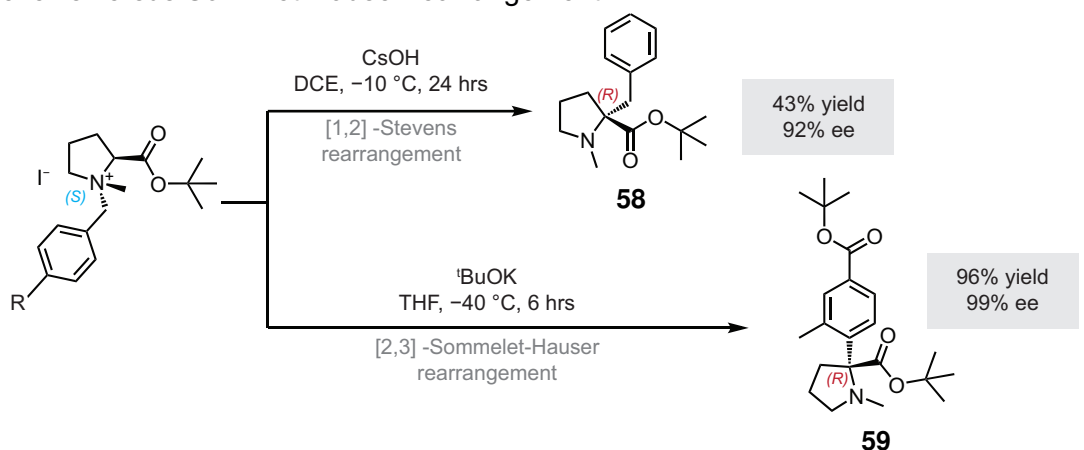


Figure 1.19: [1,2]-Stevens rearrangement and [2,3]-Sommelet-Hauser rearrangement of proline-based ammonium salts.

Enamines bearing *N*-allyl groups have the capability to partake in a [3,3] sigmatropic rearrangement commonly referred to as a 3-aza-Cope, amino-Claisen or aza-Claisen reaction.¹²⁹ It has been observed that the aza-Claisen rearrangement involving optically active 3-pyrrolidine acryl esters and diverse acid chlorides proceeds with high diastereoselectivity, through a high fidelity 1,3-stereochemical relay.¹³⁰ Nubbe-meyer and Diederich presented an *in situ* diastereoselective alkylation, in the presence of AlMe₃, to generate the necessary enolate from **61**, followed by a [3,3] sigmatropic rearrangement at low temperature, resulting in the formation of **62a**. Additional

studies into stereospecific aza-Claisen rearrangements by Maryanoff and McComsey showcased further utility for stereospecific [3,3] sigmatropic rearrangements.¹³¹ The rearrangement of salt **64** allows for the transfer of stereogenicity from the nitrogen stereocentre to the resulting quaternary carbon centre in **65**. Due to only the *trans*-iminium salt forming, it was suggested that a concerted suprafacial intramolecular rearrangement of the allyl occurred, responsible for the high stereospecificity. However, the rearrangement occurred in the presence of a chiral centre alpha to the nitrogen, which also potentially enhanced the enantioselectivity of the rearrangement (see Figure 1.20.).

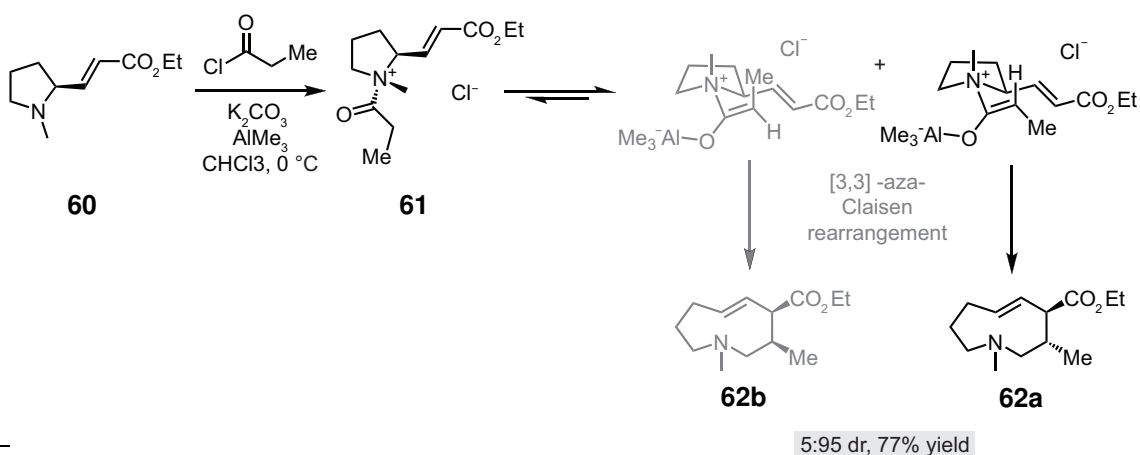
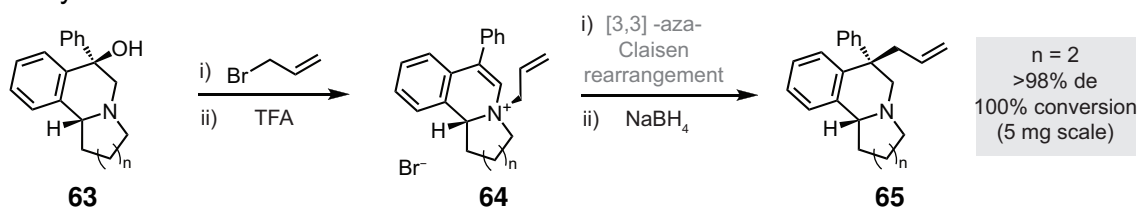
Nubbemeyer *et al.* aza-ClaisenMaryanoff *et al.* aza-Claisen

Figure 1.20: [3,3] sigmatropic rearrangements to transfer chirality from *N*-stereocentres.

Ammonium stereocentres not only govern chirality through rearrangements but they can also impart diastereoselectivity during synthesis (see Figure 1.21.). In the case of (–)-cryptaustoline, Meyers and Sielecki, demonstrated a 1,4-Michael addition selectively occurs when the amine adopts an *S* configuration.¹³² This process leads to the stereoselective formation of the configurationally stable ammonium stereocentre within the fused ring system. Next the molecule undergoes further oxidation, resulting in the formation of the conjugated enone. Interestingly, the stereoselectivity of

1.4. QUATERNARY AMMONIUM CATIONS

the subsequent reduction step is influenced by the handedness of the *N*-stereocentre, leading to inversion of the adjacent carbon stereocentre compared to the previously accessed epimer. Here, the presence of *N*-stereogenicity significantly influences the stereochemistry of the neighbouring carbon stereocentre in **66**.

(-)-cryptaustoline synthesis

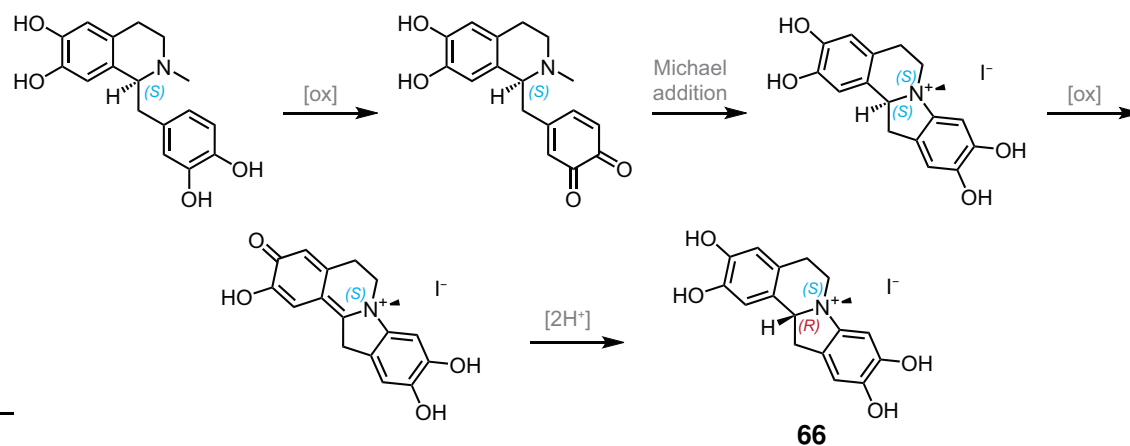


Figure 1.21: *N*-stereogenicity controlling chirality in the synthesis of (-)-cryptaustoline

1.5 Ammonium cation recognition

1.5.1 Supramolecular recognition units

Synthetic recognition systems

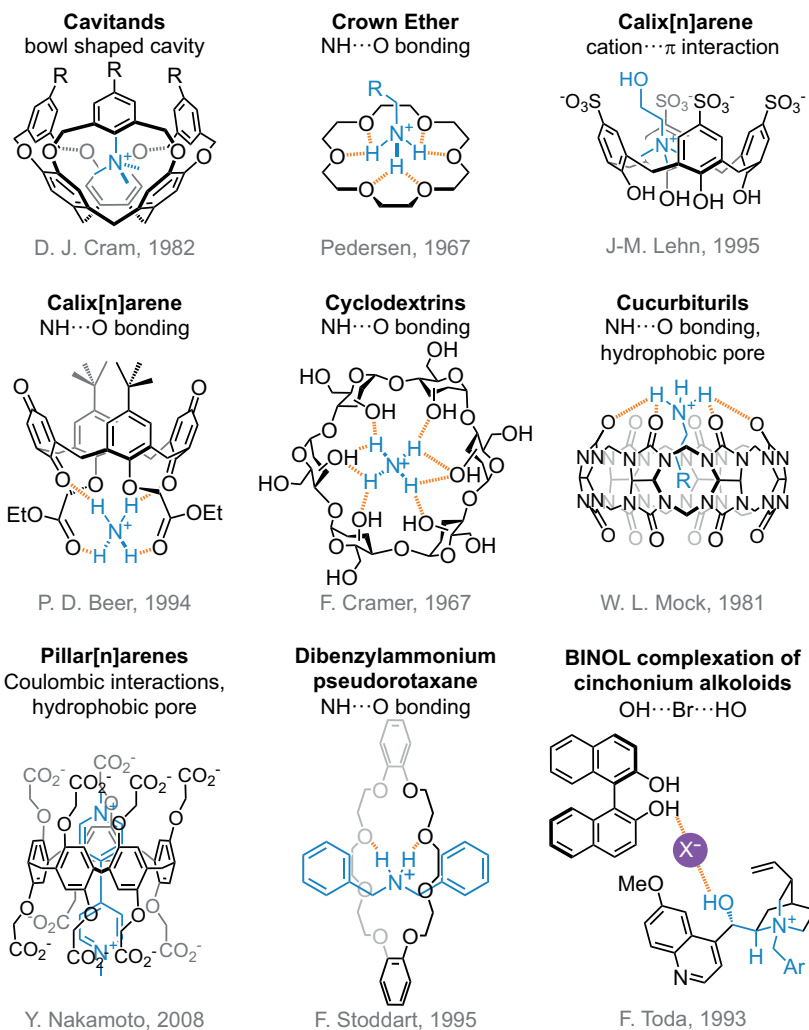


Figure 1.22: Supramolecular recognition units in ammonium cation recognition.

The field of supramolecular chemistry has made remarkable progress in designing host moieties that engage in direct non-covalent interactions with guest substrates (see Figure 1.22.). Pioneering work by Cram, Pedersen, and Lehn harnessed host molecular shape and strong directional interactions, leading to the development of complex recognition systems.^{133–135} Following this, a spectrum of synthetic ammonium recognition moieties emerged, such as calixarenes,^{136–140} cucurbiturils,^{141–143} cyclodextrins,^{144–147} and pillarenes.^{148,149} These tailored systems played a pivotal role

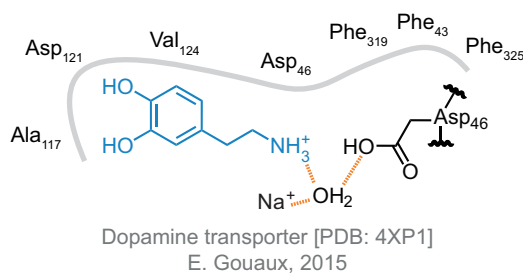
1.5. AMMONIUM CATION RECOGNITION

in advancing the field of mechanically interlocked molecules and molecular devices by providing precise positional control through their potent recognition capabilities.^{150,151}

1.5.2 Neurotransmitters

Many biological signalling pathways exploit the interaction of ammonium ions with protein receptors. This is especially evident than in the case of neurotransmitters which, after release into the synaptic cleft, bind cognate receptors on the post-synaptic cell membrane and transmit information enabling cell-to-cell communication in the nervous system.¹⁵² Histamine, dopamine, arginine, noradrenaline, gamma-aminobutyric acid (GABA), and acetylcholine (Ach), to name a few, are neurotransmitters characterised by their amine group, enabling the formation of ammonium ions in solution at biological pH. The interaction between the ammonium functionality present in these neuroactive compounds and receptors serves as a pertinent biological example of cationic nitrogen centre recognition.

Dopamine



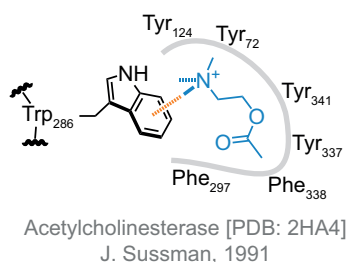
Dopamine, a biogenic amine neurotransmitter, performs a profound role in the development and function of the nervous system.¹⁵³ It also plays a key role in animal behaviour.¹⁵⁴ As a result, dopamine receptors and transporters are vital to normal neurophysiology and are thus primary

targets of many drugs; ranging from antidepressants to psychostimulants such as cocaine. Normally, the dopamine transporter eradicates dopamine from the synapse, to cease dopamine's action at its cognate G-protein coupled receptors.¹⁵⁵ Disruption of this mechanism can cause a range of effects. Cocaine for example, prolongs the activity of dopamine in the synapse by blocking the dopamine reuptake mechanism.¹⁵⁶

Dopamine, noradrenaline, and norepinephrine transporters share a conserved struc-

tural fold,¹⁵⁷ implying that these neurotransmitters form analogous interactions with their respective biological receptors. This structural motif features an aspartate residue (Asp46) crucial for accepting a hydrogen bond from the ammonium cation at a distance of 3 Å. Additionally, in the dopamine receptor, Asp46 exhibits rotational movement, facilitating indirect coordination with a sodium ion and two water molecules.¹⁵⁸ These interactions establish a molecular network linking dopamine to ion binding sites in the receptor. Notably, the specific interactions of the ammonium functionality illustrate the biological significance of cationic ammonium recognition.

Acetylcholine



Acetylcholine (ACh), an ester resulting from the combination of choline and acetic acid, assumes a crucial role in memory and learning. Its scarcity is associated with the potential development of Alzheimer's disease.¹⁵⁹ In the neural signalling process, ACh is released at the terminus of a neurone, it diffuses across the synapse and binds to

postsynaptic membrane receptors, eliciting depolarisation in the postsynaptic neurone. The enzyme acetylcholinesterase (AChase) plays a vital role in preventing overstimulation by degrading ACh (PDB: 2HA4).¹⁶⁰ However, inhibition of AChase activity, often induced by agents like organophosphates and nerve agents, can result in the accumulation of ACh. This accumulation is toxic, hyperpolarising the postsynaptic neurone and potentially contributing to the progression of conditions such as myasthenia gravis and Alzheimer's disease.¹⁶¹

Acetylcholine receptors, present on the surface of muscle cells and in the central nervous system, consist of five protein chains arranged to form a pore spanning the neuronal membrane (PDB: 2BG9).¹⁶² Upon occupancy of the two binding sites by acetylcholine, the receptor undergoes conformational change resulting in opening of the ion channel. This allows sodium, potassium, and calcium ions to cross the cell membrane, initiating an action potential in the post-synaptic neurone. Because the acetylcholine receptor plays a pivotal role in connecting muscles to the central

1.5. AMMONIUM CATION RECOGNITION

nervous system, it is a target for various neurotoxins.¹⁶³ Notably, a majority of these toxins contain at least one quaternary ammonium centre.

In the acetylcholine receptor, the tetramethylammonium cation (NMe_4^+) can serve as an agonist. Its ammonium group binds to one of the acetylcholine binding sites, interacting with a cage comprised of five aromatic side chains (Trp89, Trp143, Tyr185, Tyr192, and Trp53) and three conserved asparagine residues (Asp174, Asp180, and Asp161). This interaction prompts the movement of negatively charged residues towards the ammonium cation, believed to be the mechanism for conveying conformational change through the receptor.¹⁶⁴ Here recognition of the ammonium cation moiety is crucial to bringing about the agonistic effect.

1.6 Bioactive nitrogen stereocentres

In the context of neurotransmitters, the recognition of ammonium cations is limited to molecules devoid of *N*-stereocentres. However, given the homochiral nature of biological systems, the handedness of a nitrogen stereocentre can exert profound effects on bioactivity. Hence the identity of the *N*-epimer and control thereof becomes important in bringing about desired therapeutic effects.

Ipratropium bromide (**67**) is a bronchodilator regularly prescribed for the treatment of asthma. The drug is better known by the name it is marketed under, *Atrovent*.¹⁶⁵ Notably, both epimers of the nitrogen stereocentre are bioactive, but **67a** which possesses a (*S*)-*N*-stereocentre displays superior stability *in vivo* compared to **67b**. **67a** remains active *in vivo* for 180 mins, which is three times longer than **67b**. Consequently, when **67** is administered exclusively as the (*S*)-epimer, it demonstrates greater potency compared to a racemic mixture of both (*R*) and (*S*) epimers.¹⁶⁶ Both epimers are accessible by separation on HPLC or by manipulating the order of the alkylation in their synthesis (see Figure 1.23.).

The agonistic impact of *N*-methylnalorphine (**68**) on opiate receptors is dependent on the absolute configuration of the nitrogen epimer. Notably, in the presence of sodium, the IC₅₀ of (*S*)-*N*-methylnalorphine (**68a**, 11,500 nM) is significantly greater (over 22 times) compared to the IC₅₀ of the (*R*)-*N*-methylnalorphine epimer (**68b**, 510 nM).¹⁶⁷ Hence, **68b** is a more potent agonist (see Figure 1.23.).

Methylnaltrexone (MNTX) was formulated as a remedy for opioid-induced constipation, due to its structural resemblance to frequently prescribed opiates and the presence of a charged quaternary ammonium functionality which inhibits its crossing of the blood-brain barrier.¹⁶⁸ MNTX (**69**) functions by acting as an opiate antagonist in intestinal opiate receptors. Initially administered as a mixture of *N*-epimers, subsequent separation by HPLC and bioactivity tests revealed that only (*R*)-*N*-MNTX (**69a**) produced the desired therapeutic effect for opioid-related constipation.¹⁶⁹ Mice administered with a 10 mg kg⁻¹ dosage of (*R*)-*N*-MNTX, (**69a**) exhibited an 8% increase in intestinal motility, while (*S*)-*N*-MNTX (**69b**) resulted in an 80% decrease in

1.6. BIOACTIVE NITROGEN STEREOCENTRES

motility. This demonstrates that only **69a** offers the intended therapeutic effect for alleviating opioid-related constipation. This finding demonstrates the pharmacological significance of employing distinct nitrogen epimers in the preparation of therapeutics (see Figure 1.23.).

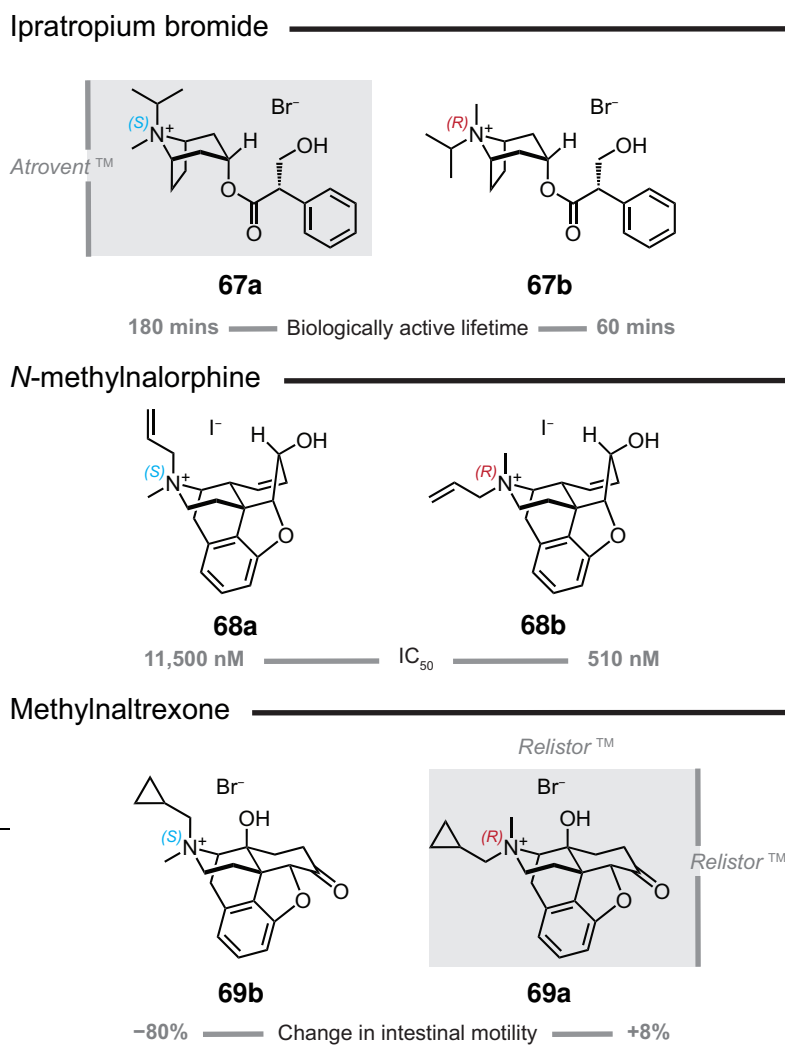


Figure 1.23: *N*-epimers of stereogenic nitrogen containing bioactive compounds.

1.7 Enantioselective preparation of *N*-stereocentres

Limited methodologies currently exist for the enantioselective preparation of nitrogen stereocentres as the sole stereogenic element in a molecule. While a few examples demonstrate diastereoselective alkylation of tertiary amines to generate a specific ammonium stereocentre,^{98,125,126,170} only recently have reports emerged of methods for the direct enantioselective preparation of nitrogen stereocentres.

In 2021, work in our group by Walsh *et al.* achieved the enantioselective synthesis of a limited range of quaternary ammonium cations, with nitrogen serving as the sole stereogenic element in a molecule, utilising a CIAT-like methodology to form a ternary complex between enantiopure BINOL and an ammonium salt.² Following this, Köhler *et al.* developed a catalytic procedure for quaternising amines under dynamic kinetic resolution conditions. They converted a range of tertiary *N*-methyltetrahydroisoquinolines into configurationally stable ammonium cations through Pd-catalysed allylation, achieving enantiomeric ratios of up to 90:10 (see ref Figure 1.24.).¹⁷¹ The absolute configuration of the *N*-stereocentre produced in this study was only characterised by SCXRD for one of the ammonium salts synthesised (CCDC access code: QIFBUG), as such the sense of the *N*-stereocentre in the selected example cannot be confirmed but is assumed to be the same. In both Walsh's and Valentin's methodologies, modest enantioenrichment is reported and the substrate scope of these procedures is limited.

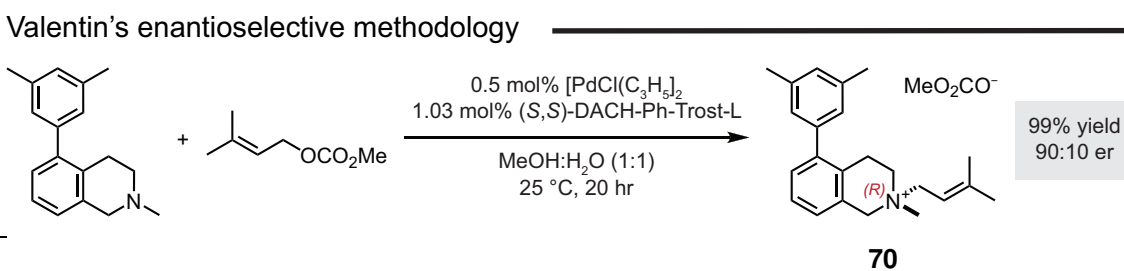


Figure 1.24: Catalytic enantioselective preparation of *N*-stereocentres.

1.8 Aims and objectives

Previous work by our group developed a method to achieve the enantioselective synthesis of a limited range of quaternary ammonium cations, where nitrogen served as the sole stereogenic element. This approach employed a CIAT-like methodology to form a ternary complex between BINOL and an ammonium salt.^{2,37} Unlike the procedure described by by Tayama *et al.* that required a hydroxyl functionalised group bonded to the ammonium centre to act as a recognition handle, this method eliminated such a necessity.

The aim of this thesis was to extend the scope of enantioselective synthesis for ammonium cations and identify potential applications for the synthesised moieties. To accomplish this goal, the task was divided into several key objectives:

- Establish the mechanism by which this supramolecular recognition of quaternary ammonium cations proceeds to better understand both the limitations and the potential of the process.
- Investigate the CIAT with enantiopure BINOL to amass a library of ammonium salts that could be enantioselectively synthesised. Interrogation of this library would provide empirical evidence for rationalisation of key requirements of the process.
- Synthesise and recrystallise multiple chiral ammonium complexes to analytically interrogate the supramolecular recognition phenomenon and reveal thermodynamic differences in diastereomeric crystallographic interactions that govern the stereoselectivity.
- Utilise highly enantioenriched ammonium salts to achieve a synthetically useful task.

Chapter 2

Recognition of achiral ammonium salts

Metal-organic frameworks (MOFs) and covalent organic frameworks (COFs) are porous materials that have been widely studied since the 1990s.¹⁷² These materials represent a class of structures that have many useful applications ranging from catalysis to drug delivery.¹⁷³ Furthermore, flexible MOFs have also been developed, that can respond to external stimuli and exhibit reversible structural transformations pointing towards potential uses in separation and sensing.¹⁷⁴

Lately, a new class of porous materials assembled from organic materials through hydrogen bonding interactions, have enticed growing interest.¹⁷⁵ They are characterised as hydrogen bonded organic frameworks (HOFs) and due to their increased flexibility compared to MOFs are suggested to be improved candidates for sensing and host-guest chemistry.¹⁷⁶ The main pitfalls of these frameworks, however, are that the majority of HOFs collapse upon removal of the solvent molecules from their pores and HOFs tend not to be functional in protic solvents which can disrupt their hydrogen bonding patterns. It has been shown that a HOF made from a counterion-BINOL framework can be used to enantioselectively encapsulate ammonium cations and upon doing so form a ternary complex which precipitates out of protic solution (EtOH).² This process thus overcomes one of the main drawbacks found with HOFs by allowing isolation in the solid state. Due to the various applications that HOFs can be used for, this observation warranted further investigation.

With this in mind we sought to establish the mechanism by which the supramolecular recognition of quaternary ammonium cations by enantiopure BINOL proceeds. Our investigation sought to determine if this mode of recognition presented distinctive differences compared to classical supramolecular systems.

2.1 Ammonium cation recognition

Ammonium cations have a fundamental role in many biological processes such as neurotransmission and plant growth (chlormequat in gibberellin biosynthesis inhibition),^{160,177} where their selective recognition fundamentally relies on their degree of substitution. In biological systems, proteins can preferentially bind more substituted ammonium cations over less substituted homologues.¹⁷⁸ To date, a general methodology to mimic this behaviour remains elusive as synthetic hosts principally observe the inverse order (i.e., $1^\circ > 2^\circ > 3^\circ > 4^\circ$). Due to the fact ammonium cations are widely used as catalysts,¹⁰⁹ reagents,¹⁰⁸ electrolytes,¹¹¹ surfactants,¹¹² structural directing agents (e.g. Zeolites),¹¹⁴ antistatic agents,¹¹³ antibacterial/antifungal agents¹¹⁶ and have long been used as recognition elements in supramolecular chemistry,^{133–135} their selective recognition based on level of substitution presents a key problem in organic chemistry.

The majority of this Chapter is based on a pre-printed manuscript titled '*Selective Recognition of Quaternary Ammonium Cations*' written by Callum S. Begg with input from Matthew O. Kitching. The author list for the said manuscript is as follows: Callum S. Begg, Mark P. Walsh, Joseph M. Phelps, Emma H. Wolpert, Emanuelle F. Fiandra, Emma F. G. Winful, Abby R. Haworth, D. Yufit, Karen E. Johnston, Clare S. Mahon, Kim E. Jelfs, and Matthew O. Kitching*. Every compound stated in this section was synthesised by Callum S. Begg and at least one data point collected. All data analysis, unless otherwise stated, was carried out by Callum S. Begg. I would like to thank all authors for their contribution to various sections of this Chapter.

2.1.1 Quaternary ammonium cation selectivity in biology

Biological receptors selectively bind key nitrogen-containing signalling molecules based on their level of substitution. The action of small neurotransmitters such as dopamine, arginine and acetylcholine is mediated by this selective ammonium cation recognition.¹⁶⁰ In enzymes such as trimethylamine dehydrogenase and dimethylamine dehydrogenase, a simple substitution of Gln to Tyr in the active site changes the cation selectivity from favouring the secondary dimethylammonium cation to the more substituted tertiary trimethylammonium cation.¹⁷⁸ Quaternary ammonium cations can also act as stronger inhibitors when in the presence of less substituted analogues, for example the tetraethylammonium cation inhibits the action of the K⁺ ion channel (Kv1.5) more strongly than its tertiary counterpart (Et₃NH⁺).¹⁷⁹ To achieve the high levels of discrimination observed in ammonium cation recognition, Nature has produced, via evolution, highly structured yet flexible hydrophobic binding cavities capable of forming multiple interactions in protein tertiary structures (see Figure 2.1.).

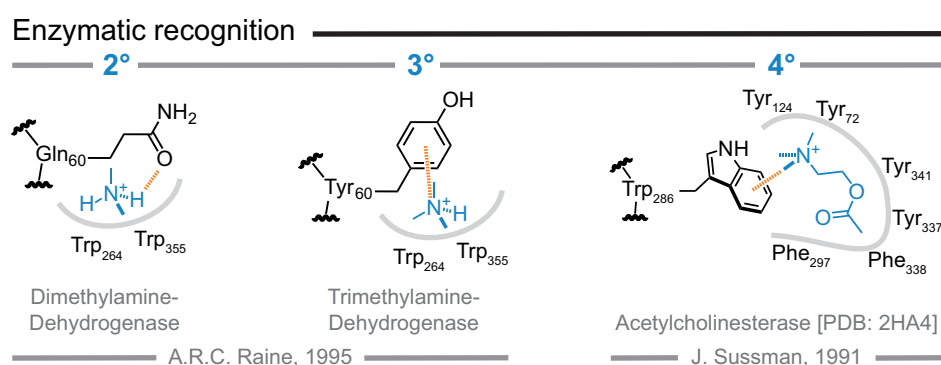


Figure 2.1: Enzymatic recognition of varyingly substituted ammonium cations.

2.1.2 Supramolecular quaternary ammonium cation selectivity

The field of supramolecular chemistry has made remarkable advances in the design of host moieties with direct non-covalent interaction to guest substrates. Seminal work by Cram, Pedersen and Lehn exploited host molecular shape and strong directional interactions in the development of complex recognition systems.^{133–135} Subsequently, a number of synthetic ammonium recognition moieties were developed, including calixarenes,^{136–140} cucurbiturils,^{141–143} cyclodextrins,^{144–147} and pillarenes.^{148,149} These systems have proven crucial in the development of mechanically

2.1. AMMONIUM CATION RECOGNITION

interlocked molecules and molecular devices through the positional control this powerful recognition affords.^{150,151} However, due to the superior hydrogen bond donor ability for less substituted ammonium cations (α parameters: $\text{Et}_3\text{NH}^+ = 4.8$, $\text{Et}_4\text{N}^+ = 2.7$),¹⁸⁰ and the strength of cation- π interactions ($\text{Me}_3\text{NH}^+ = 15.9 \text{ kcal mol}^{-1}$, $\text{Me}_4\text{N}^+ = 9.5 \text{ kcal mol}^{-1}$ – with benzene),¹⁸¹ all supramolecular recognition units that rely on strong directional interactions preferentially bind less substituted ammonium cation homologues (see Figure 2.2.). Although a limited number of systems have been designed to recognise specialised guest substrates, relying on the use of multiple functional handles or predetermined covalent molecular geometry (see Figure 2.2.),^{96,108,182–187} never has a general methodology been developed that allows quaternary ammonium cations to be selectively recognised over less substituted homologues.^{137,140,184,188–191}

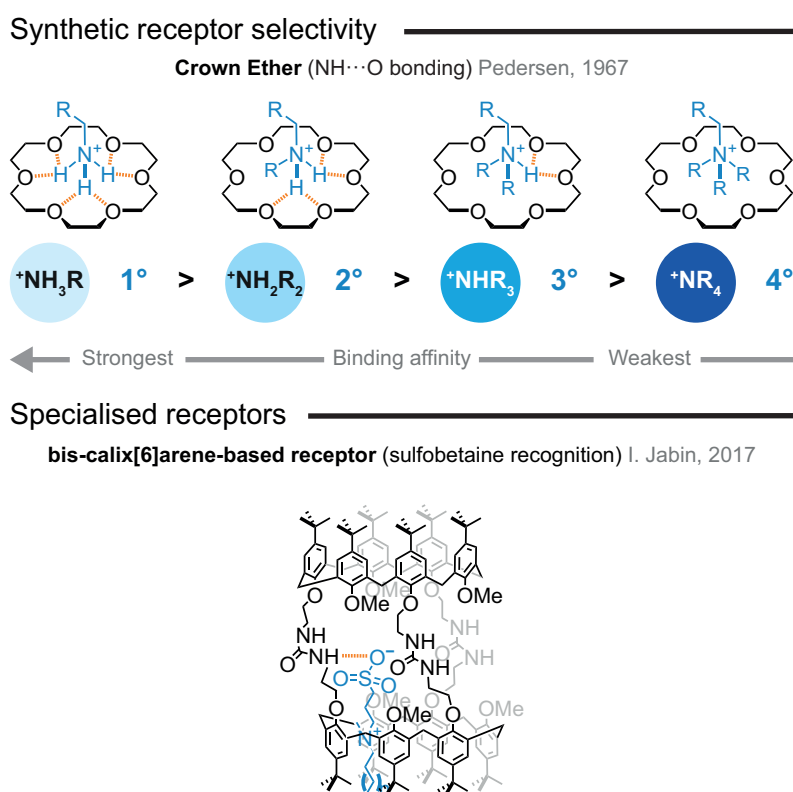


Figure 2.2: Synthetic receptor selectivity.

To realise a general method for quaternary ammonium cation recognition we reasoned that recognition principles from both natural and synthetic binding environments could be combined, through taking advantage of the solid crystalline state. The mechanism by which this supramolecular recognition of quaternary ammonium cations by

BINOL proceeds offered an ideal starting point for this. Firstly, solution-based recognition of an ammonium cation allows the formation of a ternary complex. The formation of this supramolecular complex can take advantage of strong directional interactions as commonly applied in synthetic recognition processes. Secondly, this supramolecular complex can form extended assemblies through the generation of concatenated chains. These self-assembled superstructures are highly flexible and can present a variety of binding architectures, acting as supramolecular hosts for a range of ammonium cation guests. Thirdly, abstraction of these networks to the solid phase provides a structured and hydrophobic binding environment into which an ammonium cation guest may reside. Here, multipoint binding to the cation acts to stabilise the self-assembled superstructure generating a more stable system when the quaternary ammonium cation is present. Finally, ensuring that these functional hydrogen bonded networks are equilibrating under thermodynamic control allows for selection of the more substituted ammonium cation over its less substituted congeners. We hypothesised that the recognition of quaternary ammonium salts by (*R*)-BINOL, could be utilised to overturn the energetically demanding discrimination between differentially substituted cations, by fulfilling these criteria.

2.2 Achiral ammonium salt ternary complexes with (*R*)-BINOL

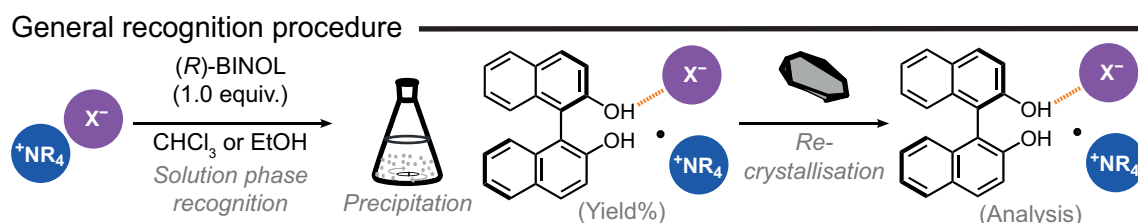


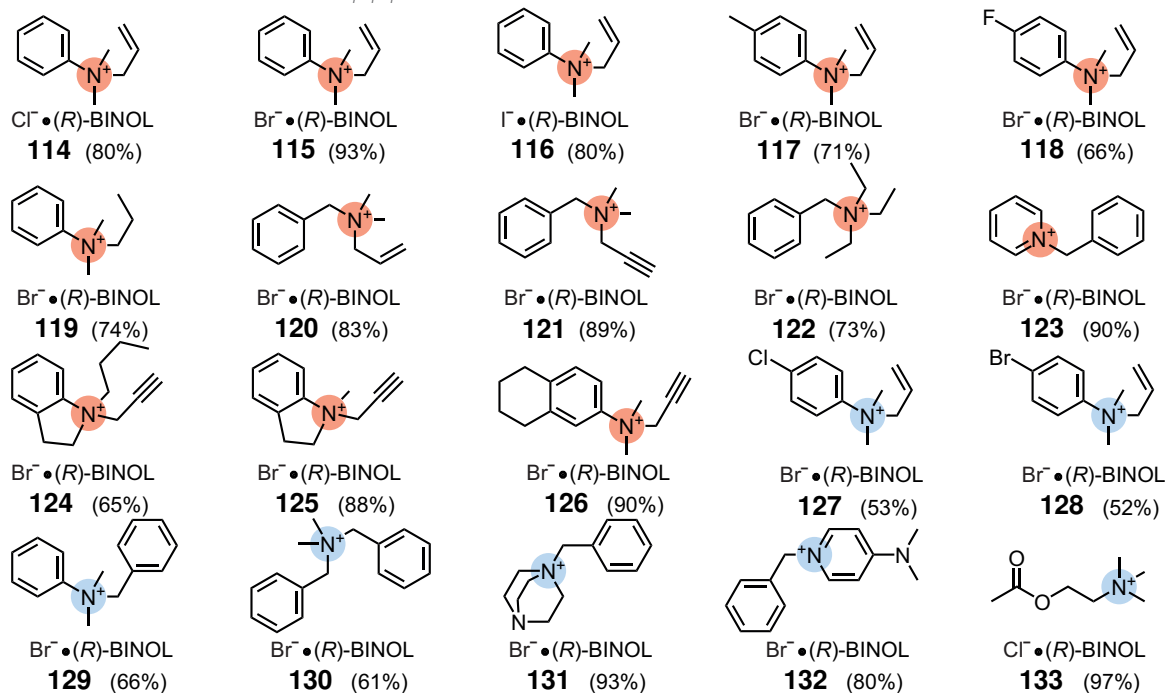
Figure 2.3: Procedure for the recognition of ammonium salts with (*R*)-BINOL.

A large and diverse range of ammonium salts derived from commonly used amines and heterocycles can be abstracted from solution to the solid phase through simple combination with (*R*)-BINOL (see Figure 2.3.). Methylation, allylation, propargylation and benzylation of several tertiary amine and pyridine substrates produced quaternary ammonium salts which could undergo complexation with (*R*)-BINOL (see Figure 2.5.). These microcrystalline solids form without the presence of any additional functional handles on the ammonium cation core. Protonation to form tertiary ammonium salts also provided suitable substrates for recognition, showing flexibility in the supramolecular behaviour. To probe the origin of this recognition, 1H NMR spectroscopy experiments were conducted. Upon addition of (*R*)-BINOL (1.0 equiv.) to a sample of **71** in a mixture of $CDCl_3:CD_3OD$ (7:1) significant upfield shifts of benzylic and methyl protons were observed, consistent with ternary complex formation (see Figure 2.6.). When conducted under suitable conditions ($CHCl_3$ or EtOH, 0.4–2.0 M), these solution phase interactions manifest as a solid-phase abstraction of the ternary complex through self-assembly of the supramolecular recognition units. The nature of the anionic counterion proves crucial to this recognition process. While the use of halogen and acetate counterions promotes supramolecular ternary complex formation through a hydrogen bonding recognition event, exchange to a non-coordinating hexafluorophosphate anion (PF_6^-) inhibits supramolecular association.

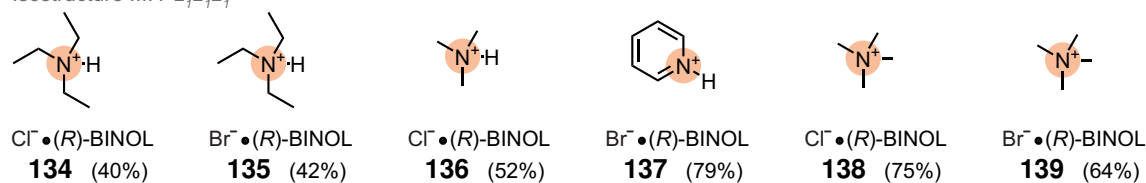
2.2. ACHIRAL AMMONIUM SALT TERNARY COMPLEXES WITH (R)-BINOL

Scope of complexation

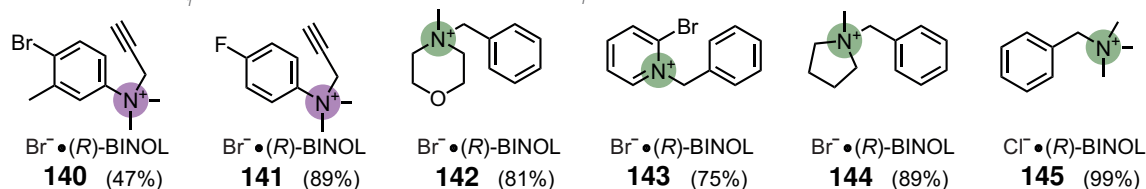
Isostructure I and Isostructure II: $P_{2,2,2,2}$



Isostructure III: $P_{2,2,2,2}$



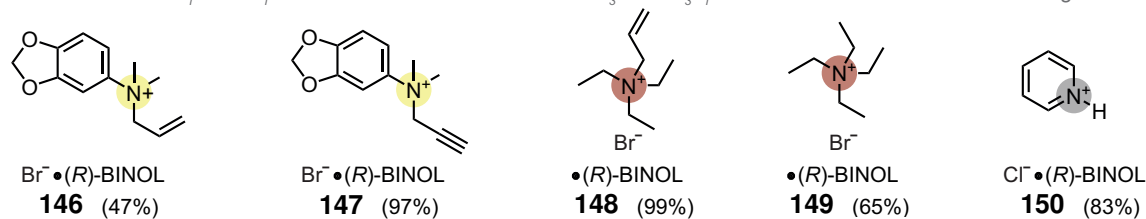
Isostructure IV: $P_{2,2}$



Isostructure VI: $P_{2,2}$ and $P_{4,2}$

Isostructure VII: $P_{4,2}$ and $P_{4,2,2}$

Unassigned



No SCXRD data

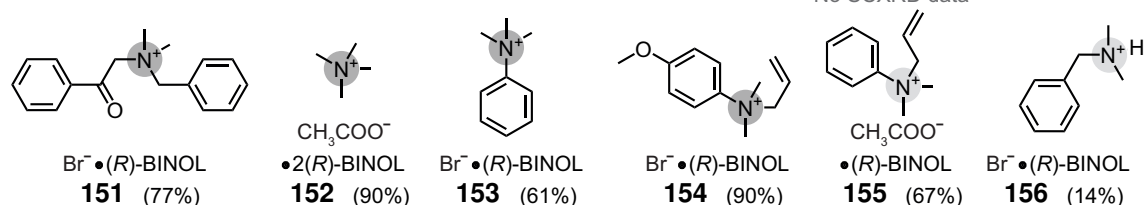
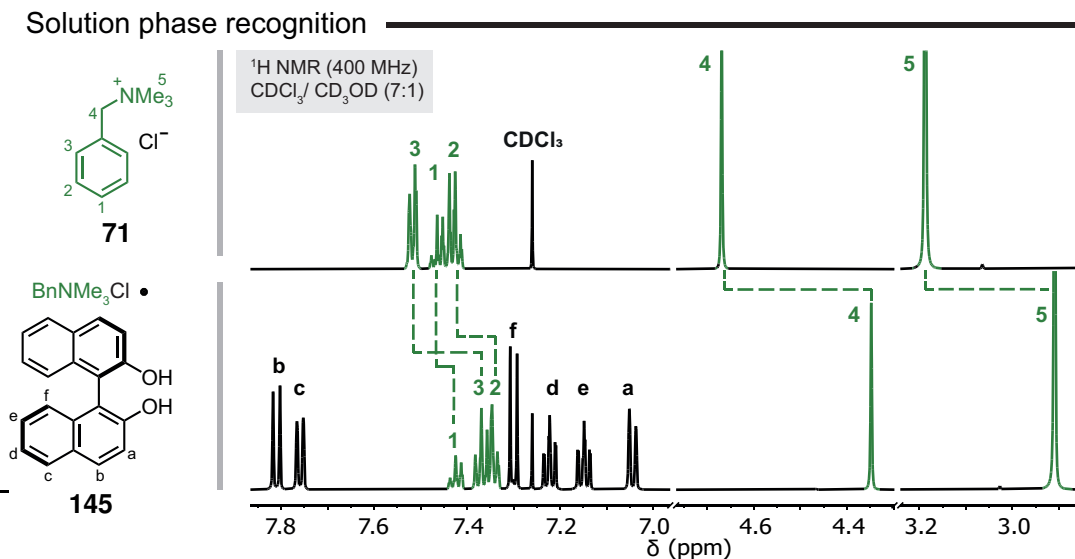


Figure 2.5: Scope of the recognition process of ammonium salts with (R)-BINOL. All yields (Yield%) refer to the solid isolated as a precipitate. Colour coding and isostructure grouping refer to COMPACK comparison results in Figure 2.10.

Figure 2.6: Solution phase recognition of **71** by (*R*)-BINOL.

2.3 Crystallographic analysis

2.3.1 Encapsulation by a hydrogen bonded network

To understand the interactions responsible for the self-assembly of the supramolecular recognition units into crystalline hosts, single crystals of each complex were grown and analysed by single crystal X-ray diffraction (SCXRD). Each SCXRD structure confirmed the existence of a continuous hydrogen bonding network between the anionic counterion and the hydroxyl functionalities of (*R*)-BINOL (e.g. **145**, C₂¹ (9), $d_{1-3} = 3.005(2)$ Å and $d_{8-1} = 3.038(2)$ Å, helix repeat length = $9.8448(4)$ Å) responsible for the formation of the helical host structure.¹⁹² In addition, multiple interactions between the ammonium cation and this helix were identified. In the SCXRD of **145**, short C–H⋯Cl contacts from α -carbon protons ($d_{\alpha 1} = 2.741$ Å, $\theta_{\alpha 1} = 144.74^\circ$, $d_{\alpha 2} = 2.813$ Å, $\theta_{\alpha 2} = 149.30^\circ$, $d_{\alpha 3} = 2.870$ Å, $\theta_{\alpha 3} = 146.32^\circ$) and an *ortho* proton of the benzyl ring ($d_{o-1} = 2.8431$ Å, $\theta_{o-1} = 153.12^\circ$) were observed alongside C–H⋯O interactions from an α -carbon proton ($d_{\alpha 3'} = 2.483$ Å, $\theta_{\alpha 3'} = 152.45^\circ$) and a further *ortho*-benzyl proton ($d_{o-2} = 2.456$ Å, $\theta_{o-2} = 140.21^\circ$). Additionally, a cation⋯ π interaction from the charged N⁺-centre to the centroid of a phenolic ring of (*R*)-BINOL ($d = 4.331$ Å) is present. The comparative significance of contacts present in the crystal structure can be illustrated on a Hirshfeld fingerprint plot. The sharp C–H⋯O (red) and C–H⋯Cl (yellow) areas of the plot exemplify the interactions observed in the crystal structure analysis of **145**.

2.3. CRYSTALLOGRAPHIC ANALYSIS

These results are consistent with multiple, weak interactions from the cationic guest acting to stabilise the assembly of the supramolecular system in the crystalline helical host (see Figure 2.7.).

Crystallographic contacts in **145**

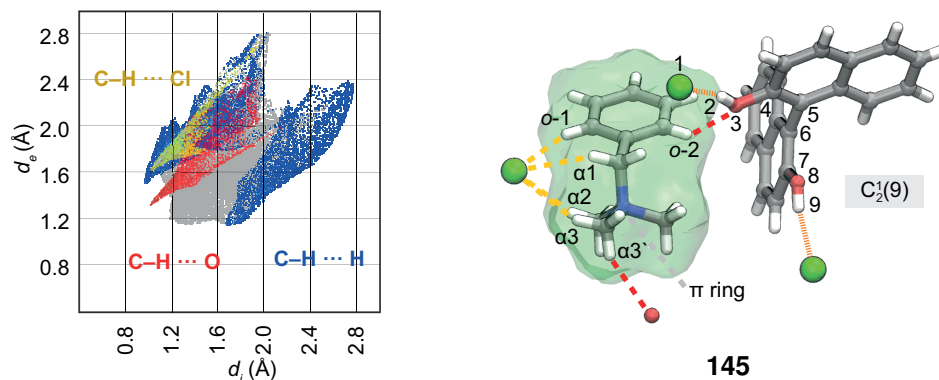


Figure 2.7: Coloured Hirshfeld plot of the ammonium cation interactions within the crystal structure **145** and a render illustrating the key contacts. The $wR2$ was 0.0887 (all data) for the crystal structure analysed. Due to the position of hydrogen atoms being calculated and refined using the riding mode in the crystal structure, no error is quoted for the distances and angles measured using these atoms.

To validate that SCXRD analysis pertaining to the host crystalline network can be propagated to the material precipitated from the reaction mixture, **145** was prepared by both precipitation and crystallisation and characterised by powder X-ray diffraction (PXRD) and solid-state NMR (SSNMR) spectroscopy (see Figure 2.8.). A comparison of the two PXRD patterns reveals that both the precipitated and crystallised forms of **145** are indistinguishable, with the same reflections observed. Solid-state ^1H magic-angle spinning (MAS) NMR, ^{13}C CPMAS NMR and ^{35}Cl MAS NMR spectra obtained for both forms of **145**, corroborate that the ^1H , ^{13}C and ^{35}Cl local environments are alike in both samples. Irrespective of the method of preparation (precipitation or re-crystallisation), identical material is produced.

2.3.2 Precipitated material versus crystallised material

PXRD traces and SSNMR spectra traces of **145**

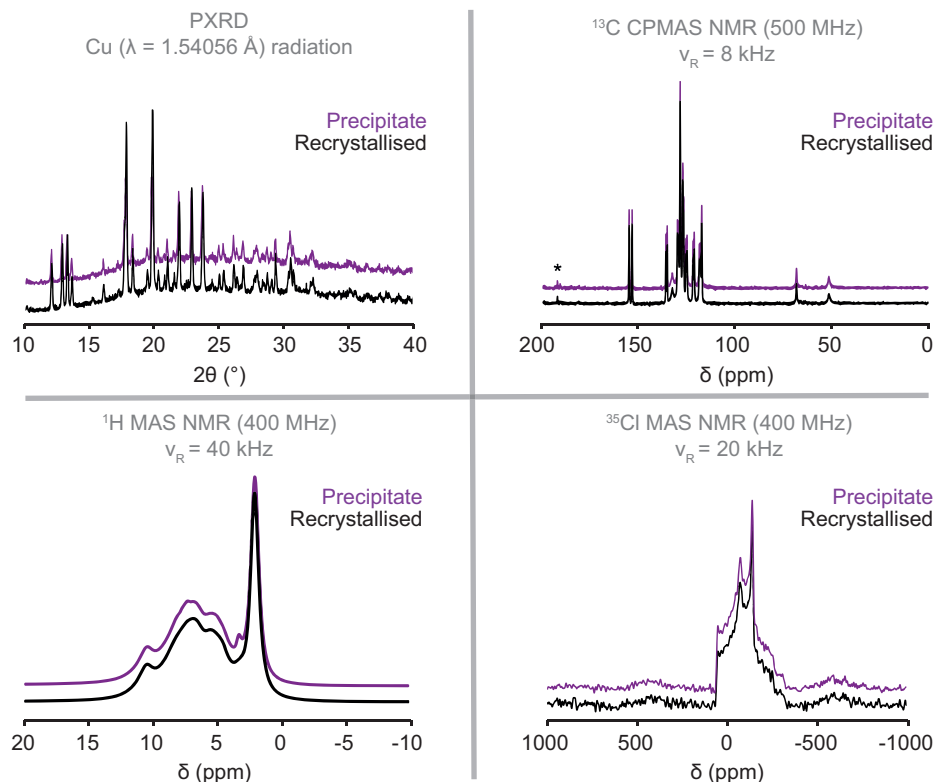


Figure 2.8: PXRD plots of crystallised and precipitated material **145** and overlaid SS-NMR spectra of precipitated and crystallised forms of **145**. Spectra run by Abby R. Haworth and Karen E. Johnston.

To confirm this conclusion could be attributed to all isolated complexes in the analysis, all precipitated samples were subject to characterisation by PXRD. The PXRD data obtained for each precipitate was then compared to a predicted PXRD pattern derived from the SCXRD data collected for the corresponding recrystallised sample. Analysis of these data verified that, for the compounds in the library, the precipitated and recrystallised materials were nearly identical (apart from minor impurities, such as excess (*R*)-BINOL, and slight variations due to discrepancies in material crystallinity in a handful of examples - more information in Chapter 3).

2.4 Isostructure analysis

COMPACK analysis

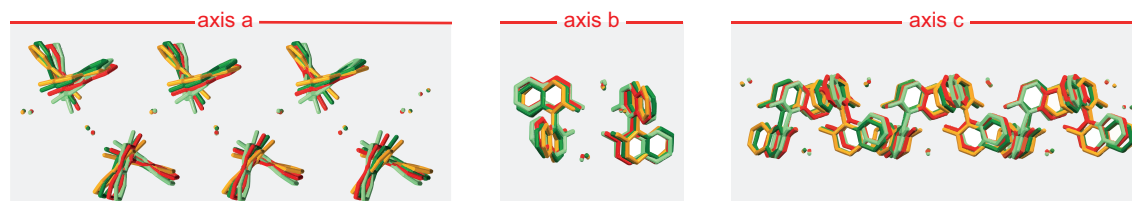


Figure 2.9: Overlays of the (*R*)-BINOL and counterion $C_2^1(9)$ network for **114**, **115**, **116** and **117** to show the isostructurality between these crystal structures. COMPACK overlays these networks in an indistinguishable way.

Global analysis of the SCXRD data reveals that a variety of helical crystalline hosts are created through supramolecular self-assembly. To explore the construction of these solid, crystalline hosts, all SCXRD structure combinations (**114–154**) were subject to an *in-silico* analysis generating a structure similarity score to establish packing isostructurality. COMPACK code (*a program used to identify crystal structures with common structural features, within specified tolerances, by mapping the relative positions and orientations of molecules between crystal structures, independent of unit cell or space group input* - see Figure 2.9.) was used to generate similarity scores between different crystal structures using the ‘Crystal packing similarity...’ in *Mercury 2020.3.0 (Build 298224)*.¹⁹³ For each structure comparison, 20 molecules within each crystal structure were analysed with a 50% leniency on both bond angle and bond length and a score of over 14/20 was empirically decided to be required for two structures to be classified as isostructural. This comparison revealed 12 distinct helical arrangements across the 41 structures analysed and identified 7 isostructural families generated from differing ammonium cations whilst retaining the same helically assembled host (see Figure 2.10.).

2.4.1 COMPACK matrix

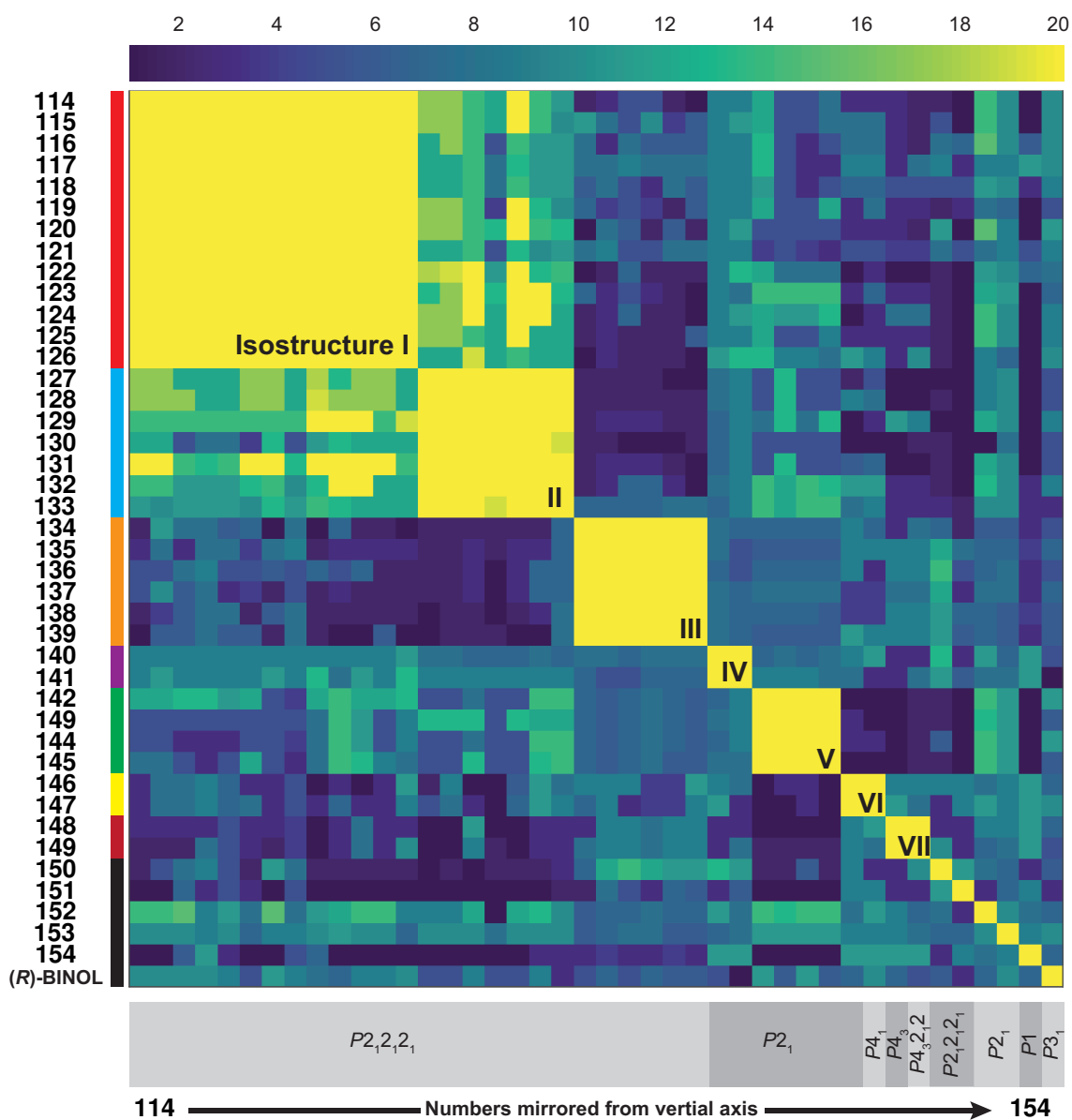


Figure 2.10: Heatmap matrix of the COMPACK comparison of 114–154. The colour bars on the y-axis correspond to the colour coding given in Figure 2.5.

2.4.2 Isostructure characterisation

Each member of an isostructural host family has an almost identical arrangement of (*R*)-BINOL and counterion participating in a C_2^1 (9) continuous hydrogen bond chain. Outside of these isostructural families, the helical host structure displayed additional flexibility. In the case of **152**, the hydrogen bonding network was further extended through incorporation of an acetate counterion into the helix affording a C_2^2 (11) hydrogen bond chain. Alternatively, in **151** the ammonium cation itself can bridge the helical arrangement through the carbonyl functionality and acidic α -C–H bonds present. In all cases a helical repeat was observed.

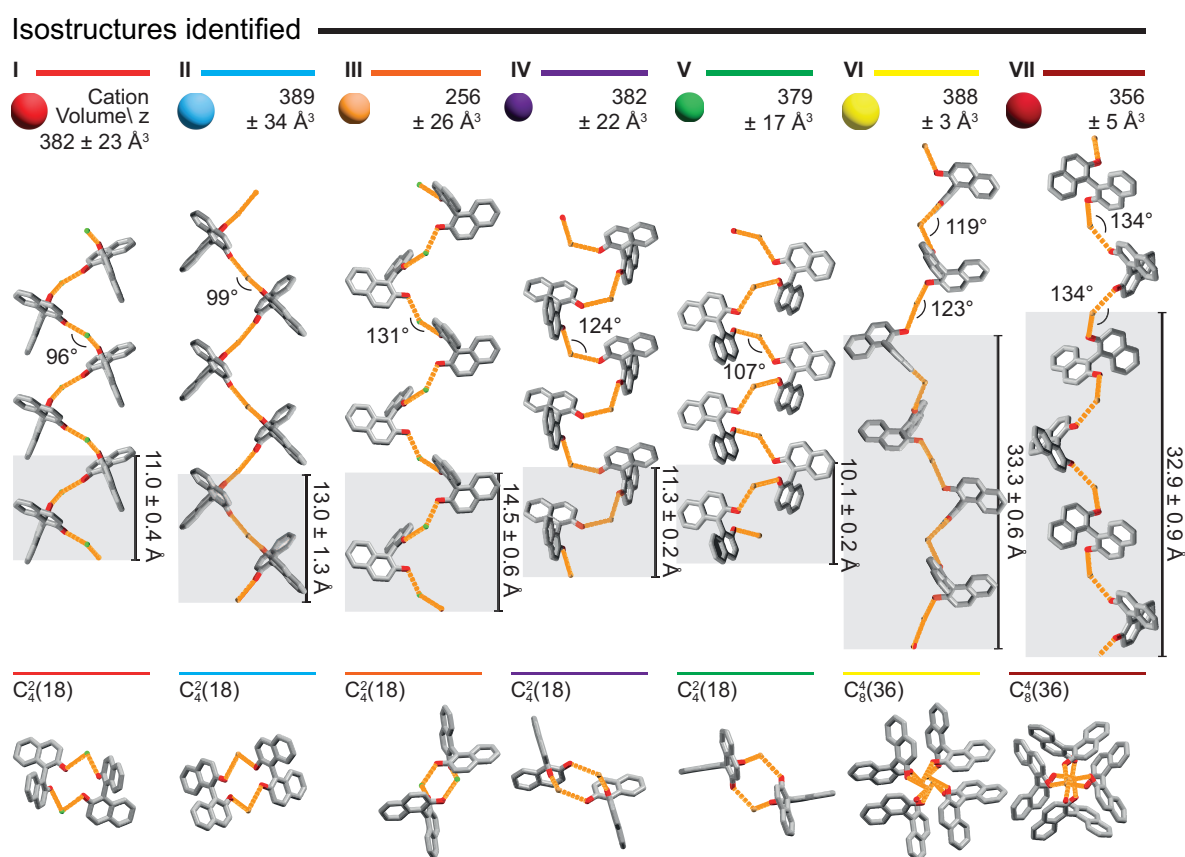


Figure 2.11: The seven isostructural families identified through COMPACK analysis. The colour coding corresponds to that given in Figure 2.5 and Figure 2.10.

Stark differences between the isostructural hosts are readily apparent. The flexible nature of the assembly of the helical host generates a wide range of helix repeat lengths (9.84–33.90 Å) and recognised ammonium cation volumes (214 – 460 Å³) that can adapt to accommodate a diverse range of ammonium cation guests.

This adaptability of the crystalline host allows a wide variety of recognition environments to be displayed to the ammonium cations enhancing its ability to sequester a diverse range of guests, without requiring any additional functionality to be present (see Figure 2.11.).

2.4.3 Composite Hirshfeld fingerprint plot analysis

Composite Hirshfeld plot generation

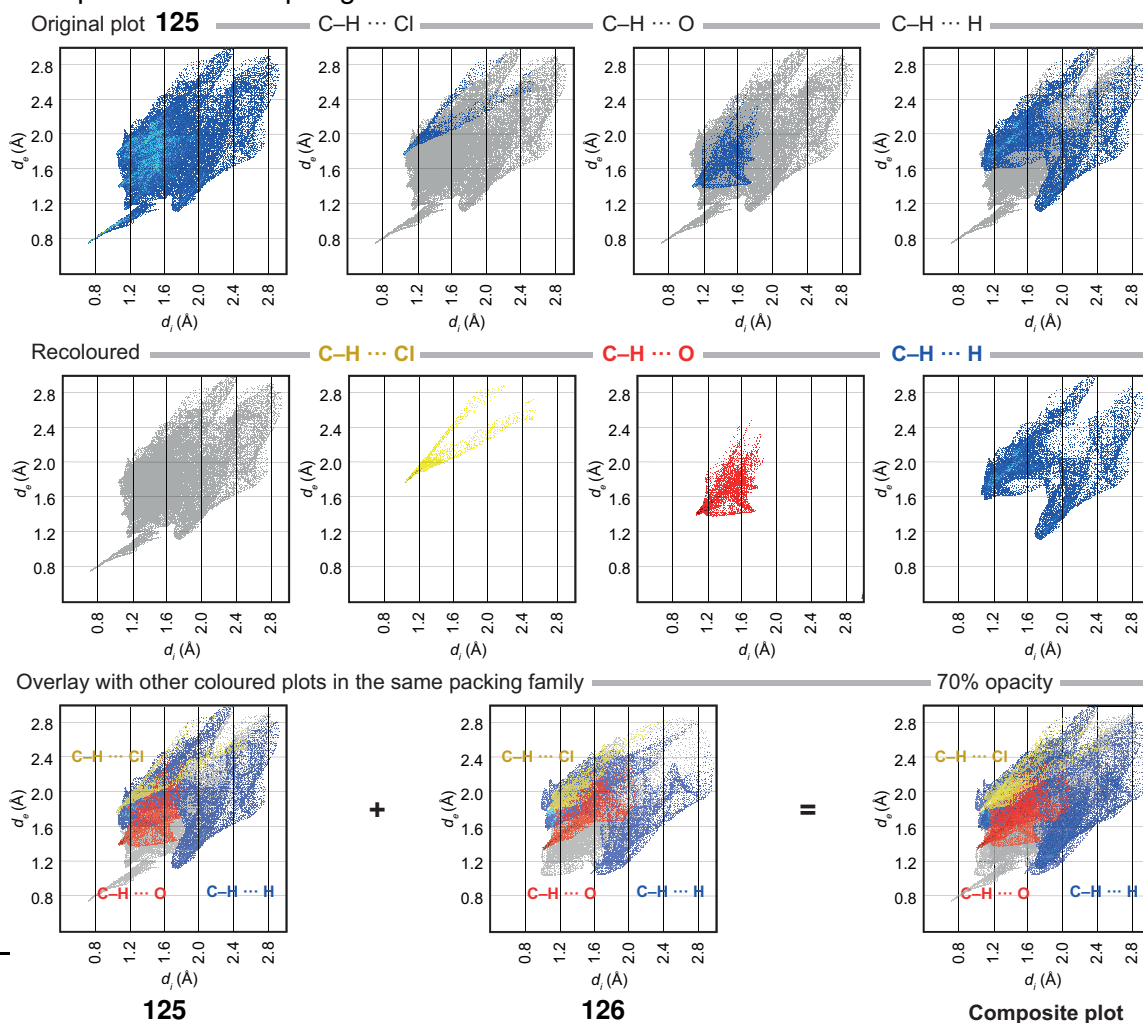


Figure 2.12: Example composite Hirshfeld plot generation by overlaying **125** and **126**.

To interrogate interactions between the guests and self-assembled supramolecular hosts across packing isostructures, composite Hirshfeld fingerprint plots were created. Composite plots were made by mapping the interactions of ammonium cations with their (*R*)-BINOL-counterion network on a 3D surface and visualising them as their

2.4. ISOSTRUCTURE ANALYSIS

own 2D Hirshfeld fingerprint plots. By colouring the specific interactions and overlaying the plots with others defined to be in the same isostructure, these overlaid Hirshfeld plots were made to illustrate the dominant interactions between ammonium cations and the host network within each isostructure (see Figure 2.12.).

Through interpretation of these plots and inspection of crystal structures, ammonium cation features that select for given superstructures can be rationalised. In all cases there is a relatively strong C–H \cdots O interaction, depicted by a pointed red area on the composite plots. This corresponds to at least one α -C–H \cdots O hydrogen bond between the ammonium cation guests and the (*R*)-BINOL network being present and is the main criteria required for isostructure I. This interaction is also seen in isostructure II, but the supramolecular recognition varies in that it must additionally incorporate a C–H \cdots π interaction between the ammonium cation and the (*R*)-BINOL network. Isostructure III encapsulates the smallest cations via forming several C–H \cdots O and C–H \cdots X contacts, whereas isostructure IV contains cations from the library which form propargylic C–H \cdots O hydrogen bonds and in isostructure V there are aromatic (edge to face) interactions which allow the guests shown to interact with multiple (*R*)-BINOL units. A methylene dioxy functionality is commonly present as a hydrogen bond acceptor in cations observed to stabilise isostructure VI and in isostructure VII two ammonium cations are seen to be bridged, non-continuously by a counter-anion. These observations are consistent with the formation of the isostructural host family being dictated through distinct multipoint interaction patterns made between the ammonium cation and the (*R*)-BINOL derived helical host (see Figure 2.13.).

Composite Hirshfeld fingerprint plots

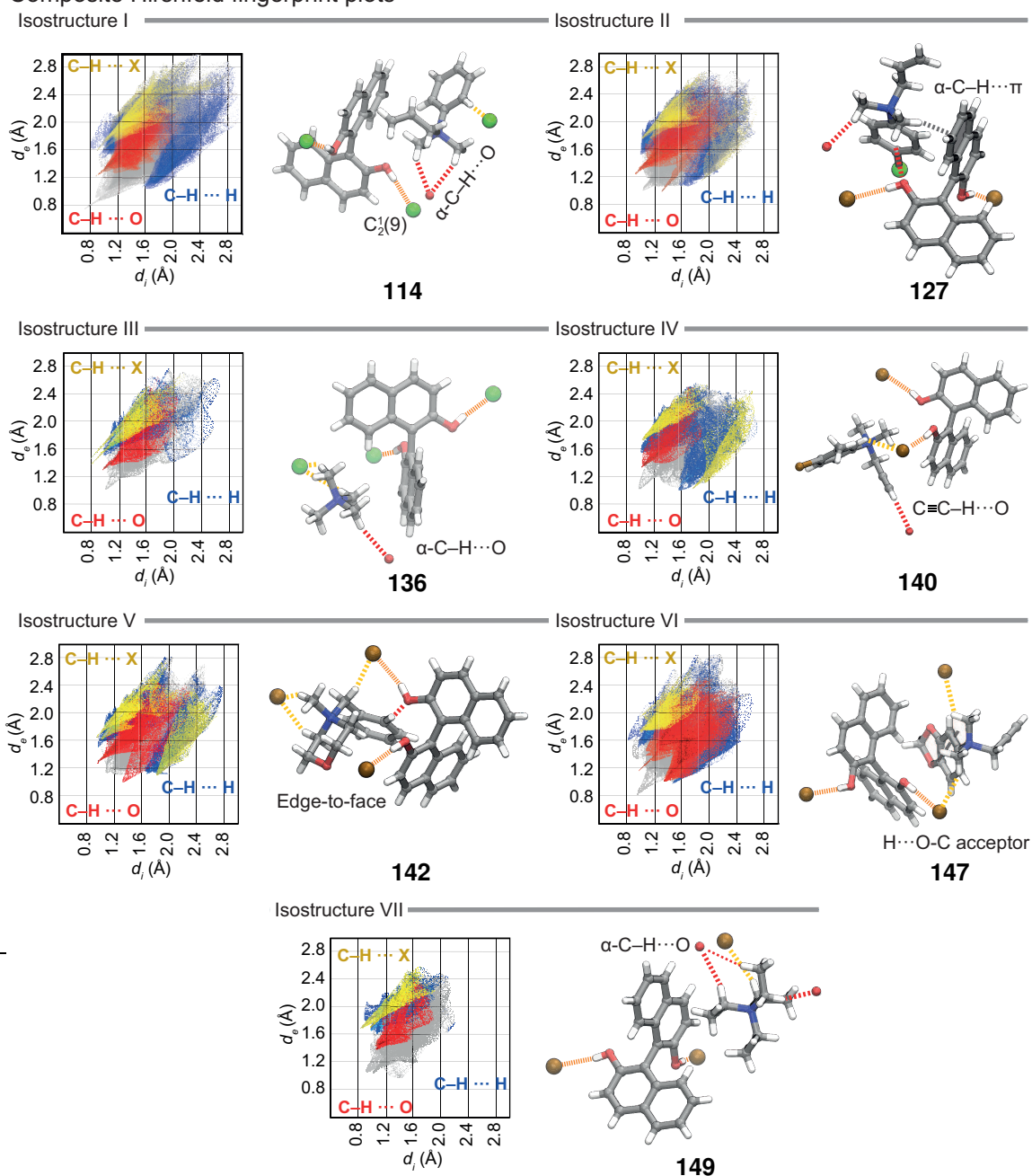


Figure 2.13: Coloured, overlaid, composite Hirshfeld plots for each isostructure and significant contacts that the ammonium cation can make to each isostructure.

2.5 Quaternary ammonium salt selectivity

Quaternary ammonium salts selectively form ternary complexes with (*R*)-BINOL when in competition with a mixture of primary, secondary and tertiary ammonium salts. Here, the selective abstraction of several analogous ammonium species from solution proceeds with the reverse selectivity than that observed by Pedersen, Cram and Lehn and is at odds with what would be expected if selectivity were to be predicted by hydrogen bond donor ability or cation- π strength (see Figure 2.14.).^{180,181}

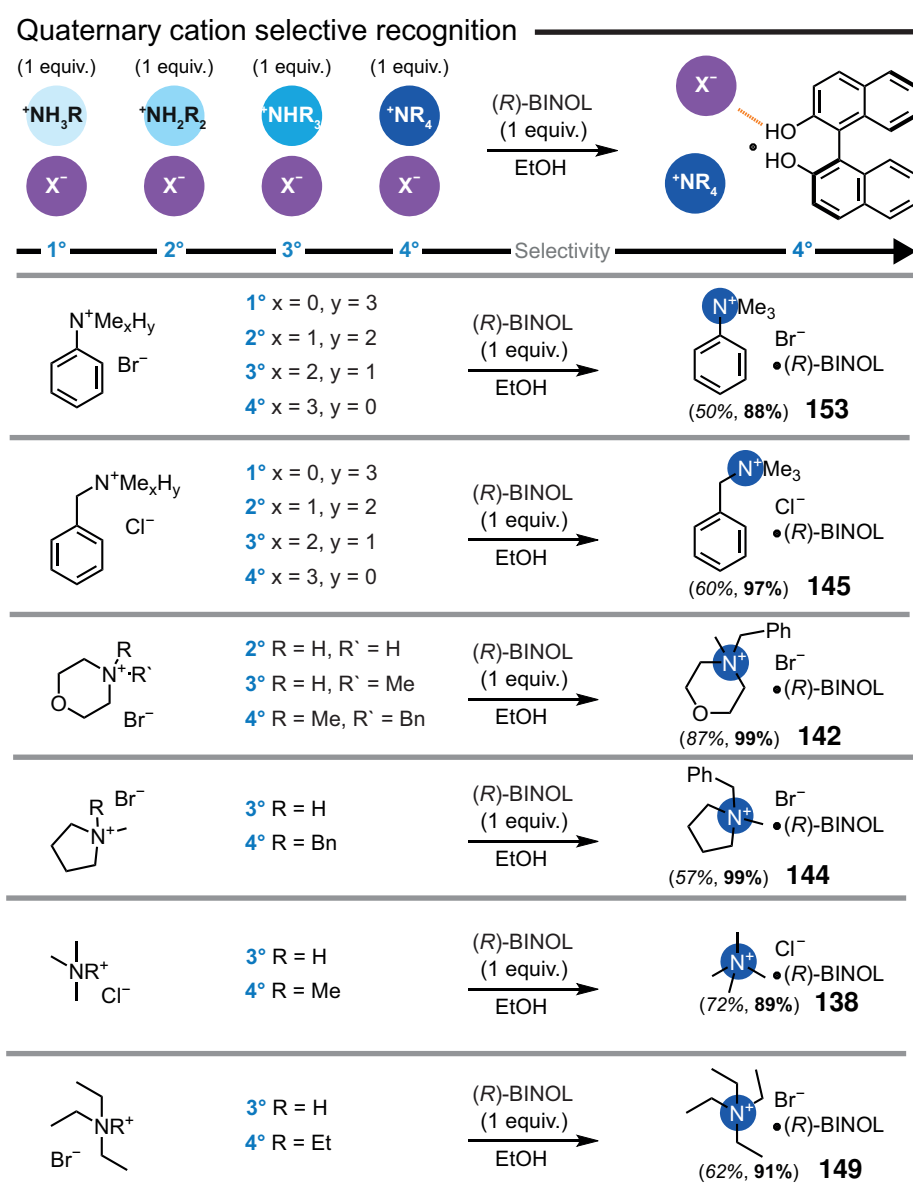


Figure 2.14: Selectivity experiments between varyingly substituted analogues of ammonium cations (*Yield%*, **Selectivity%** versus the other cations).

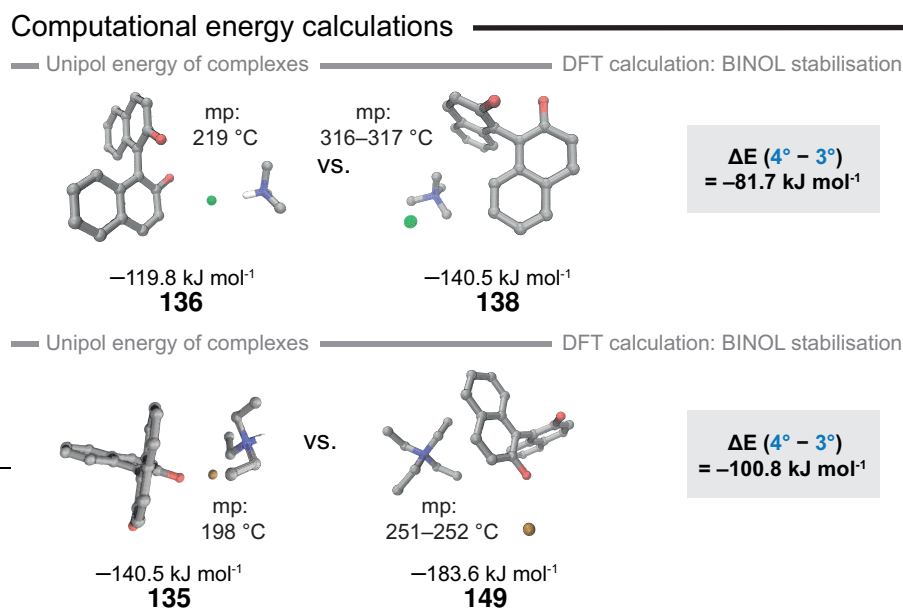
2.5.1 *In silico* calculations

Figure 2.15: Melting points, Unipol potentials and DFT calculated energy differences of the stabilising effect of (*R*)-BINOL of homologous tertiary and quaternary complexes (*DFT calculations performed by Emma P. Wolpert*).

The self-assembled host encapsulates more highly substituted cations into a lower energy superstructure than with less substituted homologues, independent of the isostructure accessed. The melting points of homologous methylammonium complexes (**136** = 219 °C, **138** = 316–317 °C) and ethylammonium complexes (**135** = 198 °C, **149** = 251–252 °C) confirm that quaternary ammonium cation complexes are more stable than complexes containing the less substituted congener. Density functional theory (DFT) calculations using the PBE functional¹⁹⁴ and Grimme-D3 dispersion correction¹⁹⁵ were used to compare the relative energies of crystal structures.^{194–199} Calculating the energy difference between crystal structures with different numbers of atoms is challenging as their lattice energies cannot be directly compared. Instead, we calculated the difference in energy of the stabilising effect of the (*R*)-BINOL by comparing the energy difference between the crystal structure and the tertiary or quaternary salt per asymmetric unit. Calculations on complexes **136** and **138** from isostructure IV reveal that the (*R*)-BINOL stabilises the quaternary tetramethyl-ammonium cation more than the analogous tertiary cation complex by 81.7 kJ mol⁻¹. The same observation is true for corresponding ammonium cations from different isostructural hosts

2.5. QUATERNARY AMMONIUM SALT SELECTIVITY

as calculations confirm that the stabilising effect of (*R*)-BINOL for the tetraethyl variant **160** (isostructure VII) is 100.8 kJ mol⁻¹ lower in energy than for the homologous *N,N,N*-triethylammonium hydrobromide complex **135** (isostructure IV) (see Figure 2.15.).

Cation replacement (thermodynamic control)

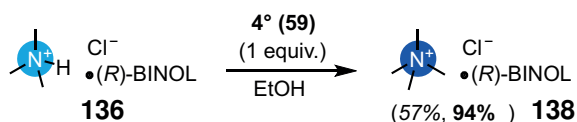


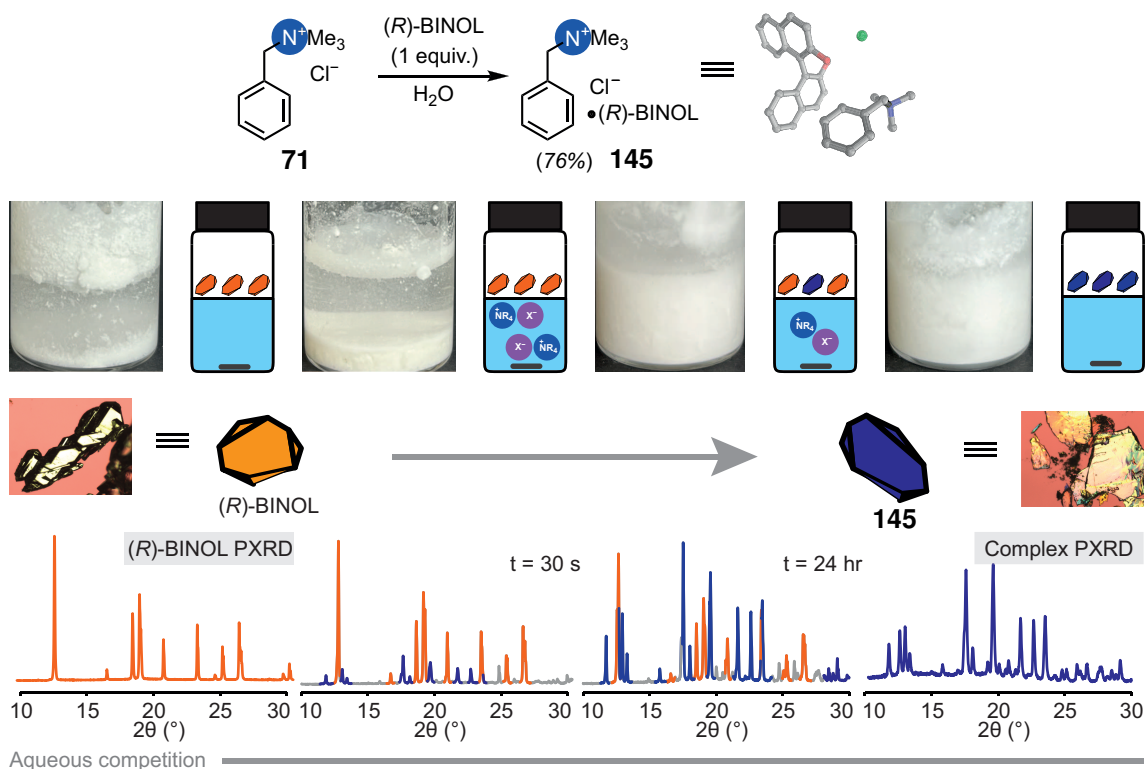
Figure 2.16: Slurry exchange from a tertiary complex to a quaternary complex (Yield%, Selectivity%).

Furthermore, Unipol binding energy calculations are in agreement with the quaternary ammonium cation complexes (**138**; $E = -140.5$ kJ mol⁻¹, **149**; $E = -183.6$ kJ mol⁻¹) proving more stable than the tertiary homologues (**136**; $E = -119.8$ kJ mol⁻¹, **135**; $E = -140.5$ kJ mol⁻¹).^{200,201} Experimental evidence additionally confirms the supramolecular solid-phase abstraction process operates under thermodynamic control (see Figure 2.16.). When tertiary ammonium complex **136** is vigorously stirred with a closely related quaternary ammonium analogue (Me₄N⁺) for 72 hours, the solid is converted to quaternary ammonium complex **138**. As the system does not require specific non-covalent interactions to be present but instead relies on multipoint binding to a spontaneously generated host, the canonical synthetic receptor selectivity is overturned.

*DFT calculations performed by Emma. H. Wolpert under the supervision of Kim. E. Jelfs.

2.6 Aqueous ammonium salt extraction and competition

Aqueous extraction experiments



Aqueous competition

Figure 2.17: Aqueous extraction of a quaternary ammonium salt and aqueous competition to bind a quaternary ammonium salt (*Yield%*, **Selectivity%**). Pictures and graphical representations of (R) -BINOL stirred with aqueous media containing **71** over varying time periods and PXRD patterns showing the composition of the solid transforms from pure (R) -BINOL to increasing levels of **145** over time. Pictures of the single crystals of pure **145** and (R) -BINOL are used to depict the morphological differences.

The same complexation phenomenon remains functional in water. By simply mixing (R) -BINOL with aqueous media containing **71**, the quaternary ammonium salt is sequestered in the form of **145**. Moreover, despite (R) -BINOL having limited solubility in water, the solid can sequester **71** into **145** with increasing yield over time. This can be tracked by PXRD to visualise the change in solid-state structure through the increase in the prevalence of **145** versus that of (R) -BINOL. Competition between the

2.6. AQUEOUS AMMONIUM SALT EXTRACTION AND COMPETITION

tertiary *N,N*-dimethylbenzylammonium hydrochloride salt (**158**) and quaternary **71** in water selectively yields **145** (93% selectivity, see Figure 2.17.). Hence, not only is the hydrogen bonded network functional in an aqueous environment but it remains highly selective towards the quaternary ammonium salt versus its less substituted congener.

Biologically relevant ammonium salt competitions

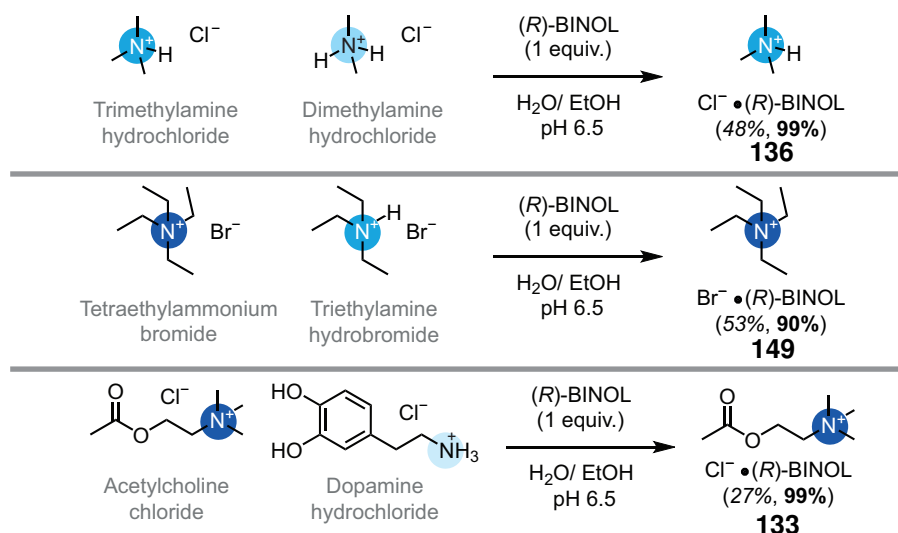


Figure 2.18: Selective recognition of acetylcholine (ACh) chloride and other biologically relevant ammonium salts from a mixture of less substituted molecules.

To test the robustness of our process we sought to reproduce the selective recognition of more substituted ammonium cations observed in Nature.^{160,178,179} The selective binding of the more substituted tertiary trimethylammonium cation in trimethylamine dehydrogenase, the K⁺ ion channels recognition of the tetraethyl ammonium cation, and the discrimination between neurotransmitters such as dopamine and acetylcholine can all be emulated by our (R)-BINOL-based recognition procedure. Addition of (R)-BINOL (1 equiv.) to a mixture of trimethyl ammonium hydrochloride (1 equiv.) and dimethyl ammonium hydrochloride (1 equiv.) in EtOH:H₂O (9:1) solution yielded the crystalline **136** in excellent yield and almost complete selectivity. Similarly, tetraethylammonium bromide and triethylammonium hydrobromide could be differentiated by our system, efficiently extracting the more substituted cation as **149** from buffered solution. Finally, competition of the neurotransmitters acetylcholine chloride and dopamine hydrochloride for inclusion in the supramolecular host, after aqueous washing to remove co-precipitated uncomplexed salts, yielded exclusively **133**. Inter-

rogation of the SCXRD of host-guest complex **133** reveals that the strong directional interactions made between (*R*)-BINOL and chloride counterion act to encapsulate the acetylcholine cation into a favourable recognition environment via providing multipoint interactions to guest (see Figure 2.19.). By exploiting this strong directionality common to synthetic systems, the host can self-assemble to provide a multipoint recognition environment delivering the same selectivity observed in the natural world.

Ach recognition environment

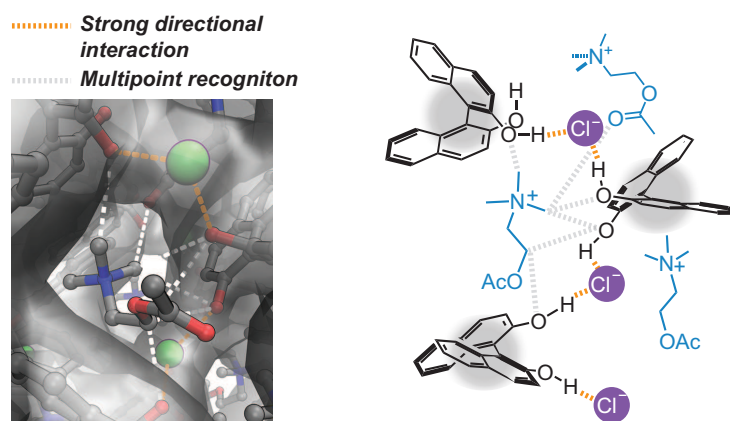


Figure 2.19: Analysis of the crystalline host's recognition environment in **133**, the grey surface represents the QuickSurf calculated isosurface of the helical host of **133**, strong directional interactions are labelled orange, interactions of ACh to the helix are shown in light grey.

2.7 Chapter 2 summary

In summary, by combining the recognition principles operative in natural and synthetic binding environments a system under thermodynamic control can be accessed in which more substituted ammonium cations can be selectively recognised. Here, the cations form ternary complexes with BINOL which acts as a supramolecular recognition unit in solution. These recognition units self-assemble into a dynamic and flexible hydrogen bonded network of (*R*)-BINOL and counterion. Subsequently the complex is abstracted into the solid phase in the form of a crystalline helical host. The isostructure of the host that encapsulates ammonium cations adapts to provide a suitable multipoint recognition environment for the cation to which it is presented. Quaternary ammonium cation complexes access a lower energy solid-state than less substituted salts and are selectively abstracted from solution. Our system overturns the

2.7. CHAPTER 2 SUMMARY

long-standing selectivity based on hydrogen bonding ability and cation- π interaction strength and competitively abstracts more substituted quaternary ammonium cations, even under aqueous conditions and from complex mixtures of biologically relevant molecules. With these advantages demonstrated, we hope that further exploration of the solid-state as a supramolecular host will lead to further unprecedented behaviour in contrast to chemistry in the solution state.

Chapter 3

Polymorphic and pseudopolymorphic ternary complexes

Polymorphism, denoting the occurrence of different crystal structures for the same molecule, holds substantial practical significance across various branches of the chemical industry, particularly within the field of organic solid-state chemistry.²⁰² In the context of pharmaceuticals for instance, over half of compounds display polymorphism.²⁰³ The first example of a polymorphic organic compound was benzamide, studied almost two centuries ago by Liebig and Wohler in 1832.²⁰⁴ As of now, benzamide is known to crystallise in three distinct forms, with forms II and III proving more challenging to crystallise (see Figure 3.1.).²⁰⁵ Despite the determination of the crystal structure of the stable form dating back to 1959 (form I),²⁰⁶ a labile polymorph was only solved in 2005 (form II),²⁰⁷ while the original metastable form studied by Liebig and Wohler wasn't solved until 2007 (form III).²⁰⁸ Benzamide exemplifies the intricate nature of crystallisation and demonstrates how control over this process can influence upon the solid morphologies of compounds.

Benzamide polymorphs

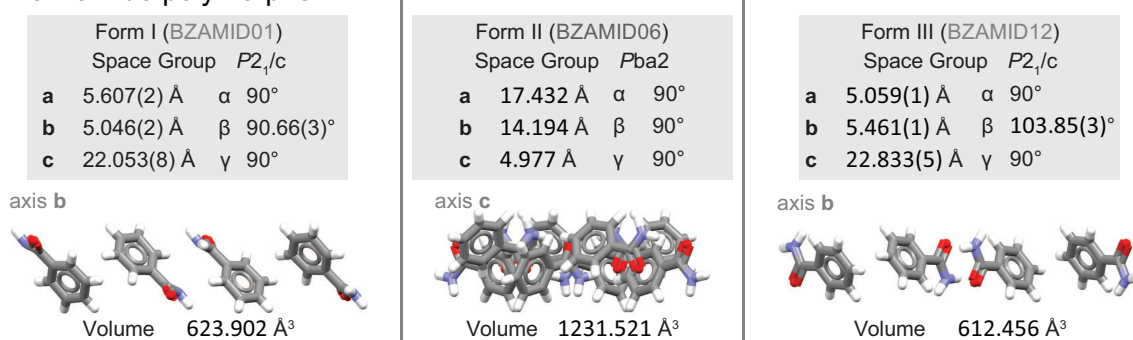


Figure 3.1: Three polymorphic forms of benzamide, their CCDC access codes and unit cell parameters.

Differences in solubility among crystal forms of pharmaceutically relevant compounds can give rise to variations in the bioavailability of solid dosage forms, especially when bioavailability is limited by dissolution.²⁰⁹ Well-known instances of drugs undergoing polymorphic transformations are aspirin, paracetamol and ritonavir. It is the presence of impurities in aspirin and paracetamol that is known to cause the transition between solid forms. Consequently, meticulous attention to synthesis and purification processes is imperative for controlling the solid-state structure of these substances.²⁰⁵ Even though aspirin has been crystallised in significant quantities since the 19th century, its second form was only unveiled in 2005 when it crystallised in the presence of the impurity, aspirin anhydride.^{210,211} Similarly, paracetamol tends to crystallise in its form II only in the presence of certain impurities, including metacetamol.²¹²

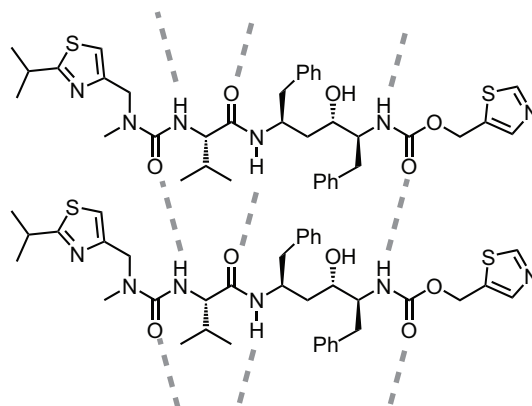
During the summer of 1998, the production of *Norvir* (**161a**), used in the treatment of Acquired Immunodeficiency Syndrome (AIDS), was at risk due to a newly identified, considerably less soluble crystal form of ritonavir (a protease inhibitor), namely form II.²⁰⁹ Intriguingly, this new polymorph exhibited an unusual combination of both high stability and difficulty of crystallisation. Ritonavir displayed conformational polymorphism, specifically in the *cis* and *trans* conformations around the carbamate linkage, resulting in two distinct crystal lattices with significantly different solubility profiles (see Figure 3.2.). The polymorph (**161b**, form II) associated with the *cis* conformation possessed a more stable packing arrangement. However, the nucleation of this polymorph necessitated the formation of a less stable *cis* conformation in solution before subsequent crystal growth could occur. This nucleation process, even when form II seeds were present, faced significant energetic barriers, except in highly supersaturated solutions. Consequently, the identification of form II might never have occurred if not for coincidence of a solution that was exceptionally supersaturated (approx. 400%) with respect to the polymorph, coupled with an unidentified nucleation enhancer capable of heterogeneously seeding the solution. This combination led to the sudden emergence of a new metastable polymorph, form II and the disappearance of form I.²¹³

Ritonavir polymorphism

Form I



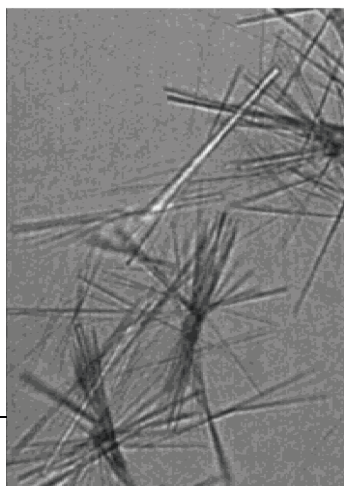
$P2_1$



Novir™

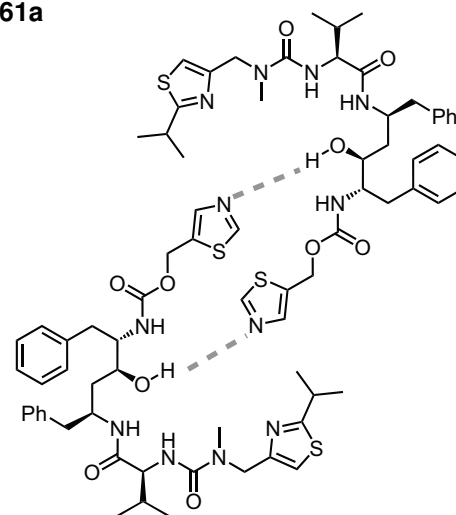
161a

Form II



$P2_12_12_1$

More stable
Harder to crystallise



161b

Figure 3.2: The two polymorphs of ritonavir (form I and II) and the arrangement of the molecules within the crystal structure. Pictures of polymorphs taken from Bauer *et al.* **2001**²⁰⁹ - 'Springer Nature allows adaptation of figures for style and formatting purposes under this license under the condition that this does not alter the meaning of the content.'

3.1 Ethanol versus chloroform

Given the importance of the solid-state to the recognition of ammonium salts by BINOL, it is imperative that polymorphic and pseudopolymorphic crystal forms of ternary complexes formed between ammonium cation, counterion and BINOL are considered. In Chapter 2, all compounds were confirmed to have the same solid-state structure by comparing the experimental PXRD evidence to a predicted PXRD pattern derived from SCXRD data, ensuring the uniformity of solid-states (see Figure 2.8.). However, for some of the recognition complexes, it was noted that different polymorphs formed dependent on the solvent from which the microcrystalline material was precipitated.

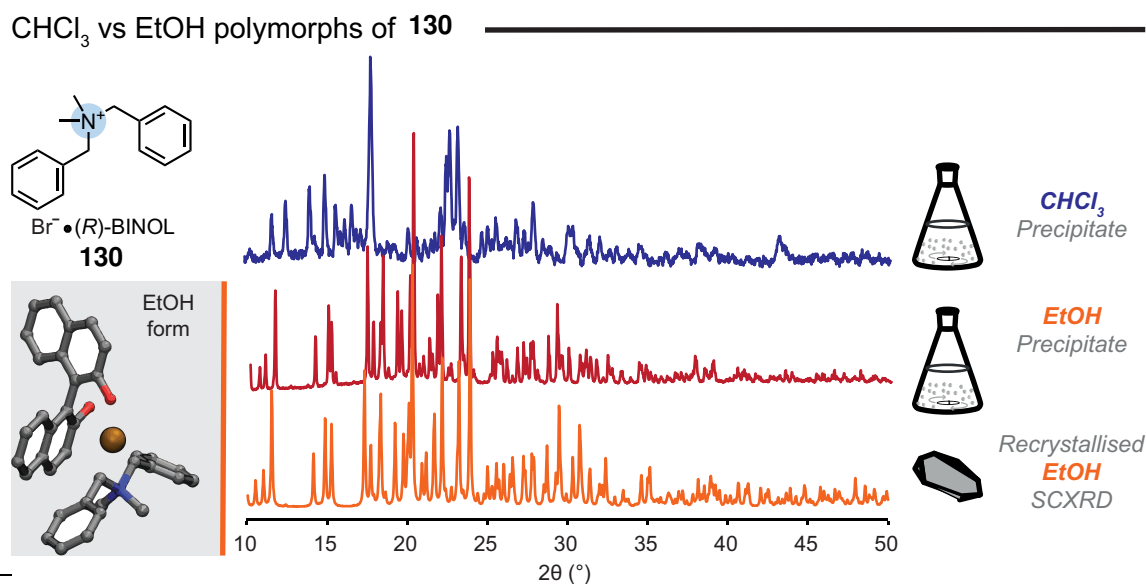


Figure 3.3: PXRD patterns of the microcrystalline material precipitated during the synthesis of **130** from CHCl₃ and EtOH, showing the SCXRD data for the compound matches the EtOH precipitate.

In the case of **130**, distinct polymorphic forms were observed depending on whether the microcrystalline solid was precipitated from CHCl₃ or EtOH (see Figure 3.3.). When analysing the PXRD patterns it becomes immediately apparent that the CHCl₃ and EtOH forms are discernibly different. Despite yielding a greater amount of precipitate in CHCl₃ (0.6 M, 95% yield compared to 61% yield in EtOH), the solid-state structure did not align with the crystal structure obtained from recrystallisation in ethanol. To ensure a consistent solid-state structure for further analysis, the material was resyn-

thesised from ethanol, to match the polymorph of the single crystal data collected. Attempts to recrystallise the compound from chloroform proved ineffective, failing to yield material of sufficient quality for SCXRD analysis.

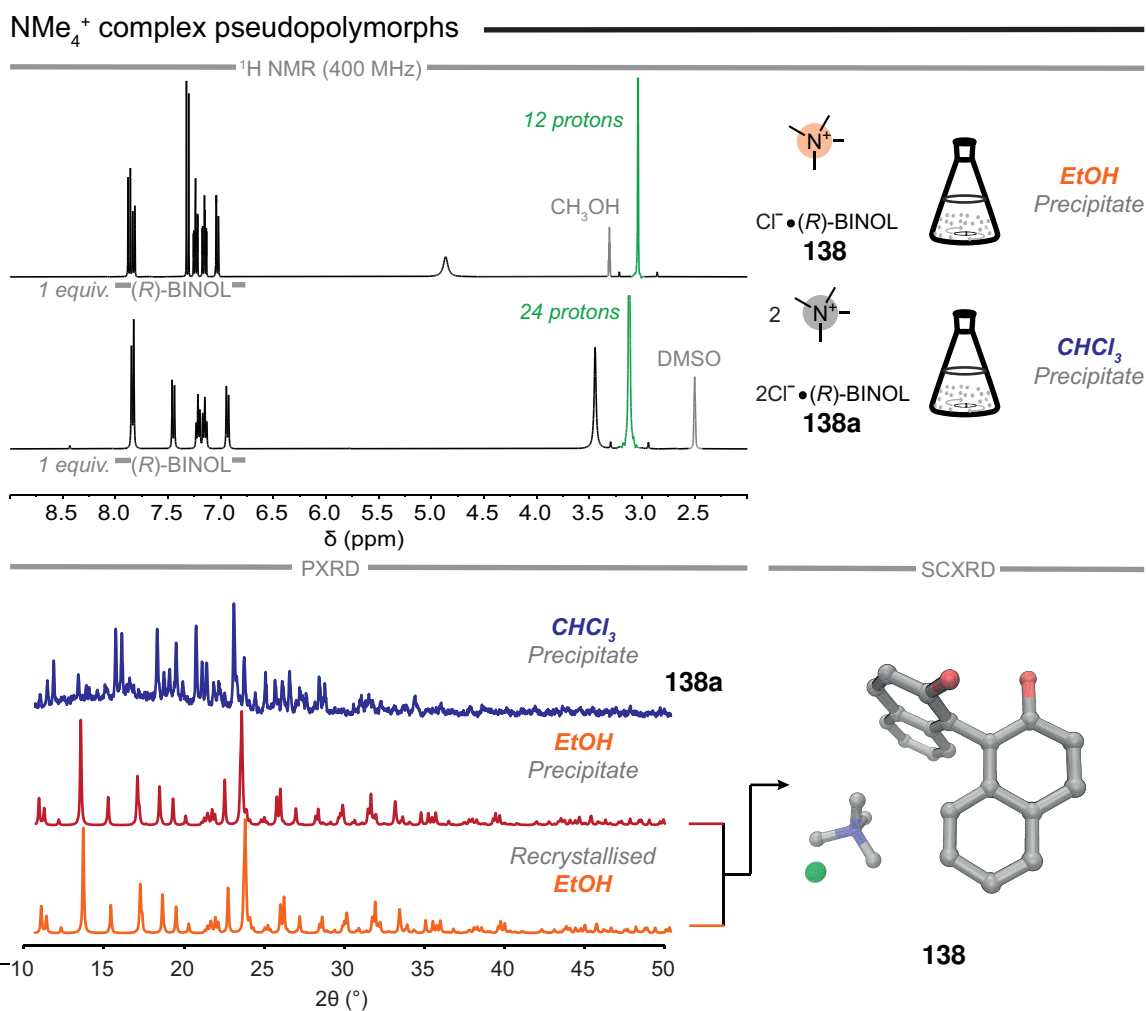


Figure 3.4: NMR, SCXRD and PXRD data showing a change in the stoichiometry of complexes dependent upon the solvent of precipitation.

In the case of complexes **138** and **152**, both featuring a tetramethylammonium cation (NMe₄⁺), the stoichiometry of the ternary complex involving the ammonium cation, counterion, and (*R*)-BINOL is determined by the choice of solvent. In CHCl₃, the stoichiometry of ammonium cation:(*R*)-BINOL in **138a** is 2:1, whereas in EtOH it is 1:1 (**138**). Conversely, for **152**, the stoichiometry is 1:1 in CHCl₃ (**152a**) but shifts to 2:1 in EtOH (**152**). Here, the change in stoichiometry is evident through ¹H NMR spectroscopy, while the consequent shift in pseudopolymorphic form is tracked via PXRD.

3.1. ETHANOL VERSUS CHLOROFORM

This phenomenon is illustrated for **138** in Figure 3.4. In this context, the solvent selection is vital in generating distinct pseudopolymorphic microcrystalline precipitate forms.

Despite a change in solvent effecting the solid form produced for **130**, **138** and **152**, analogous material can be produced through precipitation and recrystallisation from the same solvent (EtOH). In the case of 1-methylpyridinium iodide·(*R*)-1,1'-bi-2-naphthol (**162**) however, the method of preparation - precipitation or recrystallisation - also changes the solid form accessed. Hence, 4 polymorphic forms of **162** can be isolated from CHCl₃ and EtOH, dependent upon the synthesis employed (see Figure 3.5.).

To try and discern the differences in the solid-state between the precipitated material and the recrystallised material of **162**, the PXRD patterns of **162a** and **162b** were interrogated.^b The PXRD data for **162b** was initially indexed, and a Pawley fit was carried out, revealing the space group (*P2₁2₁2₁*) and unit cell dimensions (**a** = 9.297 Å, **b** = 11.783 Å, **c** = 20.673 Å), resembling the single crystal model **162c**. However, notable differences between **162c** and **162b** structures were evident during a subsequent Rietveld fit to the single crystal model. This analysis yielded refined unit cell dimensions for **162b** (**a** = 9.2982 Å, **b** = 11.775 Å, **c** = 20.650 Å). Further data analysis involving an extended 2-theta range and parameter adjustments led to excellent agreement between observed and calculated patterns (see Figure 3.5.), reflected in a low R_{wp} value of 5.64%. This agreement strongly supports the accuracy of the structural model. (*note: water content analysis was not conducted*).^b

A similar methodology was followed for **162a** to give initial unit cell dimensions of: **a** = 9.204 Å, **b** = 13.741 Å, **c** = 18.724 Å, in space group *P2₁2₁2₁*. The cell volume, 2368 Å³, compared to 2265 Å³ for **162b**, suggested potential accommodation for four additional CHCl₃ molecules in the precipitated material. Furthermore, this volume approximation was close to the SCXRD structure of **162c** (2295 Å³), hinting at possible isostructurality. However, subsequent structural analysis revealed a distinct form through precipitation from CHCl₃ (see Figure 3.5.).

^b I would like to thank and acknowledge the work of John S. O. Evans for performing Pawley structure independent fits and Rietveld fit analysis of the PXRD patterns.

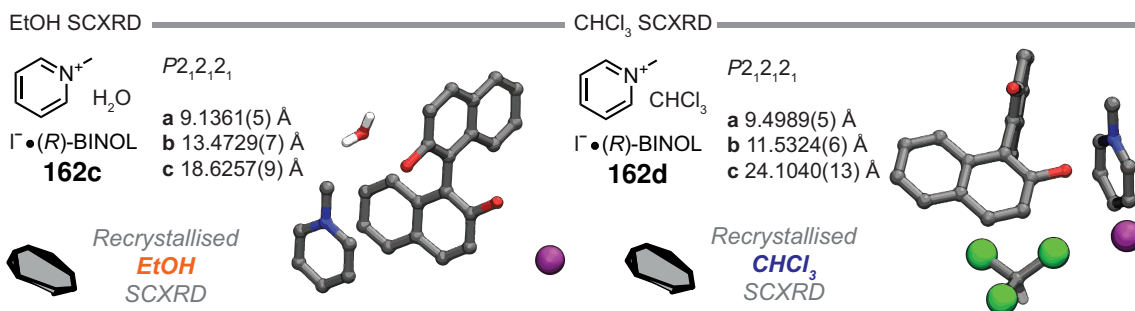
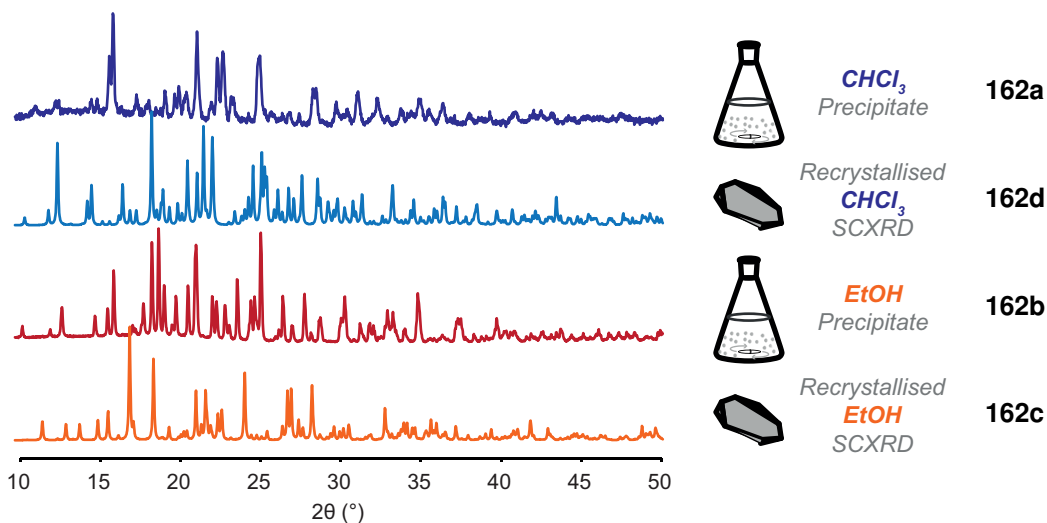
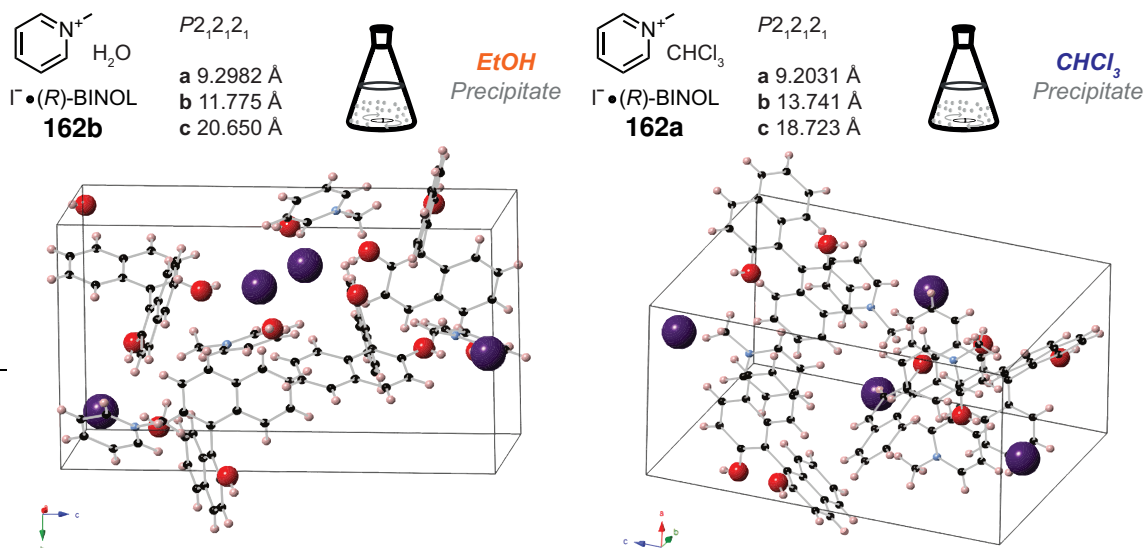
CHCl₃ vs EtOH polymorphs of **162**PXRD traces for the polymorphs of **162**PXRD structures for **162**

Figure 3.5: SCXRD crystal structures and PXRD patterns of the microcrystalline material precipitated during the synthesis of **162** from CHCl₃ and EtOH, showing the SCXRD data and PXRD for all preparations differs. PXRD solid-state structures of **162a** and **162b** based off the PXRD patterns of the microcrystalline material precipitated from the reaction mixture. *These structures were solved by John S. O. Evans.*

3.1. ETHANOL VERSUS CHLOROFORM

Single crystals were also grown for a complexes **163**, **164** and **165** from both EtOH and CHCl_3 to further demonstrate the change in solid form dependent upon the solvent in which the recognition occurs (see Figure 3.6.). In **163**, a 1:1 ((*R*)-BINOL:cation) complex is observed in EtOH, whereas it transforms into a 2:1 complex with a solvate in CHCl_3 . Conversely, in **164** a 2:1 ((*R*)-BINOL:cation) complex with a solvate structure is formed in EtOH, later shifting to a 1:1 ratio in CHCl_3 with a Z' of 2. In **165**, a 1:1 ((*R*)-BINOL:cation) complex with a solvate structure is observed in EtOH. However, this configuration transitions to a 1:1 ratio in CHCl_3 with a Z' of 2, in a non-isostructural way to **164b**.

Pseudopolymorphic recrystallisations

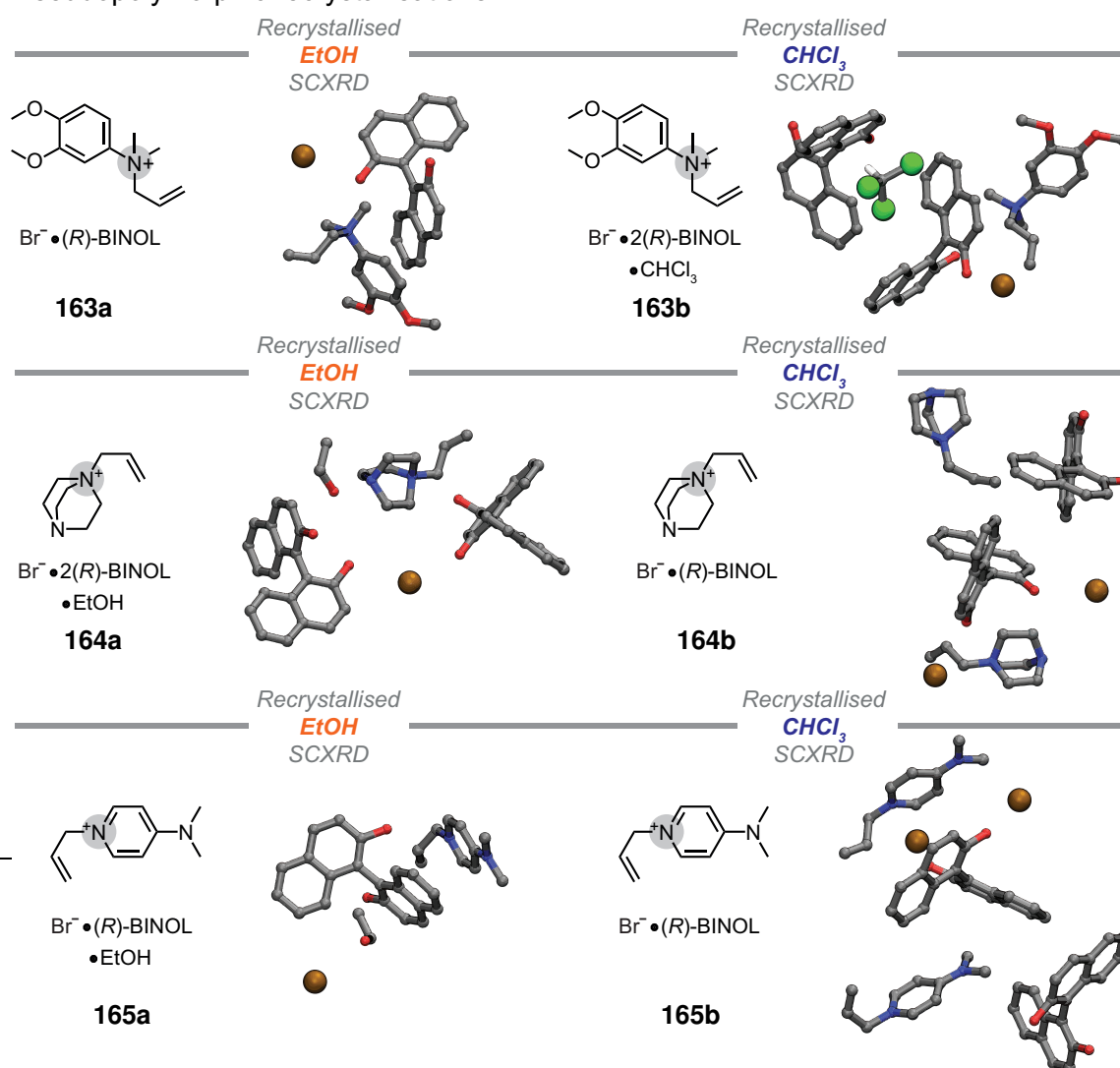


Figure 3.6: SCXRD crystal structures of **163**, **164** and **165** recrystallised from CHCl_3 and EtOH.

3.1.1 Changes in selectivity of quaternary ammonium salts

Competition experiments in EtOH prove that quaternary ammonium salts selectively form ternary complexes with (*R*)-BINOL when in competition with a mixture of primary, secondary and tertiary ammonium salts (see Figure 2.14.). Because the form of the solid-state of certain complexes changes dependent upon the solvent of precipitation, then it stands to reason that the relative stability of the tertiary to quaternary complex will shift when the solvent in which the competition proceeds is switched. Consequently, this alteration in stability will impact upon the observed level of selectivity and yield (see Figure 3.7.).

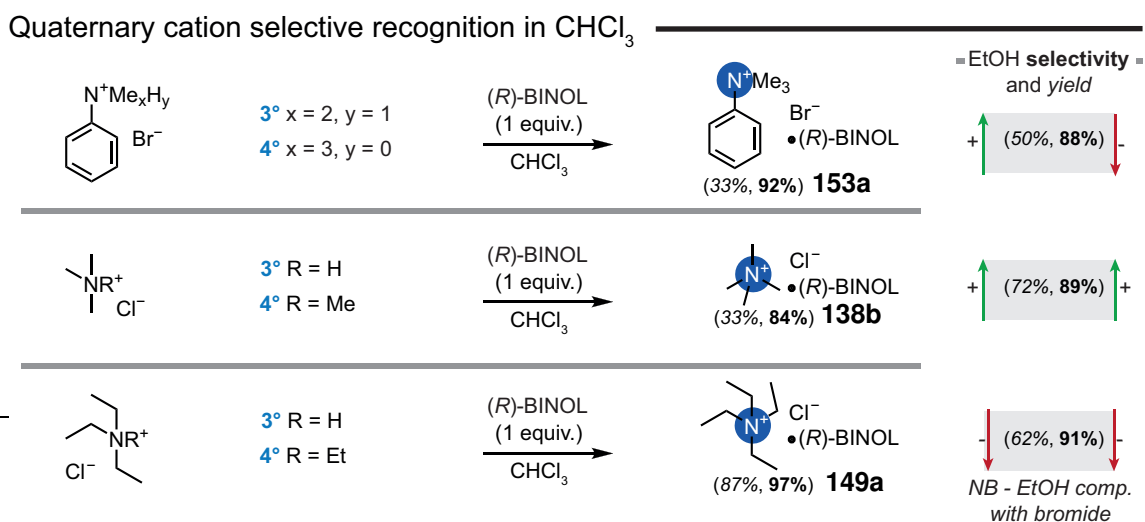


Figure 3.7: Selectivity experiments between variously substituted analogues of ammonium cations (*Yield%*, **Selectivity%**) in CHCl_3 .

Interestingly the yields and selectivities of the experiments in CHCl_3 both increase and decrease with respect to EtOH. This observation implies that alterations in the solid-state exert a more substantial influence than differences in solubility between the tertiary and quaternary complexes in the specific solvent. Otherwise, we would anticipate consistent trends when transitioning from EtOH to CHCl_3 in terms of changes to the yield and selectivity in these experiments.

3.2 Racemic versus enantiopure BINOL

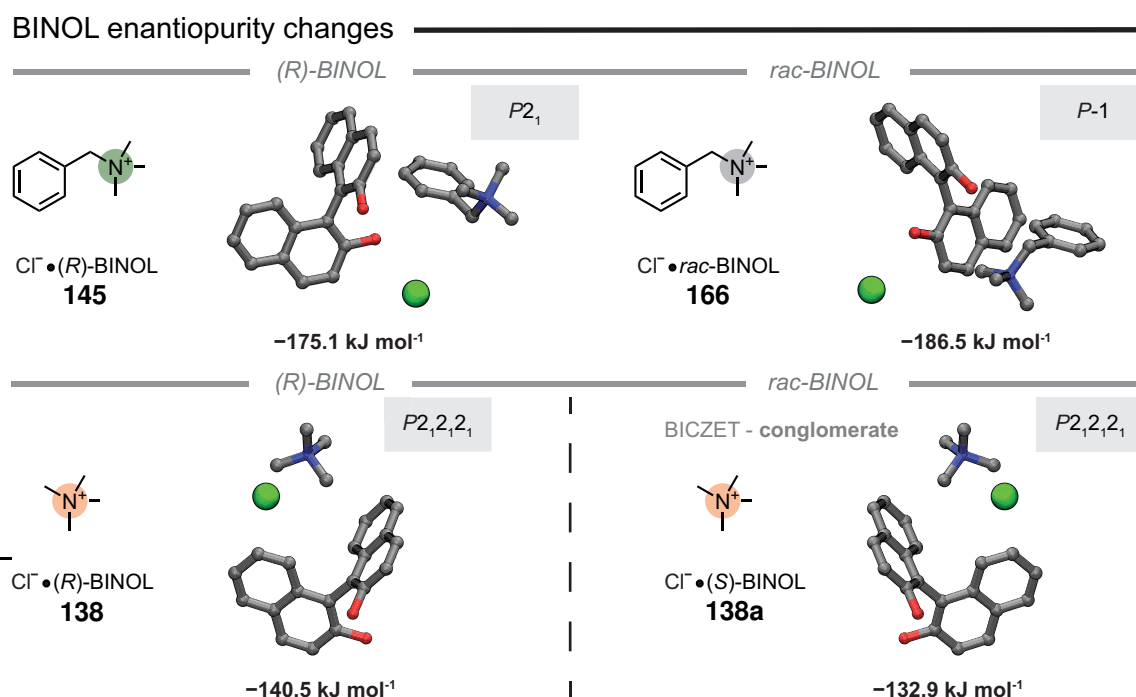


Figure 3.8: SCXRD crystal structures of ammonium salts recrystallised from EtOH in the presence of either (*R*)- or *rac*-BINOL. Unipol calculated energies are labelled below each structure.^{200,201} BICZET accessed from CCDC.²¹⁴

When varying the enantioenrichment of the BINOL used to complex the ammonium salts, different crystalline structures are observed (see Figure 3.8.). For instance, recrystallising benzyltrimethylammonium chloride (**71**, 1 equiv.) from EtOH in the presence of 1 equivalent of either (*R*)- or *rac*-BINOL yields two distinct crystal structures, **145** and **166**. The change in the solid-state of certain complexes depending on the BINOL used suggests there might also be a shift in the relative stability of the complexes. Consequently, this alteration in stability can act to change the observed level of selectivity and yield from a mixture of primary, secondary and tertiary ammonium salts when utilising (*R*)- or *rac*-BINOL. Notably, this phenomenon is not universal across all complexes, as given complexes have the ability to form conglomerates (such as **138a**), resulting in analogous crystal structures regardless of the enantioenrichment of BINOL.

In the case of **145** versus **166**, a notable shift in hydrogen bonding patterns within

the crystal structure is observed. In **145**, a C_2^1 (9) continuous hydrogen-bonded chain forms between (*R*)-BINOL and chloride anion, effectively encapsulating the benzyltrimethylammonium cation within the crystalline network. This chain and its orientation play a vital role in the construction of isostructures identified in Chapter 2 (see Figure 2.11.). In contrast, in **166**, hydrogen bonding between *rac*-BINOL and the counterion manifests as an R_4^2 (18) ring, making the construction of any crystal lattice resembling a C_2^1 (9) isostructure impossible. Hence, it is evident that the recognition event and subsequent abstraction of the complex from solution must proceed through an alternative mechanism in racemic BINOL examples like **166**, diverging from the process observed with enantiopure BINOL.

3.2.1 Changes in substitutional selectivity

Due to the change in solid-state crystal packing from **145** to **166** when using (*R*)- or *rac*-BINOL to abstract **71**, the selectivity of quaternary salt complexation over its tertiary congener decreases. In EtOH, selectivity declines from 97% with (*R*)-BINOL to 95% with *rac*-BINOL. This change is even more pronounced in H₂O, where selectivity drops by 9% (93% to 84%) upon the transition from enantiopure to racemic BINOL (see Figure 3.9.).

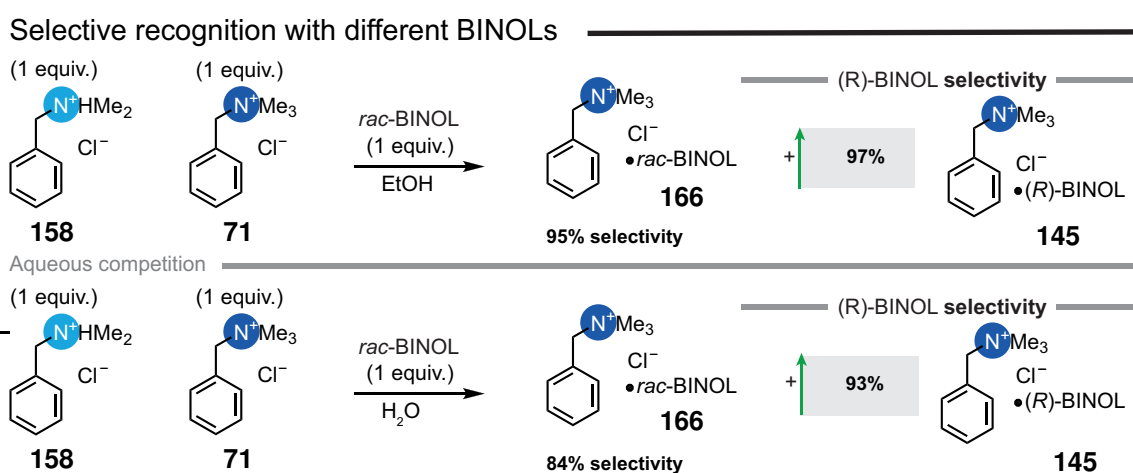


Figure 3.9: Competition experiments to determine changes in selectivity between the abstractions of **71** and **158** depending upon the enantiopurity of the BINOL used.

This trend is consistently observed across a range of competition experiments involving a variety of ammonium salts and their less substituted counterparts (see

3.2. RACEMIC VERSUS ENANTIOPURE BINOL

Figure 3.10.). Generally, the selectivity towards the more substituted quaternary cation is either reduced or there is no significant change when employing *rac*-BINOL in comparison to (*R*)-BINOL in EtOH. In the case of the trimethyl (NMe_3^+) versus tetramethyl (NMe_4^+) ammonium chloride, the selectivity and yield are almost identical to that observed in the competition experiments performed using (*R*)-BINOL due to the conglomerate nature of **138**.

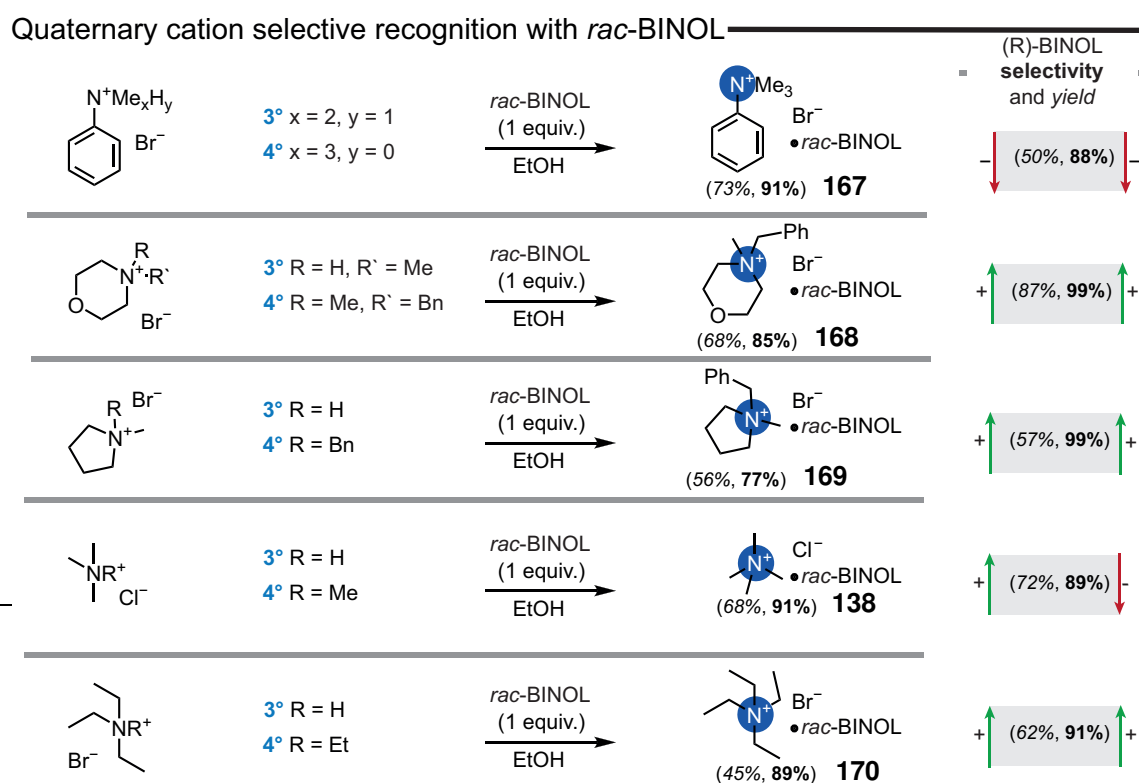


Figure 3.10: Competition experiments to determine changes in selectivity between the abstractions of tertiary versus quaternary salts across a range of ammonium salts depending upon the enantiopurity of the BINOL used.

3.3 Chapter 3 summary

In summary, the choice of solvent and the enantiopurity of the BINOL employed exert a significant influence on the resulting solid-state structures of isolated complexes. Consequently, these factors significantly impact the yield of recognition events and the selectivity observed in competition experiments. Given the importance of the crystalline state in a CIAT-like methodology, attention to both solvent selection and the enantiopurity of the chiral resolving agent is essential to control the end-point of the recognition. These considerations are crucial to a comprehensive understanding of the mechanisms governing recognition of ammonium salts by BINOL, advancing our understanding of recognition phenomenon operative within these systems.

Chapter 4

Enantioselective synthesis of *N*-methyl anilinium salts

Enantioselective synthesis is vital in the construction of many biologically and commercially relevant molecules.¹⁵ Despite having potentially wide-ranging applications, routes to synthesise enriched heteroatomic stereocentres have received less consideration than carbon-based analogues.² The use of nitrogen as a stereocentre is commonly neglected due to its ability to readily quantum tunnel at room temperature and therefore rapidly pyramidally invert (see Figure 1.2.).⁴⁷ Recent work by our group reported the first enantioselective synthesis of *N*-stereocentres via a crystallisation induced asymmetric transformation (CIAT); combining enantioselective ammonium recognition mediated by enantiopure BINOL with conditions that allow the nitrogen stereocentre to racemise.^{2,37} Here the scope of the CIAT is explored to enhance understanding and increase the utility of the methodology. The enantioselective synthesis of a diverse library of *N*-methyl anilinium cation scaffolds allows rationalisation of key requirements for the process.

4.1 Crystallisation induced asymmetric transformation

Whereas carbon stereocentres are locked, the conformational and configurational instability of amines limits the prospect of enantioenriching molecules which contain nitrogen as the sole stereogenic element (see Figure 1.3.). Despite this, the sense of *N*-epimers remains crucial for bioactivity in pharmaceutically relevant molecules (see Figure 1.23.),^{165–169} adding weight to the argument for controlling the stereochemistry of their synthesis. It is possible to resolve certain enantiomers whose chirality originates from a stereogenic nitrogen by locking the lone pair in a stable conformation and configuration, yet only a limited number of resolution processes have been established since the existence of stereogenic nitrogen was first proposed by Le Bel in 1891.⁷⁷ Despite numerous examples being reported to lock the stereochemistry

4.1. CRYSTALLISATION INDUCED ASYMMETRIC TRANSFORMATION

of the nitrogen stereocentre,^{215,216} no general methodology existed until recently to enantioselectively prepare a nitrogen stereocentre as the sole stereogenic element in a molecule.^{2,37,171}

Simple alkylation of tertiary amines with a range of electrophiles produces quaternary ammonium salts with conformationally and configurationally stable nitrogen stereocentres.²¹⁷ This method is the most common way to prevent *N*-lone pair inversion.⁴⁰ However, isolating quaternary ammonium salts with defined stereochemistry can be a challenge for organic chemists due to the inherent hygroscopicity of ammonium salts and their capacity to undergo spontaneous rearrangements at room temperature.¹¹⁷

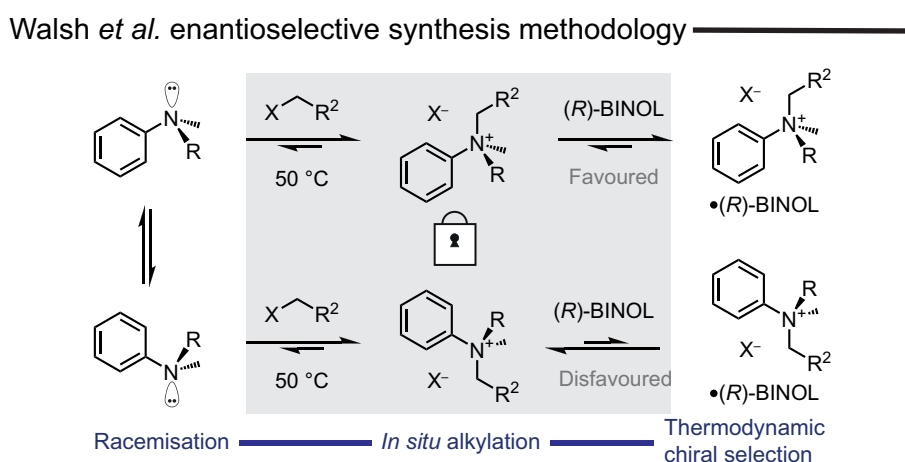


Figure 4.1: CIAT methodology employing (R) -BINOL to enantioselectively synthesise *N*-stereogenic ammonium cations.

Our group demonstrated that by merging a well-established ammonium recognition phenomenon facilitated by BINOL, with conditions that allow the nitrogen centre to racemise, it was possible to enantioselectively synthesise ammonium cations.^{2,37} This methodology is unique from kinetic resolution, as it allows for increased yield of the enantioenriched ternary complex over time. In the proposed mechanism (see Figure 4.1.) the conformationally labile amine undergoes reversible alkylation forming an equilibrium between a mixture of racemic ammonium cations and the tertiary amine. The enantiomer of the quaternary ammonium which favours ternary complexation with enantiopure BINOL is selected from solution as a precipitate. The unfavored enantiomer may also form a ternary complex at this stage, however the mismatched ternary complex preferentially re-dissolves, which releases the ammonium halide from

the solid phase back into solution.²¹⁸ In solution the ammonium is again free to dealkylate and racemise in the same equilibrium as set up previously, leading to enhanced levels of enantioenrichment as the reaction continues. Whilst significant in providing a methodology to access the illusive nitrogen stereocentre, the synthesis suffers from a small substrate scope, modest and varied enantioenrichment and a lack of application beyond kinetically resolving the axial chirality of the moiety used to originally set the stereocentre.

To overcome these drawbacks firstly a library of enantioenriched ammonium salt-BINOL complexes were synthesised using the same procedure reported by Walsh *et al.* to better understand functional group tolerance of the synthesis. Secondly, the recognition phenomenon was investigated to fully characterise and understand the key requirements for the enantioselectivity observed in the solid-state. Finally the most enriched ammonium salts were utilised to form complexes with substituted BINOL scaffolds to provide a novel resolution method for this highly utilised, functionalised, axially chiral ligand.

4.2 Tertiary aniline synthesis

The initial stage of the investigation involved synthesising a range of tertiary aniline precursors, to which various substituent groups were bound. The primary approach utilised for this purpose was a reductive amination of *N*-methyl aniline with a selected aldehyde (see Figure 4.2.). However, when attempting to employ a ketone under these specified conditions, the reaction did not reach completion. This limitation was attributed to increased steric influences about the sp^2 carbonyl functionality. The majority of aldehydes utilized for tertiary aniline synthesis were commercially available, however a subset of the anilines required synthesis by oxidation of the requisite alcohols (see 9.2.5.).

4.2. TERTIARY ANILINE SYNTHESIS

Reductive amination to make aniline cores

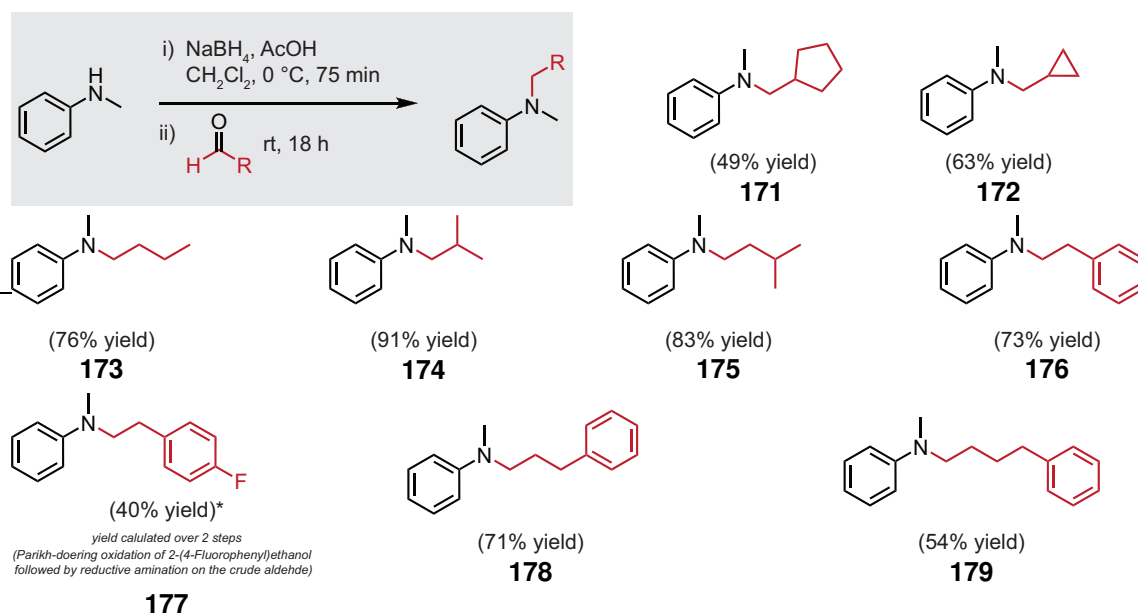


Figure 4.2: The synthesis of tertiary amine scaffolds from *N*-methyl aniline.

The reductive amination could also be performed in an alternate order to access further functionalised *N*-methyl aniline architectures. In these instances, a ketone underwent an initial reductive amination with a primary amine (aniline or 4-fluoroaniline), followed by the addition of a methyl group through a subsequent reductive amination step employing formaldehyde (see Figure 4.3.).

2-step reductive amination

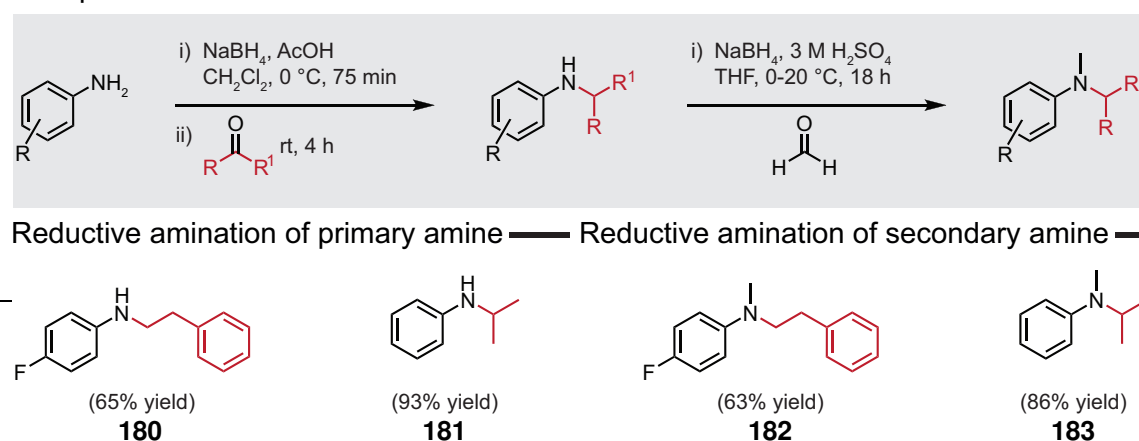


Figure 4.3: The 2-step synthesis of tertiary amine scaffolds.

A reaction sequence employing an amide coupling followed by LiAlH_4 reduction was utilised to achieve the synthesis of **185**.

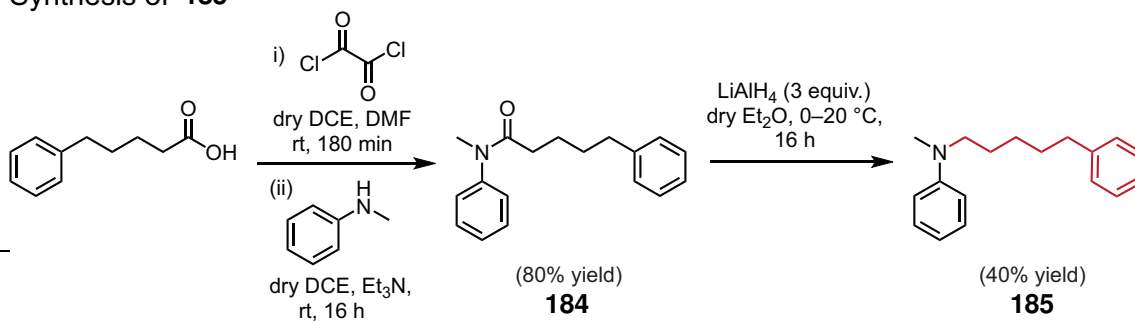
Synthesis of **185**

Figure 4.4: The 2-step synthesis of **185**. Step one: amide coupling of *N*-methyl aniline and 5-phenylvaleric acid. Step two: reduction of **184** with LiAlH_4 .

4.3 Racemic ammonium salt synthesis

Following the synthesis of the *N*-methyl tertiary aniline cores, the substrates underwent alkylation to form racemic quaternary ammonium salts (see Figure 4.5.). This alkylation, achieved through the use of corresponding bromides or iodides, added either an allyl, benzyl, or propargyl moiety to the core. However, due to the hygroscopic nature of ammonium salts, isolation of many alkylated products was challenging, resulting in variable yields for the production of several quaternary ammonium salts, with many requiring either trituration with Et₂O or recrystallisation (MeOH/Et₂O). These ammonium salts were used to test for ternary complexation with (*R*)-BINOL and would later be utilised as racemic standards for the determination of enantiopurity of enantioenriched salts.

4.3. RACEMIC AMMONIUM SALT SYNTHESIS

Alkylation to make *rac*-ammonium salts

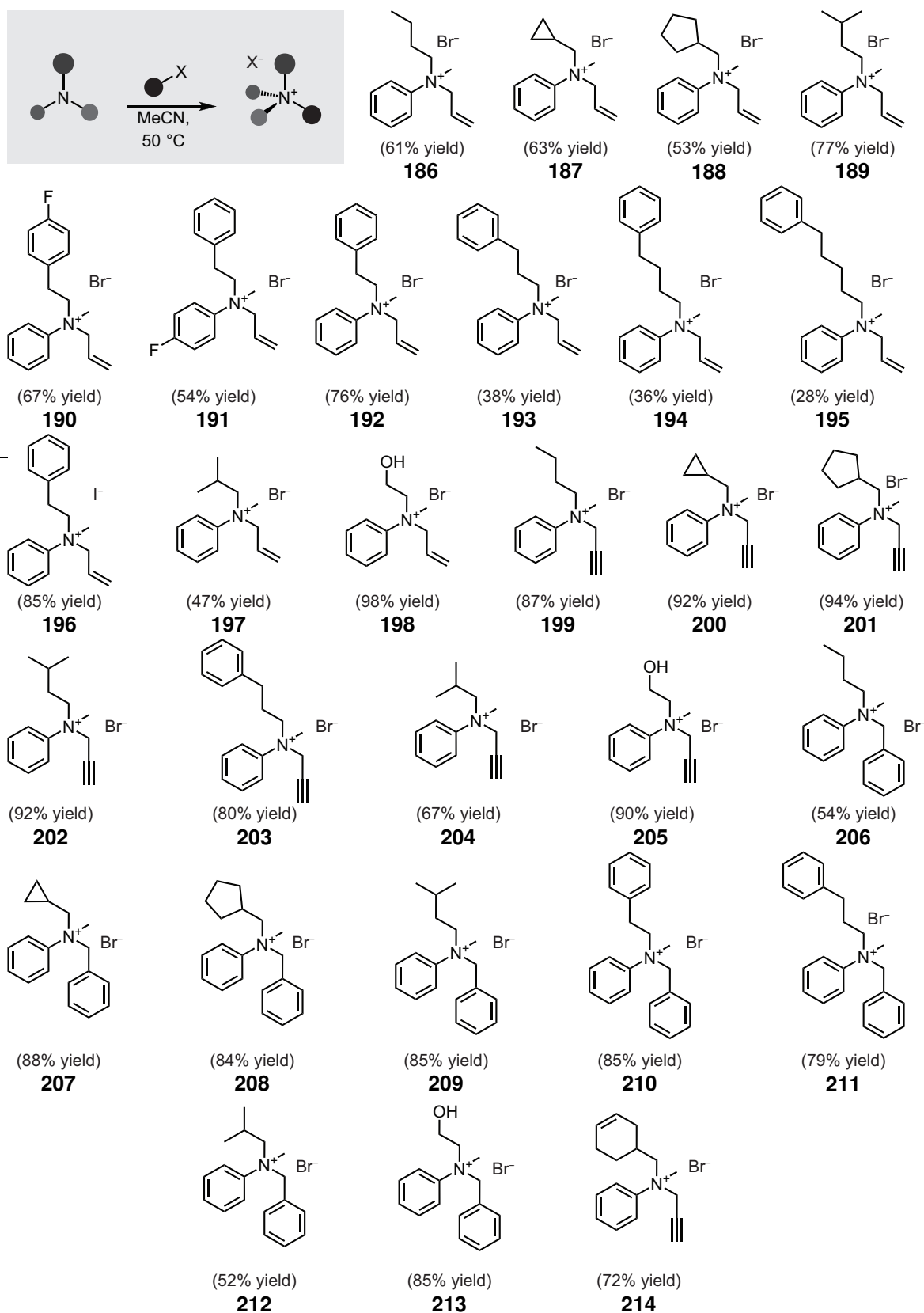


Figure 4.5: The alkylation of tertiary amine scaffolds to produce a library of *rac*-ammonium salts.

4.4 Chiral ammonium salt ternary complexes with BINOL

The racemic ammonium salts underwent testing for ternary complexation with (*R*)- and (*S*)-BINOL (0.5 equiv.) in MeCN or CHCl₃, at concentrations ranging from 0.6 M to 2.0 M. However, this process encountered a high attrition rate in identifying suitable substrates capable of forming ternary complexes and precipitating out of solution. Figure 4.6 summarises the failed kinetic resolutions. Despite the low success rate, a considerable number of salts were identified that formed precipitates in conjunction with (*R*)- and (*S*)-BINOL that could subsequently be utilised for their enantioselective synthesis. The salts found to form ternary complexes under the kinetic resolution conditions were all successful in the dynamic procedure.

Failed kinetic resolutions

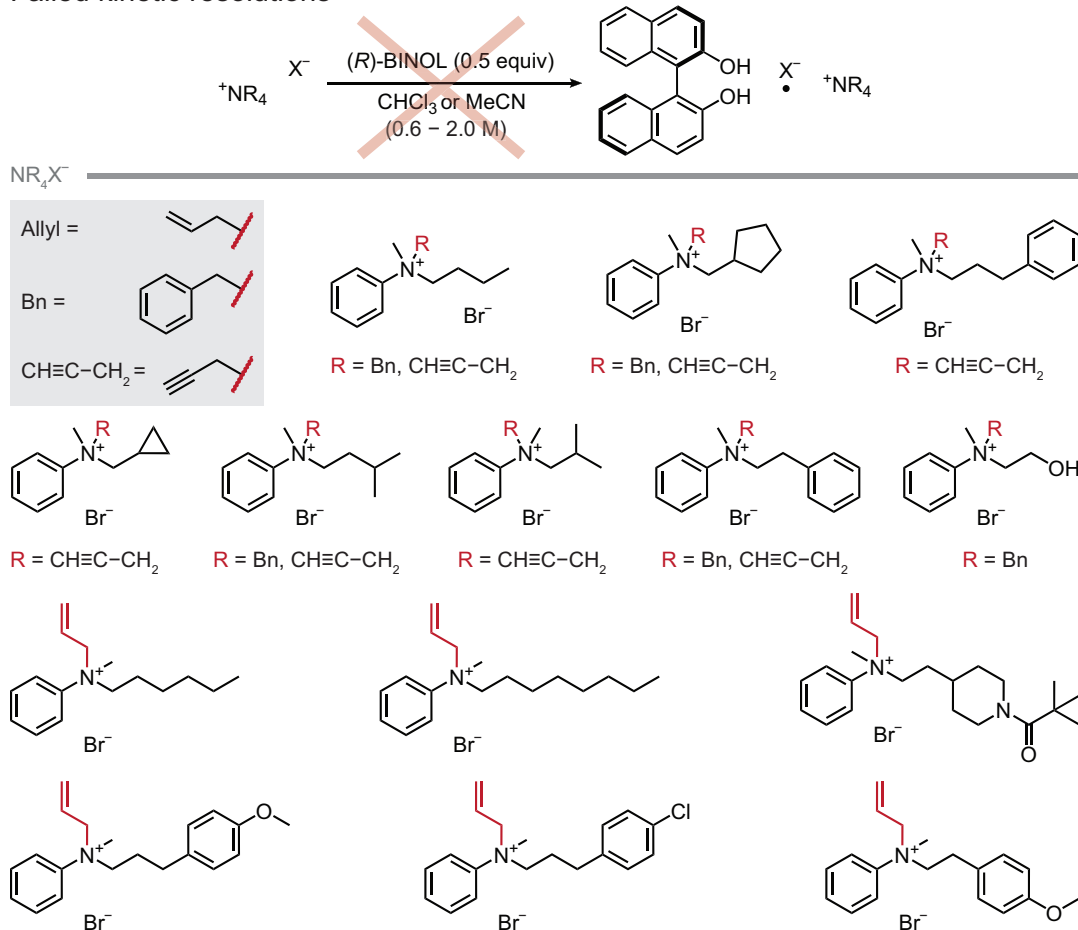


Figure 4.6: Failed kinetic complexation of racemic ammonium salts with (*R*)-BINOL.

4.4. CHIRAL AMMONIUM SALT TERNARY COMPLEXES WITH BINOL

By dissolving the library of *N*-methyl tertiary anilines in MeCN or CHCl₃ (0.6–2.0 M), depending on the conditions conducive to ternary complex formation, adding the appropriate alkylating agent and subjecting them to heating at 50 °C with vigorous stirring (1500 rpm), a diverse range of enantioselectively synthesised ammonium salts were successfully produced (see Figure 4.8. and Figure 4.9.). ¹H NMR spectroscopy and SCXRD studies were performed to confirm the formation of a 1:1 (ammonium salt:enantiopure BINOL) complex and the handedness of the *N*-stereocentre formed. Optical rotation measurements confirmed enantioenrichment of the ammonium cations; the extent of which was either measured by ¹H NMR spectroscopy employing (*R*, Λ)-BINPHAT to form diastereomers in solution or by chiral HPLC.

Enantioselective synthesis

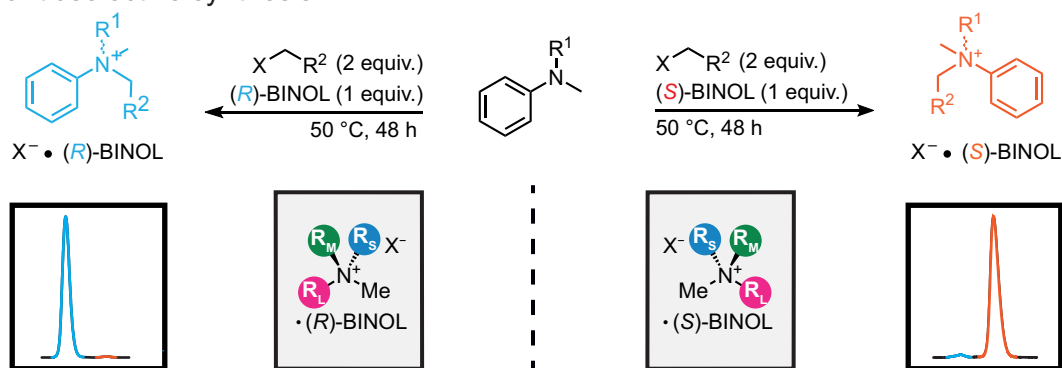


Figure 4.7: Scheme for the enantioselective synthesis of ammonium cations and model used to predict their selectivity.

4.4. CHIRAL AMMONIUM SALT TERNARY COMPLEXES WITH BINOL

(*R*)-BINOL complexes

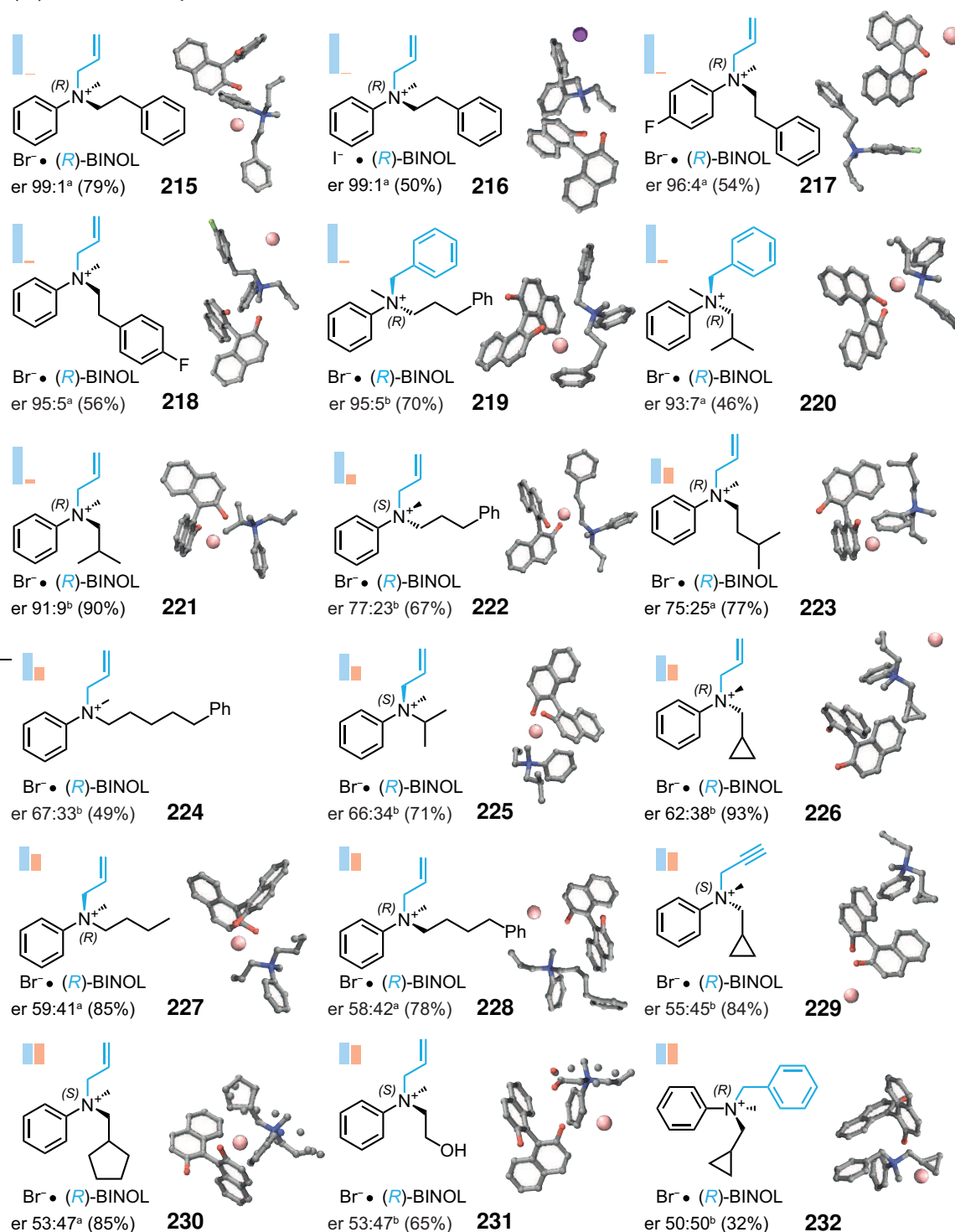


Figure 4.8: Library of chiral ammonium salts with stereogenic nitrogen complexed with (*R*)-BINOL. er measured by ¹H NMR spectroscopy using (*R*, Δ)-BINPHAT (^b) or by chiral HPLC (^a).

4.4. CHIRAL AMMONIUM SALT TERNARY COMPLEXES WITH BINOL

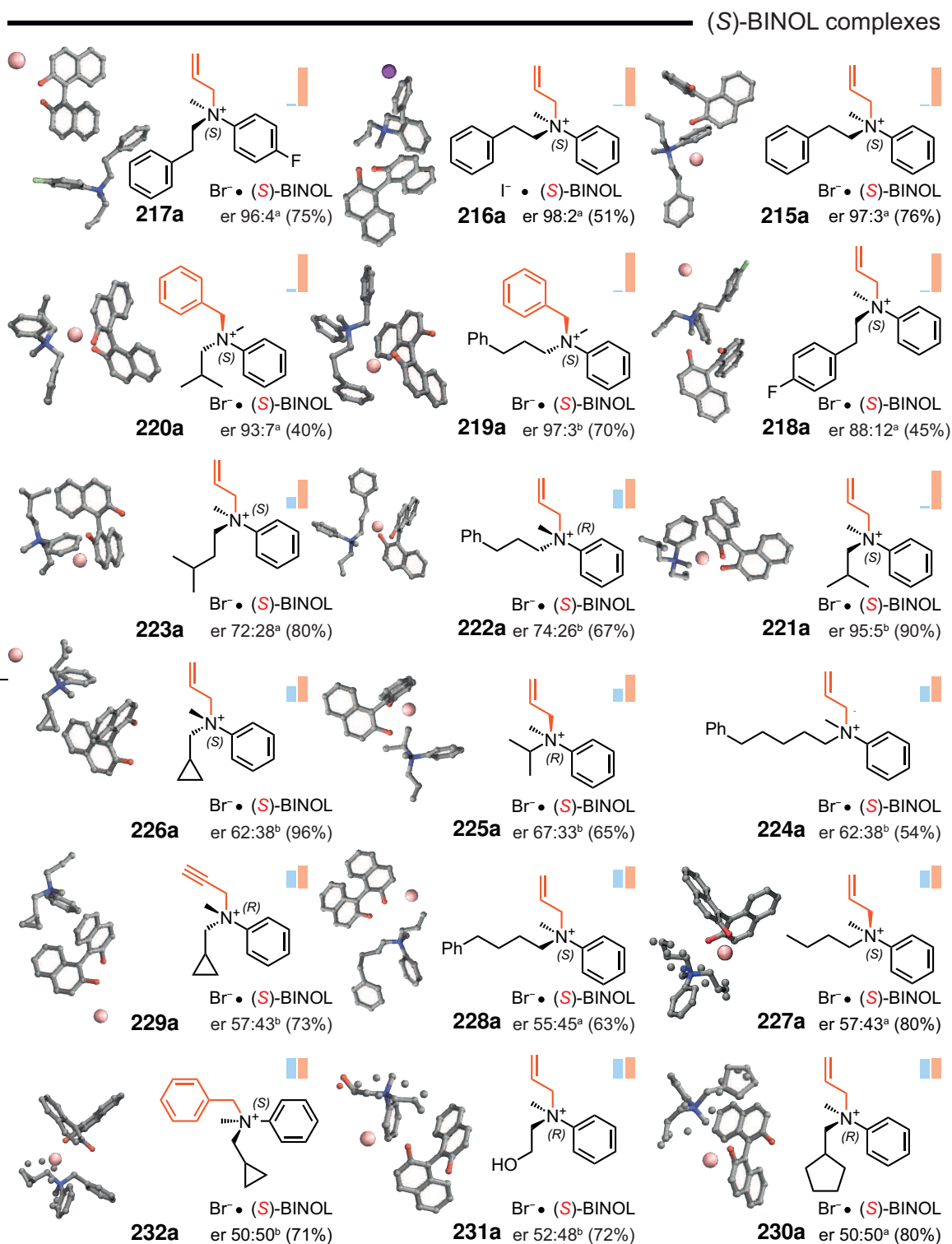


Figure 4.9: Library of chiral ammonium salts with stereogenic nitrogen complexed with (S)-BINOL. er measured by ^1H NMR spectroscopy using (*R*, Δ)-BINPHAT (^b) or by chiral HPLC (^a).

4.4. CHIRAL AMMONIUM SALT TERNARY COMPLEXES WITH BINOL

Empirical observations can be made on the library of enantioselectively synthesised complexes to give general rules towards the origins of stereoselectivity. As steric bulk is moved closer to the stereocentre there is an increase in the enantioenrichment of the anilinium cation (see Figure 4.10.). This can be seen when substituting isobutyl (**221**) for isovaleryl (**223**) and moving from allyl (**221** and **222**) to benzyl (**220** and **219**) substituents. Across the series of substituted alkyl chains with a phenyl terminus (**224**, **228**, **222** and **215**) the shorter the CH₂ alkyl spacer between the *N*-stereocentre and the phenyl group the greater the enantioenrichment of the anilinium cation.

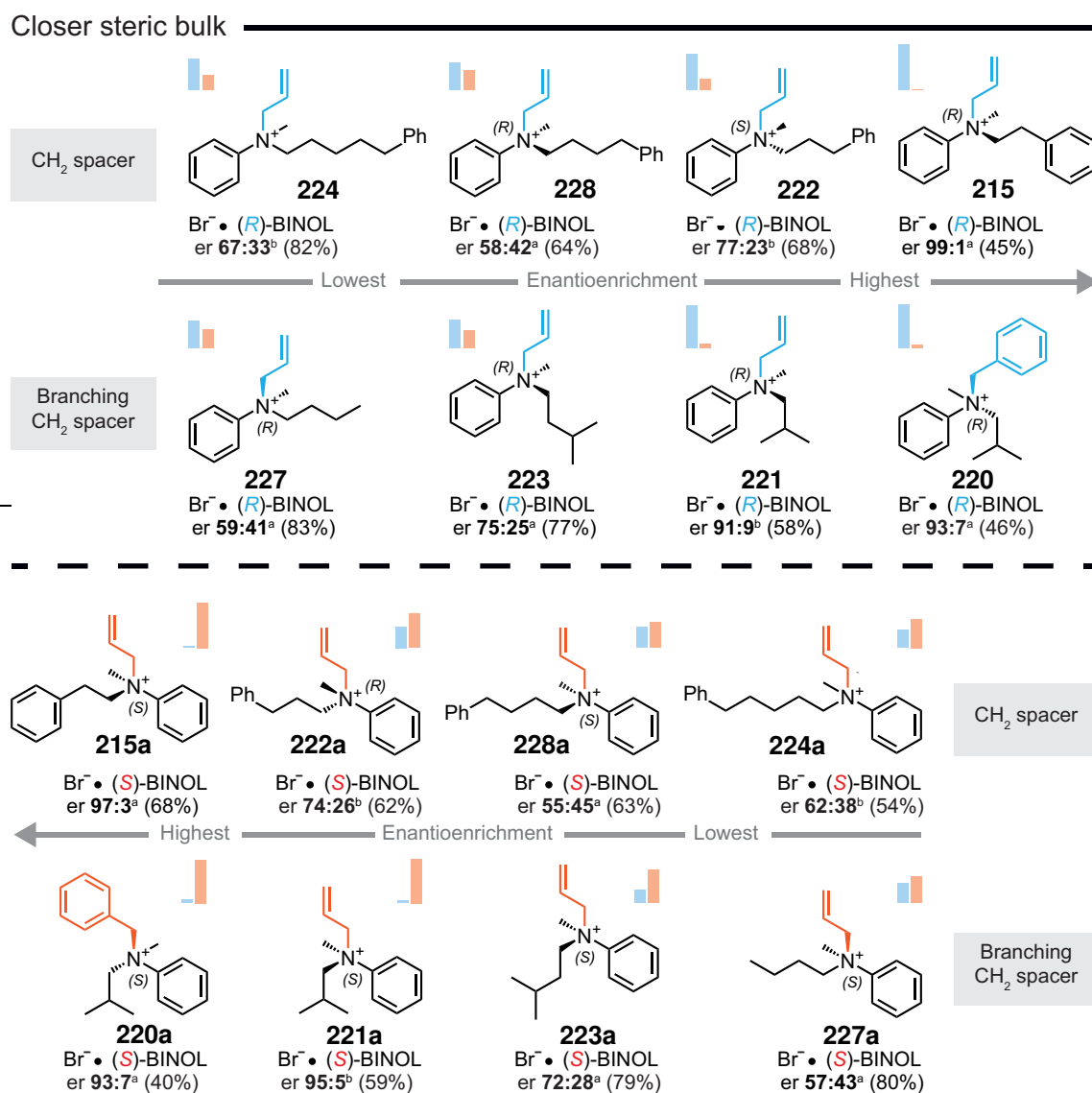


Figure 4.10: Increasing enantioenrichment as steric bulk is moved closer to the *N*-stereocentre.

4.4. CHIRAL AMMONIUM SALT TERNARY COMPLEXES WITH BINOL

As functionality with the ability to interact by either hydrogen or halogen bonding is functionalised onto a substituent group, enantioselectivity is reduced. For the hydroxy containing anilinium salt **231** the recognition results in a nearly racemic mixture of cations in the ternary complex. Moreover, when **215** is substituted with fluorine on either the aniline (**217**) or phenylacetyl ring (**218**) the enantioenrichment drops from nearly enantiopure to an ee of 92% and 88% respectively. Changing the counterion from Br⁻ to I⁻ for **215** to **216** doesn't significantly affect the stereoselectivity but the yield is greater for the bromide counterion. The CIAT works well for unfunctionalised anilinium salts with steric bulk located close to the stereocentre, but the selectivity is not well tolerated beyond this.

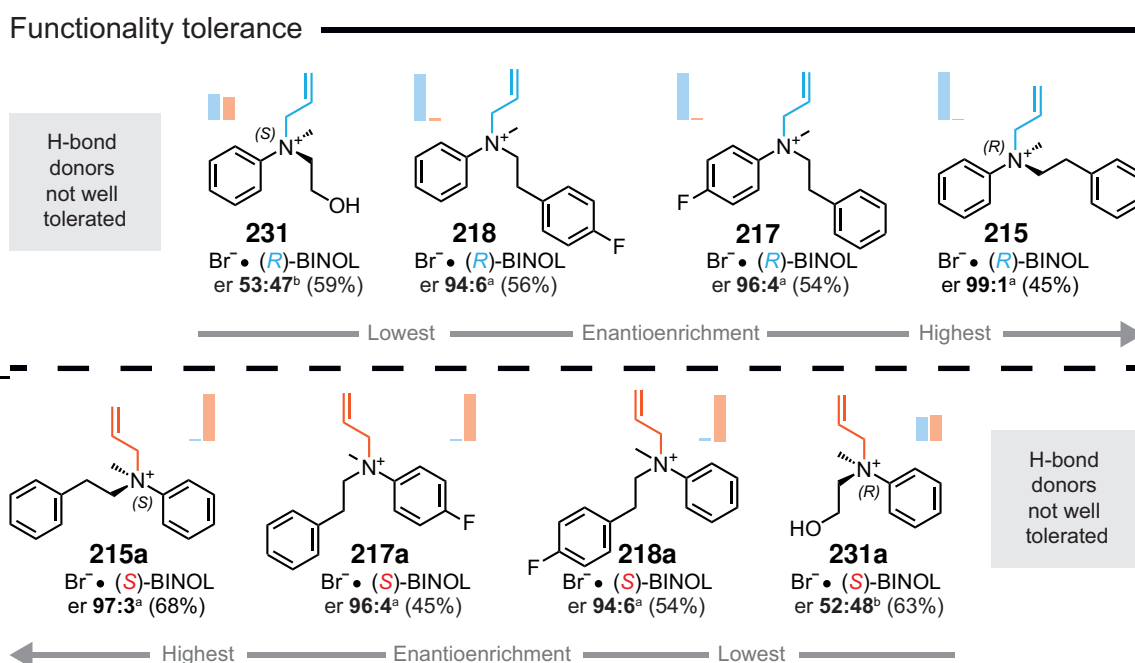


Figure 4.11: Functionality tolerance and varied enantioenrichment.

4.4. CHIRAL AMMONIUM SALT TERNARY COMPLEXES WITH BINOL

The observation that functionality is not well tolerated is further supported when attempting to perform the CIAT methodology with functionalised alkylating agents, such as substituted benzyl bromides. When employing tertiary aniline cores, recognised as allyl-derived anilinium salts, with substituted benzyl bromides and other functionalised alkylating agents, no recognition is observed across the set. (see Figure 4.12.).

Failed complexations

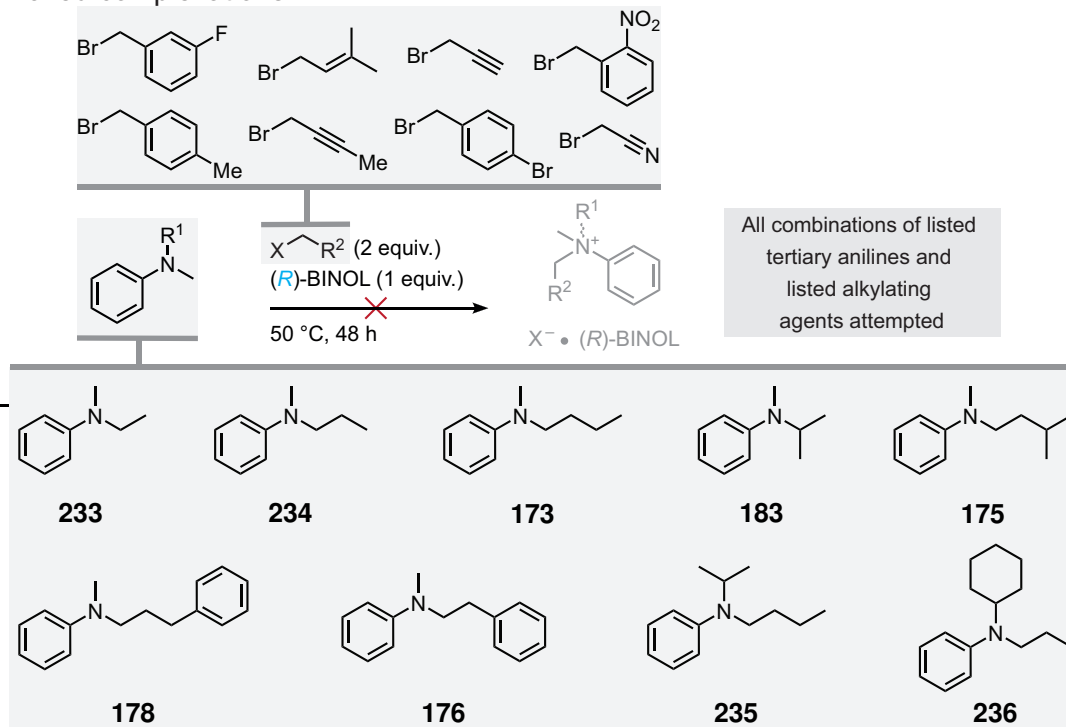


Figure 4.12: Low functionality tolerance on alkylating agents.

4.4. CHIRAL AMMONIUM SALT TERNARY COMPLEXES WITH BINOL

Almost all the complexes fit Walsh's established selectivity model. When using (*R*)-BINOL, if the aniline ring is placed on the left and methyl group on the right in a plane, then the larger remaining group will come out of the plane and the smaller will go backwards into the plane. The selectivity is flipped for (*S*)-BINOL complexes. The only complex not to obey this rule is **237**, where the larger hydrocinnamyl functionality appears to go back into the plane, with the allyl group coming forwards, in the (*R*)-BINOL complex. Interestingly this is the only complex, from which the PXRD reflections do not match the predicted SCXRD reflections (see Figure 4.13.). However, generally, the sense of the anilinium salt can be predicted and thus the appropriate enantioenriched BINOL selected if a desired enantiomer is to be produced.

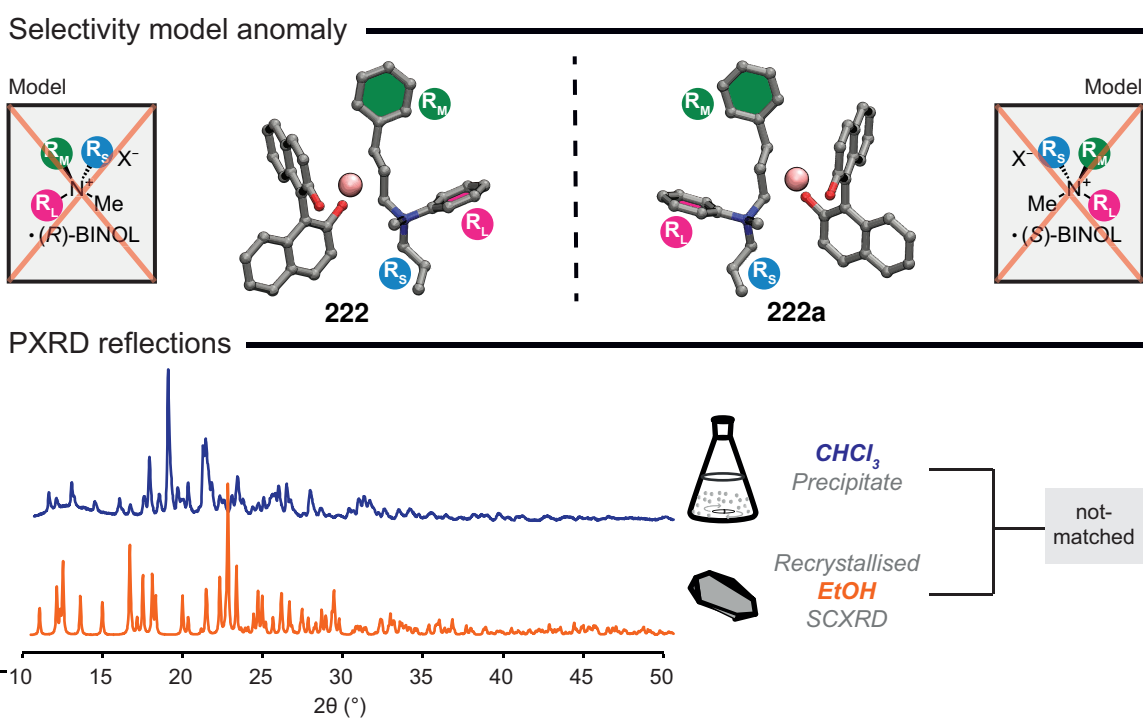


Figure 4.13: **222** and **222a** don't fit the stereoselectivity model for ammonium cation synthesis. The difference in solid morphology between precipitated material and recrystallised material is shown by the PXRD trace of precipitated **222** from CHCl_3 and a predicted SCXRD PXRD trace from the crystal structure of **222** recrystallised from EtOH.

4.5 Enantioenrichment determination

Accurate determination of enantiomeric purity is essential to validate the true enantioselectivity of a given technique. Measurement of the optical rotation of the ammonium cation complexes with BINOL was performed, however quantifying enantioenrichment solely from $[\alpha]_D$ measurements is unreliable due to the absence of an enantiopure standard and the recognised non-linear relationship between $[\alpha]_D$ and enantiomeric excess (ee).²¹⁹ Therefore, alternative techniques were necessary to accurately determine enantiomeric ratios (er).

The enantioenrichment of the synthesised ammonium salt complexes was analysed utilising two techniques, namely chiral High Performance Liquid Chromatography (HPLC) and chiral shift Nuclear Magnetic Resonance (NMR) spectroscopy. Chiral HPLC was initially employed on the set of racemic ammonium salts to identify salts responsive to enantiodifferentiation. Subsequently, NMR spectroscopy with *R*, Δ -BINPHAT was applied to those salts that could not be effectively resolved by chiral HPLC, to quantify their enantioenrichment.

4.5.1 Chiral HPLC

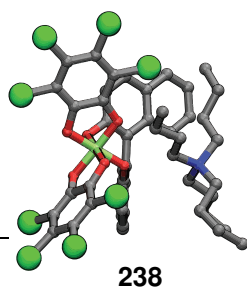
It is widely recognised that the use of chiral chromatography, such as HPLC or GC employing a chiral stationary phase, is a reliable method for measuring enantioenrichment.²²⁰ However, there is no previously reported methodology to effectively separate enantiomeric pairs of quaternary ammonium salts, whose chirality originates from a sole *N*-stereogenic element using HPLC.

Walsh experienced difficulty in developing conditions for ammonium salt enantiodifferentiation by chiral HPLC due to the absence of polar functional groups on the ammonium cations resulting in minimal interactions with the chiral stationary phase in chromatographic columns, leading to a lack of effective separation.³⁷ Several columns with different chiral stationary phases were trialled in both normal and reverse phase, but unfortunately, no effective HPLC separation method was identified to resolve enantiomers for either bromide or hexafluorophosphate quaternary ammonium salts.

Here an *Astec CHIROBIOTIC V* Chiral HPLC column (25 cm × 4.6 mm) was tested for enantiomeric separation of quaternary ammonium cations by chiral HPLC. Fortunately, the application of a vancomycin stationary phase loaded onto the column demonstrated effectiveness for this enantiodiscrimination. Presumably, the abundance of functional groups in the vancomycin stationary phase offers numerous interaction sites for effective binding with the ammonium cations, contributing to successful enantiodiscrimination. Optimisation of the methodology revealed the most effective conditions for the separation of enantiomers:

- Buffered methanol solution (MeOH:AcOH:TEA, 100:0.02:0.01) as a mobile phase (reverse phase).
- UV-detection set at 210 nm.
- Analyses conducted in an isocratic and isothermal (4 °C) manner.
- Flow rates were adjusted between 0.1–0.5 mL min⁻¹ as appropriate.

4.5.2 BINPHAT



Bis-(tetrachlorobenzenediolato)-mono-([1,1']-binaphthalenyl-2,2'-diolato)-phosphate(V) (BINPHAT, **238**) is a chiral shift reagent which can be used to split diastereomeric signals using ¹H NMR spectroscopy. From these ¹H NMR spectra the ratio of enantiomers can be determined using quantitative integration. BINPHAT has been shown to split signals for both ammonium cations with α stereogenic carbon centres²²¹ and stereogenic nitrogen centres.^{2,37}

BINPHAT was synthesised under stringent inert and dry conditions from tetrachlorocatechol in an 84% yield employing the use of enantiopure (*R*)-BINOL. ¹H NMR spectra of the product displayed only the presence of a single diastereomer. However, if water is present during the reaction or excess tris(dimethylamino)phosphine

is not sufficiently removed *in vacuo* hydrolysis of this reagent can occur, introducing an impurity that proves challenging to eliminate without degrading the BINPHAT. This increases the difficulty of the synthesis and limits the scaling up of the methodology. Attempts to recrystallise BINPHAT from acetone revealed the structure of this impurity to be a phosphorsaeure-(2-hydroxy-phenylester)-NH₂Me₂ (SCXRD quality crystals grown for **239**, see appendix), which can also be detected by a distinctive peak at –82.96 ppm in ³¹P NMR spectra.

While BINPHAT proves effective for making accurate enantiomeric ratio measurements via chiral shift ¹H NMR experiments, its synthesis introduces challenges in terms of time-consumption and potential pitfalls. Notably, the difficulty to eliminating impurities is an inherent issue. Given the necessity to measure a multitude of enantiomeric ratios in this project, chiral HPLC was the preferred method for determining the enantioselectivity.

4.6 Chiral ternary complexes crystallographic analysis

In all crystal structures a C₂¹ (9) continuous hydrogen bonded network forms between anionic counterion and hydroxyl functionalities on the enantiopure BINOL. The enantioenrichment observed for the ammonium cation can be attributed to the nature of the BINOL-counterion hydrogen bonded network formed and how well the cation is positioned in each isostructure. A COMPACK similarity matrix was generated from the SCXRD crystal structures of ternary complexes **215–232** to reveal that discrete isostructures form dependent on the identity of the ammonium species present. Across the 3 isostructures identified (labelled A, B and C), isostructure A displays poor enantioselectivity, isostructure B has poor to modest selectivity and in isostructure C there is exceptional stereoselectivity (see Figure 4.14.).

Notably the isostructures identified in Chapter 2 persist into the chiral recognition architectures. For instance, isostructure A is equivalent to isostructure VI and isostructure B is congruent with isostructure II. Isostructure C has a unique packing arrangement.

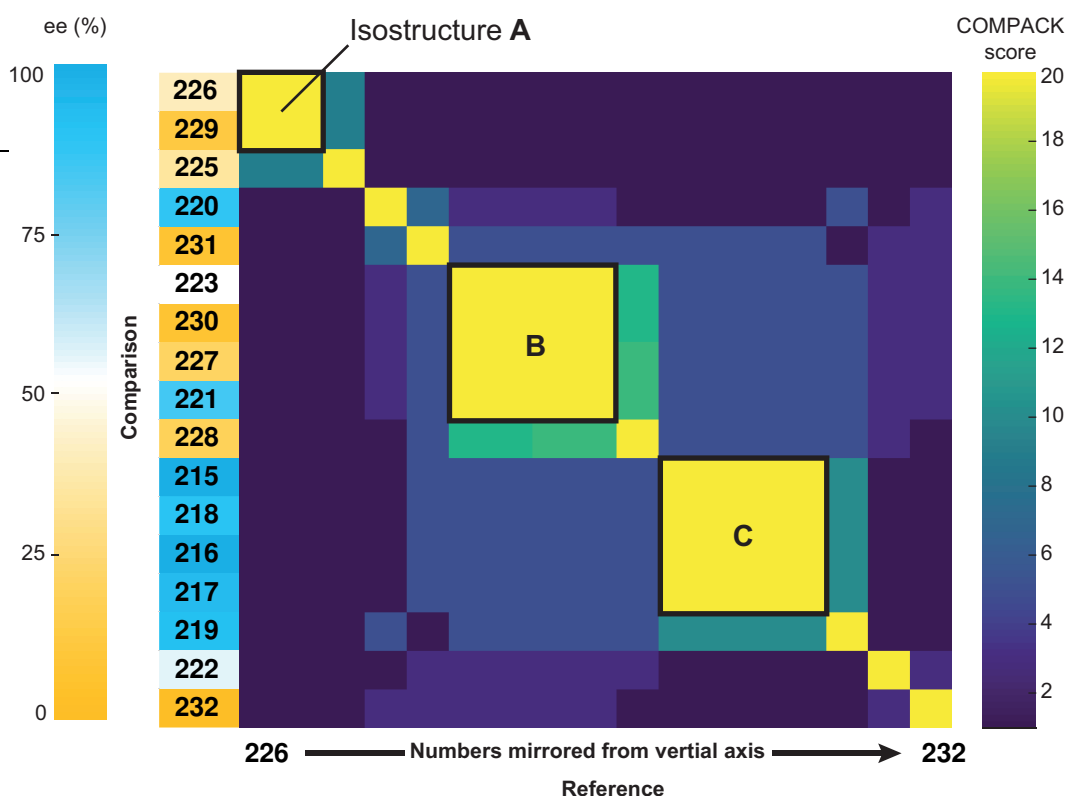
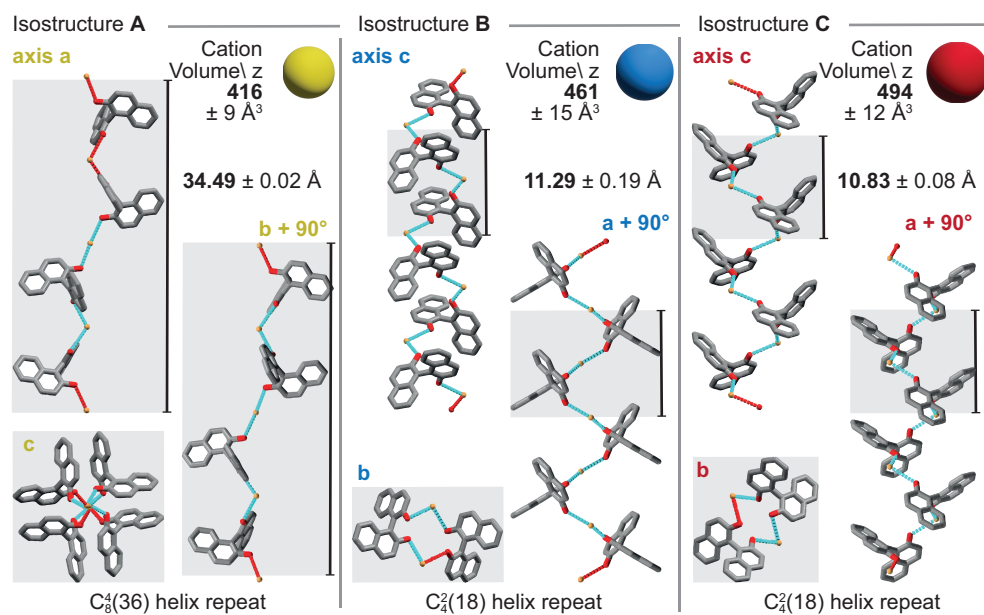


Figure 4.14: Chiral ammonium salt and (*R*)-BINOL ternary complexes COMPACK matrix.

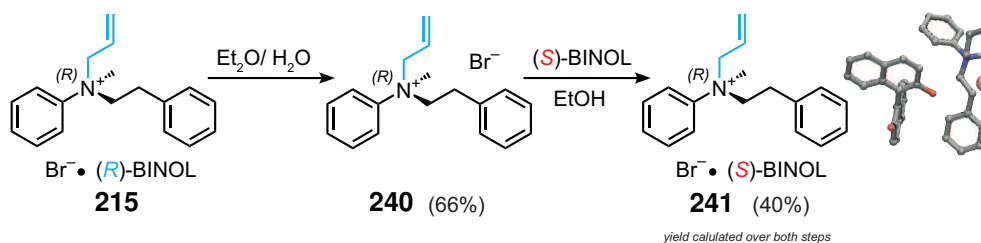
The isostructure with the shortest helix repeat length is isostructure C (10.83 ± 0.08 Å) consisting of 2 enantiopure BINOL units and 2 counterions per repeating C_4^2 (18) hydrogen bonded unit. Interestingly, as the helix repeat length increases the observed enantioselectivity decreases (isostructure B; 11.29 ± 0.09 Å, C_4^2 (18) unit, isostructure A; 34.49 ± 0.02 Å, C_8^4 (36) unit). The inverse is seen for the apparent cation volume. This value is calculated by deleting the cation from the crystal structure and subsequently measuring the void volume in the unit cell and dividing by Z; this value should represent the maximum theoretical volume available for the ammonium cation to occupy in this isostructure. The larger this value, the higher the enantioenrichment observed across the distinct isostructures (isostructure A; 416 ± 9 Å³, isostructure B; 461 ± 15 Å³, isostructure C; 494 ± 12 Å³). The construction of the continuous hydrogen bonded chain is fundamental to the enantioselectivity through providing a diastereoselective interaction pocket to encapsulate the cation.

Chiral quaternary cation isostructures

Figure 4.15: Chiral ammonium salt and (*R*)-BINOL isostructures.

To identify the variations between the diastereomeric complexes, both diastereomeric variations were prepared for the *N*-allyl, *N*-methyl, *N*-phenylacetyl anilinium bromide salt complexed with enantiopure BINOL. First, the complex resulting from the CIAT with (*R*)-BINOL was isolated to produce the matched pair **215**: (*R*)-ammonium cation·(*R*)-BINOL. To a separate batch of the matched pair (**215**), the (*R*)-BINOL was removed through extraction ($\text{Et}_2\text{O}/\text{H}_2\text{O}$) to yield **240**. To ensure there was no loss of enantiopurity when extracting the cation from the complex, the enantioenrichment of the ammonium salt measured by chiral HPLC: er 99:1 (*R*:*S*). The recovered enantioenriched ammonium salt was then complexed with (*S*)-BINOL yielding the unfavoured diastereomer (*R*)-**240**·(*S*)-BINOL (the mismatched pair, **241**, see Figure 4.16.).

Mismatched diastereomer synthesis

Figure 4.16: The isolation of **240** from **215** and subsequent recomplexation with (*S*)-BINOL to yield the mismatched diastereomer **241**.

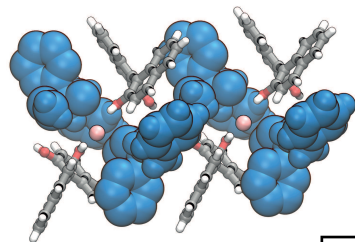
The matched pair (**215**) exhibits a more efficient packing of ternary complex (packing density $\rho = 1.352 \text{ g cm}^{-3}$) compared with its mismatched equivalent ($\rho = 1.340 \text{ g cm}^{-3}$) and has a much shorter C_4^2 (18) helix repeat length (**215**; 10.7729(7) Å, **241**; 12.2868(3) Å). Additionally, the matched pair has slightly less apparent cation volume (477.65 Å^3) than the mismatched pair (484.82 Å^3); both equate to approximately 63% of the unit cell volume and are not significantly different. In the matched pair there are C–H \cdots Br contacts from α -carbon protons on the phenylacetyl substituent ($d_{\alpha\text{phenylacetyl(C-H}\cdots\text{Br)}} = 2.985 \text{ Å}$, $d_{\text{(C}\cdots\text{Br)}} = 3.950(4) \text{ Å}$) and an *ortho*-anilinium proton ($d_{\text{ortho(C-H}\cdots\text{Br)}} = 3.040 \text{ Å}$, $d_{\text{(C}\cdots\text{Br)}} = 3.976(4) \text{ Å}$) to the same bromide counterion and it contains C–H \cdots O interactions from an α -carbon proton on the methyl group to a BINOL hydroxy functionality ($d_{\alpha\text{methyl(C-H}\cdots\text{O)}} = 2.544 \text{ Å}$, $d_{\text{(C}\cdots\text{O)}} = 2.952(6) \text{ Å}$) and an α -carbon proton from the allyl substituent to a different BINOL unit ($d_{\alpha\text{allyl(C-H}\cdots\text{O)}} = 2.521 \text{ Å}$, $d_{\text{(C}\cdots\text{O)}} = 3.506(6) \text{ Å}$). In the mismatched pair there are C–H \cdots Br contacts from α -carbon protons on each available substituent group contacting two separate anions ($d_{\alpha\text{phenylacetyl(C-H}\cdots\text{Br)}} = 2.923 \text{ Å}$, $d_{\text{(C}\cdots\text{Br)}} = 3.802(4) \text{ Å}$, $d_{\alpha\text{methyl(C-H}\cdots\text{Br)}} = 3.032 \text{ Å}$, $d_{\text{(C}\cdots\text{Br)}} = 3.935(4) \text{ Å}$, $d_{\alpha\text{allyl(C-H}\cdots\text{Br)}} = 2.919 \text{ Å}$, $d_{\text{(C}\cdots\text{Br)}} = 3.654(5) \text{ Å}$); the methyl and phenylacetyl contacting the same bromide counterion and the allyl another. The β -carbon protons on the phenylacetyl group also form a contact with the same bromide anion as the allyl α -carbon protons ($d_{\beta\text{phenylacetyl(C-H}\cdots\text{Br)}} = 2.994 \text{ Å}$, $d_{\text{(C}\cdots\text{Br)}} = 3.961(4) \text{ Å}$). The contacts were globally represented on a 3D surface and portrayed as Hirshfeld fingerprint plots,²²² to aid in interpreting the comparative significance of all contacts present in both crystal structures. Here, trends in contacts within the crystal are illustrated, with the most distinct differences between the matched and mismatched structures being the presence of more appreciable C–H \cdots Br contacts in the mismatched pair. Density functional theory was employed to calculate the relative stabilities of the two diastereomers (more information in experimental section).* These calculations reveal that the matched pair is $11.07 \text{ kJ mol}^{-1}$ more stable than the mismatched diastereomer, owing this to the variety of contacts and distribution of crystal phenomena. This finding aligns with the initially proposed mechanism, substantiating the CIAT operates using an error-checking process to favour formation of the more lower energy diastereomer (see Figure 4.17.).

4.6. CHIRAL TERNARY COMPLEXES CRYSTALLOGRAPHIC ANALYSIS

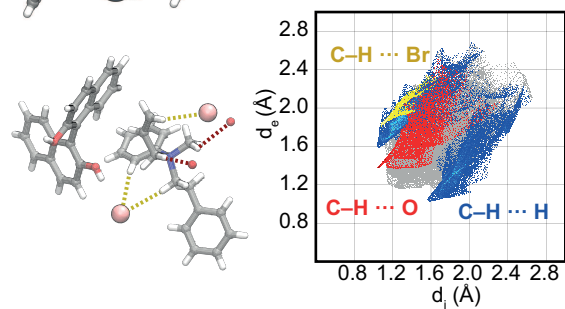
Mismatched diastereomer comparison

Matched Pair

(*R*)-cation • (*R*)-BINOL

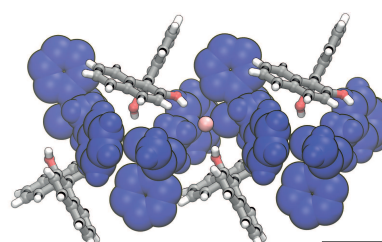


215

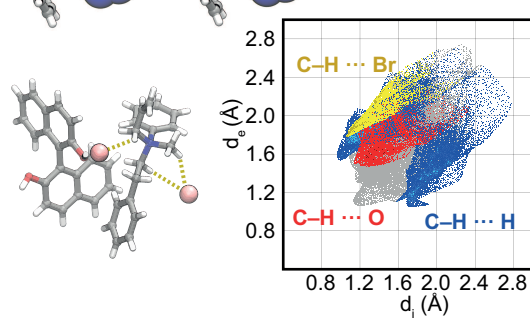


Mismatched Pair

(*R*)-cation • (*S*)-BINOL



241



Thermodynamic chiral selection

$$\Delta E_{(\text{matched vs. mismatched})} = -11.07 \text{ kJ mol}^{-1}$$

Figure 4.17: Global cation contacts to crystal structure in **215** versus **241**. The $wR2$ for the crystal structure of **215** was 0.0701 (all data) and 0.0482 (all data) for **241**.

* DFT calculations performed by Emma. H. Wolpert under the supervision of Kim. E. Jelfs.

4.7 Crystallisation variables

The enantioselectivity observed in the synthesis of ammonium cations through ternary complex formation with BINOL was noted to be concentration dependent. At higher concentrations the saturation of the liquid phase limits dissolution of the mismatched pair, limiting the racemisation of the unwanted enantiomer, therefore reducing the efficacy of the error-checking process required for the thermodynamic chiral selection. Consequently, the mismatched diastereomer becomes more prone to incorporation into the isolated solid. Additionally, the stirring rate was found to exert a notable influence, likely affecting dissolution in a similar manner. Both these anecdotal observations warranted further investigation.

4.7.1 Enantioenrichment

Initial conc. vs ee studies

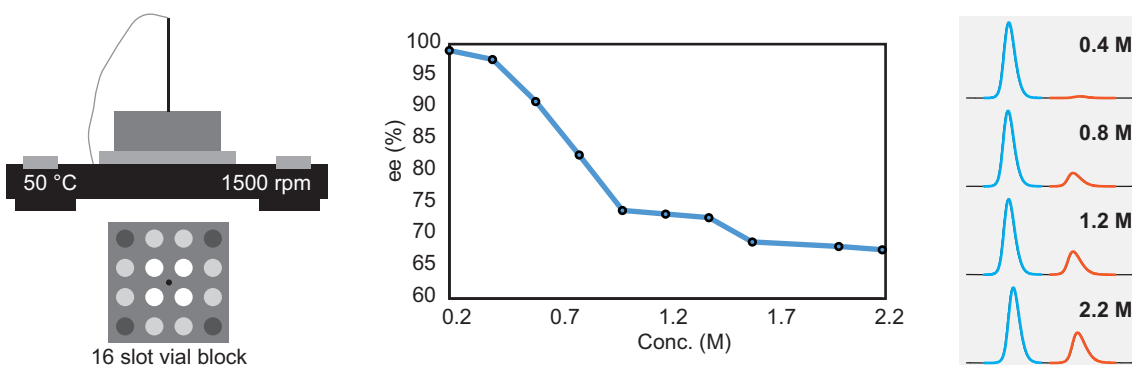


Figure 4.18: Concentration versus enantiomeric excess. Reactions done on a 16 slot heating block and ee measured by chiral HPLC.

To investigate the relationship between concentration and enantioenrichment the synthesis of **215** using the CIAT methodology was performed, and a concentration versus ee plot constructed. This synthesis utilised a 4x4 heating block on an *IKA* Plate RCT Digital Round-Top Stirring Hot Plate, Aluminium; 115 V, accommodating 10 mL vials loaded with 10 x 3 mm magnetic stirrer bars, the temperature was set to 50 °C and the stirring rate was set at 1500 rpm. Whilst this approach was valuable in illustrating the sigmoidal relationship between concentration and enantioenrichment of the ammonium salt (lower concentrations have greater enantioenrichment, see Figure 4.18.), the

4.7. CRYSTALLISATION VARIABLES

study suffered poor reproducibility. This was hypothesised to be due to the stochastic nature of crystallisation and nucleation processes introducing inherent variability, rendering the plot less consistent and therefore less reliable for analysis.²²³ Furthermore, the 16 position heating block provided 3 distinct stirring environments (i. the 4 outer corners. ii. the innermost 4 positions. iii. the remaining positions), adding another potentially confounding variable to the experiment.

To better control the stirring environment and accurately control the temperature a *Technobis* Crystal16 Benchtop Crystallisation System was used to perform the CIAT of **215**. This setup was employed to investigate four different concentrations, each subjected to four distinct stirring rates, with all conditions repeated in triplicate to ensure reliability in the experimental setup (see Figure 4.19.).

Conc. and stirring rate vs ee studies

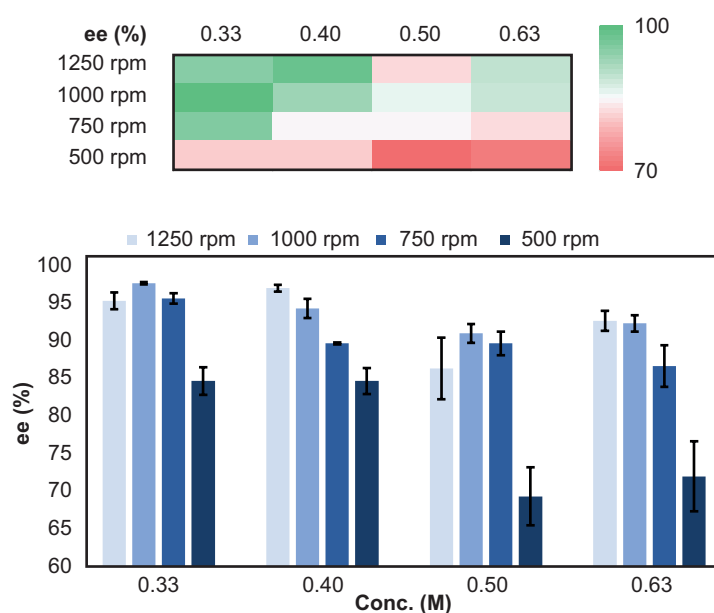


Figure 4.19: Concentration versus enantiomeric excess. Error bars are the standard deviation of the data. Reactions performed using a Crystal16 and ee measured by chiral HPLC.

The data depicts a clear trend: higher concentrations resulted in lower enantioenrichment, aligning with the notion that the solubility of the mismatched pair is lower at higher concentrations. Additionally, a higher stirring rate led to enhanced enantioenrichment. These consistent findings emphasise the significant role of dissolution of

the mismatched pair in influencing the observed selectivity. Despite precise control of both stirring rate and temperature the data still reveal an appreciable level of variance. This underscores the intrinsic stochastic nature of crystallisation and nucleation, which continues to pose a challenge in achieving consistent and reproducible results (especially at intermediate concentrations and stirring rates - either ends of the ranges display consistently significantly different results).

4.7.2 Precipitation

Stirring rate and precipitation

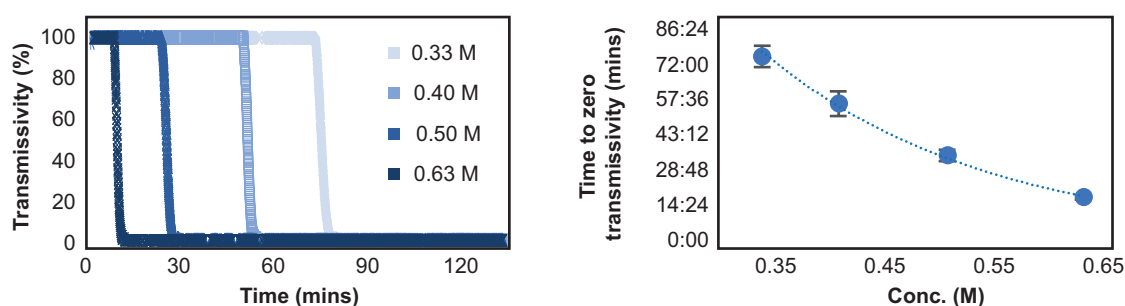


Figure 4.20: Stirring versus transmissivity. Error bars are the standard deviation of the data. Reactions performed using a Crystal16 and transmissivity measured *in situ*.

An additional observation was made by monitoring the transmissivity through the reaction vial during the experiments detailed in Figure 4.19. The data revealed a relationship between concentration and the characteristics of the system: as the concentration of the system increased, the onset of the decrease in transmissivity, and the eventual time at which the vial becomes opaque occurred more rapidly. This suggests a direct correlation between concentration and the speed at which solid precipitate appears within the reaction mixture. Furthermore, this relationship was independent of the stirring rate. By plotting all data points at a given concentration, irrespective of the stirring rate, against the time at which the transmissivity of the reaction vessel dropped to zero an exponential relationship was clearly evident (see Figure 4.20.). Moreover, the calculated regression coefficient of this curve confirmed the strength of relationship ($R^2 = 0.9972$).

The observation that stirring rate markedly impacts enantioenrichment while not

4.7. CRYSTALLISATION VARIABLES

affecting the precipitation rate, implies that stirring rate primarily influences the dissolution of the mismatched pair rather than nucleation of a potential precipitate. This deduction illustrates the critical role preferential dissolution plays in determining the stereoselectivity of the process. Additionally, the data is consistent with a dual role for concentration in the process. On one hand, it affects the rate of nucleation for the desired precipitate, while on the other, it influences the dissolution of the mismatched pair. This dual effect underscores the nuanced interplay between concentration, nucleation and dissolution in determining the overall enantioselectivity of the process.

* I would like to thank Aurora Cruz Cabeza and Fragkoulis Theodosiou for helping me set up and for allowing me to use their *Technobis* Crystal16 Benchtop Crystallisation System.

4.8. DERIVATISATION OF CHIRAL AMMONIUM CATIONS

The reactions attempted for the functionalisation of **215** are outlined in Figure 4.21. Unfortunately, the majority of these reactions proved unsuccessful due to the labile nature of the allyl group attached to the charged N⁺ centre. This group underwent dealkylation when attempting reactions with both PF₆⁻ and Br⁻ salts. Additionally, limited reactivity was attributed to the electron-withdrawing nature of the ammonium group, further complicating the desired derivatisation. As such many of the reactions attempted yielded either the starting material or the corresponding tertiary aniline (**176**) as the major product.

4.8.1 Further chiral ammonium salts application trials

Fluorescence

Tang *et al.* reported in 2022 a previously overlooked facet of aliphatic quaternary ammonium cations. Traditionally well-known as luminescence quenchers and deemed non-emissive, these compounds were found to possess intrinsic fluorescence and phosphorescence properties. Not only this, but their emissive characteristics could be finely tuned by manipulating factors such as excitation wavelength, alkyl chain length and counter-ion type.²²⁴ This posed the interesting question as to whether the enantioenrichment of newly synthesised ammonium salts could be leveraged to tailor fluorescence and phosphorescence behaviours of quaternary ammonium salts, in the context of developing novel organic electronics.^{225,226}

240, its enantiomer (**240a**) and the corresponding racemate (**192**) exhibit a striking light blue fluorescence when dissolved in either ethanol, methanol or water and irradiated with UV-light (from a UV torch). This fluorescence phenomenon extends to the iodide variants of these salts as well, however it was weaker when a PF₆⁻ counterion was present. In preliminary investigations, it was observed that the emission intensity displayed a concentration-dependent behaviour in aqueous solutions. Utilising an excitation wavelength of 345 nm with an excitation bandwidth of 5 nm, and measuring emission within the range of 350 to 600 nm, it was apparent that racemic and enantiopure samples exhibited differing emission intensities, with the racemate being more fluorescent than the enantiopure samples. However due to the emission spectrum of samples containing a combination of equal amounts of *R* and *S* enantiomer not align-

ing with the emission intensity of the racemic sample (this could be due to variations in enantiopurity of the *R* and *S* samples or small errors/inaccuracies in sample concentration etc.) and scepticism when presenting results to other academics prevalent in the field, a re-evaluation of the fluorescence study will be done in the interest of time, aiming for further clarification in future work.

Perovskites

Phenylethyl ammonium cations (of which **240** is one), along with other phenylalkyl ammonium functionalities, have been identified for their ability to stabilise perovskite surfaces, through suppressing iodide ion migration.^{227,228} This characteristic makes them invaluable moieties in the discovery of novel perovskite materials. Notably, in 2018, Ye *et al.* demonstrated that ammonium cations can also serve as building blocks in the creation of organic ferroelectrics, namely a family of metal-free organic perovskites adopting the distinctive ABX₃ three-dimensional structure.²²⁹ It was hypothesised that chiral ammonium compounds could find application in a similar context by modifying Ye's methodology. However, attempts to grow crystals with the characteristic ABX₃ structure using Ye's approach were unsuccessful, likely due to the necessity of dicationic molecules with dual ammonium functionalities in Ye's protocol.

4.9 Resolution of substituted BINOLs

BINOL, represents a prominent archetype of axially chiral molecules and was initially synthesised as a racemic mixture in 1873 by von Richter.²³⁰ Since the development of resolution methods and enantioselective syntheses of the molecular scaffold, BINOLs have emerged as highly prominent ligands in enantioselective synthetic reactions.²³¹ BINOLs have also been employed to imbue chirality within mechanically interlocked molecular structures, thus facilitating the creation of supramolecules such as chiral catenanes and rotaxanes.²³² Due to their prevalence across a diverse range of chemistries, precise control of the atropisomeric form of the molecule and its derivatives is crucial for the development of new methodologies across various fields within the chemical sciences.

4.9. RESOLUTION OF SUBSTITUTED BINOLS

To test if chiral ammonium salts were suitable for the resolution of substituted BINOLs, a range of racemic BINOLs were synthesised by aerobic oxidative coupling of the prerequisite functionalised naphthols using a CuCl_2 catalyst (see Figure 4.22.).²³³ This methodology proved effective for the synthesis of **243–246** but did not well-tolerate carboxylic acid or aldehyde functionalities substituted onto the naphthol starting materials.

Oxidative coupling of naphthols

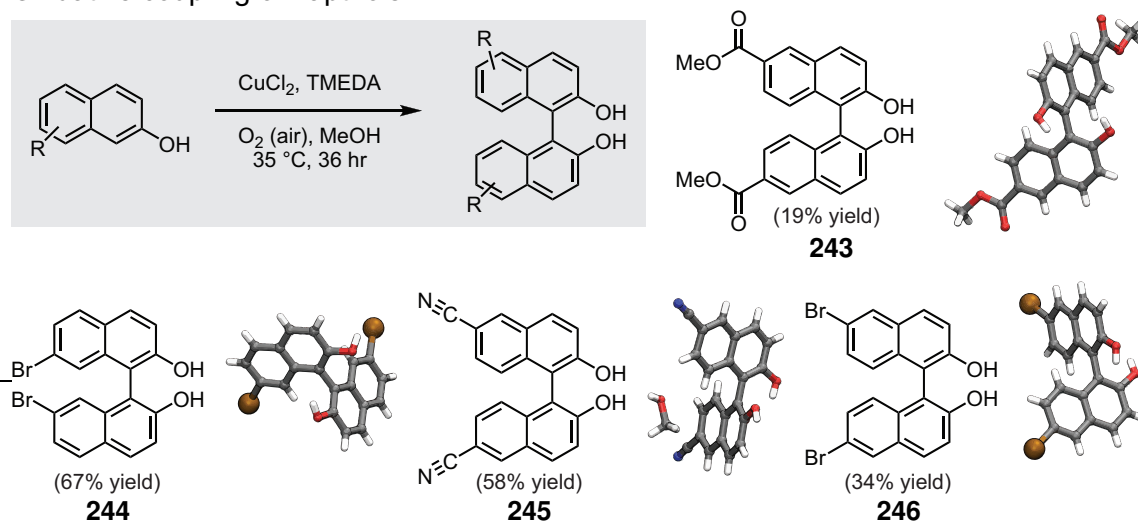


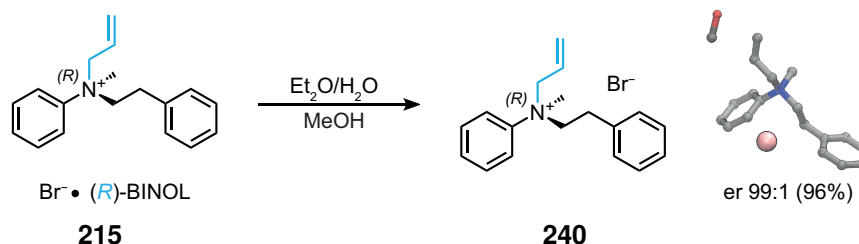
Figure 4.22: Oxidative coupling of naphthols to make functionalised *rac*-BINOLs.

Subsequently, the series of substituted *rac*-BINOL derivatives were systematically examined for ternary complexation with the most highly enantioenriched ammonium salts, aiming to investigate the potential resolution of this set of axial moieties through crystallisation. In this methodology, half an equivalent of a given enriched ammonium salt, liberated from its respective ternary complex with (*R*)-BINOL, was dissolved in either EtOH or CHCl_3 alongside one equivalent of the appropriate substituted *rac*-BINOL. The resulting solution was allowed to evaporate, testing for potential single crystal formations. This methodology enabled a comprehensive exploration of diverse ammonium salt and substituted *rac*-BINOL combinations.

Unfortunately the outcomes of these experiments proved largely unproductive, as numerous combinations failed to yield ternary complexes. Many of the combinations in fact returned single crystals of either the ammonium salt or the substituted BINOL functionality devoid of any inclusion crystals. Despite these challenges, a sin-

gular combination exhibited promise for effecting the resolution of a substituted *rac*-BINOL, utilising an enantioenriched ammonium salt from the library. The successful combination of **240** and **246** culminated in the formation of **247**, a ternary complex accompanied by a CHCl₃ solvate molecule. Encouraged by this observation, this particular combination was prioritised for the kinetic resolution of **246** in CHCl₃ (see Figure 4.23.).

Liberation of enriched ammonium salt



Resolution of substituted *rac*-BINOL

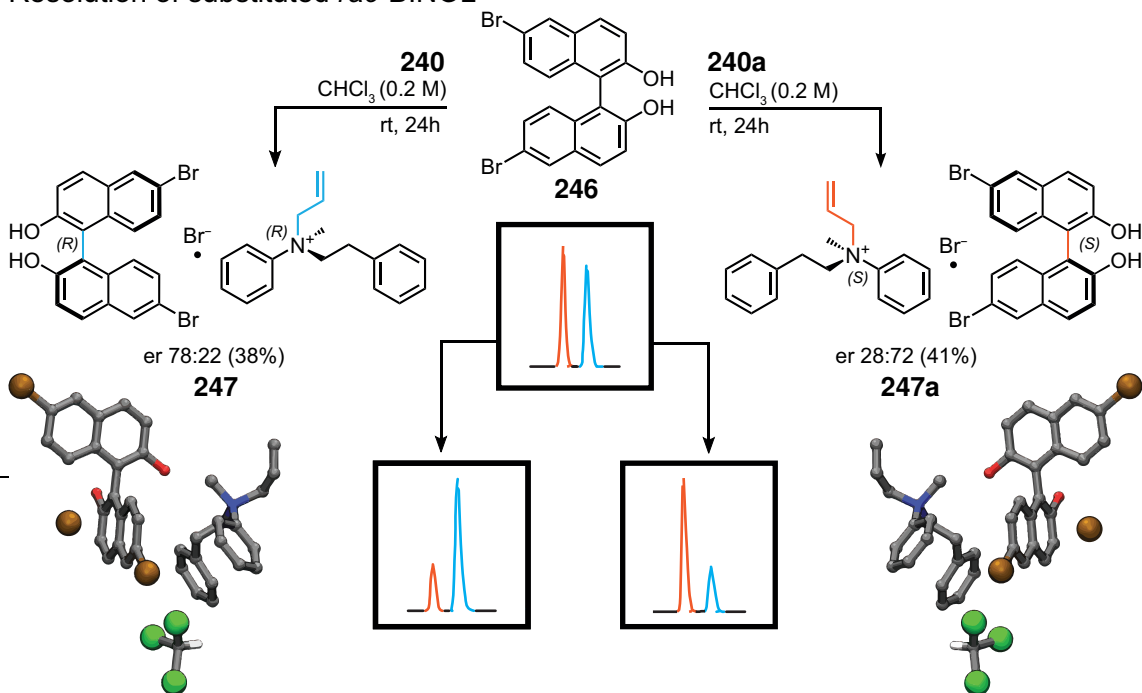


Figure 4.23: Resolution of **246** through complexation with **240**.

240 and **240a** proved effective in the kinetic resolution of **246** to yield **247** and **247a** respectively. The 6,6'-dibromo-1,1'-bi-2-naphthol molecules were resolved in the same direction as the ammonium salts (i.e. an *(R)*-ammonium salt would preferentially form a ternary complex with an *(R)*-6,6'-dibromo-BINOL and *visa versa*), in modest yield and enantioselectivity.

4.10 Chapter 4 summary

In summary, a comprehensive investigation has been performed, resulting in the enantioselective synthesis of both enantiomers of various ammonium salts through ternary complexation with enantiopure BINOL. The key synthetic requirements for achieving this synthesis have been elucidated, accenting the necessity of positioning steric bulk in close proximity to the stereocentre and the importance of minimising functionality on substituent groups. Furthermore, isostructural networks comprising BINOL and counterion have been identified, showcasing their role in facilitating varied levels of enantiodifferentiation. The thermodynamic parameters governing the preference for a specific enantiomer have been examined, revealing that diastereomeric interactions between the ammonium salt and enantiopure BINOL favour the matched pair, leading to its precipitation from the reaction mixture. Importantly, these enantiomeric enrichments are contingent upon both stirring rate and concentration. Additionally, the most enantioenriched of these salts has demonstrated utility in directing the stereochemistry of a substituted atropisomeric scaffold.

Chapter 5

Solid state enantioselectivity of ternary complexes

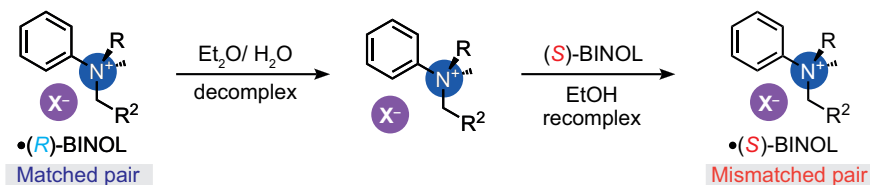
By merging a BINOL mediated recognition phenomenon with conditions that allow the nitrogen centre to racemise, it is possible to enantioselectively synthesise a range of ammonium cations. The enantioselectivity of this methodology can be rationalised with an empirical model denoting which ammonium cation will be synthesised via the CIAT (see Figure 4.7.). Moreover, the process can be reviewed to establish the key requirements for enhancing enantioselectivity; loading steric bulk closer to the stereocentre and removing functionality from substituent groups (see Figure 4.10 and Figure 4.11.). Because the system is known to operate under thermodynamic control, this section aims to more rigorously interrogate the solid-state endpoint of the CIAT to provide a thorough thermodynamic explanation for the observed enantioselectivity.

For a fully integrated model to be established then all diastereomeric interactions should be considered. Firstly, a library of matched diastereomers were synthesised and subsequently transformed into mismatched diastereomers by complexation with the opposite sense BINOL (as seen in Figure 4.16.). The energy difference of these crystal structures was calculated *in silico*. Secondly, matched diastereomers with disorder in the crystal structure were used to calculate the difference in energy between most (matched enantiomer) and least (mismatched enantiomer) occupied sites within the same bromide·BINOL network. Finally, isostructural networks of bromide·BINOL were identified between ordered and non-disordered cations. Ordered ammonium salts that were identified to crystallise in the same isostructure as disordered cations could then be modelled to reveal the theoretical position and geometry of the higher energy diastereomer and thus inform on the important interactions in enantioselectivity.

* I would like to thank and acknowledge the computational work done by Emma. H. Wolpert and Kim. E. Jelfs to calculate the energy differences by DFT throughout this chapter.

5.1 Mismatched diastereomeric pairs

Mismatched diastereomer synthesis



Change in isostructure

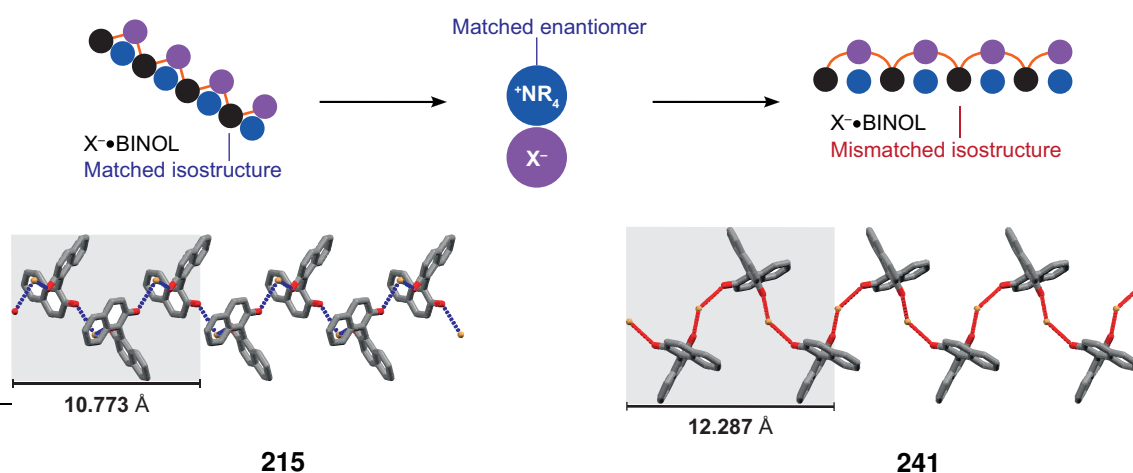


Figure 5.1: The isolation of enriched ammonium salts from (*R*)-BINOL ternary complexes and subsequent recomplexation with (*S*)-BINOL to yield mismatched diastereomers. Graphical representation of matched versus mismatched isostructures and how they vary for the more enantioenriched complexes.

In order to identify the differences inherent to the diastereomeric complexes accessible through the CIAT methodology, both diastereomeric variants were prepared for **241–255** (see Figure 5.1.). Initially, the ternary complexes resulting from the CIAT with (*R*)-BINOL were isolated to produce the matched diastereomers (ammonium salt·(*R*)-BINOL). Subsequently, to a batch of matched diastereomers, (*R*)-BINOL was removed through partition between diethyl ether (Et_2O) and water (H_2O). The resulting enantioenriched ammonium salts were then re-complexed with (*S*)-BINOL, to produce the unfavoured diastereomers (the mismatched pairs). SCXRD quality single crystals suitable for analysis were grown from ethanol (EtOH) for each complex. Examination of the crystal structures reveals that the construction of the C_2^1 (9) continuous hydrogen-bonded network made between bromide counterion and BINOL undergoes transformation between matched and mismatched diastereomeric pairs, particularly evident

when complexes exhibit greater enantioselectivity. However, for complexes with lower enantioenrichment levels (**226**, **229**, and **230**, characterised by homocyclopropyl and homocyclopentyl substituents), the packing isostructure remains consistent across the diastereomeric structures (**252**, **254**, and **255**) (see Figure 5.2.).

5.1. MISMATCHED DIASTEREOMERIC PAIRS

Mismatched diastereomer scope

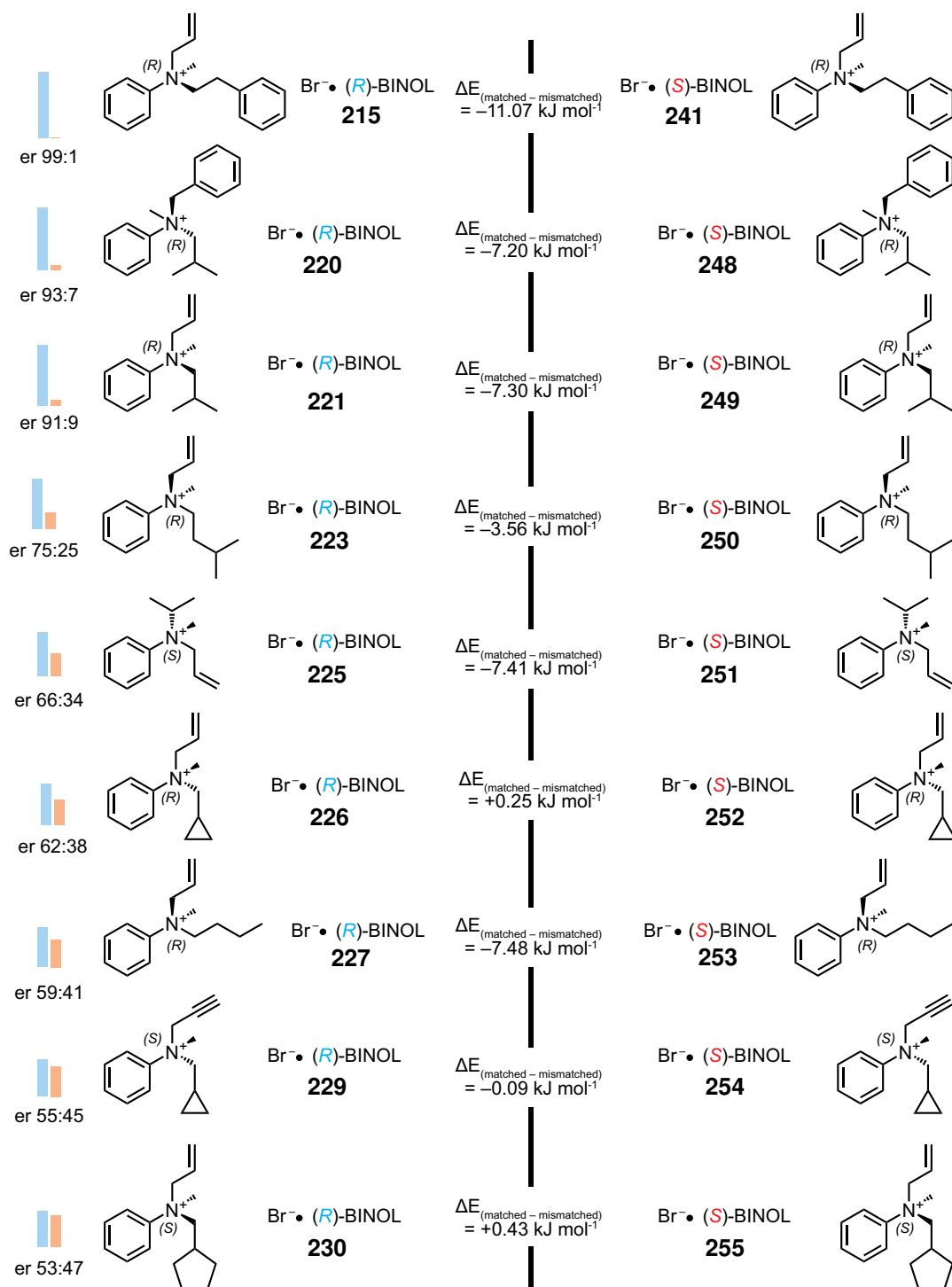


Figure 5.2: Matched versus mismatched ternary complexes and DFT calculated energy difference^a between the SCXRD structures.

^a DFT calculations performed by Emma. H. Wolpert under the supervision of Kim. E. Jelfs.

Mismatched diastereomer SCXRD

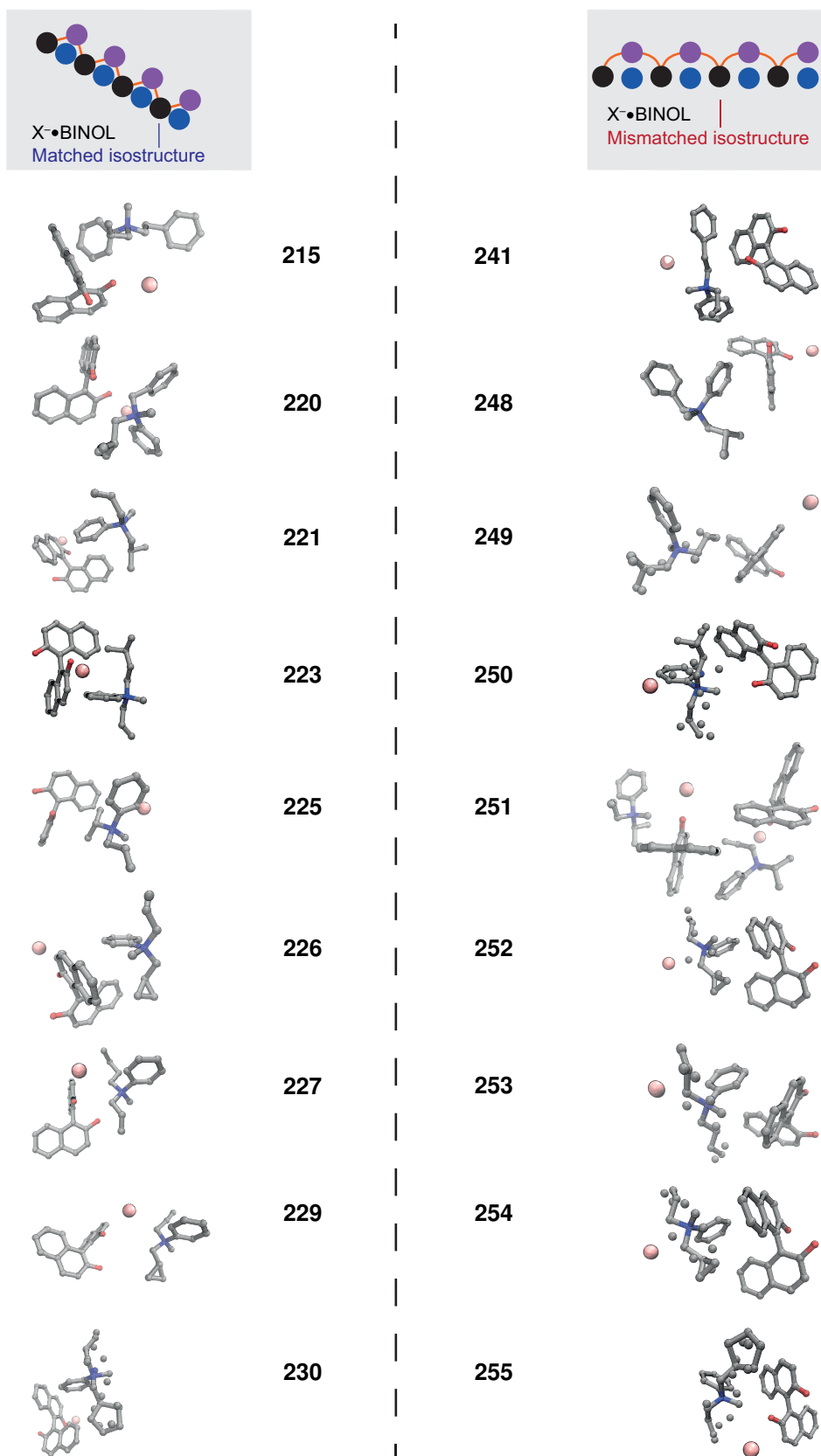


Figure 5.3: Matched versus mismatched ternary complexes SCXRD structure renders.

5.1. MISMATCHED DIASTEREOMERIC PAIRS

While it was anticipated for the matched pair to exhibit more efficient packing than the mismatched pair (as seen in Figure 4.17.), this expectation is not universally upheld across the set, as revealed by the observed variations (see Table 5.1.). Moreover, no substantial disparity in the available volume for the cation is observed between the matched and mismatched pairs, and this characteristic does not correlate with the measured enantioenrichment. Consequently, it is evident that more intricate thermodynamic parameters underlie the observed selectivity, surpassing simplistic considerations of isostructural selection for optimal crystal packing efficiency.

Table 5.1: Crystal packing parameters for diastereomer complex pairs. *Available cation volume value is calculated by deleting the cation from the crystal structure and subsequently measuring the void volume in the unit cell and dividing by Z.

Diastereomeric pair	_exptl_crystal_density_diffn	Available cation volume (\AA^3)*
215	1.352	477.6
241	1.340	484.8
220	1.336	488.9
248	1.274	530.8
221	1.303	445.3
249	1.324	433.6
223	1.287	472.5
250	1.281	476.4
225	1.345	410.5
251	1.329	414.2
226	1.362	409.8
252	1.348	416.9
227	1.292	451.9
253	1.334	428.2
229	1.343	420.2
254	1.350	412.9
230	1.309	475.1
255	1.301	480.3

For each mismatched diastereomeric pair density functional theory (DFT) calculations were used to compare the relative energies of the structures. The SCXRD crystal structure of each complex were fully optimised,^{194–198} in two steps. First the atomic positions were relaxed with fixed cell parameters, and then both the cell parameters and the atomic positions were relaxed. The cut-off for the plane wave grid used in these calculations differed depending on the cation (see experimental section). After the optimisation process, the ammonium cations were extracted from the optimised structure, and a single point energy calculation was performed on the resulting cation. To determine the energetics of the BINOL and counterion network in each of the structures, the lattice energies from the optimisation were divided by the number of formula units in the structure, and the energy difference between that and the single point energy calculation of the ammonium cation were calculated. The differences in energy between the BINOL and counterion network formed between the diastereomeric pairs were then calculated by subtracting the energy of the matched BINOL and counterion network from that of the mismatched (see Figure 5.2.).

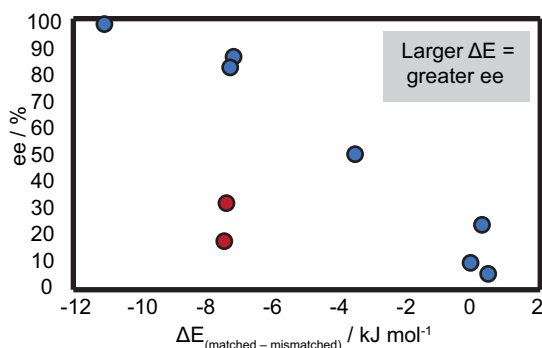


Figure 5.4: Diastereomer DFT calculated energy difference versus measured enantioselectivity.

Previously it has been reasoned that this must be due to the modulation of solubility of the mismatched pair with respect to the matched pair, thus influencing the error checking capacity of the CIAT (see Figure 4.17.). This would also explain the observation that enantioselectivity is dependent upon concentration; with higher concentrations destroying the enantioselectivity due to the mismatched pair becoming less soluble in the more saturated liquid phase.

The enantioselectivity of the isolated ammonium salt correlates (although with anomalies - red circles) with the DFT calculated energy difference of the matched and mismatched pair (see Figure 5.4.), hence revealing that this diastereomeric selectivity is necessary for providing the observed stereoselectivity.

5.2 Long range order

If the solubility of the mismatched pair with respect to the matched pair is the main factor determining the error checking capacity of the CIAT, then the mismatched diastereomer (**241**) should be present in the microcrystalline precipitate formed through the synthesis of **215** at higher concentrations (because at higher concentration there is decreased enantioenrichment). Powder X-ray diffraction (PXRD) experiments were performed on **215** synthesised at concentrations between 0.4–1.8 M. Despite the enantiomeric excess (ee) ranging from 99% to 35%, the PXRD patterns are identical suggesting that the long-range order in the microcrystalline precipitate is unchanged and that there is no entrainment of **241** into the precipitate of **215** at higher concentration. Hence, the energetic difference between the matched and mismatched diastereomers cannot be the only factor affecting the enantioenrichment; it is necessary but not sufficient.

PXRD at various conc. values

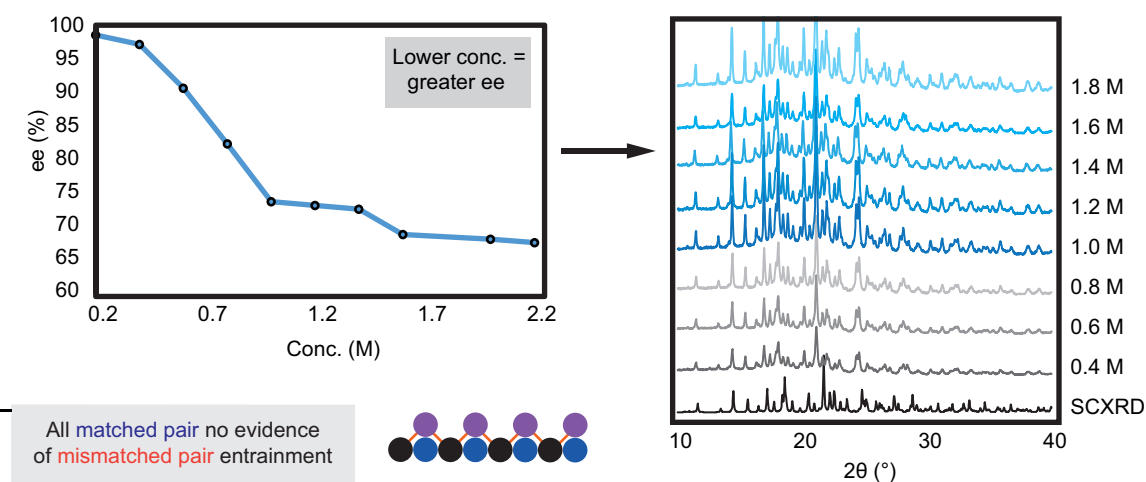


Figure 5.5: Concentration versus ee plot for **215** and PXRD traces at 0.2 M interval concentration values.

5.3 Disordered cations

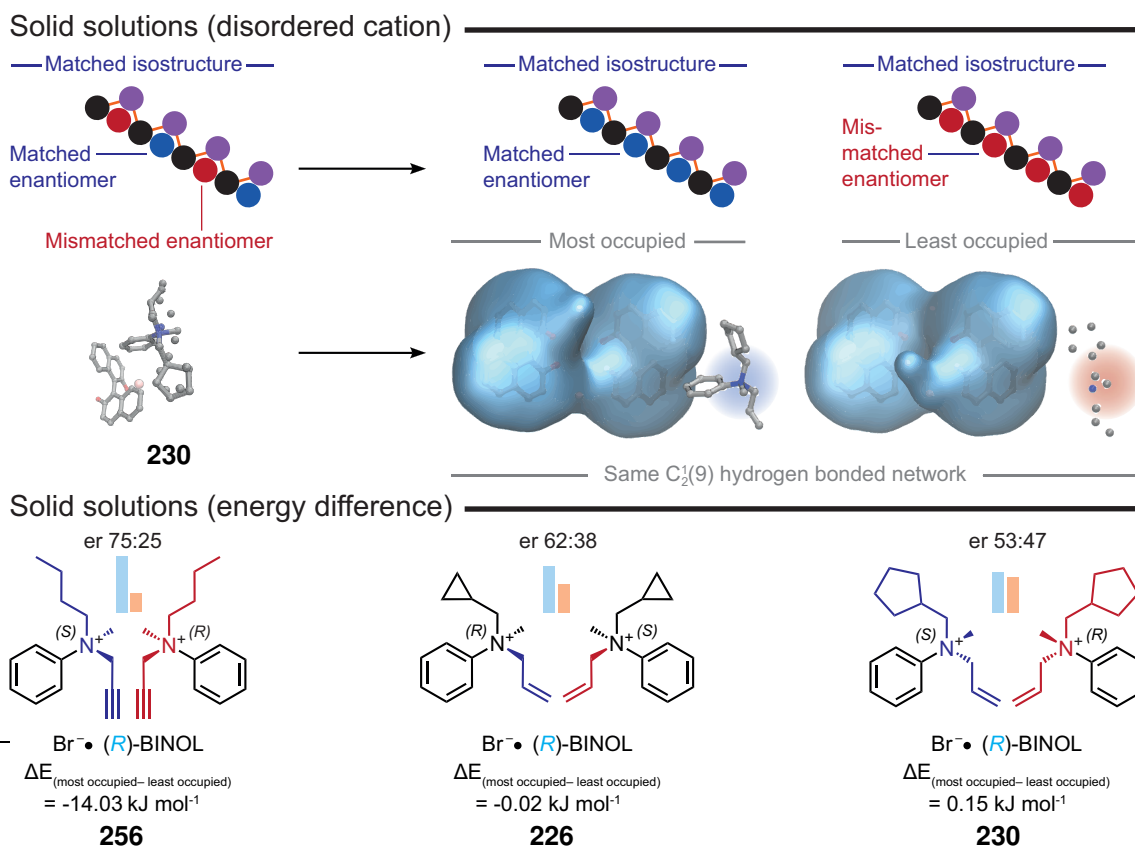


Figure 5.6: Solid solutions from SCXRD data.

To investigate the diastereomeric interactions between two mirror image cations existing as a solid solution in the same $C_2^1(9)$ (*R*)-BINOL·bromide isostructure, three crystal structures with disorder about the cation were identified (**256**, **226** and **230** - the disorder represents two enantiomers in the same isostructural superstructure) (see Figure 5.6.). Taking the most occupied sites as the matched cation and the least occupied sites as the mismatched cation, DFT calculations were performed to calculate the energy difference between the two enantiomers in the same (*R*)-BINOL·bromide isostructure. The greater the energy difference between the most and least occupied sites, the greater the enantiodiscrimination between the two cations, within the crystallographic solid solution of enantiomers. Furthermore, there is a greater energy difference between the disordered cations in the same isostructure for the lower selectivity complex **256** (er 75:25, -14.3 kJ mol⁻¹) than the highly enantioselective complex **215** (er 99:1, **215** – **241** = -11.1 kJ mol⁻¹) displays across mismatched diastereomeric

5.4. ISOSTRUCTURAL BASIS SET

pairs with different isostructures. Hence, the energy difference between enantiomeric cations in the same isostructure is likely more significant in the determination of enantioselectivity than the mismatched diastereomeric effect across different isostructures. However there is no direct way to compare the energy difference between the ammonium enantiomers in more enantioselective examples due to the fact that they do not crystallise as solid solutions of enantiomers, thus no disorder exists about the *N*-stereocentre in the crystal structure for these examples.

5.4 Isostructural basis set

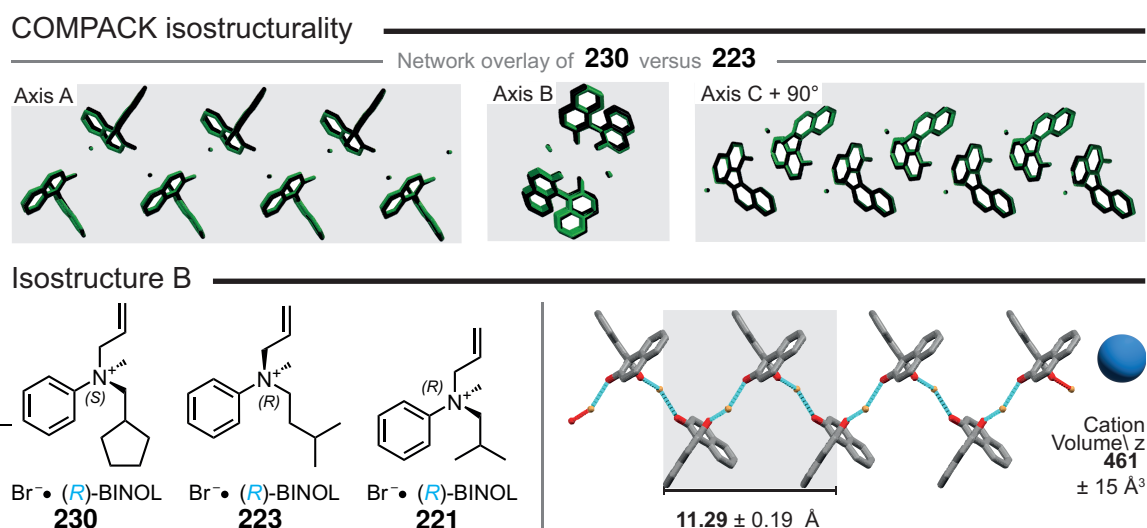


Figure 5.7: COMPACK analysis to determine isostructurality between solid solutions and non-solid solutions.

COMPACK analysis was performed across the set of ternary complexes to identify isostructural crystal structures of ammonium salts complexed with (*R*)-BINOL (see Figure 4.14.).¹⁹³ This study revealed **221** and **223** to form an analogous bromide·(*R*)-BINOL hydrogen bonded chains with **230** (20/20 similarity, 20% leniency on bond angle and bond length, see Figure 5.7.). **230** exists as a solid solution, where **221** and **223** are well defined as one enantiomer with no disorder about the ammonium cation in their SCXRD structures. Due to the isostructural nature of these crystal structures the cations in **221** and **223** occupy the same space as the most occupied cation from **230** within the crystallographic units. Therefore, **230** can be used to model disorder

onto **221** and **223** and thus provide a theoretic position and orientation for the opposite sense ammonium cation enantiomer for these crystal structures.

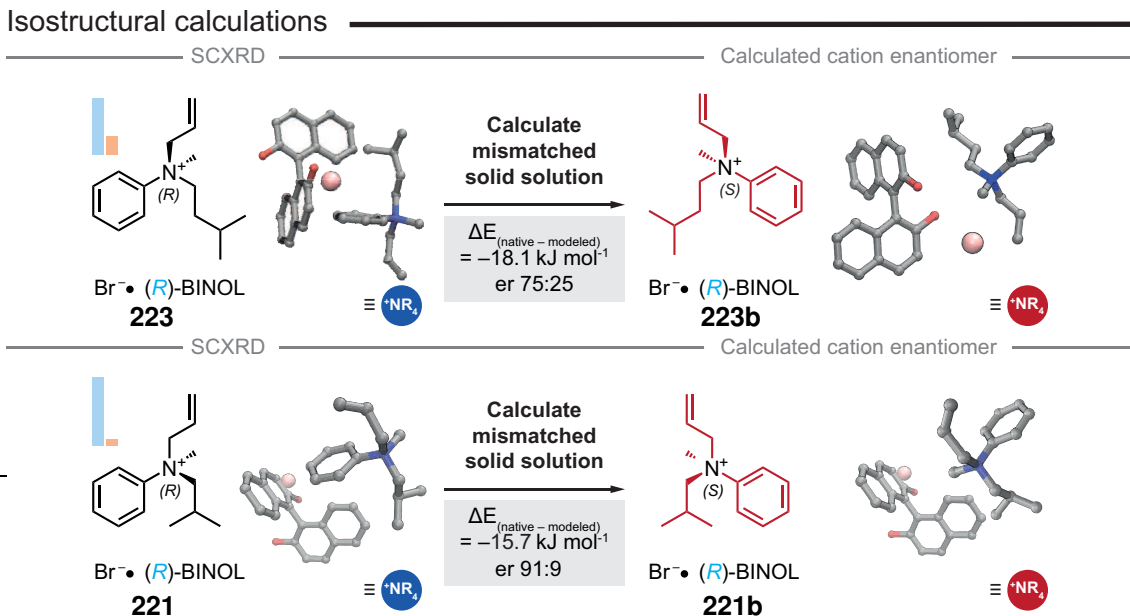


Figure 5.8: DFT calculated energy differences between the two cationic enantiomers in **221** and **223** using **230** as a basis set due to isostructurality in their C_2^1 (9) networks.

DFT calculations were used to compare the relative energies of the two cationic enantiomers of **221** and **223** in complex with (*R*)-BINOL, as theoretical solid solutions. Experimentally, only the (*R*)-ammonium enantiomer cation forms a complex with the (*R*)-BINOL. In order to obtain the structure of the (*S*)-ammonium enantiomer cation complexed with (*R*)-BINOL in **221** and **223**, the atomic positions of the allyl and methyl groups from the SCXRD structure were replaced with that of the (*S*) enantiomer, of the *N*-allyl, *N*-methyl, *N*-homocyclopentyl anilinium bromide in **230**. To compare the energy difference between the two structures, the SCXRD structure of the (*R*)-ammonium cation enantiomer and the substituted *N*-homocyclopentyl enantiomer were fully optimised. To determine the relative energies of the structures formed with (*R*)- and (*S*)-ammonium cation enantiomer in **221** and **223**, the total lattice energy was divided by the number of formula units in each crystal structure to directly compare the energies. The energy difference between the two structures was then calculated. In **223** this was determined to be $-18.1 \text{ kJ mol}^{-1}$ and in **221** $-15.7 \text{ kJ mol}^{-1}$. These energy differences were the largest diastereomeric differences calculated across the study and suggest that enantioselectivity must be most dependent upon this thermo-

5.4. ISOSTRUCTURAL BASIS SET

dynamic discriminator; the energy difference of the ammonium cation enantiomers within the same matched pair isostructure.

To understand the key differences in interactions made between the two ammonium cation enantiomers and within the favoured (*R*)-BINOL-bromide hydrogen bonded network in **223**, the contacts were globally represented on a 3D surface and portrayed as coloured Hirshfeld fingerprint plots.²²² Visual trends in contacts within the crystal can easily be seen, with the most distinct contrast being the presence of more appreciable C–H⋯H contacts in the mismatched pair. These close C–H⋯H interactions represent increased steric clashes in the mismatched enantiomer which increases energy of the mismatched enantiomer versus that of the matched, thus promoting matched enantiomer enantioselectivity.

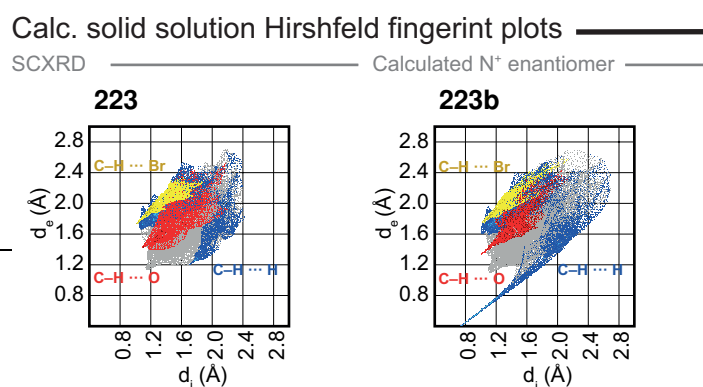


Figure 5.9: Coloured Hirshfeld fingerprint plots depicting cation contacts to the rest of the SCXRD crystal structure for a cation calculated to be in Isostructure B.

^a DFT calculations performed by Emma. H. Wolpert under the supervision of Kim. E. Jelfs.

5.5 Chapter 5 summary

In conclusion, to explain the observed enantioselectivity of the CIAT process in the synthesis of stereogenic nitrogen two main solid-state factors must be considered. Firstly, there must be a significant energy disparity between the matched and mismatched diastereomeric pair bromide·BINOL isostructures. The preferential formation of the lower energy isostructure is driven by the construction of a continuous hydrogen-bonded network that favourably accommodates a specific enantiomer. Additionally, there must be an appreciable energy difference between the enantiomers of the ammonium cation within the matched pair isostructure, crucial for providing stereoselectivity and preventing the formation of a solid solution. The latter is best described as a steric effect and depends on both the architecture of the bromide·BINOL C₂¹ (9) hydrogen bonded network and how well each mirror image cation is incorporated.

Chapter 6

Chiral crystallographic phenomena

The property of existing as non-superposable mirror images, known as enantiomers, is defined as chirality in molecular compounds. Given the geometrical essence of chirality, it significantly influences the crystallisation behaviour of compounds which possess this characteristic.²³⁴ In this chapter the influence of chirality in organic crystals is considered.

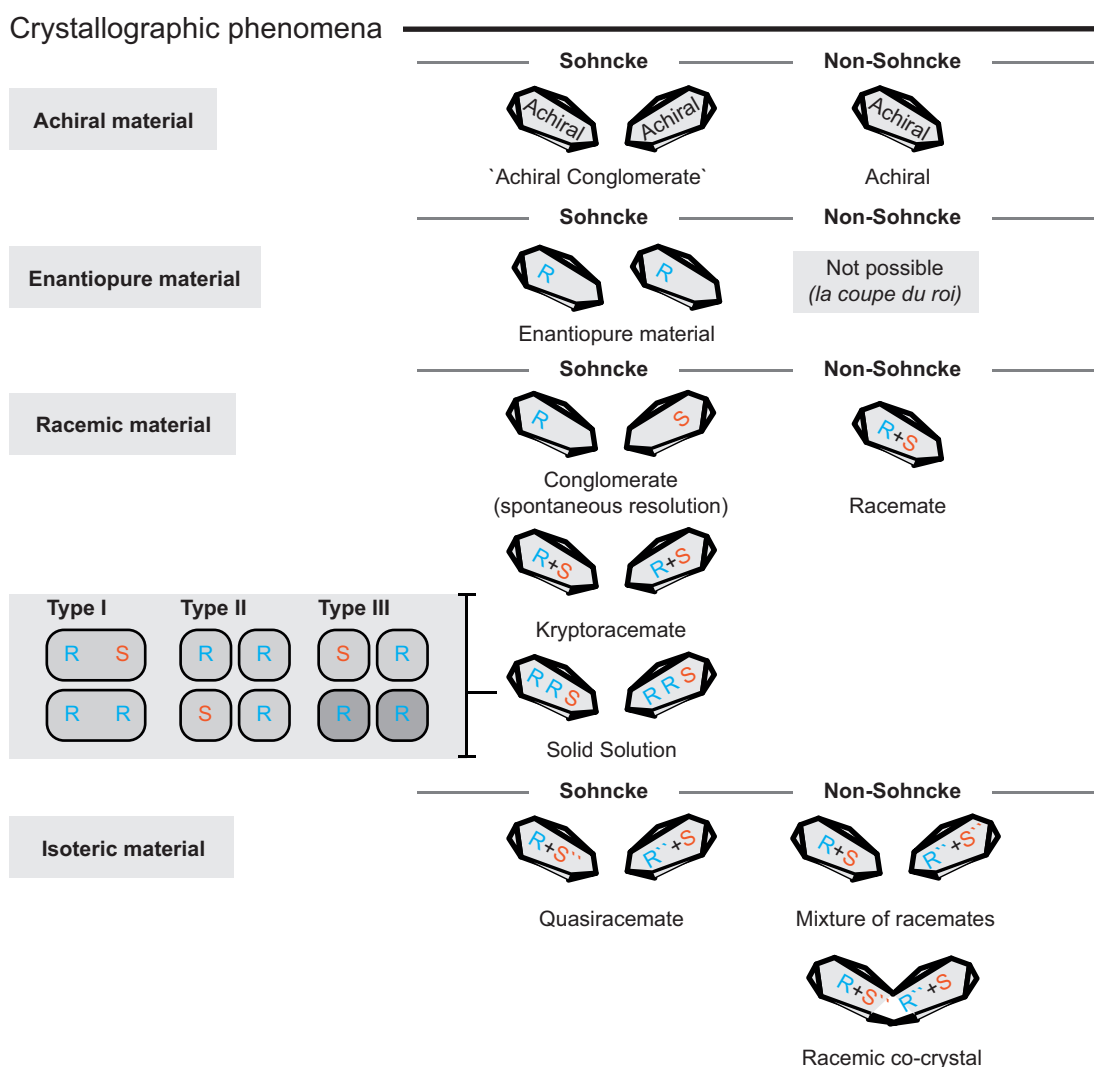


Figure 6.1: Crystallographic phenomena.

Achiral molecules can crystallise within any of the 230 space groups, encompass-

ing those featuring an inversion or mirror symmetry operation and those without. In contrast, single-enantiomer molecules are confined to only crystallise within the 65 Sohncke space groups.²³⁵ These space groups do not contain any inversion or mirror symmetry operations and therefore may only contain a single enantiomer by definition.²³⁶ Racemic chiral compounds can access all 230 space groups owing to their inherent inversion and mirror symmetry. Generally there is little crystallographic difference between racemic compounds and achiral compounds, due to their symmetry permitting both to crystallise in either Sohncke or non-Sohncke space groups, yet useful and distinct crystallographic behaviours can be observed between the classes.

When pure racemic material is crystallised, there are four possible crystallographic outcomes (see Figure 6.1.):³⁷

Racemate

Here the crystal exists in a non-Sohncke space group. The crystal is not optically active due to both enantiomers coupling together through an inversion and/or mirror symmetry described by the space group. Racemates are the most common crystallisation behaviour for racemic material. Interestingly, racemic crystals are thought to be denser (approx 1% on average) than their enantioenriched congeners - a much contested phenomenon known as Wallach's 1895 rule based on the density of *D,L*-alanine being greater than that of *L*-alanine.^{237,238}

Kryptoracemate

Kryptoracemates are racemic compounds that can crystallise as enantiomeric pairs in Sohncke space groups ($Z' > 1$).^{239,240} The two symmetry-independent enantiomers cannot be transformed onto each another by any symmetry element present in the crystal, hence they fulfil the requirement to crystallise in a Sohncke space group. Only 0.1% of racemic crystals are thought to crystallise as this phenomenon.²⁴¹

Quasiracemates form when an additional enantiopure, isosteric compound is present alongside an analogous enantiopure isostere.²⁴² There is no requirement for these crystal structures to crystallise in a Sohncke space group and they may crystallise in an analogous way to a racemate. However, when pseudoenantiomers crystallise

into chiral space group, these crystals can be thought of as "pseudo-kryptoracemates" where the two symmetry-independent isosteres cannot be transformed onto each another by any pseudosymmetry element present in the crystal and therefore crystallise into a Sohncke space group with $Z' > 1$.

Conglomerate (spontaneous resolution)

Conglomerate crystallisation, also known as spontaneous resolution, is the spontaneous generation of individually enantioenriched, optically active crystals from a racemic material.^{103,104,107} Approximately 5–10% of racemic crystals crystallise in this fashion.⁸⁶

Solid solution or pseudoracemate (scalemic crystallographic mixture)

When a molecule exhibits comparable affinities toward its own enantiomer and its opposite during crystallisation a crystal structure forms wherein both enantiomers are present in what appears as a random and disordered arrangement. This distinction can be further broken down to give distinct types of solid solution.²⁴³ The definitions broken down in Figure 6.1 are adapted and expanded from Chion *et al* and Rekiş:^{243,244}

Type I - a mixture of diastereomers that contain stereogenic elements located on the same molecule but vary in the absolute configuration about one (or more) of the stereogenic elements whilst one remains the same. **Type II** - a scalemic mixture of enantiomers in an asymmetric unit. i.e. the ratio of *R* to *S* is unbalanced. **Type III** - a two or more component crystal system in which one of the components is enantiopure and the other is either racemic or scalemic.

Throughout this chapter these various crystallographic phenomena will be discussed.

6.1 Spontaneous resolution

Responsible for the discovery of molecular chirality by Pasteur,⁴ conglomerate crystallisation is the spontaneous formation of individually enantioenriched crystals from a non-enantioenriched material. Despite its significance, this phenomenon remains largely under-documented, lacking a comprehensive database for materials established to crystallise in this manner. The scarcity of recorded instances comes from the tendency of synthetic chemists, who predominantly generate and publish chiral conglomerate crystals, to overlook and rarely leverage the implications of this phenomenon on the enantiopurity of their crystalline products. Through a manual examination of the Cambridge Structural Database (CSD), over 2000 chiral molecules capable of spontaneous resolution were discovered, thus uncovering a novel chiral pool distinct from biological sources.^{103,104}

Spontaneous resolution offers advantages over the natural chiral pool, including the potential for enantioenrichment across a diverse range of molecular architectures, independence from specific organisms for compound production, equal accessibility to both enantiomers through crystallisation (controlled through bias or seeding), enhanced scalability and the fact that as synthetic chemists continue to synthesise and crystallise new materials, an increase in the discovery of conglomerate crystals is also anticipated giving rise to a potentially limitless source of chiral information.²⁴⁵ Given these attributes, a catalogue of materials capable of spontaneous resolution via conglomerate crystallisation holds substantial value for the synthetic chemistry community.

* The majority of this section is based on two collaborative publications and is a summary thereof. I would like to thank the authors for their contribution to this work. The author list is as follows: (*JACS Au*, **2022**)¹⁰³ Mark P. Walsh, James A. Barclay, Callum S. Begg, Jinyi Xuan, Natalie T. Johnson, Jason C. Cole, and Matthew O. Kitching*; (*Cryst. Growth Des.*, **2023**)¹⁰⁴ Mark P. Walsh, James A. Barclay, Callum S. Begg, Jinyi Xuan and Matthew O. Kitching*.

To generate a list of potential conglomerates, initially queries were generated using *Conquest*, with CSD version 5.41 (November 2019)¹⁰³ and CSD version 5.43 (November 2021)¹⁰⁴ being used for the searches. To reduce the total number of manual searches required whilst checking through CSD entries, the following queries were employed:

- Must exist in a Sohncke space group AND $Z' = 1$.
- Must NOT be a member of carbohydrate, steroid, peptide or nucleoside/nucleotide classes.
- Must have carbon centre with C(Non-metal)₄ OR H-C(Non-metal)₃.
- Must be organic, non-polymeric, a single crystal, $R_1 < 0.075$ and no errors (disorder and salts were allowed).
- Crystals published as only *CSD Communications* were removed because their synthesis could not be interrogated.
- Text strings including; “isolated”, “sourced from”, “extracted”, “bark”, “marine”, “sponge”, “penicillium” were removed.
- Text strings common to natural products including; “cinchonine”, “strychnine”, “Striatin A” were removed from *JACS Au*, **2022**¹⁰³ and “D-(+)-xylose”, “crokonoid B”, “wortmannolol” were removed from *Cryst. Growth Des.*, **2023**.¹⁰⁴
- Compound names with the following; (+), (−), *D*, *L*, (*R*) and (*S*), were removed from the list.
- *Additionally the (November 2021) search was limited to crystals published between 2021–2022 to prevent duplicate entries appearing.*

These searches of the CSD returned 26,563 crystal entries (21,098 - November 2019 and 5,465 - November 2021) to be manually sorted through to identify conglomerates. The manual search of reported syntheses was performed by firstly confirming the enantioenrichment of the crystal (i.e. checking that the crystal was not an achiral conglomerate), secondly interrogating the publication to which the crystal was linked and finally inspecting the synthesis to determine whether the crystal was synthesised

6.1. SPONTANEOUS RESOLUTION

from racemic or enantioenriched material. Essential to confirming conglomerate behaviour was the ability to track the stereochemical enrichment in the starting materials and ruling out the use of any enantioselective methodology during the synthesis.

Following these laborious manual searches, an inventory of 2,179 materials exhibiting spontaneous resolution was compiled. Within this library, conglomerate behaviour was observed across a varied array of chiral compounds, exhibiting a lack of apparent structural constraints determining the occurrence of this phenomenon. Selected compounds of note are depicted in Figure 6.2 but comprehensive lists are compiled in the Supporting Information sections of the corresponding publications (*JACS Au*, **2022**,¹⁰³ *Cryst. Growth Des.*, **2023**,¹⁰⁴ follow "Supporting Info" tab).

Conglomerate crystals

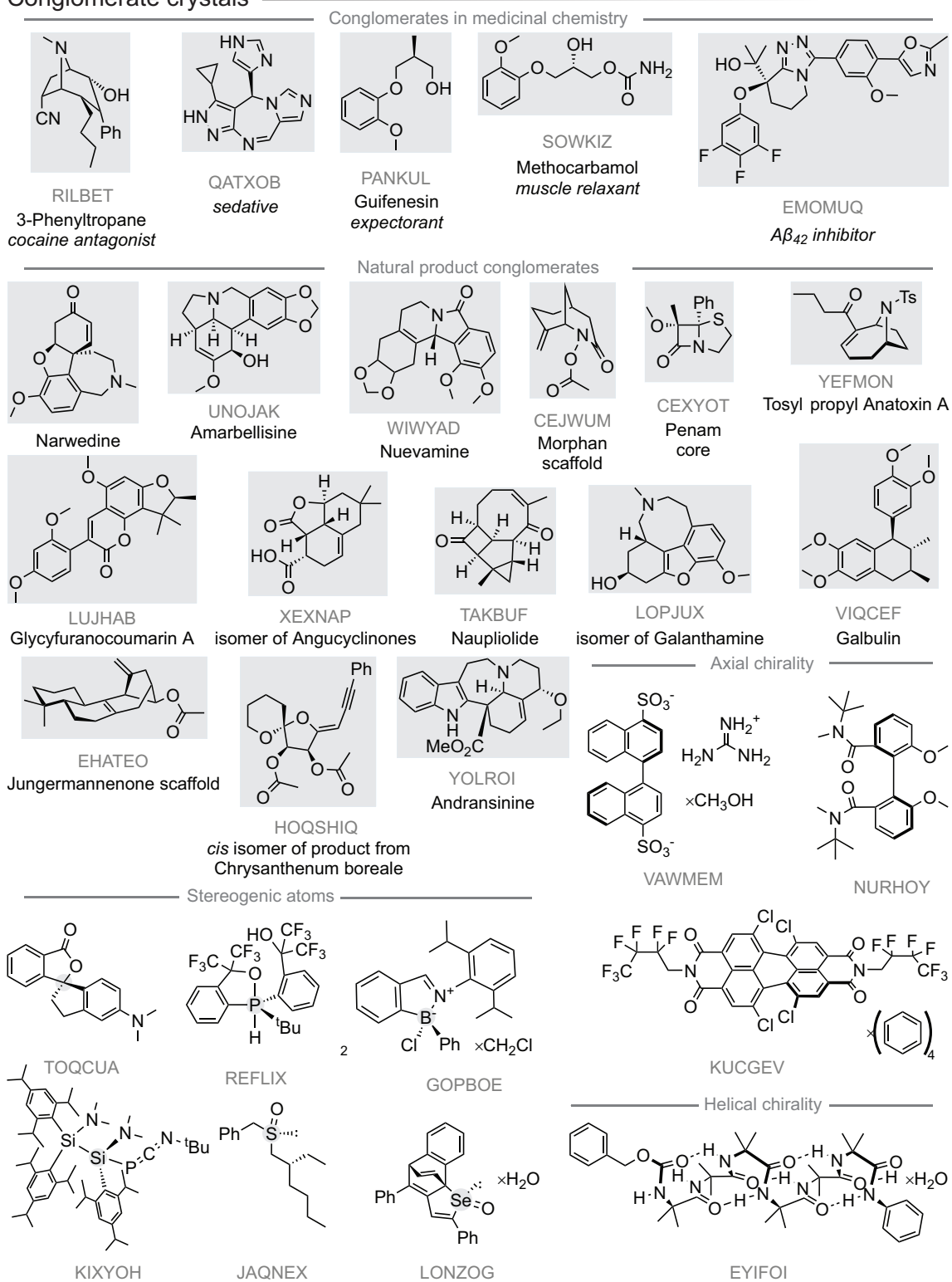
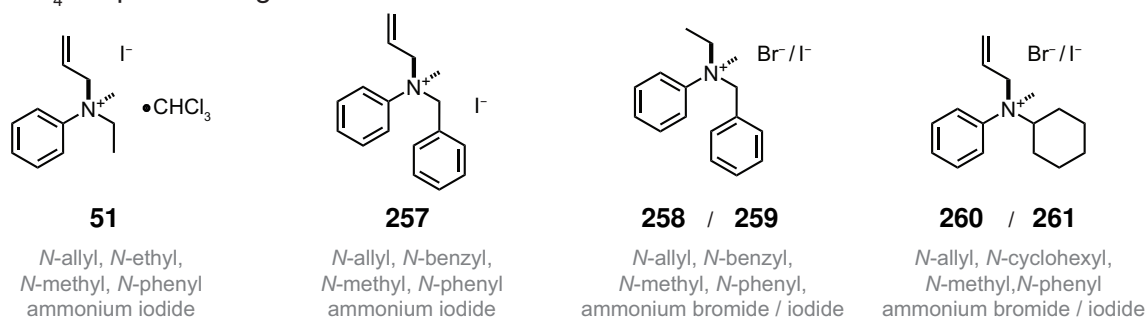


Figure 6.2: Notable crystals reported to be conglomerates from a manual search of the CSD.

6.1.1 Quaternary ammonium salt conglomerates

The main focus of this thesis is based around quaternary ammonium salts containing an *N*-stereogenic functionality, yet it is notable that a scarce number of quaternary ammonium salts meeting this criteria have been reported to crystallise as conglomerates (6 documented, Figure 6.3).^{2,107,246} Spontaneous resolution could act as a valuable tool for accessing the elusive *N*-stereocentre, therefore the identification of quaternary ammonium salts capable of crystallising as conglomerates would enhance practical utility in this field.

NR₄X reported conglomerates

New quaternary ammonium salt conglomerates

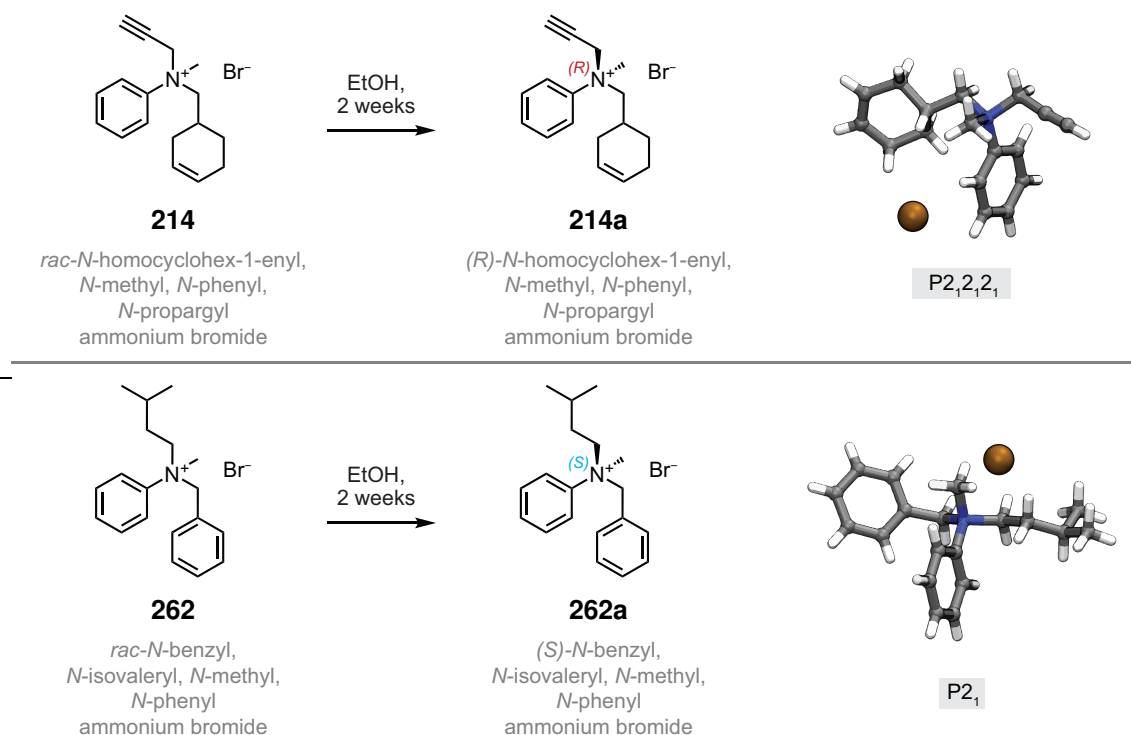


Figure 6.3: Reported quaternary ammonium salts that crystallise as conglomerates. All previously reported conglomerate salts crystallise in the space group $P2_12_12_1$ (no. 19). The spontaneous resolution of **214** and **262** is shown below.

Through recrystallisation of a library of racemic quaternary ammonium salts, two additional quaternary ammonium salts with the potential to spontaneously resolve were identified (**214** and **262**). Through recrystallisation in EtOH, the (*R*)-enantiomer of **214** ($P2_12_12_1$, **214a**) and the (*S*)-enantiomer of **262** ($P2_1$, **262b**) were obtained as single crystals suitable for SCXRD analysis from the racemic mixture (see Figure 6.3.).

Viedma Ripening

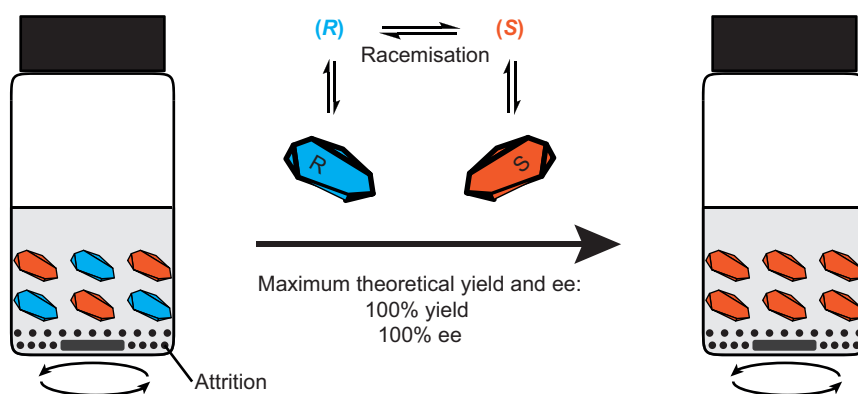


Figure 6.4: Viedma ripening protocol.

Due to the presence of a labile alkyl group substituted onto the quaternary ammonium salts identified to crystallise as conglomerates, these salts are suitable for integration into a Viedma ripening protocol. This process, founded on conglomerate crystallisation, attrition and racemisation, facilitates the enantioenrichment of racemic material, achieving enantiomeric excess (ee) levels of up to 100% for either the *R* or *S* enantiomer without reliance on external chiral information.^{247–251} Conglomerate crystallisation produces a system in which discrete enantiopure crystals are physically separated from one another. Concurrently, attrition introduces a stochastic element which leads to a breakdown of one enantiomeric crystal faster than the other, culminating in a biased Ostwald ripening phenomenon wherein the larger enantioenriched crystals prevail in the competitive growth against the crystals of the opposing enantiomer. Racemisation allows all material to be converted to the enantiomer which has been randomly favoured in the crystallisation process (seeding can be used to bias the protocol towards a desired enantiomer). This technique has demonstrated efficacy in the enantioselective synthesis of functionalised BINOL-like scaffolds²⁵² as well as amino acids,²⁵³ showcasing its versatility and applicability across diverse chemical contexts.

6.1. SPONTANEOUS RESOLUTION

It is hoped that future work will develop a methodology to extend the Viedma ripening to spontaneously resolving quaternary ammonium salts in a bid to supplement the enantioselective synthesis of ammonium salts.

6.2 $Z' > 1$ conglomerate search

The initial examinations of the CSD yielded 2,179 conglomerate crystals, as reported in recent studies.^{103,104} Notably, the majority of these crystals were limited to $Z' = 1$ as a pragmatic approach to manually searching the massive data set. However, this constraint is not physically essential for conglomerate crystallisations. Consequently, a segment of the CSD dataset was not interrogated in this analysis.

To explore potential conglomerate crystals within this chemical space, a new search was conducted. Initially, a list of potentially spontaneously resolved crystals was generated using CSD version 5.42 (Feb 2021) and *Conquest*. The same approach utilised in previous searches was employed to streamline the manual search process through combining additional queries within the *Conquest* search. Notably, unlike the aforementioned search, the requirement of $Z' = 1$ was changed to Z' MUST > 1 and only non-disordered crystal structures were permitted (see Table 6.1.). The search returned 11,338 crystals that had the potential to be conglomerates and crystallised with more than one molecule in the asymmetric unit.

Filters: 3D coordinates determined, $R_1 < 0.075$, only non-disordered, no errors, non-polymeric, only single crystal structures and only organics.

Table 6.1: Queries used to streamline the search for conglomerates with $Z' > 1$.

Must have	Must not have
Allows enantiopure substance (Sohncke)	Carbohydrates
$Z' > 1$	Nucleosides and nucleotides
	Amino acids, peptides and complexes
	Porphyrins, corrins and complexes
	Steroids
	Terpenes
	Alkaloids
	Organic polymers
	<i>CSD Communications</i>

* The manual search was performed by Callum S. Begg, James A. Barclay and Jinyi Xuan.

6.2. $Z' > 1$ CONGLOMERATE SEARCH

In an effort to increase the efficiency of the literature review process, a strategy involving the analysis of source tags to exclude crystals originating from biological sources was employed. This decision was based on the presumption that substances isolated or extracted from biological sources would inherently possess a degree of enantioenrichment due to the homochiral nature of biology, hence the conglomerate behaviour of any such compound could not be confirmed. This removed 709 entries. Selected examples of these source tags that would lead to a crystal being removed from the search include: 'extracted from the seed of *Euonymus maackii*', 'isolated from a soil-derived fungus *Bipolaris zeicola*' and 'derived from adenosine.' The next stage of the search involved excluding compounds designated with prefixes such as (+), (-), *D*, *L*, (*R*), and/or (*S*). This streamlining was based on the assumption that the synthesis and stereochemistry of these compounds had been controlled to achieve the given prefix assignment. Finally the manual search was performed on remaining list of compounds to interrogate the crystal structures and their respective syntheses to identify enantiopure crystal structures that had been recrystallised from non-enantioenriched (i.e. racemic) material. In contrast to the previous searches, where $Z' = 1$, additional complexity was introduced for $Z' > 1$ crystal structures. Here, it had to be manually verified that molecules within the crystallographic asymmetric unit were identical and accurately defined with their Z' value and further it had to be ensured that there was uniform enantioenrichment across all molecules within the asymmetric unit.

After performing the manual search by firstly confirming the enantioenrichment of the crystal, secondly interrogating the publication to which the crystal was linked and finally inspecting the synthesis to determine whether the crystal was synthesised from racemic or enantioenriched material, 149 conglomerates were identified (a 1.31% success rate in the $Z' > 1$ crystallographic space).

6.2.1 What does Z' mean?

The International Union of Crystallography (IUCr) defines Z as 'the number of the formula units in the unit cell.'²⁵⁴ This number can be further broken down to give the number of symmetry-independent molecules in a crystal structure, known as Z' - a parameter referring to the number of formula units in the asymmetric unit of a crystal structure (i.e. the number of symmetry unrelated molecules of the same compound that are crystallographically unique in a crystal system).²⁵⁵ As such the Z' value is dependent on the subjective deduction of a 'formula unit' by a given crystallographer. The correct derivation of Z' involves dividing the the number of formula units in the unit cell (Z) by the number of independent general positions and has been reported to range in value between 0.125 and 56.^{255,256}

A survey of the CSD reveals that 11.8% of organic and 8.8% of all deposited crystal structures possess a Z' value greater than 1.²⁵⁷ Furthermore, the majority of crystal structures, accounting for 95.3% of all entries, are distributed among the Z' values of 0.5, 1, and 2.²⁵⁸ Notably, the occurrence of $Z' > 1$ in Sohncke space groups is almost 5% greater than the overall frequency in the CSD (14.6%), with specific chiral structures demonstrating a further heightened occurrence of $Z' > 1$; such as nucleosides and nucleotides at a frequency of 20.8% and steroids at a frequency of 18.8%.²⁵⁸ This observation could offer one potential explanation as to the low success rate for conglomerate identification in structures with $Z' > 1$ (1.31% versus approx. 8–10% overall) due to the greater prevalence of enantiopure materials in this crystallographic space compared to $Z' = 1$.

High Z' structures are thought to come about through competition between two or more opposing factors. Generally they tend to form as a compromise between an optimisation of hydrogen bonding and crystal packing within the crystal lattice.²⁵⁹ Numerous studies have explored the link between structures with Z' values greater than 1 and the phenomenon of polymorphism,²⁶⁰ aiming to elucidate the factors influencing their formation and thus control the solid-state of these materials.^{261,262} The effect of this phenomenon on the properties of such crystalline compounds can be illustrated across series of 1,3-disubstituted benzenes that display pseudopolymorphism through

6.2. $Z' > 1$ CONGLOMERATE SEARCH

modification of their Z' values ($Z' = 0.5\text{--}5.0$).²⁶³ A critical question involving both high Z' structures and polymorphs is: are these solid forms simply kinetic products formed under non equilibrium conditions, or rather do they represent a thermodynamic minima?^{261,264}

6.2.2 Conglomerates with $Z' > 1$

149 conglomerates were identified to crystallise with $Z' > 1$, with the largest number of symmetry independent molecules found in a conglomerate crystal structure being 6 (WAKWEM). Interestingly, as Z' increases the number of conglomerates decreases, with a distribution that mirrors the same trend seen by all organic crystals with Z' greater than 1 in Sohncke space groups in the CSD.

Distributions of $Z' > 1$ conglomerates

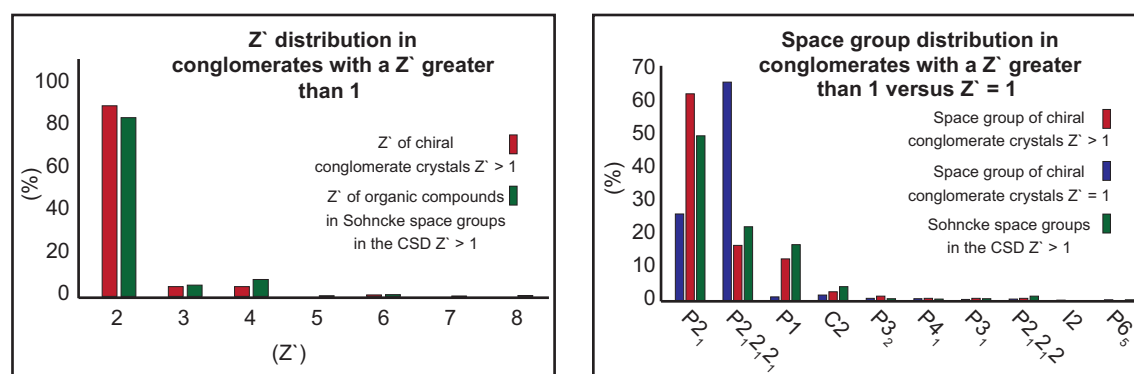


Figure 6.5: Bar charts showing the distribution of Z' and the distribution of space groups in conglomerates found to crystallise with $Z' > 1$. Note that only Z' values and space groups in which a conglomerate was found are shown.

The distribution of conglomerate space groups with $Z' = 1$ closely mirrors the distribution of Sohncke space groups observed in the CSD (see Figure 6.5.). However, significant differences are observed when Z' is greater than 1. Notably, the $P2_1$ space group is the most prevalent for conglomerates with Z' greater than 1, in contrast to the higher symmetry $P2_12_12_1$ space group observed when $Z' = 1$. This pattern aligns with the general trend seen in all organic crystals with Z' greater than 1 in Sohncke space groups in the CSD, where $P2_1$ (50.3%) is more abundant compared to $P2_12_12_1$ (22.5%). This the trend is further inflated for conglomerates, with $P2_1$ accounting for 63.1% and $P2_12_12_1$ 16.8% of the crystals. This disparity between the frequency of the two space groups when Z' is greater than 1 could potentially be attributed to the

increased challenge of accessing a higher symmetry environment for higher Z' values. Additionally, this tendency is exemplified by the absence of the space groups $P4_12_12$ and $P4_32_12$ constituting approximately 1% of conglomerates when $Z' = 1$ but are absent in conglomerates with Z' greater than 1.

Within this library documenting Z' greater than 1 conglomerates, a diverse range of chiral compounds were exhibited. Compounds of potential interest are illustrated in Figure 6.6 but the full list of 149 conglomerate refcodes can be found in the experimental section of this thesis.

Conglomerate crystals ($Z' > 1$)

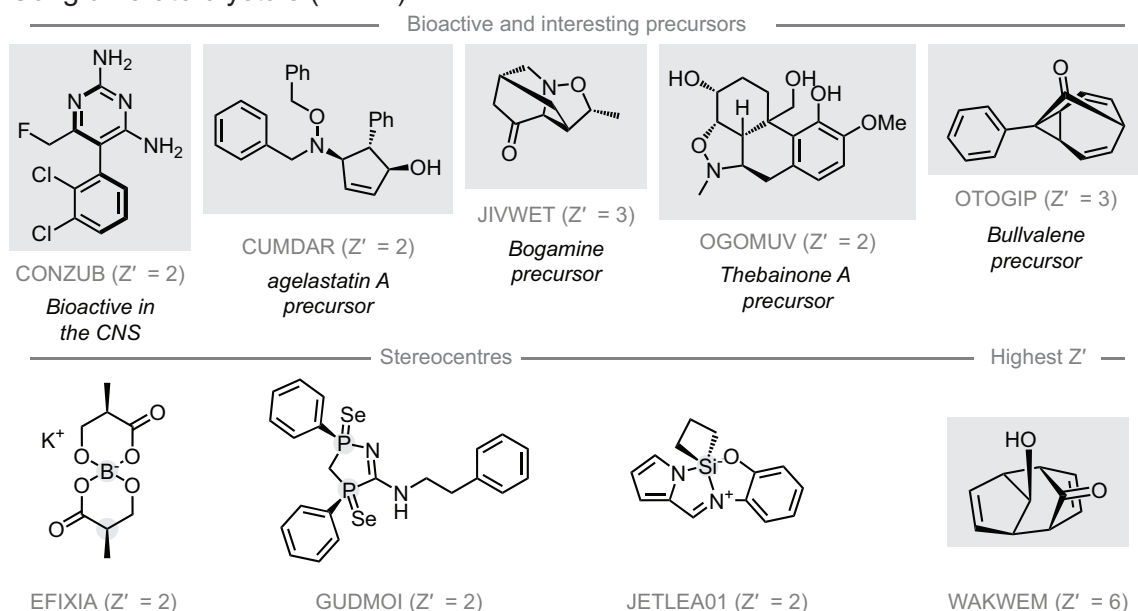


Figure 6.6: Notable crystals with Z' greater than 1 reported to be conglomerates from a manual search of the CSD.

6.2.3 Kryptoracemates

Kryptoracemates, sometimes referred to as false conglomerates,²⁶⁵ are a rare crystallographic class in which two enantiomers exist as crystallographically independent functional units. Their scarceness is attributed to the intrinsic molecular inclination to adopt inversion symmetry whenever possible (seen in 99% of molecules),²⁶⁶ hence mixtures of enantiomers tend to crystallise as racemates in a non-Sohncke space group.

Table 6.2: The number of kryptoracemates identified in Fabian *et al.*²⁴¹ list versus newly generated list of kryptoracemates, plus combined. Refcodes removed from the list due to the crystal being solved in a space group of too low symmetry.

Total number of kryptoracemates uncovered in CSD search	466
Total number of kryptoracemates in Fábíán <i>et al.</i> list	181
Number that appear in both lists	32
Total number of unique values across the two lists	578
Potentially too low symmetry	GIWRIO, LIMHIZ, RIGSEF, WASWAO, YIZGEU
Total number of kryptoracemates	461

During the $Z' > 1$ CSD search (aiming to identify conglomerate crystals), the specific search criteria used allowed for parallel compilation of a list of organic kryptoracemates. A prior automated search of the database had already identified 181 organic kryptoracemates,²⁴¹ although the definition of kryptoracemate varied in this study (in that their definition included solid solutions of enantiomers). However, usefully Fábíán *et al.* identified crystal structures that had been solved with too low symmetry and were not true kryptoracemates, thus their automated search proved effective in applying constraints to the manual CSD search. In our initial manual survey a total of 466 kryptoracemic crystals were uncovered. Analysis and subsequent amalgamation of the two datasets resulted in a comprehensive catalogue of 461 kryptoracemates from our CSD search (see Table 6.2.), by removing the previously identified crystals of too low symmetry to be true kryptoracemates.

The manual search for kryptoracemates returned a hit rate of 4.1% for organic crystals in non-Sohncke space groups within the CSD. Interestingly, this hit rate is approximately three times higher than that observed for conglomerates under identical search conditions. This disparity prompts an intriguing question: could this discrep-

ancy arise from the inherent symmetry of these systems, making them more prone to crystallise in Sohncke space groups, or is it more likely to be attributed to potential misinterpretations of crystallographic data leading to incorrect space group selection?

Care must be taken when reporting a Z' value of greater than 1 to ensure that there are no missing symmetry elements that could describe a relationship between the two 'crystallographically independent' moieties. In approximately one-third of structures where chiral molecules crystallise in $P1$ with $Z = 2$ ($Z' = 2$), the two molecules are related by an approximate centre of inversion.²⁶⁷ Therefore, a more accurate description as $P\bar{1}$ with $Z = 2$ and $Z' = 1$ is appropriate. Consequently, many potential kryptoracemates should be properly identified as strictly racemic compounds. Furthermore, compounds in the $C2$ space group may also benefit from a revised symmetry description with an added centre of inversion, prompting a change to $C2/m$ and resulting in a decrease in the values of both Z and Z' . This alteration would once again reclassify a potential kryptoracemate as racemic crystal.²⁶⁸

The aim of this search was not to correct any literature nor the corresponding crystallographic data, as such the crystal structures catalogued were assumed to be solved correctly in the appropriate space group. The only exception to this were those that could be identified as being solved with too lower symmetry by comparing the newly generated list to the previously reported list, from which 5 kryptoracemates had been removed based on this suspicion (GIWRIO, LIMHIZ, RIGSEF, WASWAO, YIZGEU).²⁴¹

6.2. $Z' > 1$ CONGLOMERATE SEARCH

Distributions of $Z' > 1$ conglomerates

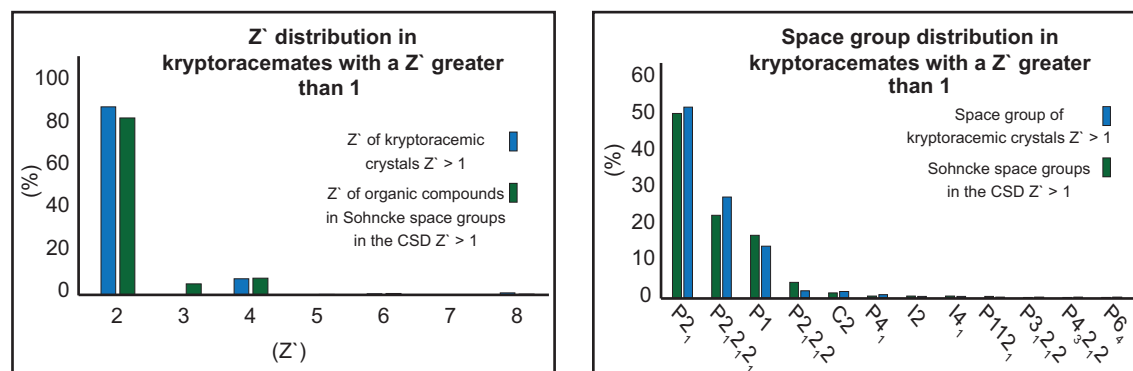


Figure 6.7: Bar charts showing the distribution of Z' and the distribution of space groups in kryptoracemates found to crystallise with $Z' > 1$. Note that only Z' values and space groups in which kryptoracemates were found are shown.

The distribution of kryptoracemic space groups resembles the distribution of all organic crystals with Z' greater than 1 in Sohncke space groups within CSD (see Figure 6.7.). This observation also holds broadly true for the distribution of Z' values, with a notable difference being the absence of odd Z' values in kryptoracemates. This stems from the necessity of kryptoracemates to exhibit an even Z' value to facilitate the pairing of enantiomers within an asymmetric unit. Furthermore, there is a slight increase in the percentage of kryptoracemates observed at $Z' = 8$ (1.1%) compared to $Z' = 6$ (0.65%). This suggests an intriguing preference in kryptoracemates for Z' values that are 2^n as opposed to merely even integers (see Figure 6.7.).

The kryptoracemic crystal structure identified to contain the highest number of formula units per asymmetric unit is (2-bromophenyl)(pentafluorophenyl)methanol (OTOGOW, $Z' = 16$). Unfortunately, inspection of the crystal structure suggests that symmetry elements might be missing in the $P1$ space group description to cause the heightened Z' value in this instance. The next highest Z' value is 8, notably observed in five kryptoracemic instances (HUYBIN, IGAKAI, LIWMOW, LUMJUJ, YAQVUK). In these cases, upon visual inspection, the choice of space groups (either $P2_1$ or $P2_12_12_1$) appears to align more reasonably with the observed structural symmetry in the crystal structure.

It is important for synthetic chemists wishing to exploit these crystallographic phenomena to recognise the distinction between kryptoracemates and conglomerate crys-

tals. While the suggested compilation of chiral conglomerate crystals, spanning all Z' values, can be conceived as an innovative chiral pool independent of biologically derived chiral information, advancing the development of preferential crystallisation and spontaneous deracemisation techniques, it is crucial to recognise that not all racemates crystallising into Sohncke space groups are invariably resolved into distinct enantiopure crystals.

Selected kryptoracemates are depicted in Figure 6.8 but the full list of kryptoracemate refcodes can be found in the appendix of this thesis.

6.2. $Z' > 1$ CONGLOMERATE SEARCH

Kryptoracemate crystals

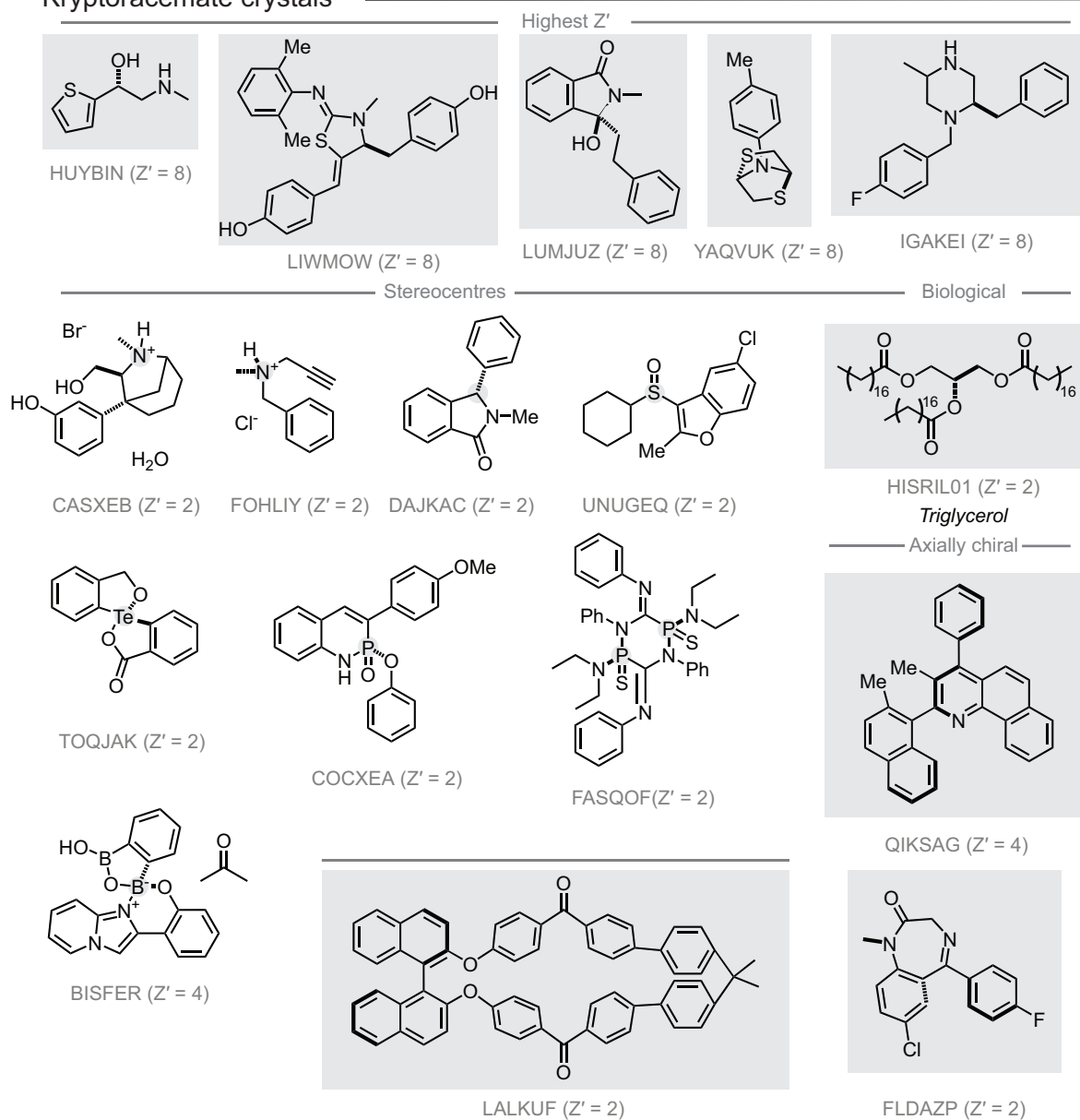


Figure 6.8: Notable kryptoracemic crystals from a manual search of the CSD.

6.2.4 Solid solutions of enantiomers

Solid solutions of enantiomers, rarer than conglomerates, are sparsely documented within the literature.²⁴⁴ Rekiş classified them into two distinct types:²⁴³ *type 1* enantiomer solid solutions represent crystalline phases where each molecular site can be equally occupied by either enantiomer, while *type 2* solid solutions (the more prominent type) manifest as crystalline phases where enantiomers are distinctly identified as separate entities within the crystal structure. The precise factors driving their formation remain elusive, prompting numerous intriguing inquiries into crystal packing. As such, cataloguing of this phenomenon's occurrence holds significant importance to the crystallographic community.

When searching the CSD for organic crystals with $Z' > 1$ in Sohncke space groups, an observation emerged: this space hosts a notable quantity of solid solutions of enantiomers. Consequently, these crystals were documented alongside conglomerates and kryptoracemates. A total of 94 instances were uncovered and subsequently categorised for further analysis.

Here the formation of solid solutions of enantiomers has been further broken down into 3 categories (see Figure 6.9.). **Type I** solid solutions refer to a mixture of diastereomers that contain a undefined epimer about one of the stereocentres, on a single molecule. **Type II** solid solutions refer to a scalemic mixture of enantiomers in an asymmetric unit i.e. the ratio of *R* to *S* is unbalanced. These most closely resemble the *type 1* definition given by Rekiş and must not equal 2 molecules per asymmetric unit. **Type III** solid solutions can be thought of as 'failed resolutions,' in that they comprise of a two or more component crystal system in which one of the components is enantiopure and the other is either racemic or scalemic.

The breakdown of frequency of the solid solution types (see Figure 6.10.) shows that most of the crystals manifest as **Type I**, wherein there is a mixture of diastereomers in an asymmetric unit that crystallises in a Sohncke space group. The next most common occurrence was **type II**, followed by **type III**. The highest Z' value was 8.

6.2. $Z' > 1$ CONGLOMERATE SEARCH

Solid solution categories

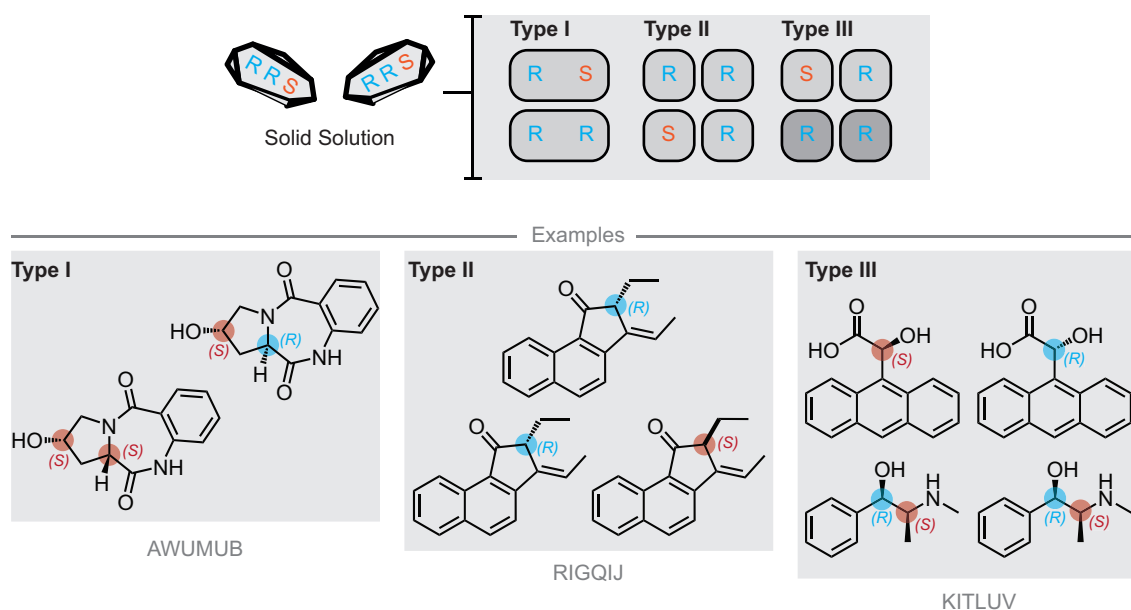
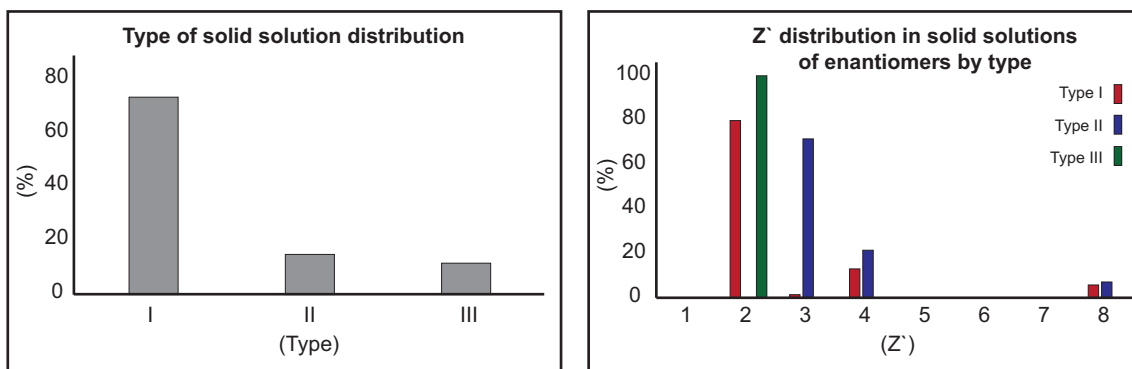


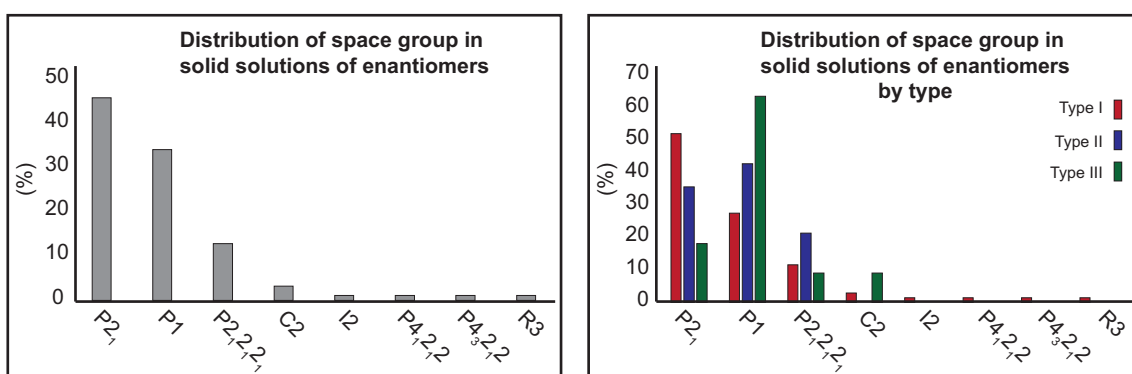
Figure 6.9: Solid solutions and the categories they have been broken down into.

An interesting question arises when considering Z' and solid solutions: is a **type I** solid solution with $Z' = 2$, better described as a mixture of diastereomers in a solid solution or would it better be modelled as a single crystallographic entity ($Z' = 1$) with disorder about the epimeric stereocentre? i.e. Do solid solutions of enantiomers actually exist as a crystallographic phenomenon or are they a limitation of our definition of Z' and the subjectivity of what defines a 'formula unit'?

Much like with kryptoracemates, the selection of space group when solving structures that might be solid solutions is imperative. To illustrate how Z' modification can occur through space group selection one can consider the case of Emycin E (LIPYUE).²⁶⁹ Emycin E, crystallises as two molecules within a triclinic unit cell. These structures can be solved and refined either in the centrosymmetric space group $P\bar{1}$, with disorder about one of the stereocentres, or in the non-centrosymmetric space group $P1$, denoting mixtures of two diastereomers without disorder. Significantly, only the latter interpretation aligns with chemical and spectroscopic evidence, confirming the structure as a solid solution in this instance and not just a structure with disorder about a stereocentre.

Distributions of type and Z' of solid solutions

Distributions of space group for solid solutions

Figure 6.10: Solid solution of enantiomers Z' and space group distributions broken down by type assigned in Figure 6.9.

When analysing the Z' distribution, several intriguing patterns emerge dependent upon the type of solid solution of enantiomers formed. **Type I** solid solutions of enantiomers exhibit a trend akin to kryptoracemates, favouring Z' values of 2^n , with a decrease in relative frequency as Z' increases. Similarly, **Type II** solid solutions of enantiomers, unable to accommodate two molecules in an asymmetric unit (otherwise they would become kryptoracemates or conglomerates depending upon the identity of the given stereocentres), also showcase a decline in frequency as Z' escalates. Interestingly, **Type III** solid solutions of enantiomers are exclusively present at $Z' = 2$.

Despite $P2_1$ being the dominant space group across the entire dataset, a notable trend emerges across all solid solutions of enantiomers. There is an increased prevalence of $P1$ compared to $P2_12_12_1$ in contrast to conglomerates, kryptoracemates, and all organic crystals with $Z' > 1$ in Sohncke space groups. This trend is particularly pronounced in **type II** and **type III** solid solutions of enantiomers, where $P1$ surpasses

6.2. $Z' > 1$ CONGLOMERATE SEARCH

$P2_1$ to become the most common space group. The assignment of this lower symmetry space group raises concerns regarding potential missing symmetry elements in the assignment of space groups for these crystal structures, possibly leading to inaccuracies in identifying them as solid solutions. However, the objective of this work did not involve correcting any existing literature or the corresponding crystallographic data. As a result, the catalogued crystal structures were presumed to have been correctly solved within the designated space groups.

Solid solution of enantiomers crystals

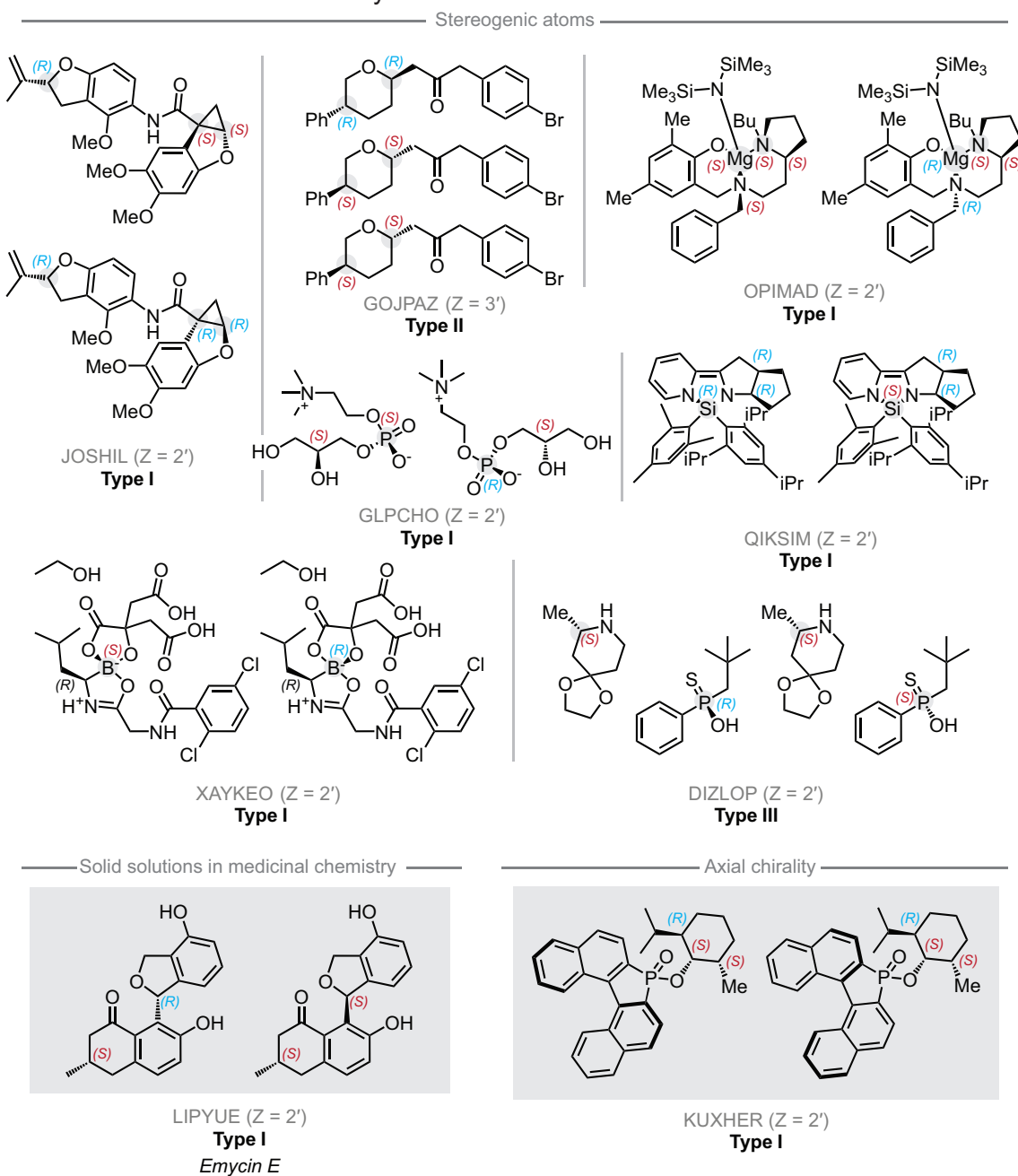


Figure 6.11: Solid solution of enantiomers examples from manual CSD search.

6.2.5 Quasiracemates

Quasiracemates, characterised by pairs of co-crystalline pseudoenantiomers, exhibit patterns mirroring the inversion relationships seen in their racemic counterparts.²⁷⁰ These crystals are not obligated to crystallise in Sohncke space groups, however in an analogous way to their kryptoracemic counterparts, there exists the possibility for them to do so.

During the search of the CSD, a group of co-crystal (N-benzoyl)methylbenzylamines were identified from Craddock *et al.* that exhibited this unique behaviour. All crystallised in P1 with a Z' values of 2. (see Figure 6.12.).

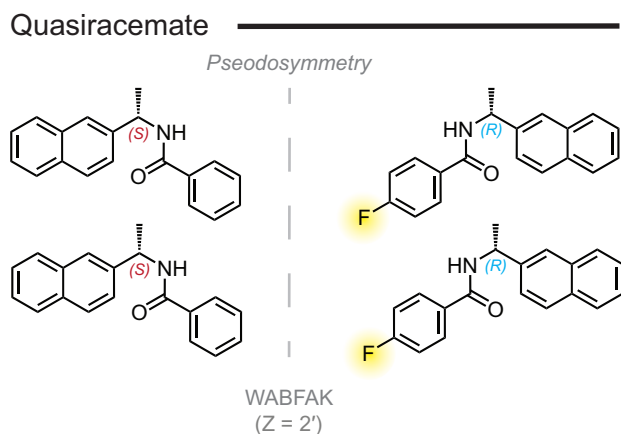


Figure 6.12: Quasiracemate identified from Craddock *et al.*²⁷⁰

6.3 Chapter 6 summary

A list of 2328 conglomerate crystals (2179, $Z' = 1$; 149, $Z' > 1$), 461 kryptoracemates and 96 solid solutions of enantiomers were identified from a manual search of the CSD and literature. Encouraging synthetic chemists to share crystal structures along with comprehensive synthetic procedures and reagent details, even for seemingly unremarkable crystals or synthesis processes, is the most effective approach for discovering new conglomerate crystals. The proposed list of chiral conglomerate crystals (across all values of Z') can be envisioned as a novel chiral pool, devoid of reliance on biologically derived chiral information. It is anticipated that curating this conglomerate crystal list will facilitate the advancement of preferential crystallisation and spontaneous deracemisation procedures, enhancing the comprehension of conglomerate crystal behaviour. Furthermore, the characterisation of both kryptoracemic and solid solutions of enantiomers phenomena is expected to provide insight for those aiming to gain a deeper understanding and impart control over chiral crystallisations of organic material.

Chapter 7

Additional projects

7.1 Chiral protonated ammonium cation complexes

Tertiary ammonium salts can be resolved in EtOH using a modified protocol from the one detailed in Figure 4.1. Intriguingly, specific alkyl groups such as 2-ethylbutyl, exhibit better tolerance in tertiary ammonium cation recognition by enantiopure BINOL compared to their quaternary counterparts. The *N*-methyl, *N*-2-ethylbutyl aniline derived quaternary ammonium salts were not recognised using the general CIAT like procedure, yet the *N*-methyl, *N*-2-ethylbutyl anilinium hydrobromide formed a ternary complex (**266**). However, overall the tertiary ammonium salts suffered an even greater rate of attrition when testing for their complexation with enantiopure BINOL compared to the quaternary alkylated variants. This discrepancy can be attributed to the comparatively lower stability of tertiary ammonium cations in the crystalline state, thus limiting their scope in comparison to the quaternary salts (see Figure 2.15.).

Chiral tertiary complexes

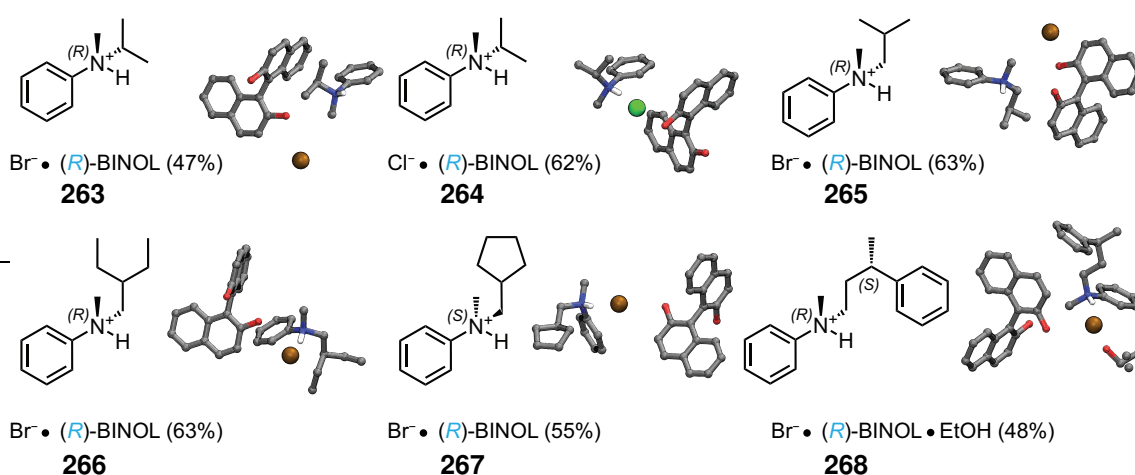


Figure 7.1: Chiral tertiary ammonium salt complexes with (*R*)-BINOL (yield%).

In Figure 7.1, six instances of tertiary ammonium hydrobromide and hydrochloride salts complexed with (*R*)-BINOL are presented. Surprisingly these ternary complexes displayed optical activity in solution that was distinct from what would be expected for

pure (*R*)-BINOL. Unfortunately, it is assumed that these complexes will lack practical utility beyond their synthesis due to their tendency to undergo rapid deprotonation in solution upon re-dissolution of the complex. Furthermore, the tendency of these tertiary ammonium salts to undergo deprotonation poses a significant challenge in accurately measuring the enantioenrichment of given complexes. Techniques such as chiral HPLC and the utilisation of a chiral shift reagent become impractical in this context.

7.2 Amine catalysed Suzuki-Miyaura coupling

A recent report in *Nature Catalysis* detailed the potentially groundbreaking organocatalysis of a Suzuki-Miyaura type cross-coupling of aryl halides with aryl boronic acids, catalysed by a simple amine species.²⁷¹ Across multiple academic and industrial laboratories, a reinvestigation of key claims in this paper was conducted showing that the observed catalytic activity cannot be due to the amine, but rather is due to tricyclohexylphosphine palladium complexes that are readily entrained during the purification of the amine.²⁷²

After reproducing experiments done by Xu *et al.* it was evident that the ligand **269**, synthesised in accordance with their procedures, did indeed exhibit catalytic activity in the Suzuki-Miyaura type cross-coupling of aryl halides with aryl boronic acids. However, this catalytic activity was not owed to the amine **269**. Instead it was determined that a palladium complex was readily entrained during the purification of **269** by column chromatography, leading to the observed catalytic behaviour. Notably, the tricyclohexylphosphine palladium complexes were also shown to be robust enough to survive two rounds of column chromatography while retaining sufficient loading to catalyse the cross-coupling. When ligand **269** was purified by recrystallisation and when the palladium impurity from **269** was removed by reaction with PhB(OH)₂ and K₂CO₃ the catalytic activity was lost. Moreover, both purification methods led to the removal of tricyclohexylphosphine palladium complexes, which were detected via ³¹P NMR spectroscopy. These data strongly suggest that tricyclohexylphosphine complexes are likely the species responsible for the observed catalytic activity in the work

of Xu *et al.*

This evidence along with experimental data from several other groups conclusively proves that the catalysis reported by Xu *et al.* was not metal free.^{272–274} Consequently, the report of an “amine catalysed Suzuki-Miyaura-type coupling of aryl halides and arylboronic acids,” could not be substantiated. Following publication of the discussed results, the article published by Xu *et al.* was retracted.

Organocatalytic Suzuki-Miyaura type cross-coupling

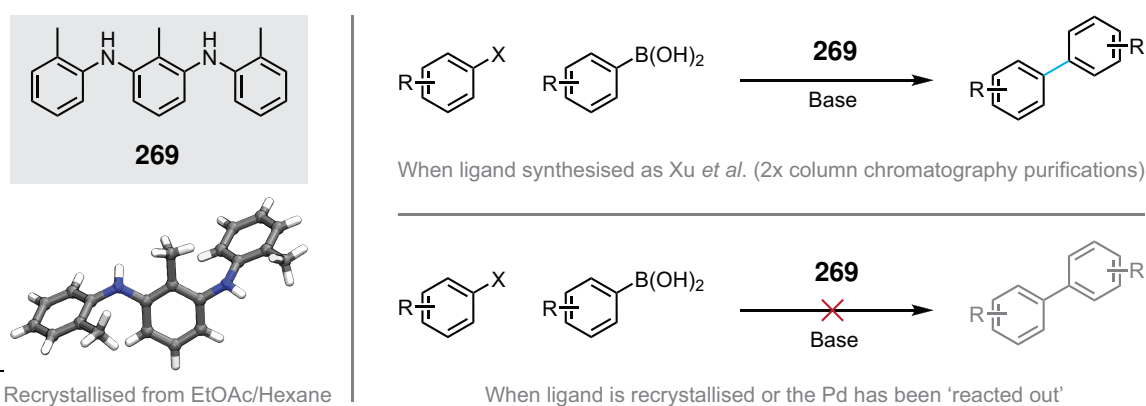


Figure 7.2: Crystal structure of ligand **269** obtained by SCXRD and the reactions carried out with the ligand purified in different ways as a part of this investigation.

7.3 EthR booster drug development

Currently Tuberculosis (TB) is amongst the top ten causes of death worldwide and in 2022 was the second most deadly infectious agent globally.²⁷⁵ The causal bacillus, *Mycobacterium tuberculosis* has, in certain strains, begun to develop resistance to frontline antimycobacterial drugs, with 450,00 cases of multidrug-resistant TB confirmed in the past year. It is vital that new medicines are developed to tackle the growing demand for therapy and prevent deadly outbreaks of the disease.

Ethionamide (ETH), a structural analogue of isoniazid, is a second line drug which inhibits mycolic acid synthesis in *M.tuberculosis*.^{276,277} Before interacting with its cellular target ETH must first be activated *in situ* by *S*-oxidation. The process is catalysed by the mycobacterial monooxygenase EthA, the biosynthesis of which is controlled by the transcriptional repressor EthR – a homodimer of two, nine α helix monomers. Up-regulating EthA expression, via EthR inhibition, increases the bioavailability of active ETH and therefore boosts the potency of the second line drug against *M. tuberculosis*.²⁷⁸ The binding of small ligands to a hydrophobic cavity in EthR induces conformational change in the DNA binding domain, reducing DNA binding affinity and perturbing repressor function.^{279–282}

In this study, we synthesised and screened a library of novel 4-methylpiperidine-based scaffolds to assess their binding affinity and inhibition potential against EthR. Utilising a thermal shift assay for biophysical screening, we identified correlations between functionality and the observed melting temperatures (ranging from $-0.4 - +11.6$ °C). These findings were further validated through growth inhibition assays. Additionally, co-crystal structures of EthR in complex with four newly identified ligands were determined, providing insights into their binding modes and inactivation mechanisms. Notably, growth inhibition assays highlighted that five out of the twenty initial biophysical hits exhibited the ability to enhance ETH activity *in vitro*, with the most promising novel scaffold displaying an EC₅₀ of 34 μ M. These results hold significant promise for future lead development in combatting TB.

7.3. ETHR BOOSTER DRUG DEVELOPMENT

EthR inhibition by a library of urea-based ligands

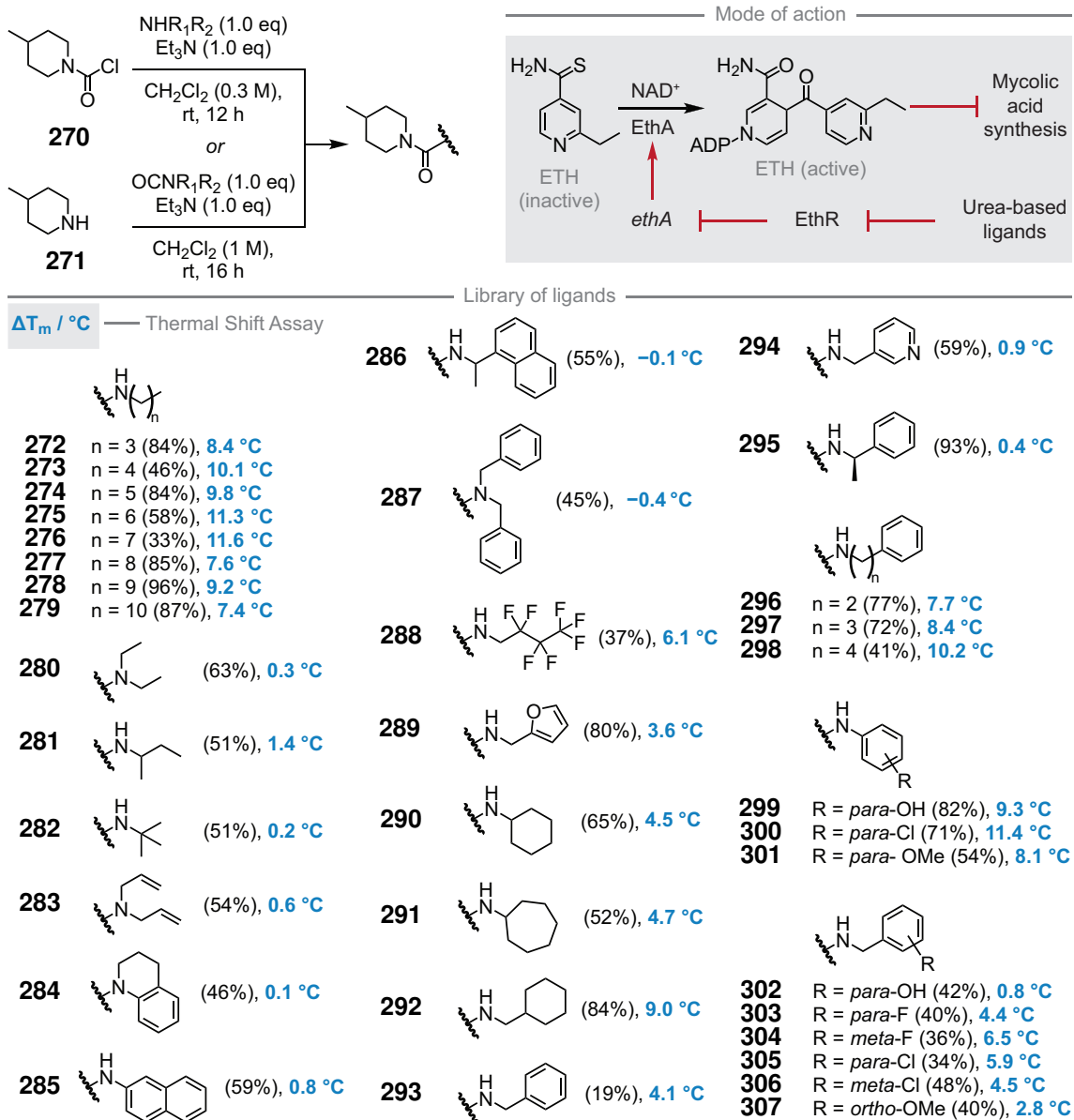


Figure 7.3: General procedures to synthesise urea-based ligands and the method of ETH action and prodrug action in *Mycobacterium tuberculosis*.

* This section is based on a draft manuscript in collaboration with: Natalie J. Tatum, Charles W. E. Tomlinson, Roseangela Frita, Rose Bennett, Alain R. Baulard, Callum S. Begg, Ehmke Pohl* and Matthew O. Kitching*. Callum S. Begg synthesised and characterised several of the urea-based compounds presented.

7.4 Tetrahalopyridyl crystallinity

In this research, we focused on enhancing the solid-state properties and crystallinity of various substituted aromatic compounds by incorporating tetrahalopyridyl groups. These functionalities proved to be highly effective in establishing stabilising interactions within the solid state, leading to the formation of highly crystalline systems. The incorporation of these functionalities was found to be straightforward and high yielding, necessitating minimal purification.²⁸³ Notably, the presence of tetrahalopyridyl groups significantly increased the melting point of materials and provided a useful tool for determining absolute chirality. This study sheds light on the potential of tetrafluoro- and tetrachloropyridine groups as versatile tools to tailor the solid-state properties of compounds.

In recent years, there has been a significant focus on the development of fluorinated moieties due to the distinct physical and chemical properties they confer to molecules.^{284–287} This trend has been particularly prevalent in the field of medicinal chemistry, with approximately 20% of small-molecule drugs now incorporating one or more fluorine atoms. Notably, among the top 100 best-selling drugs worldwide, 13 contain fluorine.²⁸⁸ Beyond pharmaceutical applications, fluorination is also employed to adjust material hydrophobicity, as seen in polytetrafluoroethylene (PTFE), a versatile fluorinated polymer used in everyday products like cookware and waterproof clothing.^{289–292} Given the broad relevance of fluorination in various scientific domains, exploring new fluorinated molecular scaffolds and understanding their chemical and physical characteristics is a crucial avenue of research. We hypothesised that introducing tetrahalopyridine (THP) groups, including tetrafluoropyridine (TFP), into various compound classes (such as ethers, thioethers, and amines) that are traditionally challenging to crystallise, could promote the formation of highly crystalline materials. This approach positions THP installation as a complement to conventional crystallisation methods such as salt formation,^{293–295} co-crystallisation,²⁹⁶ introduction of *para*-bromo or *para*-nitro aryl functionalities,^{297–300} and the use of "crystal sponges" (porous complexes).³⁰¹ Notably, this synthetic approach employs readily available reagents and operates under mild conditions without necessitating product purification, potentially offering advantages over other methodologies in the field.

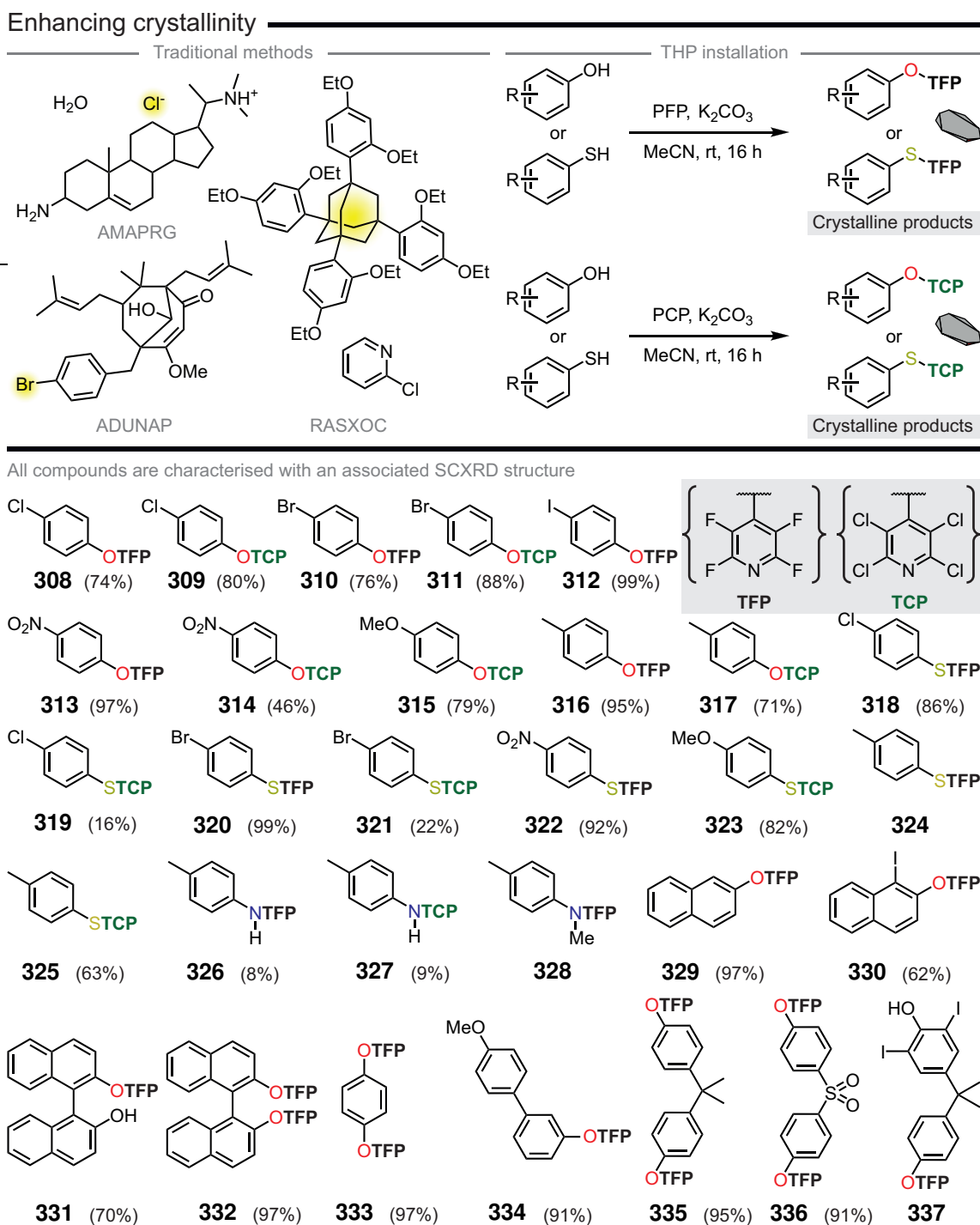


Figure 7.4: Traditional methods for enhancing crystallinity and TFP and TCP derivatisation as a supplementary tool.

* This section is based on a draft manuscript in collaboration with: Callum S. Begg, Viktoriya G. Drago-manova, Dmitry S. Yufit, Toby J. Blundell, Matthew O. Kitching*, Steven L. Cobb* and William D. G. Brittain*. Callum S. Begg performed SCXRD experiments on the library of compounds and wrote the draft manuscript.

7.4. TETRAHALOPYRIDYL CRYSTALLINITY

The analysis of compounds derivatised with a tetrahalopyridyl group revealed a diverse array of stabilising interactions in the solid state facilitated by the presence of this functionality. These interactions encompassed $X\cdots X$ halogen bonds (with distances less than the sum of Van der Waals radii), $X\cdots\pi$ interactions (with distances less than 4 Å), $N\cdots\pi$ interactions (with distances less than 4 Å), $\pi\cdots\pi$ interactions (with distances less than 4 Å), and $N\cdots H$ interactions (with distances less than the sum of Van der Waals radii). The nature and relative strength of these interactions were contingent upon the specific substituent groups present on the aromatics to be derivatised and the halogen's identity on the THP group, whether it be fluorine or chlorine.

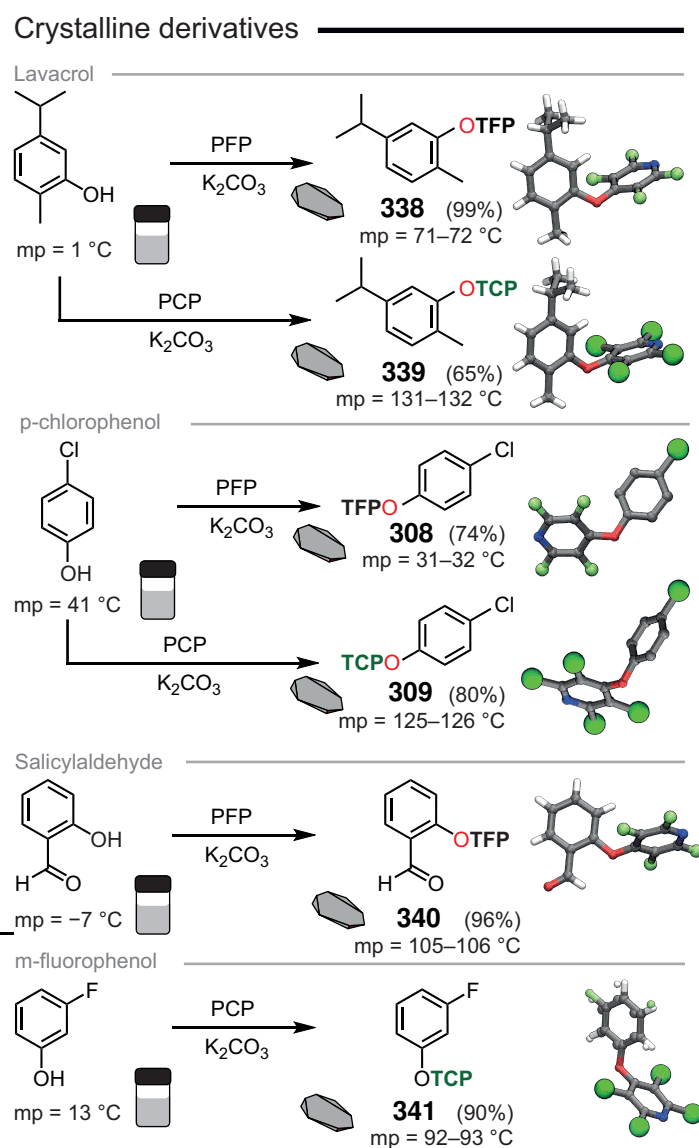


Figure 7.5: Enhancing crystallinity and increasing melting point through and TFP and TCP derivatisation.

Absolute chirality

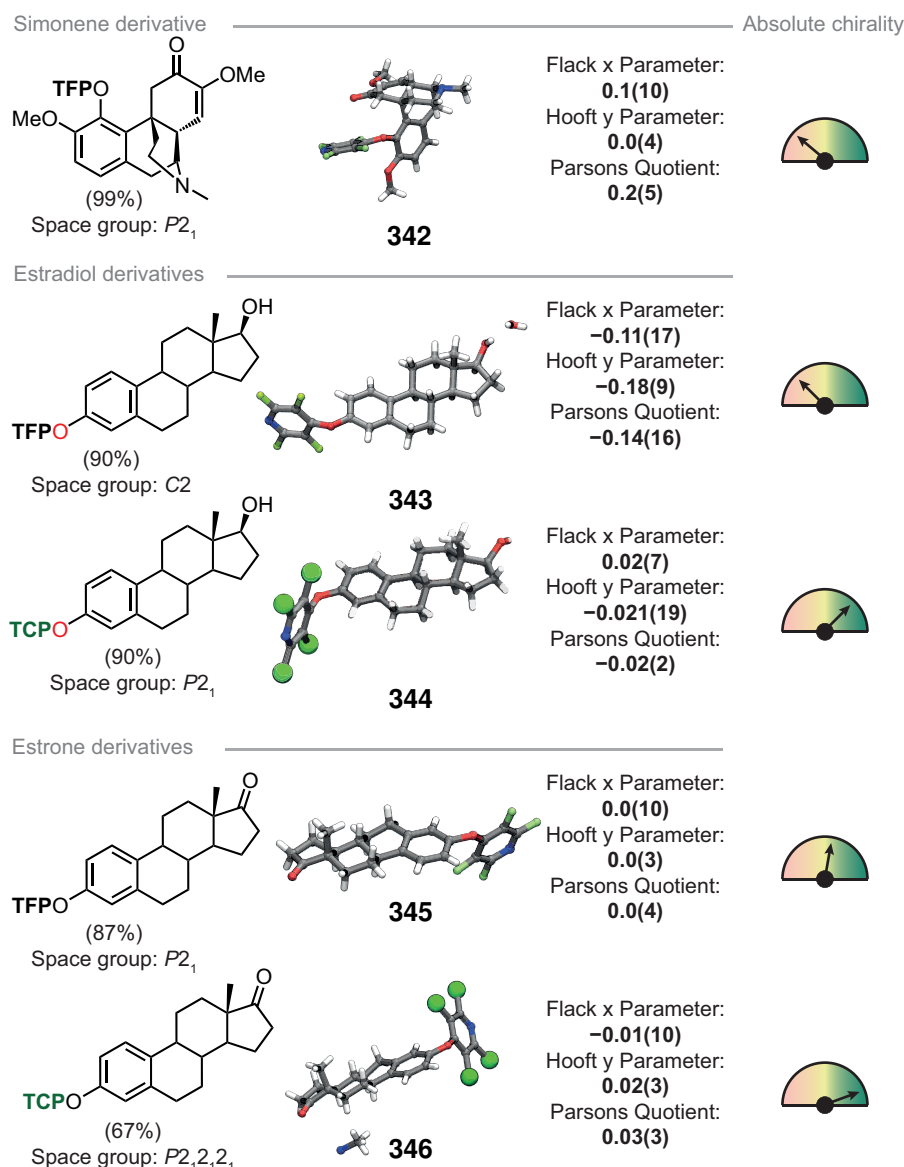


Figure 7.6: Determining absolute chirality through and TFP and TCP derivatisation.

Utilising the stabilising interactions facilitated by tetrahalopyridyl groups in the solid state, we then explored their application in synthetic chemistry, by employing THP as synthetic tags to enhance the crystallinity of materials that are typically non-crystalline. By introducing THP groups, liquid monoterpene phenolic natural product Lavacrol was successfully modified to produce compounds **338** and **339** in high yield (99% and 65% respectively). Notably, both **338** and **339** exhibited significantly increased melting points (71–72 °C and 131–132 °C) compared to the parent phenol (1 °C). This transformation from liquid to crystalline solid was replicated in other compounds such as

7.4. TETRAHALOPYRIDYL CRYSTALLINITY

p-chlorophenol, salicylaldehyde, and *m*-fluorophenol, showing a notable increase in melting points upon THP installation (see Figure 7.5.). Furthermore, the incorporation of the TCP group led to a more substantial increase in melting point compared to TFP analogues, aligning with observed trends in packing energies.

Due to the localisation of electron density onto the halogen atoms substituted on the THP ring the functional groups can also behave as synthetic handles for absolute determination of chirality via SCXRD. The reduction of TFP-estrone (**345**) to TFP-estradiol (**343**) is known to be diastereoselective but the absolute configuration of the newly generated stereocentre is unconfirmed by NMR spectroscopic analysis. Through recrystallising this material in CH₂Cl₂ the structure was successfully determined to be (*S*) at the hydroxyl carbon with a flack parameter of (−0.11(17)) which allowed us to tentatively assign the absolute structure of the compound. Given the heightened crystallinity observed with TCP derivatives and the increased electron density of chlorine atoms compared to fluorine, we postulated that integrating a TCP group could provide more useful in the ascertaining of absolute configuration (see Figure 7.6.). While the TCP group offers superior parameters for determining chirality, its relatively more challenging installation compared to TFP renders it less suitable for utilisation with certain substrates.

In summary, THP groups demonstrate a general facile installability and an ability to transform liquids into crystalline solids. Additionally, TCP groups act as a valuable tool for determining the absolute chirality of compounds, while TFP groups are more easily deployable and versatile for incorporation across a broad range of molecular scaffolds.

Chapter 8

Future work

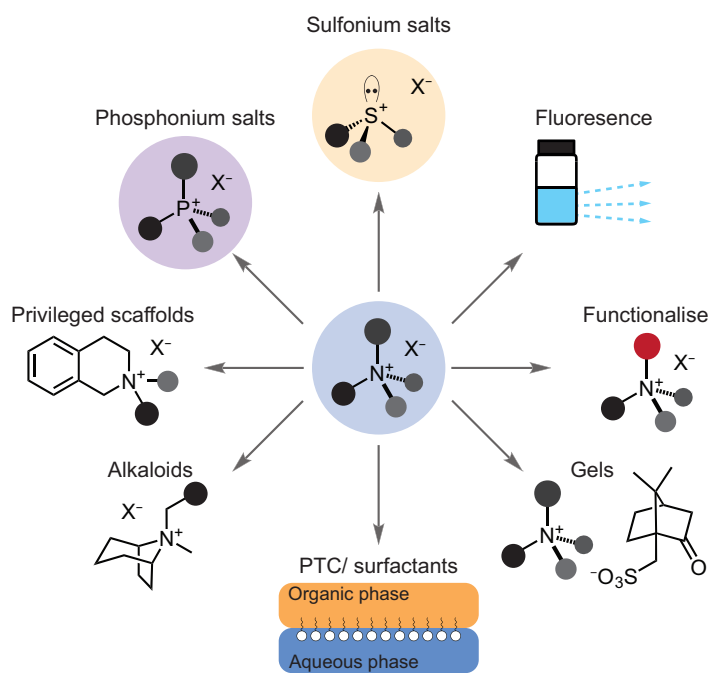


Figure 8.1: Future research based on enantioenriched ammonium cations.

8.1 Application of enantioenriched ammonium salts

Future investigations could focus on advancing the derivatisation and rearrangement chemistry of enantioenriched ammonium salts, aiming to yield more synthetically and practically valuable molecular entities. These derivatised scaffolds could be used as chiral phase transfer catalysts, surfactants or in a plethora of other applications. Additionally, an exploration into the potential of ammonium salts to serve as novel chiral organic fluorescence and phosphorescence electronics could be undertaken, with a particular emphasis on fluorescence. A promising avenue includes perovskite synthesis on dicationic quaternary ammonium salts, offering the prospect of a novel family of metal-free chiral organic ferroelectrics.

Empirical observations have also highlighted the preferential gel formation of quaternary ammonium salts with (*R*)-camphorsulfonic acid, dependent on the sense of the *N*-stereocentre. This phenomenon could be investigated and the rheology quantified, presenting a unique methodology for the development of chiral gels. Notably, it has been observed that quaternary ammonium cations are unable to cross the blood-brain barrier. This observation suggests a potential advantage in drug delivery design, particularly in the context of incorporating these cations into therapeutics that form gels with sulfonic acid-containing drugs, such as ursodoxicoltaurine. This approach could potentially hold promise for the treatment of diseases such as amyotrophic lateral sclerosis.³⁰³ The chirality of the *N*-stereocentre is anticipated to exert influence on both the morphology of any potential gel and its interaction with the homochiral biological system, underscoring the significance of *N*-stereocentre chirality.

8.2 Enantioselective synthesis of other scaffolds

The dynamic behaviour of ammonium cations, coupled with BINOL complexation, presents a viable avenue for synthesising and controlling the stereochemistry of the nitrogen stereocentre in natural alkaloids, including tropane and camphidine. The method of racemisation and epimerisation could also be adapted from the S_N2 /retro- S_N2 like procedure to allow improved synthesis of these molecular architectures. More-

over, while the kinetic resolution of tetrahydroisoquinolinium salts has been established (by Sam F. Fidler, MChem report, 2022), enhancing this methodology requires obtaining and optimising conditions for the dynamic kinetic resolution of tetrahydroisoquinolinium bromides. Achieving reversible alkylation and dealkylation under dynamic conditions, potentially employing similar conditions to Valentin,¹⁷¹ is pivotal for enabling a one-pot enantioselective synthesis of these privileged scaffolds.

8.3 Expansion to additional heteroatoms

Boron, silicon, phosphorus, sulfur, and oxygen have been documented as stereogenic elements in the literature.^{1,22–27} The cationic variants of phosphorus and sulfur, specifically phosphonium and sulfonium cations, emerge as viable options for extending the established CIAT methodology and governing the stereochemistry of these stereocentres. Notably, phosphonium salts, within this framework, have demonstrated recognition by (*R*)-BINOL, as evidenced by Walsh and Kitching,³⁰⁴ indicating the potential for extending this recognition to enable enantioselective synthesis similar to ammonium salts. Initial findings also indicate that sulfonium salts can be prepared using a comparable CIAT-like methodology, although further investigations are required to validate their enantioenrichment and utility. The envisaged applications of these salts encompass enantioselective ylide formation and their role in the synthesis of *S*-adenosylmethionine (SAM).

8.4 High throughput crystallography

Examination of the compiled conglomerate list indicates a significant occurrence of chromone-like structures. These structures can be synthesised through a straightforward three-component reaction. Utilising a high-throughput crystallography approach, this reaction can be parallelised to efficiently identify potential candidates for new spontaneously resolving materials.³⁰⁵

8.4. HIGH THROUGHPUT CRYSTALLOGRAPHY

Simple 3 component synthesis

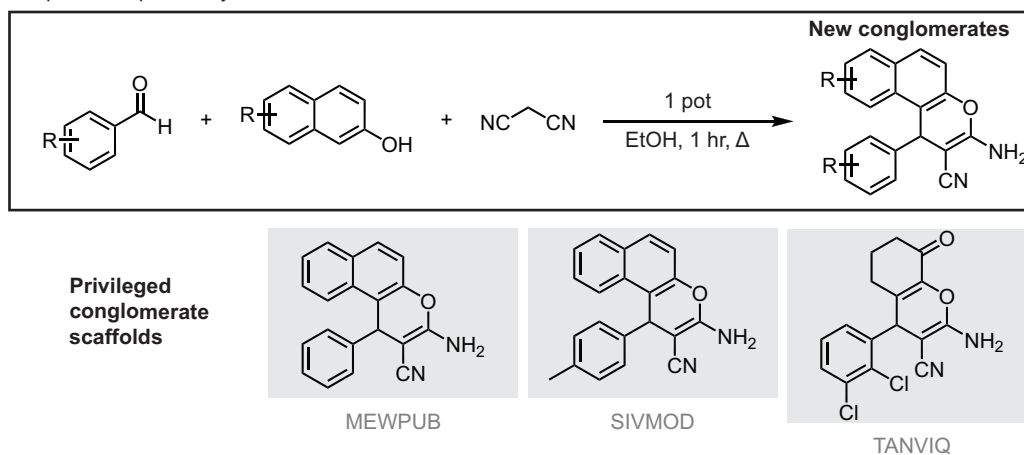


Figure 8.2: Future research into spontaneous resolution.

Chapter 9

Experimental

9.1 Experimental specifications

All reagents and solvents are commercially available (*Sigma Aldrich*, *Fisher*, *Fluorochem*, and *TCl*) and were used without further purification, unless stated otherwise. Dried solvents were obtained from in-house SPS (*Innovative Technology PureSolv MD 5* solvent purification system), or were dried using standard inert distillation procedures and were stored under Ar atmosphere and molecular sieves. Column chromatography was typically carried out using 60 Å (70 – 230 mesh) silica gel from *Fisher Scientific*. TLC was conducted using 2 cm x 5 cm aluminium backed plates coated with silica matrix (0.2 mm) and fluorescent indicator (254 nm). Visualisation of TLC was carried out using a UV lamp and/or staining (KMnO₄, PMA, ninhydrin).

Solution-state NMR spectra were recorded at 298 K on either: a *Bruker Avance III-HD-400* spectrometer with operating frequencies of 400.07 MHz for ¹H, 100.60 MHz for ¹³C, 376.45 MHz for ¹⁹F, 161.95 MHz for ³¹P; a *Bruker Avance III-HD-400* spectrometer with operating frequencies of 400.07 MHz for ¹H, 128.36 MHz, 100.60 MHz for ¹³C, 376.45 MHz for ¹⁹F, 161.95 MHz for ³¹P; a *Bruker Neo-400* spectrometer with operating frequencies of 400.20 MHz for ¹H, 100.63 MHz for ¹³C, 376.57 MHz for ¹⁹F, 162.00 MHz for ³¹P; a *Varian VNMRS-600* spectrometer with operating frequencies of 599.42 MHz for ¹H, 150.72 MHz for ¹³C, 564.02 MHz for ¹⁹F, 242.65 MHz for ³¹P; or a *Varian VNMRS-700* spectrometer with operating frequencies of 699.73 MHz for ¹H, 175.95 MHz for ¹³C, 658.41 MHz for ¹⁹F, 283.25 MHz for ³¹P. Spectra were processed using *MestReNova* (V 12.0) software. ¹H NMR Chemical shifts were referenced to residual non-deuterated solvent peaks within the NMR solvent; CHCl₃ (δH = 7.26 ppm), CH₃CN (δH = 1.94 ppm), CH₃OH (δH = 3.31 ppm), DMSO (δH = 2.50 ppm).³⁰⁶ The multiplicity of ¹H signals are indicated as: s = singlet; d = doublet; t = triplet; q = quartet; quint. = quintet; sex. = sextet; sept. = septet; m = multiplet; br = broad; apt. = apparent; and combinations thereof. Coupling constants (*J*) are quoted in Hz and are reported to the nearest 0.1 Hz. Chemical shifts for ¹³C NMR spectra

9.1. EXPERIMENTAL SPECIFICATIONS

were referenced to deuterated solvent peaks in the NMR solvent; CDCl_3 ($\delta\text{C} = 77.16$ ppm), CD_3CN ($\delta\text{C} = 1.32$ ppm), CD_3OD ($\delta\text{C} = 49.00$ ppm), $\text{DMSO}-d_6$ ($\delta\text{C} = 39.52$ ppm).³⁰⁶ All ^{13}C resonances are reported to the nearest 0.1 ppm in general, or to 0.01 ppm to aid in the differentiation of closely resolved signals.

All mass spectrometry was carried out using tandem Acquity UPLC (*Waters Ltd*) and a TQD with ESI mass spectrometer (set to EI^+ mode and EI^- mode where appropriate). The UPLC was equipped with an Acquity UPLC BEH C_{18} 1.7 μm (2.1 mm x 50 mm) column, and mobile phase composition of H_2O containing formic acid (0.1% v/v): methanol mobile phase (gradient elution; $t = 0$ min, 95% : 0%, $t = 4$ min, 5% : 95%), set at 0.6 mL min^{-1} .

X-ray single crystal data was collected using $\lambda\text{MoK}\alpha$ radiation ($\lambda = 0.71073$ Å) on an *Agilent XCalibur* (Sapphire-3 CCD detector, fine-focus sealed tube, graphite monochromator) and *Bruker D8 Venture* (Photon100 CMOS detector, μm Microsource, focusing mirrors). Diffractometers are equipped with the *Cryostream* (Oxford Cryosystems) open-flow nitrogen cryostats at a temperature of 120.0 K. All structures were solved by direct methods and refined by full-matrix least squares on F2 for all data using *Olex2*³⁰⁷ and *SHELXTL*^{308,309} software. Non-disordered non-hydrogen atoms were refined anisotropically, the hydrogen atoms were placed in the calculated positions and refined in riding mode. Crystallographic data and related CIFs for the structures related to submitted publications have been deposited with the Cambridge Crystallographic Data Centre as supplementary publications: Chapter 2 - CCDC 2283502 – 2283521, 2283524 – 2283544.

Optical rotation measurements (α) were conducted on a *Schmidt & Haensch UniPol L2000* polarimeter, equipped with a 589.44 nm Na light source. The temperature was controlled using a *Brookfield TC-550MX* circulating water bath, and a jacketed 100 mm quartz cell. Samples were prepared using HPLC grade solvents. Rotation measurements were repeated in quadruplicate and are reported as an average specific rotation ($[\alpha]_D$), along with the concentration (c) and solvent used for the measurement.

Solid-state NMR spectra were acquired using a *Bruker Avance III-HD*-spectrometer

equipped with a wide-bore 9.4 or 11.7 T magnet. At 9.4 T, Larmor frequencies of 39.20 MHz and 400.13 MHz were used for ^{35}Cl and ^1H respectively. At 11.7 T, Larmor frequencies of 49.00 MHz, 125.76 MHz, and 500.13 MHz were used for ^{13}C , ^{35}Cl , and ^1H respectively. All samples were finely ground and packed into 4 or 1.9 mm ZrO_2 rotors and magic-angle spinning (MAS) rates of either 8, 10, 20 or 40 kHz were applied. ^1H and ^{13}C chemical shifts were referenced using adamantane and ^{35}Cl chemical shifts were referenced to 0.1 M $\text{NaCl}_{(\text{aq})}$. At 9.4 T, ^1H MAS NMR spectra were acquired using a background suppression (DEPTH) experiment with typical $\pi/2$ and π pulse lengths of 2.4 μs and 5.2 μs , respectively and a recycle delay of 4 s. At 11.7 T, ^1H MAS NMR spectra were obtained using a single pulse experiment with an optimised pulse length of 3.4 μs and a recycle delay of 7 s. ^{13}C cross-polarization (CP) MAS NMR spectra were acquired using a 1 ms contact time and total sideband suppression using TOSS. ^{35}Cl MAS NMR spectra were acquired using a *Hahn-echo* pulse sequence ($90_x\text{-}\tau\text{-}180_y$) with optimised 90_x pulse lengths of 2.6 μs and 4.0 μs at 9.4 and 11.7 T respectively and an optimised recycle delay of 0.6 s.

Powder X-ray diffraction experiments were performed with a *Bruker* d8 diffractometer using $\text{Cu K}\alpha_1$ ($\lambda = 1.54056 \text{ \AA}$) radiation. Samples were ground in mortar and pestle prior to being applied to a moderately greased slide using a 250 micron sieve. Diffraction patterns were acquired over a $2\theta = 10 - 75^\circ$ in steps of 0.02 degrees. Predicted PXRD plots were generated from the appropriate .cif files using *Mercury 2020.3.0* (Build 298224), ensuring that the predicted spectrum was predicted using Cu radiation ($\lambda = 1.54056 \text{ \AA}$).

Melting points of solid and crystalline products were measured using a *Sanyo Gallenkamp* variable heater equipped with a 300 $^\circ\text{C}$ mercury thermometer. Melting points are uncorrected and solvents of crystallisation are listed along with the observed melting point range where appropriate.

Infra-red spectra were acquired using a *Perkin Elmer* Spectrum 100 FT-IR spectrometer equipped with a UATR attachment and CsI window. Spectra were recorded from a range of 4,000 – 380 cm^{-1} . Absorbance shape and intensity are described as w = weak; m = medium; s = strong; sh = sharp; br = broad.

9.1. EXPERIMENTAL SPECIFICATIONS

The enantiomeric excesses (ee%) of resolution products determined by HPLC analyses were performed on a *Waters Arc* UHPLC with a diode array detector and an *Astec CHIROBIOTIC V* Chiral HPLC column (25 cm × 4.6 mm); using buffered methanol solution (MeOH:AcOH:TEA, 100:0.02:0.01) as a mobile phase (reverse phase). The wavelength of UV-detection was set at 210 nm and analyses were conducted in an isocratic and isothermal (4 °C) manner. Flow rates were adjusted between 0.1 – 0.5 mL min⁻¹ as appropriate.

COMPACT code was used to generate similarity scores between different crystal structures using the ‘Crystal packing similarity...’ in *Mercury* 2020.3.0 (Build 298224).¹⁹³ For each structure comparison 20 molecules within each crystal were analysed with a 50% leniency on both bond angle and bond length when assigning a match. These raw comparisons were compiled together and the similarity scores for the matches between crystal structures depicted on a heatmap matrix using *MATLAB*. Crystallographic data and related CIFs for structures related to *rac*-BINOL and (*R*)-BINOL in the COMPACT similarity matrix were accessed from the Cambridge Crystallographic Data Centre as supplementary publications with codes: BIRCOC01 and WANNII respectively. The images for the overlaid BINOL-counterion networks within each packing family was done using *Hermes 1.10.4* where the structure overlay was done manually within the program to align the BINOL-counterion networks.

Distances and angles within the crystal structures were determined using *Mercury* 2020.3.0 (Build 298224). Errors, when provided, are denoted in parentheses following the respective measurement values. However, for hydrogen atoms, whose positions were calculated and refined using the riding mode and therefore lack associated measurement errors, the error related to the distance to the nearest anisotropically refined atom is specified alongside the measurement. The influence of individual measurement errors on the average isostructural distances and angles was disregarded due to the predominance of the standard deviation of these averages over the errors associated with individual distances and angles.

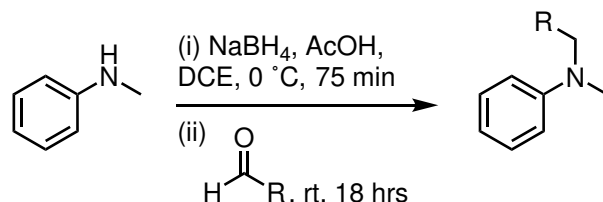
Apparent cation volumes were determined by deleting the ammonium cation(s)

from the crystal structure using *Mercury* 2020.3.0 (Build 298224) and saving the coordinates of the remaining BINOL and counterion as a .mol2 file. Subsequently, this file was reloaded into *Mercury* 2020.3.0 (Build 298224), and the 'Voids...' tool was employed to calculate the void within the structure excluding the cation (using a 0.2 Å Probe Radius, 0.2 Å Approx. Grid Spacing, and calculated with the Contact Surface method). This calculated volume was then divided by Z to represent the maximum theoretical volume available for the ammonium cation to occupy in each crystal structure.

Crystal explorer v17.5 was used to generate Hirshfeld surface plots for specific interactions (C-H—halogen, C-H—O and C-H—H). These plots were re-coloured in *Adobe Illustrator v26.0.1*. Composite Hirshfeld surface plots can be made from individual plots by overlaying the plots with others defined to be in the same isostructure and scaling the opacity of each plot.

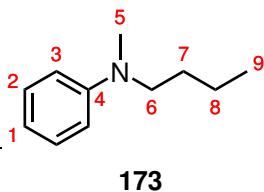
9.2 Tertiary aniline synthesis

9.2.1 General procedure for reductive amination: A



Scheme 9.1: Reductive amination adapted from Clayden *et al.* for the synthesis of tertiary aniline compounds.

Adapted from Clayden *et al.*³¹⁰ NaBH₄ (1.5 equiv.) and dry DCE (0.3 M) were added to an oven-dried dry 2-necked round bottom flask charged with a flow of argon or nitrogen. The suspension was cooled to 0 °C using an ice bath, and glacial acetic acid (4.5 equiv.) was added slowly, whilst ensuring the reaction temperature was maintained below 5 °C. The mixture was allowed to react for 30 minutes at 0 °C before being warmed to rt. and subsequently being allowed to react for a further 45 minutes. *N*-methyl aniline (1.0 equiv.) was added, along with another addition of glacial acetic acid (1.5 equiv.). After the mixture was fully mixed, the desired aldehyde (1.5 equiv.) was added dropwise. The reaction was allowed to react at room temperature for 16 hours before diluting with distilled water (40 mL) and neutralised with NaOH pellets. The reaction mixture was extracted with EtOAc (3 x 40 mL) and the combined organic phases were washed with brine (40 mL), dried with MgSO₄, concentrated and purified by flash column chromatography (hexanes:EtOAc) to afford the desired tertiary aniline product.

***N*-methyl, *N*-butylaniline**

Following the general procedure outlined in 9.2.1 using *N*-methylaniline (4.95 mL, 46.7 mmol, 1.0 equiv.) and butyraldehyde (6.31 mL, 70.0 mmol, 1.5 equiv.). Purification by flash column chromatography (hexanes) afforded **173** as a pale yellow oil (5.78 g, 76% yield).

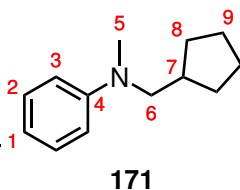
^1H NMR (599 MHz, CDCl_3) δ 7.28 – 7.22 (2H, m, H_2), 6.73 (2H, d, $J = 8.6$ Hz, H_3), 6.70 (1H, t, $J = 7.0$ Hz, H_1), 3.36 – 3.31 (2H, m, H_6), 2.95 (3H, s, H_5), 1.59 (2H, tt, $J = 7.7, 6.6$ Hz, H_7), 1.37 (2H, apt. sext., $J = 7.4$ Hz, H_8), 0.98 (3H, t, $J = 7.4$ Hz, H_9).

^{13}C NMR (151 MHz, CDCl_3) δ 149.5 (C_4), 129.3 (C_2), 115.9 (C_1), 112.2 (C_3), 52.7 (C_6), 38.4 (C_5), 29.0 (C_7), 20.5 (C_8), 14.2 (C_9).

LRMS (ESI-TOF) m/z : 164.7 ($[\text{M}+\text{H}]^+$, 100%).

HRMS (ESI-TOF) m/z : $[\text{M}+\text{H}]^+$ calculated for $\text{C}_{11}\text{H}_{18}\text{N}^+$: 164.1439, found 164.1441.

IR ($\text{max}/\text{cm}^{-1}$): 2958br, 1598m, 1505s, 744s, 690m.

***N*-methyl, *N*-homocyclopentylaniline**

Following the general procedure outlined in 9.2.1 using *N*-methylaniline (2.00 mL, 18.5 mmol, 1.0 equiv.) and cyclopentanecarboxaldehyde (2.10 mL, 19.7 mmol, 1.1 equiv.). Purification by flash column chromatography (hexanes) afforded **171** as a pale yellow oil (2.15 g, 49% yield).

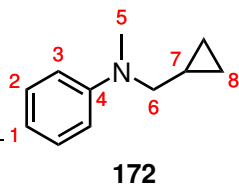
^1H NMR (599 MHz CDCl_3) δ 7.33 – 7.28 (2H, m, H_2), 6.78 (2H, d, $J = 8.7$ Hz, H_3), 6.75 (1H, t, $J = 7.1$ Hz, H_1), 3.34 – 3.31 (2H, d, $J = 7.3$ Hz, H_6), 3.03 (3H, s, H_5), 2.40 – 2.31 (1H, m, H_7), 1.87– 1.78 (2H, m, H_8), 1.77 – 1.68 (2H, m, H_9), 1.67 – 1.58 (2H, m, H_9'), 1.35 – 1.27 (2H, m, H_8').

^{13}C NMR (151 MHz, CDCl_3) δ 149.7 (C_4), 129.2 (C_2), 115.8 (C_1), 112.1 (C_3), 57.9 (C_6), 39.1 (C_5), 39.0 (C_7), 30.9 (C_8), 25.1 (C_9).

LRMS (ESI-TOF) m/z : 190.7 ($[\text{M}+\text{H}]^+$, 100%).

HRMS (ESI-TOF) m/z : $[\text{M}+\text{H}]^+$ calculated for $\text{C}_{13}\text{H}_{20}\text{N}^+$: 190.1596, found 190.1596.

IR ($\text{max}/\text{cm}^{-1}$): 2949m, 1597m, 1505s, 744s, 690m.

***N*-methyl, *N*-homocyclopropylaniline**

Following the general procedure outlined in 9.2.1 using *N*-methylaniline (3.25 mL, 30.0 mmol, 1.0 equiv.) and cyclopropanecarboxaldehyde (3.50 mL, 46.8 mmol, 1.6 equiv.). Purification by flash column chromatography (hexanes) afforded **172** as a pale yellow oil (2.37 g, 63% yield).

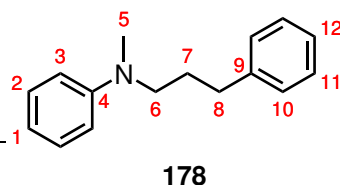
^1H NMR (599 MHz, CDCl_3) δ 7.28 – 7.20 (2H, m, H_2), 6.85 – 6.79 (2H, d, $J = 8.6$ Hz, H_3), 6.72 (1H, t, $J = 7.3$ Hz, H_1), 3.23 (2H, d, $J = 6.3$ Hz, H_6), 2.99 (3H, s, H_5), 1.09 – 0.96 (1H, m, H_7), 0.58 – 0.44 (2H, m, H_8), 0.28 – 0.18 (2H, m, H_8).

^{13}C NMR (151 MHz, CDCl_3) δ 149.8 (C_4), 129.1 (C_2), 116.3 (C_1), 112.7 (C_3), 57.1 (C_6), 38.4 (C_5), 8.8 (C_7), 3.3 (C_8).

LRMS (ESI-TOF) m/z : 162.5 ($[\text{M}+\text{H}]^+$, 100%).

HRMS (ESI-TOF) m/z : $[\text{M}+\text{H}]^+$ calculated for $\text{C}_{11}\text{H}_{16}\text{N}^+$: 162.1283, found 162.1280.

IR (max/ cm^{-1}): 3000m, 1597m, 1504s, 743s, 690m.

***N*-methyl, *N*-hydrocinnamylaniline**

Following the general procedure outlined in 9.2.1 using *N*-methylaniline (4.95 mL, 46.7 mmol, 1.0 equiv.) and hydrocinnamaldehyde (9.21 mL, 70.0 mmol, 1.5 equiv.). Purification by flash column chromatography (hexanes) afforded **178** as a pale yellow oil (7.49 g, 71% yield).

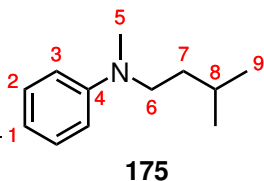
^1H NMR (599 MHz, CDCl_3) δ 7.41 – 7.35 (2H, m, H_{11}), 7.33 – 7.27 (4H, m, H_{2+10}), 7.27 – 7.26 (1H, m, H_{12}), 6.81 – 6.73 (3H, m, H_{1+3}), 3.45 – 3.40 (2H, m, H_6), 3.00 (3H, s, H_5), 2.74 (2H, t, $J = 7.7$ Hz, H_8), 2.05 – 1.96 (2H, apt. p, $J = 7.4$, H_7).

^{13}C NMR (151 MHz, CDCl_3) δ 149.4 (C_4), 141.9 (C_9), 129.3 (C_2), 128.48 (C_{10}), 128.45 (C_{12}), 126.0 (C_{11}), 116.2 (C_1), 112.3 (C_3), 52.3 (C_6), 38.4 (C_5), 33.4 (C_8), 28.3 (C_7).

LRMS (ESI-TOF) m/z : 226.9 ($[\text{M}+\text{H}]^+$, 100%).

HRMS (ESI-TOF) m/z : $[\text{M}+\text{H}]^+$ calculated for $\text{C}_{16}\text{H}_{20}\text{N}^+$: 226.1596, found 226.1601.

IR (max/ cm^{-1}): 2948m, 1598m, 1506s, 744s, 691s.

***N*-methyl, *N*-isovalerylaniline**

Following the general procedure outlined in 9.2.1 using *N*-methylaniline (4.95 mL, 46.7 mmol, 1.0 equiv.) and isovaleraldehyde (7.51 mL, 70.0 mmol, 1.5 equiv.). Purification by flash column chromatography (hexanes) afforded **175** as a pale yellow oil (6.87 g, 83% yield).

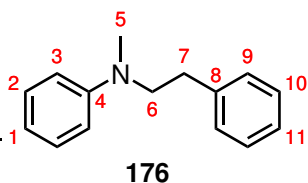
^1H NMR (599 MHz, CDCl_3) δ 7.23 (2H, t, $J = 7.9$ Hz, H_2), 6.70 (2H, d, $J = 7.9$ Hz, H_3), 6.67 (1H, t, $J = 7.2$ Hz, H_1), 3.33 (2H, m, H_6), 2.92 (3H, s, H_5), 1.61 (1H, sept., $J = 6.3$ Hz, H_8), 1.48 – 1.43 (2H, m, H_7), 0.95 (6H, d, $J = 6.3$ Hz, H_9).

^{13}C NMR (151 MHz, CDCl_3) δ 149.5 (C_4), 129.3 (C_2), 116.0 (C_1), 112.3 (C_3), 51.2 (C_6), 38.3 (C_5), 35.3 (C_7), 26.4 (C_8), 22.8 (C_9).

LRMS (ESI-TOF) m/z : 178.4 ($[\text{M}+\text{H}]^+$, 100%).

HRMS (ESI-TOF) m/z : $[\text{M}+\text{H}]^+$ calculated for $\text{C}_{12}\text{H}_{20}\text{N}^+$: 178.1596, found 178.1596.

IR ($\text{max}/\text{cm}^{-1}$): 2955m, 1599m, 1506s, 745s, 689s.

***N*-methyl, *N*-phenylacetylaniline**

Following the general procedure outlined in 9.2.1 using *N*-methylaniline (4.95 mL, 46.7 mmol, 1.0 equiv.) and phenylacetaldehyde (7.79 mL, 70.0 mmol, 1.5 equiv.). Purification by flash column chromatography (hexanes) afforded **176** as a pale yellow oil which solidified upon cooling (7.22

g, 73% yield).

^1H NMR (599 MHz, CDCl_3) δ 7.36 – 7.28 (2H, m, H_{10}), 7.30 – 7.25 (3H, m, H_{2+11}), 7.24 (2H, d, $J = 7.9$ Hz, H_9), 6.77 (2H, d, $J = 7.9$ Hz, H_3), 6.74 (1H, t, $J = 7.2$ Hz, H_1), 3.62 – 3.56 (2H, m, H_6), 2.92 (3H, s, H_5), 2.90 – 2.85 (2H, t, $J = 7.6$ Hz, H_7).

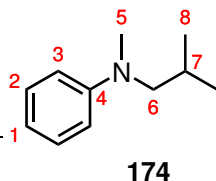
^{13}C NMR (151 MHz, CDCl_3) δ 149.0 (C_4), 140.0 (C_8), 129.4 (C_2), 129.0 (C_{10}), 128.7 (C_9), 126.3 (C_{11}), 116.3 (C_1), 112.3 (C_3), 54.9 (C_6), 38.6 (C_5), 33.1 (C_7).

LRMS (ESI-TOF) m/z : 212.7 ($[\text{M}+\text{H}]^+$, 100%).

HRMS (ESI-TOF) m/z : $[\text{M}+\text{H}]^+$ calculated for $\text{C}_{15}\text{H}_{18}\text{N}^+$: 212.1439, found 212.1447.

IR ($\text{max}/\text{cm}^{-1}$): 2932m, 1596m, 1503m, 1227w, 1191w, 738s, 692s, 494s.

mp: 29 °C (hexanes precipitate).

***N*-methyl, *N*-isobutylaniline**

Following the general procedure outlined in 9.2.1 using *N*-methylaniline (4.95 mL, 46.7 mmol, 1.0 equiv.) and isobutyraldehyde (6.39 mL, 70.0 mmol, 1.5 equiv.). Purification by flash column chromatography (hexanes) afforded **174** as a pale yellow oil (6.97 g, 91% yield).

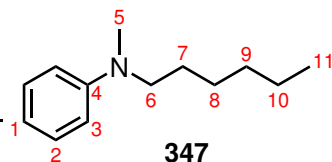
^1H NMR (599 MHz, CDCl_3) δ 7.31 – 7.25 (2H, m, H_2), 6.77 – 6.70 (3H, m, H_{1+3}), 3.15 (2H, d, $J = 7.3$ Hz, H_6), 3.01 (3H, s, H_5), 2.16 – 2.07 (1H, m, H_7), 0.99 (6H, d, $J = 6.7$ Hz, H_8).

^{13}C NMR (151 MHz, CDCl_3) δ 149.7 (C_4), 129.1 (C_2), 115.6 (C_1), 111.8 (C_3), 61.0 (C_6), 39.4 (C_5), 27.4 (C_7), 20.5 (C_8).

LRMS (ESI-TOF) m/z : 164.6 ($[\text{M}+\text{H}]^+$, 100%).

HRMS (ESI-TOF) m/z : $[\text{M}+\text{H}]^+$ calculated for $\text{C}_{11}\text{H}_{18}\text{N}^+$: 164.1439, found 164.1438.

IR ($\text{max}/\text{cm}^{-1}$): 2956m, 1598m, 1505s, 993w, 744s, 689m.

***N*-methyl, *N*-hexylaniline**

Following the general procedure outlined in 9.2.1 using *N*-methylaniline (5.06 mL, 46.7 mmol, 1.0 equiv.) and hexanal (8.60 mL, 56.2 mmol, 1.2 equiv.). Purification by flash column chromatography (hexanes) afforded **347** as a pale yellow oil (8.88 g, 99% yield).

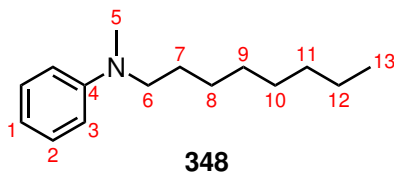
^1H NMR (599 MHz, CDCl_3) δ 7.32 – 7.25 (2H, m, H_2), 6.79 – 6.71 (3H, m, H_{1+3}), 3.39 – 3.33 (2H, m, H_6), 2.98 (3H, s, H_5), 1.63 (2H, tt, $J = 7.3, 5.8$ Hz, H_7), 1.43 – 1.35 (6H, m, H_{8+9+10}), 0.96 (3H, t, $J = 4.4$ Hz, H_{11}).

^{13}C NMR (151 MHz, CDCl_3) δ 149.5 (C_4), 129.2 (C_2), 115.9 (C_1), 112.2 (C_3), 53.0 (C_6), 38.4 (C_5), 31.9 (C_8), 27.0 (C_9), 26.8 (C_7), 22.8 (C_{10}), 14.2 (C_{11}).

LRMS (ESI-TOF) m/z : 192.3 ($[\text{M}+\text{H}]^+$, 100%).

HRMS (ESI-TOF) m/z : $[\text{M}+\text{H}]^+$ calculated for $\text{C}_{13}\text{H}_{22}\text{N}^+$: 192.1752, found 192.1760.

IR ($\text{max}/\text{cm}^{-1}$): 2927m, 1599m, 1506s, 990m, 745s, 690s, 513w..

***N*-methyl, *N*-octylaniline**

Following the general procedure outlined in 9.2.1 using *N*-methylaniline (5.06 mL, 46.7 mmol, 1.0 equiv.) and octanal (10.94 mL, 70.5 mmol, 1.5 equiv.). Purification by flash column chromatography (hexanes) afforded **348** as a pale yellow oil

(10.09 g, 99% yield).

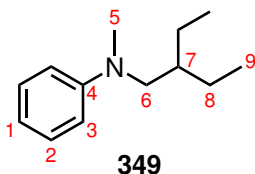
^1H NMR (599 MHz, CDCl_3) δ 7.32 (2H, t, $J = 9.1$ Hz, H_2), 6.81 – 6.75 (3H, m, H_{1+3}), 3.39 (2H, dd, $J = 9.4, 6.8$ Hz, H_6), 3.01 (3H, s, H_5), 1.67 (2H, q, $J = 6.9$ Hz, H_7), 1.45 – 1.34 (10H, m, $\text{H}_{8+9+10+11+12}$), 1.00 (3H, t, $J = 7.1$ Hz, H_{13}).

^{13}C NMR (151 MHz, CDCl_3) δ 149.5 (C_4), 129.4 (C_2), 116.0 (C_1), 112.2 (C_3), 53.0 (C_6), 38.3 (C_5), 32.0 (C_8), 29.7 (C_9), 29.4 (C_{10}), 27.3 (C_{11}), 26.8 (C_7), 22.8 (C_{12}), 14.2 (C_{13}).

LRMS (ESI-TOF) m/z : 220.3 ($[\text{M}+\text{H}]^+$, 100%).

HRMS (ESI-TOF) m/z : $[\text{M}+\text{H}]^+$ calculated for $\text{C}_{15}\text{H}_{26}\text{N}^+$: 220.2065, found 220.2070.

IR (max/cm $^{-1}$): 2923br 2852m, 1598m, 1505s, 991w, 744s, 689s, 513w..

***N*-methyl, *N*-2-ethylbutylaniline**

Following the general procedure outlined in 9.2.1 using *N*-methylaniline (5.06 mL, 46.7 mmol, 1.0 equiv.) and 2-ethylbutyraldehyde (9.36 mL, 76.1 mmol, 1.6 equiv.). Purification by flash column chromatography (hexanes) afforded **347** as a pale yellow oil (7.51 g, 84% yield).

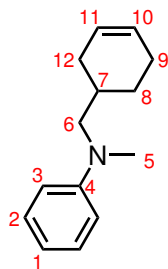
^1H NMR (599 MHz, CDCl_3) δ 7.28 – 7.22 (2H, m, H_2), 6.74 – 6.67 (3H, m, H_{1+3}), 3.21 (2H, d, $J = 7.4$ Hz, H_6), 2.97 (3H, s, H_5), 1.74 (1H, sept., $J = 6.8$ Hz, H_7), 1.47 – 1.31 (4H, m, H_8), 0.94 (6H, t, $J = 7.5$ Hz, H_9).

^{13}C NMR (151 MHz, CDCl_3) δ 150.0 (C_4), 129.2 (C_2), 115.7 (C_1), 112.0 (C_3), 57.0 (C_6), 39.51 (C_5), 39.47 (C_7), 23.6 (C_8), 10.9 (C_9).

LRMS (ESI-TOF) m/z : 192.3 ($[\text{M}+\text{H}]^+$, 100%).

HRMS (ESI-TOF) m/z : $[\text{M}+\text{H}]^+$ calculated for $\text{C}_{13}\text{H}_{21}\text{N}^+$: 192.1752, found 192.1755.

IR (max/cm $^{-1}$): 2961m, 1598m, 1505s, 993m, 745s, 690s, 514w.

rac-N-methyl, N-homocyclohex-2-enyl aniline

Following the general procedure outlined in 9.2.1 using *N*-methylaniline (4.95 mL, 46.7 mmol, 1.0 equiv.) and cyclohex-2-enecarboxaldehyde (8.20 mL, 70.0 mmol, 1.5 equiv.). Purification by flash column chromatography (hexanes) afforded **350** as a pale yellow oil (7.47 g, 80% yield).

$^1\text{H NMR}$ (599 MHz, CDCl_3) δ 7.23 (2H, t, $J = 7.9$ Hz, H_2), 6.71 (2H, d, $J = 8.0$ Hz, H_3), 6.68 (1H, t, $J = 7.2$ Hz, H_1), 5.72 – 5.64 (2H, m, H_{10+11}), 3.26 (1H, dd, $J = 7.3, 6.7$ Hz, H_6), 3.20 (1H, dd, $J = 7.3,$

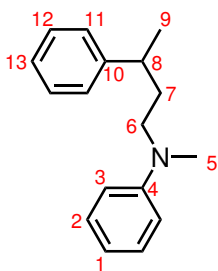
6.7 Hz, H_6), 2.98 (3H, s, H_5), 2.15 – 1.99 (4H, m, H_{7+8+12}), 1.85 – 1.78 (1H, m, H_9), 1.79 – 1.71 (1H, m, H_8), 1.35 – 1.25 (1H, m, H_9).

$^{13}\text{C NMR}$ (151 MHz, CDCl_3) δ 149.8 (C_4), 129.2 (C_2), 127.3 (C_{11}), 126.1 (C_{10}), 115.8 (C_1), 112.0 (C_3), 58.8 (C_6), 39.6 (C_5), 32.9 (C_{12}), 29.7 (C_8), 26.9 (C_9), 24.9 (C_7).

LRMS (ESI-TOF) m/z : 202.7 ($[\text{M}+\text{H}]^+$, 100%).

HRMS (ESI-TOF) m/z : $[\text{M}+\text{H}]^+$ calculated for $\text{C}_{14}\text{H}_{20}\text{N}^+$: 202.1596, found 202.1610.

IR ($\text{max}/\text{cm}^{-1}$): 2901m, 1597m, 1505s, 744s, 691m, 654m.

***rac-N*-methyl, *N*-3-phenylbutyl aniline****351**

Following the general procedure outlined in 9.2.1 using *N*-methylaniline (4.95 mL, 46.7 mmol, 1.0 equiv.) and 3-phenylbutyraldehyde (11.38 mL, 70.0 mmol, 1.5 equiv.). Purification by flash column chromatography (hexanes) afforded **351** as a pale yellow oil (7.78 g, 70% yield).

^1H NMR (599 MHz, CDCl_3) δ 7.52 – 7.48 (2H, m, H_{12}), 7.42 – 7.37 (5H, m, $\text{H}_{2+11+13}$), 6.87 (1H, tt, $J = 7.2, 0.9$ Hz, H_1), 6.81 – 6.77 (2H, m, H_3), 3.46 – 3.40 (1H, m, H_6), 3.38 – 3.32 (1H, m, H_6), 3.03 (3H, s, H_5), 2.95 – 2.87 (1H, m, H_8), 2.09 – 2.02 (2H, m, H_7), 1.48 (3H, d, $J = 7.0$ Hz, H_9).

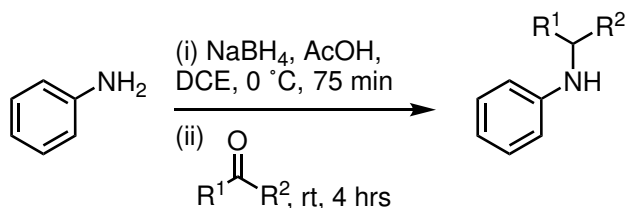
^{13}C NMR (151 MHz, CDCl_3) δ 148.8 (C_4), 146.5 (C_{10}), 129.0 (C_2), 128.3 (C_{12}), 126.8 (C_{11}), 126.0 (C_{13}), 115.8 (C_1), 112.0 (C_3), 50.9 (C_6), 38.0 (C_5), 37.8 (C_8), 34.2 (C_7), 22.7 (C_9).

LRMS (ESI-TOF) m/z : 240.9 ($[\text{M}+\text{H}]^+$, 100%).

HRMS (ESI-TOF) m/z : $[\text{M}+\text{H}]^+$ calculated for $\text{C}_{17}\text{H}_{22}\text{N}^+$: 240.1752, found 240.1761.

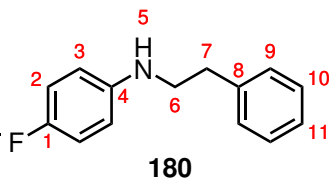
IR ($\text{max}/\text{cm}^{-1}$): 2961m, 1598m, 1505s, 745s, 689s.

9.2.2 General procedure for reductive amination: B



Scheme 9.2: Reductive amination adapted from Clayden *et al.* for the synthesis of secondary aniline compounds.

Adapted from Clayden *et al.*³¹⁰ NaBH₄ (1.5 equiv.) and dry DCE (0.3 M) were added to a dry 2-necked round bottom flask charged with a flow of argon or nitrogen. The suspension was cooled to 0 °C using an ice bath, and glacial acetic acid (4.5 equiv.) was added slowly to ensure the temperature was maintained below 5 °C. The reaction mixture was allowed to react for 30 minutes at 0 °C before being warmed to rt. and allowed to react for a further 45 minutes. The desired aniline (1.0 equiv.) was added, along with another addition of glacial acetic acid (1.5 equiv.). After the mixture was fully mixed, the desired ketone (1.5 equiv.) was added dropwise. The reaction was allowed to react at room temperature for 4 – 16 hrs before diluting with distilled water (40 mL) and quenched with NaOH pellets. The reaction mixture was extracted with EtOAc (3 x 40 mL) and the combined organic phases were washed with brine (40 mL), dried with MgSO₄, concentrated and purified by flash column chromatography (hexanes:EtOAc) to afford the desired secondary aniline product.

4-fluoro-*N*-phenylacetylaniline

Following the general procedure outlined in 9.2.2 using 4-fluoroaniline (3.34 g, 30.1 mmol, 1.0 equiv.) and phenylacetaldehyde (1.48 mL, 20.0 mmol, 1.0 equiv.). Purification by flash column chromatography (hexanes:EtOAc, 98:2) afforded **180** as a yellow oil (4.18 g, 65% yield).

^1H NMR (700 MHz, CDCl_3) δ 7.22 – 7.18 (2H, m, H_9), 7.15 – 7.11 (1H, m, H_{11}), 7.10 (2H, d, $J = 7.5$ Hz, H_{10}), 6.77 (2H, t, $J = 8.4$ Hz, H_3), 6.40 (2H, dd, $J = 8.9, 4.4$ Hz, H_2), 3.35 (1H, s, H_5), 3.22 (2H, t, $J = 7.0$ Hz, H_6), 2.77 (2H, t, $J = 7.0$ Hz, H_7).

^{13}C NMR (176 MHz, CDCl_3) δ 155.9 (d, $J = 233.4$ Hz, C_1), 144.4 (C_4), 139.3 (C_8), 128.9 (C_9), 128.6 (C_{10}), 126.6 (C_{11}), 115.8 (d, $J = 23.0$ Hz, C_3), 113.9 (d, $J = 7.6$ Hz, C_2), 45.8 (C_6), 35.5 (C_7).

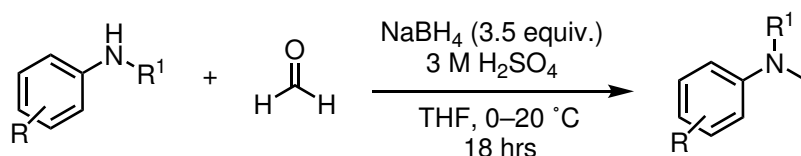
^{19}F NMR (376 MHz, CDCl_3) δ -127.87.

LRMS (ESI-TOF) m/z : 216.2 ($[\text{M}+\text{H}]^+$, 100%).

HRMS (ESI-TOF) m/z : $[\text{M}+\text{H}]^+$ calculated for $\text{C}_{14}\text{H}_{15}\text{NF}^+$: 216.1189, found 216.1181.

IR ($\text{max}/\text{cm}^{-1}$): 3409br, 2942m, 1508s, 1213m, 1254m, 818s, 698s, 495m.

9.2.3 General procedure for reductive amination: C



Scheme 9.3: Reductive amination adapted from Walsh *et al.* for the synthesis of tertiary aniline compounds.

Adapted from Walsh *et al.*² The relevant aniline (1.0 equiv.) and powdered NaBH₄ (3.5 equiv.) are combined and made into a slurry with THF (0.5 M). A second solution composed of 37% aqueous formaldehyde (3.0 equiv.), 3 M H₂SO₄ (1 mL per 1 mmol of aniline) and THF (0.2 M) was prepared and chilled to 0 °C. The aniline/NaBH₄ slurry was then added slowly to the acidic formaldehyde solution slowly, so as to maintain a reaction temperature of less than 20 °C. Once half of the aniline mixture has been added the pH of the reaction is checked and additional 3 M H₂SO₄ is added if the pH greater than 2. Once all of the aniline has been added (over the course of 30 minutes), the reaction is removed from the ice bath and is allowed to stir at room temperature overnight.

The reaction mixture is diluted with 50 mL of water and is made strongly basic using solid NaOH pellets. The basic reaction mixture is then extracted with diethyl ether (3 x 20 mL), dried with MgSO₄ and concentrated to give the tertiary aniline product.

***N*-methyl, *N*-isopropylaniline****183**

Following the general procedure outlined in 9.2.3 using *N*-isopropyl aniline (2.00 g, 14.8 mmol, 1.0 equiv.). Purification by flash column chromatography (hexanes:EtOAc, 96:4) afforded **183** as a pale yellow oil (1.90 g, 86% yield).

^1H NMR (400 MHz, CDCl_3) δ 7.29 – 7.21 (2H, m, H_2), 6.81 (2H, d, $J = 8.3$ Hz, H_3), 6.71 (1H, t, $J = 7.5$ Hz, H_1), 4.11

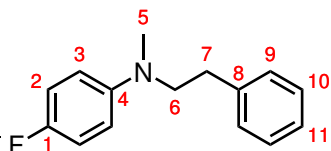
(1H, sept., $J = 6.6$ Hz, H_5), 2.74 (3H, s, H_7), 1.18 (6H, d, $J = 6.3$ Hz, H_6).

^{13}C NMR (101 MHz, CDCl_3) δ 150.3 (C_4), 129.2 (C_2), 116.6 (C_1), 113.5 (C_3), 49.1 (C_5), 29.9 (C_7), 19.4 (C_6).

LRMS (ESI-TOF) m/z : 150.1 ($[\text{M}+\text{H}]^+$, 100%).

HRMS (ESI-TOF) m/z : $[\text{M}+\text{H}]^+$ calculated for $\text{C}_{10}\text{H}_{16}\text{N}^+$: 150.1283, found 150.1276.

IR (max/ cm^{-1}): 2999m, 2976m, 1491m, 1382w, 1117m, 1001m, 959m, 790s, 552m.

4-fluoro-*N*-methyl, *N*-phenylacetylaniline**182**

Following the general procedure outlined in 9.2.3 using **180** (4.18 g, 19.4 mmol, 1.0 equiv.). Purification by flash column chromatography (hexanes) afforded **182** as a colourless oil, which solidified upon cooling (2.81 g, 63% yield).

^1H NMR (599 MHz, CDCl_3) δ 7.33 – 7.29 (2H, m, H_{10}), 7.25 – 7.22 (1H, m, H_{11}), 7.22 – 7.19 (2H, m, H_9), 6.97 (2H, t, $J = 8.7$ Hz, H_3), 6.71 – 6.63 (2H, m, H_2), 3.53 (2H, dd, $J = 8.2, 7.2$ Hz, H_6), 2.87 (3H, s, H_5), 2.84 (2H, dd, $J = 9.0, 6.5$ Hz, H_7).

^{13}C NMR (151 MHz, CDCl_3) δ 155.5 (d, $J = 229.8$ Hz, C_1), 145.7 (C_4), 139.9 (C_8), 128.9 (C_{10}), 128.7 (C_9), 126.4 (C_{11}), 115.7 (d, $J = 22.9$ Hz, C_3), 113.6 (br, C_2), 55.6 (C_6), 39.0 (C_5), 32.9 (C_7).

^{19}F NMR (376 MHz, CDCl_3) δ -129.58.

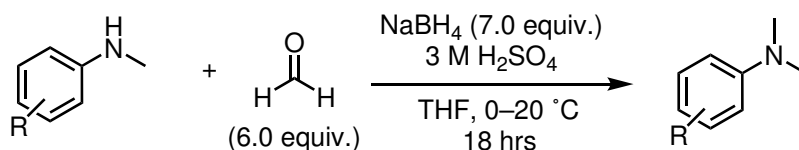
LRMS (ESI-TOF) m/z : 230.1 ($[\text{M}+\text{H}]^+$, 100%).

HRMS (ESI-TOF) m/z : $[\text{M}+\text{H}]^+$ calculated for $\text{C}_{15}\text{H}_{17}\text{NF}^+$: 230.1345, found 230.1348.

IR (max/ cm^{-1}): 2936w, 1509m, 1221m, 810s, 751m, 704s, 494s.

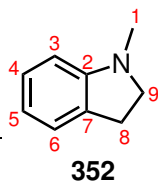
mp: 40 °C (hexanes precipitate).

9.2.4 General procedure for reductive amination: D

Scheme 9.4: Reductive amination adapted from Giumanini *et al.*

Adapted from Giumanini *et al.* reported reductive amination procedure.³¹¹ Aniline (1.0 equiv.) and powdered NaBH₄ (7.0 equiv.) are combined and made into a slurry with THF (0.3 M). A second solution composed of 37% aqueous formaldehyde (6.0 equiv.), 3 M H₂SO₄ (2 mL per 1 mmol of aniline) and THF (0.3 M) is prepared and chilled to 0 °C. The aniline/NaBH₄ slurry is then added slowly to the acidic formaldehyde solution, so as to maintain a reaction temperature less than 20 °C. Once half of the aniline mixture has been added, the pH of the reaction is checked and additional 3 M H₂SO₄ is added if the pH is greater than 2. Once all of the aniline has been added, the reaction is removed from the ice bath and is allowed to stir at room temperature overnight.

The reaction mixture is diluted with 40 mL of water, and is made strongly basic using solid NaOH pellets. The basic reaction mixture is then extracted with diethyl ether (3 x 20 mL), dried with MgSO₄ and concentrated to give crude permethylated tertiary aniline product, which was purified using a silica gel plug (hexanes/EtOAc).

N-methylindoline

Following the method outlined in 9.2.1 using indoline (3.0 mL, 26.7 mmol) and purification using a silica gel plug (hexane), afforded the methylated indoline **352** as a yellow oil (0.89 g, 25% yield).

^1H NMR (400 MHz, CDCl_3) δ 7.14 – 7.04 (2H, m, H_{4+6}), 6.68 (1H, td, $J = 7.4, 1.0$ Hz, H_5), 6.51 (1H, dd, $J = 8.1, 1.0$ Hz, H_3), 3.30 (2H, t, $J = 8.1$ Hz, H_9), 2.95 (2H, t, $J = 8.1$ Hz, H_8), 2.77 (3H, s, H_1).

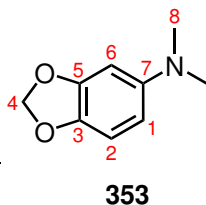
^{13}C NMR (101 MHz, CDCl_3) δ 153.5 (C_2), 130.4 (C_7), 127.4 (C_4), 124.4 (C_6), 117.9 (C_5), 107.4 (C_3), 56.3 (C_9), 36.4 (C_1), 28.9 (C_8).

LRMS (ESI-TOF) m/z : 134.1 ($[\text{M}+\text{H}]^+$, 100%).

HRMS (ESI-TOF) m/z : $[\text{M}+\text{H}]^+$ Calculated for $\text{C}_9\text{H}_{12}\text{N}^+$: 134.0970, found 134.0977.

IR ($\nu_{\text{max}}/\text{cm}^{-1}$): 2992w, 2949m, 2808m, 1609s, 1266s, 742s.

This compound was also synthesised by Emmanuelle F. Fiandra.

N,N-dimethyl-3,4-(methylenedioxy)aniline

Following the method outlined in 9.2.1 using 3,4-(methylenedioxy)aniline (2.98 g, 21.8 mmol) and purification using a silica gel plug (95:5 hexane:EtOAc), afforded the permethylated tertiary aniline **353** as a brown oil (2.76 g, 77% yield).

^1H NMR (400 MHz, CDCl_3) δ 6.74 (1H, d, $J = 8.51$ Hz, H_2), 6.44 (1H, d, $J = 2.50$, H_6), 6.19 (1H, dd, $J = 8.51, 2.50$ Hz, H_1), 5.88 (2H, s, H_4), 2.87 (6H, s, H_8).

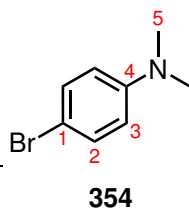
^{13}C NMR (101 MHz, CDCl_3) δ 148.3 (C_7), 147.2 (C_5), 139.4 (C_3), 108.4 (C_6), 105.2 (C_2), 100.7 (C_1), 96.5 (C_4), 41.9 (C_8).

LRMS (ESI-TOF) m/z : 166.4 ($[\text{M}+\text{H}]^+$, 100%).

HRMS (ESI-TOF) m/z : $[\text{M}+\text{H}]^+$ Calculated for $\text{C}_9\text{H}_{12}\text{NO}_2^+$: 166.0851, found 166.0868.

IR ($\nu_{\text{max}}/\text{cm}^{-1}$): 2874m, 1631w, 1504s, 1319w, 1224s, 1035s, 933s, 813s.

This compound was also synthesised by Emmanuelle F. Fiandra and Emma F.G. Winful.

4-bromo-*N,N*-dimethylaniline

Following the method outlined in 9.2.1 using 4-bromoaniline (3.08 g, 17.9 mmol) and purification using a silica gel plug (99:1 hexane:EtOAc), afforded the permethylated tertiary aniline **354** as an off-white solid (2.96 g, 83% yield).

^1H NMR (400 MHz, CDCl_3) δ 7.30 (2H, dt, $J = 9.3, 2.4$ Hz, H_2), 6.59 (2H, dt, $J = 9.3, 2.4$ Hz, H_3), 2.93 (6H, s, H_5).

^{13}C NMR (101 MHz, CDCl_3) δ 149.6 (C_4), 131.8 (C_2), 114.2 (C_3), 108.6 (C_1), 40.7 (C_5).

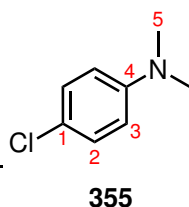
LRMS (ESI-TOF) m/z : 201.3 ($[\text{M}+\text{H}]^+$, 100%).

HRMS (ESI-TOF) m/z : $[\text{M}+\text{H}]^+$ Calculated for $\text{C}_8\text{H}_{11}\text{BrN}^+$: 200.0075, found 200.0084.

IR ($\nu_{\text{max}}/\text{cm}^{-1}$): 2976m, 2808m, 1583m, 1441m, 1353m, 803s, 500m.

mp: 48 – 50 °C (EtOAc/hexanes).

This compound was also synthesised by Emmanuelle F. Fiandra.

4-chloro-*N,N*-dimethylaniline

Following the method outlined in 9.2.1 using 4-chloroaniline (2.93 g, 23.0 mmol) and purification using a silica gel plug (99:1 hexane:EtOAc), afforded the permethylated tertiary aniline **355** as a yellow oil which later solidified (2.41 g, 68% yield).

^1H NMR (400 MHz, CDCl_3) δ 7.18 (2H, dt, $J = 9.1, 2.2$ Hz, H_2), 6.64 (2H, dt, $J = 9.1, 2.2$ Hz, H_3), 2.93 (6H, s, H_5).

^{13}C NMR (101 MHz, CDCl_3) δ 149.6 (C_4), 129.2 (C_1), 121.8 (C_2), 114.1 (C_3), 41.1 (C_5).

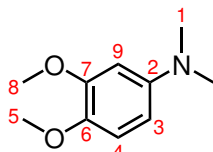
LRMS (ESI-TOF) m/z : 156.9 ($[\text{M}+\text{H}]^+$, 100%).

HRMS (ESI-TOF) m/z : $[\text{M}+\text{H}]^+$ Calculated for $\text{C}_8\text{H}_{11}\text{ClN}^+$: 156.0580, found 156.0569.

IR ($\nu_{\text{max}}/\text{cm}^{-1}$): 2876m, 2798m, 1596m, 809s, 611s.

mp: 30 – 32 °C (EtOAc/hexanes).

This compound was also synthesised by Emmanuelle F. Fiandra.

***N,N*-dimethyl, 3,4-dimethoxyaniline****356**

Following the method outlined in 9.2.1 using 3,4-dimethoxyaniline (3.02 g, 19.7 mmol) and purification using a silica gel plug (4:1 hexane:EtOAc), afforded the permethylated tertiary aniline **356** as an off-white solid (2.83 g, 79% yield).

^1H NMR (400 MHz, CDCl_3) δ 6.81 (1H, d, $J = 8.7$ Hz, H_4), 6.42 (1H, d, $J = 2.8$ Hz, H_9), 6.29 (1H, dd, $J = 8.7, 2.8$ Hz, H_3), 3.88 (3H, s, H_8), 3.82 (3H, s, H_5), 2.89 (6H, s, H_1).

^{13}C NMR (101 MHz, CDCl_3) δ 149.8 (C_2), 146.5 (C_7), 141.6 (C_6), 113.0 (C_3), 104.9 (C_4), 99.6 (C_9), 56.7 (C_8), 55.9 (C_5), 41.9 (C_1).

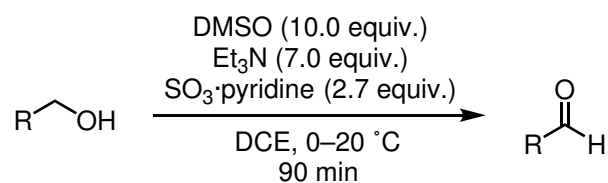
LRMS (ESI-TOF) m/z : 182.5 ($[\text{M}+\text{H}]^+$, 100%).

HRMS (ESI-TOF) m/z : $[\text{M}+\text{H}]^+$ Calculated for $\text{C}_{10}\text{H}_{16}\text{NO}_2^+$: 182.1181, found 182.1187.

IR ($\nu_{\text{max}}/\text{cm}^{-1}$): 2991m, 1581m, 1234s, 815s, 680m.

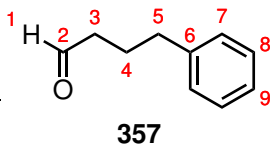
mp: 56 – 58 °C (EtOAc/hexanes).

This compound was also synthesied by Emmanuelle F. Fiandra.

9.2.5 General procedure for oxidation of primary alcohols

Scheme 9.5: Selective oxidation of primary alcohol to aldehyde adapted from Parikh *et al.*

Adapted from Parikh *et al.*³¹² The desired alcohol (1.0 equiv.), anhydrous Et₃N (7.0 equiv.) and DMSO dried over 4 Å molecular sieves (10.0 equiv.) were added to an oven-dried 2-necked round bottom flask charged with a flow of argon or nitrogen. The solution was cooled to 0 °C. To a second oven-dried 2-necked round bottom flask charged with a flow of argon or nitrogen was added sulphur trioxide pyridine complex (2.7 equiv.) which was subsequently dissolved into dry CH₂Cl₂ (0.8 M). The sulphur trioxide pyridine complex solution was added dropwise to the solution of alcohol at 0 °C, before being allowed to warm to room temperature and left to react for 90 minutes. The reaction was quenched by the addition of distilled water (40 mL), extracted with CH₂Cl₂ (3 x 40 mL), washed with water (3 x 40 mL) and brine (3 x 40 mL) and dried over MgSO₄. The crude product was purified by flash column chromatography (hexanes:EtOAc) to afford the desired aldehyde product.

4-phenyl-1-butyraldehyde

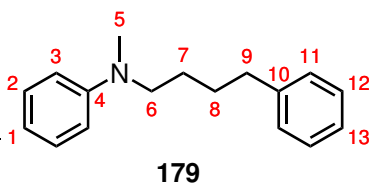
Following the general procedure outlined in 9.2.5 using 4-phenyl-1-butanol (4.92 g, 32.8 mmol, 1.0 equiv.). Purification by flash column chromatography (hexanes:EtOAc, 30:1) afforded **357** as a colourless oil (2.99 g, 61% yield).

^1H NMR (599 MHz, CDCl_3) δ 9.76 (1H, s, H_1), 7.34 – 7.28 (2H, m, H_8), 7.28 – 7.17 (3H, m, H_{7+9}), 2.67 (2H, t, $J = 7.6$ Hz, H_5), 2.46 (2H, td, $J = 7.3, 1.7$ Hz, H_3), 1.98 (2H, p, $J = 7.6$ Hz, H_4).

^{13}C NMR (151 MHz, CDCl_3) δ 202.3 (C_2), 141.3 (C_6), 128.50 (C_7), 128.49 (C_8), 126.1 (C_9), 43.1 (C_3), 35.0 (C_5), 23.7 (C_4).

IR (max/ cm^{-1}): 2940w, 1721s, 1454w, 747m, 699s, 491m.

Data consistent with literature values.³¹³

***N*-methyl, *N*-4-phenylbutylaniline**

Following the general procedure outlined in 9.2.1 using *N*-methylaniline (1.90 mL, 17.5 mmol, 1.0 equiv.) and **357** (2.56 g, 17.3 mmol, 1.0 equiv.). Purification by flash column chromatography (hexanes) afforded **179** as an orange oil (2.23

g, 54% yield).

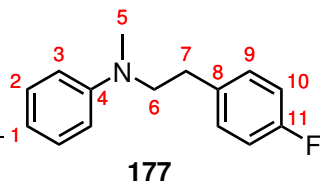
^1H NMR (700 MHz, CDCl_3) δ 7.33 (2H, apt. t, $J = 7.8$ Hz, H_{12}), 7.30 – 7.26 (2H, m, H_2), 7.26 – 7.22 (3H, m, H_{11+13}), 6.76 – 6.71 (3H, m, H_{1+3}), 3.40 – 3.35 (2H, m, H_9), 2.96 (3H, s, H_5), 2.70 (2H, t, $J = 7.3$ Hz, H_6), 1.75 – 1.65 (4H, m, H_{7+8}).

^{13}C NMR (176 MHz, CDCl_3) δ 149.4 (C_4), 142.4 (C_{10}), 129.3 (C_2), 128.5 (C_{11}), 128.4 (C_{12}), 125.9 (C_{13}), 116.0 (C_1), 112.2 (C_3), 52.8 (C_9), 38.4 (C_5), 35.9 (C_6), 29.2 (C_7), 26.5 (C_8).

LRMS (ESI-TOF) m/z : 240.2 ($[\text{M}+\text{H}]^+$, 100%).

HRMS (ESI-TOF) m/z : $[\text{M}+\text{H}]^+$ calculated for $\text{C}_{17}\text{H}_{22}\text{N}^+$: 240.1752, found 240.1763.

IR (max/ cm^{-1}): 2937w, 1598s, 1504s, 744s, 692s, 516w.

***N*-methyl, *N*-4-fluoro-phenylacetylaniline**

Following the general procedure outlined in 9.2.5 using 4-fluorophenethyl alcohol (3.20 mL, 25.6 mmol, 1.0 equiv.) was afforded crude 4-fluorophenylacetylaldehyde as a yellow oil. Following the general procedure outlined in 9.2.1 using *N*-methylaniline (2.87 mL, 26.5 mmol, 1.1 equiv.)

and crude 4-fluorophenylacetylaldehyde (3.33 g, 24.0 mmol, 1.0 equiv.) yielded crude **177**. The crude tertiary aniline was dissolved into Et₂O and cooled to 0 °C. 37% HCl was added dropwise until a precipitate was observed and the solution filtered. The resulting solid was dissolved into 15% NaOH_(aq), extracted with CHCl₃ (3 x 20 mL) and washed with 15% NaOH_(aq) (3 x 20 mL), H₂O (3 x 20 mL) and brine (3 x 20 mL). Purification by flash column chromatography (hexanes) afforded **177** as an orange oil which solidified upon cooling and was pure enough for further synthesis (2.36 g, 40% yield).

¹H NMR (700 MHz, CDCl₃) δ 7.35 – 7.30 (2H, m, H₃), 7.24 – 7.19 (2H, m, H₁₀), 7.08 – 7.01 (2H, m, H₉), 6.85 – 6.75 (3H, m, H₁₊₃), 3.60 (2H, t, J = 7.7 Hz, H₆), 2.92 (3H, s, H₅), 2.89 (2H, t, J = 7.5 Hz, H₇).

¹³C NMR (176 MHz, CDCl₃) δ 162.3 (d, J = 244.0 Hz, C₁₁), 148.8 (C₄), 135.6 (d, J = 3.0 Hz, C₈), 130.3 (d, J = 7.7 Hz, C₁₀), 129.4 (C₂), 116.3 (C₁), 115.3 (d, J = 21.7 Hz, C₉), 112.2 (C₁), 54.9 (d, J = 1.2 Hz, C₆), 38.6 (C₅), 32.2 (C₇).

¹⁹F NMR (376 MHz, CDCl₃) δ –117.0

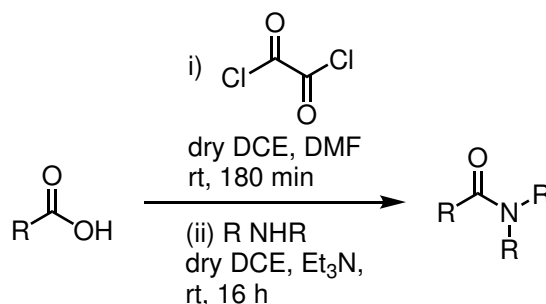
LRMS (ESI-TOF) m/z: 230.1 ([M+H]⁺, 100%).

HRMS (ESI-TOF) m/z: [M+H]⁺ calculated for C₁₅H₁₇NF⁺: 230.1345, found 230.1342.

IR (max/cm⁻¹): 2939m, 1599m, 1504s, 1355m, 1219s, 1112m, 990m, 824m, 746s, 691m, 518m.

mp: 41 °C (hexanes precipitate).

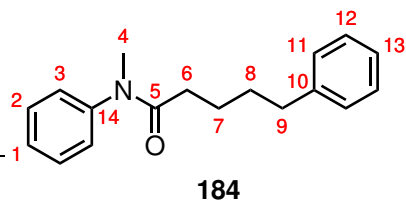
9.2.6 General procedure for amide coupling



Scheme 9.6: Coupling of carboxylic acid to aniline.

The relevant carboxylic acid (1.0 equiv.) and dry DCE (0.6 M) were added to an oven-dried 2-necked round bottom flask charged with a flow of argon or nitrogen. Oxalyl chloride (1.1 equiv.) and DMF (0.05 equiv.) were added dropwise and the solution was left to stir for 3 hours. The solvent was removed under reduced pressure to yield the crude acid chloride.

A second dry 2-necked round bottom flask was charged with a flow of argon or nitrogen and to it was added the relevant amine (1.0 equiv.), anhydrous Et₃N (2.2 equiv.) and dry DCE (1.0 M). The crude acid chloride was dissolved into dry DCE (1.0 M) and added dropwise the amine solution. The reaction was stirred overnight. The reaction was quenched by the addition of distilled water (40 mL), extracted with CH₂Cl₂ (3 x 40 mL), washed with water (3 x 40 mL) and brine (3 x 40 mL) and dried over MgSO₄. The crude product was purified by flash column chromatography (hexanes:EtOAc) to afford the desired amide product.

***N*-methyl, *N*-phenyl-5-phenylvalerylamide**

Following the general procedure outlined in 9.2.6 using 5-phenylvaleric acid (5.36 g, 30.0 mmol, 1.0 equiv.) and *N*-methyl aniline (3.25 mL, 30.6 mmol, 1.0 equiv.). Purification by flash column chromatography (hexanes:EtOAc, 3:1) afforded **184** as a pale orange oil (6.42 g, 80% yield).

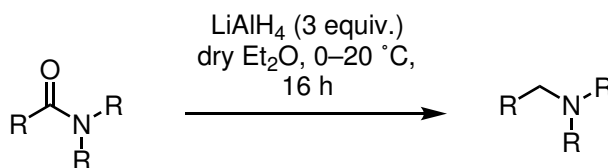
^1H NMR (599 MHz, CDCl_3) δ 7.40 (2H, dd, $J = 8.3, 7.0$ Hz, H_2), 7.33 (1H, t, $J = 7.4$ Hz, H_{13}), 7.24 (2H, t, $J = 7.6$ Hz, H_{12}), 7.18 – 7.12 (3H, m, H_{3+1}), 7.10 (2H, d, $J = 7.4$ Hz, H_{11}), 3.26 (3H, s, H_4), 2.53 (2H, t, $J = 7.7$ Hz, H_6), 2.09 (2H, t, $J = 7.1$ Hz, H_9), 1.62 (2H, p, $J = 7.4$ Hz, H_8), 1.53 (2H, p, $J = 7.4$ Hz, H_7).

^{13}C NMR (151 MHz, CDCl_3) δ 173.2 (C_5), 144.4 (C_{14}), 142.5 (C_{10}), 129.9 (C_2), 128.5 (C_{11}), 128.3 (C_{12}), 127.8 (C_{13}), 127.4 (C_1), 125.8 (C_3), 37.4 (C_4), 35.8 (C_6), 34.1 (C_9), 31.2 (C_7), 25.3 (C_8).

LRMS (ESI-TOF) m/z : 268.2 ($[\text{M}+\text{H}]^+$, 100%).

HRMS (ESI-TOF) m/z : $[\text{M}+\text{H}]^+$ calculated for $\text{C}_{18}\text{H}_{22}\text{NO}^+$: 268.1701, found 268.1707.

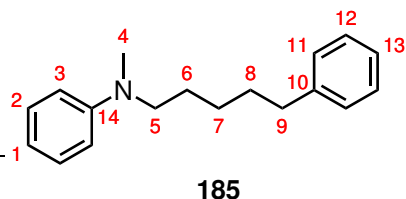
IR ($\text{max}/\text{cm}^{-1}$): 2936m, 1653s, 1495m, 1383m, 1119m, 697s, 558m, 411w.

9.2.7 General procedure for amide reduction

Scheme 9.7: Reduction of amide to aniline.

LiAlH₄ (3 equiv.) and dry Et₂O (0.3 M) were added to an oven-dried 2-necked round bottom flask charged with a flow of argon or nitrogen and cooled to 0 °C. The desired amide (1.0 equiv.) and dry Et₂O (1.0 M) were added to a second dry 2-necked round bottom flask charged with a flow of argon or nitrogen and the amide solution was added dropwise to the LiAlH₄ solution. Once the addition was complete the reaction mixture was allowed to warm to rt and left to stir for 16 hours.

The reaction was diluted with Et₂O and cooled to 0 °C. Water (x mL = g of LiAlH₄ used) was added dropwise to the reaction, followed by the addition of 15% NaOH_(aq) solution (y mL = g of LiAlH₄ used) and the addition of more water (z mL = 3 x g of LiAlH₄ used). The reaction mixture was warmed to rt and left to stir for 30 minutes. MgSO₄ was added to the reaction mixture, followed by filtering. The filtrate was reduced down under reduced pressure to yield the crude product, which was purified by flash column chromatography (hexanes:EtOAc) to afford the desired aniline product.

N-methyl, 5-phenylvalerylaniline

Following the general procedure outlined in 9.2.7 using **184** (3.41 g, 12.8 mmol, 1.0 equiv.) and LiAlH₄ (1.48 mL, 39.0 mmol, 3.0 equiv.). Purification by flash column chromatography (hexanes) afforded **185** as a colourless oil (1.31 g, 40% yield).

¹H NMR (700 MHz, CDCl₃) δ 7.33 (2H, apt. t, *J* = 8.3, 6.9 Hz, H₁₂), 7.30 – 7.25 (2H, m, H₂), 7.25 – 7.23 (1H, m, H₁₃), 7.23 – 7.20 (2H, m, H₁₁), 6.76 – 6.71 (3H, m, H₁₊₃), 3.34 (2H, t, *J* = 7.6 Hz, H₉), 2.95 (3H, s, H₄), 2.66 (2H, t, *J* = 7.7 Hz, H₅), 1.74 – 1.68 (2H, m, H₆), 1.68 – 1.61 (2H, m, H₈), 1.44 – 1.37 (2H, m, H₇).

¹³C NMR (176 MHz, CDCl₃) δ 149.4 (C₁₄), 142.7 (C₁₀), 129.3 (C₂), 128.5 (C₁₁), 128.4 (C₁₂), 125.8 (C₁₃), 115.9 (C₁), 112.2 (C₃), 52.8 (C₉), 38.4 (C₄), 36.1 (C₅), 31.5 (C₆), 26.9 (C₈), 26.6 (C₇).

LRMS (ESI-TOF) *m/z*: 254.2 ([M+H]⁺, 100%).

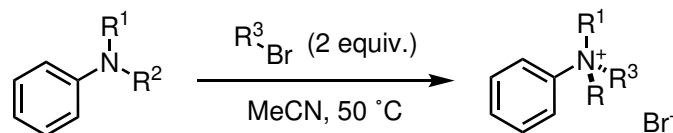
HRMS (ESI-TOF) *m/z*: [M+H]⁺ calculated for C₁₈H₂₄N⁺: 254.1909, found 254.1917.

IR (max/cm⁻¹): 2931w, 2855w, 1599m, 1505s, 744s, 690s.

For anilines and tertiary amines that haven't been characterised in this experimental section but are listed to have been alkylated to form corresponding ammonium salts in this thesis, see M.P. Walsh's thesis, E.F. Fiandra's report or E.W. Winful's report for full characterisation. Callum S. Begg synthesised these amines but did not fully characterise them due to the data already being available.

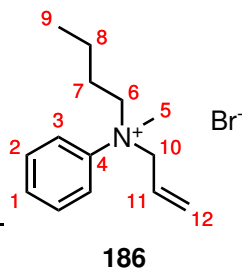
9.3 Racemic and achiral ammonium salt synthesis

9.3.1 General procedure for alkylation



Scheme 9.8: General alkylation procedure for the synthesis of quaternary ammonium salts.

Procedure adapted from Lehn *et al.*³¹⁴ The selected tertiary amine (1.0 equiv.) and MeCN (1.0 M) were added into a round bottom flask. With stirring, the desired alkylating agent (1.1 – 2.0 equiv.) was added to the tertiary aniline. The reaction mixture was then heated to 50 °C, until all starting material was consumed, and in most cases the desired salt has precipitated from the reaction. The reaction mixture was triturated with diethyl ether to ensure all the ammonium salt had precipitated. The crude solid salt was filtered and washed with diethyl ether (3 x 10 mL) to remove excess alkylating agent and unreacted amine. The quaternary ammonium salt can be recrystallised to purity using a number of solvents (MeOH, EtOH, MeOH/Et₂O, MeCN).

***N*-allyl, *N*-butyl, *N*-methyl anilinium bromide**

Following the general procedure outlined in 9.3.1 using **173** (0.33 g, 2.05 mmol, 1.0 equiv.) and allyl bromide (0.26 mL, 3.00 mmol, 1.5 equiv.) afforded **186** as a pale pink solid (0.35 g, 61% yield).

^1H NMR (599 MHz, CD_3OD) δ 7.87 (2H, d, $J = 8.2$ Hz, H_3), 7.62 (2H, t, $J = 8.2$ Hz, H_2), 7.51 (1H, t, $J = 7.6$ Hz, H_1), 5.69 – 5.60 (2H, m, $\text{H}_{11+12\text{-trans}}$), 5.55 (1H, dt, $J = 9.2$,

2.0 Hz, $\text{H}_{12\text{-cis}}$), 4.69 (1H, dd, $J = 13.3, 5.5$ Hz, H_{10}), 4.47 (1H, dd, $J = 13.0, 6.9$ Hz, H_{10}), 4.09 (1H, td, $J = 12.6, 4.3$ Hz, H_6), 3.86 (1H, td, $J = 11.8, 5.0$ Hz, H_6), 3.57 (3H, s, H_5), 1.74 – 1.63 (1H, m, H_7), 1.38 – 1.33 (2H, m, H_8), 1.25 – 1.15 (1H, m, H_7), 0.90 (3H, t, $J = 7.4$ Hz, H_9).

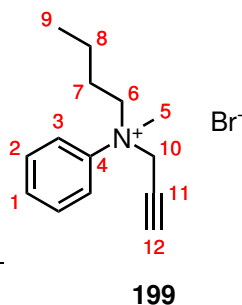
^{13}C NMR (151 MHz, CD_3OD) δ 143.4 (C_4), 131.7 (C_2), 131.6 (C_1), 129.2 (C_{12}), 126.2 (C_{11}), 122.9 (C_3), 72.5 (C_{10}), 69.0 (C_6), 47.9 (C_5), 25.9 (C_7), 20.4 (C_8), 13.8 (C_9).

LRMS (ESI-TOF) m/z : 204.2 ($[\text{M}]^+$, 100%).

HRMS (ESI-TOF) m/z : $[\text{M}]^+$ calculated for $\text{C}_{14}\text{H}_{22}\text{N}^+$: 204.1752, found 204.1758.

IR ($\text{max}/\text{cm}^{-1}$): 3462m, 3382m, 2972m, 1617w, 1462m, 938m, 860m, 769m, 565s, 487m.

mp: 82 – 83 °C (MeCN precipitate).

***N*-butyl, *N*-methyl, *N*-propargyl anilinium bromide**

Following the general procedure outlined in 9.3.1 using **173** (0.33 g, 2.00 mmol, 1.0 equiv.) and 80% propargyl bromide solution (0.34 mL, 3.82 mmol, 1.9 equiv.) afforded **199** as a pale pink solid (0.49 g, 87% yield).

^1H NMR (599 MHz, $\text{DMSO}-d_6$) δ 7.87 – 7.81 (2H, m, H_3), 7.66 (2H, t, $J = 7.8$ Hz, H_2), 7.60 (1H, t, $J = 7.3$ Hz, H_1), 5.15 (1H, dd, $J = 16.4, 2.5$ Hz, H_{10}), 4.97 (1H, dd, $J = 16.2, 2.5$ Hz, H_{10}), 4.04 (1H, apt. td, $J = 12.5, 4.6$ Hz, H_6),

3.90 (1H, apt. td, $J = 12.2, 4.8$ Hz, H_6), 3.89 – 3.85 (1H, m, H_{12}), 3.66 (3H, s, H_5), 1.57 – 1.47 (1H, m, H_7), 1.22 (2H, qp, $J = 13.5, 6.5$ Hz, H_8), 1.12 (1H, apt. ddd, $J = 13.7, 9.9, 5.5$ Hz, H_7), 0.80 (3H, t, $J = 7.3$ Hz, H_9).

^{13}C NMR (151 MHz, $\text{DMSO}-d_6$) δ 142.3 (C_4), 130.3 (C_2), 130.2 (C_1), 121.9 (C_3), 82.9

(C₁₂), 72.5 (C₁₁), 66.7 (C₁₀), 57.3 (C₆), 48.6 (C₅), 24.5 (C₇), 18.8 (C₈), 13.3 (C₉).

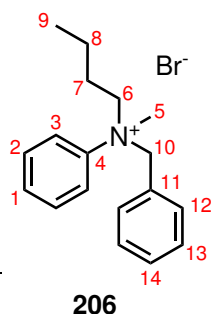
LRMS (ESI-TOF) m/z: 202.2 ([M]⁺, 100%).

HRMS (ESI-TOF) m/z: [M]⁺ calculated for C₁₄H₂₀N⁺: 202.1596, found 202.1604.

IR (max/cm⁻¹): 3156, 2939, 2119, 1463, 872, 698s.

mp: 178 – 180 °C (MeCN precipitate).

N-benzyl, *N*-butyl, *N*-methyl anilinium bromide



Following the general procedure outlined in 9.3.1 using **173** (0.331 g, 2.03 mmol, 1.0 equiv.) and benzyl bromide (0.35 mL, 2.94 mmol, 1.5 equiv.) afforded **206** as a white solid (0.369 g, 54% yield).

¹H NMR (599 MHz, CD₃OD) δ 7.74 – 7.67 (2H, m, H₂), 7.66 – 7.59 (3H, m, H₁₊₃), 7.45 – 7.39 (1H, m, H₁₄), 7.32 – 7.27 (2H, m, H₁₃), 7.07 – 7.02 (2H, m, H₁₂), 5.14 (1H, d, *J* = 12.8 Hz, H₁₀), 4.96 (1H, d, *J* = 12.8 Hz, H₁₀), 4.32 (1H,

td, *J* = 12.7, 4.3 Hz, H₆), 3.92 (1H, td, *J* = 13.1, 5.1 Hz, H₆), 3.48 (3H, s, H₅), 1.78 – 1.68 (1H, m, H₇), 1.49 – 1.33 (2H, m, H₈), 1.24 – 1.18 (1H, m, H₇), 0.93 (3H, t, *J* = 7.4 Hz, H₉).

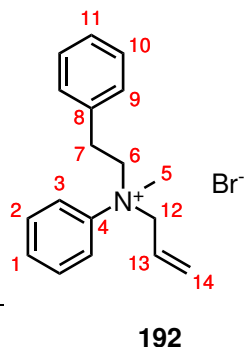
¹³C NMR (151 MHz, CD₃OD) δ 142.9 (C₄), 133.9 (C₁₂), 131.8 (C₁₄), 131.7 (C₁), 131.6 (C₂), 129.8 (C₁₃), 128.7 (C₁₁), 123.5 (C₃), 75.2 (C₁₀), 68.5 (C₆), 47.1 (C₅), 26.1 (C₇), 20.6 (C₈), 13.8 (C₉).

LRMS (ESI-TOF) m/z: 254.2 ([M]⁺, 100%).

HRMS (ESI-TOF) m/z: [M]⁺ calculated for C₁₈H₂₄N⁺: 254.1909, found 254.1911.

mp: 152 °C (MeCN precipitate).

IR (max/cm⁻¹): 2981m, 1493m, 1455m, 773m, 695s.

***N*-allyl, *N*-methyl, *N*-phenylacetyl anilinium bromide**

Following the general procedure outlined in 9.3.1 using **176** (0.43 g, 2.03 mmol, 1.0 equiv.) and allyl bromide (0.26 mL, 3.00 mmol, 1.5 equiv.) afforded **192** as a pale red solid (0.51 g, 76% yield).

$^1\text{H NMR}$ (599 MHz, CD_3OD) δ 7.93 – 7.87 (2H, d, $J = 8.5$ Hz, H_3), 7.71 (2H, t, $J = 7.1$ Hz, H_2), 7.65 (1H, t, $J = 7.3$ Hz, H_1), 7.30 (2H, t, $J = 7.2$ Hz, H_{10}), 7.27 – 7.21 (1H, m, H_{11}), 7.20 – 7.15 (2H, d, $J = 8.0$ Hz, H_9), 5.71 – 5.53 (3H, m, H_{13+14}), 4.71 (1H, dd, $J = 13.2, 5.8$ Hz, H_{12}), 4.50 (1H,

dd, $J = 12.6, 5.6$ Hz, H_{12}), 4.30 (1H, td, $J = 12.5, 4.7$ Hz, H_6), 4.09 (1H, td, $J = 12.8, 5.6$ Hz, H_6), 3.67 (3H, s, H_5), 3.04 (1H, td, $J = 12.5, 5.6$ Hz, H_7), 2.54 (1H, td, $J = 12.3, 4.7$ Hz, H_7).

$^{13}\text{C NMR}$ (151 MHz, CD_3OD) δ 143.2 (C_4), 136.7 (C_8), 131.9 (C_2), 131.8 (C_1), 130.01 (C_9), 129.95 (C_{10}), 129.4 (C_{14}), 128.4 (C_{11}), 126.1 (C_{13}), 123.0 (C_3), 72.7 (C_{12}), 69.7 (C_6), 48.0 (C_5), 30.4 (C_7).

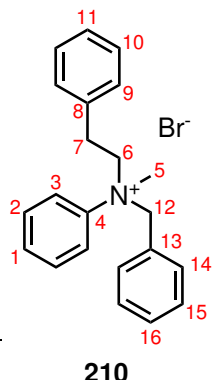
LRMS (ESI-TOF) m/z : 252.2 ($[\text{M}]^+$, 100%).

HRMS (ESI-TOF) m/z : $[\text{M}]^+$ calculated for $\text{C}_{18}\text{H}_{22}\text{N}^+$: 252.1752, found 252.1760

IR ($\text{max}/\text{cm}^{-1}$): 3406br, 3000m, 2491m, 1597m, 1497m, 1491m, 864m, 748m, 695s, 549m.

mp: 96 – 98 °C (MeCN precipitate).

XRD: A portion of the racemic ammonium salt was crystallised in H_2O and with a few drops of HBr and 1 equivalent of NH_4Cl to give clear colourless blocks. Crystal data for $\text{C}_{36}\text{H}_{46}\text{Br}_2\text{N}_2\text{O}$ ($m = 682.57$ g/mol): Monoclinic, space group $P2_1/n$ (no. 14).

***N*-benzyl, *N*-methyl, *N*-phenylacetyl anilinium bromide**

Following the general procedure outlined in 9.3.1 using **176** (0.417 g, 1.97 mmol, 1.0 equiv.) and benzyl bromide (0.35 mL, 2.94 mmol, 1.5 equiv.) afforded **210** as a white solid (0.640 g, 85% yield).

^1H NMR (599 MHz, CD_3OD) δ 7.80 (2H, dt, $J = 6.3, 1.3$ Hz, H_3), 7.72 – 7.63 (3H, m, H_{1+2}), 7.43 (1H, t, $J = 7.5$ Hz, H_{16}), 7.35 – 7.24 (5H, m, $\text{H}_{10+11+15}$), 7.21 (2H, d, $J = 7.3$ Hz, H_9), 7.05 (2H, d, $J = 8.3$ Hz, H_{14}), 5.18 (1H, d, $J = 12.8$ Hz, H_{12}), 5.00 (1H, d, $J = 12.8$ Hz, H_{12}), 4.55 (1H, td,

$J = 12.5, 4.6$ Hz, H_6), 4.19 (1H, td, $J = 13.1, 5.7$ Hz, H_6), 3.59 (3H, s, H_5), 3.09 (1H, td, $J = 12.6, 5.7$ Hz, H_7), 2.55 (1H, td, $J = 13.1, 4.6$ Hz, H_7).

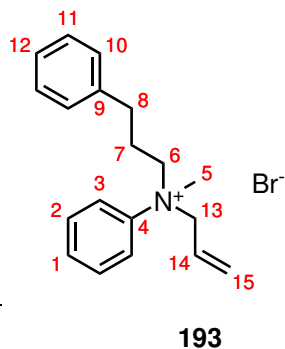
^{13}C NMR (151 MHz, CD_3OD) δ 142.7 (C_4), 136.8 (C_8), 133.9 (C_{14}), 131.94 (C_{16}), 131.92 (C_1), 131.8 (C_2), 130.1 (C_{15}), 130.0 (C_9), 129.9 (C_{10}), 128.54 (C_{13}), 128.45 (C_{11}), 123.6 (C_3), 75.3 (C_{12}), 69.4 (C_6), 47.1 (C_5), 30.4 (C_7).

LRMS (ESI-TOF) m/z : 302.2 ($[\text{M}]^+$, 100%).

HRMS (ESI-TOF) m/z : $[\text{M}]^+$ calculated for $\text{C}_{22}\text{H}_{24}\text{N}^+$: 302.1909, found 302.1909.

mp: 114 – 115 °C (MeCN).

IR ($\text{max}/\text{cm}^{-1}$): 2981, 1456m, 748, 693s, 640, 570.

***N*-allyl, *N*-hydrocinnamyl, *N*-methyl anilinium bromide**

Following the general procedure outlined in 9.3.1 using **178** (0.46 g, 2.03 mmol, 1.0 equiv.) and allyl bromide (0.26 mL, 3.00 mmol, 1.5 equiv.) afforded **193** as a pale pink solid (0.27 g, 38% yield).

$^1\text{H NMR}$ (599 MHz, CD_3OD) δ 7.79 – 7.73 (2H, d, $J = 8.4$ Hz, H_3), 7.62 (2H, t, $J = 7.6$ Hz, H_2), 7.58 (1H, t, $J = 7.2$ Hz, H_1), 7.25 (2H, t, $J = 7.5$ Hz, H_{11}), 7.17 (1H, t, $J = 7.3$ Hz, H_{12}), 7.13 (2H, d, $J = 7.8$ Hz, H_{10}), 5.63 – 5.53 (2H, m, $\text{H}_{14, 15}$), 5.52 – 5.49 (1H, m, H_{15}), 4.70 – 4.65 (1H, m,

H_{13}), 4.49 – 4.44 (1H, m, H_{13}), 4.10 (1H, td, $J = 12.7, 4.1$ Hz, H_6), 3.91 (1H, td, $J = 13.2, 5.2$ Hz, H_6), 3.56 (3H, s, H_5), 2.73 – 2.63 (1H, m, H_8), 2.65 – 2.56 (1H, m, H_8), 2.05 (1H, oct., $J = 5.8$ Hz, H_7), 1.55 – 1.46 (1H, m, H_7).

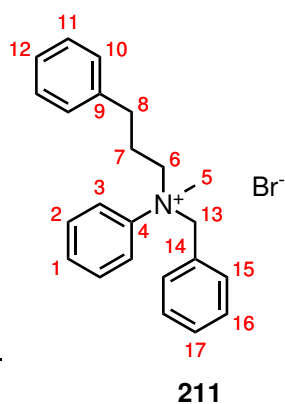
$^{13}\text{C NMR}$ (151 MHz, CD_3OD) δ 143.2 (C_4), 141.1 (C_9), 131.7 (C_2), 131.5 (C_1), 129.6 (C_{11}), 129.4 (C_{10}), 129.3 (C_{15}), 127.5 (C_{12}), 126.1 (C_{14}), 122.9 (C_3), 72.4 (C_{13}), 68.3 (C_6), 48.1 (C_5), 32.8 (C_8), 25.8 (C_7).

LRMS (ESI-TOF) m/z : 266.2 ($[\text{M}]^+$, 100%).

HRMS (ESI-TOF) m/z : $[\text{M}]^+$ calculated for $\text{C}_{19}\text{H}_{24}\text{N}^+$: 266.1909, found 266.1912.

IR ($\text{max}/\text{cm}^{-1}$): 3000m, 1597w, 1493m, 1490m, 956m, 866m, 753m, 689s, 505m.

mp: 108 – 109 °C (MeCN precipitate).

***N*-benzyl, *N*-hydrocinnamyl, *N*-methyl anilinium bromide**

Following the general procedure outlined in 9.3.1 using **178** (0.45 g, 1.99 mmol, 1.0 equiv.) and benzyl bromide (0.35 mL, 2.94 mmol, 1.5 equiv.) afforded **211** as a white solid (0.62 g, 79% yield).

$^1\text{H NMR}$ (599 MHz, CD_3OD) δ 7.62 – 7.55 (5H, m, H_{3+2+1}), 7.41 (1H, t, $J = 7.5$ Hz, H_{17}), 7.30 – 7.24 (4H, m, H_{11+16}), 7.24 – 7.18 (1H, m, H_{12}), 7.15 (2H, d, $J = 7.6$ Hz, H_{10}), 7.00 (2H, d, $J = 8.2$ Hz, H_{15}), 5.10 (1H, d, $J = 12.8$ Hz, H_{13}), 4.94 (1H, d, $J = 13.0$ Hz, H_{13}), 4.27 (1H, td, $J = 12.8,$

4.0 Hz, H_6), 3.93 (1H, td, $J = 13.5, 5.2$ Hz, H_6), 3.47 (3H, s, H_5), 2.74 (1H, dt, $J = 14.2, 7.2$ Hz, H_8), 2.65 (1H, dt, $J = 14.2, 7.4$ Hz, H_8), 2.15 – 2.05 (1H, m, H_7), 1.57 – 1.48

(1H, m, H₇).

¹³C NMR (151 MHz, CD₃OD) δ 142.8 (C₄), 141.0 (C₉), 133.9 (C₁₅), 131.8 (C₁), 131.7 (C₁₇), 131.6 (C₂), 129.8 (C₁₀), 129.7 (C₁₆), 129.5 (C₁₁), 128.6 (C₁₄), 127.6 (C₁₂), 123.4 (C₃), 75.2 (C₁₃), 67.6 (C₆), 47.3 (C₅), 32.9 (C₈), 25.8 (C₇).

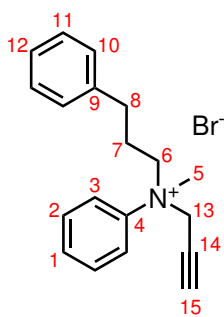
LRMS (ESI-TOF) m/z: 316.2 ([M]⁺, 100%).

HRMS (ESI-TOF) m/z: [M]⁺ calculated for C₂₃H₂₆N⁺: 316.2065, found 316.2066

IR (max/cm⁻¹): 2981, 1491m, 1458m, 743m, 692s.

mp: 108 – 110 °C (MeCN precipitate).

***N*-propargyl, *N*-hydrocinnamyl, *N*-methyl anilinium bromide**



203

Following the general procedure outlined in 9.3.1 using **178** (0.455 g, 2.02 mmol) and 80% propargyl bromide solution (0.34 mL, 3.82 mmol, 1.9 equiv.) afforded **203** as a pink solid (0.555 g, 80% yield).

¹H NMR (599 MHz, DMSO-d₆) δ 7.92 – 7.87 (2H, m, H₃), 7.64 (2H, t, *J* = 8.7 Hz, H₂), 7.59 (1H, t, *J* = 7.2 Hz, H₁), 7.26 (2H, t, *J* = 7.5 Hz, H₁₁), 7.18 (1H, t, *J* = 7.3 Hz, H₁₂), 7.14 – 7.10 (2H, m, H₁₀), 5.15 (1H, dd, *J* = 16.4, 2.5 Hz, H₁₃), 4.97 (1H, dd, *J* = 16.4, 2.5 Hz, H₁₃), 4.04 (1H, td, *J*

= 12.5, 4.6 Hz, H₆), 3.92 (1H, td, *J* = 12.3, 4.8 Hz, H₆), 3.87 (1H, t, *J* = 2.11 Hz, H₁₅), 3.66 (3H, s, H₅), 2.55 (2H, td, *J* = 14.4, 6.1 Hz, H₈), 1.90 (1H, dp, *J* = 20.7, 5.5 Hz, H₇), 1.50 – 1.40 (1H, m, H₇).

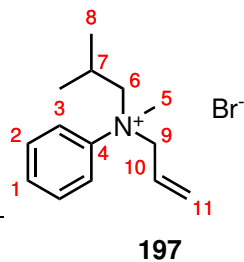
¹³C NMR (151 MHz, DMSO-d₆) δ 142.2 (C₄), 139.8 (C₉), 130.4 (C₁), 130.1 (C₂), 128.4 (C₁₀), 128.2 (C₁₁), 126.2 (C₁₂), 121.9 (C₃), 83.0 (C₁₅), 72.5 (C₁₄), 66.4 (C₆), 57.4 (C₁₃), 48.7 (C₅), 31.2 (C₈), 24.3 (C₇).

LRMS (ESI-TOF) m/z: 264.2 ([M]⁺, 100%).

HRMS (ESI-TOF) m/z: [M]⁺ calculated for C₁₉H₂₂N⁺: 264.1752, found 264.1760.

mp: 118 °C (MeCN).

IR (max/cm⁻¹): 2982, 1492, 766m, 695s.

***N*-allyl, *N*-isobutyl, *N*-methyl anilinium bromide**

Following the general procedure outlined in 9.3.1 using **174** (0.34 g, 2.02 mmol, 1.0 equiv.) and allyl bromide (0.26 mL, 3.00 mmol, 1.5 equiv.) afforded **197** as a pale pink solid (0.28 g, 47% yield).

^1H NMR (599 MHz, CD_3OD) δ 7.87 (2H, d, $J = 8.5$ Hz, H_3), 7.67 (2H, t, $J = 7.9$ Hz, H_2), 7.61 (1H, t, $J = 7.4$ Hz, H_1), 5.64 – 5.55 (2H, m, H_{10+11}), 5.57 – 5.51 (1H, m, H_{11}),

4.73 – 4.65 (1H, m, H_9), 4.46 – 4.40 (1H, m, H_9), 4.04 (1H, dd, $J = 13.5, 6.1$ Hz, H_6), 3.75 (1H, dd, $J = 13.4, 4.7$ Hz, H_6), 3.60 (3H, s, H_5), 1.98 (1H, apt. non, $J = 6.4$ Hz, H_7), 1.04 (3H, d, $J = 6.8$ Hz, H_8), 0.62 (3H, d, $J = 6.7$ Hz, H_8).

^{13}C NMR (151 MHz, CD_3OD) δ 143.6 (C_4), 131.70 (C_2), 131.65 (C_1), 129.3 (C_{11}), 126.0 (C_{10}), 123.3 (C_3), 76.6 (C_9), 73.4 (C_6), 47.8 (C_5), 25.6 (C_7), 22.8 (C_8), 22.0 (C_8).

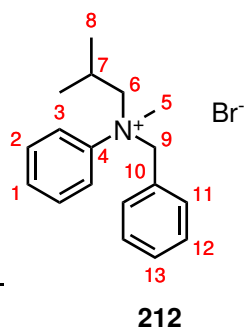
LRMS (ESI-TOF) m/z : 204.2. ($[\text{M}]^+$, 100%).

HRMS (ESI-TOF) m/z : $[\text{M}]^+$ calculated for $\text{C}_{14}\text{H}_{22}\text{N}^+$: 204.1752, found 204.1757.

IR ($\text{max}/\text{cm}^{-1}$): 3439br, 2962m, 1598w, 1466m, 955m, 871m, 704s, 493m.

mp: 116 °C (MeCN precipitate).

XRD: Crystallised in EtOH to give clear colourless blocks. Crystal data for $\text{C}_{36}\text{H}_{46}\text{Br}_2\text{N}_2\text{O}$ ($m = 682.57$ g/mol): Monoclinic, space group $P2_1/n$ (no. 14).

***N*-benzyl, *N*-isobutyl, *N*-methyl anilinium bromide**

Following the general procedure outlined in 9.3.1 using **174** (0.33 g, 1.99 mmol, 1.0 equiv.) and benzyl bromide (0.35 mL, 2.94 mmol, 1.5 equiv.) afforded **212** as a white solid (0.35 g, 52% yield).

^1H NMR (599 MHz, CD_3OD) δ 7.78 – 7.73 (2H, m, H_3), 7.65 – 7.60 (3H, m, H_{1+2}), 7.42 (1H, td, $J = 7.6, 1.1$ Hz, H_{13}), 7.32 – 7.26 (2H, m, H_{12}), 7.07 – 6.99 (2H, m, H_{11}), 5.16 (1H, d, $J = 12.8$ Hz, H_9), 4.91 (1H, d, $J = 12.8$ Hz,

H_9), 4.30 (1H, dd, $J = 13.5, 5.9$ Hz, H_6), 3.83 (1H, dd, $J = 13.6, 4.8$ Hz, H_6), 3.50 (3H, s, H_5), 2.00 – 1.94 (1H, m, H_7), 1.11 (3H, d, $J = 6.7$ Hz, H_8), 0.68 (3H, d, $J = 6.8$ Hz, H_8).

^{13}C NMR (151 MHz, CD_3OD) δ 143.1 (C_4), 133.9 (C_{11}), 131.89 (C_{13}), 131.86 (C_1), 131.5 (C_2), 129.9 (C_{12}), 128.5 (C_{10}), 123.8 (C_3), 76.2 (C_6), 75.8 (C_9), 46.9 (C_5), 25.8 (C_7), 23.0 (C_8), 22.1 (C_8').

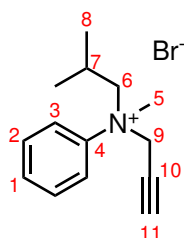
LRMS (ESI-TOF) m/z : 254.2 ($[\text{M}]^+$, 100%).

HRMS (ESI-TOF) m/z : $[\text{M}]^+$ calculated for $\text{C}_{18}\text{H}_{24}\text{N}^+$: 254.1909, found 254.1914.

IR (max/ cm^{-1}): 2982m, 1489m, 775s, 705s, 569m.

mp: 138 – 140 °C (MeCN precipitate).

***N*-propargyl, *N*-isobutyl, *N*-methyl anilinium bromide**



204

Following the general procedure outlined in 9.3.1 using **174** (0.322 g, 1.97 mmol) and 80% propargyl bromide solution (0.34 mL, 3.82 mmol) afforded **204** as a pale lilac solid (0.373 g, 67% yield).

^1H NMR (599 MHz, $\text{DMSO}-d_6$) δ 7.97 (2H, d, $J = 8.5$ Hz, H_3), 7.66 (2H, t, $J = 7.8$ Hz, H_2), 7.61 (1H, t, $J = 7.3$ Hz, H_1), 5.14 (1H, dd, $J = 16.3, 2.5$ Hz, H_9), 4.92 (1H, dd, $J = 16.4, 2.5$ Hz, H_9), 3.92 (1H, dd, $J = 13.3, 5.8$ Hz, H_6), 3.86

(1H, t, $J = 2.5$ Hz, H_{11}), 3.80 (1H, dd, $J = 13.3, 4.7$ Hz, H_6), 3.67 (3H, s, H_5), 1.90 – 1.85 (1H, m, H_7), 0.84 (3H, d, $J = 6.7$ Hz, H_8), 0.54 (3H, d, $J = 6.7$ Hz, H_8').

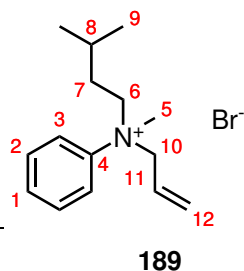
^{13}C NMR (151 MHz, $\text{DMSO}-d_6$) δ 142.4 (C_4), 130.5 (C_1), 130.1 (C_2), 122.1 (C_3), 83.0 (C_{11}), 74.3 (C_9), 72.5 (C_{10}), 57.9 (C_5), 23.7 (C_7), 21.9 (C_8), 21.4 (C_8').

LRMS (ESI-TOF) m/z : 202.1 ($[\text{M}]^+$, 100%).

HRMS (ESI-TOF) m/z : $[\text{M}]^+$ calculated for $\text{C}_{14}\text{H}_{20}\text{N}^+$: 202.1596, found 202.1601.

mp: 179 °C (MeCN).

IR (max/ cm^{-1}): 3171, 2118w, 1462, 958, 697s.

***N*-allyl, *N*-isovaleryl, *N*-methyl anilinium bromide**

Following the general procedure outlined in 9.3.1 using **175** (0.35 g, 1.97 mmol, 1.0 equiv.) and allyl bromide (0.26 mL, 3.00 mmol, 1.5 equiv.) afforded **189** as a pink solid (0.45 g, 77% yield).

^1H NMR (599 MHz, CD_3OD) δ 7.85 (2H, d, $J = 7.8$ Hz, H_3), 7.67 (2H, t, $J = 6.6$ Hz, H_2), 7.61 (1H, t, $J = 7.3$ Hz, H_1), 5.69 – 5.57 (2H, m, H_{11+12}), 5.56 – 5.52 (1H, m, H_{12}),

4.72 (1H, dd, $J = 13.2, 5.0$ Hz, H_{10}), 4.49 (1H, dd, $J = 13.6, 6.9$ Hz, H_{10}), 4.15 (1H, td, $J = 12.5, 4.2$ Hz, H_6), 3.90 (1H, td, $J = 12.3, 6.1$ Hz, H_6), 3.57 (3H, s, H_5), 1.67 – 1.55 (2H, m, H_{7+8}), 1.12 – 1.02 (1H, m, H_7), 0.92 (3H, d, $J = 6.5$ Hz, H_9), 0.87 (3H, d, $J = 6.5$ Hz, H_9).

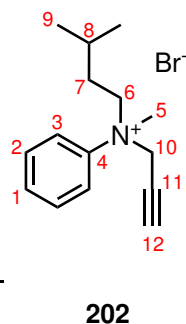
^{13}C NMR (151 MHz, CD_3OD) δ 143.3 (C_4), 131.7 (C_2), 131.6 (C_1), 129.2 (C_{12}), 126.2 (C_{11}), 123.0 (C_3), 72.6 (C_{10}), 68.2 (C_6), 47.8 (C_5), 32.4 (C_7), 27.2 (C_8), 22.6 (C_9), 22.5 (C_9).

LRMS (ESI-TOF) m/z : 218.2 ($[\text{M}]^+$, 100%).

HRMS (ESI-TOF) m/z : $[\text{M}]^+$ calculated for $\text{C}_{15}\text{H}_{24}\text{N}^+$: 218.1909, found 218.1903.

IR ($\text{max}/\text{cm}^{-1}$): 2960m, 1427w, 868m, 770m, 701m.

mp: 134 – 135 °C (MeCN precipitate).

***N*-propargyl, *N*-isovaleryl, *N*-methyl anilinium bromide**

Following the general procedure outlined in 9.3.1 using **175** (0.350 g, 1.97 mmol) and 80% propargyl bromide solution (0.34 mL, 3.82 mmol) afforded **202** as a white solid (0.539 g, 92% yield).

^1H NMR (599 MHz, $\text{DMSO}-d_6$) δ 7.91 (2H, d, $J = 8.5$ Hz, H_3), 7.67 (2H, dd, $J = 8.7, 7.1$ Hz, H_2), 7.60 (1H, t, $J = 7.3$ Hz, H_1), 5.09 (1H dd, $J = 16.4, 2.5$ Hz, H_{10}), 4.90 (1H, dd, $J = 16.4, 2.5$ Hz, H_{10}), 4.04 (1H, td, $J = 12.5, 4.5$ Hz, H_6),

3.92 – 3.86 (2H, m, H_{6+12}), 3.63 (3H, s, H_5), 1.56 – 1.39 (2H, m, H_7), 1.02 – 0.98 (1H, m, H_8), 0.81 (3H, d, $J = 6.6$ Hz, H_9), 0.80 (3H, d, $J = 6.6$ Hz, H_9).

^{13}C NMR (151 MHz, $\text{DMSO}-d_6$) δ 142.2 (C_4), 130.4 (C_1), 130.2 (C_2), 121.8 (C_3), 83.0 (C_{12}), 72.5 (C_{11}), 65.8 (C_6), 57.3 (C_{10}), 48.6 (C_5), 30.8 (C_7), 25.4 (C_8), 22.0 (C_9), 21.9

(C₉).

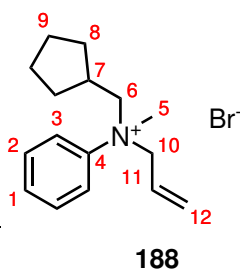
LRMS (ESI-TOF) m/z : 216.2 ([M]⁺, 100%).

HRMS (ESI-TOF) m/z : [M]⁺ calculated for C₁₅H₂₂N⁺: 216.1752, found 216.1755.

mp: 182–183 °C (MeCN).

IR (max/cm⁻¹): 3184, 2972, 2119, 1459, 869m, 695s.

***N*-allyl, *N*-homocyclopentyl, *N*-methyl anilinium bromide**



Following the general procedure outlined in 9.3.1 using **171** (0.37 g, 1.93 mmol, 1.0 equiv.) and allyl bromide (0.26 mL, 3.00 mmol, 1.5 equiv.) afforded **188** as a pale pink solid (0.32 g, 53% yield).

¹H NMR (599 MHz, CD₃OD) δ 7.89 – 7.79 (2H, m, H₃), 7.67 (2H, t, $J = 7.8$ Hz, H₂), 7.61 (1H, td, $J = 7.4, 1.1$ Hz, H₁), 5.68 – 5.56 (2H, m, H₁₁₊₁₂), 5.58 – 5.51 (1H, m, H₁₂),

4.75 – 4.69 (1H, m, H₁₀), 4.47 – 4.41 (1H, m, H₁₀), 4.18 (1H, dd, $J = 13.4, 6.3$ Hz, H₆), 3.92 (1H, dd, $J = 13.3, 5.5$ Hz, H₆), 3.59 (3H, s, H₅), 2.06 – 1.98 (1H, m, H₇), 1.94 – 1.85 (1H, m, H₈), 1.68 – 1.57 (1H, m, H₉), 1.59 – 1.46 (2H, m, H₉), 1.43 – 1.34 (1H, m, H₉), 1.35 – 1.27 (1H, m, H₈), 1.27 – 1.24 (1H, m, H₈), 0.97 – 0.87 (1H, m, H₈).

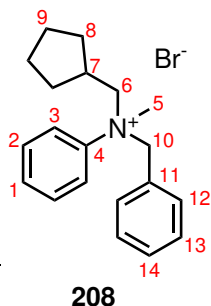
¹³C NMR (151 MHz, CD₃OD) δ 143.7 (C₄), 131.66 (C₂), 131.65 (C₁), 129.2 (C₁₂), 126.2 (C₁₁), 123.3 (C₃), 75.1 (C₆), 72.8 (C₁₀), 48.0 (C₅), 36.7 (C₇), 33.3 (C₈), 32.9 (C₈), 25.7 (C₉), 25.5 (C₉).

LRMS (ESI-TOF) m/z : 230.2 ([M]⁺, 100%).

HRMS (ESI-TOF) m/z : [M]⁺ calculated for C₁₆H₂₄N⁺: 230.1909, found 230.1915.

IR (max/cm⁻¹): 2953m, 1421m, 958m, 870m, 773w, 704s.

mp: 141 – 142 °C (MeCN precipitate).

***N*-benzyl, *N*-homocyclopentyl, *N*-methyl anilinium bromide**

Following the general procedure outlined in 9.3.1 using **171** (0.286 g, 1.51 mmol, 1.0 equiv.) and benzyl bromide (0.35 mL, 2.94 mmol, 2.0 equiv.) afforded **208** as a white solid (0.46 g, 84% yield).

^1H NMR (599 MHz, CD_3OD) δ 7.79 – 7.74 (2H, m, H_3), 7.67 – 7.59 (3H, m, H_{1+2}), 7.41 (1H, t, $J = 7.5$ Hz, H_{14}), 7.28 (2H, t, $J = 7.8$ Hz, H_{13}), 7.04 (2H, d, $J = 8.0$ Hz, H_{12}), 5.19 (1H, d, $J = 12.8$ Hz, H_{10}), 4.96 (1H, d, $J = 12.8$ Hz,

H_{10}), 4.46 (1H, dd, $J = 13.4, 5.7$ Hz, H_6), 4.02 (1H, dd, $J = 13.4, 5.7$ Hz, H_6), 3.51 (3H, s, H_5), 2.05 – 1.91 (1H, m, H_7), 1.71 – 1.62 (1H, m, H_8), 1.62 – 1.48 (2H, m, H_9), 1.46 – 1.28 (3H, m, $\text{H}_{8'+9'}$), 1.07 – 0.97 (1H, m, $\text{H}_{8'}$).

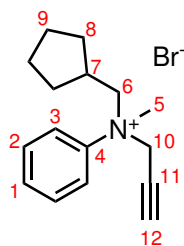
^{13}C NMR (151 MHz, CD_3OD) δ 143.3 (C_4), 133.9 (C_{12}), 131.81 (C_{14}), 131.78 (C_1), 131.5 (C_2), 129.8 (C_{13}), 128.7 (C_{11}), 123.8 (C_3), 75.2 (C_{10}), 74.5 (C_6), 47.2 (C_5), 36.9 (C_7), 33.5 (C_8), 33.1 ($\text{C}_{8'}$), 25.7 (C_9), 25.5 ($\text{C}_{9'}$).

LRMS (ESI-TOF) m/z : 280.2 ($[\text{M}]^+$, 100%).

HRMS (ESI-TOF) m/z : $[\text{M}]^+$ calculated for $\text{C}_{20}\text{H}_{26}\text{N}^+$: 280.2065, found 280.2076.

mp: 157 – 158 °C (MeCN).

IR ($\text{max}/\text{cm}^{-1}$): 2960, 1457, 774m, 704s.

***N*-propargyl, *N*-homocyclopentyl, *N*-methyl anilinium bromide**

Following the general procedure outlined in 9.3.1 using **171** (0.380 g, 2.01 mmol) and 80% propargyl bromide solution (0.34 mL, 3.82 mmol) afforded **201** as a pale pink solid (0.583 g, 94% yield).

^1H NMR (599 MHz, $\text{DMSO}-d_6$) δ 7.98 – 7.93 (2H, m, H_3), 7.65 (2H, t, $J = 7.0$ Hz, H_2), 7.60 (1H, t, $J = 7.3$ Hz, H_1), 5.15 (1H, dd, $J = 16.5, 2.5$ Hz, H_{10}), 4.93 (1H, dd, $J = 16.4, 2.5$ Hz, H_{10}), 4.07 (1H, dd, $J = 13.2, 6.3$ Hz, H_6),

3.97 (1H, dd, $J = 13.2, 5.5$ Hz, H_6), 3.86 (1H, t, $J = 2.4$ Hz, H_{12}), 3.67 (3H, s, H_5), 1.97 – 1.93 (1H, m, H_7), 1.68 – 1.65 (1H, m, H_8), 1.53 – 1.40 (2H, m, $\text{H}_{9+9'}$), 1.41 – 1.33 (1H, m, $\text{H}_{9'}$), 1.33 – 1.24 (1H, m, H_9), 1.24 – 1.17 (1H, m, $\text{H}_{8'}$), 1.09 (1H, apt. dq, $J = 12.4, 8.8$ Hz, H_8), 0.81 (1H, apt. dq, $J = 12.4, 8.9$ Hz, $\text{H}_{8'}$).

^{13}C NMR (151 MHz, $\text{DMSO}-d_6$) δ 142.6 (C_4), 130.4 (C_1), 130.1 (C_2), 122.1 (C_3), 83.0 (C_{12}), 72.62 (C_6), 72.56 (C_{11}), 57.5 (C_{10}), 48.8 (C_5), 34.8 (C_7), 31.4 (C_8), 31.1 (C_9), 24.3 (C_9), 24.1 (C_9).

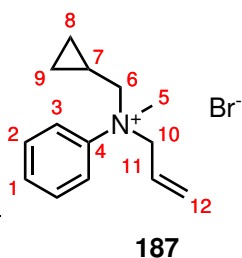
LRMS (ESI-TOF) m/z : 228.2 ($[\text{M}]^+$, 100%).

HRMS (ESI-TOF) m/z : $[\text{M}]^+$ calculated for $\text{C}_{16}\text{H}_{22}\text{N}^+$: 228.1752, found 228.1754.

mp: 179 – 181 °C (MeCN).

IR ($\text{max}/\text{cm}^{-1}$): 3160, 2946, 2121, 1490, 763m, 693s.

***N*-allyl, *N*-homocyclopropyl, *N*-methyl anilinium bromide**



Following the general procedure outlined in 9.3.1 using **172** (0.31 g, 1.94 mmol, 1.0 equiv.) and allyl bromide (0.26 mL, 3.00 mmol, 1.5 equiv.) afforded **187** as a pale pink solid (0.35 g, 63% yield).

^1H NMR (599 MHz, CD_3OD) δ 7.92 (2H, d, $J = 8.1$ Hz, H_3), 7.71 – 7.65 (2H, m, H_2), 7.61 (1H, t, $J = 7.4$ Hz, H_1), 5.66 – 5.58 (2H, m, H_{11+12}), 5.57 – 5.50 (1H, m, H_{12}), 4.83 – 4.77 (1H, m, H_{10}), 4.54 – 4.48 (1H, m, H_{10}), 4.14 (1H, dd, $J = 13.3, 6.2$ Hz, H_6), 3.75 (1H, dd, $J = 13.3, 8.0$ Hz, H_6), 3.68 (3H, s, H_5), 0.92 – 0.82 (1H, m, H_7), 0.77 – 0.68 (1H, m, H_8), 0.58 – 0.48 (2H, m, H_{8+9}), 0.22 – 0.14 (1H, m, H_9).

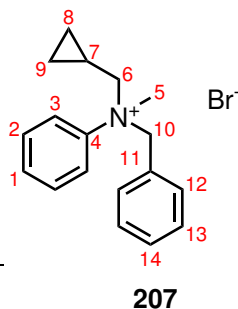
^{13}C NMR (151 MHz, CD_3OD) δ 143.9 (C_4), 131.6 (C_2), 131.5 (C_1), 129.0 (C_{12}), 126.2 (C_{11}), 123.3 (C_3), 74.7 (C_6), 71.2 (C_{10}), 48.0 (C_5), 6.0 (C_7), 5.8 (C_8), 4.1 (C_9).

LRMS (ESI-TOF) m/z : 202.2 ($[\text{M}]^+$, 100%).

HRMS (ESI-TOF) m/z : $[\text{M}]^+$ calculated for $\text{C}_{14}\text{H}_{20}\text{N}^+$: 202.1596, found 202.1603.

IR ($\text{max}/\text{cm}^{-1}$): 3000w, 1414w, 970m, 965m, 935m, 855m, 779m, 702m.

mp: 136 °C (MeCN precipitate).

***N*-benzyl, *N*-homocyclopropyl, *N*-methyl anilinium bromide**

Following the general procedure outlined in 9.3.1 using **172** (0.27 g, 1.70 mmol, 1.0 equiv.) and benzyl bromide (0.35 mL, 2.94 mmol, 1.7 equiv.) afforded **207** as a white solid (0.495 g, 88% yield).

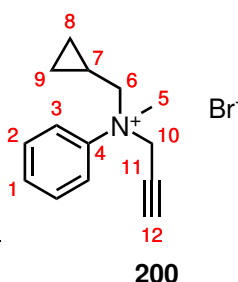
^1H NMR (599 MHz, CD_3OD) δ 7.80 (2H, d, $J = 7.6$ Hz, H_3), 7.67 – 7.58 (3H, m, H_{1+2}), 7.43 – 7.38 (1H, t, $J = 7.5$ Hz, H_{14}), 7.28 (2H, t, $J = 7.6$ Hz, H_{13}), 7.06 (2H, d, $J = 8.0$ Hz, H_{12}), 5.20 (1H, d, $J = 12.8$ Hz, H_{10}), 4.98 (1H, d, $J = 12.8$ Hz, $\text{H}_{10'}$), 4.47 (1H, dd, $J = 13.4, 5.5$ Hz, H_6), 3.77 (1H, dd, $J = 13.4, 8.3$ Hz, H_6'), 3.59 (3H, s, H_5), 0.88 – 0.81 (1H, m, H_7), 0.78 – 0.72 (1H, m, H_8), 0.64 – 0.52 (2H, m, $\text{H}_{8'+9}$), 0.29 – 0.23 (1H, m, H_9).

^{13}C NMR (151 MHz, CD_3OD) δ 143.5 (C_4), 133.8 (C_{12}), 131.72 (C_{14}), 131.65 (C_1), 131.5 (C_2), 129.8 (C_{13}), 128.7 (C_{11}), 123.8 (C_3), 74.0 (C_{10}), 73.9 (C_6), 47.1 (C_5), 6.4 (C_8), 6.1 (C_7), 3.9 (C_9).

HRMS (ESI-TOF) m/z : $[\text{M}]^+$ calculated for $\text{C}_{18}\text{H}_{22}\text{N}^+$: 252.1752, found 252.1760.

IR (max/ cm^{-1}): 2980, 1413, 872, 774m, 706s, 693m, 567.

mp: 148 – 149 °C (MeCN precipitate).

***N*-homocyclopropyl, *N*-methyl, *N*-propargyl anilinium bromide**

Following the general procedure outlined in 9.3.1 using **172** (0.33 g, 2.04 mmol, 1.0 equiv.) and 80% propargyl bromide solution (0.34 mL, 3.82 mmol, 1.9 equiv.) afforded **200** as a pale pink solid (0.53 g, 92% yield).

^1H NMR (599 MHz, $\text{DMSO}-d_6$) δ 7.99 – 7.94 (2H, m, H_3), 7.66 (2H, dd, $J = 8.7, 7.0$ Hz, H_2), 7.60 (1H, t, $J = 7.3$ Hz, H_1), 5.18 (1H, dd, $J = 16.5, 2.5$ Hz, H_{10}), 4.95 (1H, dd, $J = 16.4, 2.5$ Hz, H_{10}), 3.96 (1H, dd, $J = 13.2, 6.7$ Hz, H_6), 3.87 – 3.83 (1H, m, H_{12}), 3.79 (1H, dd, $J = 13.2, 7.5$ Hz, H_6), 3.70 (3H, s, H_5), 0.80 (1H, dtp, $J = 12.5, 7.9, 3.8$ Hz, H_7), 0.58 (1H, ddt, $J = 8.3, 7.9, 4.7$ Hz, H_8), 0.48 (1H, ddt, $J = 13.7, 8.6, 4.9$ Hz, H_9), 0.33 (1H, dt, $J = 10.1, 5.0$ Hz, H_8'), 0.13 (1H, dt, $J = 10.1, 5.0$ Hz, H_9').

^{13}C NMR (151 MHz, $\text{DMSO}-d_6$) δ 143.0 (C_4), 130.3 (C_1), 130.0 (C_2), 122.0 (C_3), 82.9 (C_{12}), 72.7 (C_{11}), 72.2 (C_6), 56.0 (C_{10}), 48.6 (C_5), 4.9 (C_7), 4.4 (C_8), 3.6 (C_9).

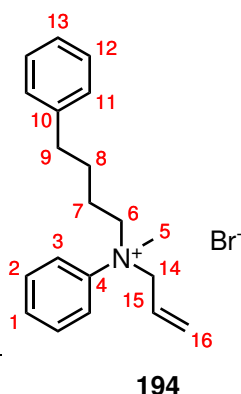
LRMS (ESI-TOF) m/z : 200.1 ($[M]^+$, 100%).

HRMS (ESI-TOF) m/z : $[M]^+$ calculated for $C_{14}H_{18}N^+$: 200.1439, found 200.1433

IR ($\text{max}/\text{cm}^{-1}$): 3175m, 2980m, 2119m, 1459m, 696s.

mp: 154 – 155 °C (MeCN precipitate).

***N*-allyl, *N*-4-phenylbutyl, *N*-methyl anilinium bromide**



Following the general procedure outlined in 9.3.1 using **179** (120 mg, 0.52 mmol, 1.0 equiv.) and allyl bromide (0.10 mL, 1.15 mmol, 2.2 equiv.) afforded **194** as a hygroscopic red solid (70 mg, 36% yield).

^1H NMR (599 MHz, CD_3OD) δ 7.79 – 7.75 (2H, m, H_3), 7.67 – 7.61 (2H, m, H_2), 7.61 – 7.56 (1H, m, H_1), 7.25 – 7.17 (2H, m, H_{12}), 7.16 – 7.08 (3H, m, H_{11+13}), 5.67 – 5.58 (2H, m, H_{15+16}), 5.57 – 5.52 (1H, m, H_{16}), 4.64 (1H, dd, $J = 13.2, 5.9$ Hz, H_{14}), 4.41 (1H, dd, $J = 13.2, 7.2$ Hz, H_{14}),

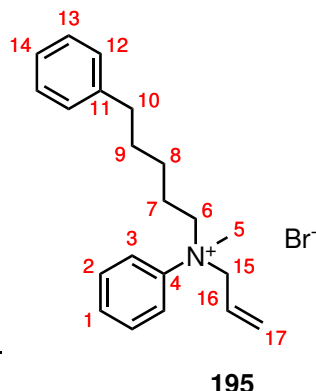
4.08 (1H, td, $J = 12.4, 4.4$ Hz, H_6), 3.84 (1H, ddd, $J = 13.0, 11.9, 4.8$ Hz, H_6), 3.52 (3H, s, H_5), 2.58 (2H, t, $J = 7.5$ Hz, H_9), 1.76 – 1.56 (3H, m, H_{7+8}), 1.29 – 1.20 (1H, m, H_7).

^{13}C NMR (151 MHz, CD_3OD) δ 143.4 (C_4), 142.5 (C_{10}), 131.8 (C_2), 131.6 (C_1), 129.44 (C_{12}), 129.36 (C_{11}), 129.3 (C_{16}), 127.1 (C_{13}), 126.1 (C_{15}), 122.9 (C_3), 72.5 (C_{14}), 68.9 (C_6), 47.9 (C_5), 35.8 (C_9), 28.8 (C_8), 23.3 (C_7).

LRMS (ESI-TOF) m/z : 280.2 ($[M]^+$, 100%).

HRMS (ESI-TOF) m/z : $[M]^+$ calculated for $\text{C}_{20}\text{H}_{26}\text{N}^+$: 280.2065, found 280.2052.

IR ($\text{max}/\text{cm}^{-1}$): 3415br, 2981m, 1599w, 1455m, 957m, 862m, 694s.

***N*-allyl, *N*-5-phenylvaleryl, *N*-methyl anilinium bromide**

Following the general procedure outlined in 9.3.1 using **185** (130 mg, 0.50 mmol, 1.0 equiv.) and allyl bromide (0.10 mL, 1.15 mmol, 2.3 equiv.) afforded **195** as a pink solid (51 mg, 28% yield).

$^1\text{H NMR}$ (599 MHz, CD_3OD) δ 7.82 – 7.77 (2H, m, H_3), 7.70 – 7.63 (2H, m, H_2), 7.63 – 7.58 (1H, m, H_1), 7.25 – 7.19 (2H, m, H_{13}), 7.16 – 7.08 (3H, m, H_{12+14}), 5.67 – 5.58 (2H, m, H_{16+17}), 5.57 – 5.52 (1H, m, H_{17}), 4.64 (1H, dd, $J = 13.2, 5.7$ Hz, H_{15}), 4.41 (1H, dd, $J = 13.2, 7.0$ Hz, H_{15}),

4.03 (1H, td, $J = 12.6, 4.2$ Hz, H_6), 3.80 (1H, ddd, $J = 12.9, 11.6, 5.0$ Hz, H_6), 3.54 (3H, s, H_5), 2.54 (2H, t, $J = 7.5$ Hz, H_{10}), 1.75 – 1.66 (1H, , m, H_7), 1.59 (2H, p, $J = 7.6$ Hz, H_9), 1.41 – 1.18 (3H, m, H_{7+8}).

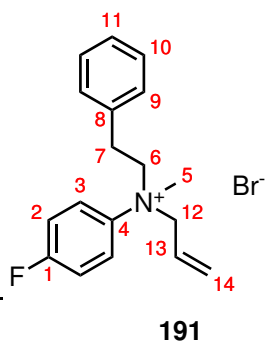
$^{13}\text{C NMR}$ (151 MHz, CD_3OD) δ 143.4 (C_4), 143.1 (C_{11}), 131.8 (C_2), 131.6 (C_1), 129.4 (C_{12}), 129.3 (C_{13}), 129.2 (C_{17}), 126.8 (C_{14}), 126.1 (C_{16}), 122.9 (C_3), 72.5 (C_{15}), 69.0 (C_6), 47.9 (C_5), 36.3 (C_{10}), 31.7 (C_9), 26.5 (C_8), 23.8 (C_7).

LRMS (ESI-TOF) m/z : 294.2 ($[\text{M}]^+$, 100%).

HRMS (ESI-TOF) m/z : $[\text{M}]^+$ calculated for $\text{C}_{21}\text{H}_{28}\text{N}^+$: 294.2222, found 294.2232.

IR ($\text{max}/\text{cm}^{-1}$): 3350br, 2926m, 1599w, 1455m, 954m, 861m, 749m, 697s.

mp: 111 °C (MeCN precipitate).

***N*-allyl, *N*-phenylacetyl, *N*-methyl-4-fluoroanilinium bromide**

Following the general procedure outlined in 9.3.1 using **182** (105 mg, 0.46 mmol, 1.0 equiv.) and allyl bromide (0.10 mL, 1.15 mmol, 2.5 equiv.) afforded **191** as a white solid (91 mg, 54% yield).

$^1\text{H NMR}$ (599 MHz, CD_3OD) δ 7.96 – 7.90 (2H, m, H_3), 7.47 – 7.40 (2H, m, H_3), 7.34 – 7.28 (2H, m, H_2), 7.28 – 7.22 (1H, m, H_{11}), 7.22 – 7.15 (2H, m, H_9), 5.75 – 5.65 (1H, m, H_{13}), 5.63 – 5.56 (2H, m, H_{14}), 4.67 (1H, dd, $J =$

13.2, 6.4 Hz, H_{12}), 4.47 (1H, dd, $J = 13.2, 7.7$ Hz, H_{12}), 4.28 (1H, td, $J = 12.4, 4.9$ Hz, H_6), 4.07 (1H, ddd, $J = 13.1, 11.4, 5.6$ Hz, H_6), 3.67 (3H, s, H_5), 3.05 (1H, td, $J = 12.0, 5.6$ Hz, H_7), 2.60 (1H, ddd, $J = 13.2, 11.4, 4.9$ Hz, H_7).

^{13}C NMR (151 MHz, CD_3OD) δ 164.2 (d, $J = 264.6$ Hz, C_1), 139.0 (C_4), 136.5 (C_8), 129.9 (C_{10}), 129.8 (C_9), 129.5 (C_{14}), 128.3 (C_{11}), 125.8 (C_{13}), 125.6 (d, $J = 9.1$ Hz, C_3), 118.5 (d, $J = 23.7$ Hz, C_2), 72.9 (C_{12}), 69.9 (C_6), 48.3 (C_5), 30.2 (C_7).

^{19}F NMR (376 MHz, CD_3OD) δ -111.67.

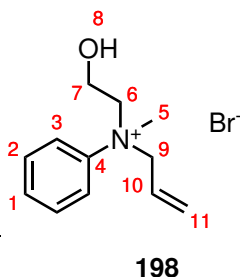
LRMS (ESI-TOF) m/z : 270.2 ($[\text{M}]^+$, 100%).

HRMS (ESI-TOF) m/z : $[\text{M}]^+$ calculated for $\text{C}_{18}\text{H}_{21}\text{NF}^+$: 270.1658, found 270.1671.

IR ($\text{max}/\text{cm}^{-1}$): 2981m, 1604w, 1514s, 1494m, 1250s, 1174m, 956m, 870s, 752m, 706m, 548m.

mp: 85 – 87 °C (MeCN precipitate).

***N*-allyl, *N*-2-hydroxyethyl, *N*-methyl anilinium bromide**



Following the general procedure outlined in 9.3.1 using *N*-2-hydroxyethyl, *N*-methyl-aniline (0.31 g, 2.03 mmol, 1.0 equiv.) and allyl bromide (0.26 mL, 3.00 mmol, 1.5 equiv.) afforded **198** as a blue solid (0.54 g, 98% yield).

^1H NMR (599 MHz, CD_3OD) δ 7.90 – 7.85 (2H, d, $J = 7.9$ Hz, H_3), 7.71 – 7.65 (2H, t, $J = 7.9$ Hz, H_2), 7.64 – 7.59 (1H, t, $J = 7.4$ Hz, H_1), 5.68 – 5.58 (2H, m, H_{10+11}), 5.60 –

5.53 (1H, m, H_{11}), 4.76 (1H, dd, $J = 12.4, 4.0$ Hz, H_9), 4.61 – 4.54 (1H, m, H_9), 4.22 (1H, dt, $J = 13.9, 3.9$ Hz, H_6), 4.05 (1H, ddd, $J = 13.9, 8.2, 3.5$ Hz, H_6), 3.76 (1H, dt, $J = 13.6, 4.2$ Hz, H_7), 3.72 (3H, s, H_5), 3.58 (1H, ddd, $J = 13.6, 8.2, 3.2$ Hz, H_7).

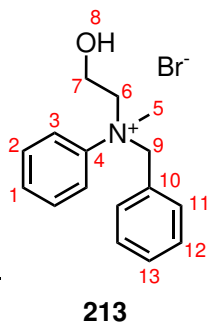
^{13}C NMR (151 MHz, CD_3OD) δ 143.4 (C_4), 131.7 (C_2), 131.6 (C_1), 129.4 (C_{11}), 126.1 (C_{10}), 123.2 (C_3), 72.9 (C_9), 70.7 (C_6), 57.1 (C_7), 49.8 (C_5).

LRMS (ESI-TOF) m/z : 192.1 ($[\text{M}]^+$, 100%).

HRMS (ESI-TOF) m/z : $[\text{M}]^+$ calculated for $\text{C}_{12}\text{H}_{18}\text{NO}^+$: 192.1388, found 192.1381.

IR ($\text{max}/\text{cm}^{-1}$): 3232s, 1599w, 1464m, 1415m, 1350m, 1097m, 1034m, 955s, 877m, 876m, 697s, 613s, 509s.

mp: 100 – 102 °C (MeCN precipitate).

***N*-benzyl, *N*-2-hydroxyethyl, *N*-methyl anilinium bromide**

Following the general procedure outlined in 9.3.1 using *N*-2-hydroxyethyl, *N*-methyl-aniline (0.314 g, 2.08 mmol, 1.0 equiv.) and benzyl bromide (0.35 mL, 2.94 mmol, 1.5 equiv.) afforded **213** as a white solid (0.571 g, 85% yield). ^1H NMR (599 MHz, CD_3OD) δ 7.45 – 7.39 (2H, m, H_3), 7.35 – 7.28 (3H, m, H_{1+2}), 7.14 – 7.08 (1H, $J = 7.5$ Hz, H_{13}), 6.98 (2H, t, $J = 7.8$ Hz, H_{12}), 6.76 – 6.72 (2H, m, H_{11}), 4.86 (1H, d, $J = 12.8$ Hz, H_9), 4.73 (1H, d, $J = 12.7$

Hz, H_9), 4.11 (1H, dt, $J = 13.9, 3.9$ Hz, H_6), 3.80 (1H, td, $J = 13.9, 3.5$ Hz, H_6), 3.50 (1H, dt, $J = 13.7, 4.0$ Hz, H_7), 3.31 (3H, s, H_5), 3.33 – 3.26 (1H, m, H_7). H_{11} is missing from the ^1H NMR spectrum, presumably due to exchange with the solvent.

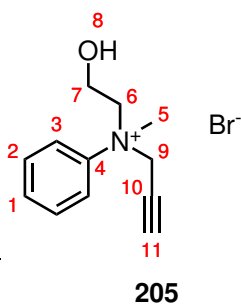
^{13}C NMR (151 MHz, CD_3OD) δ 143.0 (C_4), 134.0 (C_{11}), 131.9 (C_{13}), 131.8 (C_1), 131.6 (C_2), 129.8 (C_{12}), 128.6 (C_{10}), 123.7 (C_3), 75.5 (C_9), 70.2 (C_6), 57.2 (C_7), 48.9 (C_5).

LRMS (ESI-TOF) m/z : 242.1 ($[\text{M}]^+$, 100%).

HRMS (ESI-TOF) m/z : $[\text{M}]^+$ calculated for $\text{C}_{16}\text{H}_{20}\text{NO}^+$: 242.1545, found 242.1551.

mp: 106 °C (MeCN).

IR (max/ cm^{-1}): 3357br, 2982m, 1036m, 705s.

***N*-2-hydroxyethyl, *N*-methyl, *N*-propargyl anilinium bromide**

Following the general procedure outlined in 9.3.1 using *N*-2-hydroxyethyl, *N*-methyl-aniline (0.30 g, 1.97 mmol, 1.0 equiv.) and 80% propargyl bromide solution (0.34 mL, 3.82 mmol, 1.9 equiv.) afforded **205** as a hygroscopic blue solid (0.48 g, 90% yield).

^1H NMR (599 MHz, CDCl_3) δ 8.00 (2H, d, $J = 7.8$ Hz, H_3), 7.87 (2H, t, $J = 9.1$ Hz, H_2), 7.82 (1H, t, $J = 7.3$ Hz, H_1), 5.15 (1H, dd, $J = 16.4, 2.5$ Hz, H_9), 5.04 (1H, dd, $J = 16.3,$

2.5 Hz, H_9), 4.41 (1H, td, $J = 14.1, 5.9$ Hz, H_6), 4.27 (1H, td, $J = 14.0, 7.1$ Hz, H_6), 4.01 (3H, s, H_5), 3.96 (1H, td, $J = 14.0, 5.9$ Hz, H_7), 3.89 (1H, td, $J = 14.1, 7.1$ Hz, H_7).

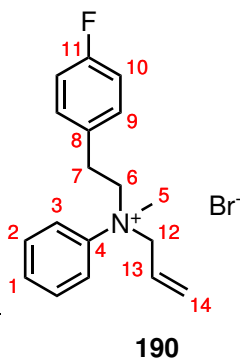
^{13}C NMR (151 MHz, CDCl_3) δ 140.3 (C_4), 129.4 (C_1), 129.1 (C_2), 119.9 (C_3), 80.4 (C_{11}), 69.7 (C_{10}), 67.1 (C_6), 57.4 (C_9), 54.3 (C_7), 49.0 (C_5).

LRMS (ESI-TOF) m/z : 190.1 ($[\text{M}+\text{H}]^+$, 100%).

HRMS (ESI-TOF) m/z : $[M+h]^+$ calculated for $C_{12}H_{16}NO^+$: 190.1232, found 190.1227.

IR (max/cm⁻¹): 3347s, 1227w, 1599w, 1459m, 1042m, 689s.

***N*-allyl, *N*-4-fluorophenylacetyl, *N*-methyl anilinium bromide**



Following the general procedure outlined in 9.3.1 using **177** (0.117 g, 0.51 mmol, 1.0 equiv.) and allyl bromide (0.20 mL, 2.31 mmol, 4.5 equiv.) afforded **190** as a red solid (0.120 g, 67% yield).

¹H NMR (400 MHz, CD₃OD) δ 7.94 – 7.78 (2H, m, H₃), 7.76 – 7.65 (2H, m, H₂), 7.68 – 7.57 (1H, m, H₂), 7.26 – 7.16 (2H, m, H₁₀), 7.08 – 6.97 (2H, m, H₉), 5.74 – 5.51 (3H, m, H₁₃₊₁₄), 4.72 (1H, dd, J = 13.1, 5.3 Hz, H₁₂), 4.54 – 4.41 (1H, m, H₁₂), 4.30 (1H, td, J = 12.4, 4.9 Hz, H₆),

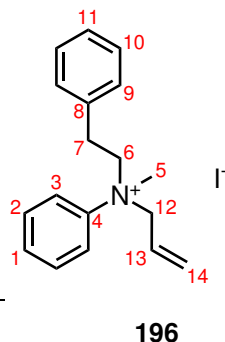
4.09 (1H, ddd, J = 13.0, 11.5, 5.5 Hz, H₆), 3.68 (3H, s, H₅), 3.04 (1H, td, J = 12.5, 5.5 Hz, H₇), 2.54 (1H, ddd, J = 13.2, 11.5, 4.8 Hz, H₇).

¹³C NMR (101 MHz, CD₃OD) δ 164.4 (d, J = 244.0 Hz, C₁₁), 143.2 (C₄), 132.6 (d, J = 3.7 Hz, C₈), 131.92 (C₂), 131.89 (C₁), 131.82 (d, J = 2.0 Hz, C₉), 129.5 (C₁₄), 126.1 (C₁₃), 123.0 (C₃), 116.6 (d, J = 21.5 Hz, C₁₀), 72.7 (C₁₂), 69.6 (C₆), 48.0 (C₅), 29.5 (C₇).

LRMS (ESI-TOF) m/z : 270.3 ($[M]^+$, 100%).

IR (max/cm⁻¹): 3009m, 1601w, 1510s, 1221m, 959m, 829m, 762s, 699s, 500m.

mp: 93 – 95 °C (MeCN precipitate).

***N*-allyl, *N*-methyl, *N*-phenylacetyl anilinium iodide**

Following the general procedure outlined in 9.3.1 using **176** (0.988 g, 4.68 mmol, 1.0 equiv.) and allyl iodide (1.00 mL, 10.9 mmol, 2.3 equiv.) afforded **196** as a yellow solid (1.510 g, 85% yield).

^1H NMR (400 MHz, CD_3OD) δ 7.98 – 7.93 (2H, m, H_3), 7.75 – 7.69 (2H, m, H_2), 7.65 – 7.59 (1H, m, H_1), 7.32 – 7.19 (5H, m, $\text{H}_{9+10+11}$), 5.72 – 5.57 (2H, m, H_{14}), 5.57 – 5.50 (1H, m, H_{13}), 4.81 – 4.73 (1H, m, H_{12}), 4.64 – 4.53

(1H, m, H_{12}), 4.33 (1H, td, $J = 12.5, 4.8$ Hz, H_6), 4.16 (1H, ddd, $J = 13.0, 11.5, 5.6$ Hz, H_6), 3.72 (3H, s, H_5), 3.05 (1H, td, $J = 12.5, 5.6$ Hz, H_7), 2.53 (1H, ddd, $J = 13.1, 11.5, 4.7$ Hz, H_7).

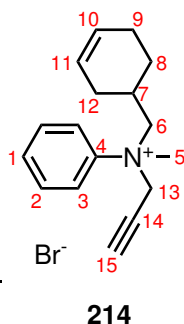
^{13}C NMR (101 MHz, CD_3OD) δ 143.1 (C_4), 136.6 (C_8), 131.9 (C_2), 131.7 (C_1), 130.1 (C_9), 129.9 (C_{10}), 129.5 (C_{14}), 128.3 (C_{11}), 126.0 (C_{13}), 123.1 (C_3), 72.5 (C_{12}), 69.6 (C_6), 48.3 (C_5), 30.3 (C_7).

LRMS (ESI-TOF) m/z : 252.1 ($[\text{M}]^+$, 100%).

HRMS (ESI-TOF) m/z : $[\text{M}]^+$ calculated for $\text{C}_{18}\text{H}_{22}\text{N}^+$: 252.1752, found 252.1751.

IR ($\text{max}/\text{cm}^{-1}$): 3000m, 1497m, 1491m, 970w, 859m, 748m, 696s, 551m.

mp: 110 – 111 °C (MeCN precipitate).

***N*-cyclohex-2-enyl, *N*-methyl, *N*-propargyl anilinium bromide**

Following the general procedure outlined in 9.3.1 using **350** (0.394 g, 1.96 mmol, 1.0 equiv.) and 80% propargyl bromide solution (0.34 mL, 3.82 mmol, 1.9 equiv.) afforded **214** as a pink solid (0.453 g, 72% yield). The product was isolated as a mixture of diastereomers (**214:214'**, 51:49).

^1H NMR (599 MHz, CDCl_3) δ 7.99 (2H, d, $J = 9.0$ Hz, $\text{H}_{3+3'}$), 7.67 (2H, t, $J = 7.1$ Hz, $\text{H}_{2+2'}$), 7.61 (1H, t, $J = 7.3$ Hz, $\text{H}_{1+1'}$), 5.63 – 5.57 (1H, m, $\text{H}_{10+10'}$), 5.58 – 5.51

(0.51H, m, H_{11}), 5.42 – 5.36 (0.49H, m, $\text{H}_{11'}$), 5.18 (1H, dd, $J = 18.4, 2.5$ Hz, $\text{H}_{13+13'}$), 4.95 (1H, dt, $J = 16.4, 2.4$ Hz, $\text{H}_{13+13'}$), 4.01 (1H, td, $J = 13.4, 5.2$ Hz, $\text{H}_{6+6'}$), 3.95 – 3.80 (2H, m, $\text{H}_{6+6'+15+15'}$), 3.71 (1.53H, s, H_5), 3.70 (1.47H, s, H_5), 2.02 – 1.89 (1.49H, m, H_{8+12}), 1.89 – 1.77 (1.98H, m, $\text{H}_{7+7'+8}$), 1.76 – 1.72 (0.49H, m, H_{12}), 1.55 – 1.51

(0.49H, m, H_{9'}), 1.48 – 1.44 (1.02H, m, H₁₂), 1.29 – 1.25 (0.49H, m, H₉), 1.17 – 1.11 (0.51H, m, H₉), 1.05 – 1.02 (0.51H, m, H₉).

¹³C NMR (151 MHz, CDCl₃) δ 142.5 (C₄), 142.4 (C_{4'}), 130.5 (C₁), 130.10 (C₂), 130.08 (C_{2'}), 126.68 (C₁₀), 126.67 (C_{10'}), 125.1 (C₁₁), 125.0 (C_{11'}), 122.10 (C₃), 122.06 (C_{3'}), 83.1 (C₁₅), 83.0 (C_{15'}), 72.9 (C_{6'}), 72.8 (C₆), 72.51 (C₆), 72.46 (C_{6'}), 57.8 (C₁₃), 57.4 (C_{13'}), 49.1 (C₅), 48.6 (C_{5'}), 30.5 (C_{12'}), 30.2 (C₁₂), 28.52 (C_{7'}), 28.45 (C₇), 27.5 (C₉), 26.8 (C_{9'}), 23.8 (C₈), 23.6 (C_{8'}).

LRMS (ESI-TOF) m/z: 240.2 ([M]⁺, 100%).

HRMS (ESI-TOF) m/z: [M]⁺ calculated for C₁₇H₂₂N⁺: 240.1752, found 240.1762.

IR (max/cm⁻¹): 3216, 2917, 1463, 853, 695m, 662m.

mp: 174 °C (MeCN precipitate).

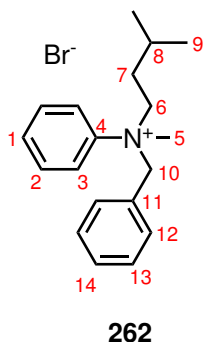
XRD: A portion of the salt was crystallised in EtOH to give clear colourless planks.

Crystal data for C₁₇H₂₂BrN (m = 320.26 g/mol): Orthorhombic, space group *P*2₁2₁2₁ (no. 19). The ammonium salt crystallised as a conglomerate (**214a**).

XRD: A portion of the salt was crystallised in EtOH to give clear colourless planks.

Crystal data for C₁₇H₂₂BrN (m = 320.26 g/mol): Orthorhombic, space group *P*2₁2₁2₁ (no. 19). The ammonium salt crystallised as a conglomerate (**214b**).

N-benzyl, *N*-isovaleryl, *N*-methyl anilinium bromide



Following the general procedure outlined in 9.3.1 using **358** (0.350 g, 1.97 mmol, 1.0 equiv.) and benzyl bromide (0.35 mL, 2.94 mmol, 1.5 equiv.) afforded **262** as a yellow solid (0.587 g, 85% yield).

¹H NMR (599 MHz, CD₃OD) δ 7.74 – 7.68 (2H, m, H₃), 7.67 – 7.59 (3H, m, H₁₊₂), 7.42 (1H, t, *J* = 7.6 Hz, H₁₄), 7.29 (2H, t, *J* = 7.8 Hz, H₁₃), 7.06 – 7.01 (2H, m, H₁₂), 5.16 (1H, d, *J* = 12.8 Hz, H₁₀), 4.98 (1H, d, *J* = 12.8 Hz,

H₁₀), 4.38 (1H, td, *J* = 12.6, 4.1 Hz, H₆), 3.97 (1H, td, *J* = 12.9, 4.9 Hz, H₆), 3.46 (3H, s, H₅), 1.73 – 1.60 (2H, m, H₇), 1.12 – 1.06 (1H, m, H₈), 0.96 (3H, d, *J* = 6.5 Hz, H₉), 0.91 (3H, d, *J* = 6.4 Hz, H₉).

¹³C NMR (151 MHz, CD₃OD) δ 142.8 (C₄), 133.9 (C₁₂), 131.9 (C₁₄), 131.8 (C₁), 131.6 (C₂), 129.9 (C₁₃), 128.7 (C₁₁), 123.5 (C₃), 75.2 (C₁₀), 67.8 (C₆), 46.9 (C₅), 32.5 (C₈), 27.4 (C₇), 22.58 (C₉), 22.56 (C₉).

9.3. RACEMIC AND ACHIRAL AMMONIUM SALT SYNTHESIS

LRMS (ESI-TOF) m/z : 268.2 ($[M]^+$, 100%).

HRMS (ESI-TOF) m/z : $[M]^+$ calculated for $C_{23}H_{26}N^+$: 268.2065, found 268.2078..

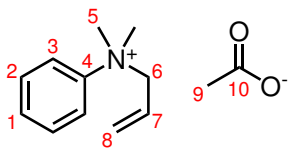
IR ($\text{max}/\text{cm}^{-1}$): 2960, 1493, 1457m, 773s, 705s, 571.

mp: 161 °C (MeCN precipitate).

XRD: A portion of the salt was crystallised in EtOH to give clear colourless planks.

Crystal data for $C_{19}H_{26}BrN$ ($m = 348.32$ g/mol): Monoclinic, space group $P2_1$ (no. 4).

The ammonium salt crystallised as a conglomerate (**262a**).

***N*-allyl-*N,N*-dimethylanilinium acetate****112**

A counterion swap was conducted by flushing an *Amblyst* A26 OH⁻ form, 6 inches, 30 mm \varnothing column) resin with a saturated aqueous solution of sodium acetate, until the eluted solution had a neutral pH. The corresponding bromide salt **73** (1.19 g, 4.91 mmol) was dissolved into methanol, and eluted through the ion exchange resin. Af-

ter collecting 3 columns lengths worth of eluent, the fractions were combined and concentrated to dryness to give the desired acetate salt, **112** as a brown hygroscopic solid (1.01 g, 93% yield).

¹H NMR (400 MHz, CDCl₃) δ 7.84 – 7.73 (2H, m, H₃), 7.50 (2H, dd, J = 8.9, 7.1 Hz, H₂), 7.42 (1H, t, J = 7.3 Hz, H₁), 5.60 (1H, dd, J = 15.8, 2.3 Hz, H₇), 5.42 – 5.26 (2H, m, H₈), 4.82 (2H, d, J = 6.5 Hz, H₆), 3.74 (6H, s, H₅), 1.87 (3H, s, H₉).

¹³C NMR (101 MHz, CDCl₃) δ 177.3 (C₁₀), 144.6 (C₄), 130.5 (C₂), 130.3 (C₁), 129.1 (C₈), 125.0 (C₇), 120.8 (C₃), 70.9 (C₆), 49.6 (C₅), 25.4 (C₉).

LRMS (ESI-TOF, EI⁺) m/z : 162.6 ([M]⁺, 100%).

HRMS (ESI-TOF) m/z : [M]⁺ Calculated for C₁₁H₁₆N⁺: 162.1283, found 162.1273.

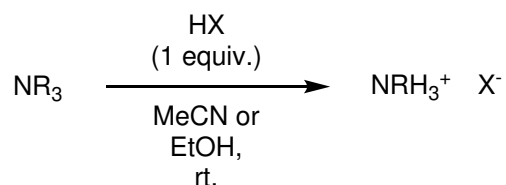
mp: 318 °C (MeOH).

IR ($\nu_{\text{max}}/\text{cm}^{-1}$): 3276br, 1560s, 1393s, 1000m, 921m, 620s.

For quaternary ammonium salts that haven't been characterised in this experimental section but are listed to have been complexed with BINOL in this thesis, see M.P. Walsh's thesis, E.F. Fiandra's report or E.W. Winful's report for full characterisation. Callum S. Begg synthesised these salts but did not fully characterise them due to the data already being available.²

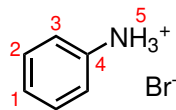
9.4 Protonated ammonium salt synthesis

9.4.1 General procedure for preparation of protonated ammonium salts



Scheme 9.9: Protonation of amines to produce primary, secondary and tertiary ammonium salts.

The selected amine (1.0 equiv.) was placed into a 10 mL vial and dissolved into MeCN or EtOH (1.0 – 2.0 M) and cooled to 0 °C. With stirring, the desired acid was added dropwise to the amine solution. The reaction mixture was warmed to room temperature and stirred until all starting material was consumed. The solvent was removed *in vacuo* and the resulting crude solid was washed with diethyl ether to remove unreacted amine. The desired ammonium salt can be recrystallised to purity using a number of solvents (MeOH, EtOH, MeOH/Et₂O, MeCN).

Anilinium hydrobromide**359**

Aniline (0.928 g, 10.0 mmol) was dissolved in MeCN (5.0 mL, 2.0 M). 48% HBr solution (4.53 mL, 4.0 equiv.) was then added dropwise with stirring to the solution. This solution was allowed to stir at room temperature for 2 hours.

The solvent was removed *in vacuo* and the crude **359** was washed with diethyl ether to remove excess acid and unreacted amine. The resulting white precipitate was isolated by vacuum filtration (1.658 g, 96% yield).

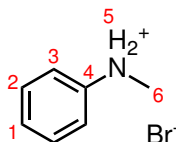
^1H NMR (400 MHz, DMSO- d_6) δ 10.03 (3H, s, H₅), 7.54 - 7.46 (2H, m, H₃), 7.44 - 7.35 (3H, m, H₁₊₂).

^{13}C NMR (101 MHz, DMSO- d_6) δ 131.8 (C₄), 129.9 (C₂), 128.1 (C₁), 123.1 (C₃).

mp: 262 - 264 °C (MeCN).

IR (vmax/cm⁻¹): 2824br, 1491m, 741s, 680s, 474s.

*Data consistent with literature values.*³¹⁵

N-methylanilinium hydrobromide**360**

N-methyl aniline (1.088 g, 10.2 mmol) was dissolved in MeCN (5.0 mL, 2.0 M). 48% HBr solution (3.39 mL, 3.0 equiv.) was then added dropwise with stirring to the solution. This solution was allowed to stir at room temperature for 2 hours. The solvent was removed *in vacuo* and the crude **360** was washed with diethyl ether to remove excess acid and unreacted amine. The resulting off white precipitate was isolated by vacuum filtration (1.705 g, 89% yield).

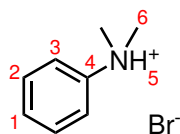
^1H NMR (400 MHz, DMSO- d_6) δ 10.23 (2H, br, H₅), 7.56 - 7.50 (4H, m, H₂₊₃), 7.47 - 7.42 (1H, m, H₁), 2.94 (3H, s, H₆).

^{13}C NMR (101 MHz, DMSO- d_6) δ 137.9 (C₄), 130.0 (C₂), 128.5 (C₁), 122.0 (C₃), 36.0 (C₆).

mp: 96 °C (MeCN).

IR (vmax/cm⁻¹): 2870br, 1472m, 1395m, 1122m, 754s, 688s, 563s. 487s.

*Data consistent with literature values.*³¹⁶

***N,N*-dimethylanilinium hydrobromide****361**

N,N-dimethyl aniline (1.222 g, 10.1 mmol) was dissolved in MeCN (5.0 mL, 2.0 M). 48% HBr solution (2.27 mL, 2.0 equiv.) was then added dropwise with stirring to the solution. This solution was allowed to stir at room temperature for 2 hours. The solvent was removed *in vacuo* and the crude **361** was washed with diethyl ether to remove excess acid and unreacted amine. The resulting hydroscopic off-white precipitate was

isolated by vacuum filtration (1.790 g, 88% yield).

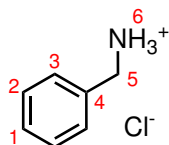
^1H NMR (400 MHz, DMSO- d_6) δ 7.83 (2H, d, J = 8.0 Hz, H₃), 7.55 (2H, t, J = 7.4 Hz, H₂), 7.68 (1H, t, J = 7.4 Hz, H₁), 4.83 (1H, s, H₅), 3.17 (6H, s, H₆).

^{13}C NMR (101 MHz, DMSO- d_6) δ 143.2 (C₄), 130.1 (C₂), 129.5 (C₁), 120.9 (C₃), 45.8 (C₆).

mp: 75 °C (MeCN).

IR (vmax/cm⁻¹): 3424br, 2434m, 1495m, 1130m, 898m, 766s, 691s, 529s.

*Data consistent with literature values.*³¹⁷

Benzylammonium hydrochloride**362**

Benzylamine (1.10 mL, 10.0 mmol) was dissolved in MeCN (5.0 mL, 2.0 M). 37% HCl solution (3.34 mL, 4.0 equiv.) was then added dropwise with stirring to the solution. This solution was allowed to stir at room temperature for 3 hours. The solvent was removed *in vacuo* and the crude **362** was washed with diethyl ether to remove excess acid and unreacted amine. The resulting off white precipitate was isolated by vacuum filtration (1.427 g, 100% yield).

isolated by vacuum filtration (1.427 g, 100% yield).

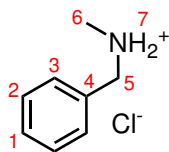
^1H NMR (400 MHz, DMSO- d_6) δ 8.63 (3H, s, H₆), 7.55 – 7.46 (2H, m, H₃), 7.44 – 7.30 (3H, m, H₁₊₂), 4.01 – 3.96 (2H, m, H₅).

^{13}C NMR (101 MHz, DMSO- d_6) δ 134.2 (C₄), 129.0 (C₂), 128.6 (C₃), 128.4 (C₁), 42.1 (C₅).

mp: 230 – 232 °C (MeCN).

IR (vmax/cm⁻¹): 2965br, 1596m, 1112m, 744s, 692s, 576m, 481m.

*Data consistent with literature values.*³¹⁸

N-methyl benzylammonium hydrochloride**363**

N-methyl benzylamine (1.30 mL, 10.0 mmol) was dissolved in MeCN (5.0 mL, 2.0 M). 37% HCl solution (2.51 mL, 3.0 equiv.) was then added dropwise with stirring to the solution. This solution was allowed to stir at room temperature for 3 hours. The solvent was removed *in vacuo* and the crude **363** was washed with diethyl ether to remove excess acid and unreacted amine. The resulting

off white precipitate was isolated by vacuum filtration (0.401 g, 25% yield).

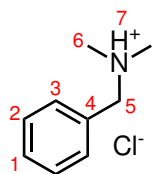
^1H NMR (400 MHz, DMSO- d_6) δ 9.36 (2H, s, H₇), 7.56 – 7.51 (2H, m, H₃), 7.46 – 7.38 (3H, m, H₁₊₂), 4.09 (2H, t, J = 6.0 Hz, H₅), 2.50 (3H, s, H₆).

^{13}C NMR (101 MHz, DMSO- d_6) δ 134.1 (C₄), 130.0 (C₂), 128.9 (C₁), 128.7 (C₃), 51.1 (C₅), 31.9 (C₇).

mp: 104 – 106 °C (MeCN).

IR (vmax/cm⁻¹): 3356br, 2930br(m), 2433w, 2270m, 1435m, 1025m, 748s, 702s.

*Data consistent with literature values.*³¹⁹

***N,N*-dimethylbenzylammonium hydrochloride****364**

A solution of *N,N*-dimethylbenzylamine (1.57 mL, 11.1 mmol) in ethanol (1.0 M, 11.0 mL) was prepared and cooled on an ice bath. With stirring, concentrated HCl was added dropwise until a strongly acidic solution was observed. The excess HCl and solvent were removed under reduced pressure with the aid of a base trap to neutralise acidic vapours. After thorough drying, **364** was yielded as a

white crystalline solid (1.90 g, 100% yield).

^1H NMR (400 MHz, CDCl₃) δ 12.62 (1H, s, H₇), 7.59 (2H, dd, J = 5.1, 2.6 Hz, H₃), 7.48 – 7.35 (3H, m, H₁₊₂), 4.18 (2H, d, J = 5.3 Hz, H₅), 2.74 (6H, d, J = 5.0 Hz, H₆).

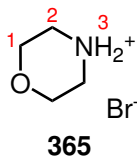
^{13}C NMR (101 MHz, CDCl₃) δ 131.0 (C₄), 130.2 (C₂), 129.3 (C₁), 128.4 (C₃), 61.0 (C₅), 42.0 (C₆).

LRMS (ESI-TOF, EI⁺) m/z : 136.1 ([M]⁺, 100%).

HRMS (ESI-TOF) m/z : [M]⁺ Calculated for C₉H₁₄N⁺: 136.1126, found: 136.1131.

mp: 94 °C (MeCN).

IR (vmax/cm⁻¹): 3377br, 2958w, 2573m, 2480m, 1455m, 944m, 743s, 697s.

Morpholinium hydrobromide

Morpholine (0.44 mL, 5.0 mmol) was dissolved in MeCN (2.5 mL, 2.0 M). 48% HBr solution (2.00 mL, 3.6 equiv.) was then added dropwise with stirring to the solution. This solution was allowed to stir at room temperature for 2 hours. The solvent was removed *in vacuo* and the crude **365** was washed with diethyl ether to remove

excess acid and unreacted amine. The resulting white precipitate was isolated by vacuum filtration (0.672 g, 80% yield).

^1H NMR (400 MHz, DMSO- d_6) δ 8.98 (2H, s, H₃), 3.80 – 3.73 (4H, m, H₁), 3.13 – 3.06 (4H, m, H₂).

^{13}C NMR (101 MHz, DMSO- d_6) δ 63.1 (C₁), 43.8 (C₂).

mp: 205 °C (MeCN).

IR (vmax/cm⁻¹): 3395br, 2945br, 1096m, 868m.

*Data consistent with literature values.*³²⁰

N-methyl morpholinium hydrobromide

N-methyl morpholine (0.47 mL, 4.3 mmol) was dissolved in MeCN (2.5 mL, 2.0 M). 48% HBr solution (1.13 mL, 2.3 equiv.) was then added dropwise with stirring to the solution. This solution was allowed to stir at room temperature for 2 hours. The solvent was removed *in vacuo* and the crude **366** was washed with diethyl ether

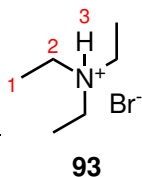
to remove excess acid and unreacted amine. The resulting white precipitate was isolated by vacuum filtration (0.650 g, 83% yield).

^1H NMR (400 MHz, DMSO- d_6) δ 10.02 (1H, s, H₃), 3.96 (2H, dd, J = 12.9, 3.6 Hz, H₁), 3.67 (2H, t, J = 11.5 Hz, H_{1'}), 3.36 (2H, d, J = 12.9 Hz, H₂), 3.14 – 3.02 (2H, m, H_{2'}), 2.79 (3H, d, J = 4.7 Hz, H₄).

^{13}C NMR (101 MHz, DMSO- d_6) δ 63.3 (C₁), 52.5 (C₄), 42.4 (C₂).

mp: 74 °C (MeCN).

IR (vmax/cm⁻¹): 3363br, 2912m, 2612m, 1467m, 1089m, 862s.

***N,N,N*-triethylammonium hydrobromide**

Triethylamine (anhydrous) (0.61 mL, 5.0 mmol) was dissolved in MeCN (2.00 mL, 2.5 M). 48% HBr solution (0.85 mL, 1.5 equiv.) was then added dropwise with stirring to the solution. This solution was allowed to stir at room temperature for 2 hours. The solvent was removed *in vacuo* and the crude **93** was washed with diethyl

ether to remove excess acid and unreacted amine. The resulting orange precipitate was isolated by vacuum filtration (0.895 g, 98% yield).

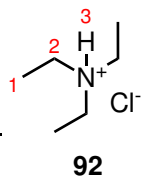
^1H NMR (400 MHz, DMSO- d_6) δ 9.47 (1H, s, H₃), 3.09 (6H, qd, $J = 7.3, 4.8$ Hz, H₂), 1.19 (9H, t, $J = 7.3$ Hz, H₁).

^{13}C NMR (101 MHz, DMSO- d_6) δ 45.6 (C₂), 8.6 (C₁).

mp: 234 – 236 °C (MeCN).

IR ($\nu_{\text{max}}/\text{cm}^{-1}$): 2938m, 2676m, 1397m, 1170m, 1034s, 804s.

*Data consistent with literature values.*³²¹

***N,N,N*-triethylammonium hydrochloride**

A solution of triethylamine (3.00 g, 29.6 mmol) in ethanol (1.0 M, 30 mL) was prepared and cooled on an ice bath. With stirring, concentrated HCl was added dropwise until a strongly acidic solution was observed. The excess HCl and solvent were removed under reduced pressure with the aid of a base trap to neutralise acidic

vapours. After thorough drying, **92** was yielded as a white crystalline solid (4.07 g, 100% yield).

^1H NMR (400 MHz, CDCl₃) δ 3.08 (6H, qd, $J = 7.3, 4.8$ Hz, H₂), 1.38 (9H, t, $J = 7.3$ Hz, H₁).

^{13}C NMR (101 MHz, CDCl₃) δ 45.8 (C₂), 8.6 (C₁).

LRMS (ESI-TOF, EI⁺) m/z : 102.1 ([M]⁺, 100%).

HRMS (ESI-TOF) m/z : [M]⁺ Calculated for C₆H₁₆N⁺: 102.1283, found: 102.1290.

mp: 260 – 262 °C (MeCN).

*Data consistent with literature values.*³²²

4-dimethylaminopyridinium hydrobromide

4-Dimethylaminopyridine (0.608 g, 5.0 mmol) was dissolved in MeCN (3.00 mL, 1.7 M). 48% HBr solution (0.85 mL, 1.5 equiv.) was then added dropwise with stirring to the solution. This solution was allowed to stir at room temperature for 2 hours. The solvent was removed *in vacuo* and the crude **367** was washed with diethyl ether to remove excess acid and unreacted amine. The resulting

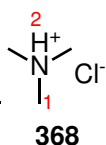
white precipitate was isolated by vacuum filtration (0.610 g, 60% yield).

^1H NMR (400 MHz, DMSO- d_6) δ 8.27 – 8.19 (2H, m, H₂), 6.98 (2H, d, J = 7.0 Hz, H₃), 3.17 (6H, s, H₅).

^{13}C NMR (101 MHz, DMSO- d_6) δ 156.9 (C₄), 139.0 (C₂), 107.0 (C₃), 39.8 (C₅).

mp: 210 – 212 °C (MeCN).

IR (vmax/cm⁻¹): 3053br, 2891br, 1640m, 1556s, 1393m, 1206s, 993m, 801s, 510s.

***N,N,N*-trimethyl ammonium hydrochloride**

37% HCl solution (1.25 mL, 3.0 equiv.) was added dropwise with stirring to a solution of trimethylamine 35% wt in EtOH (1.19 mL, 5.0 mmol). This solution was allowed to stir at room temperature for 2 hours. The solvent was removed *in vacuo* and the crude **94** was washed with diethyl ether to remove excess acid and unreacted amine. The resulting orange precipitate was isolated by vacuum filtration (0.895

g, 98% yield).

^1H NMR (400 MHz, DMSO- d_6) δ 11.06 (1H, s, H₂), 2.70 (9H, d, J = 4.9 Hz, H₁).

^{13}C NMR (101 MHz, DMSO- d_6) δ 43.7 (C₁).

IR (vmax/cm⁻¹): 2959w, 2595m, 2473m, 1482m, 988s.

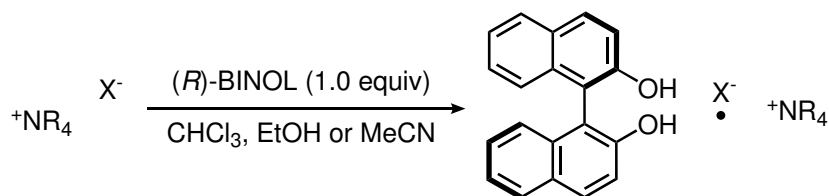
mp: 283 – 285 °C (MeCN).

*Data consistent with literature values.*³²²

For achiral protonated ammonium salts that haven't been characterised in this experimental section but are listed to have been complexed with BINOL in this thesis, see M.P. Walsh's thesis for full characterisation. Callum S. Begg synthesised these salts but did not fully characterise them due to the data already being available.

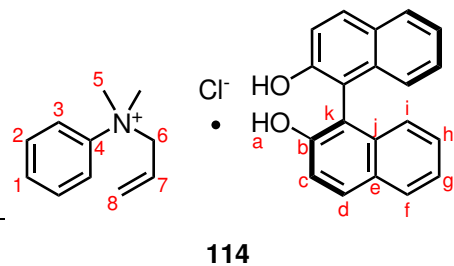
9.5 Recognition of ammonium salts

9.5.1 General procedure for recognition of ammonium salts



Scheme 9.10: General procedure for recognition of ammonium salts by (R) -BINOL.

The selected ammonium salt was dissolved into $CHCl_3$, MeCN or EtOH (0.6 – 2.0 M), solid (R) -BINOL was added to the solution and the reaction mixture was stirred vigorously at room temperature. A white precipitate is generally observed 5 – 30 minutes after (R) -BINOL addition. After 24 hours the reaction is filtered and washed with reaction solvent to yield a white solid precipitate which can be recrystallised (MeOH, $CHCl_3$, EtOH) to yield SCXRD quality crystals.

***N*-allyl-*N,N*-dimethylanilinium chloride · (*R*)-1,1'-bi-2-naphthol**

The quaternary ammonium chloride salt **72** (0.030 g, 0.15 mmol) was dissolved in CHCl_3 (0.40 mL, 0.4 M) in a 10 mL vial. Solid (*R*)-BINOL (0.043 g, 1.0 equiv.) was then added with stirring to the solution, resulting in a pale yellow homogeneous solution. This solution was allowed to stir at room temper-

ature overnight, which produced the desired complexed product **114** as a white precipitate. The resulting complex was isolated by vacuum filtration (0.058 g, 80% yield).

Analysis by ^1H NMR spectroscopy ensured that a 1:1 complex had formed.

^1H NMR (400 MHz, CD_3OD) δ 7.87 (2H, dd, $J = 9.0, 0.8$ Hz, H_d), 7.83 (2H, dt, $J = 8.2, 0.9$ Hz, H_f), 7.81 – 7.77 (2H, m, H_3), 7.66 – 7.54 (3H, m, H_{1+2}), 7.30 (2H, d, $J = 8.9$ Hz, H_i), 7.24 (2H, ddd, $J = 8.1, 6.8, 1.3$ Hz, H_g), 7.16 (2H, ddd, $J = 8.3, 6.8, 1.3$ Hz, H_h), 7.05 – 6.99 (2H, m, H_c), 5.66 – 5.47 (3H, m, H_{7+8}), 4.45 (2H, d, $J = 5.7$ Hz, H_6), 3.55 (6H, s, H_5).

^{13}C NMR (101 MHz, CD_3OD) δ 154.2, 144.9, 135.8, 131.65, 130.64, 130.56, 130.4, 129.3, 129.0, 127.1, 126.3, 125.8, 123.9, 122.0, 119.3, 116.2, 72.6, 54.3.

LRMS (ESI-TOF, EI^+) m/z : 162.2 ($[\text{M}]^+$, 100%).

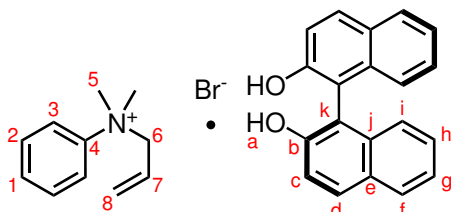
LRMS (ESI-TOF, EI^-) m/z : 285.3 ($[\text{M}-\text{H}]^-$, 100%).

HRMS (ESI-TOF) m/z : $[\text{M}]^+$ calculated for $\text{C}_{11}\text{H}_{16}\text{N}^+$: 162.1283, found 162.1282. $[\text{M}-\text{H}]^-$ calculated for $\text{C}_{20}\text{H}_{13}\text{O}_2^-$: 285.0916, found 285.0916.

mp: 148 °C, decomposes to red oil (CHCl_3).

IR ($\nu_{\text{max}}/\text{cm}^{-1}$): 3048br, 2982m, 1622m, 1505m, 1273m, 819m.

XRD: A portion of the complex was crystallised in EtOH to give clear colourless prisms. Crystal data for $\text{C}_{30}\text{H}_{28}\text{NO}_2\text{Cl}$ ($m = 469.98$ g/mol): Orthorhombic, space group $\text{P2}_1\text{2}_1\text{2}_1$ (no. 19).

***N*-allyl-*N,N*-dimethylanilinium bromide · (*R*)-1,1'-bi-2-naphthol****115**

The quaternary ammonium bromide salt **73** (0.230 g, 0.95 mmol) was dissolved in CHCl_3 (0.50 mL, 2.0 M) in a 10 mL vial. Solid (*R*)-BINOL (0.292 g, 1.0 equiv.) was then added with stirring to the solution, resulting in a pale yellow homogeneous solution. This solution was allowed to stir at room temper-

ature overnight, which produced the desired complexed product **115** as a white precipitate. The resulting complex was isolated by vacuum filtration (0.445 g, 93% yield). Analysis by ^1H NMR spectroscopy ensured that a 1:1 complex had formed.

^1H NMR (400 MHz, CD_3OD) δ 7.87 (2H, dd, $J = 9.0, 0.7$ Hz, H_d), 7.83 (2H, dd, $J = 8.2, 0.9$ Hz, H_f), 7.79 (2H, d, $J = 8.2$ Hz, H_3), 7.64 – 7.54 (3H, m, H_{1+2}), 7.30 (2H, d, $J = 8.9$ Hz, H_i), 7.24 (2H, ddd, $J = 8.1, 6.7, 1.3$ Hz, H_g), 7.15 (2H, ddd, $J = 8.2, 6.8, 1.4$ Hz, H_h), 7.02 (2H, dq, $J = 8.5, 0.9$ Hz, H_c), 5.68 – 5.45 (3H, m, H_{7+8}), 4.45 (2H, d, $J = 5.6$ Hz, H_6), 3.54 (3H, s, H_5).

^{13}C NMR (101 MHz, CD_3OD) δ 154.1, 145.8, 135.7, 131.6, 131.5, 130.5, 130.3, 129.4, 129.1, 127.2, 126.1, 125.8, 123.9, 122.9, 119.3, 116.3, 72.5, 54.2.

LRMS (ESI-TOF, EI^+) m/z : 162.3 ($[\text{M}]^+$, 100%).

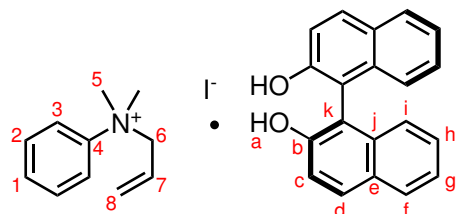
LRMS (ESI-TOF, EI^-) m/z : 285.3 ($[\text{M}-\text{H}]^-$, 100%).

HRMS (ESI-TOF) m/z : $[\text{M}]^+$ Calculated for $\text{C}_{13}\text{H}_{20}\text{N}^+$: 162.1283, found 162.1288. $[\text{M}-\text{H}]^-$ calculated for $\text{C}_{20}\text{H}_{13}\text{O}_2^-$: 285.0916, found 285.0915.

mp: 150 °C, decomposes to red oil (EtOH).

IR ($\nu_{\text{max}}/\text{cm}^{-1}$): 3115br, 1625m, 1506m, 1430m, 1271m, 816m.

XRD: A portion of the complex was crystallised in EtOH to give clear colourless plates. Crystal data for $\text{C}_{31}\text{H}_{30}\text{BrNO}_2$ ($m = 528.47$ g/mol): Orthorhombic, space group $P2_12_12_1$ (no. 19).

***N*-allyl-*N,N*-dimethylanilinium iodide · (*R*)-1,1'-bi-2-naphthol****116**

The quaternary ammonium iodide salt **74** (0.144 g, 1.00 mmol) was dissolved in CHCl_3 (1.25 mL, 0.8 M) in a 10 mL vial. Solid (*R*)-BINOL (0.286 g, 1.0 equiv.) was then added with stirring to the solution, resulting in a pale red homogeneous solution. This solution was allowed to stir at room temperature overnight,

which produced the desired complexed product **116** as a white precipitate. The resulting complex was isolated by vacuum filtration (0.229 g, 80% yield). Analysis by ^1H NMR spectroscopy ensured that a 1:1 complex had formed.

^1H NMR (400 MHz, CD_3OD) δ 7.87 (2H, dd, $J = 9.0, 0.7$ Hz, H_d), 7.85 – 7.81 (4H, m, H_{f+3}), 7.70 – 7.59 (3H, m, H_{1+2}), 7.29 (2H, d, $J = 8.9$ Hz, H_i), 7.24 (2H, ddd, $J = 8.0, 6.7, 1.3$ Hz, H_g), 7.16 (2H, ddd, $J = 8.3, 6.8, 1.4$ Hz, H_h), 7.02 (2H, dd, $J = 8.5, 1.1$ Hz, H_c), 5.72 – 5.52 (3H, m, H_{7+8}), 4.51 (2H, d, $J = 6.2$ Hz, H_6), 3.61 (6H, s, H_5).

^{13}C NMR (101 MHz, CD_3OD) δ 154.2, 145.6, 135.8, 131.6, 130.6, 130.4, 129.4, 129.0, 127.1, 126.3, 125.8, 123.9, 122.0, 119.3, 116.2, 72.6, 54.4. *Spectrum missing a resonance due to the coincidence of C_2 and C_d signals.*

LRMS (ESI-TOF, EI^+) m/z : 162.2 ($[\text{M}]^+$, 100%), 130.3 (2), 110.1 (6).

LRMS (ESI-TOF, EI^-) m/z : 285.2 ($[\text{M}-\text{H}]^-$, 100%).

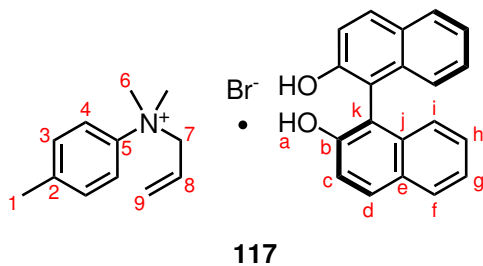
HRMS (ESI-TOF) m/z : $[\text{M}]^+$ calculated for $\text{C}_{11}\text{H}_{16}\text{N}^+$: 162.1283, found 162.1278. $[\text{M}-\text{H}]^-$ calculated for $\text{C}_{20}\text{H}_{13}\text{O}_2^-$: 285.0916, found 285.0916.

mp: 154 °C (CHCl_3).

IR ($\nu_{\text{max}}/\text{cm}^{-1}$): 3185br, 1621m, 1317m, 1145m, 952m, 815s,.

XRD: A portion of the complex was crystallised in EtOH to give clear colourless plates.

Crystal data for $\text{C}_{31}\text{H}_{30}\text{INO}_2$ ($m = 575.46$ g/mol): Orthorhombic, space group $P2_12_12_1$ (no. 19).

***N*-allyl-4-methyl-*N,N*-dimethylanilinium bromide · (*R*)-1,1'-bi-2-naphthol**

The quaternary ammonium bromide salt **75** (0.249 g, 1.0 mmol) was dissolved in CHCl_3 (0.75 mL, 1.3 M) in a 10 mL vial. Solid (*R*)-BINOL (0.287 g, 1.0 equiv.) was then added with stirring to the solution, resulting in a homogeneous solution. This solution was allowed to stir at room temperature overnight,

which produced the desired complexed product **117** as a white precipitate. The resulting complex was isolated by vacuum filtration (0.384 g, 71% yield). Analysis by ^1H NMR spectroscopy ensured that a 1:1 complex had formed.

^1H NMR (599 MHz, CD_3OD) δ 7.87 (2H, d, $J = 8.9$ Hz, H_d), 7.83 (2H, d, $J = 8.5$ Hz, H_f), 7.71 – 7.65 (2H, m, H_4), 7.47 – 7.41 (2H, m, H_3), 7.29 (2H, d, $J = 8.9$ Hz, H_i), 7.24 (2H, ddd, $J = 8.0, 6.6, 1.2$ Hz, H_g), 7.16 (2H, ddd, $J = 8.1, 6.7, 1.3$ Hz, H_h), 7.02 (2H, d, $J = 8.4$ Hz, H_c), 5.66 – 5.58 (1H, m, H_8), 5.58 – 5.52 (2H, m, H_9), 4.46 (2H, d, $J = 6.8$ Hz, H_7), 3.56 (6H, s, H_6), 2.41 (3H, s, H_1).

^{13}C NMR (151 MHz, CD_3OD) δ 154.2, 142.4, 135.8, 132.0, 130.6, 130.5, 129.2, 129.0, 127.1, 126.4, 125.8, 123.8, 121.8, 119.3, 116.2, 72.6, 54.3, 20.8. *Spectrum missing a resonance due to the coincidence of C_2 and C_d signals.*

LRMS (ESI-TOF, EI^+) m/z : 176.2 ($[\text{M}]^+$, 100%), 135.09 (28).

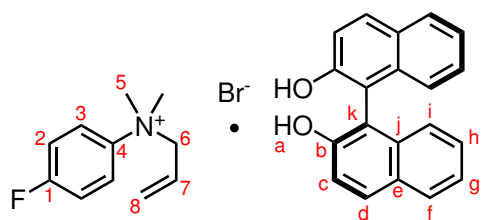
LRMS (ESI-TOF, EI^-) m/z : 285.1 ($[\text{M}-\text{H}]^-$, 100%).

HRMS (ESI-TOF) m/z : $[\text{M}]^+$ calculated for $\text{C}_{12}\text{H}_{18}\text{N}^+$: 176.1439, found 176.1438. $[\text{M}-\text{H}]^-$ calculated for $\text{C}_{20}\text{H}_{13}\text{O}_2^-$: 285.0916, found 285.0926.

mp: 144 – 147 °C (CHCl_3).

IR ($\nu_{\text{max}}/\text{cm}^{-1}$): 3128br, 1622m, 1431s, 1270s, 953s, 757s.

XRD: A portion of the complex was crystallised in EtOH to give colourless plates. Crystal data for $\text{C}_{32}\text{H}_{32}\text{BrNO}_2$ ($m = 542.49$ g/mol): Orthorhombic, space group $P2_12_12_1$ (no. 19).

***N*-allyl-4-fluoro-*N,N*-dimethylanilinium bromide · (*R*)-1,1'-bi-2-naphthol****118**

The quaternary ammonium bromide salt **76** (0.156 g, 0.6 mmol) was dissolved in CHCl_3 (0.29 mL, 2.0 M) in a 10 mL vial. Solid (*R*)-BINOL (0.169 g, 1.0 equiv.) was then added with stirring to the solution, resulting in a homogeneous solution. This solution was allowed to stir at room temperature overnight,

which produced the desired complexed product **118** as a white precipitate. The resulting complex was isolated by vacuum filtration (0.209 g, 66% yield). Analysis by ^1H NMR spectroscopy ensured that a 1:1 complex had formed.

^1H NMR (599 MHz, CD_3OD) δ 7.92 – 7.88 (2H, m, H_2), 7.87 (2H, d, $J = 9.0$ Hz, H_d), 7.83 (2H, d, $J = 8.3$ Hz, H_f), 7.41 – 7.36 (2H, m, H_3), 7.29 (2H, d, $J = 8.9$ Hz, H_i), 7.27 – 7.22 (2H, m, H_g), 7.16 (2H, ddd, $J = 8.2, 6.7, 1.3$ Hz, H_h), 7.02 (2H, d, $J = 8.6$ Hz, H_c), 5.71 – 5.63 (1H, m, H_7), 5.61 – 5.54 (2H, m, H_8), 4.49 (2H, dd, $J = 7.1, 2.8$ Hz, H_6), 3.61 (6H, s, H_5).

^{13}C NMR (151 MHz, CD_3OD) δ 164.3 (d, $J = 250.7$ Hz), 154.2, 142.0, 135.8, 130.5 (d, $J = 16.3$ Hz), 129.6, 129.0, 127.1, 126.2, 125.8, 124.8 (d, $J = 8.9$ Hz), 123.8, 119.3, 118.4, 118.2, 116.2, 73.0, 54.6.

^{19}F NMR (376 MHz, CHCl_3) δ – 108.62.

LRMS (ESI-TOF, EI^+) m/z : 180.1 ($[\text{M}]^+$, 100%).

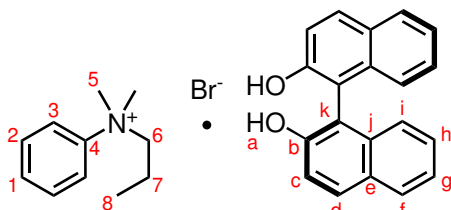
LRMS (ESI-TOF, EI^-) m/z : 285.1 ($[\text{M}-\text{H}]^-$, 100%).

HRMS (ESI-TOF) m/z : $[\text{M}]^+$ calculated for $\text{C}_{11}\text{H}_{15}\text{NF}^+$: 180.1189, found 180.1185. $[\text{M}-\text{H}]^-$ calculated for $\text{C}_{20}\text{H}_{13}\text{O}_2^-$: 285.0916, found 285.0909.

mp: 142 – 144 °C (CHCl_3).

IR ($\nu_{\text{max}}/\text{cm}^{-1}$): 3122br, 1621br, 1504m, 1271s, 957s, 819s.

XRD: A portion of the complex was crystallised in MeOH to give yellow plates. Crystal data for $\text{C}_{31}\text{H}_{29}\text{BrFNO}_2$ ($m = 546.46$ g/mol): Orthorhombic, space group $P2_12_12_1$ (no. 19).

***N,N*-dimethyl-*N*-propylanilinium · (*R*)-1,1'-bi-2-naphthol****119**

The quaternary ammonium bromide salt **77** (0.100 g, 0.41 mmol) was dissolved in CHCl_3 (1.0 mL, 0.4 M) in a 10 mL vial. Solid (*R*)-BINOL (0.117 g, 1.0 equiv.) was then added with stirring to the solution, resulting in a pale yellow homogeneous solution. This solution was allowed to stir at room temperature

overnight, which produced the desired complexed product **119** as a white precipitate. The resulting complex was isolated by vacuum filtration (0.162 g, 74% yield). Analysis by ^1H NMR spectroscopy ensured that a 1:1 complex had formed.

^1H NMR (400 MHz, CD_3OD) δ 7.90 – 7.85 (2H, m, H_d), 7.85 – 7.81 (2H, m, H_f), 7.79 – 7.74 (2H, m, H_3), 7.66 – 7.53 (3H, m, H_{1+2}), 7.30 (2H, d, $J = 8.9$ Hz, H_i), 7.24 (2H, ddd, $J = 8.1, 6.7, 1.3$ Hz, H_g), 7.15 (2H, ddd, $J = 8.2, 6.7, 1.3$ Hz, H_h), 7.02 (2H, ddt, $J = 8.5, 1.5, 0.8$ Hz, H_c), 3.84 – 3.73 (2H, m, H_6), 3.53 (6H, s, H_5), 1.47 – 1.31 (2H, m, H_7), 0.87 (3H, t, $J = 7.4$ Hz, H_8).

^{13}C NMR (101 MHz, CD_3OD) δ 154.2, 145.8, 135.8, 131.7, 131.5, 130.6, 130.4, 129.0, 127.1, 125.8, 123.9, 121.8, 119.3, 116.2, 71.3, 56.2, 17.3, 9.9.

LRMS (ESI-TOF, EI^+) m/z : 164.7 ($[\text{M}]^+$, 100%), 121.0 (1).

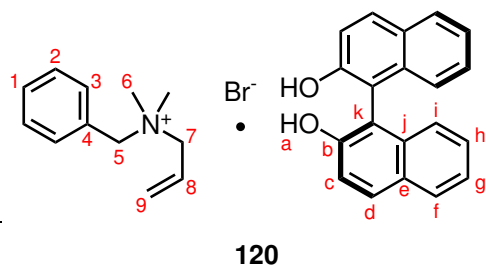
LRMS (ESI-TOF, EI^-) m/z : 285.3 ($[\text{M}-\text{H}]^-$, 100%).

HRMS (ESI-TOF) m/z : $[\text{M}]^+$ calculated for $\text{C}_{11}\text{H}_{18}\text{N}^+$: 164.1439, found 164.1431. $[\text{M}-\text{H}]^-$ calculated for $\text{C}_{20}\text{H}_{13}\text{O}_2^-$: 285.0916, found 285.0903.

mp: 184 – 186 °C (EtOH).

IR ($\nu_{\text{max}}/\text{cm}^{-1}$): 3122br, 1339m, 1271m, 818m, 756m, 685m.

XRD: A portion of the complex was crystallised in EtOH to give clear colourless plates. Crystal data for $\text{C}_{31}\text{H}_{32}\text{BrNO}_2$ ($m = 599.24$ g/mol): orthorhombic, space group $P2_12_12_1$ (no. 19).

***N*-benzyl-*N,N*-dimethylprop-2-en-1-aminium bromide · (*R*)-1,1'-bi-2-naphthol**

The quaternary ammonium bromide salt **78** (0.256 g, 1.00 mmol) was dissolved in CHCl_3 (2.5 mL, 0.4 M) in a 10 mL vial. Solid (*R*)-BINOL (0.286 g, 1.0 equiv.) was then added with stirring to the solution, resulting in a pale yellow homogeneous solution. This solution was allowed to stir at room temperature

overnight, which produced the desired complexed product **120** as a white precipitate. The resulting complex was isolated by vacuum filtration (0.449 g, 83% yield). Analysis by ^1H NMR spectroscopy ensured that a 1:1 complex had formed.

^1H NMR (400 MHz, CD_3OD) δ 7.87 (2H, d, $J = 8.9$ Hz, H_d), 7.82 (2H, dd, $J = 7.9, 1.2$ Hz, H_f), 7.58 – 7.47 (5H, m, H_{1+2+3}), 7.29 (2H, d, $J = 8.8$ Hz, H_i), 7.26 – 7.21 (2H, m, H_g), 7.15 (2H, ddd, $J = 8.2, 6.7, 1.4$ Hz, H_h), 7.02 (2H, dd, $J = 8.4, 1.2$ Hz, H_c), 6.12 (1H, ddt, $J = 17.4, 10.3, 7.3$ Hz, H_8), 5.78 – 5.65 (2H, m, H_9), 4.47 (2H, s, H_5), 3.94 (2H, d, $J = 7.3$ Hz, H_7), 2.92 (6H, s, H_6).

^{13}C NMR (101 MHz, CD_3OD) δ 154.2, 135.8, 134.1, 131.9, 130.6, 130.4, 130.3, 129.6, 129.0, 128.7, 127.1, 126.2, 125.8, 123.8, 119.2, 116.2, 68.9 (dd, $J = 5.0, 2.8$ Hz), 67.9 (dd, $J = 6.3, 3.0$ Hz), 49.8 (dd, $J = 8.5, 4.1$ Hz).

LRMS (ESI-TOF, EI^+) m/z : 176.2 ($[\text{M}]^+$, 100%), 110.0 (4).

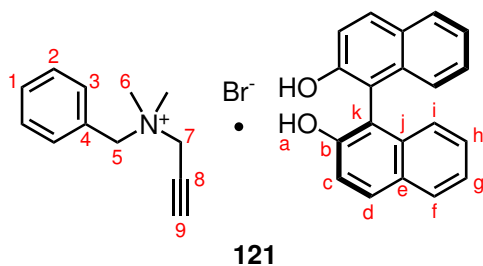
LRMS (ESI-TOF, EI^-) m/z : 286.2 ($[\text{M}-\text{H}]^-$, 100%).

HRMS (ESI-TOF) m/z : $[\text{M}]^+$ calculated for $\text{C}_{12}\text{H}_{18}\text{N}^+$: 176.1439, found 176.1439. $[\text{M}-\text{H}]^-$ calculated for $\text{C}_{20}\text{H}_{13}\text{O}_2^-$: 285.0916, found 285.0906.

mp: 194 – 196 °C (CHCl_3).

IR ($\nu_{\text{max}}/\text{cm}^{-1}$): 3126br, 1620m, 1504m, 1271s, 968m, 815s.

XRD: A portion of the complex was crystallised in EtOH to give clear colourless plates. Crystal data for $\text{C}_{32}\text{H}_{32}\text{NO}_2\text{Br}$ ($m = 542.49$ g/mol): Orthorhombic, space group $P2_12_12_1$ (no. 19).

***N,N*-dimethyl-*N*-(prop-1-yne)-*N*-benzylammonium bromide · (*R*)-1,1'-bi-2-naphthol**

Ammonium salt **79** (0.306 g, 1.0 mmol) was dissolved in CHCl_3 (1.67 mL, 0.6 M) in a 10 mL vial. Solid (*R*)-BINOL (0.286 g, 1.0 equiv.) was then added with stirring to the solution. This solution was allowed to stir at room temperature overnight, which produced the desired complexed product **121** as a white precipitate.

The resulting complex was isolated by vacuum filtration (0.483 g, 89% yield). Analysis by ^1H NMR spectroscopy ensured that a 1:1 complex had formed.

^1H NMR (400 MHz, $\text{DMSO}-d_6$) δ 9.22 (2H, s, H_a), 7.91 – 7.80 (4H, m, H_{d+f}), 7.66 – 7.51 (5H, m, H_{1+2+3}), 7.33 (2H, d, $J = 8.9$ Hz, H_i), 7.24 (2H, ddd, $J = 8.1, 6.7, 1.3$ Hz, H_g), 7.17 (2H, ddd, $J = 8.2, 6.7, 1.5$ Hz, H_h), 6.94 (2H, dd, $J = 8.4, 1.3$ Hz, H_c), 4.62 (2H, s, H_5), 4.32 (2H, d, $J = 2.5$ Hz, H_7), 4.19 (1H, t, $J = 2.5$ Hz, H_9), 3.06 (6H, s, H_6).
 ^{13}C NMR (101 MHz, $\text{DMSO}-d_6$) δ 153.5, 134.6, 133.3, 131.0, 129.6, 129.1, 128.6, 128.3, 128.1, 126.3, 124.9, 122.7, 119.0, 115.8, 84.1, 73.0, 66.2, 53.4, 49.8.

LRMS (ESI-TOF, EI^+) m/z : 174.1 ($[\text{M}]^+$, 100%).

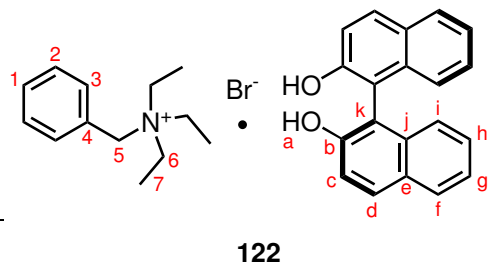
LRMS (ESI-TOF, EI^-) m/z : 286.2 ($[\text{M}-\text{H}]^-$, 100%).

HRMS (ESI-TOF) m/z : $[\text{M}]^+$ calculated for $\text{C}_{12}\text{H}_{16}\text{N}^+$: 174.1283, found: 174.1282. $[\text{M}-\text{H}]^-$ calculated for $\text{C}_{20}\text{H}_{13}\text{O}_2^-$: 285.0916, found: 285.0915.

mp: 178 – 180 °C (EtOH).

IR ($\nu_{\text{max}}/\text{cm}^{-1}$): 3157br, 2980m, 1504m, 1272m, 813m, 755m.

XRD: A portion of the complex was crystallised in EtOH to give clear colourless prisms. Crystal data for $\text{C}_{32}\text{H}_{30}\text{BrNO}_2$ ($m = 540.48$ g/mol): Orthorhombic, space group $P2_12_12_1$ (no. 19).

***N*-benzyl-*N,N*-triethylethanaminium bromide · (*R*)-1,1'-bi-2-naphthol**

The quaternary ammonium bromide salt **80** (0.100 g, 0.37 mmol) was dissolved in CHCl_3 (1.00 mL, 0.4 M) in a 10 mL vial. Solid (*R*)-BINOL (0.105 g, 1.0 equiv.) was then added with stirring to the solution, resulting in a pale yellow homogeneous solution. This solution was allowed to stir at room temper-

ature overnight, which produced the desired complexed product **122** as a white precipitate. The resulting complex was isolated by vacuum filtration (0.149 g, 73% yield).

Analysis by ^1H NMR spectroscopy ensured that a 1:1 complex had formed.

^1H NMR (400 MHz, CD_3OD) δ 7.87 (2H, dd, $J = 8.9, 0.8$ Hz, H_d), 7.83 (2H, dt, $J = 8.1, 0.9$ Hz, H_f), 7.59 – 7.47 (5H, m, H_{1+2+3}), 7.29 (2H, d, $J = 8.9$ Hz, H_i), 7.24 (2H, ddd, $J = 8.1, 6.8, 1.3$ Hz, H_g), 7.16 (2H, ddd, $J = 8.2, 6.8, 1.4$ Hz, H_h), 7.02 (2H, dd, $J = 8.4, 1.1$ Hz, H_c), 4.44 (2H, s, H_5), 3.21 (6H, q, $J = 7.3$ Hz, H_6), 1.49 – 1.28 (9H, m, H_7).

^{13}C NMR (101 MHz, CD_3OD) δ 154.2, 135.8, 133.6, 131.8, 130.6, 130.5, 130.4, 129.0, 128.7, 127.1, 125.8, 123.8, 119.3, 116.2, 61.4, 53.6, 8.1.

LRMS (ESI-TOF, EI^+) m/z : 192.2 ($[\text{M}]^+$, 100%), 110.1 (4).

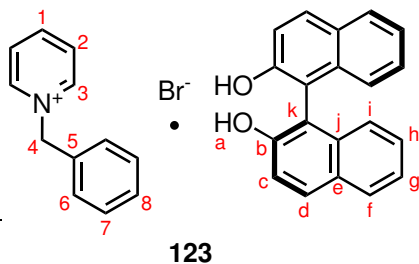
LRMS (ESI-TOF, EI^-) m/z : 285.3 ($[\text{M}-\text{H}]^-$, 100%).

HRMS (ESI-TOF) m/z : $[\text{M}]^+$ calculated for $\text{C}_{13}\text{H}_{22}\text{N}^+$: 192.1752, found 192.1745. $[\text{M}-\text{H}]^-$ calculated for $\text{C}_{20}\text{H}_{13}\text{O}_2^-$: 285.0916, found 285.0911.

mp: 191 – 192 °C (CHCl_3).

IR ($\nu_{\text{max}}/\text{cm}^{-1}$): 3120br, 1619m, 1331s, 1274s, 817s, 750s.

XRD: A portion of the complex was crystallised in ethanol to produce clear colourless blocks. Crystal data for $\text{C}_{32}\text{H}_{36}\text{NO}_2\text{Br}$ ($m = 546.53$ g/mol): Orthorhombic, space group $P2_12_12_1$ (no. 19).

1-benzylpyridinium bromide · (*R*)-1,1'-bi-2-naphthol

Ammonium salt **81** (0.250 g, 1.0 mmol) was dissolved in CHCl_3 (1.50 mL, 0.6 M) in a 10 mL vial. Solid (*R*)-BINOL (0.286 g, 1.0 equiv.) was then added with stirring to the solution, resulting in a pale yellow homogeneous solution. This solution was allowed to stir at room temperature overnight, which produced the desired complex **123** as a

white precipitate. The resulting complex was isolated by vacuum filtration (0.480 g, 90% yield). Analysis by ^1H NMR spectroscopy ensured that a 1:1 complex had formed. ^1H NMR (400 MHz, $\text{DMSO}-d_6$) δ 9.28 – 9.25 (2H, m, H_3), 9.24 (2H, s, H_a), 8.63 (1H, tt, $J = 7.8, 1.4$ Hz, H_1), 8.25 – 8.13 (2H, m, H_2), 7.89 – 7.79 (4H, m, H_{d+f}), 7.55 (2H, dd, $J = 7.6, 2.0$ Hz, H_6), 7.48 – 7.41 (3H, m, H_{7+8}), 7.34 (2H, d, $J = 8.8$ Hz, H_i), 7.22 (2H, ddd, $J = 8.1, 6.7, 1.3$ Hz, H_g), 7.16 (2H, ddd, $J = 8.2, 6.7, 1.4$ Hz, H_h), 6.93 (2H, dd, $J = 8.4, 1.2$ Hz, H_c), 5.90 (2H, s, H_4).

^{13}C NMR (101 MHz, $\text{DMSO}-d_6$) δ 153.0, 146.0, 144.8, 134.3, 134.1, 129.4, 129.3, 128.8, 128.6, 128.5, 128.1, 127.9, 125.8, 124.4, 122.3, 118.6, 115.4, 63.2.

LRMS (ESI-TOF, EI^+) m/z : 170.1 ($[\text{M}]^+$, 100%).

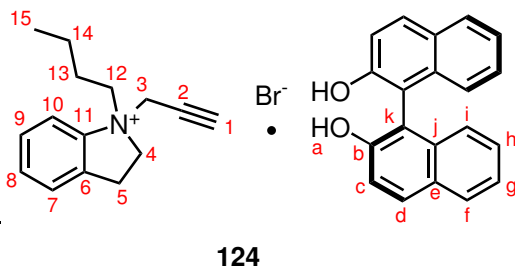
LRMS (ESI-TOF, EI^-) m/z : 285.2 ($[\text{M}-\text{H}]^-$, 100%).

HRMS (ESI-TOF) m/z : $[\text{M}]^+$ calculated for $\text{C}_{12}\text{H}_{12}\text{N}^+$: 170.0970, found: 170.0958. $[\text{M}-\text{H}]^-$ calculated for $\text{C}_{20}\text{H}_{13}\text{O}_2^-$: 285.0916, found: 285.0924.

mp: 204 °C (EtOH).

IR ($\nu_{\text{max}}/\text{cm}^{-1}$): 3141br, 2980m, 1625m, 1271m, 817m.

XRD: A portion of the complex was crystallised in EtOH, to give clear colourless irregular crystals. Crystal data for $\text{C}_{32}\text{H}_{26}\text{NO}_2\text{Br}$ ($m = 536.45$ g/mol): Orthorhombic, space group $P2_12_12_1$ (no. 19).

***rac*-1-butyl-1-(prop-2-yne)indolin-1-ium bromide · (*R*)-1,1'-bi-2-naphthol**

80% w/w propargyl bromide in toluene (0.14 mL, 1.3 mmol, 1.3 equiv.) was added to **82** (0.177 g, 1.01 mmol, 1.0 equiv.) in MeCN (0.50 mL, 2.0 M) and heated at 50 °C for 10 minutes. (*R*)-BINOL (0.289 g, 1.01 mmol, 1.0 equiv.) was added

and the reaction mixture was stirred vigorously at room temperature for 69 hrs, which produced the desired complexed product **124** as a white precipitate. The resulting complex was isolated by vacuum filtration (0.382 g, 65% yield). Analysis by ¹H NMR spectroscopy ensured that a 1:1 complex had formed.

¹H NMR (599 MHz, DMSO-*d*₆) δ 9.19 (2H, s, H_a), 7.89 – 7.81 (4H, m, H_{f+d}), 7.82 (1H, d, *J* = 7.6 Hz, H₁₀), 7.59 – 7.54 (3H, m, H₇₊₈₊₉), 7.32 (2H, d, *J* = 8.8 Hz, H_i), 7.23 (2H, ddd, *J* = 8.1, 6.7, 1.3 Hz, H_g), 7.17 (2H, ddd, *J* = 8.2, 6.7, 1.5 Hz, H_h), 6.93 (2H, d, *J* = 8.4 Hz, H_c), 4.93 – 4.85 (2H, m, H₃), 4.32 (1H, ddd, *J* = 12.0, 8.2, 6.2 Hz, H₄), 4.24 (1H, dt, *J* = 12.2, 7.8 Hz, H_{4'}), 3.89 – 3.84 (1H, m, H₁₂), 3.88 (1H, t, *J* = 2.5 Hz, H₁), 3.73 (1H, dd, *J* = 12.5, 4.0 Hz, H_{12'}), 3.40 – 3.35 (2H, m, H₅), 1.70 – 1.62 (1H, m, H₁₃), 1.34 – 1.23 (3H, m, H_{13'+14}), 0.87 (3H, t, *J* = 7.1 Hz, H₁₅).

¹³C NMR (151 MHz, DMSO-*d*₆) δ 153.0, 142.5, 135.4, 134.1, 131.1, 128.7, 128.6, 128.1, 127.8, 126.6, 125.8, 124.4, 122.2, 119.0, 118.5, 115.4, 82.4, 72.8, 64.1, 62.6, 54.8, 27.8, 24.5, 18.9, 13.4.

LRMS (ESI-TOF, EI⁺) *m/z*: 214.5 ([M]⁺, 100%).

LRMS (ESI-TOF, EI⁻) *m/z*: 285.4 ([M-H]⁻, 100%).

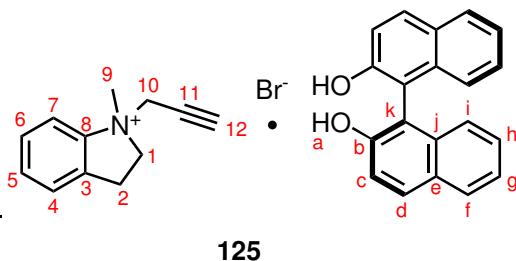
HRMS (ESI-TOF) *m/z*: [M]⁺ calculated for C₁₅H₂₀N⁺: 214.1596, found 214.1606. [M-H]⁻ calculated for C₂₀H₁₃O₂⁻: 285.0916, found 285.0913.

mp: 136 – 138 °C (CHCl₃).

[α]_D = +12.85 (c = 1.03, MeOH).

IR (ν_{max}/cm⁻¹): 3137br, 2960m, 1623m, 1270s, 816s, 753s.

XRD: A portion of the complex was crystallised in EtOH to give colourless plates. Crystal data for C₃₅H₃₄BrNO₂ (m = 580.54 g/mol): Orthorhombic, space group *P*2₁2₁2₁ (no. 19).

***rac*-1-(prop-2-yne)-1-methylindolin-1-ium bromide · (*R*)-1,1'-bi-2-naphthol**

The quaternary ammonium bromide salt **83** (0.265 g, 1.05 mmol) was dissolved in CHCl_3 (1.80 mL, 0.6 M) in a 10 mL vial. Solid (*R*)-BINOL (0.307 g, 1.0 equiv.) was then added with stirring to the solution, resulting in a homogeneous solution. This solution was allowed to stir at

room temperature overnight, which produced the desired complexed product **125** as a white precipitate. The resulting complex was isolated by vacuum filtration (0.500 g, 88% yield). Analysis by ^1H NMR spectroscopy ensured that a 1:1 complex had formed. *When a kinetic resolution is performed using (R)-BINOL (0.5 equiv.) the dr is reported to be 80:20 (R:S).*

^1H NMR (599 MHz, $\text{DMSO}-d_6$) δ 9.19 (2H, s, H_a), 7.87 (1H, d, $J = 7.5$ Hz, H_7), 7.86 – 7.83 (4H, m, H_{d+f}), 7.59 – 7.53 (3H, m, H_{4+5+6}), 7.32 (2H, d, $J = 8.9$ Hz, H_i), 7.22 (2H, ddd, $J = 8.7, 6.9, 1.7$ Hz, H_g), 7.16 (2H, ddd, $J = 8.2, 6.7, 1.5$ Hz, H_h), 6.93 (2H, dd, $J = 8.5, 1.2$ Hz, H_c), 4.90 (2H, t, $J = 2.4$ Hz, H_{10}), 4.31 (1H, dt, $J = 11.8, 7.3$ Hz, H_1), 4.20 (1H, dt, $J = 11.7, 7.3$ Hz, H_1), 3.94 (1H, t, $J = 2.5$ Hz, H_{12a}), 3.54 (3H, s, H_9), 3.41 (2H, t, $J = 7.3$ Hz, H_2).

^{13}C NMR (151 MHz, $\text{DMSO}-d_6$) δ 153.0, 144.7, 134.5, 134.1, 131.1, 128.7, 128.6, 128.1, 127.8, 126.5, 125.8, 124.4, 122.2, 118.5, 118.3, 115.4, 82.5, 72.9, 65.4, 55.4, 52.5, 27.1.

LRMS (ESI-TOF, EI^+) m/z : 172.6 ($[\text{M}]^+$, 100%).

LRMS (ESI-TOF, EI^-) m/z : 285.4 ($[\text{M}-\text{H}]^-$, 100%).

HRMS (ESI-TOF) m/z : $[\text{M}]^+$ calculated for $\text{C}_{12}\text{H}_{14}\text{N}^+$: 172.1126, found 172.1132. $[\text{M}-\text{H}]^-$ calculated for $\text{C}_{20}\text{H}_{13}\text{O}_2^-$: 285.0916, found 285.0928.

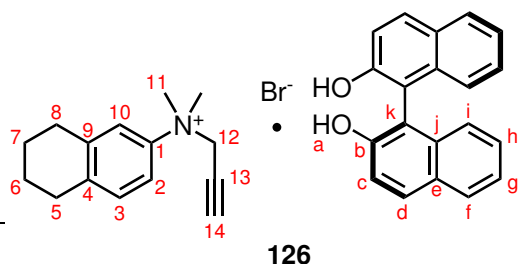
mp: 164 – 166 °C (CHCl_3).

IR ($\nu_{\text{max}}/\text{cm}^{-1}$): 3280w, 3121br, 2979m, 2135w, 1621m, 759s.

XRD: A portion of the complex was crystallised in EtOH to give clear colourless irregular crystal. Crystal data for $\text{C}_{32}\text{H}_{28}\text{BrNO}_2$ ($m = 538.46$ g/mol): Orthorhombic, space group $P2_12_12_1$ (no. 19).

The data for this compound is consistent with literature values.²

***N,N*-dimethyl-*N*-(prop-2-yn-1-yl)-5,6,7,8-tetrahydronaphthalen-2-aminium bromide
·(*R*)-1,1'-bi-2-naphthol**



The quaternary ammonium bromide salt **84** (0.299 g, 1.0 mmol) was dissolved in CHCl_3 (0.50 mL, 2.0 M) in a 10 mL vial. Solid (*R*)-BINOL (0.297 g, 1.0 equiv.) was then added with stirring to the solution, resulting in a homogeneous solution. This solu-

tion was allowed to stir at room temperature overnight, which produced the desired complexed product **126** as a white precipitate. The resulting complex was isolated by vacuum filtration (0.529 g, 90% yield). Analysis by ^1H NMR spectroscopy ensured that a 1:1 complex had formed.

^1H NMR (599 MHz, $\text{DMSO}-d_6$) δ 9.20 (2H, s, H_a), 7.88 – 7.83 (4H, apt. dd, $J = 8.6$, 5.1 Hz, H_{d+f}), 7.68 (1H, d, $J = 3.2$ Hz, H_{10}), 7.63 (1H, dd, $J = 8.6$, 2.9 Hz, H_2), 7.33 (2H, dd, $J = 8.8$, 2.9 Hz, H_i), 7.29 (1H, d, $J = 8.4$ Hz, H_3), 7.22 (2H, ddd, $J = 8.0$, 6.6, 1.5 Hz, H_g), 7.16 (2H, ddd, $J = 8.1$, 6.7, 1.3 Hz, H_h), 6.93 (2H, d, $J = 8.4$ Hz, H_c), 4.97 (2H, d, $J = 7.8$ Hz, H_{12}), 3.87 (1H, t, $J = 2.4$ Hz, H_{14}), 3.60 (6H, s, H_{11}), 2.79 (2H, t, $J = 6.1$ Hz, H_5), 2.76 (2H, t, $J = 6.1$ Hz, H_8), 1.76 – 1.73 (4H, m, H_{6+7}).

^{13}C NMR (151 MHz, $\text{DMSO}-d_6$) δ 153.0, 142.4, 139.2, 138.7, 134.1, 130.2, 128.6, 128.1, 127.8, 125.8, 124.4, 122.2, 121.2, 118.5, 117.9, 115.4, 82.7, 72.9, 57.9, 53.7, 29.0, 28.1, 22.2, 22.1.

LRMS (ESI-TOF, EI^+) m/z : 214.6 ($[\text{M}]^+$, 100%).

LRMS (ESI-TOF, EI^-) m/z : 285.4 ($[\text{M}-\text{H}]^-$, 100%).

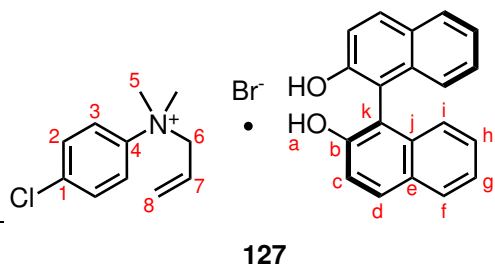
HRMS (ESI-TOF) m/z : $[\text{M}]^+$ calculated for $\text{C}_{15}\text{H}_{20}\text{N}^+$: 214.1596, found 214.1607. $[\text{M}-\text{H}]^-$ calculated for $\text{C}_{20}\text{H}_{13}\text{O}_2^-$: 285.0916, found 285.0914.

mp: 124 – 126 °C (CHCl_3).

IR ($\nu_{\text{max}}/\text{cm}^{-1}$): 3280m, 3120br, 2936m, 1620m, 1267s, 819s.

XRD: A portion of the complex was crystallised in EtOH to give colourless prisms.

Crystal data for $\text{C}_{35}\text{H}_{34}\text{BrNO}_2$ ($m = 580.54$ g/mol): Orthorhombic, space group $P2_12_12_1$ (no. 19).

***N*-allyl-4-chloro-*N,N*-dimethylanilinium bromide · (*R*)-1,1'-bi-2-naphthol**

The quaternary ammonium bromide salt **85** (0.212 g, 0.8 mmol) was dissolved in CHCl_3 (0.38 mL, 2.0 M) in a 10 mL vial. Solid (*R*)-BINOL (0.221 g, 1.0 equiv.) was then added with stirring to the solution, resulting in a homogeneous solution. This solution was allowed to stir at room temperature overnight,

which produced the desired complexed product **127** as a white precipitate. The resulting complex was isolated by vacuum filtration (0.227 g, 53% yield). Analysis by ^1H NMR spectroscopy ensured that a 1:1 complex had formed.

^1H NMR (599 MHz, CD_3OD) δ 7.87 (2H, d, $J = 8.9$ Hz, H_d), 7.86 – 7.81 (4H, m, H_{2+f}), 7.69 – 7.63 (2H, m, H_3), 7.29 (2H, d, $J = 8.9$ Hz, H_i), 7.24 (2H, ddd, $J = 8.1, 6.7, 1.2$ Hz, H_g), 7.16 (2H, ddd, $J = 8.1, 6.7, 1.3$ Hz, H_h), 7.02 (2H, d, $J = 8.5$ Hz, H_c), 5.72 – 5.64 (1H, m, H_7), 5.61 – 5.55 (2H, m, H_8), 4.49 (2H, d, $J = 7.1$ Hz, H_6), 3.61 (6H, s, H_5).

^{13}C NMR (151 MHz, CD_3OD) δ 154.2, 144.4, 137.5, 135.8, 131.5, 130.6, 130.4, 129.7, 129.0, 127.2, 126.0, 125.8, 124.1, 123.9, 119.3, 116.3, 72.8, 54.4.

LRMS (ESI-TOF, EI^+) m/z : 196.1 ($[\text{M}]^+$, 100%).

LRMS (ESI-TOF, EI^-) m/z : 285.1 ($[\text{M}-\text{H}]^-$, 100%).

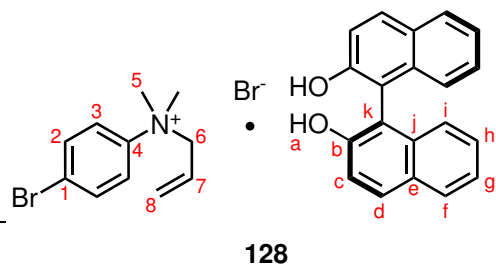
HRMS (ESI-TOF) m/z : $[\text{M}]^+$ calculated for $\text{C}_{11}\text{H}_{15}\text{NCl}^+$: 196.0893, found 196.0899.

$[\text{M}-\text{H}]^-$ calculated for $\text{C}_{20}\text{H}_{13}\text{O}_2^-$: 285.0916, found 285.0923.

mp: 126 – 128 °C (CHCl_3).

IR ($\nu_{\text{max}}/\text{cm}^{-1}$): 3118br, 1621m, 1271s, 964s, 746s, 688s.

XRD: A portion of the complex was crystallised in EtOH to give colourless plates. Crystal data for $\text{C}_{31}\text{H}_{29}\text{BrClNO}_2$ ($m = 562.91$ g/mol): Orthorhombic, space group $P2_12_12_1$ (no. 19).

***N*-allyl-4-bromo-*N,N*-dimethylanilinium bromide · (*R*)-1,1'-bi-2-naphthol**

The quaternary ammonium bromide salt **86** (0.311 g, 1.0 mmol) was dissolved in CHCl_3 (0.77 mL, 1.3 M) in a 10 mL vial. Solid (*R*)-BINOL (0.300 g, 1.1 equiv.) was then added with stirring to the solution, resulting in a homogeneous solution. This solution was allowed to stir at room temperature overnight,

which produced the desired complexed product **128** as a white precipitate. The resulting complex was isolated by vacuum filtration (0.308 g, 52% yield). Analysis by ^1H NMR spectroscopy ensured that a 1:1 complex had formed.

^1H NMR (599 MHz, CD_3OD) δ 7.87 (2H, d, $J = 8.9$ Hz, H_d), 7.85 – 7.78 (4H, m, H_{2+f}), 7.76 (2H, d, $J = 8.8$ Hz, H_3), 7.29 (2H, d, $J = 8.9$ Hz, H_i), 7.24 (2H, ddd, $J = 8.3, 6.7, 1.3$ Hz, H_g), 7.16 (2H, ddd, $J = 8.2, 6.7, 1.4$ Hz, H_h), 7.01 (2H, d, $J = 8.5$ Hz, H_c), 5.72 – 5.62 (1H, m, H_7), 5.60 – 5.54 (2H, m, H_8), 4.48 (2H, d, $J = 7.0$ Hz, H_6), 3.59 (6H, s, H_5).

^{13}C NMR (151 MHz, CD_3OD) δ 154.2, 145.1, 135.8, 134.7, 130.6, 130.4, 129.8, 129.0, 127.1, 126.1, 125.8, 125.6, 124.3, 123.8, 119.3, 116.2, 72.9, 54.4.

LRMS (ESI-TOF, EI^+) m/z : 242.2 ($[\text{M}]^+$, 100%), 240.06 (82), 161.12 (96).

LRMS (ESI-TOF, EI^-) m/z : 285.1 ($[\text{M}-\text{H}]^-$, 100%).

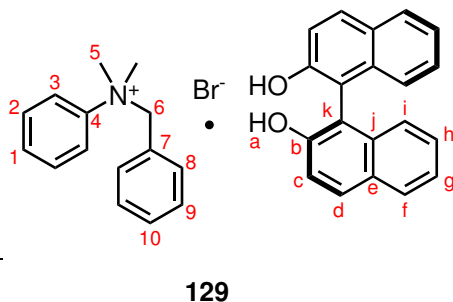
HRMS (ESI-TOF) m/z : $[\text{M}]^+$ calculated for $\text{C}_{11}\text{H}_{15}\text{NBr}^+$: 240.0388, found 240.0392.

$[\text{M}-\text{H}]^-$ calculated for $\text{C}_{20}\text{H}_{13}\text{O}_2^-$: 285.0916, found 285.0923.

mp: 136 – 139 °C (CHCl_3).

IR ($\nu_{\text{max}}/\text{cm}^{-1}$): 3113br, 1621br, 1271s, 930br, 817sh, 687m.

XRD: A portion of the complex was crystallised in EtOH to give colourless plates. Crystal data for $\text{C}_{31}\text{H}_{29}\text{Br}_2\text{NO}_2$ ($m = 607.37$ g/mol): Orthorhombic, space group $P2_12_12_1$ (no. 19).

***N*-benzyl-*N,N*-dimethylanilinium bromide · (*R*)-1,1'-bi-2-naphthol**

The quaternary ammonium bromide salt **87** (0.100 g, 0.34 mmol) was dissolved in CHCl_3 (0.85 mL, 0.4 M) in a 10 mL vial. Solid (*R*)-BINOL (0.097 g, 1.0 equiv.) was then added with stirring to the solution, resulting in a pale yellow homogeneous solution. This solution was allowed to stir at room temperature

overnight, which produced the desired complexed product as a white precipitate. The resulting complex **129** was isolated by vacuum filtration (0.131 g, 66% yield). Analysis by ^1H NMR spectroscopy ensured that a 1:1 complex had formed.

^1H NMR (400 MHz, CD_3OD) δ 7.87 (2H, dd, $J = 9.0, 0.7$ Hz, H_d), 7.83 (2H, dd, $J = 8.3, 1.3$ Hz, H_f), 7.75 – 7.67 (2H, m, H_3), 7.62 – 7.55 (3H, m, H_{1+2}), 7.43 (1H, tt, $J = 7.7, 1.5$ Hz, H_{10}), 7.33 – 7.27 (4H, m, H_{9+i}), 7.24 (2H, ddd, $J = 8.1, 6.7, 1.3$ Hz, H_g), 7.15 (2H, ddd, $J = 8.2, 6.7, 1.4$ Hz, H_h), 7.03 (4H, td, $J = 8.5, 1.2$ Hz, H_{8+i}), 4.98 (2H, s, H_6), 3.60 (6H, s, H_5).

^{13}C NMR (101 MHz, CD_3OD) δ 154.2, 145.7, 135.8, 133.7, 131.9, 131.7, 131.4, 130.6, 130.4, 129.9, 129.0, 128.9, 127.1, 125.8, 123.8, 122.6, 119.3, 116.2, 74.6, 53.8.

LRMS (ESI-TOF, EI^+) m/z : 212.2 ($[\text{M}]^+$, 100%), 130.69 (3).

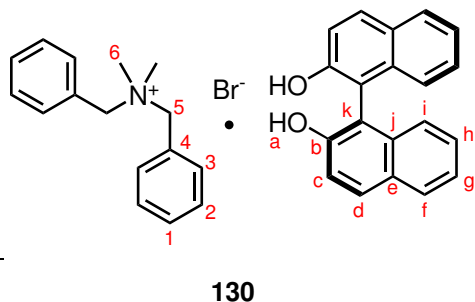
LRMS (ESI-TOF, EI^-) m/z : 285.2 ($[\text{M}-\text{H}]^-$, 100%).

HRMS (ESI-TOF) m/z : $[\text{M}]^+$ calculated for $\text{C}_{15}\text{H}_{18}\text{N}^+$: 212.1439, found 212.1450. $[\text{M}-\text{H}]^-$ calculated for $\text{C}_{20}\text{H}_{13}\text{O}_2^-$: 285.0916, found 285.0931.

mp: 160 – 162 °C, decomposes to blue oil (CHCl_3).

IR ($\nu_{\text{max}}/\text{cm}^{-1}$): 3142br, 1623m, 1505m, 1431m, 1272s, 816s.

XRD: A portion of the complex was crystallised in EtOH to give clear colourless plates. Crystal data for $\text{C}_{33}\text{H}_{32}\text{NO}_2\text{Br}$ ($m = 578.52$ g/mol): Orthorhombic, space group $P2_12_12_1$ (no. 19).

***N,N*-dimethyl-*N,N*-dibenzylammonium bromide · (*R*)-1,1'-bi-2-naphthol**

Ammonium salt **88** (0.201 g, 0.66 mmol) was dissolved in EtOH (1.10 mL, 0.6 M) in a 10 mL vial. Solid (*R*)-BINOL (0.188 g, 1.0 equiv.) was then added with stirring to the solution. This solution was allowed to stir at room temperature overnight, which produced the desired product **130** as a white precipitate.

The resulting complex was isolated by vacuum filtration (0.237 g, 61% yield). Analysis by ^1H NMR spectroscopy ensured that a 1:1 complex had formed.

^1H NMR (599 MHz, CD_3OD) δ 7.86 (2H, d, $J = 8.9$ Hz, H_d), 7.81 (2H, d, $J = 8.2$ Hz, H_f), 7.54 – 7.44 (10H, m, H_{1+2+3}), 7.31 (2H, d, $J = 8.9$ Hz, H_i), 7.22 (2H, ddd, $J = 8.1$, 6.7, 1.2 Hz, H_g), 7.12 (2H, ddd, $J = 8.3$, 6.8, 1.4 Hz, H_h), 7.02 (2H, dd, $J = 8.5$, 1.1 Hz, H_c), 4.53 (4H, s, H_5), 2.79 (6H, s, H_6).

^{13}C NMR (151 MHz, $\text{DMSO}-d_6$) δ 154.1, 135.8, 134.3, 131.9, 130.6, 130.4, 130.3, 129.1, 128.6, 127.2, 125.8, 123.9, 119.1, 116.3, 69.6, 49.1.

LRMS (ESI-TOF, EI^+) m/z : 226.2 ($[\text{M}]^+$, 100%).

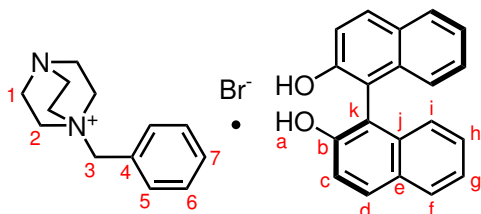
LRMS (ESI-TOF, EI^-) m/z : 285.2 ($[\text{M}-\text{H}]^-$, 100%).

HRMS (ESI-TOF) m/z : $[\text{M}]^+$ calculated for $\text{C}_{16}\text{H}_{20}\text{N}^+$: 226.1596, found: 226.1597. $[\text{M}-\text{H}]^-$ calculated for $\text{C}_{20}\text{H}_{13}\text{O}_2^-$: 285.0916, found: 285.0930.

mp: 168 – 169 °C (EtOH).

IR ($\nu_{\text{max}}/\text{cm}^{-1}$): 3138br, 1271s, 810, 748, 724.

XRD: A portion of the complex was crystallised in EtOH to give clear colourless blocks. Crystal data for $\text{C}_{36}\text{H}_{34}\text{BrNO}_2$ ($m = 592.55$ g/mol): Orthorhombic, space group $P2_12_12_1$ (no. 19).

1-benzyl-1,4-diazabicyclo[2.2.2]octan-1-ium bromide · (*R*)-1,1'-bi-2-naphthol**131**

Ammonium salt **89** (0.283 g, 1.0 mmol) was dissolved in CHCl_3 (1.67 mL, 0.6 M) in a 10 mL vial. Solid (*R*)-BINOL (0.286 g, 1.0 equiv.) was then added with stirring to the solution. This solution was allowed to stir at room temperature overnight, which produced the desired complexed product **131** as a white precipitate.

The resulting complex was isolated by vacuum filtration (0.527 g, 93% yield).

^1H NMR (400 MHz, $\text{DMSO}-d_6$) δ 9.23 (2H, s, H_a), 7.89 – 7.81 (4H, m, H_{d+f}), 7.52 (5H, d, $J = 2.4$ Hz, H_{5+6+7}), 7.32 (2H, d, $J = 8.9$ Hz, H_i), 7.23 (2H, ddd, $J = 8.1, 6.8, 1.3$ Hz, H_g), 7.16 (2H, ddd, $J = 8.3, 6.8, 1.5$ Hz, H_h), 6.93 (2H, dd, $J = 8.3, 1.2$ Hz, H_c), 4.52 (2H, s, H_3), 3.29 (6H, t, $J = 7.5$ Hz, H_2), 3.01 (6H, dd, $J = 8.9, 6.1$ Hz, H_1).

^{13}C NMR (101 MHz, $\text{DMSO}-d_6$) δ 153.5, 134.6, 133.7, 130.7, 129.5, 129.1, 128.6, 128.2, 127.6, 126.3, 124.9, 122.7, 119.0, 115.9, 66.9, 52.0, 45.1.

LRMS (ESI-TOF, EI^+) m/z : 203.2 ($[\text{M}]^+$, 100%).

LRMS (ESI-TOF, EI^-) m/z : 285.2 ($[\text{M}-\text{H}]^-$, 100%).

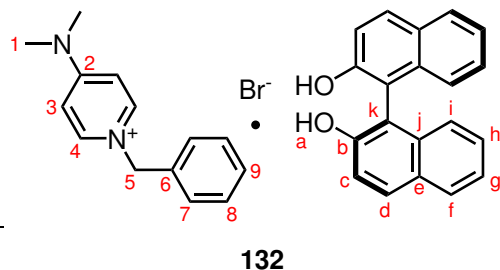
HRMS (ESI-TOF) m/z : $[\text{M}]^+$ calculated for $\text{C}_{13}\text{H}_{19}\text{N}_2^+$: 203.1548, found: 203.1539.

$[\text{M}-\text{H}]^-$ calculated for $\text{C}_{20}\text{H}_{13}\text{O}_2^-$: 285.0916, found: 285.0917.

mp: 222 – 223 °C (EtOH).

IR ($\nu_{\text{max}}/\text{cm}^{-1}$): 3190br, 1623m, 1503m, 1336m, 1270m, 816m.

XRD: A portion of the complex was crystallised in EtOH, to give clear colourless prisms. Crystal data for $\text{C}_{33}\text{H}_{34}\text{BrN}_2\text{O}_2$ ($m = 570.53$ g/mol): Orthorhombic, space group $P2_12_12_1$ (no. 19).

1-benzyl-4-(dimethylamino)pyridin-1-ium bromide · (*R*)-1,1'-bi-2-naphthol

Ammonium salt **90** (0.293 g, 1.0 mmol) was dissolved in CHCl_3 (1.67 mL, 0.6 M) in a 10 mL vial. Solid (*R*)-BINOL (0.286 g, 1.0 equiv.) was then added with stirring to the solution. This solution was allowed to stir at room temperature overnight, which produced the desired complex **132** as a white precipitate. The

complex was isolated by vacuum filtration (0.465 g, 80% yield). Analysis by ^1H NMR spectroscopy ensured that a 1:1 complex had formed.

^1H NMR (400 MHz, $\text{DMSO}-d_6$) δ 9.22 (2H, s, H_a), 8.45 – 8.38 (2H, m, H_3), 7.88 – 7.81 (4H, m, H_{d+f}), 7.46 – 7.35 (5H, m, H_{7+8+9}), 7.32 (2H, d, $J = 8.8$ Hz, H_i), 7.23 (2H, ddd, $J = 8.1, 6.7, 1.3$ Hz, H_g), 7.16 (2H, ddd, $J = 8.2, 6.8, 1.4$ Hz, H_h), 7.07 – 7.02 (2H, m, H_4), 6.93 (2H, d, $J = 8.3$ Hz, H_c), 5.41 (2H, s, H_5), 3.17 (6H, s, H_1).

^{13}C NMR (101 MHz, $\text{DMSO}-d_6$) δ 155.9, 153.0, 142.0, 135.8, 134.1, 129.1, 128.7, 128.6, 128.1, 128.0, 127.8, 125.8, 124.4, 122.2, 118.5, 115.4, 108.0, 59.3.

LRMS (ESI-TOF, EI^+) m/z : 213.1 ($[\text{M}]^+$, 100%).

LRMS (ESI-TOF, EI^-) m/z : 285.2 ($[\text{M}-\text{H}]^-$, 100%).

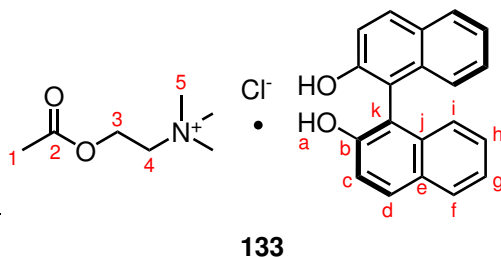
HRMS (ESI-TOF) m/z : $[\text{M}]^+$ calculated for $\text{C}_{14}\text{H}_{17}\text{N}_2^+$: 213.1392, found: 213.1382.

$[\text{M}-\text{H}]^-$ calculated for $\text{C}_{20}\text{H}_{13}\text{O}_2^-$: 285.0916, found: 285.0912.

mp: 200 – 201 °C (EtOH).

IR ($\nu_{\text{max}}/\text{cm}^{-1}$): 3169br, 2981w, 1653m, 1439m, 1170m, 808m.

XRD: A portion of the complex was crystallised in EtOH, to give clear colourless prisms. Crystal data for $\text{C}_{34}\text{H}_{31}\text{BrN}_2\text{O}_2$ ($m = 579.52$ g/mol): Orthorhombic, space group $P2_12_12_1$ (no. 19).

Acetylcholine chloride · (*R*)-1,1'-bi-2-naphthol

Acetylcholine chloride (**91**, 0.183 g, 1.0 mmol) was dissolved in EtOH (1.00 mL, 1.0 M) in a 10 mL vial. Solid (*R*)-BINOL (0.284 g, 1.0 equiv.) was then added with stirring to the solution. This solution was allowed to stir at room temperature overnight, which produced the desired complexed product **133**

as a white precipitate. The resulting complex was isolated by vacuum filtration (0.449 g, 97% yield). Analysis by ^1H NMR spectroscopy ensured that a 1:1 complex had formed.

^1H NMR (599 MHz, CD_3OD) δ 7.87 (2H, d, $J = 9.1$ Hz, H_d), 7.82 (2H, d, $J = 8.1$ Hz, H_f), 7.33 (2H, d, $J = 8.9$ Hz, H_i), 7.24 (2H, ddd, $J = 8.1, 6.7, 1.2$ Hz, H_g), 7.15 (2H, ddd, $J = 8.1, 6.7, 1.3$ Hz, H_h), 7.04 (2H, d, $J = 8.4$ Hz, H_c), 4.39 (2H, dq, $J = 7.6, 2.6$ Hz, H_3), 3.54 – 3.50 (2H, m, H_4), 3.03 (9H, s, H_5), 2.05 (3H, s, H_1).

^{13}C NMR (151 MHz, CD_3OD) δ 171.5, 154.1, 135.8, 130.6, 130.4, 129.1, 127.2, 125.8, 123.9, 119.3, 116.2, 65.9 (t, $J = 3.5$ Hz), 58.8, 54.3 (t, $J = 3.6$ Hz), 20.6.

LRMS (ESI-TOF, EI^+) m/z : 146.1 ($[\text{M}]^+$, 100%).

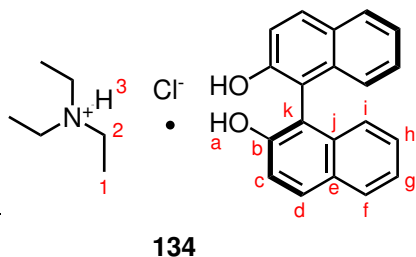
LRMS (ESI-TOF, EI^-) m/z : 285.2 ($[\text{M}-\text{H}]^-$, 100%).

HRMS (ESI-TOF) m/z : $[\text{M}]^+$ calculated for $\text{C}_7\text{H}_{16}\text{NO}_2$: 146.1181, found 146.1177. $[\text{M}-\text{H}]^-$ calculated for $\text{C}_{20}\text{H}_{13}\text{O}_2^-$: 285.0916, found 285.0910.

mp: 142 – 143 °C (EtOH).

IR ($\nu_{\text{max}}/\text{cm}^{-1}$): 3000br, 1741m, 1623m, 1432m, 1238s, 933m, 816s, 753s.

XRD: A portion of the complex was crystallised in MeOH, to give clear colourless blocks. Crystal data for $\text{C}_{27}\text{H}_{30}\text{ClNO}_4$ ($m = 467.97$ g/mol): Orthorhombic, space group $P2_12_12_1$ (no. 19).

***N,N,N*-triethylammonium hydrochloride · (*R*)-1,1'-bi-2-naphthol**

Ammonium salt **92** (0.137 g, 1.0 mmol) was dissolved in CHCl_3 (1.50 mL, 0.6 M) in a 10 mL vial. Solid (*R*)-BINOL (0.286 g, 1.0 equiv.) was then added with stirring to the solution. This solution was allowed to stir at room temperature overnight, which produced the desired complex **134** as a white precipitate. The resulting complex was iso-

lated by vacuum filtration (0.170 g, 40% yield). Analysis by ^1H NMR spectroscopy ensured that a 1:1 complex had formed.

^1H NMR (400 MHz, $\text{DMSO}-d_6$) δ 10.39 (1H, s, H_3), 9.30 (2H, d, $J = 2.3$ Hz, H_a), 7.85 (4H, apt. dd, $J = 8.7, 2.8$ Hz, H_{d+f}), 7.36 (2H, dd, $J = 8.8, 1.3$ Hz, H_i), 7.27 – 7.19 (2H, m, H_g), 7.16 (2H, dd, $J = 8.3, 6.7$ Hz, H_h), 6.94 (2H, d, $J = 8.4$ Hz, H_c), 3.04 (6H, q, $J = 7.3$ Hz, H_2), 1.19 (9H, t, $J = 7.3$ Hz, H_1).

^{13}C NMR (101 MHz, $\text{DMSO}-d_6$) δ 153.1, 134.1, 128.6, 128.1, 127.9, 125.8, 124.4, 122.3, 118.6, 115.4, 45.3, 8.4.

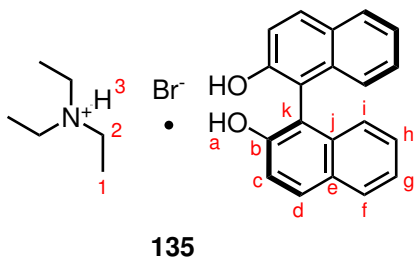
LRMS (ESI-TOF, EI^-) m/z : 285.2 ($[\text{M}-\text{H}]^-$, 100%).

HRMS (ESI-TOF) m/z : $[\text{M}]^+$ calculated for $\text{C}_6\text{H}_{16}\text{N}^+$: 102.1283, found: 102.1276. $[\text{M}-\text{H}]^-$ calculated for $\text{C}_{20}\text{H}_{13}\text{O}_2^-$: 285.0916, found: 285.0922.

mp: 189 – 191 °C (EtOH).

IR ($\nu_{\text{max}}/\text{cm}^{-1}$): 3415br, 2981m, 1526m, 1351m, 812sh, 742sh.

XRD: A portion of the complex was crystallised in EtOH, to give clear colourless prisms. Crystal data for $\text{C}_{26}\text{H}_{30}\text{ClNO}_2$ ($m = 423.96$ g/mol): Orthorhombic, space group $P2_12_12_1$ (no. 19).

Triethylammonium hydrobromide · (*R*)-1,1'-bi-2-naphthol

93 (0.543 g, 3.00 mmol) was dissolved in EtOH (3.00 mL, 1.0 M) in a 10 mL vial. Solid (*R*)-BINOL (0.860 g, 1.0 equiv.) was then added with stirring to the solution. This solution was allowed to stir at room temperature overnight, which produced the desired complex **135** as a white precipitate.

The resulting complex was isolated by vacuum filtration (0.583 g, 42% yield). Analysis by ^1H NMR spectroscopy ensured that a 1:1 complex had formed.

^1H NMR (599 MHz, CD_3OD) δ 7.87 (2H, d, $J = 8.8$ Hz, H_d), 7.83 (2H, d, $J = 8.3$ Hz, H_f), 7.31 (2H, dd, $J = 8.9, 1.8$ Hz, H_i), 7.24 (2H, ddd, $J = 8.0, 6.7, 1.2$ Hz, 2H_g), 7.16 (2H, ddd, $J = 8.2, 6.8, 1.3$ Hz, H_h), 7.03 (2H, d, $J = 8.4$ Hz, H_c), 3.10 (6H, q, $J = 7.4$ Hz, H_2), 1.24 (9H, t, $J = 7.3$ Hz, H_1).

^{13}C NMR (151 MHz, CD_3OD) δ 154.2, 135.8, 130.6, 130.4, 129.0, 127.1, 125.8, 123.8, 119.3, 116.2, 47.9, 9.2.

LRMS (ESI-TOF, EI^+) m/z : 102.3 ($[\text{M}]^+$, 100%).

LRMS (ESI-TOF, EI^-) m/z : 285.2 ($[\text{M}-\text{H}]^-$, 100%).

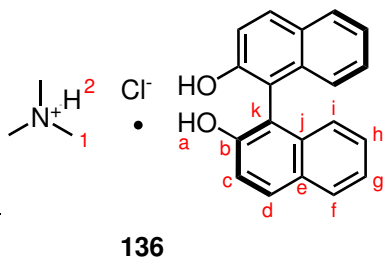
HRMS (ESI-TOF) m/z : $[\text{M}]^+$ calculated for $\text{C}_6\text{H}_{16}\text{N}^+$: 102.1283, found: 102.1274. $[\text{M}-\text{H}]^-$ calculated for $\text{C}_{20}\text{H}_{13}\text{O}_2^-$: 285.0916, found: 285.0923.

mp: 202 °C (EtOH).

IR ($\nu_{\text{max}}/\text{cm}^{-1}$): 3245br, 1270s, 981w, 815s, 748s.

XRD: A portion of the complex was crystallised in EtOH to give clear colourless blocks.

Crystal data for $\text{C}_{78}\text{H}_{90}\text{Br}_3\text{N}_3\text{O}_6$ ($m = 1405.25$ g/mol): Orthorhombic, space group $P2_12_12_1$ (no. 19).

Trimethylammonium hydrochloride · (*R*)-1,1'-bi-2-naphthol

Trimethylammonium hydrochloride (**94**, 0.096 g, 1.0 mmol) was dissolved in CHCl_3 (1.67 mL, 0.6 M) in a 10 mL vial. Solid (*R*)-BINOL (0.286 g, 1.0 equiv.) was then added with stirring to the solution. This solution was allowed to stir at room temperature overnight, which produced the desired product **136** as a white precipitate. The resulting

complex was isolated by vacuum filtration (0.199 g, 52% yield). Analysis by ^1H NMR spectroscopy ensured that a 1:1 complex had formed.

^1H NMR (400 MHz, CDCl_3) δ 10.61 (1H, s, H_2), 9.29 (2H, s, H_a), 7.91 – 7.77 (4H, m, H_{d+f}), 7.35 (2H, d, $J = 8.9$ Hz, H_i), 7.23 (2H, m, H_g), 7.20 – 7.11 (2H, m, H_h), 7.03 – 6.95 (2H, m, H_c), 2.71 (9H, s, H_1).

^{13}C NMR (101 MHz, CDCl_3) δ 153.0, 134.1, 128.6, 128.1, 127.8, 125.8, 124.4, 122.2, 118.6, 115.4, 43.8.

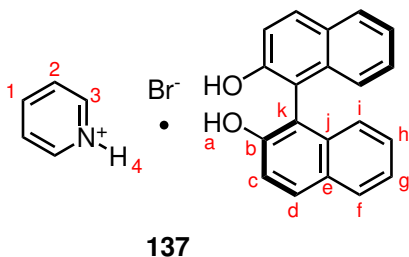
LRMS (ESI-TOF, EI^-) m/z : 285.2 ($[\text{M}-\text{H}]^-$, 100%).

HRMS (ESI-TOF) m/z : $[\text{M}]^-$ calculated for $\text{C}_{20}\text{H}_{13}\text{O}_2^-$: 285.0916, found: 285.0920.

mp: 219 °C (EtOH).

IR ($\nu_{\text{max}}/\text{cm}^{-1}$): 3181br, 2725br, 1270s, 964m, 820s, 752s.

XRD: A portion of the complex was crystallised in EtOH, to give clear colourless prisms. Crystal data for $\text{C}_{23}\text{H}_{24}\text{ClNO}_2$ ($m = 381.88$ g/mol): Orthorhombic, space group $P2_12_12_1$ (no. 19).

Pyridinium hydrobromide · (*R*)-1,1'-bi-2-naphthol

Ammonium salt **95** (0.200 g, 1.0 mmol) was dissolved in EtOH (1.67 mL, 0.6 M) in a 10 mL vial. Solid (*R*)-BINOL (0.218 g, 1.0 equiv.) was then added with stirring to the solution. This solution was allowed to stir at room temperature overnight, which produced the desired complex **137** as a white precipitate. The resulting complex was iso-

lated by vacuum filtration (0.353 g, 79% yield). Analysis by ^1H NMR spectroscopy ensured that a 1:1 complex had formed.

^1H NMR (400 MHz, DMSO- d_6) δ 9.20 (1H, br, H_4), 9.00 – 8.84 (2H, m, H_3), 8.59 (1H, tt, $J = 7.8, 1.6$ Hz, H_1), 8.13 – 7.99 (2H, m, H_2), 7.92 – 7.77 (4H, m, H_{d+f}), 7.33 (2H, d, $J = 8.9$ Hz, H_i), 7.22 (2H, ddd, $J = 8.1, 6.7, 1.3$ Hz, H_g), 7.16 (2H, ddd, $J = 8.3, 6.8, 1.4$ Hz, H_h), 6.93 (2H, d, $J = 8.3$ Hz, H_c).

^{13}C NMR (101 MHz, DMSO- d_6) δ 153.0, 146.0, 142.5, 134.1, 128.7, 128.1, 127.9, 127.1, 125.9, 124.4, 122.2, 118.6, 115.4.

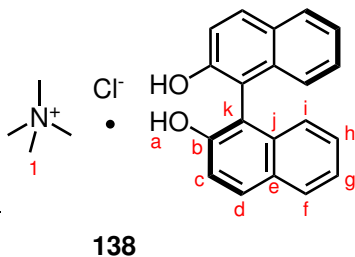
LRMS (ESI-TOF, EI^-) m/z : 285.2 ($[\text{M}-\text{H}]^-$, 100%).

HRMS (ESI-TOF) m/z : $[\text{M}]^+$ calculated for $\text{C}_5\text{H}_6\text{N}^+$: 80.0500, found: 80.0494. $[\text{M}-\text{H}]^-$ calculated for $\text{C}_{20}\text{H}_{13}\text{O}_2^-$: 285.0916, found: 285.0907.

mp: 209 – 210 °C (EtOH).

IR ($\nu_{\text{max}}/\text{cm}^{-1}$): 3224br, 2980m, 1622m, 1270s, 816s, 740s.

XRD: A portion of the complex was crystallised in EtOH, to give clear colourless prisms. Crystal data for $\text{C}_{25}\text{H}_{20}\text{BrNO}_2$ ($m = 446.33$ g/mol): Orthorhombic, space group $P2_12_12_1$ (no. 19).

Tetramethylammonium chloride · (*R*)-1,1'-bi-2-naphthol

Tetramethylammonium chloride (**96**, 0.207 g, 1.89 mmol) was dissolved in EtOH (1.89 mL, 1.0 M) in a 10 mL vial. Solid (*R*)-BINOL (0.501 g, 0.93 equiv.) was then added with stirring to the solution. This solution was allowed to stir at room temperature overnight, which produced the desired complex **138** as a white precipitate. The resulting

complex was isolated by vacuum filtration (0.534 g, 77% yield). Analysis by ^1H NMR spectroscopy revealed that a 1:1 complex had formed.

^1H NMR (400 MHz, CD_3OD) δ 7.91 – 7.77 (4H, m, $\text{H}_{\text{d+f}}$), 7.31 (2H, d, $J = 8.8$ Hz, H_i), 7.24 (2H, ddd, $J = 8.1, 6.7, 1.3$ Hz, H_g), 7.16 (2H, ddd, $J = 8.2, 6.7, 1.4$ Hz, H_h), 7.03 (2H, apt. d, $J = 8.4$ Hz, H_c), 3.04 (12H, s, H_1).

^{13}C NMR (101 MHz, CD_3OD) δ 154.2, 135.8, 130.6, 130.4, 129.1, 127.2, 125.8, 123.9, 119.3, 116.3, 55.8 (t, $J = 4.0$ Hz).

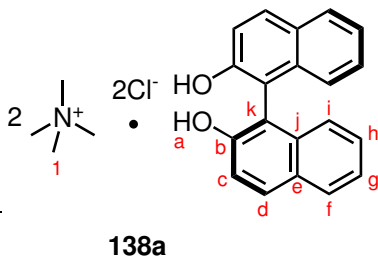
LRMS (ESI-TOF, EI^-) m/z : 285.4 ($[\text{M}]^-$, 100%).

HRMS (ESI-TOF) m/z : $[\text{M-H}]^-$ calculated for $\text{C}_{20}\text{H}_{13}\text{O}_2^-$: 285.0916, found 285.0913.

mp: 316 – 317 °C (EtOH).

IR ($\nu_{\text{max}}/\text{cm}^{-1}$): 3050br, 1622m, 1481s, 1274s, 949s, 822s,.

XRD: A portion of the complex was crystallised in EtOH, to give clear colourless plates. Crystal data for $\text{C}_{24}\text{H}_{26}\text{ClNO}_2$ ($m = 395.91$ g/mol): Orthorhombic, space group $P2_12_12_1$ (no. 19).

Tetramethylammonium chloride · (*R*)-1,1'-bi-2-naphthol

Tetramethyl ammonium chloride (**96**, 0.142 g, 1.298 mmol) was dissolved in CHCl_3 (1.30 mL, 1.0 M) in a 10 mL vial. Solid (*R*)-BINOL (0.143 g, 1.0 equiv.) was then added with stirring to the solution. This solution was allowed to stir at room temperature overnight, which produced the desired complex **138a** as a white precipitate. The

resulting complex was isolated by vacuum filtration (0.385 g, 75% yield). Analysis by ^1H NMR spectroscopy revealed that a 2:1 (ammonium:BINOL) complex had formed.

^1H NMR (400 MHz, $\text{DMSO}-d_6$) δ 9.52 (2H, s, H_a), 7.87 – 7.80 (4H, m, H_{d+f}), 7.45 (2H, d, $J = 8.8$ Hz, H_i), 7.22 (2H, t, $J = 8.1$ Hz, H_g), 7.15 (2H, t, $J = 8.2$ Hz, H_h), 6.93 (2H, d, $J = 8.3$ Hz, H_c), 3.12 (24H, s, H_1).

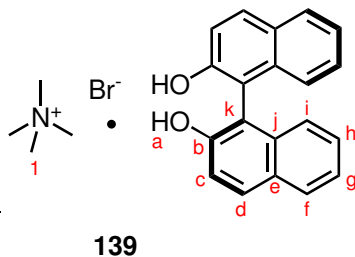
^{13}C NMR (101 MHz, $\text{DMSO}-d_6$) δ 153.2, 134.1, 128.5, 128.0, 127.9, 125.8, 124.4, 122.2, 118.6, 115.4, 53.4 (t, $J = 4.0$ Hz).

LRMS (ESI-TOF, EI^-) m/z : 285.4 ($[\text{M}]^-$, 100%).

HRMS (ESI-TOF) m/z : $[\text{M}-\text{H}]^-$ calculated for $\text{C}_{20}\text{H}_{13}\text{O}_2^-$: 285.0916, found 285.0913.

mp: 310 °C (CHCl_3).

PXRD data for 138a displays different indices than the EtOH precipitated material 138.

Tetramethylammonium bromide · (*R*)-1,1'-bi-2-naphthol

Tetramethylammonium bromide (**97**, 0.154 g, 1.0 mmol) was dissolved in EtOH (1.67 mL, 0.6 M) in a 10 mL vial. Solid (*R*)-BINOL (0.286 g, 1.0 equiv.) was then added with stirring to the solution. This solution was allowed to stir at room temperature overnight, which produced the desired complex **139** as a white precipitate. The resulting

complex was isolated by vacuum filtration (0.281 g, 64% yield). Analysis by ^1H NMR spectroscopy ensured that a 1:1 complex had formed.

^1H NMR (400 MHz, $\text{DMSO}-d_6$) δ 9.23 (2H, s, H_a), 7.89 – 7.81 (4H, m, H_{d+f}), 7.33 (2H, d, $J = 8.8$ Hz, H_i), 7.23 (2H, ddd, $J = 8.1, 6.7, 1.3$ Hz, H_g), 7.16 (2H, ddd, $J = 8.2, 6.7, 1.5$ Hz, H_h), 6.93 (2H, dd, $J = 8.4, 1.3$ Hz, H_c), 3.11 (12H, s, H_1).

^{13}C NMR (101 MHz, $\text{DMSO}-d_6$) δ 153.0, 134.1, 128.6, 128.1, 127.8, 125.8, 124.4, 122.2, 118.5, 115.4, 54.3 (t, $J = 4.1$ Hz).

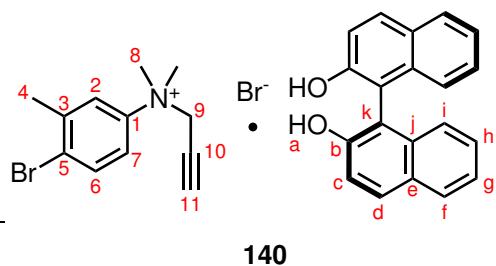
LRMS (ESI-TOF, EI^-) m/z : 285.2 ($[\text{M}]^-$, 100%).

HRMS (ESI-TOF) m/z : $[\text{M}-\text{H}]^-$ calculated for $\text{C}_{20}\text{H}_{13}\text{O}_2^-$: 285.0916, found 285.0924.

mp: 261 – 263 °C (EtOH).

IR ($\nu_{\text{max}}/\text{cm}^{-1}$): 3130br, 2980m, 1620m, 1270s, 820s.

XRD: A portion of the complex was crystallised in EtOH, to give clear colourless prisms. Crystal data for $\text{C}_{24}\text{H}_{26}\text{BrNO}_2$ ($m = 440.37$ g/mol): Orthorhombic, space group $P2_12_12_1$ (no. 19).

4-bromo-3,*N,N*-trimethyl-*N*-(prop-2-yne)anilinium bromide · (*R*)-1,1'-bi-2-naphthol

The quaternary ammonium bromide salt **98** (0.198 g, 0.6 mmol) was dissolved in CHCl_3 (0.50 mL, 1.2 M) in a 10 mL vial. Solid (*R*)-BINOL (0.172 g, 1.0 equiv.) was then added with stirring to the solution, resulting in a homogeneous solution. This solution was allowed to stir at room temperature overnight,

which produced the desired complexed product **140** as a white precipitate. The resulting complex was isolated by vacuum filtration (0.174 g, 47% yield). Analysis by ^1H NMR spectroscopy ensured that a 1:1 complex had formed.

^1H NMR (599 MHz, $\text{DMSO}-d_6$) δ 9.20 (2H, s, H_a), 8.07 (1H, d, $J = 3.7$ Hz, H_2), 7.88 (1H, dd, $J = 8.9, 1.5$ Hz, H_7), 7.85 (4H, apt. dd, $J = 8.7, 4.9$ Hz, H_{d+f}), 7.74 (1H, dd, $J = 8.8, 4.0$ Hz, H_6), 7.33 (2H, dd, $J = 8.9, 1.4$ Hz, H_i), 7.23 (2H, ddd, $J = 8.1, 6.7, 1.4$ Hz, H_g), 7.16 (2H, ddd, $J = 8.2, 6.7, 1.5$ Hz, H_h), 6.93 (2H, d, $J = 8.5$ Hz, H_c), 5.01 (2H, d, $J = 2.5$ Hz, H_9), 3.91 (1H, q, $J = 2.5$ Hz, H_{11}), 3.65 (6H, s, H_8), 2.45 (3H, s, H_4).

^{13}C NMR (151 MHz, $\text{DMSO}-d_6$) δ 153.0, 144.1, 139.6, 134.1, 133.3, 128.6, 128.1, 127.8, 126.0, 125.8, 124.4, 123.9, 122.2, 120.8, 118.5, 115.4, 83.1, 72.6, 58.2, 53.8, 22.7.

LRMS (ESI-TOF, EI^+) m/z : 252.4 ($[\text{M}]^+$, 100%).

LRMS (ESI-TOF, EI^-) m/z : 285.4 ($[\text{M}-\text{H}]^-$, 100%).

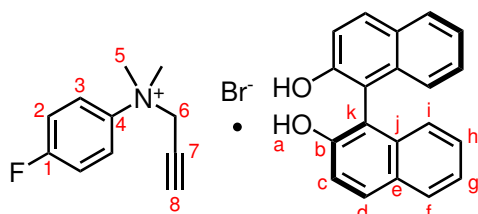
HRMS (ESI-TOF) m/z : $[\text{M}]^+$ calculated for $\text{C}_{12}\text{H}_{15}\text{NBr}^+$: 252.0388, found 252.0386.

$[\text{M}-\text{H}]^-$ calculated for $\text{C}_{20}\text{H}_{13}\text{O}_2^-$: 285.0916, found 285.0919.

mp: 120 – 121 °C (CHCl_3).

IR ($\nu_{\text{max}}/\text{cm}^{-1}$): 3243m, 3135br, 2977m, 1622m, 824s.

XRD: A portion of the complex was crystallised in methanol, resulting in colourless blocks. Crystal data for $\text{C}_{32}\text{H}_{29}\text{Br}_2\text{NO}_2$ ($m = 619.38$ g/mol): Monoclinic, space group $P2_1$ (no. 4).

4-fluoro-*N,N*-dimethyl-*N*-(prop-2-yn-1-yl)anilinium bromide · (*R*)-1,1'-bi-2-naphthol**141**

The quaternary ammonium bromide salt **99** (0.203 g, 0.79 mmol) was dissolved in CHCl_3 (1.60 mL, 0.5 M) in a 10 mL vial. Solid (*R*)-BINOL (0.226 g, 1.0 equiv.) was then added with stirring to the solution, resulting in a homogeneous solution. This solution was allowed to stir at room temperature overnight,

which produced the desired complexed product **141** as a white precipitate. The resulting complex was isolated by vacuum filtration (0.382 g, 89% yield). Analysis by ^1H NMR spectroscopy ensured that a 1:1 complex had formed.

^1H NMR (599 MHz, $\text{DMSO}-d_6$) δ 9.23 (2H, s, H_a), 8.10 (2H, dd, $J = 9.3, 4.0$ Hz, H_3), 7.88 – 7.82 (4H, m, H_{d+f}), 7.52 (2H, t, $J = 8.7$ Hz, H_2), 7.38 (2H, d, $J = 8.9$ Hz, H_i), 7.22 (2H, t, $J = 6.9$ Hz, H_g), 7.16 (2H, t, $J = 7.9$ Hz, H_h), 6.96 (2H, d, $J = 8.5$ Hz, H_c), 5.14 (2H, d, $J = 2.6$ Hz, H_6), 3.91 (1H, t, $J = 2.6$ Hz, H_8), 3.72 (6H, s, H_5).

^{13}C NMR (151 MHz, $\text{DMSO}-d_6$) δ 162.1 (d, $J = 248.6$ Hz), 153.0, 141.0 (d, $J = 2.8$ Hz), 134.1, 128.6, 128.1, 127.8, 125.8, 124.4, 124.2 (d, $J = 9.4$ Hz), 122.2, 118.6, 116.8 (d, $J = 23.5$ Hz), 115.4, 83.0, 72.6, 58.4, 54.0.

^{19}F NMR (376 MHz, $\text{DMSO}-d_6$) δ -110.87.

LRMS (ESI-TOF, EI^+) m/z : 178.4 ($[\text{M}]^+$, 100%).

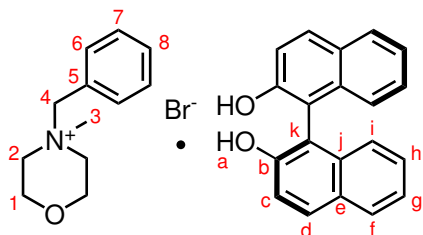
LRMS (ESI-TOF, EI^-) m/z : 285.4 ($[\text{M}-\text{H}]^-$, 100%).

HRMS (ESI-TOF) m/z : $[\text{M}]^+$ calculated for $\text{C}_{11}\text{H}_{13}\text{NF}^+$: 178.1032, found 178.1041. $[\text{M}-\text{H}]^-$ calculated for $\text{C}_{20}\text{H}_{13}\text{O}_2^-$: 285.0916, found 285.0924.

mp: 160 – 162 °C (CHCl_3).

IR ($\nu_{\text{max}}/\text{cm}^{-1}$): 3249m, 3106br, 1624m, 815s, 756s, 631m.

XRD: A portion of the complex was crystallised in EtOH to give colourless plates. Crystal data for $\text{C}_{31}\text{H}_{27}\text{BrNO}_2$ ($m = 544.44$ g/mol): Monoclinic, space group $P2_1$ (no. 4).

1-benzyl-1-methyl-morpholinium bromide · (*R*)-1,1'-bi-2-naphthol**142**

Ammonium salt **100** (0.272 g, 1.0 mmol) was dissolved in CHCl_3 (1.67 mL, 0.6 M) in a 10 mL vial. Solid (*R*)-BINOL (0.286 g, 1.0 equiv.) was then added with stirring to the solution. This solution was allowed to stir at room temperature overnight, which produced the desired complexed product **142** as a white precipitate.

The resulting complex was isolated by vacuum filtration (0.600 g, 81% yield). ^1H NMR (400 MHz, $\text{DMSO}-d_6$) δ 9.22 (2H, s, H_a), 7.88 – 7.81 (4H, m, H_{d+f}), 7.61 – 7.47 (5H, m, H_{6+7+8}), 7.32 (2H, d, $J = 8.8$ Hz, H_i), 7.23 (2H, ddd, $J = 8.1, 6.7, 1.3$ Hz, H_g), 7.16 (2H, ddd, $J = 8.3, 6.7, 1.5$ Hz, H_h), 6.93 (2H, dd, $J = 8.3, 1.2$ Hz, H_c), 4.71 (2H, s, H_4), 4.08 – 3.88 (4H, m, H_2), 3.53 (2H, ddd, $J = 13.1, 8.7, 4.4$ Hz, H_1), 3.31 (2H, dt, $J = 13.2, 2.9$ Hz, $\text{H}_{1'}$), 3.06 (3H, s, H_3).

^{13}C NMR (101 MHz, $\text{DMSO}-d_6$) δ 153.5, 134.5, 133.7, 130.8, 129.4, 129.1, 128.6, 128.3, 127.7, 126.3, 124.9, 122.7, 119.0, 115.9, 67.8, 60.3, 58.9, 45.4.

LRMS (ESI-TOF, EI^+) m/z : 192.1 ($[\text{M}]^+$, 100%).

LRMS (ESI-TOF, EI^-) m/z : 285.2 ($[\text{M}-\text{H}]^-$, 100%).

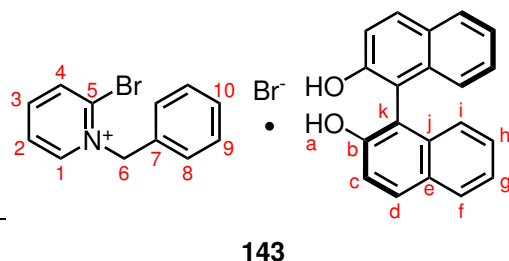
HRMS (ESI-TOF) m/z : $[\text{M}]^+$ calculated $\text{C}_{12}\text{H}_{18}\text{NO}^+$: 192.1388, found: 192.1373. $[\text{M}-\text{H}]^-$ calculated for $\text{C}_{20}\text{H}_{13}\text{O}_2^-$: 285.0916, found: 285.0911.

mp: 212 – 214 °C (EtOH).

IR ($\nu_{\text{max}}/\text{cm}^{-1}$): 3245br, 2980w, 1620m, 1274m, 1124m, 751m.

XRD: A portion of the complex was crystallised in EtOH, to give clear colourless blocks.

Crystal data for $\text{C}_{32}\text{H}_{32}\text{BrNO}_3$ ($m = 558.49$ g/mol): Monoclinic, space group $P2_1$ (no. 4).

2-bromo-1-benzylpyridinium bromide · (*R*)-1,1'-bi-2-naphthol

Ammonium salt **101** (0.165 g, 0.501 mmol) was dissolved in EtOH (0.84 mL, 0.6 M) in a 10 mL vial. Solid (*R*)-BINOL (0.143 g, 1.0 equiv.) was then added with stirring to the solution. This solution was allowed to stir at room temperature overnight, which produced the desired

complex **143** as a white precipitate. The resulting complex was isolated by vacuum filtration (0.230 g, 75% yield). Analysis by ^1H NMR spectroscopy ensured that a 1:1 complex had formed.

^1H NMR (400 MHz, CDCl_3) δ 9.40 (1H, dd, $J = 6.3, 1.5$ Hz, H_1), 9.22 (2H, s, H_a), 8.62 – 8.48 (2H, m, H_{2+4}), 8.23 (1H, ddd, $J = 7.7, 6.3, 1.9$ Hz, H_3), 7.87 – 7.83 (4H, m, H_{d+f}), 7.44 (3H, qd, $J = 7.6, 6.4, 3.6$ Hz, H_{9+10}), 7.33 – 7.28 (4H, m, H_{8+i}), 7.26 – 7.20 (2H, m, H_g), 7.16 (2H, ddd, $J = 8.3, 6.7, 1.4$ Hz, H_h), 6.93 (2H, d, $J = 8.4$ Hz, H_c), 6.04 (2H, s, H_6).

^{13}C NMR (101 MHz, CDCl_3) δ 153.0, 148.7, 147.0, 139.1, 134.7, 134.1, 132.9, 129.2, 128.9, 128.6, 128.1, 127.9, 127.8, 127.4, 125.9, 124.4, 122.3, 118.5, 115.4, 64.6.

LRMS (ESI-TOF, EI^+) m/z : 248.0 ($[\text{M}]^+$, 100%).

LRMS (ESI-TOF, EI^-) m/z : 285.2 ($[\text{M}]^-$, 100%).

HRMS (ESI-TOF) m/z : $[\text{M}]^+$ calculated for $\text{C}_{12}\text{H}_{11}\text{NBr}^+$: 248.0075, found: 248.0059.

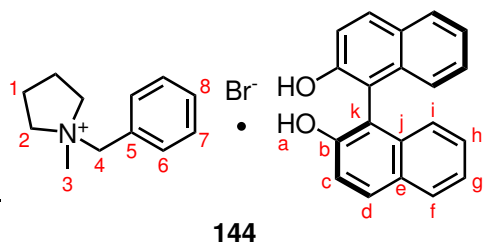
$[\text{M-H}]^-$ calculated for $\text{C}_{20}\text{H}_{13}\text{O}_2^-$: 285.0916, found: 285.0924.

mp: 160 – 161 °C (EtOH).

IR ($\nu_{\text{max}}/\text{cm}^{-1}$): 2980s, 1382m, 1272m, 1156m, 951m.

XRD: A portion of the complex was crystallised in EtOH, to give clear colourless plates.

Crystal data for $\text{C}_{32}\text{H}_{25}\text{Br}_2\text{NO}_2$ ($m = 615.35$ g/mol): Monoclinic, space group $P2_1$ (no. 4).

***N*-benzyl-*N*-methylpyrrolidinium bromide · (*R*)-1,1'-bi-2-naphthol**

Ammonium salt **102** (0.256 g, 1.0 mmol) was dissolved in CHCl_3 (1.67 mL, 0.6 M) in a 10 mL vial. Solid (*R*)-BINOL (0.286 g, 1.0 equiv.) was then added with stirring to the solution. This solution was allowed to stir at room temperature overnight, which produced the desired complexed product **144** as a white precipitate.

The resulting complex was isolated by vacuum filtration (0.484 g, 89% yield). Analysis by ^1H NMR spectroscopy ensured that a 1:1 complex had formed.

^1H NMR (400 MHz, $\text{DMSO}-d_6$) δ 9.23 (2H, s, H_a), 7.87 – 7.83 (4H, m, H_{d+i}), 7.70 – 7.46 (5H, m, H_{6+7+8}), 7.34 (2H, d, $J = 8.9$ Hz, H_i), 7.23 (2H, t, $J = 7.0$ Hz, H_g), 7.16 (2H, ddd, $J = 8.2, 6.7, 1.4$ Hz, H_h), 6.94 (2H, d, $J = 8.4$ Hz, H_c), 4.61 (2H, s, H_4), 3.58 (2H, q, $J = 8.9, 6.8$ Hz, H_2), 3.44 – 3.33 (2H, m, $\text{H}_{2'}$), 2.90 (3H, s, H_3), 2.27 – 2.02 (4H, m, H_1).

^{13}C NMR (101 MHz, $\text{DMSO}-d_6$) δ 153.0, 134.1, 132.5, 130.2, 129.1, 129.0, 128.6, 128.1, 127.9, 125.8, 124.4, 122.3, 118.6, 115.4, 65.0, 62.6, 47.2, 20.8.

LRMS (ESI-TOF, EI^+) m/z : 176.1 ($[\text{M}]^+$, 100%).

LRMS (ESI-TOF, EI^-) m/z : 285.2 ($[\text{M}-\text{H}]^-$, 100%).

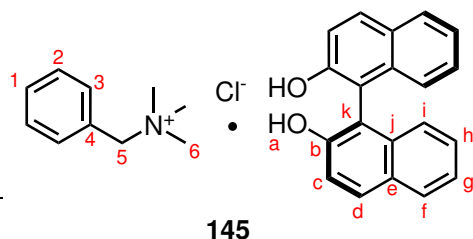
HRMS (ESI-TOF) m/z : $[\text{M}]^+$ calculated for $\text{C}_{12}\text{H}_{18}\text{N}^+$: 176.1439, found: 176.1433. $[\text{M}-\text{H}]^-$ calculated for $\text{C}_{20}\text{H}_{13}\text{O}_2^-$: 285.0916, found 285.0930.

mp: 197 – 198 °C (EtOH).

IR ($\nu_{\text{max}}/\text{cm}^{-1}$): 3141br, 1622m, 1504m, 1271m, 811m, 748m.

XRD: A portion of the complex was crystallised in EtOH, to give clear colourless blocks.

Crystal data for $\text{C}_{31}\text{H}_{32}\text{NO}_2\text{Br}$ ($m = 530.48$ g/mol): Monoclinic, space group $P2_1$ (no. 4).

Benzyltrimethylammonium chloride · (*R*)-1,1'-bi-2-naphthol

Benzyltrimethylammonium chloride (**71**, 0.186 g, 1.0 mmol) was dissolved in CHCl_3 (1.60 mL, 0.6 M) in a 10 mL vial. Solid (*R*)-BINOL (0.286 g, 1.0 equiv.) was then added with stirring to the solution, resulting in a pale yellow homogeneous solution. This solution was allowed to stir at room temperature overnight,

which produced the desired complexed product **145** as a white precipitate. The resulting complex was isolated by vacuum filtration (0.472 g, 100% yield). Analysis by ^1H NMR spectroscopy ensured that a 1:1 complex had formed.

^1H NMR (400 MHz, $\text{DMSO}-d_6$) δ 9.37 (2H, s, H_a), 7.87 – 7.83 (4H, m, H_{d+f}), 7.52 – 7.48 (5H, m, H_{1+2+3}), 7.39 (2H, d, $J = 8.8$ Hz, H_i), 7.26 – 7.19 (2H, m, H_g), 7.16 (2H, apt. t, $J = 7.8$ Hz, H_h), 6.93 (2H, d, $J = 8.4$ Hz, H_c), 4.59 (2H, s, H_5), 3.04 (9H, s, H_6).

^{13}C NMR (101 MHz, $\text{DMSO}-d_6$) δ 153.6, 134.6, 133.3, 130.7, 129.4, 129.0, 128.9, 128.5, 128.3, 126.2, 124.9, 122.7, 119.0, 115.9, 68.1, 52.1 (t, $J = 4.1$ Hz).

LRMS (ESI-TOF, EI^+) m/z : 150.1 ($[\text{M}]^+$, 100%).

LRMS (ESI-TOF, EI^-) m/z : 285.2 ($[\text{M}-\text{H}]^-$, 100%).

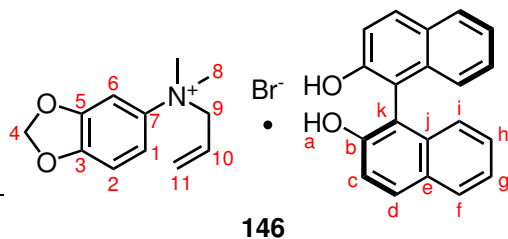
HRMS (ESI-TOF) m/z : $[\text{M}]^+$ calculated for $\text{C}_{10}\text{H}_{16}\text{N}^+$: 150.1283, found: 150.1278. $[\text{M}-\text{H}]^-$ calculated for $\text{C}_{20}\text{H}_{13}\text{O}^-$: 285.0916, found 285.0923.

mp: 205 – 207 °C (CHCl_3).

IR ($\nu_{\text{max}}/\text{cm}^{-1}$): 3142br, 2988m, 1621m, 1281m, 955m, 740m.

XRD: A portion of the complex was crystallised in EtOH to give clear colourless blocks.

Crystal data for $\text{C}_{30}\text{H}_{30}\text{ClNO}_2$ ($m = 472.00$ g/mol): Monoclinic, space group $P2_1$ (no. 4).

***N*-allyl-3,4-(methylenedioxy)-*N,N*-dimethylanilinium bromide · (*R*)-1,1'-bi-2-naphthol**

The quaternary ammonium bromide salt **103** (0.253 g, 1.0 mmol) was dissolved in EtOH (0.44 mL, 2.0 M) in a 10 mL vial. Solid (*R*)-BINOL (0.253 g, 1.0 equiv.) was then added with stirring to the solution, resulting in a homogeneous solution.

This solution was allowed to stir at room temperature overnight, which produced the desired complexed product **146** as a pale brown precipitate. The resulting complex was isolated by vacuum filtration (0.238 g, 47% yield). Analysis by ^1H NMR spectroscopy ensured that a 1:1 complex had formed.

^1H NMR (599 MHz, CD_3OD) δ 7.86 (2H, d, $J = 8.9$ Hz, H_d), 7.82 (2H, d, $J = 8.2$ Hz, H_f), 7.37 (1H, d, $J = 2.8$ Hz, H_6), 7.31 (2H, d, $J = 2.8$ Hz, H_i), 7.24 (2H, ddd, $J = 8.1$, 6.7, 1.2 Hz, H_g), 7.19 – 7.12 (3H, m, H_{1+h}), 7.03 (2H, d, $J = 8.4$ Hz, H_c), 6.91 (1H, d, $J = 8.7$ Hz, H_2), 6.07 (2H, s, H_4), 5.63 – 5.55 (2H, m, H_{11}), 5.56 – 5.48 (1H, m, H_{10}), 4.35 (2H, d, $J = 6.4$ Hz, H_9), 3.44 (6H, s, H_8).

^{13}C NMR (151 MHz, CD_3OD) δ 154.2, 150.7, 150.4, 139.7, 135.8, 130.6, 130.4, 129.2, 129.0, 127.1, 126.3, 125.8, 123.9, 119.3, 116.2, 115.9, 109.2, 104.4, 103.3, 72.8, 54.70.

LRMS (ESI-TOF, EI^+) m/z : 206.1 ($[\text{M}]^+$, 100%), 165.08 (74).

LRMS (ESI-TOF, EI^-) m/z : 285.1 ($[\text{M}-\text{H}]^-$, 100%).

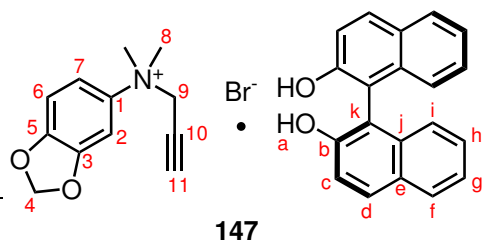
HRMS (ESI-TOF) m/z : $[\text{M}]^+$ calculated for $\text{C}_{12}\text{H}_{16}\text{NO}_2^+$: 206.1181, found 206.1193.

$[\text{M}-\text{H}]^-$ calculated for $\text{C}_{20}\text{H}_{13}\text{O}_2^-$: 285.0916, found 285.0934.

mp: 128 °C (EtOH).

IR ($\nu_{\text{max}}/\text{cm}^{-1}$): 3210br, 1483, 1247s, 818, 625.

XRD: A portion of the complex was crystallised in EtOH to give colourless plates. Crystal data for $\text{C}_{33}\text{H}_{34}\text{BrNO}_4$ ($m = 588.52$ g/mol): Monoclinic, space group $P2_1$ (no. 4).

3,4-methylenedioxy-*N,N*-dimethyl-*N*-(prop-2-yne)anilinium bromide · (*R*)-1,1'-bi-2-naphthol

The quaternary ammonium bromide salt **104**

(0.236 g, 0.83 mmol) was dissolved in EtOH (1.40 mL, 0.6 M) in a 10 mL vial. Solid (*R*)-BINOL (0.228 g, 1.0 equiv.) was then added with stirring to the solution, resulting in a homogeneous solution. This solution was allowed to stir at room temperature overnight,

which produced the desired complexed product **147** as a white precipitate. The resulting complex was isolated by vacuum filtration (0.462 g, 97% yield). Analysis by ^1H NMR spectroscopy ensured that a 1:1 complex had formed.

^1H NMR (599 MHz, $\text{DMSO}-d_6$) δ 9.21 (2H, s, H_a), 7.87 – 7.83 (4H, m, H_{d+f}), 7.73 (1H, d, $J = 2.6$ Hz, H_2), 7.41 (1H, dd, $J = 8.2, 2.2$ Hz, H_7), 7.35 (2H, dd, $J = 8.9, 1.2$ Hz, H_i), 7.22 (2H, ddd, $J = 7.4, 6.6, 1.4$ Hz, H_g), 7.16 (2H, ddd, $J = 7.9, 6.6, 1.4$ Hz, H_h), 7.11 (1H, d, $J = 8.7$ Hz, H_6), 6.94 (2H, d, $J = 8.5$ Hz, H_c), 6.19 (2H, s, H_4), 5.01 (2H, s, H_9), 3.90 (1H, t, $J = 2.7$ Hz, H_{11}), 3.63 (6H, s, H_8).

^{13}C NMR (151 MHz, $\text{DMSO}-d_6$) δ 153.0, 148.4, 148.3, 138.8, 134.1, 128.6, 128.1, 127.8, 125.8, 124.4, 122.2, 118.5, 115.4, 115.2, 107.9, 102.84, 102.79, 82.8, 72.8, 58.4, 54.1.

LRMS (ESI-TOF, EI^+) m/z : 204.5 ($[\text{M}]^+$, 100%).

LRMS (ESI-TOF, EI^-) m/z : 285.4 ($[\text{M}-\text{H}]^-$, 100%).

HRMS (ESI-TOF) m/z : $[\text{M}]^+$ calculated for $\text{C}_{12}\text{H}_{14}\text{NO}_2^+$: 204.1025, found 204.1032.

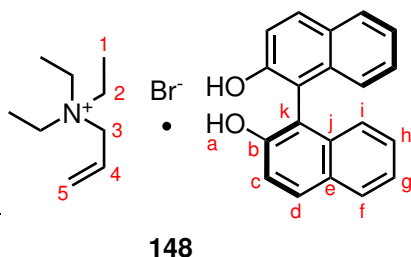
$[\text{M}-\text{H}]^-$ calculated for $\text{C}_{20}\text{H}_{13}\text{O}_2^-$: 285.0916, found 285.0905.

mp: 160 – 162 °C (EtOH).

IR ($\nu_{\text{max}}/\text{cm}^{-1}$): 3195br, 2980m, 2952m, 1623m, 1274s, 634s.

XRD: A portion of the complex was crystallised in EtOH to give colourless blocks of **147**. Crystal data for $\text{C}_{32}\text{H}_{28}\text{BrNO}_4$ ($m = 570.46$ g/mol): Tetragonal, space group $P4_1$ (no. 76).

Another sample was also crystallised in EtOH to give colourless blocks of **147**. Crystal data for $\text{C}_{32}\text{H}_{28}\text{BrNO}_4 \cdot \text{H}_2\text{O}$ ($m = 574.97$ g/mol): Tetragonal, space group $P4_1$ (no. 76). The predicted PXRD trace for this crystal structure did not match that produced from the precipitate.

***N,N,N*-triethylprop-2-en-1-aminium bromide · (*R*)-1,1'-bi-2-naphthol**

The quaternary ammonium bromide salt **105** (0.222 g, 1.00 mmol) was dissolved in CHCl_3 (2.50 mL, 0.4 M) in a 10 mL vial. Solid (*R*)-BINOL (0.286 g, 1.0 equiv.) was then added with stirring to the solution, resulting in a pale yellow homogeneous solution. This solution was allowed to stir at room temperature overnight, which produced the desired complexed product **148** as a white precipitate. The resulting complex was isolated by vacuum filtration (0.568 g, 100% yield).

Analysis by ^1H NMR spectroscopy ensured that a 1:1 complex had formed.

^1H NMR (400 MHz, CD_3OD) δ 7.89 – 7.85 (2H, m, H_d), 7.83 (2H, dt, $J = 8.2, 0.9$ Hz, H_f), 7.31 (2H, d, $J = 8.9$ Hz, H_i), 7.24 (2H, ddd, $J = 8.1, 6.8, 1.3$ Hz, H_g), 7.16 (2H, ddd, $J = 8.2, 6.7, 1.4$ Hz, H_h), 7.05 – 7.00 (2H, m, H_c), 5.93 (1H, ddt, $J = 17.3, 10.1, 7.2$ Hz, H_4), 5.71 – 5.59 (2H, m, H_5), 3.77 (2H, d, $J = 7.1$ Hz, H_3), 3.18 (6H, q, $J = 7.2$ Hz, H_2), 1.23 (9H, tt, $J = 7.3, 1.8$ Hz, H_1).

^{13}C NMR (101 MHz, CD_3OD) δ 154.2, 135.8, 130.5, 130.4, 129.0, 128.5, 127.1, 125.80, 125.77, 123.8, 119.3, 116.2, 60.3 (dd, $J = 5.7, 3.0$ Hz), 53.7 (dd, $J = 5.5, 2.6$ Hz), 7.7.

LRMS (ESI-TOF, EI^+) m/z : 142.2 ($[\text{M}]^+$, 100%).

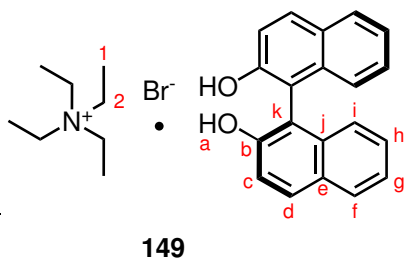
LRMS (ESI-TOF, EI^-) m/z : 285.3 ($[\text{M}-\text{H}]^-$, 100%).

HRMS (ESI-TOF) m/z : $[\text{M}]^+$ calculated for $\text{C}_9\text{H}_{20}\text{N}^+$: 142.1596, found 142.1593. $[\text{M}-\text{H}]^-$ calculated for $\text{C}_{20}\text{H}_{13}\text{O}_2^-$: 285.0916, found 285.0921.

mp: 220 – 222 °C (CHCl_3).

IR ($\nu_{\text{max}}/\text{cm}^{-1}$): 3175br, 1504m, 1435m, 1273m, 818m, 750m.

XRD: A portion of the complex was crystallised in EtOH to give clear colourless prisms. Crystal data for $\text{C}_{29}\text{H}_{34}\text{NO}_2\text{Br}$ ($m = 508.48$ g/mol): Tetragonal, space group $P4_3$ (no. 78).

Tetraethylammonium bromide · (*R*)-1,1'-bi-2-naphthol

Tetraethylammonium bromide (**106**, 0.367 g, 1.75 mmol) was dissolved in CHCl_3 (1.75 mL, 1.0 M) in a 10 mL vial. Solid (*R*)-BINOL (0.500 g, 1.0 equiv.) was then added with stirring to the solution. This solution was allowed to stir at room temperature overnight, which produced the desired complex **149** as a white precipitate. The resulting

complex was isolated by vacuum filtration (0.564 g, 65% yield). Analysis by ^1H NMR spectroscopy ensured that a 1:1 complex had formed.

^1H NMR (400 MHz, $\text{DMSO}-d_6$) δ 9.22 (2H, s, H_a), 7.87 – 7.85 (2H, m, H_d), 7.85 – 7.83 (2H, m, H_f), 7.34 (2H, d, $J = 8.9$ Hz, H_i), 7.23 (2H, ddd, $J = 8.1, 6.7, 1.3$ Hz, H_g), 7.16 (2H, ddd, $J = 8.2, 6.7, 1.4$ Hz, H_h), 6.93 (2H, dd, $J = 8.3, 1.2$ Hz, H_c), 3.20 (8H, q, $J = 7.3$ Hz, H_2), 1.15 (12H, tt, $J = 7.3, 1.9$ Hz, H_1).

^{13}C NMR (101 MHz, $\text{DMSO}-d_6$) δ 153.0, 134.1, 128.6, 128.1, 127.9, 125.8, 124.3, 122.3, 118.5, 115.4, 79.3, 51.4.

LRMS (ESI-TOF, EI^+) m/z : 130.4 ($[\text{M}]^+$, 100%).

LRMS (ESI-TOF, EI^-) m/z : 285.2 ($[\text{M}]^-$, 100%).

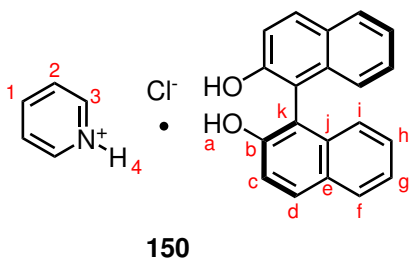
HRMS (ESI-TOF) m/z : $[\text{M}]^+$ calculated for $\text{C}_8\text{H}_{20}\text{N}^+$: 130.1596, found: 130.1594. $[\text{M}-\text{H}]^-$ calculated for $\text{C}_{20}\text{H}_{13}\text{O}_2^-$: 285.0916, found: 285.0916.

mp: 251 – 252 °C (CHCl_3).

mp: 264 °C (EtOH).

IR ($\nu_{\text{max}}/\text{cm}^{-1}$): 3120br, 1274s, 821s, 751s.

XRD: A portion of the complex was crystallised in EtOH, to give clear colourless needles. Crystal data for $\text{C}_{28}\text{H}_{34}\text{BrNO}_2$ ($m = 496.47$ g/mol): Tetragonal, space group $P4_32_12$ (no. 96).

Pyridinium hydrochloride · (*R*)-1,1'-bi-2-naphthol

Ammonium salt **107** (0.115 g, 1.0 mmol) was dissolved in CHCl_3 (1.67 mL, 0.6 M) in a 10 mL vial. Solid (*R*)-BINOL (0.286 g, 1.0 equiv.) was then added with stirring to the solution. This solution was allowed to stir at room temperature overnight, which produced the desired complex **150** as a white precipitate. The resulting complex was iso-

lated by vacuum filtration (0.333 g, 83% yield). Analysis by ^1H NMR spectroscopy ensured that a 1:1 complex had formed.

^1H NMR (400 MHz, $\text{DMSO}-d_6$) δ 9.32 (2H, s, H_a), 8.97 – 8.86 (2H, m, H_3), 8.67 – 8.46 (1H, m, H_1), 8.14 – 7.98 (2H, m, H_2), 7.92 – 7.73 (4H, m, H_{d+f}), 7.37 (2H, d, $J = 8.9$ Hz, H_i), 7.22 (2H, ddd, $J = 8.0, 6.7, 1.3$ Hz, H_g), 7.16 (2H, ddd, $J = 8.2, 6.7, 1.4$ Hz, H_h), 6.97 – 6.88 (2H, m, H_c).

^{13}C NMR (101 MHz, $\text{DMSO}-d_6$) δ 153.1, 145.7, 142.2, 134.1, 128.6, 128.1, 127.9, 127.1, 125.8, 124.4, 122.3, 118.6, 115.4.

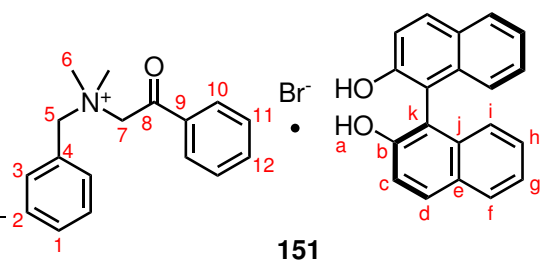
LRMS (ESI-TOF, EI^-) m/z : 285.2 ($[\text{M}-\text{H}]^-$, 100%).

HRMS (ESI-TOF) m/z : $[\text{M}]^+$ calculated for $\text{C}_5\text{H}_6\text{N}^+$: 80.0500, found: 80.0492. $[\text{M}-\text{H}]^-$ calculated for $\text{C}_{20}\text{H}_{13}\text{O}_2^-$: 285.0916, found: 285.0918.

mp: 196 – 197 °C (EtOH).

IR ($\nu_{\text{max}}/\text{cm}^{-1}$): 3190br, 1615m, 1489m, 1266m, 967m, 812m.

XRD: A portion of the complex was crystallised in EtOH, to give clear colourless needles. Crystal data for $\text{C}_{25}\text{H}_{20}\text{ClNO}_2$ ($m = 401.87$ g/mol): Orthorhombic, space group $P2_12_12_1$ (no. 19).

***N*-benzyl-*N,N*-dimethyl-2-oxo-2-phenylethan-1-aminium bromide · (*R*)-1,1'-bi-2-naphthol**

The quaternary ammonium salt **108** (0.100 g, 0.30 mmol) was dissolved in EtOH (0.38 mL, 0.8 M) in a 1 mL vial. Solid (*R*)-BINOL (0.085 g, 1.0 equiv.) was then added with stirring to the solution, resulting in a pale yellow homogeneous solution. This solution was allowed to stir at room temperature for 15 minutes, which produced the desired complexed product **151** as a white precipitate. The resulting complex was isolated by vacuum filtration (0.139 g, 77% yield). Analysis by ¹H NMR spectroscopy ensured that a 1:1 complex had formed.

Analysis by ¹H NMR spectroscopy ensured that a 1:1 complex had formed.

¹H NMR (400 MHz, CDCl₃) δ 8.00 (2H, d, *J* = 7.6 Hz, H_d), 7.91 (2H, d, *J* = 8.9 Hz, H_f), 7.86 (2H, d, *J* = 8.1 Hz, H₃), 7.58 (1H, t, *J* = 7.3 Hz, H₁), 7.50 – 7.44 (9H, m, H_{2+10+11+12+i}), 7.34 (2H, t, *J* = 7.4 Hz, H_g), 7.26 (2H, dd, *J* = 16.1, 8.1 Hz, H_h), 7.14 (2H, d, *J* = 8.4 Hz, H_c), 6.12 (2H, s, H₅), 5.45 – 5.33 (2H, m, H₇), 4.98 (2H, s, H_a), 3.30 (6H, s, H₆).

¹³C NMR (101 MHz, CDCl₃) δ 191.3, 152.8, 135.1, 134.1, 133.8, 133.2, 131.1, 130.8, 129.4, 129.3, 129.1, 128.5, 128.4, 127.2, 126.9, 124.6, 123.8, 118.2, 112.4, 68.0, 66.0, 50.6.

LRMS (ESI-TOF, EI⁺) *m/z*: 254.1 ([M]⁺, 100%).

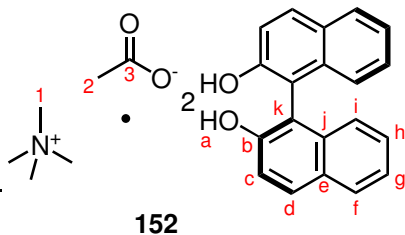
LRMS (ESI-TOF, EI⁻) *m/z*: 285.2 ([M-H]⁻, 100%).

HRMS (ESI-TOF) *m/z*: [M]⁺ calculated for C₁₇H₂₀NO⁺: 254.1538, found: 254.1541.

[M-H]⁻ calculated for C₂₀H₁₃O⁻: 285.0916, found: 285.0930.

mp: 120 – 121 °C (CHCl₃).

XRD: A portion of the complex was crystallised in MeCN to give clear colourless needles. Crystal data for C₃₇H₃₄NO₃Br (*m* = 620.56 g/mol): orthorhombic, space group *P*2₁2₁2₁ (no. 19).

Tetramethylammonium acetate · (*R*)-1,1'-bi-2-naphthol

Tetramethylammonium acetate (**109**, 0.301 g, 2.26 mmol) was dissolved in EtOH (2.30 mL, 1.0 M) in a 10 mL vial. Solid (*R*)-BINOL (0.648 g, 1.0 equiv.) was then added with stirring to the solution. This solution was allowed to stir at room temperature overnight, which produced the desired

product **152** as a white precipitate. The resulting complex was isolated by vacuum filtration (0.706 g, 75% yield). Analysis by ^1H NMR spectroscopy revealed that a 2:1 ((*R*)-BINOL:ammonium salt) complex had formed.

^1H NMR (400 MHz, CD_3OD) δ 7.92 – 7.77 (4H, m, $\text{H}_{\text{d+f}}$), 7.31 (2H, d, $J = 8.9$ Hz, H_i), 7.23 (2H, ddd, $J = 8.1, 6.8, 1.3$ Hz, H_g), 7.15 (2H, ddd, $J = 8.3, 6.8, 1.4$ Hz, H_h), 7.06 – 7.01 (2H, m, H_c), 2.98 (6H, s, H_1) 1.91 (1.50H, s, H_2).

^{13}C NMR (101 MHz, CD_3OD) δ 180.2, 154.2, 135.8, 130.5, 130.4, 129.0, 127.1, 125.8, 123.8, 119.3, 116.3, 55.7 (t, $J = 3.9$ Hz), 24.3.

LRMS (ESI-TOF, EI^+) m/z : 74.1 ($[\text{M}]^+$, 100%).

LRMS (ESI-TOF, EI^-) m/z : 285.2 ($[\text{M}-\text{H}]^-$, 100%).

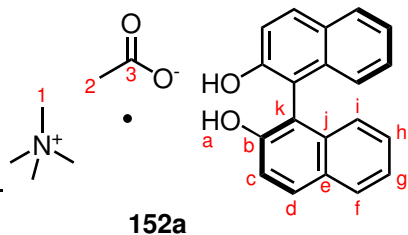
HRMS (ESI-TOF) m/z : $[\text{M}]^+$ calculated for $\text{C}_4\text{H}_{12}\text{N}^+$: 74.0964, found: 74.0958. $[\text{M}-\text{H}]^-$ calculated $\text{C}_{20}\text{H}_{13}\text{O}_2^-$: 285.0916, found: 285.0927.

mp: 224 – 226 °C (EtOH).

IR ($\nu_{\text{max}}/\text{cm}^{-1}$): 3052br, 2980m, 1564m, 1338s, 949m, 812m.

XRD: A portion of the complex was crystallised in EtOH, to give clear colourless plates.

$\text{C}_{46}\text{H}_{43}\text{NO}_6$ ($m = 705.81$ g/mol): Monoclinic, space group $P2_1$ (no. 4). The crystal structure confirmed the 2:1 ((*R*)-BINOL:ammonium salt) complex had formed.

Tetramethylammonium acetate · (*R*)-1,1'-bi-2-naphthol

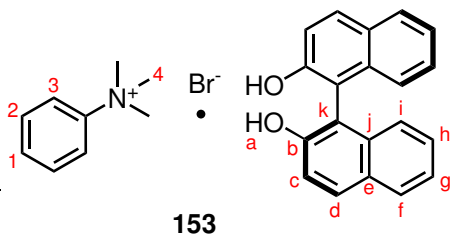
Tetramethylammonium acetate (0.133 g, 1.0 mmol) was dissolved in CHCl_3 (1.60 mL, 0.6 M) in a 10 mL vial. Solid (*R*)-BINOL (0.286 g, 1.0 equiv.) was then added with stirring to the solution. This solution was allowed to stir at room temperature overnight, which produced the desired

product **152** as a white precipitate. The resulting complex was isolated by vacuum filtration (0.379 g, 90% yield). Analysis by ^1H NMR spectroscopy ensured that a 1:1 complex had formed.

^1H NMR (400 MHz, $\text{DMSO}-d_6$) δ 7.77 (4H, t, $J = 8.5$ Hz, H_{d+f}), 7.33 (2H, d, $J = 8.8$ Hz, H_i), 7.16 (2H, ddd, $J = 8.0, 6.7, 1.4$ Hz, H_g), 7.09 (2H, ddd, $J = 8.2, 6.7, 1.4$ Hz, H_h), 6.99 – 6.90 (2H, m, H_c), 3.07 (12H, s, H_1) 1.67 (3H, s, H_2).

^{13}C NMR (101 MHz, $\text{DMSO}-d_6$) δ 173.4, 155.4, 134.3, 128.1, 127.8, 127.6, 125.2, 124.8, 121.5, 119.9, 116.1, 54.4 (t, $J = 3.9$ Hz), 24.6.

PXRD data for **152a** displays different indices than the *EtOH* precipitated material **152** indicating that the two solid forms are not alike.

***N,N,N*-trimethyl anilinium bromide · (*R*)-1,1'-bi-2-naphthol**

N,N,N-trimethyl anilinium bromide (**110**, 0.317 g, 1.47 mmol) was dissolved in CHCl_3 (1.46 mL, 1.0 M) in a 10 mL vial. Solid (*R*)-BINOL (0.419 g, 1.0 equiv.) was then added with stirring to the solution. This solution was allowed to stir at room temperature overnight, which

produced the desired complex **153** as a white precipitate. The resulting complex was isolated by vacuum filtration (0.449 g, 61% yield). Analysis by ^1H NMR spectroscopy ensured that a 1:1 complex had formed.

^1H NMR (400 MHz, $\text{DMSO}-d_6$) δ 9.23 (2H, s, H_a), 8.02 – 7.97 (2H, m H_3), 7.88 – 7.82 (4H, m, H_{d+f}), 7.66 – 7.60 (2H, m, H_2), 7.60 – 7.54 (1H, m, H_1), 7.35 (2H, d, $J = 8.8$ Hz, H_i), 7.23 (2H, ddd, $J = 8.0, 6.7, 1.4$ Hz, H_g), 7.16 (2H, ddd, $J = 8.0, 6.7, 1.4$ Hz, H_h), 6.94 (2H, dd, $J = 8.1, 1.2$ Hz, H_c), 3.63 (9H, s, H_4).

^{13}C NMR (101 MHz, $\text{DMSO}-d_6$) δ 153.5, 147.8, 134.6, 130.5, 129.1, 128.6, 128.3, 126.3, 124.9, 122.7, 120.9, 119.0, 115.8, 56.8.

LRMS (ESI-TOF, EI^+) m/z : 136.4 ($[\text{M}]^+$, 100%).

LRMS (ESI-TOF, EI^-) m/z : 285.2 ($[\text{M}]^-$, 100%).

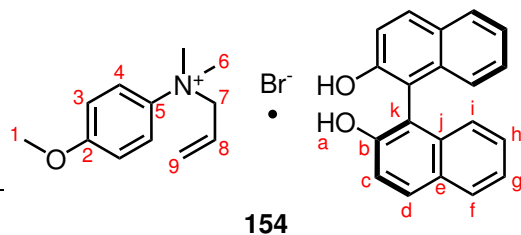
HRMS (ESI-TOF) m/z : $[\text{M}]^+$ calculated for $\text{C}_9\text{H}_{14}\text{N}^+$: 136.1126, found: 136.1121. $[\text{M}-\text{H}]^-$ calculated for $\text{C}_{20}\text{H}_{13}\text{O}_2^-$: 285.0916, found: 285.0920.

mp: 186 – 187 °C (CHCl_3).

IR ($\nu_{\text{max}}/\text{cm}^{-1}$): 3173br, 1274s, 814s, 752s, 681w.

XRD: A portion of the complex was crystallised in EtOH, to give clear colourless plates.

$\text{C}_{29}\text{H}_{28}\text{NO}_2\text{Br}$ ($m = 502.43$ g/mol): Monoclinic, space group $P2_1$ (no. 4).

***N*-allyl-4-methoxy-*N,N*-dimethylanilinium bromide · (*R*)-1,1'-bi-2-naphthol**

The quaternary ammonium bromide salt **111** (0.282 g, 1.0 mmol) was dissolved in CHCl_3 (0.50 mL, 2.0 M) in a 10 mL vial. Solid (*R*)-BINOL (0.291 g, 1.0 equiv.) was then added with stirring to the solution, resulting in a homogeneous solution.

This solution was allowed to stir at room temperature overnight, which produced the desired complexed product **154** as a white precipitate. The resulting complex was isolated by vacuum filtration (0.507 g, 90% yield). Analysis by ^1H NMR spectroscopy ensured that a 1:1 complex had formed.

^1H NMR (599 MHz, CD_3OD) δ 7.87 (2H, d, $J = 8.9$ Hz, H_d), 7.83 (2H, d, $J = 8.2$ Hz, H_f), 7.71 – 7.65 (2H, m, H_3), 7.30 (2H, d, $J = 8.9$ Hz, H_i), 7.24 (2H, ddd, $J = 8.0, 6.7, 1.0$ Hz, H_g), 7.15 (2H, ddd, $J = 8.1, 6.7, 1.0$ Hz, H_h), 7.11 – 7.05 (2H, m, H_4), 7.02 (2H, d, $J = 8.6$ Hz, H_c), 5.64 – 5.56 (1H, m, H_8), 5.56 – 5.50 (2H, m, H_9), 4.40 (2H, d, $J = 6.6$ Hz, H_7), 3.83 (3H, s, H_1), 3.50 (6H, s, H_6).

^{13}C NMR (151 MHz, CD_3OD) δ 162.0, 154.2, 138.4, 135.8, 130.6, 130.4, 129.2, 129.0, 127.1, 126.4, 125.8, 123.9, 123.4, 119.3, 116.2, 79.0, 72.7, 56.3, 54.5.

LRMS (ESI-TOF, EI^+) m/z : 192.1 ($[\text{M}]^+$, 100%), 151.1 (98).

LRMS (ESI-TOF, EI^-) m/z : 285.1 ($[\text{M}-\text{H}]^-$, 100%).

HRMS (ESI-TOF) m/z : $[\text{M}]^+$ calculated for $\text{C}_{12}\text{H}_{18}\text{NO}^+$: 192.1388, found 192.1396.

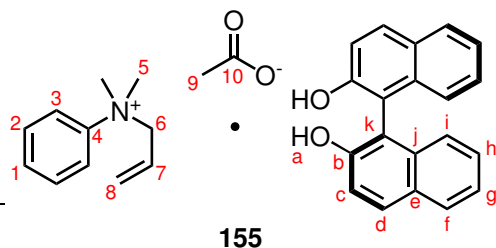
$[\text{M}-\text{H}]^-$ calculated for $\text{C}_{20}\text{H}_{13}\text{O}_2^-$: 285.0916, found 285.0916.

mp: 155 – 157 °C (CHCl_3).

IR ($\nu_{\text{max}}/\text{cm}^{-1}$): 3191br, 2980br, 1620m, 1328s, 1268s, 814s.

XRD: A portion of the complex was crystallised in EtOH to give colourless plates.

Crystal data for $\text{C}_{32}\text{H}_{32}\text{BrNO}_4$ ($m = 558.49$ g/mol): Triclinic, space group *P*1 (no. 1).

***N*-allyl-*N,N*-dimethylanilinium acetate · (*R*)-1,1'-bi-2-naphthol**

Ammonium salt **112** (0.221 g, 1.0 mmol) was dissolved in CHCl_3 (1.67 mL, 0.6 M) in a 10 mL vial. Solid (*R*)-BINOL (0.286 g, 1.0 equiv.) was then added with stirring to the solution. This solution was allowed to stir at room temperature overnight, which produced the desired complexed product **155** as a white precipitate.

The resulting complex was isolated by vacuum filtration (0.338 g, 67% yield). Analysis by ^1H NMR spectroscopy ensured that a 1:1 complex had formed.

^1H NMR (400 MHz, $\text{DMSO}-d_6$) δ 7.93 – 7.85 (2H, m, H_3), 7.82 – 7.72 (4H, m, H_{d+f}), 7.62 (2H, dd, $J = 8.1, 6.9$ Hz, H_2), 7.59 – 7.51 (1H, m, H_1), 7.32 (2H, d, $J = 8.8$ Hz, H_i), 7.14 (2H, ddd, $J = 8.0, 6.7, 1.4$ Hz, H_g), 7.08 (2H, ddd, $J = 8.2, 6.7, 1.5$ Hz, H_h), 6.93 (2H, dd, $J = 8.4, 1.3$ Hz, H_c), 5.58 (1H, ddt, $J = 17.2, 9.2, 6.9$ Hz, H_7), 5.50 – 5.39 (2H, m, H_8), 4.52 (2H, d, $J = 7.0$ Hz, H_6), 3.55 (6H, s, H_5), 1.68 (3H, s, H_9).

^{13}C NMR (101 MHz, $\text{DMSO}-d_6$) δ 173.5, 155.6, 144.7, 134.3, 130.1, 128.0, 127.84, 127.75, 127.7, 127.5, 125.8, 125.1, 124.8, 121.33, 121.25, 120.1, 116.2, 70.3, 53.1, 24.7.

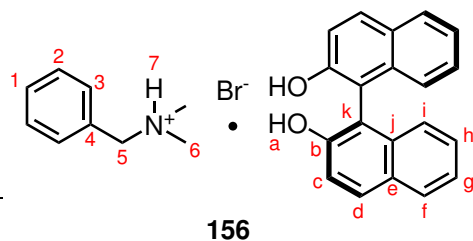
LRMS (ESI-TOF, EI^+) m/z : 162.1 ($[\text{M}]^+$, 100%).

LRMS (ESI-TOF, EI^-) m/z : 285.2 ($[\text{M}-\text{H}]^-$, 100%).

HRMS (ESI-TOF) m/z : $[\text{M}]^+$ calculated for $\text{C}_{11}\text{H}_{16}\text{N}^+$: 162.1283, found 162.1275. $[\text{M}-\text{H}]^-$ calculated for $\text{C}_{20}\text{H}_{13}\text{O}_2^-$: 285.0916, found: 285.0928.

mp: 189 – 191 °C (EtOH).

IR ($\nu_{\text{max}}/\text{cm}^{-1}$): 2972br, 1550m, 1341s, 819s, 761s, 693s.

***N,N*-dimethylbenzylammonium hydrobromide · (*R*)-1,1'-bi-2-naphthol**

Ammonium salt **113** (0.216 g, 1.0 mmol) was dissolved in EtOH (1.67 mL, 0.6 M) in a 10 mL vial. Solid (*R*)-BINOL (0.286 g, 1.0 equiv.) was then added with stirring to the solution. This solution was allowed to stir at room temperature overnight, which produced the desired complexed product **156** as a white pre-

precipitate. The resulting complex was isolated by vacuum filtration (0.071 g, 14% yield). Analysis by ^1H NMR spectroscopy ensured that a 1:1 complex had formed.

^1H NMR (400 MHz, DMSO- d_6) δ 9.68 (1H, s, H₇), 9.21 (2H, s, H_a), 7.97 – 7.75 (4H, m, H_{d+f}), 7.57 – 7.42 (5H, m, H₁₊₂₊₃), 7.32 (2H, d, J = 8.9 Hz, H_i), 7.23 (2H, ddd, J = 8.1, 6.7, 1.3 Hz, H_g), 7.16 (2H, ddd, J = 8.2, 6.7, 1.4 Hz, H_h), 6.93 (2H, dd, J = 8.3, 1.2 Hz, H_c), 4.29 (2H, s, H₅), 2.72 (6H, s, H₆).

^{13}C NMR (101 MHz, DMSO- d_6) δ 153.0, 134.1, 131.0, 130.4, 129.6, 128.9, 128.6, 128.1, 127.9, 125.9, 124.4, 122.3, 118.5, 115.4, 59.7, 41.8.

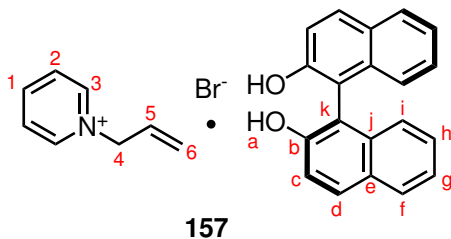
LRMS (ESI-TOF, EI⁺) m/z : 136.1 ([M]⁺, 100%).

LRMS (ESI-TOF, EI⁻) m/z : 285.2 ([M-H]⁻, 100%).

HRMS (ESI-TOF) m/z : [M]⁺ calculated for C₉H₁₄N⁺: 136.1126, found: 136.1115. [M-H]⁻ calculated for C₂₀H₁₃O₂⁻: 285.0916, found: 285.0920.

mp: 142 °C (EtOH).

IR ($\nu_{\text{max}}/\text{cm}^{-1}$): 3135br, 2725m, 1620m, 1271s, 814s, 745s.

1-allyl-pyridinium bromide · (*R*)-1,1'-bi-2-naphthol

The quaternary ammonium salt **369** (0.150 g, 0.75 mmol) was dissolved in EtOH (0.93 mL, 0.8 M) in a 5 mL vial. Solid (*R*)-BINOL (0.214 g, 1.0 equiv.) was then added with stirring to the solution. This solution was allowed to stir at room temperature for 15 minutes, which produced the desired complexed product **157**

as a white precipitate. The resulting complex **157** was isolated by vacuum filtration (0.271 g, 75% yield). Analysis by ^1H NMR spectroscopy ensured that a 1:1 complex had formed.

^1H NMR (400 MHz, DMSO- d_6) δ 9.22 (2H, s, H_a), 9.10 – 9.02 (2H, m, H_3), 8.64 (1H, tt, $J = 7.8, 1.4$ Hz, H_1), 8.28 – 8.15 (2H, m, H_2), 7.92 – 7.77 (4H, m, H_{d+f}), 7.33 (2H, d, $J = 8.9$ Hz, H_i), 7.23 (2H, ddd, $J = 8.1, 6.7, 1.3$ Hz, H_g), 7.16 (2H, ddd, $J = 8.2, 6.7, 1.5$ Hz, H_h), 6.97 – 6.85 (2H, m, H_c), 6.17 (1H, ddt, $J = 16.6, 10.2, 6.2$ Hz, H_5), 5.51 – 5.35 (2H, m, H_6), 5.30 (2H, dt, $J = 6.2, 1.4$ Hz, H_4).

^{13}C NMR (101 MHz, DMSO- d_6) δ 153.0, 145.9, 144.8, 134.1, 131.8, 128.6, 128.3, 128.1, 127.9, 125.9, 124.4, 122.3, 121.9, 118.5, 115.4, 62.4.

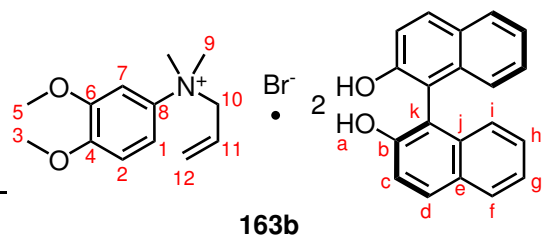
LRMS (ESI-TOF, EI^+) m/z : 120.1 ($[\text{M}]^+$, 100%).

LRMS (ESI-TOF, EI^-) m/z : 285.2 ($[\text{M}-\text{H}]^-$, 100%).

HRMS (ESI-TOF) m/z : $[\text{M}]^+$ calculated for $\text{C}_8\text{H}_{10}\text{N}^+$: 120.0808, found: 120.0804. $[\text{M}-\text{H}]^-$ calculated for $\text{C}_{20}\text{H}_{13}\text{O}_2^-$: 285.0916, found: 285.0914

mp: 149 – 151 °C (EtOH).

IR ($\nu_{\text{max}}/\text{cm}^{-1}$): 3411br, 2981m, 1427m, 1212m, 744sh, 701s.

***N*-allyl-3,4-dimethoxy-*N,N*-dimethylanilinium bromide · (*R*)-1,1'-bi-2-naphthol**

The quaternary ammonium bromide salt **370** (0.227 g, 0.8 mmol) was dissolved in CHCl_3 (0.77 mL, 1.3 M) in a 10 mL vial. Solid (*R*)-BINOL (0.213 g, 1.0 equiv.) was then added with stirring to the solution, resulting in a homogeneous solution.

This solution was allowed to stir at room temperature overnight, which produced the desired complexed product **163b** as a white precipitate. The resulting complex was isolated by vacuum filtration (0.241 g, 55% yield). Analysis by ^1H NMR spectroscopy showed that a 2:1 complex ((*R*)-BINOL:ammonium salt) had formed.

^1H NMR (599 MHz, CD_3OD) δ 7.87 (4H, d, $J = 9.0$ Hz, H_d), 7.83 (4H, d, $J = 8.3$ Hz, H_f), 7.31 (1H, d, $J = 3.1$ Hz, H_7), 7.29 (4H, d, $J = 8.8$ Hz, H_i), 7.26 – 7.21 (5H, m, H_{g+1}), 7.16 (4H, ddd, $J = 8.2, 6.7, 1.3$ Hz, H_h), 7.05 – 7.00 (5H, m, H_{c+2}), 5.64 – 5.50 (3H, m, H_{11+12}), 4.43 (2H, d, $J = 6.4$ Hz, H_{10}), 3.91 (3H, s, H_5), 3.85 (3H, s, H_3), 3.51 (6H, s, H_9).

^{13}C NMR (151 MHz, CD_3OD) δ 154.2, 151.9, 151.6, 138.5, 135.8, 130.6, 130.4, 129.01, 128.98, 127.1, 126.5, 125.8, 123.8, 119.2, 116.2, 114.4, 112.4, 106.1, 72.6, 57.2, 56.7, 54.5.

LRMS (ESI-TOF, EI^+) m/z : 222.1 ($[\text{M}]^+$, 100%), 181.10 (52).

LRMS (ESI-TOF, EI^-) m/z : 285.1 ($[\text{M}-\text{H}]^-$, 100%).

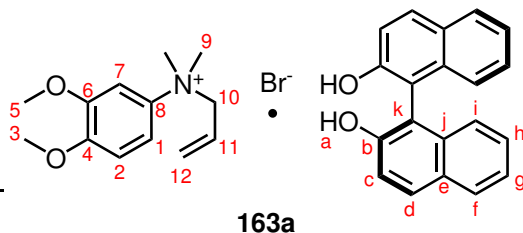
HRMS (ESI-TOF) m/z : $[\text{M}]^+$ calculated for $\text{C}_{13}\text{H}_{20}\text{NO}_2^+$: 222.1494, found 222.1496.

$[\text{M}-\text{H}]^-$ calculated for $\text{C}_{20}\text{H}_{13}\text{O}_2^-$: 285.0916, found 285.0928.

mp: 136 – 140 °C (CHCl_3).

IR ($\nu_{\text{max}}/\text{cm}^{-1}$): 3177br, 1505s, 1432s, 1322s, 1274s, 824s.

XRD: A portion of the complex was crystallised in CHCl_3 to give brown blocks of **163b**. Crystal data for $0.5(\text{C}_{54}\text{H}_{49}\text{BrCl}_3\text{NO}_6)$ ($m = 497.10$ g/mol): Monoclinic, space group $P2_1$ (no. 4).

***N*-allyl-3,4-dimethoxy-*N,N*-dimethylanilinium bromide · (*R*)-1,1'-bi-2-naphthol**

The quaternary ammonium bromide salt **370** (0.253 g, 0.84 mmol) was dissolved in EtOH (0.65 mL, 1.3 M) in a 10 mL vial. Solid (*R*)-BINOL (0.213 g, 1.0 equiv.) was then added with stirring to the solution, resulting in a homogeneous solution.

This solution was allowed to stir at room temperature overnight, which produced the desired complexed product **163a** as a white precipitate. The resulting complex was isolated by vacuum filtration (0.263 g, 53% yield). Analysis by ^1H NMR spectroscopy ensured that a 1:1 complex had formed.

^1H NMR (599 MHz, CD_3OD) δ 7.86 (2H, d, $J = 9.0$ Hz, H_d), 7.82 (2H, d, $J = 8.3$ Hz, H_f), 7.33 – 7.28 (3H, m, H_{7+i}), 7.23 (2H, ddd, $J = 8.1, 6.7, 1.2$, H_g), 7.19 – 7.12 (3H, m, H_{1+h}), 7.03 (2H, dd $J = 8.5, 1.3$ Hz, H_c), 6.98 (1H, d, $J = 9.0$ Hz, H_2), 5.60 – 5.51 (2H, m, H_{12}), 5.51 – 5.47 (1H, m, H_{11}), 4.41 (2H, d, $J = 5.8$ Hz, H_{10}), 3.89 (3H, s, H_5), 3.82 (3H, s, H_3), 3.47 (6H, s, H_9).

^{13}C NMR (151 MHz, CD_3OD) δ 154.2, 151.8, 151.5, 138.5, 135.8, 130.6, 130.4, 129.04, 128.99, 127.2, 126.5, 125.8, 123.9, 119.3, 116.2, 114.4, 112.4, 106.1, 72.5, 57.3, 56.7, 54.5.

LRMS (ESI-TOF, EI^+) m/z : 222.1 ($[\text{M}]^+$, 100%).

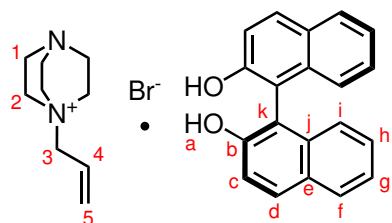
LRMS (ESI-TOF, EI^-) m/z : 285.1 ($[\text{M}-\text{H}]^-$, 100%).

mp: 126 – 128 °C (EtOH).

IR ($\nu_{\text{max}}/\text{cm}^{-1}$): 3190br, 1516s, 1269s, 820s, 754m.

XRD: A portion of the complex was crystallised in EtOH to give brown plates of **163a**. Crystal data for $\text{C}_{33}\text{H}_{34}\text{BrNO}_4$ ($m = 588.52$ g/mol): Orthorhombic, space group $P2_12_12_1$ (no. 19).

Solids of 163 isolated from CHCl_3 and EtOH display different PXRD indices. See Figure 3.6.

1-allyl-1,4-diazabicyclo[2.2.2]octan-1-ium bromide · (*R*)-1,1'-bi-2-naphthol**164**

The quaternary ammonium bromide salt **371** (0.222 g, 0.95 mmol) was dissolved in EtOH (2.4 mL, 0.4 M) in a 10 mL vial. Solid (*R*)-BINOL (0.272 g, 1.0 equiv.) was then added with stirring to the solution, resulting in a pale yellow homogeneous solution. This solution was allowed to stir at room temperature

overnight, which produced the desired complexed product **164a** as a white precipitate. The resulting complex was isolated by vacuum filtration (0.384 g, 78% yield). *If the same complexation is performed in CHCl₃ (0.4 M) a 64% yield is achieved.*

¹H NMR (400 MHz, DMSO-d₆) δ 9.23 (2H, s, H_a), 7.90 – 7.81 (4H, m, H_{d,f}), 7.35 (2H, d, *J* = 8.8 Hz, H_i), 7.23 (2H, ddd, *J* = 8.0, 6.7, 1.3 Hz, H_g), 7.16 (2H, ddd, *J* = 8.2, 6.7, 1.4 Hz, H_h), 7.00 – 6.88 (2H, m, H_c), 6.00 (1H, ddt, *J* = 16.3, 10.7, 7.3 Hz, H₄), 5.66 – 5.54 (2H, m, H₅), 3.92 (2H, d, *J* = 7.5 Hz, H₃), 3.39 – 3.25 (6H, m, H₂), 3.03 – 3.00 (6H, m, H₁).

¹³C NMR (101 MHz, DMSO-d₆) δ 153.0, 134.1, 128.6, 128.1, 127.8, 127.3, 125.8, 125.4, 124.4, 122.2, 118.5, 115.4, 65.1, 51.6, 44.6.

LRMS (ESI-TOF, EI⁺) *m/z*: 153.2 ([M]⁺, 100%).

LRMS (ESI-TOF, EI⁻) *m/z*: 285.3 ([M-H]⁻, 100%).

HRMS (ESI-TOF) *m/z*: [M]⁺ calculated for C₉H₁₂N₂⁺: 153.1392, found 153.1390. [M-H]⁻ calculated for C₂₀H₁₃O₂⁻: 285.0916, found 285.0915.

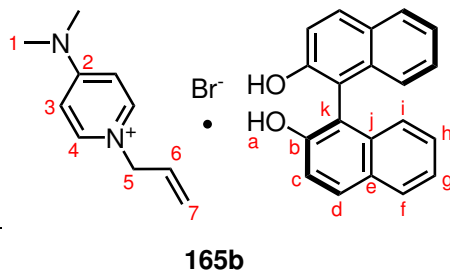
mp: 180 °C (CHCl₃).

IR (ν_{max}/cm⁻¹): 3185br, 1624m, 1338m, 1272s, 1054m, 811s.

XRD: A portion of the complex was crystallised in EtOH to give clear colourless prisms of **164a**. Crystal data for C_{25.50}H_{25.50}Br_{0.50}NO_{2.50} (*m* = 425.92 g/mol): Orthorhombic, space group *P*2₁2₁2₁ (no. 19).

XRD: A portion of the complex was crystallised in CHCl₃ to give clear colourless prisms of **164b**. Crystal data for C₅₈H₆₂Br₂N₄O₄ (*m* = 1038.93 g/mol): Monoclinic, space group *P*2₁ (no. 4).

Solids of 164 isolated from CHCl₃ and EtOH display different PXRD indices. See Figure 3.6.

1-allyl-4-(dimethylamino)pyridin-1-ium bromide · (*R*)-1,1'-bi-2-naphthol

The quaternary ammonium bromide salt **372** (0.243 g, 1.00 mmol) was dissolved in CHCl_3 (2.5 mL, 0.4 M) in a 10 mL vial. Solid (*R*)-BINOL (0.286 g, 1.0 equiv.) was then added with stirring to the solution, resulting in a pale yellow homogeneous solution. This solution was allowed to stir at room temperature

overnight, which produced the desired complexed product **165b** as a white precipitate. The resulting complex was isolated by vacuum filtration (0.385 g, 71% yield). Analysis by ^1H NMR spectroscopy ensured that a 1:1 complex had formed.

^1H NMR (599 MHz, CD_3OD) δ 7.97 (2H, d, $J = 7.8$ Hz, H_4), 7.89 – 7.83 (2H, m, H_d), 7.83 – 7.79 (2H, m, H_f), 7.29 (2H, d, $J = 8.8$ Hz, H_i), 7.23 (2H, ddd, $J = 8.1, 6.8, 1.3$ Hz, H_g), 7.15 (2H, ddd, $J = 8.2, 6.7, 1.4$ Hz, H_h), 7.02 (2H, dd, $J = 8.5, 1.3$ Hz, H_c), 6.86 (2H, d, $J = 7.8$ Hz, H_3), 6.00 (1H, ddt, $J = 17.1, 10.3, 6.0$ Hz, H_6), 5.37 (1H, dd, $J = 10.3, 1.1$ Hz, $\text{H}_{7\text{-cis}}$), 5.27 (1H, dtd, $J = 17.1, 1.6, 0.9$ Hz, $\text{H}_{7\text{-trans}}$), 4.68 (2H, dt, $J = 6.0, 1.5$ Hz, H_5), 3.15 (6H, s, H_1).

^{13}C NMR (151 MHz, CD_3OD) δ 157.8, 154.2, 142.9, 135.8, 133.0, 130.5, 130.4, 129.0, 127.1, 125.8, 123.8, 121.2, 119.3, 116.3, 108.9, 60.5, 40.3.

LRMS (ESI-TOF, EI^+) m/z : 163.6 ($[\text{M}]^+$, 100%).

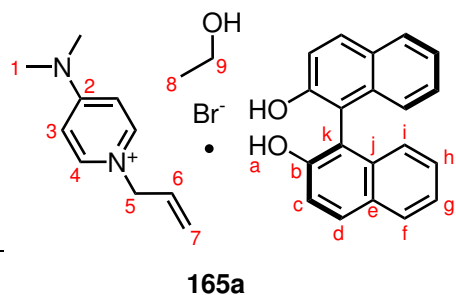
LRMS (ESI-TOF, EI^-) m/z : 285.3 ($[\text{M-H}]^-$, 100%).

HRMS (ESI-TOF) m/z : $[\text{M}]^+$ calculated for $\text{C}_{10}\text{H}_{15}\text{N}_2^+$: 163.1235, found 163.1229. $[\text{M-H}]^-$ calculated for $\text{C}_{20}\text{H}_{13}\text{O}_2^-$: 285.0916, found 285.0914.

mp: 186 °C (CHCl_3).

IR ($\nu_{\text{max}}/\text{cm}^{-1}$): 3073br, 1653s, 1567s, 1273s, 813s, 751s.

XRD: A portion of the complex was crystallised in CHCl_3 to give clear colourless prisms of **165b**. Crystal data for $\text{C}_{60}\text{H}_{58}\text{Br}_2\text{N}_4\text{O}_4$ ($m = 1058.92$ g/mol): Monoclinic, space group $P2_1$ (no. 4).

1-allyl-4-(dimethylamino)pyridin-1-ium bromide · (*R*)-1,1'-bi-2-naphthol

The quaternary ammonium bromide salt **372** (0.252 g, 1.04 mmol) was dissolved in EtOH (2.1 mL, 0.5 M) in a 10 mL vial. Solid (*R*)-BINOL (0.296 g, 1.0 equiv.) was then added with stirring to the solution, resulting in a pale yellow homogeneous solution. This solution was allowed to stir at room temperature

overnight, which produced the desired complexed product **165a** as a white precipitate. The resulting complex was isolated by vacuum filtration (0.509 g, 93% yield). Analysis by ^1H NMR spectroscopy ensured that a 1:1 complex had formed with one equivalent of an EtOH solvate.

^1H NMR (400 MHz, CD_3OD) δ 7.92 – 7.76 (6H, m, $\text{H}_{4+\text{d+f}}$), 7.30 (2H, d, $J = 8.9$ Hz, H_i), 7.22 (2H, ddd, $J = 8.1, 6.7, 1.3$ Hz, H_g), 7.13 (2H, ddd, $J = 8.1, 6.7, 1.4$ Hz, H_h), 7.02 (2H, ddd, $J = 8.5, 1.3, 0.7$ Hz, H_c), 6.81 – 6.73 (2H, m, H_3), 5.95 (1H, ddt, $J = 17.1, 10.3, 6.0$ Hz, H_6), 5.34 (1H, dd, $J = 10.3, 1.1$ Hz, $\text{H}_{7-\text{cis}}$), 5.24 (1H, dq, $J = 17.1, 1.4$ Hz, $\text{H}_{7-\text{trans}}$), 4.62 (2H, dt, $J = 6.1, 1.5$ Hz, H_5), 3.61 (2H, q, $J = 7.0$ Hz, H_9), 3.09 (6H, s, H_1), 1.18 (3H, t, $J = 7.0$ Hz, H_8).

^{13}C NMR (101 MHz, CD_3OD) δ 157.7, 154.2, 142.8, 135.8, 132.9, 130.5, 130.3, 129.1, 127.1, 125.8, 123.8, 121.2, 119.3, 116.3, 108.8, 60.4, 58.3, 40.3, 18.4.

LRMS (ESI-TOF, EI^+) m/z : 163.6 ($[\text{M}]^+$, 100%).

LRMS (ESI-TOF, EI^-) m/z : 285.3 ($[\text{M}-\text{H}]^-$, 100%).

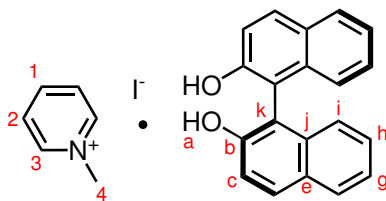
HRMS (ESI-TOF) m/z : $[\text{M}]^+$ calculated for $\text{C}_{10}\text{H}_{15}\text{N}_2^+$: 163.1235, found 163.1229. $[\text{M}-\text{H}]^-$ calculated for $\text{C}_{20}\text{H}_{13}\text{O}_2^-$: 285.0916, found 285.0914.

mp: 158 – 160 °C (EtOH).

IR ($\nu_{\text{max}}/\text{cm}^{-1}$): 3225br, 1654, 1570, 1272s, 812s, 758.

XRD: A portion of the complex was crystallised in EtOH to give clear colourless prisms of **165a**. Crystal data for $\text{C}_{32}\text{H}_{35}\text{BrN}_2\text{O}_3$ ($m = 575.53$ g/mol): Orthorhombic, space group $P2_12_12_1$ (no. 19).

Solids of 165 isolated from CHCl_3 and EtOH display different PXRD indices. See Figure 3.6.

1-methylpyridinium iodide · (*R*)-1,1'-bi-2-naphthol**162**

Ammonium salt **373** (0.129 g, 0.5 mmol) was dissolved in CHCl_3 (1.60 mL, 0.6 M) in a 10 mL vial. Solid (*R*)-BINOL (0.143 g, 1.0 equiv.) was then added with stirring to the solution. This solution was allowed to stir at room temperature overnight, which produced the desired complex **162c** as a white precipitate. The resulting complex was iso-

lated by vacuum filtration (0.252 g, 99% yield). Analysis by ^1H NMR spectroscopy ensured that a 1:1 complex had formed.

^1H NMR (400 MHz, $\text{DMSO}-d_6$) δ 9.21 (2H, s, H_a), 9.04 – 8.93 (2H, m, H_3), 8.57 (1H, tt, $J = 7.8, 1.5$ Hz, H_1), 8.13 (2H, t, $J = 7.0$ Hz, H_2), 7.89 – 7.81 (4H, m, H_{d+f}), 7.31 (2H, d, $J = 8.9$ Hz, H_i), 7.23 (2H, ddd, $J = 8.1, 6.7, 1.4$ Hz, H_g), 7.16 (2H, ddd, $J = 8.2, 6.7, 1.5$ Hz, H_h), 6.93 (2H, dd, $J = 8.4, 1.2$ Hz, H_c), 4.35 (3H, s, H_4).

^{13}C NMR (101 MHz, $\text{DMSO}-d_6$) δ 153.0, 145.5, 145.1, 134.1, 128.6, 128.1, 127.8, 127.7, 125.8, 124.4, 122.3, 118.5, 115.4, 44.0.

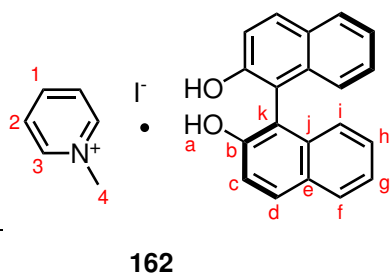
LRMS (ESI-TOF, EI^-) m/z : 285.2 ($[\text{M}-\text{H}]^-$, 100%).

HRMS (ESI-TOF) m/z : $[\text{M}]^+$ calculated $\text{C}_6\text{H}_8\text{N}^+$: 94.0657, found: 94.0648. $[\text{M}-\text{H}]^-$ calculated for $\text{C}_{20}\text{H}_{13}\text{O}_2^-$: 285.0916, found: 285.0930.

mp: 187 – 189 °C (EtOH).

IR ($\nu_{\text{max}}/\text{cm}^{-1}$): 3155br, 2980m, 1625m, 1271m, 954m, 740m.

XRD: A portion of the complex was crystallised in EtOH, to give clear colourless prisms of **162a**. Crystal data for $\text{C}_{26}\text{H}_{24}\text{INO}_3$ ($m = 525.36$ g/mol): Orthorhombic, space group $P2_12_12_1$ (no. 19).

1-methylpyridinium iodide · (*R*)-1,1'-bi-2-naphthol

Ammonium salt **373** (0.245 g, 1.11 mmol) was dissolved in EtOH (1.85 mL, 0.6 M) in a 10 mL vial. Solid (*R*)-BINOL (0.3174 g, 1.0 equiv.) was then added with stirring to the solution. This solution was allowed to stir at room temperature overnight, which produced the desired complex **162d** as a white precipitate. The resulting complex

was isolated by vacuum filtration (0.402 g, 71% yield). Analysis by ^1H NMR spectroscopy ensured that a 1:1 complex had formed.

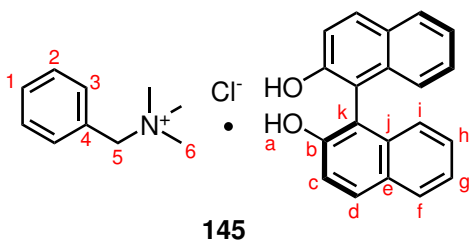
^1H NMR (400 MHz, $\text{DMSO}-d_6$) δ 8.73 – 8.63 (2H, m, H_3), 8.40 (1H, tt, $J = 7.9, 1.5$ Hz, H_1), 7.90 (2H, t, $J = 7.0$ Hz, H_2), 7.88 – 7.77 (4H, m, H_{d+f}), 7.30 (2H, d, $J = 8.9$ Hz, H_i), 7.23 (2H, ddd, $J = 8.1, 6.7, 1.3$ Hz, H_g), 7.15 (2H, ddd, $J = 8.3, 6.7, 1.4$ Hz, H_h), 7.02 (2H, dd, $J = 8.5, 1.1$ Hz, H_c), 4.86 (2H, s, br, $\text{H}_{\text{H}_2\text{O}}$), 4.24 (3H, s, H_4). ^{13}C NMR (101 MHz, $\text{DMSO}-d_6$) δ 154.1, 146.5, 146.3, 135.7, 130.6, 130.3, 129.04, 129.00, 127.2, 125.8, 123.9, 119.2, 116.3.

XRD: A portion of the complex was crystallised in CHCl_3 , to give clear colourless prisms of **162b**. Crystal data for $\text{C}_{27}\text{H}_{23}\text{Cl}_3\text{INO}_2$ ($m = 626.71$ g/mol): Monoclinic, space group $P2_1$ (no. 4).

All precipitates and single crystals of 162 display different PXRD indices. See Figure 3.5.

9.6 Aqueous ammonium cation recognition

Benzyltrimethylammonium chloride · (*R*)-1,1'-bi-2-naphthol



Benzyltrimethylammonium chloride (0.186 g, 1.0 mmol) was dissolved in H₂O (1.0 mL, 1.0 M) in a 10 mL vial. Solid (*R*)-BINOL (0.286 g, 1.0 equiv.) was then added with stirring to the solution, resulting in a slurried mixture. This reaction mixture was allowed to stir vigorously at

room temperature for 16 hours, which produced a mixture of the desired complexed product **145** and (*R*)-BINOL. The resulting solid was isolated by vacuum filtration (0.237 g). Analysis by ¹H NMR spectroscopy showed that the solid consisted of both **145** and (*R*)-BINOL. **145** accounted for 76% of the molar ratio by integration of the NMR spectrum.

To yield exclusively **145** the precipitate was slurried with CHCl₃ for 10 mins and isolated by vacuum filtration with washing (CHCl₃ and EtOH). Analysis by ¹H NMR spectroscopy ensured a 1:1 complex had been isolated (0.176 g, 37% yield).

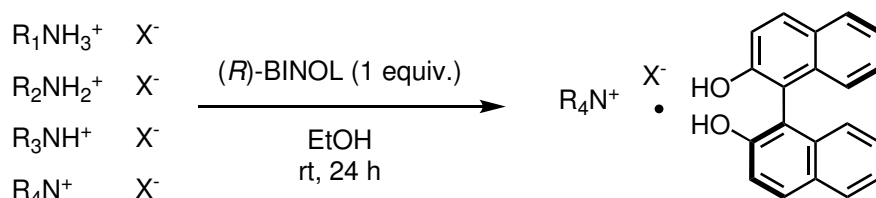
¹H NMR (400 MHz, DMSO-*d*₆) δ 9.38 (2H, s, H_a), 7.89 – 7.80 (4H, m, H_{d+i}), 7.61 – 7.46 (5H, m, H₁₊₂₊₃), 7.40 (2H, d, *J* = 8.9 Hz, H_i), 7.22 (2H, ddd, *J* = 8.2, 6.7, 1.2 Hz, H_g), 7.15 (2H, ddd, *J* = 8.4, 6.7, 1.3 Hz, H_h), 6.94 (2H, dt, *J* = 8.4, 1.0 Hz, H_c), 4.60 (2H, s, H₅), 3.04 (9H, s, H₆).

¹³C NMR (101 MHz, DMSO-*d*₆) δ 153.1, 134.1, 132.8, 130.2, 128.9, 128.49, 128.45, 128.1, 127.8, 125.7, 124.4, 122.2, 118.6, 115.4, 67.5 (t, *J* = 2.9 Hz), 51.6 (t, *J* = 4.0 Hz).

Data consistent with 145 isolated from EtOH.

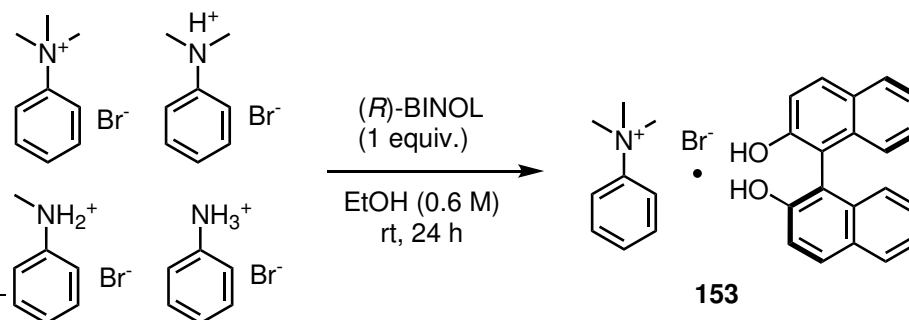
9.7 Selective recognition experiments

9.7.1 General procedure for selective complexation experiments



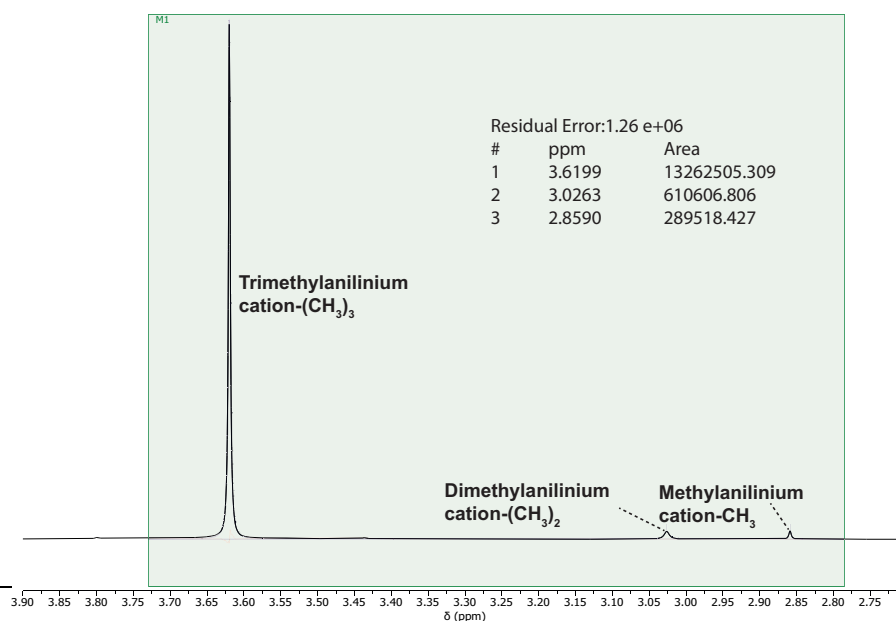
Scheme 9.11: Selective complexation with (*R*)-BINOL from a mixture of primary, secondary, tertiary and quaternary ammonium salts.

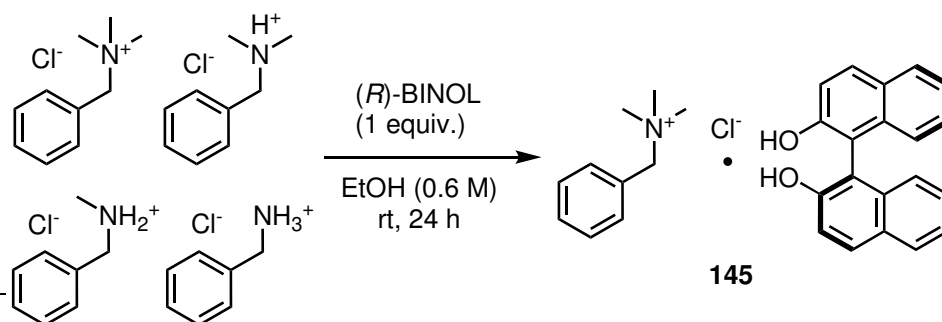
Primary (1.0 equiv.), secondary (1.0 equiv.), tertiary (1.0 equiv.) and quaternary (1.0 equiv.) salts from selected ammonium species were combined and dissolved in EtOH (0.3 – 0.6 M) in a 10 mL vial. Solid (*R*)-BINOL was then added with stirring to the solution, resulting in a homogeneous solution. This solution was allowed to stir at room temperature overnight, to produce complexed product. The resulting complex was isolated by vacuum filtration and analysed by 1H NMR spectroscopy to confirm the identity of the precipitate and to ensure that a 1:1 complex had formed. All yields are calculated with respect to (*R*)-BINOL and assume a 1:1 complex with the quaternary ammonium cation.

Anilinium bromides selectivity with (*R*)-BINOL

Scheme 9.12: Selective complexation with (*R*)-BINOL from a mixture of primary, secondary, tertiary and quaternary anilinium salts.

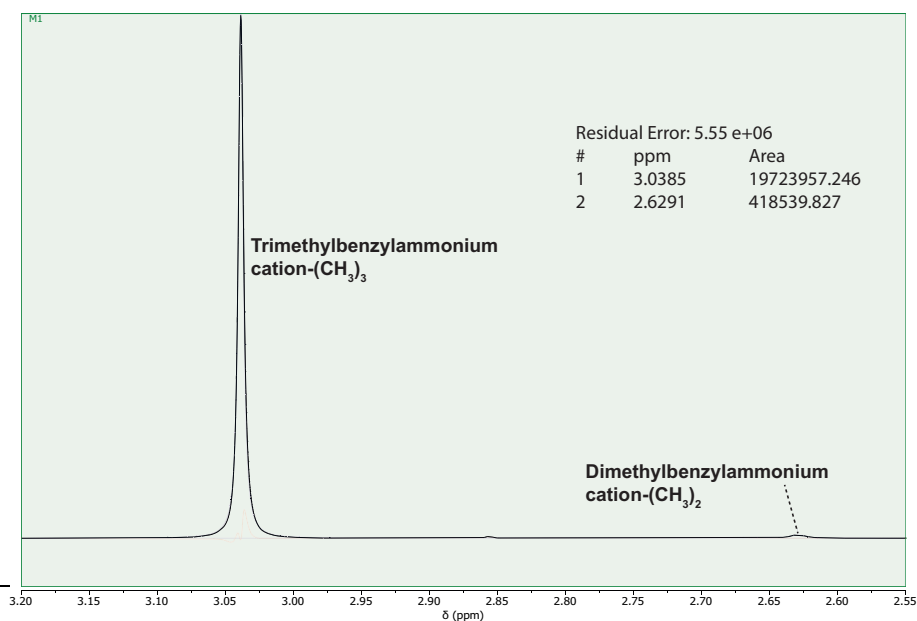
359 (0.174 g, 1.0 mmol), **360** (0.189 g, 1.0 mmol), **361** (0.202 g, 1.0 mmol) and trimethyl anilinium bromide (0.216 g, 1.0 mmol) were dissolved in EtOH (1.67 mL, 0.6 M) in a 10 mL vial. Solid (*R*)-BINOL (0.279 g, 1.0 equiv.) was then added with stirring to the solution, resulting in a pale yellow homogeneous solution. This solution was allowed to stir at room temperature overnight, which produced the desired complexed product **153** as a white precipitate. The resulting complex was isolated by vacuum filtration (0.243 g, 50% yield, 88% selectivity). Analysis by ¹H NMR spectroscopy (400 MHz, DMSO-*d*₆) ensured that a 1:1 complex had formed.

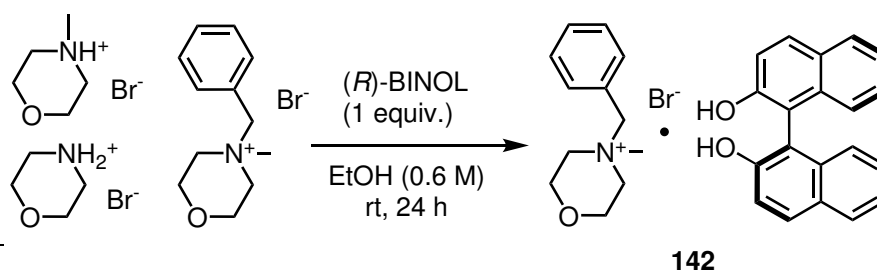


Benzylammonium chlorides selectivity with (*R*)-BINOL

Scheme 9.13: Selective complexation with (*R*)-BINOL from a mixture of primary, secondary, tertiary and quaternary benzylammonium salts.

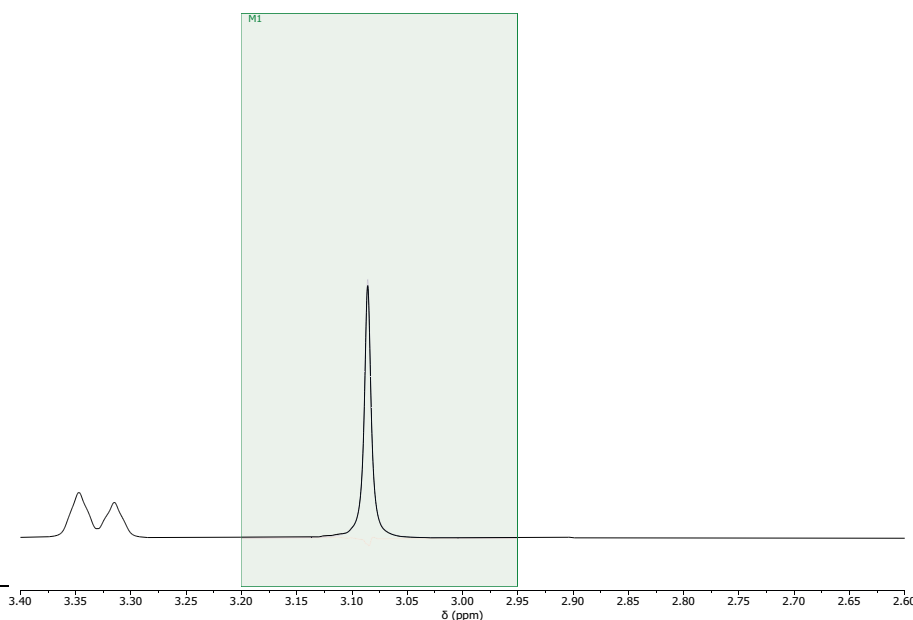
362 (0.145 g, 1.0 mmol), **363** (0.158 g, 1.0 mmol), **364** (0.172 g, 1.0 mmol) and *N,N,N*-trimethyl benzylammonium chloride (0.186 g, 1.0 mmol) were dissolved in EtOH (1.67 mL, 0.6 M) in a 10 mL vial. Solid (*R*)-BINOL (0.285 g, 1.0 equiv.) was then added with stirring to the solution, resulting in a colourless homogeneous solution. This solution was allowed to stir at room temperature overnight, which produced the desired complexed product **145** as a white precipitate. The resulting complex was isolated by vacuum filtration (0.323 g, 69% yield, 97% selectivity). Analysis by ^1H NMR spectroscopy (400 MHz, DMSO- d_6) ensured that a 1:1 complex had formed.

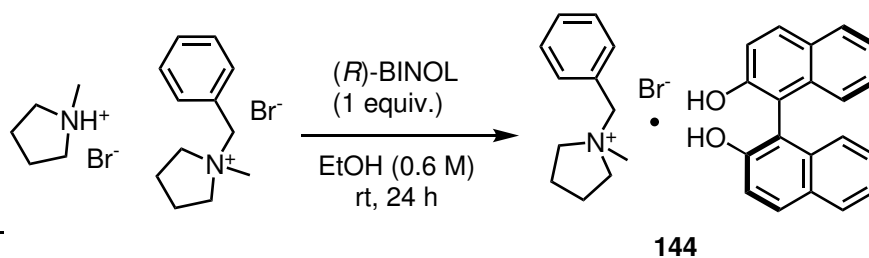


Morpholinium bromides selectivity with (*R*)-BINOL

Scheme 9.14: Selective complexation with (*R*)-BINOL from a mixture of secondary, tertiary and quaternary morpholinium salts.

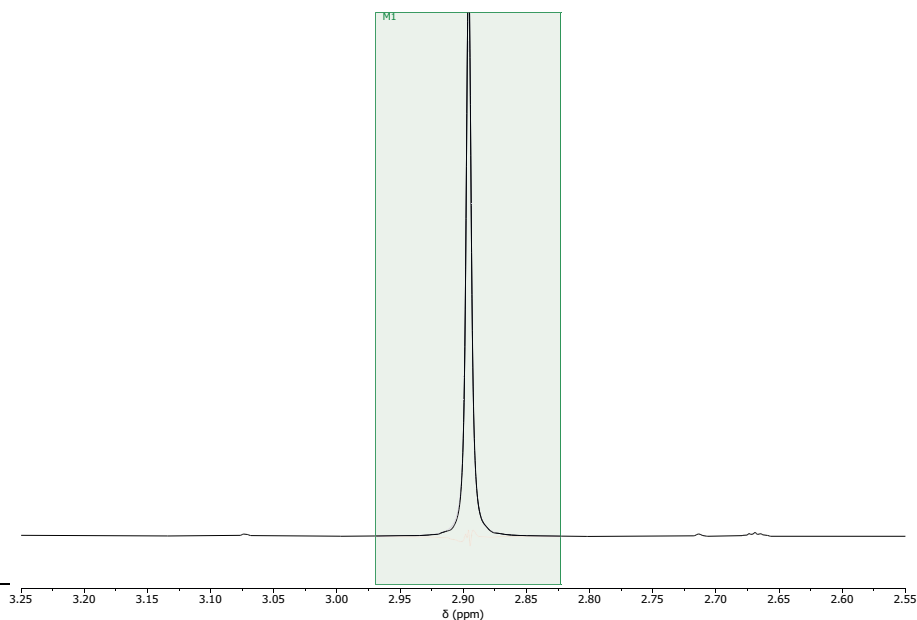
377 (0.168 g, 1.0 mmol), **366** (0.182 g, 1.0 mmol) and **100** (0.271g, 1.0 mmol) were dissolved in EtOH (1.67 mL, 0.6 M) in a 10 mL vial. Solid (*R*)-BINOL (0.285 g, 1.0 equiv.) was then added with stirring to the solution, resulting in a pale yellow homogeneous solution. This solution was allowed to stir at room temperature overnight, which produced the desired complexed product **142** as a white precipitate. The resulting complex was isolated by vacuum filtration (0.485 g, 87% yield, >99% selectivity). Analysis by ^1H NMR spectroscopy (400 MHz, $\text{DMSO}-d_6$) ensured that a 1:1 complex had formed.

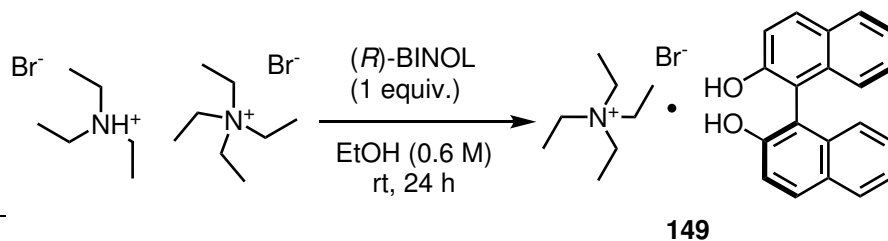


Pyrrolidinium bromides selectivity with (*R*)-BINOL

Scheme 9.15: Selective complexation with (*R*)-BINOL from a mixture of tertiary and quaternary pyrrolidinium salts.

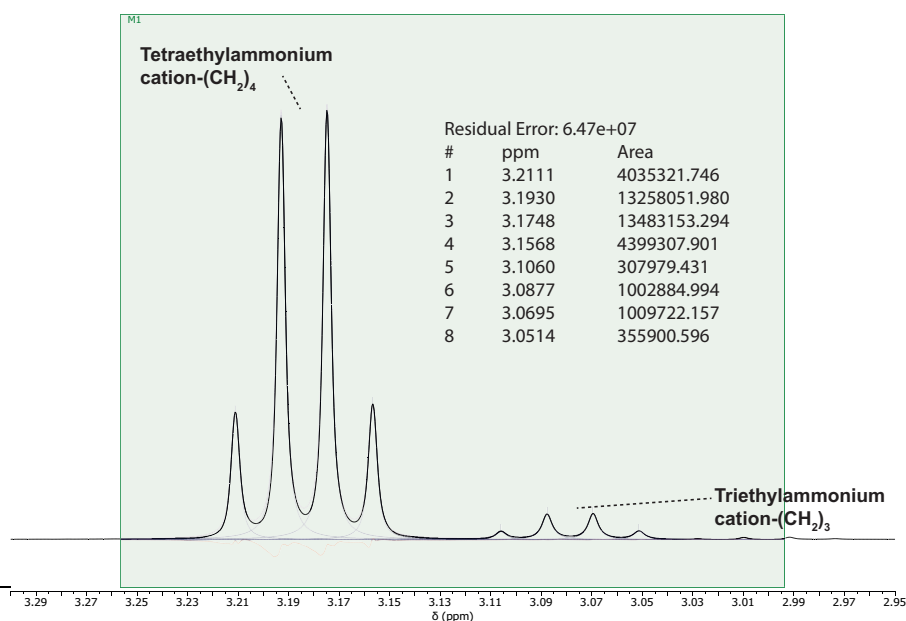
379 (0.168 g, 1.0 mmol), and **102** (0.257 g, 1.0 mmol) were dissolved in EtOH (2.00 mL, 0.5 M) in a 10 mL vial. Solid (*R*)-BINOL (0.284 g, 1.0 equiv.) was then added with stirring to the solution, resulting in a colourless homogeneous solution. This solution was allowed to stir at room temperature overnight, which produced the desired complexed product **144** as a white precipitate. The resulting complex was isolated by vacuum filtration (0.310 g, 57% yield, >99% selectivity) and analysis by ^1H NMR spectroscopy (400 MHz, DMSO- d_6) ensured that a 1:1 complex had formed.

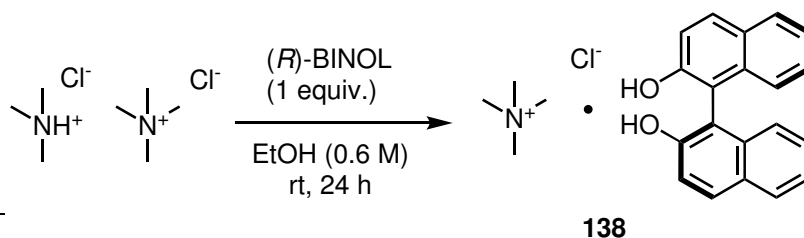


***N*-ethyl bromides selectivity with (*R*)-BINOL**

Scheme 9.16: Selective complexation with (*R*)-BINOL from a mixture of tertiary and quaternary *N*-ethylammonium bromide salts.

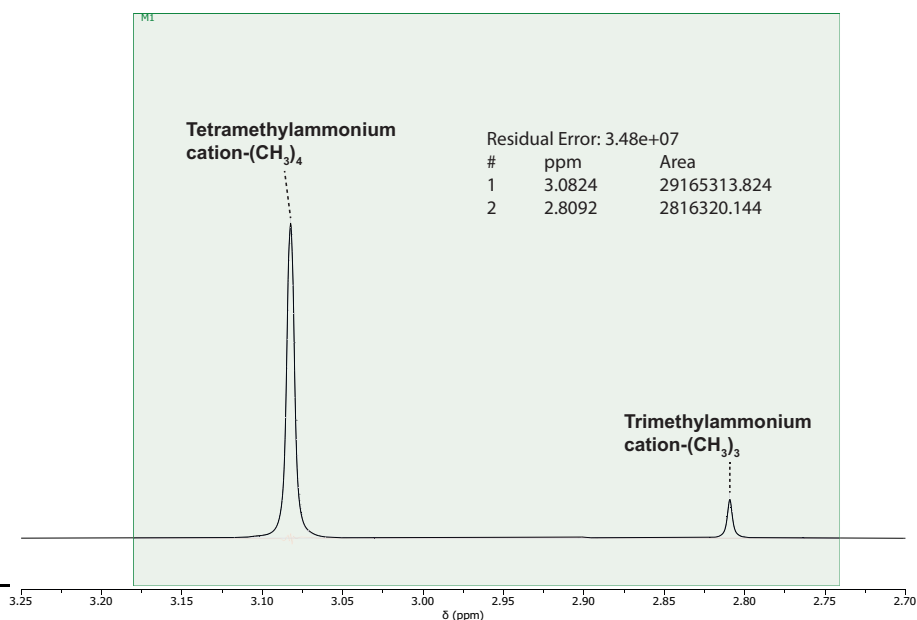
93 (0.187 g, 1.0 mmol), and tetraethylammonium bromide (0.218 g, 1.0 mmol) were dissolved in EtOH (1.67 mL, 0.6 M) in a 10 mL vial. Solid (*R*)-BINOL (0.285 g, 1.0 equiv.) was then added with stirring to the solution, resulting in a colourless homogeneous solution. This solution was allowed to stir at room temperature overnight, which produced the desired complexed product **149** as a white precipitate. The resulting complex was isolated by vacuum filtration (0.314 g, 62% yield, 91% selectivity) and analysis by ^1H NMR spectroscopy (400 MHz, DMSO- d_6) ensured that a 1:1 complex had formed.

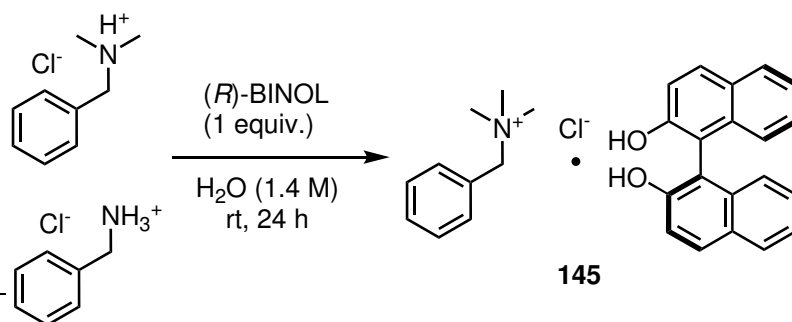


***N*-methyl ammonium chloride salts selectivity with (*R*)-BINOL**

Scheme 9.17: Selective complexation with (*R*)-BINOL from a mixture of tertiary and quaternary *N*-methylammonium bromide salts.

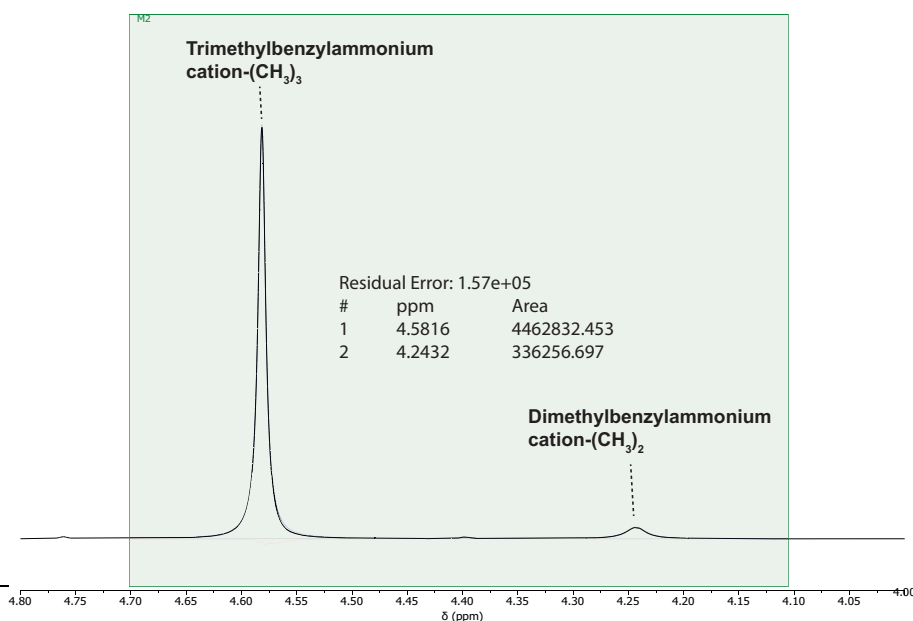
368 (0.050 g, 0.5 mmol) and tetramethylammonium chloride (0.059 g, 0.5 mmol) were dissolved in EtOH (1.67 mL, 0.3 M) in a 10 mL vial. Solid (*R*)-BINOL (0.131 g, 0.9 equiv.) was then added with stirring to the solution, resulting in a colourless homogeneous solution. This solution was allowed to stir at room temperature overnight, which produced the desired complexed product **138** as a white precipitate. The resulting complex was isolated by vacuum filtration (0.143 g, 72% yield, 89% selectivity) and analysis by ^1H NMR spectroscopy (400 MHz, DMSO- d_6) ensured that a 1:1 complex had formed.



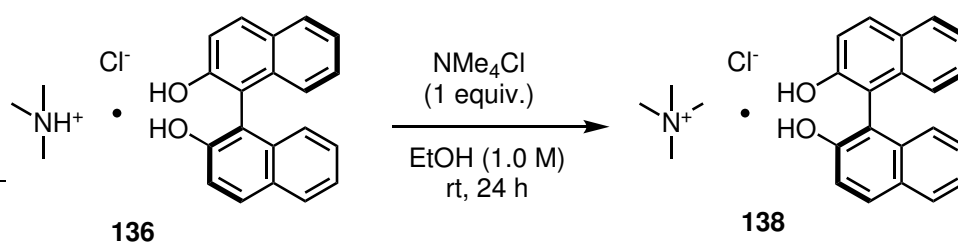
***N*-methylbenzylammonium chloride salts selectivity with (*R*)-BINOL**

Scheme 9.18: Selective complexation with (*R*)-BINOL from a mixture of tertiary and quaternary *N*-methylbenzylammonium bromide salts in water .

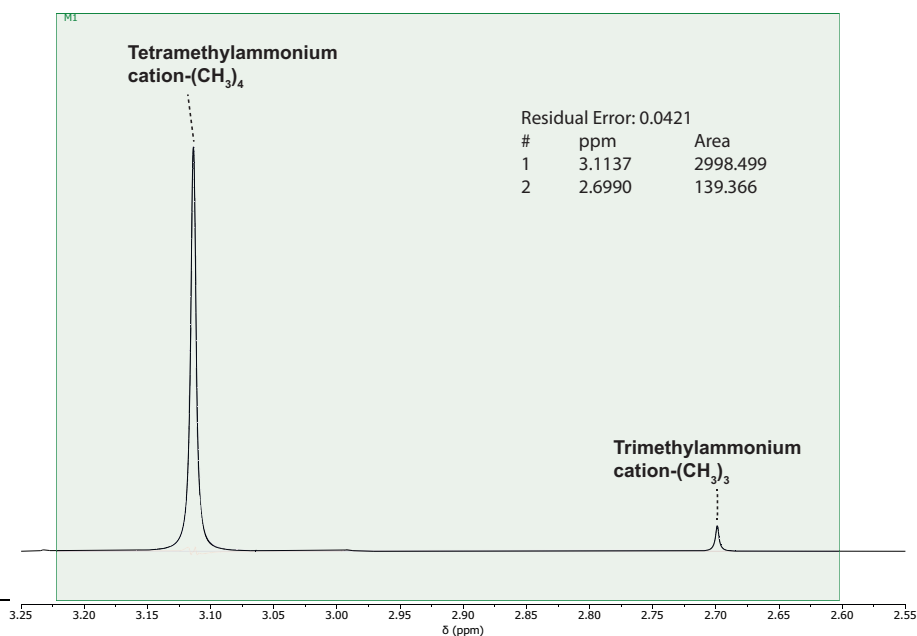
364 (0.170 g, 1.0 mmol) and benzyltrimethylammonium chloride (0.186 g, 1.0 mmol) were dissolved in H₂O (0.70 mL, 1.4 M) in a 10 mL vial. Solid (*R*)-BINOL (0.287 g, 1.0 equiv.) was then added with stirring to the solution, resulting slurred mixture. This solution was allowed to stir at room temperature overnight, which produced the desired product **145** as a white precipitate. The resulting complex was isolated by vacuum filtration (0.357 g). Analysis by ¹H NMR spectroscopy (599 MHz, DMSO-*d*₆) showed that (*R*)-BINOL had extracted benzyltrimethylammonium chloride as **145**, accounting for 57% of the total solid mass with a 93% selectivity (38% yield) versus the less substituted cation **364**.



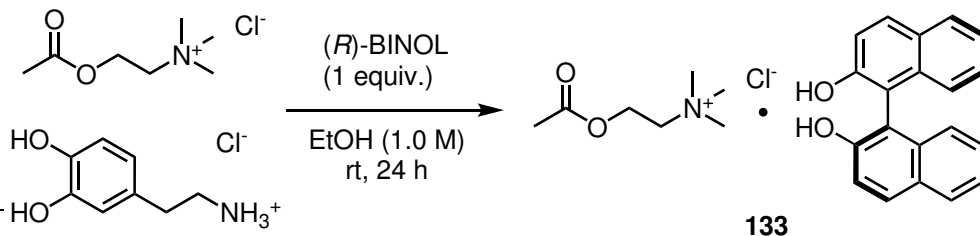
9.7.2 Ammonium cation replacement experiment

Scheme 9.19: Ammonium cation replacement from **136** to **138**.

136 (0.0716 g, 0.12 mmol, 1.0 equiv.) was stirred with EtOH (0.20 mL, 1.0 M) in a 10 mL vial. Solid tetramethylammonium chloride (0.0259 g, 1.0 equiv.) was then added with vigorous stirring to the mixture, resulting in a cloudy slurry. This was allowed to stir at room temperature for 72 hours, to produce **138**. The resulting complex was isolated by vacuum filtration and analysed by ^1H NMR spectroscopy (400 MHz, $\text{DMSO}-d_6$) to confirm the identity of the precipitate and to ensure that a 1:1 complex had formed (0.0424 g, 57% yield, 94% selectivity).

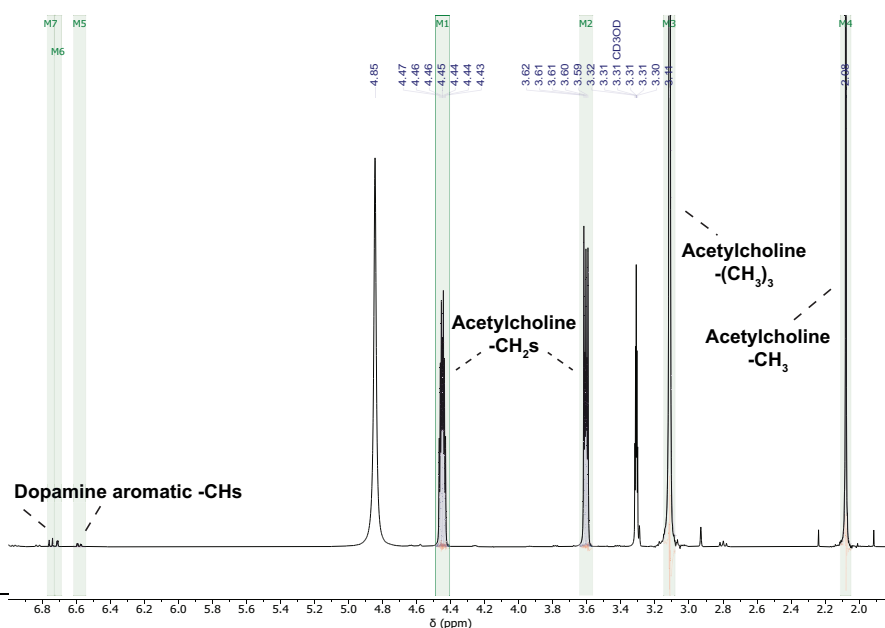


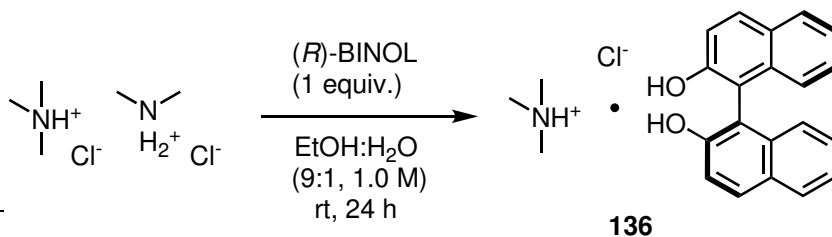
9.7.3 Selective recognition from biology

Neurotransmitter chloride and hydrochloride salts selectivity with (*R*)-BINOL

Scheme 9.20: Selective complexation with (*R*)-BINOL from a mixture of neurotransmitter chloride salts.

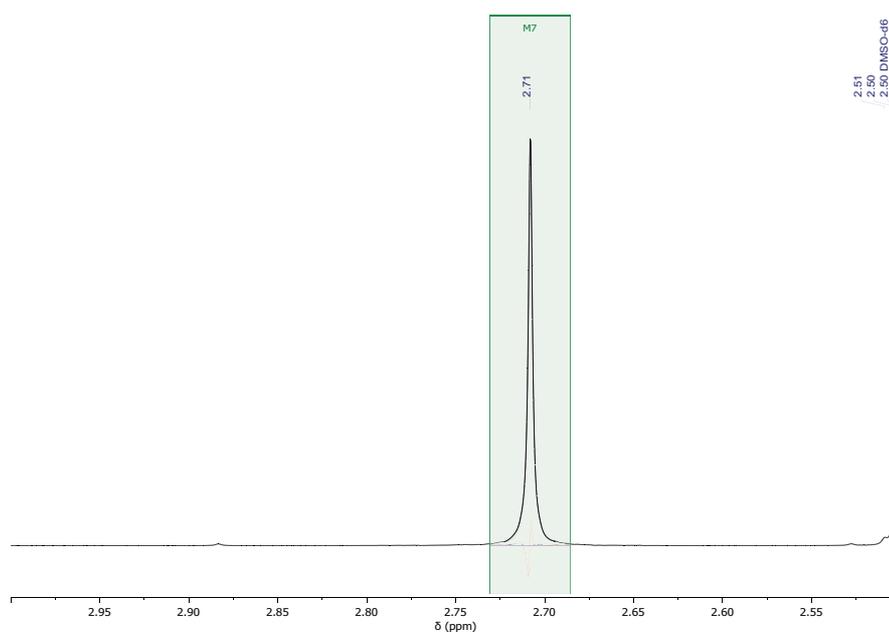
Acetylcholine chloride (0.182 g, 1.0 mmol) and dopamine hydrochloride (0.190 g, 1.0 mmol) were partially dissolved into EtOH (1.00 mL) in a 10 mL vial. Solid (*R*)-BINOL (0.286 g, 1.0 equiv.) was then added with stirring to the solution, resulting in a white cloudy slurry. This solution was allowed to stir at room temperature overnight, which produced the desired complexed product **133** as a white precipitate. The resulting complex was isolated by vacuum filtration and subsequently stirred in H₂O (0.50 mL) for 20 seconds before being filtered again. The complex was washed with EtOH and CHCl₃ and analysed by ¹H NMR spectroscopy (400 MHz, CD₃OD) to ensure the washing had yielded a 1:1 complex and to determine the selectivity of the ammonium salts. **133** was yielded as a white precipitate (126.3 mg, 27% yield, 98% selectivity).

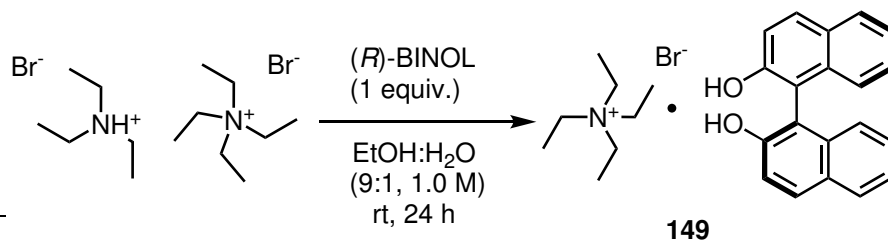


***N*-methylammonium hydrochloride salts selectivity with (*R*)-BINOL**

Scheme 9.21: Selective complexation with (*R*)-BINOL from a mixture of *N*-methylammonium hydrochloride salts.

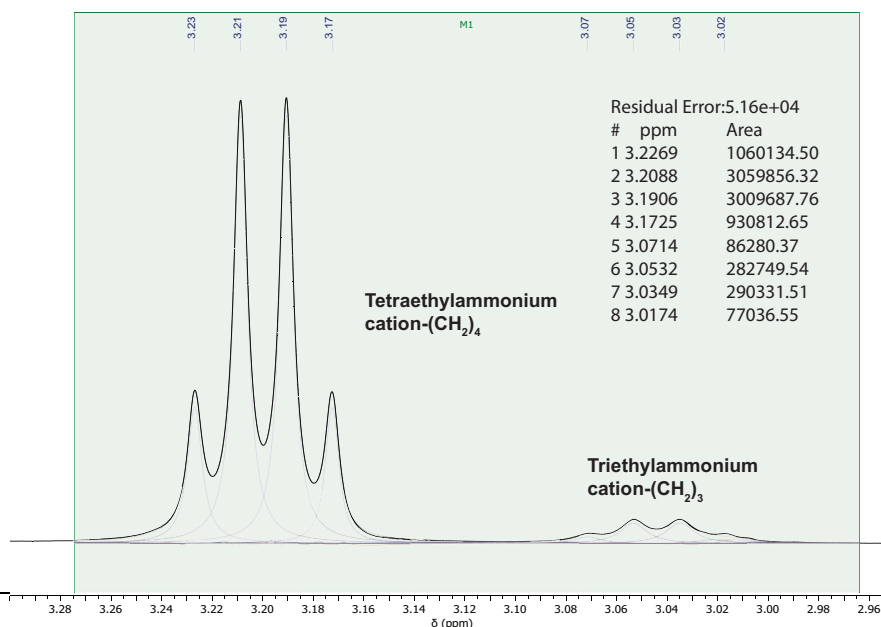
Trimethylammonium hydrochloride (0.096 g, 1.0 mmol) and dimethylammonium hydrochloride (0.082 g, 1.0 mmol) were dissolved into EtOH (0.90 mL) and H₂O (0.10 mL) in a 10 mL vial. Solid (*R*)-BINOL (0.287 g, 1.0 equiv.) was then added with stirring to the solution, resulting in a colourless homogeneous solution. This solution was allowed to stir at room temperature overnight, which produced the desired complexed product **136** as a white precipitate. The resulting complex was isolated by vacuum filtration, washed with EtOH, H₂O and CHCl₃ and analysed by ¹H NMR spectroscopy (400 MHz, DMSO-d₆) to ensure a 1:1 complex had formed and to determine the selectivity of the ammonium salts. **136** was isolated as a white precipitate with >99% selectivity (0.183, 48% yield).

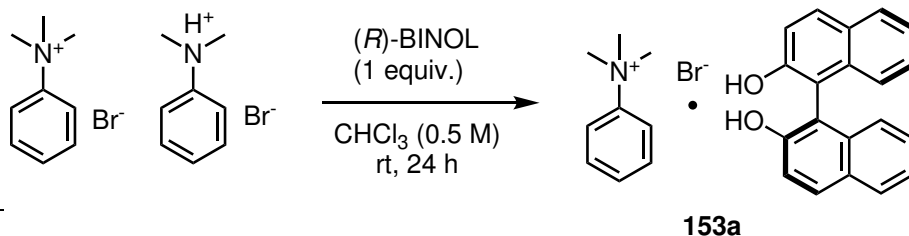


***N*-ethylammonium bromide and hydrobromide salts selectivity with (*R*)-BINOL.**

Scheme 9.22: Selective complexation with (*R*)-BINOL from a mixture of *N*-ethylammonium hydrobromide salts.

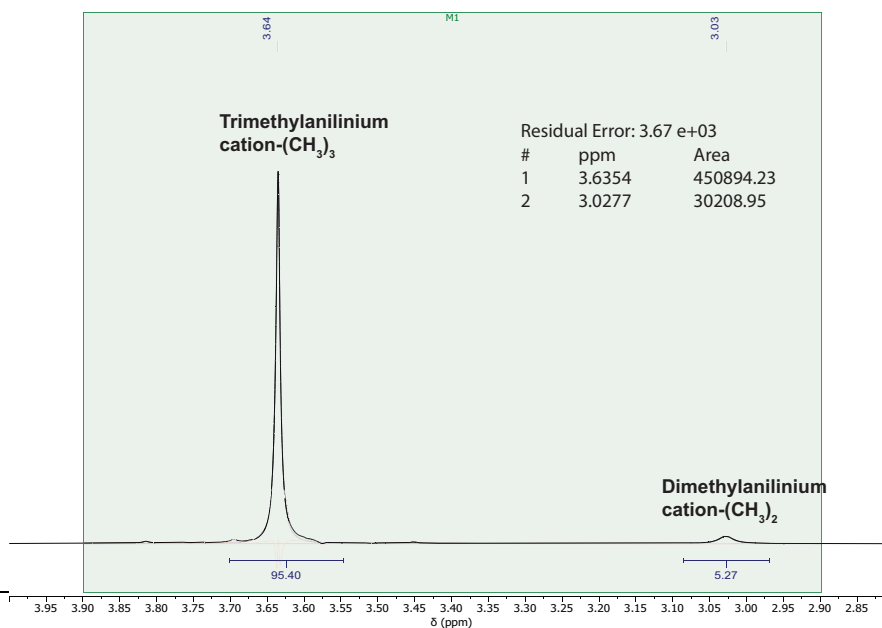
Tetraethylammonium bromide (0.211 g, 1.0 mmol) and triethylammonium hydrobromide (0.182 g, 1.0 mmol) were dissolved into EtOH (0.90 mL) and H₂O (0.10 mL) in a 10 mL vial. Solid (*R*)-BINOL (0.285 g, 1.0 equiv.) was then added with stirring to the solution, resulting in a colourless homogeneous solution. This solution was allowed to stir at room temperature overnight, which produced the desired complexed product **149** as a white precipitate. The resulting complex was isolated by vacuum filtration, washed with EtOH, H₂O and CHCl₃ and analysed by ¹H NMR spectroscopy (400 MHz, DMSO-*d*₆) to ensure a 1:1 complex had formed and to determine the selectivity of the ammonium salts. **149** was isolated as a white precipitate with 90% selectivity (0.283 g, 53% yield).

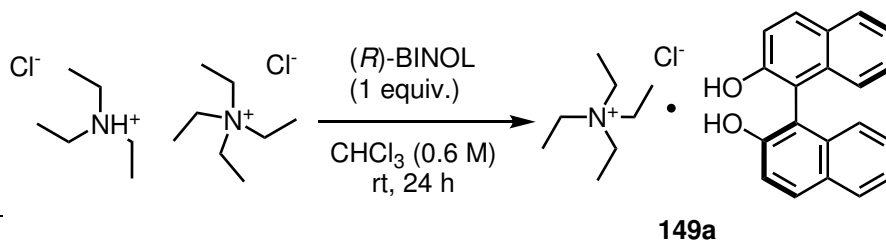


9.7.4 Selective complexation experiments in CHCl_3 Anilinium bromides selectivity with (*R*)-BINOL in CHCl_3 

Scheme 9.23: Selective complexation with (*R*)-BINOL from a mixture of primary, secondary, tertiary and quaternary anilinium salts in CHCl_3 .

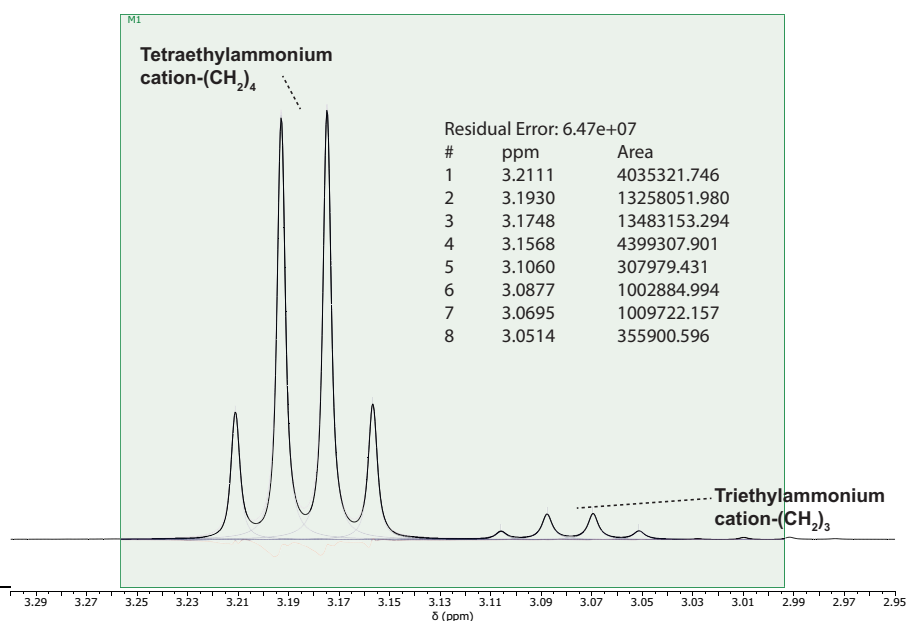
361 (0.261 g, 1.3 mmol) and trimethyl anilinium bromide (0.289 g, 1.3 mmol) were dissolved in CHCl_3 (1.67 mL, 0.6 M) in a 10 mL vial. Solid (*R*)-BINOL (0.282 g, 0.75 equiv.) was then added with stirring to the solution, resulting in a pale yellow homogeneous solution. This solution was allowed to stir at room temperature overnight, which produced the desired complexed product **153a** as a white precipitate. The resulting complex was isolated by vacuum filtration (0.177 g, 33% yield, 92% selectivity). Analysis by ^1H NMR spectroscopy (400 MHz, $\text{DMSO}-d_6$) ensured that a 1:1 complex had formed.

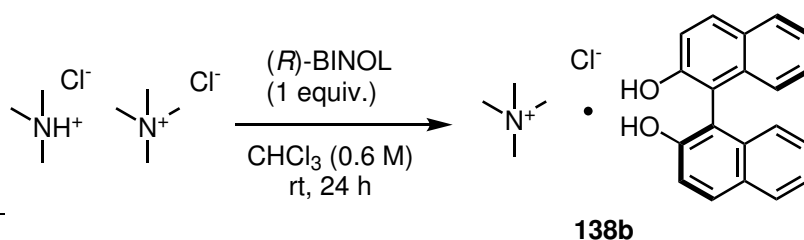


***N*-ethyl bromides selectivity with (*R*)-BINOL in CHCl₃**

Scheme 9.24: Selective complexation with (*R*)-BINOL from a mixture of tertiary and quaternary *N*-ethylammonium bromide salts in CHCl₃.

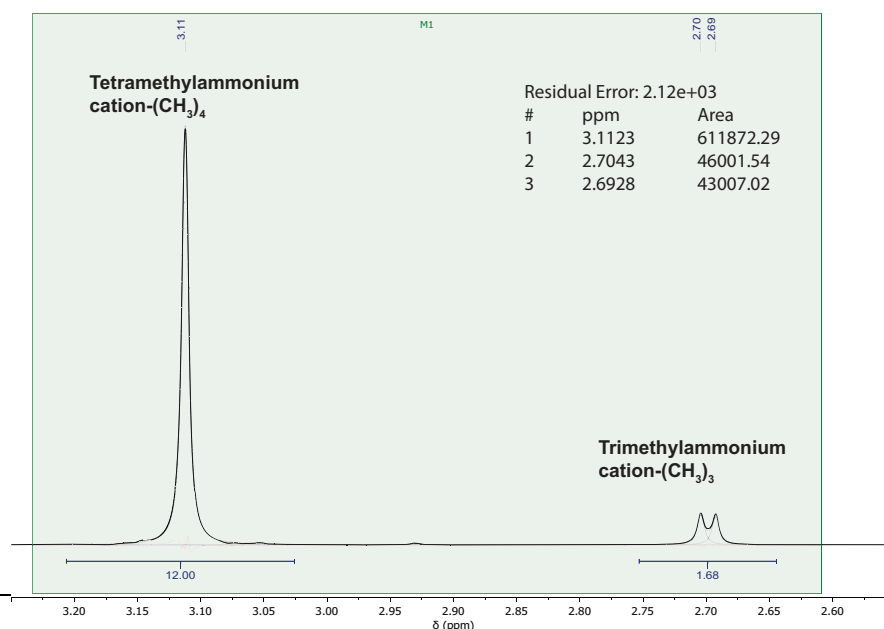
Triethylammonium hydrochloride (0.138 g, 1.0 mmol), and tetraethylammonium chloride (0.164 g, 1.0 mmol) were dissolved in CHCl₃ (1.67 mL, 0.6 M) in a 10 mL vial. Solid (*R*)-BINOL (0.281 g, 1.0 equiv.) was then added with stirring to the solution, resulting in a colourless homogeneous solution. This solution was allowed to stir at room temperature overnight, which produced the desired complexed product **149a** as a white precipitate. The resulting complex was isolated by vacuum filtration (0.314 g, 87% yield, 97% selectivity) and analysis by ¹H NMR spectroscopy (400 MHz, DMSO–d₆) ensured that a 1:1 complex had formed.

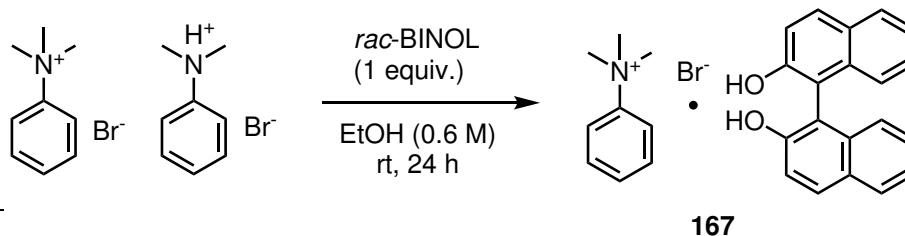


***N*-methyl ammonium chloride salts selectivity with (*R*)-BINOL in CHCl₃**

Scheme 9.25: Selective complexation with (*R*)-BINOL from a mixture of tertiary and quaternary *N*-methylammonium bromide salts in CHCl₃.

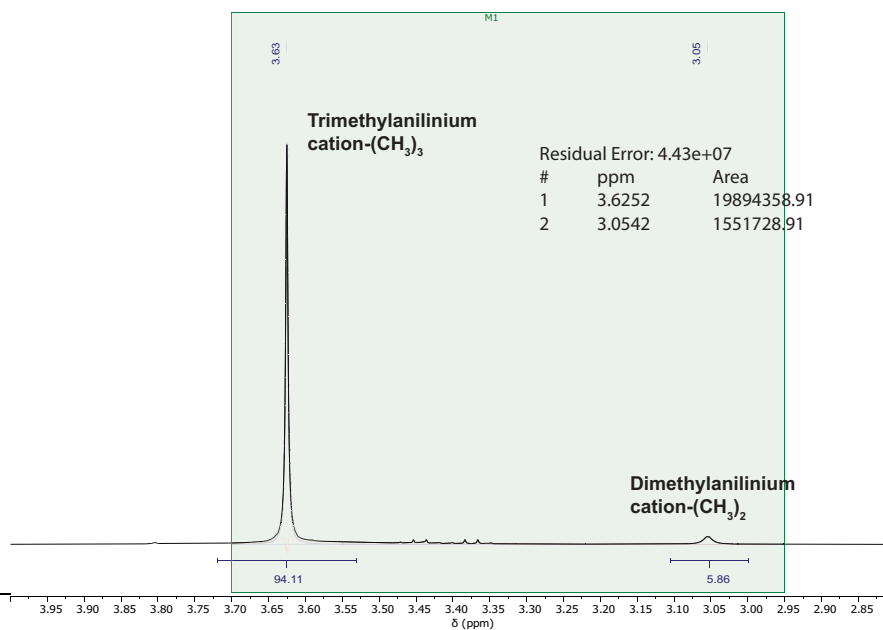
368 (0.096 g, 1.0 mmol) and tetramethylammonium chloride (0.107 g, 1.0 mmol) were dissolved in CHCl₃ (1.67 mL, 0.3 M) in a 10 mL vial. Solid (*R*)-BINOL (0.286 g, 1.0 equiv.) was then added with stirring to the solution, resulting in a colourless homogeneous solution. This solution was allowed to stir at room temperature overnight, which produced the desired complexed product **138b** as a white precipitate. The resulting complex was isolated by vacuum filtration (0.155 g, 33% yield, 84% selectivity) and analysis by ¹H NMR spectroscopy (400 MHz, DMSO–d₆) ensured that a 1:1 complex had formed.

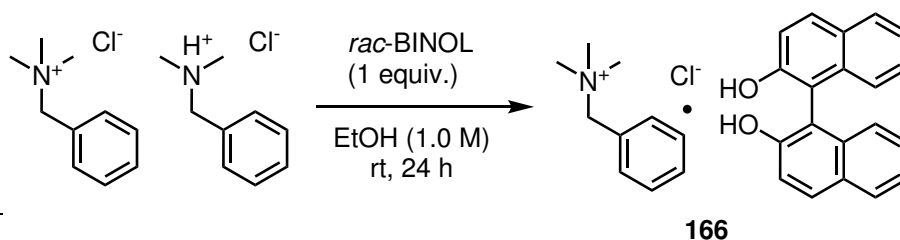


9.7.5 Selective complexation experiments with *rac*-BINOLAnilinium bromides selectivity with *rac*-BINOL

Scheme 9.26: Selective complexation with *rac*-BINOL from a mixture of primary, secondary, tertiary and quaternary anilinium salts.

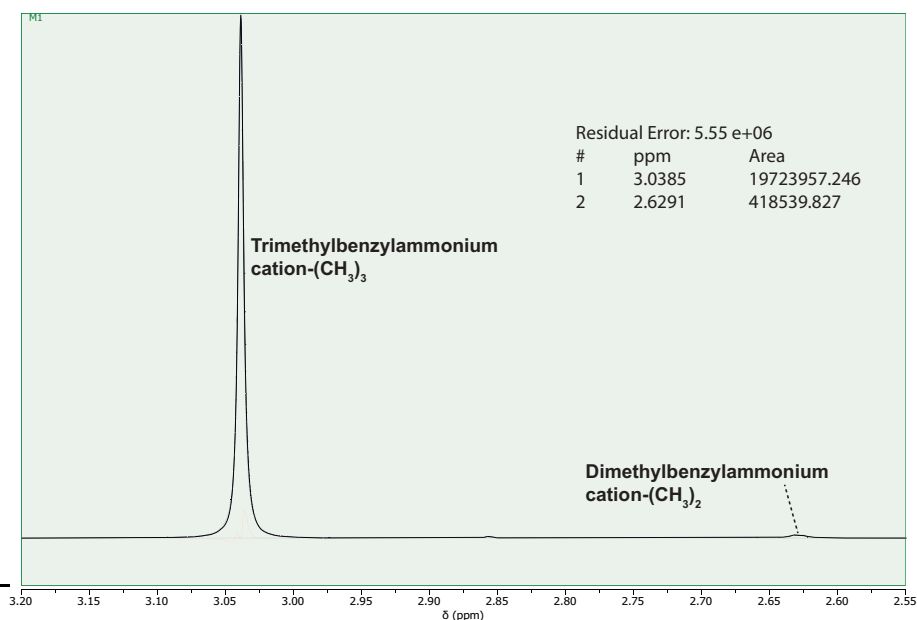
361 (0.202 g, 1.0 mmol) and trimethyl anilinium bromide (0.216 g, 1.0 mmol) were dissolved in EtOH (1.67 mL, 0.6 M) in a 10 mL vial. Solid *rac*-BINOL (0.286 g, 1.0 equiv.) was then added with stirring to the solution, resulting in a pale yellow homogeneous solution. This solution was allowed to stir at room temperature overnight, which produced the desired complexed product **167** as a white precipitate. The resulting complex was isolated by vacuum filtration (0.416 g, 73% yield, 91% selectivity). Analysis by ^1H NMR spectroscopy (400 MHz, $\text{DMSO}-d_6$) ensured that a 1:1 complex had formed.

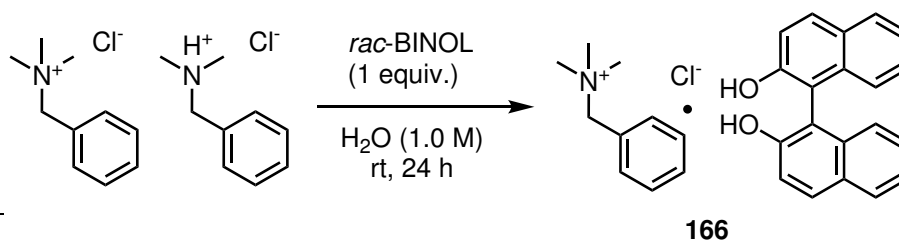


Benzylammonium chlorides selectivity with *rac*-BINOL

Scheme 9.27: Selective complexation with *rac*-BINOL from a mixture of primary, secondary, tertiary and quaternary benzylammonium salts.

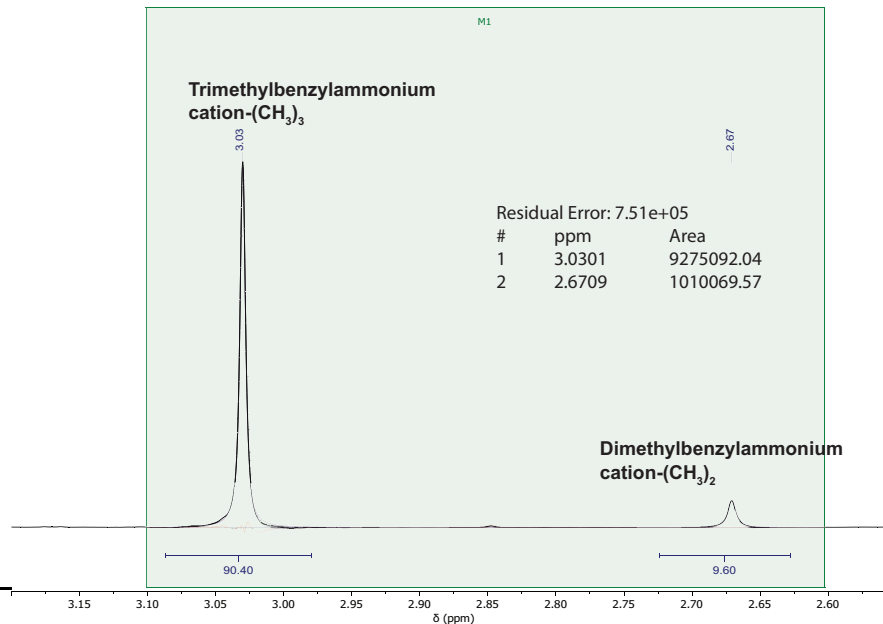
364 (0.170 g, 1.0 mmol) and *N,N,N*-trimethyl benzylammonium chloride (0.181 g, 1.0 mmol) were dissolved in EtOH (1.00 mL, 1.0 M) in a 10 mL vial. Solid *rac*-BINOL (0.287 g, 1.0 equiv.) was then added with stirring to the solution, resulting in a colourless homogeneous solution. This solution was allowed to stir at room temperature overnight, which produced the desired complexed product **166** as a white precipitate. The resulting complex was isolated by vacuum filtration (0.306 g, 67% yield, 95% selectivity). Analysis by ^1H NMR spectroscopy (400 MHz, $\text{DMSO}-d_6$) ensured that a 1:1 complex had formed.

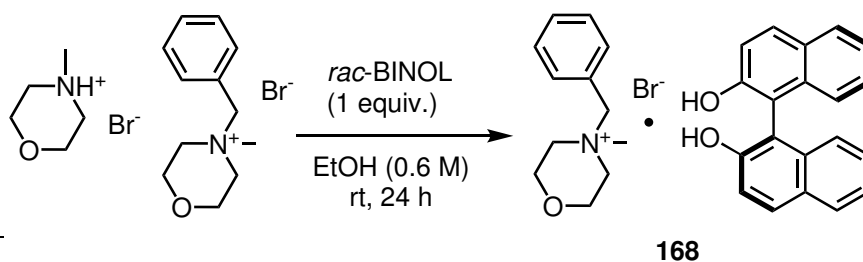


Benzylammonium chlorides selectivity with *rac*-BINOL in H₂O

Scheme 9.28: Selective complexation with *rac*-BINOL from a mixture of primary, secondary, tertiary and quaternary benzylammonium salts in H₂O.

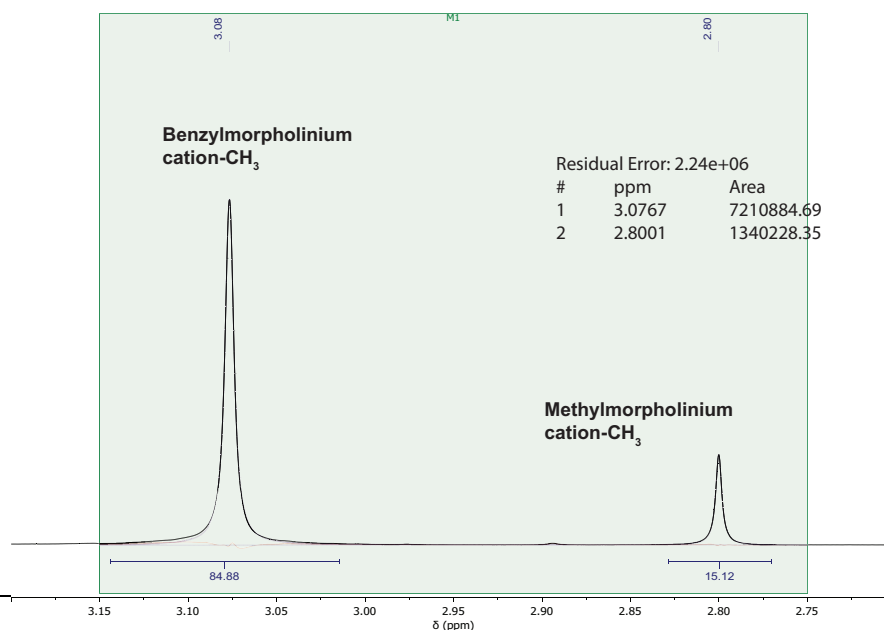
364 (0.170 g, 1.0 mmol) and *N,N,N*-trimethyl benzylammonium chloride (0.187 g, 1.0 mmol) were dissolved in H₂O (1.00 mL, 1.0 M) in a 10 mL vial. Solid *rac*-BINOL (0.286 g, 1.0 equiv.) was then added with stirring to the solution, resulting in a cloudy slurry. This slurry was allowed to stir at room temperature overnight, which produced the desired complexed product **166** as a white precipitate. The resulting complex was isolated by vacuum filtration (0.188 g, 40% yield, 84% selectivity). Analysis by ¹H NMR spectroscopy (400 MHz, DMSO-*d*₆) ensured that a 1:1 complex had formed.

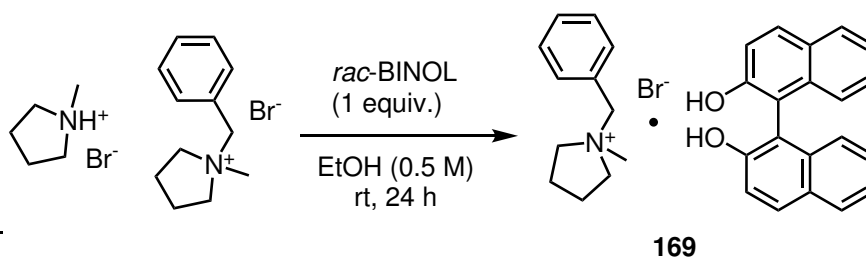


Morpholinium bromides selectivity with *rac*-BINOL

Scheme 9.29: Selective complexation with *rac*-BINOL from a mixture of secondary, tertiary and quaternary morpholinium salts.

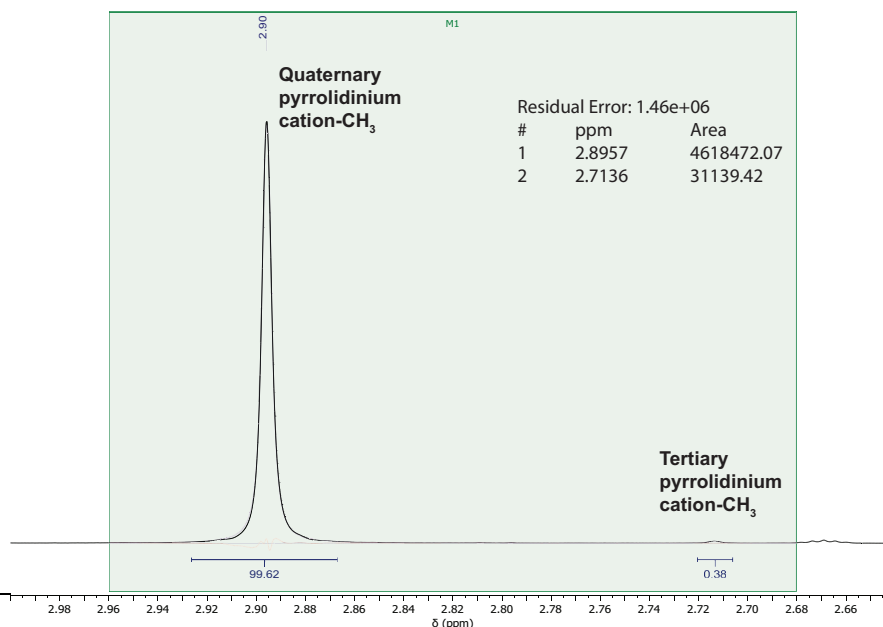
366 (0.182 g, 1.0 mmol) and **100** (0.272 g, 1.0 mmol) were dissolved in EtOH (1.67 mL, 0.6 M) in a 10 mL vial. Solid *rac*-BINOL (0.288 g, 1.0 equiv.) was then added with stirring to the solution, resulting in a pale yellow homogeneous solution. This solution was allowed to stir at room temperature overnight, which produced the desired complexed product **168** as a white precipitate. The resulting complex was isolated by vacuum filtration (0.447 g, 68% yield, 85% selectivity). Analysis by ^1H NMR spectroscopy (400 MHz, $\text{DMSO}-d_6$) ensured that a 1:1 complex had formed.

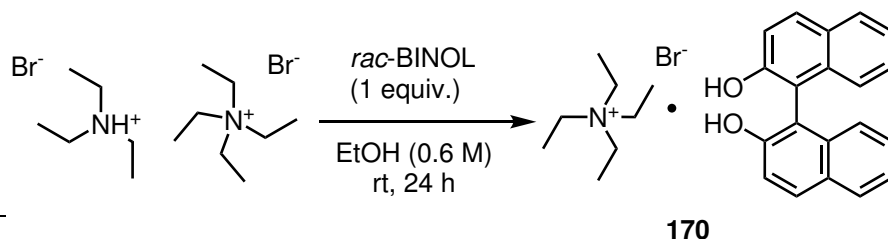


Pyrrolidinium bromides selectivity with *rac*-BINOL

Scheme 9.30: Selective complexation with *rac*-BINOL from a mixture of tertiary and quaternary pyrrolidinium salts.

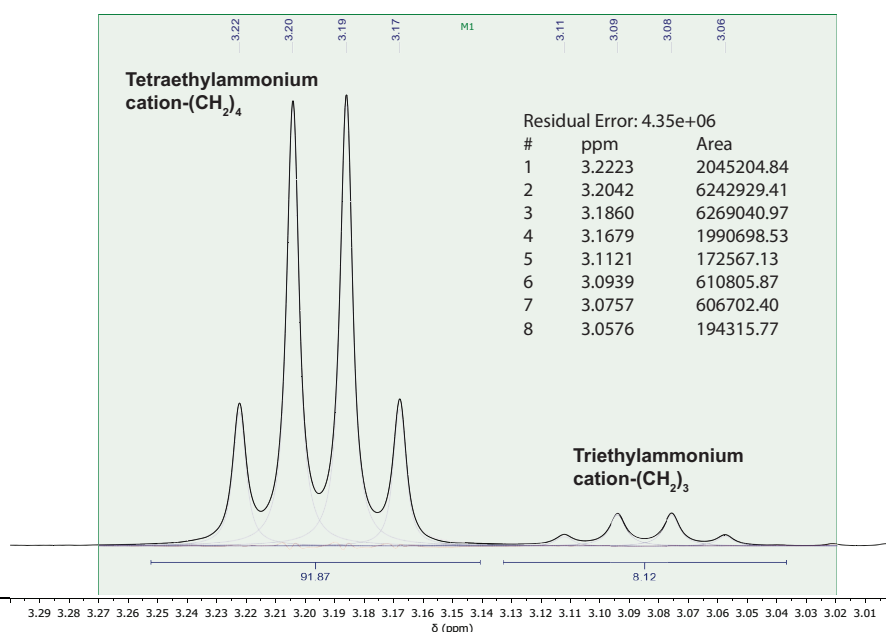
379 (0.168 g, 1.0 mmol), and **102** (0.256 g, 1.0 mmol) were dissolved in EtOH (2.00 mL, 0.5 M) in a 10 mL vial. Solid *rac*-BINOL (0.284 g, 1.0 equiv.) was then added with stirring to the solution, resulting in a colourless homogeneous solution. This solution was allowed to stir at room temperature overnight, which produced the desired complexed product **169** as a white precipitate. The resulting complex was isolated by vacuum filtration (0.397 g, 56% yield, 77% selectivity) and analysis by ^1H NMR spectroscopy (400 MHz, $\text{DMSO}-d_6$) ensured that a 1:1 complex had formed.

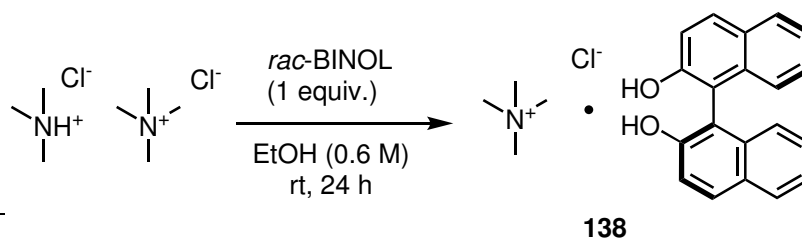


***N*-ethyl bromides selectivity with *rac*-BINOL**

Scheme 9.31: Selective complexation with *rac*-BINOL from a mixture of tertiary and quaternary *N*-ethylammonium bromide salts.

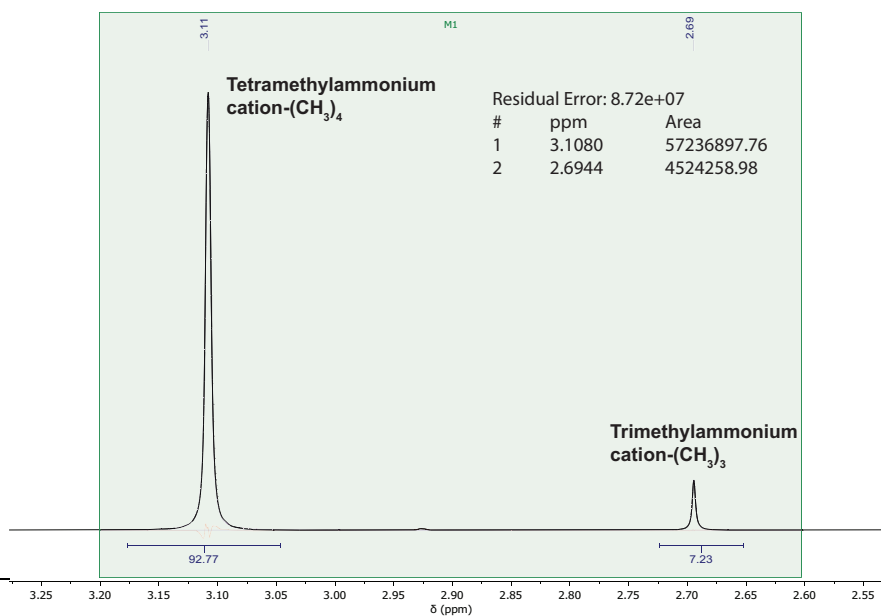
93 (0.182 g, 1.0 mmol), and tetraethylammonium bromide (0.208 g, 1.0 mmol) were dissolved in EtOH (1.67 mL, 0.6 M) in a 10 mL vial. Solid *rac*-BINOL (0.286 g, 1.0 equiv.) was then added with stirring to the solution, resulting in a colourless homogeneous solution. This solution was allowed to stir at room temperature overnight, which produced the desired complexed product **170** as a white precipitate. The resulting complex was isolated by vacuum filtration (0.241 g, 45% yield, 89% selectivity) and analysis by ^1H NMR spectroscopy (400 MHz, $\text{DMSO}-d_6$) ensured that a 1:1 complex had formed.



***N*-methyl ammonium chloride salts selectivity with *rac*-BINOL**

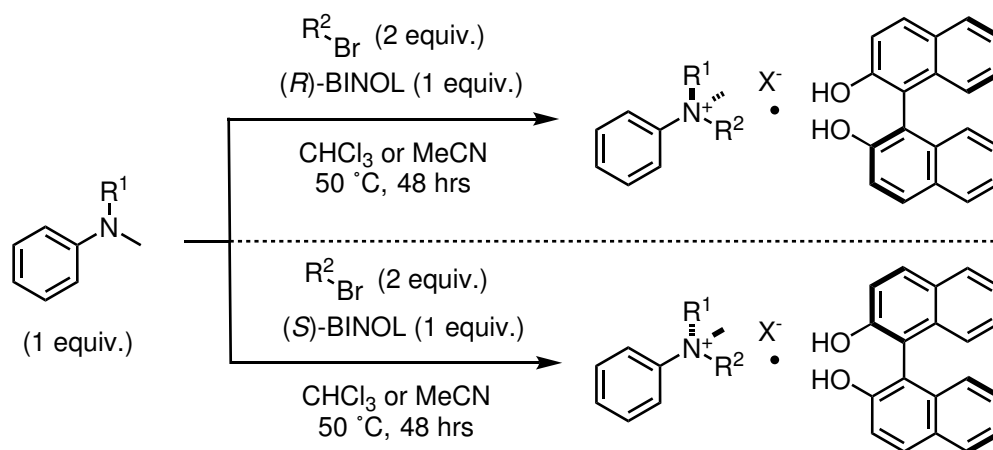
Scheme 9.32: Selective complexation with *rac*-BINOL from a mixture of tertiary and quaternary *N*-methylammonium bromide salts.

368 (0.096 g, 0.5 mmol) and tetramethylammonium chloride (0.110 g, 0.5 mmol) were dissolved in EtOH (1.67 mL, 0.3 M) in a 10 mL vial. Solid *rac*-BINOL (0.279 g, 1.0 equiv.) was then added with stirring to the solution, resulting in a colourless homogeneous solution. This solution was allowed to stir at room temperature overnight, which produced the desired complexed product **138** as a white precipitate. The resulting complex was isolated by vacuum filtration (0.295 g, 68% yield, 91% selectivity) and analysis by ^1H NMR spectroscopy (400 MHz, DMSO- d_6) ensured that a 1:1 complex had formed.



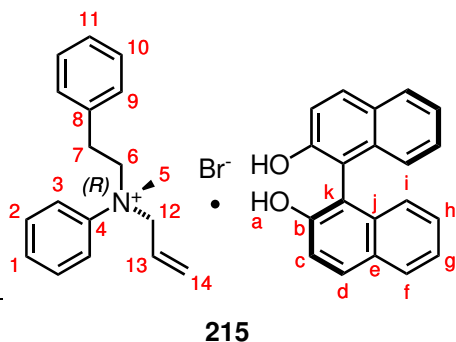
9.8 CIAT of ammonium salts

9.8.1 General procedure for CIAT of ammonium cations



Scheme 9.33: Crystallisation induced asymmetric transformation from Walsh *et al* for the one-pot synthesis of enantioenriched quaternary ammonium salt complexes with 1,1'-bi-2-naphthol.

Adapted from Walsh *et al.*² The selected tertiary aniline (1.0 equiv.) was dissolved into $CHCl_3$ or MeCN. With stirring, the desired alkylating agent (2.0 equiv.) was added to the tertiary aniline solution. The reaction mixture was heated to $50\text{ }^\circ\text{C}$ and left to stir for 10 minutes. Solid (R) -BINOL or (S) -BINOL (1.0 equiv.) was then added with stirring to the solution, resulting in a clear homogenous solution. This solution was allowed to stir at $50\text{ }^\circ\text{C}$ for 48 h, which produced the desired complex as a white precipitate. The product was isolated by vacuum filtration and washed with a few drops of reaction solvent. Analysis by ^1H NMR spectroscopy ensured that a 1:1 complex had formed. Single crystals for XRD analysis can be grown from EtOH.

(R)-N-allyl, N-methyl, N-phenylacetyl anilinium bromide · (R)-1,1'-bi-2-naphthol

Following the general procedure outlined in 9.8.1, **176** (0.216 g, 1.02 mmol) was dissolved in CHCl_3 (1.67 mL, 0.6 M) and allyl bromide (0.17 mL, 2.00 mmol) was added and stirred for 10 minutes at 50 °C. (*R*)-BINOL (0.284 g, 0.99 mmol) was added, and the mixture was stirred at 50 °C for 48 hours.

A white precipitate formed which was isolated by vacuum filtration to yield **215** (0.483 g, 79% yield).

Enantioenrichment of the ammonium salt measured by chiral HPLC: er 99:1 (*R*:*S*).

^1H NMR (599 MHz, CD_3OD) δ 7.88 – 7.81 (6H, m, d_{df+3}), 7.71 (2H, apt. t, $J = 8.3$ Hz, H_2), 7.65 (1H, apt. t, $J = 7.3$ Hz, H_1), 7.32 – 7.27 (4H, m, H_{9+i}), 7.25 – 7.22 (3H, m, H_{11+g}), 7.18 – 7.14 (4H, m, H_{10+h}), 7.01 (2H, d, $J = 8.5$ Hz, H_c), 5.64 (1H, dddd, $J = 16.8, 9.4, 7.4, 5.9$ Hz, H_{13}), 5.61 – 5.55 (2H, m, H_{14}), 4.65 (1H, dd, $J = 13.2, 5.9$ Hz, H_{12}), 4.43 (1H, dd, $J = 13.1, 7.3$ Hz, $\text{H}_{12'}$), 4.25 (1H, td, $J = 12.5, 4.7$ Hz, H_6), 4.03 (1H, ddd, $J = 13.0, 11.6, 5.6$ Hz, H_6'), 3.62 (3H, s, H_5), 3.00 (1H, td, $J = 12.5, 5.6$ Hz, H_7), 2.52 (1H, ddd, $J = 13.0, 11.5, 4.7$ Hz, H_7').

^{13}C NMR (151 MHz, CD_3OD) δ 154.2 (C_b), 143.2 (C_4), 136.6 (C_8), 135.8 (C_j), 131.94 (C_2), 131.88 (C_1), 130.6 (C_d), 130.5 (C_e), 130.1 (C_9), 129.9 (C_{10}), 129.4 (C_{13}), 129.0 (C_f), 128.5 (C_{11}), 127.1 (C_h), 126.0 (C_{14}), 125.8 (C_c), 123.8 (C_g), 122.9 (C_3), 119.3 (C_i), 116.2 (C_k), 72.7 (C_{12}), 69.7 (C_6), 47.9 (C_5), 30.3 (C_7).

.LRMS (ESI-TOF, EI^+) m/z : 252.8 ($[\text{M}]^+$, 100%).

LRMS (ESI-TOF, EI^-) m/z : 285.4 ($[\text{M}-\text{H}]^-$, 100%).

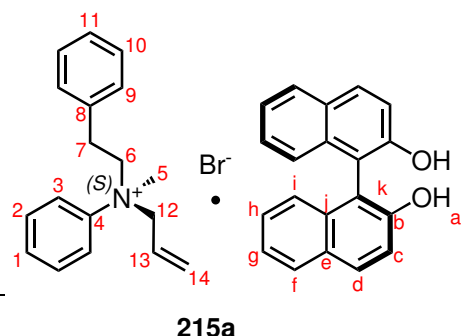
HRMS (ESI-TOF) m/z : $[\text{M}]^+$ calculated for $\text{C}_{18}\text{H}_{22}\text{N}^+$: 252.1752, found 252.1763. $[\text{M}-\text{H}]^-$ calculated for $\text{C}_{20}\text{H}_{13}\text{O}_2^-$: 285.0916, found 285.0929.

mp: 148 °C (CHCl_3 precipitate).

Optical rotation: $[\alpha]_D^{20} = -10.17$ (MeOH, $c = 1.40$).

IR ($\text{max}/\text{cm}^{-1}$): 3157br, 1624m, 1506m, 1431m, 1328m, 1271s, 952s, 818s, 750s, 691s.

XRD: A portion of the complex was crystallised in EtOH to give clear colourless needles. Crystal data for $\text{C}_{38}\text{H}_{36}\text{BrNO}_2$ ($m = 618.59$ g/mol): Orthorhombic, space group $P2_12_12$ (no. 18).

(S)-N-allyl, N-methyl, N-phenylacetyl anilinium bromide · (S)-1,1'-bi-2-naphthol

Following the general procedure outlined in 9.8.1, **176** (0.210 g, 0.99 mmol) was dissolved in CHCl_3 (1.67 mL, 0.6 M) and allyl bromide (0.17 mL, 2.00 mmol) was added and stirred for 10 minutes at 50 °C. (S)-BINOL (0.285 g, 1.00 mmol) was added, and the mixture was stirred at 50 °C for 48 hours. A white precipitate formed which was isolated

by vacuum filtration to yield **215a** (0.466 g, 76% yield).

Enantioenrichment of the ammonium salt measured by chiral HPLC: er 3:97 (*R*:*S*).

^1H NMR (599 MHz, CD_3OD) identical to that of **215**.

^{13}C NMR (151 MHz, CD_3OD) identical to that of **215**.

LRMS (ESI-TOF, EI^+) m/z : 252.2 ($[\text{M}]^+$, 100%).

LRMS (ESI-TOF, EI^-) m/z : 285.4 ($[\text{M}-\text{H}]^-$, 100%).

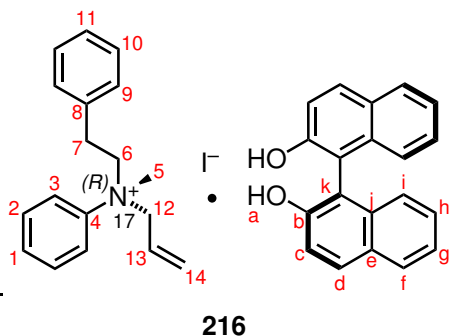
HRMS (ESI-TOF) m/z : $[\text{M}]^+$ calculated for $\text{C}_{18}\text{H}_{22}\text{N}^+$: 252.1752, found 252.1764.

mp: 149 °C (CHCl_3 precipitate).

Optical rotation: $[\alpha]_{\text{D}}^{20} = +10.60$ (MeOH, $c = 1.50$).

IR ($\text{max}/\text{cm}^{-1}$): 3162br, 1624w, 1506w, 1431w, 1331m, 1271s, 981w, 818s, 750s, 691s.

XRD: A portion of the complex was crystallised in EtOH to give clear colourless needles. Crystal data for $\text{C}_{38}\text{H}_{36}\text{BrNO}_2$ ($m = 618.59$ g/mol): Orthorhombic, space group $P2_12_12$ (no. 18).

(R)-N-allyl, N-methyl, N-phenylacetyl anilinium iodide · (R)-1,1'-bi-2-naphthol

Following the general procedure outlined in 9.8.1, **176** (0.204 g, 0.97 mmol) was dissolved in CHCl_3 (1.67 mL, 0.6 M) and allyl iodide (0.18 mL, 1.97 mmol) was added and stirred for 10 minutes at 50 °C. (*R*)-BINOL (0.286 g, 1.00 mmol) was added, and the mixture was stirred at 50 °C for 48 hours. A white precipitate formed which was isolated

by vacuum filtration to yield **216** (0.324 g, 50% yield).

Enantioenrichment of the ammonium salt measured by chiral HPLC: er 99:1 (*R*:*S*).

^1H NMR (700 MHz, CD_3OD) δ 7.90 – 7.81 (6H, m, $\text{H}_{\text{d+f+3}}$), 7.73 – 7.67 (2H, m, H_2), 7.67 – 7.61 (1H, m, H_1), 7.32 – 7.28 (4H, m, $\text{H}_{\text{i+9}}$), 7.26 – 7.22 (3H, m, $\text{H}_{\text{11+g}}$), 7.17 – 7.14 (4H, m, $\text{H}_{\text{10+h}}$), 7.02 (2H, d, $J = 8.5$ Hz, H_c), 5.64 (1H, dddd, $J = 16.8, 9.4, 7.4, 5.9$ Hz, H_{13}), 5.61 – 5.57 (1H, m, H_{14}), 5.55 (1H, dd, $J = 9.7, 1.8$ Hz, H_{14}), 4.66 (1H, dd, $J = 13.3, 5.9$ Hz, H_{12}), 4.44 (1H, dd, $J = 13.2, 7.4$ Hz, $\text{H}_{12'}$), 4.25 (1H, td, $J = 12.5, 4.7$ Hz, H_6), 4.04 (1H, ddd, $J = 13.1, 11.6, 5.6$ Hz, H_6'), 3.62 (3H, s, H_5), 3.00 (1H, td, $J = 12.5, 5.6$ Hz, H_7), 2.52 (1H, td, $J = 12.3, 4.7$ Hz, H_7').

^{13}C NMR (176 MHz, CD_3OD) δ 154.2 (C_b), 143.2 (C_4), 136.6 (C_8), 135.8 (C_j), 131.9 (C_2), 131.8 (C_1), 130.6 (C_d), 130.4 (C_e), 130.0 (C_9), 129.9 (C_{10}), 129.5 (C_{13}), 129.0 (C_f), 128.4 (C_{11}), 127.1 (C_h), 126.0 (C_{14}), 125.8 (C_c), 123.8 (C_g), 123.0 (C_3), 119.3 (C_i), 116.2 (C_k), 72.7 (C_{12}), 69.7 (C_6), 48.0 (C_5), 30.3 (C_7).

LRMS (ESI-TOF, EI^+) m/z : 252.2 ($[\text{M}]^+$, 100%).

LRMS (ESI-TOF, EI^+) m/z : 287.1 ($[\text{M}+\text{H}]^+$, 100%).

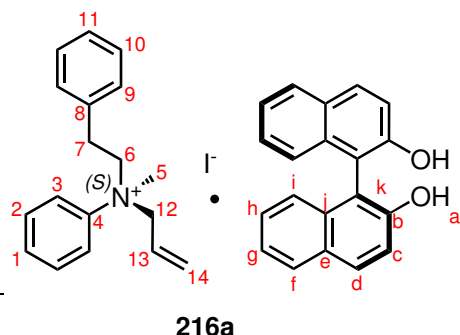
HRMS (ESI-TOF) m/z : $[\text{M}]^+$ calculated for $\text{C}_{18}\text{H}_{22}\text{N}^+$: 252.1752, found 252.1763.

mp: 164 – 165 °C (CHCl_3 precipitate).

Optical rotation: $[\alpha]_\text{D}^{20} = -9.52$ (MeOH, $c = 0.49$).

IR (max/cm^{-1}): 3227br, 1624w, 1507w, 1321m, 1286s, 816s, 751s, 700s.

XRD: A portion of the complex was crystallised in EtOH to give clear colourless needles. Crystal data for $\text{C}_{38}\text{H}_{36}\text{INO}_2$ ($m = 665.60$ g/mol): Orthorhombic, space group $P2_12_12$ (no. 18).

(S)-N-allyl, N-methyl, N-phenylacetyl anilinium iodide · (S)-1,1'-bi-2-naphthol

Following the general procedure outlined in 9.8.1, **176** (0.211 g, 1.00 mmol) was dissolved in CHCl_3 (1.67 mL, 0.6 M) and allyl iodide (0.17 mL, 2.00 mmol) was added and stirred for 10 minutes at 50 °C. (S)-BINOL (0.286 g, 1.00 mmol) was added, and the mixture was stirred at 50 °C for 48 hours. A white precipitate formed which was isolated

by vacuum filtration to yield **216a** (0.342 g, 51% yield).

Enantioenrichment of the ammonium salt measured by chiral HPLC: er 2:98 (*R*:*S*).

^1H NMR (599 MHz, CD_3OD) *identical to that of 216*.

^{13}C NMR (151 MHz, CD_3OD) *identical to that of 216*.

LRMS (ESI-TOF, EI^+) m/z : 252.2 ($[\text{M}]^+$, 100%).

LRMS (ESI-TOF, EI^-) m/z : 285.4 ($[\text{M}-\text{H}]^-$, 100%).

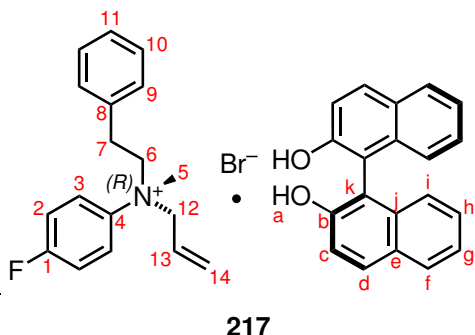
HRMS (ESI-TOF) m/z : $[\text{M}]^+$ calculated for $\text{C}_{18}\text{H}_{22}\text{N}^+$: 252.1752, found 252.1764.

mp: 165 °C (CHCl_3 precipitate).

Optical rotation: $[\alpha]_{\text{D}}^{20} = +8.46$ (MeOH, $c = 0.52$).

IR ($\text{max}/\text{cm}^{-1}$): 3227br, 1624w, 1507w, 1321m, 1269s, 980w, 816s, 750s, 700s.

XRD: A portion of the complex was crystallised in EtOH to give clear colourless needles. Crystal data for $\text{C}_{38}\text{H}_{36}\text{INO}_2$ ($m = 665.60$ g/mol): Orthorhombic, space group $P2_12_12$ (no. 18).

(R)-N-allyl, N-methyl, N-phenylacetyl 4-fluoroanilinium bromide · (R)-1,1'-bi-2-naphthol

Following the general procedure outlined in 9.8.1, **182** (0.235 g, 1.02 mmol) was dissolved in CHCl_3 (0.50 mL, 2.0 M) and allyl bromide (0.17 mL, 2.00 mmol) was added and stirred for 10 minutes at 50 °C. (R)-BINOL (0.288 g, 1.00 mmol) was added, and the mixture was stirred at 50 °C for 48 hours.

A white precipitate formed which was isolated by vacuum filtration to yield **217** (0.350 g, 54% yield).

Enantioenrichment of the ammonium salt measured by chiral HPLC: er 96:4 (*R*:*S*).

^1H NMR (400 MHz, CD_3OD) δ 7.88 – 7.78 (6H, m, $\text{H}_{\text{d+f+3}}$), 7.39 – 7.32 (2H, m, H_2), 7.32 – 7.28 (2H, m, H_i), 7.28 – 7.20 (5H, m, H_{9+11+g}), 7.17 – 7.11 (4H, m, $\text{H}_{\text{h+10}}$), 7.03 (2H, dq, $J = 8.5, 0.9$ Hz, H_c), 5.64 – 5.48 (3H, m, H_{13+14}), 4.56 (1H, dd, $J = 13.2, 6.4$ Hz, H_{12}), 4.36 (1H, dd, $J = 13.2, 6.5$ Hz, $\text{H}_{12'}$), 4.23 – 4.10 (1H, m, H_6), 3.98 (1H, ddd, $J = 12.9, 11.3, 5.5$ Hz, H_6), 3.52 (3H, s, H_5), 2.95 (1H, td, $J = 12.4, 5.5$ Hz, H_7), 2.49 (1H, ddd, $J = 13.1, 11.3, 4.9$ Hz, H_7).

^{13}C NMR (101 MHz, CD_3OD) δ 164.3 (d, $J = 245.8$ Hz, C_1), 154.2 (C_b), 143.1 (C_4), 135.8 (C_j), 132.6 (d, $J = 15.8$ Hz, C_2), 131.9 (d, $J = 14.4$ Hz, C_3), 131.78 (C_{11}), 131.7 (C_8), 130.6 (C_d), 130.4 (C_e), 129.5 (C_{13}), 129.0 (C_f), 127.1 (C_h), 126.0 (C_{14}), 125.8 (C_c), 123.8 (C_g), 122.9 (C_{10}), 119.3 (C_i), 116.7 (d = 21.8 Hz, C_9), 116.2 (C_k), 72.7 (C_{12}), 69.5 (C_6), 47.9 (C_5), 29.5 (C_7).

^{19}F NMR (376 MHz, CD_3OD) δ -111.61.

LRMS (ESI-TOF, EI^+) m/z : 270.1 ($[\text{M}]^+$, 100%).

LRMS (ESI-TOF, EI^-) m/z : 287.1 ($[\text{M}+\text{H}]^+$, 100%).

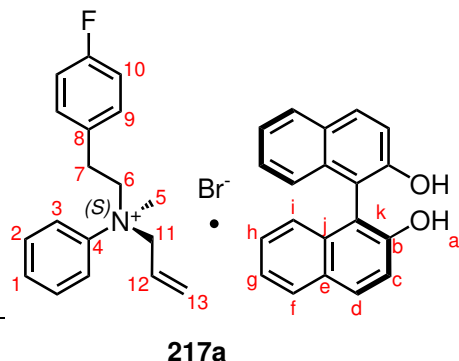
HRMS (ESI-TOF) m/z : $[\text{M}]^+$ calculated for $\text{C}_{18}\text{H}_{21}\text{NF}^+$: 270.1658 found 270.1664.

mp: 121 °C (CHCl_3 precipitate).

Optical rotation: $[\alpha]_{\text{D}}^{20} = +2.14$ (MeOH, $c = 0.57$).

IR (max/cm^{-1}): 3161br, 1622m, 1507m, 1431m, 1326m, 1270s, 863m, 818s, 748s, 698m.

XRD: A portion of the complex was crystallised in EtOH to give clear colourless needles. Crystal data for $\text{C}_{38}\text{H}_{35}\text{FBrNO}_2$ ($m = 636.58$ g/mol): Orthorhombic, space group $P2_12_12$ (no. 18).

(S)-N-allyl, N-methyl, N-phenylacetyl 4-fluoroanilinium bromide · (S)-1,1'-bi-2-naphthol

Following the general procedure outlined in 9.8.1, **182** (0.229 g, 1.00 mmol) was dissolved in CHCl_3 (0.50 mL, 2.0 M) and allyl bromide (0.17 mL, 2.00 mmol) was added and stirred for 10 minutes at 50 °C. (*R*)-BINOL (0.284 g, 0.99 mmol) was added, and the mixture was stirred at 50 °C for 48 hours. A white precipitate formed which was isolated by vacuum filtration to yield **217a** (0.476 g,

75% yield).

Enantioenrichment of the ammonium salt measured by chiral HPLC: er 4:96 (*R*:*S*).

^1H NMR (599 MHz, CD_3OD) δ identical to that of **217**

^{13}C NMR (151 MHz, CD_3OD) δ identical to that of **217**

^{19}F NMR (376 MHz, CD_3OD) δ identical to that of **217**

LRMS (ESI-TOF, EI^+) m/z : 270.2 ($[\text{M}]^+$, 100%).

LRMS (ESI-TOF, EI^-) m/z : 285.2 ($[\text{M}-\text{H}]^-$, 100%).

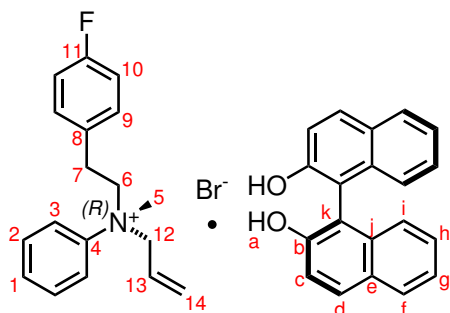
HRMS (ESI-TOF) m/z : $[\text{M}]^+$ calculated for $\text{C}_{18}\text{H}_{21}\text{NF}^+$: 270.1658, found 270.1663.

mp: 120 – 121 °C (CHCl_3 precipitate).

Optical rotation: $[\alpha]_{\text{D}}^{20} = -2.09$ (MeOH, $c = 0.51$).

IR ($\text{max}/\text{cm}^{-1}$): 3153br, 1622w, 1506m, 1270m, 817s, 748s.

XRD: A portion of the complex was crystallised in EtOH to give clear colourless needles. Crystal data for $\text{C}_{38}\text{H}_{35}\text{FBrNO}_2$ ($m = 636.59$ g/mol): Orthorhombic, space group $P2_12_12$ (no. 18).

(R)-N-allyl, N-methyl, N-para-fluorophenylacetyl anilinium bromide · (R)-1,1'-bi-2-naphthol**218**

Following the general procedure outlined in 9.8.1, **177** (0.236 g, 1.02 mmol) was dissolved in CHCl_3 (1.67 mL, 0.6 M) and allyl bromide (0.17 mL, 2.00 mmol) was added and stirred for 10 minutes at 50 °C. (*R*)-BINOL (0.286 g, 1.00 mmol) was added, and the mixture was stirred at 50 °C for 48 hours. A white precipitate formed which was isolated by vacuum filtration to yield **218** (0.286 g,

56% yield).

Enantioenrichment of the ammonium salt measured by chiral HPLC: er 95:5 (*R*:*S*).

^1H NMR (599 MHz, CD_3OD) δ 7.89 – 7.81 (6H, m, $\text{H}_{3+\text{d}+\text{f}}$), 7.73 – 7.67 (2H, m, H_2), 7.66 – 7.61 (1H, m, H_1), 7.29 (2H, d, $J = 8.8$ Hz, H_i), 7.24 (2H, ddd, $J = 8.1, 6.7, 1.2$ Hz, H_g), 7.19 – 7.14 (4H, m, $\text{H}_{9+\text{h}}$), 7.06 – 6.99 (4H, m, $\text{H}_{10+\text{c}}$), 5.65 – 5.53 (3H, m, $\text{H}_{12+\text{13}}$), 4.66 (1H, dd, $J = 13.2, 6.0$ Hz, H_{12}), 4.43 (1H, dd, $J = 13.2, 7.5$ Hz, $\text{H}_{12'}$), 4.25 (1H, td, $J = 12.5, 4.8$ Hz, H_6), 4.02 (1H, ddd, $J = 13.1, 11.5, 5.5$ Hz, H_6'), 3.63 (3H, s, H_5), 3.01 (1H, td, $J = 12.6, 5.5$ Hz, H_7), 2.53 (1H, ddd, $J = 13.4, 11.6, 4.8$ Hz, H_7').

^{13}C NMR (151 MHz, CD_3OD) δ 162.9 (d, $J = 241.1$ Hz, C_{11}), 152.8 (C_b), 141.8 (C_4), 134.4 (C_j), 131.2 (d, $J = 3.0$ Hz, C_8), 130.5 (C_2), 130.44 (C_1), 130.35 (d, $J = \text{C}_9$), 129.2 (C_d), 129.1 (C_e), 128.1 (C_{14}), 127.6 (C_f), 125.7 (C_h), 124.6 (C_{13}), 124.4 (C_c), 122.5 (C_g), 121.5 (C_3), 117.9 (C_i), 115.2 (d, $J = 21.8$ Hz, C_{10}), 114.8 (C_k), 71.4 (C_{12}), 68.1 (C_6), 46.5 (C_5), 28.1 (C_7).

^{19}F NMR (376 MHz, CD_3OD) δ -117.38 (p, $J = 7.6$ Hz).

LRMS (ESI-TOF, EI^+) m/z : 270.2 ($[\text{M}]^+$, 100%).

LRMS (ESI-TOF, EI^-) m/z : 285.4 ($[\text{M}-\text{H}]^-$, 100%).

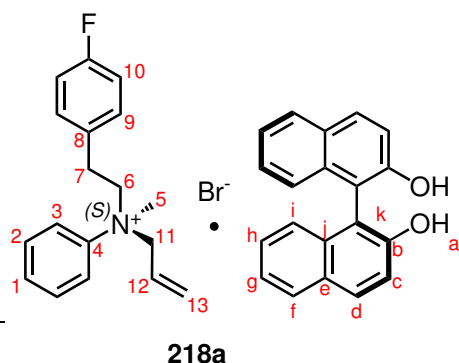
HRMS (ESI-TOF) m/z : $[\text{M}]^+$ calculated for $\text{C}_{18}\text{H}_{21}\text{NF}^+$: 270.1665, found 270.1664.

mp: 136 – 137 °C (CHCl_3 precipitate).

Optical rotation: $[\alpha]_D^{20} = -12.18$ (MeOH, $c = 0.17$).

IR ($\text{max}/\text{cm}^{-1}$): 3141br, 1623w, 1508s, 1430w, 1328m, 1272s, 816s, 749s, 691s.

XRD: A portion of the complex was crystallised in EtOH to give clear colourless needles. Crystal data for $\text{C}_{38}\text{H}_{35}\text{BrFNO}_2$ ($m = 636.58$ g/mol): Orthorhombic, space group $P2_12_12$ (no. 18).

(S)-N-allyl, N-methyl, N-para-fluorophenylacetyl anilinium bromide · (S)-1,1'-bi-2-naphthol

Following the general procedure outlined in 9.8.1, **177** (0.225 g, 0.98 mmol) was dissolved in CHCl_3 (1.67 mL, 0.6 M) and allyl bromide (0.17 mL, 2.00 mmol) was added and stirred for 10 minutes at 50 °C. (S)-BINOL (0.284 g, 0.99 mmol) was added, and the mixture was stirred at 50 °C for 48 hours. A white precipitate formed which was isolated by vacuum filtration to yield **218a** (0.281 g,

45% yield).

Enantioenrichment of the ammonium salt measured by chiral HPLC: er 12:88 (*R*:*S*).

^1H NMR (599 MHz, CD_3OD) identical to that of **218**.

^{13}C NMR (151 MHz, CD_3OD) identical to that of **218**.

LRMS (ESI-TOF, EI^+) m/z : 270.2 ($[\text{M}]^+$, 100%).

LRMS (ESI-TOF, EI^-) m/z : 285.4 ($[\text{M}-\text{H}]^-$, 100%).

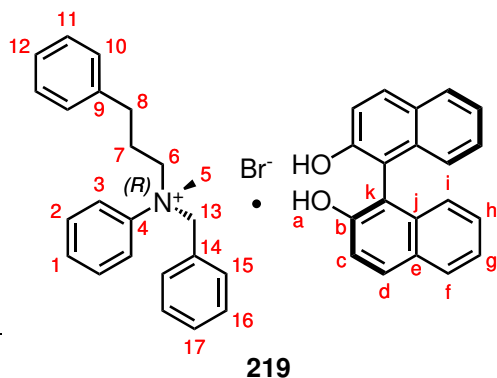
HRMS (ESI-TOF) m/z : $[\text{M}]^+$ calculated for $\text{C}_{18}\text{H}_{21}\text{NF}^+$: 270.1658, found 270.1663.

mp: 155 – 156 °C (CHCl_3 precipitate).

Optical rotation: $[\alpha]_{\text{D}}^{20} = +13.17$ (MeOH, $c = 0.20$).

IR ($\text{max}/\text{cm}^{-1}$): 3138br, 1623w, 1508s, 1431m, 1329m, 1272s, 1229m, 816s, 749s, 690s.

XRD: A portion of the complex was crystallised in EtOH to give clear colourless needles. Crystal data for $\text{C}_{38}\text{H}_{35}\text{BrFNO}_2$ ($m = 636.58$ g/mol): Orthorhombic, space group $P2_12_12$ (no. 18).

(R)-N-benzyl, N-methyl, N-hydrocinnamyl anilinium bromide · (R)-1,1'-bi-2-naphthol

Following the general procedure outlined in 9.8.1, **178** (0.228 g, 1.01 mmol) was dissolved in MeCN (0.50 mL, 2.0 M) and benzyl bromide (0.24 mL, 2.00 mmol) was added and stirred for 10 minutes at 50 °C. (*R*)-BINOL (0.286 g, 1.00 mmol) was added, and the mixture was stirred at 50 °C for 48 hours. A white precipitate formed which was isolated by vacuum filtration to yield **219** (0.474 g,

70% yield).

Enantioenrichment of the ammonium salt measured by ^1H NMR spectroscopy using (Δ ,*R*)-BINPHAT as a chiral shift reagent: er 95:5 (*R*:*S*).

^1H NMR (599 MHz, CD_3OD) δ 7.87 (2H, d, J = 8.9 Hz, H_d), 7.83 (2H, d, J = 8.1 Hz, H_f), 7.58 – 7.48 (5H, m, H_{1+2+3}), 7.41 – 7.36 (1H, m, H_{17}), 7.30 (2H, d, J = 8.9 Hz, H_i), 7.28 – 7.22 (6H, m, $\text{H}_{11+16+g}$), 7.22 – 7.18 (1H, m, H_{12}), 7.17 – 7.11 (4H, m, H_{10+h}), 7.02 (2H, d, J = 8.5 Hz, H_c), 6.96 (2H, dd, J = 8.2, 1.4 Hz, H_{15}), 5.02 (1H, d, J = 12.8 Hz, H_{13}), 4.86 (1H, d, J = 12.6 Hz, $\text{H}_{13'}$), 4.20 (1H, td, J = 12.7, 4.0 Hz, H_6), 3.85 (1H, td, J = 12.9, 5.2 Hz, $\text{H}_{6'}$), 3.39 (3H, s, H_5), 2.70 (1H, dt, J = 14.2, 7.2 Hz, H_8), 2.62 (1H, dt, J = 14.2, 7.4 Hz, $\text{H}_{8'}$), 2.05 (1H, ttd, J = 12.6, 5.9, 4.2 Hz, H_7), 1.48 (1H, ttd, J = 11.8, 7.5, 3.9 Hz, $\text{H}_{7'}$).

^{13}C NMR (151 MHz, CD_3OD) δ 154.2 (C_b), 142.7 (C_4), 141.0 (C_{14}), 135.8 (C_j), 133.8 (C_{15}), 131.8 (C_{17}), 131.7 (C_1), 131.6 (C_2), 130.6 (C_d), 130.4 (C_e), 129.8 (C_{16}), 129.7 (C_{11}), 129.5 (C_{10}), 129.0 (C_f), 128.5 (C_9), 127.6 (C_{12}), 127.1 (C_h), 125.8 (C_c), 123.8 (C_g), 123.3 (C_3), 119.3 (C_i), 116.2 (C_k), 75.2 (C_{13}), 67.6 (C_6), 47.3 (C_5), 32.9 (C_8), 25.7 (C_7).

LRMS (ESI-TOF, EI^+) m/z : 316.9 ($[\text{M}]^+$, 100%).

LRMS (ESI-TOF, EI^-) m/z : 285.4 ($[\text{M}-\text{H}]^-$, 100%).

HRMS (ESI-TOF) m/z : $[\text{M}]^+$ calculated for $\text{C}_{19}\text{H}_{24}\text{N}^+$: 316.2065, found 316.2075. $[\text{M}-\text{H}]^-$ calculated for $\text{C}_{20}\text{H}_{13}\text{O}_2^-$: 285.0916, found 285.0906.

mp: 142 °C (MeCN precipitate).

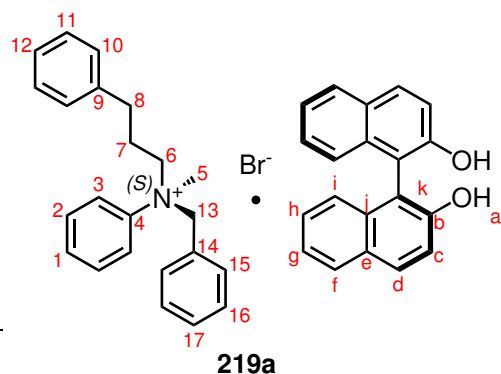
Optical rotation: $[\alpha]_D^{20} = -28.48$ (MeOH, $c = 1.21$).

IR ($\text{max}/\text{cm}^{-1}$): 3161br, 1620w, 1505w, 1430w, 1323m, 1271s, 816s, 748s, 686s.

9.8. CIAT OF AMMONIUM SALTS

XRD: A portion of the complex was crystallised in EtOH to give clear colourless prisms. Crystal data for $C_{43}H_{40}BrNO_2 \cdot 0.2(H_2O)$ ($m = 686.27$ g/mol): Orthorhombic, space group $P2_12_12_1$ (no. 19).

(S)-N-benzyl, N-methyl, N-hydrocinnamyl anilinium bromide · (S)-1,1'-bi-2-naphthol



Following the general procedure outlined in 9.8.1, **178** (0.223 g, 0.99 mmol) was dissolved in MeCN (0.50 mL, 2.0 M) and benzyl bromide (0.24 mL, 2.00 mmol) was added and stirred for 10 minutes at 50 °C. (S)-BINOL (0.283 g, 0.99 mmol) was added, and the mixture was stirred at 50 °C for 48 hours. A white precipitate formed which was isolated by vacuum filtration to yield **219a** (0.473 g,

70% yield).

Enantioenrichment of the ammonium salt measured by 1H NMR spectroscopy using (Δ,R)-BINPHAT as a chiral shift reagent: er 3:97 ($R:S$).

1H NMR (599 MHz, CD_3OD) identical to that of **219**.

^{13}C NMR (151 MHz, CD_3OD) identical to that of **219**.

LRMS (ESI-TOF, EI^+) m/z : 316.2 ($[M]^+$, 100%).

LRMS (ESI-TOF, EI^-) m/z : 285.4 ($[M-H]^-$, 100%).

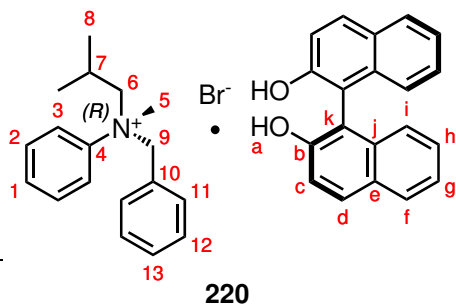
HRMS (ESI-TOF) m/z : $[M]^+$ calculated for $C_{23}H_{26}N^+$: 316.2065, found 316.2070.

mp: 148 – 149 °C ($CHCl_3$ precipitate).

Optical rotation: $[\alpha]_D^{20} = +30.12$ (MeOH, $c = 1.44$).

IR (max/cm^{-1}): 3154br, 1623w, 1505w, 1431w, 1329m, 1270s, 822s, 754s, 700s.

A portion of the complex was crystallised in EtOH to give clear colourless prisms. Crystal data for $C_{43}H_{40}BrNO_2 \cdot 0.2(H_2O)$ ($m = 686.27$ g/mol): Orthorhombic, space group $P2_12_12_1$ (no. 19).

(R)-N-benzyl, N-methyl, N-isobutyl anilinium bromide · (R)-1,1'-bi-2-naphthol

Following the general procedure outlined in 9.8.1, **174** (0.160 g, 0.98 mmol) was dissolved in MeCN (1.00 mL, 1.0 M) and benzyl bromide (0.24 mL, 2.00 mmol) was added and stirred for 10 minutes at 50 °C. (*R*)-BINOL (0.287 g, 1.00 mmol) was added, and the mixture was stirred at 50 °C for 48 hours.

A white precipitate formed which was isolated by vacuum filtration to yield **220** (0.279 g, 46% yield).

Enantioenrichment of the ammonium salt measured by chiral HPLC: er 93:7 (*R*:*S*).

¹H NMR (599 MHz, CD₃OD) δ 7.87 (2H, d, *J* = 8.9 Hz, H_d), 7.83 (2H, d, *J* = 8.1 Hz, H_f), 7.76 – 7.71 (2H, m, H₃), 7.64 – 7.59 (3H, m, H₁₊₂), 7.44 – 7.38 (1H, m, H₁₃), 7.29 (4H, dd, *J* = 8.3, 6.3 Hz, H_{12+i}), 7.27 – 7.22 (2H, m, H_g), 7.16 (2H, ddd, *J* = 8.3, 6.8, 1.4 Hz, H_h), 7.04 – 6.98 (4H, m, H_{11+c}), 5.13 (1H, d, *J* = 12.8 Hz, H₉), 4.88 (1H, d, *J* = 12.8 Hz, H₉), 4.28 (1H, dd, *J* = 13.6, 5.9 Hz, H₆), 3.80 (1H, dd, *J* = 13.6, 4.8 Hz, H₆), 3.46 (3H, s, H₅), 1.95 (1H, apt. dp, *J* = 12.9, 6.6 Hz, H₇), 1.09 (3H, d, *J* = 6.8 Hz, H₈), 0.67 (3H, d, *J* = 6.8 Hz, H₈).

¹³C NMR (151 MHz, CD₃OD) δ 154.2 (C_b), 143.1 (C₄), 135.8 (C_j), 133.9 (C₁₁), 131.9 (C₁₂), 131.9 (C₁), 131.5 (C₂), 130.6 (C_d), 130.5 (C_e), 129.8 (C₁₃), 129.0 (C_f), 128.5 (C₁₀), 127.1 (C_h), 125.8 (C_c), 123.83 (C_g), 123.78 (C₃), 119.3 (C_i), 116.2 (C_k), 76.2 (C₉), 75.8 (C₆), 46.8 (C₅), 25.8 (C₇), 22.9 (C₈), 22.1 (C₈).

LRMS (ESI-TOF, EI⁺) *m/z*: 254.8 ([M]⁺, 100%).

LRMS (ESI-TOF, EI⁻) *m/z*: 285.4 ([M-H]⁻, 100%).

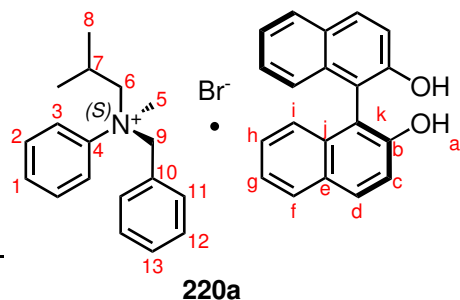
HRMS (ESI-TOF) *m/z*: [M]⁺ calculated for C₁₄H₂₂N⁺: 254.1909, found 254.1901. [M-H]⁻ calculated for C₂₀H₁₃O₂⁻: 285.0916, found 285.0916.

mp: 141 °C (CHCl₃ precipitate).

Optical rotation: [α]_D²⁰ = -35.09 (MeOH, c = 1.16).

IR (max/cm⁻¹): 3108br, 1621w, 1500w, 1337m, 1271s, 965w, 815s, 750s, 686s.

XRD: A portion of the complex was crystallised in EtOH to give clear colourless blocks. Crystal data for C₃₈H₃₈BrNO₂ (*m* = 620.60 g/mol): Orthorhombic, space group *P*2₁2₁2₁ (no. 19).

(S)-N-benzyl, N-methyl, N-isobutyl anilinium bromide · (S)-1,1'-bi-2-naphthol

Following the general procedure outlined in 9.8.1, **174** (0.163 g, 1.00 mmol) was dissolved in MeCN (1.00 mL, 1.0 M) and benzyl bromide (0.24 mL, 2.00 mmol) was added and stirred for 10 minutes at 50 °C. (S)-BINOL (0.287 g, 1.00 mmol) was added, and the mixture was stirred at 50 °C for 48 hours.

A white precipitate formed which was isolated

by vacuum filtration to yield **220a** (0.248 g, 40% yield).

Enantioenrichment of the ammonium salt measured by chiral HPLC: er 7:93 (*R*:*S*).

¹H NMR (599 MHz, CD₃OD) *identical to that of 220*.

¹³C NMR (151 MHz, CD₃OD) *identical to that of 220*.

LRMS (ESI-TOF, EI⁺) *m/z*: 254.2 ([M]⁺, 100%).

LRMS (ESI-TOF, EI⁻) *m/z*: 285.4 ([M-H]⁻, 100%).

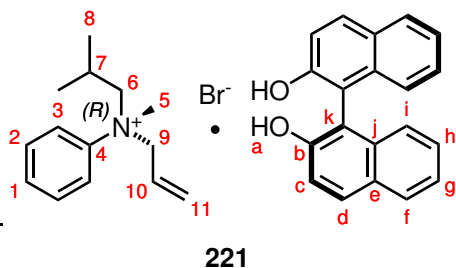
HRMS (ESI-TOF) *m/z*: [M]⁺ calculated for C₁₈H₂₄N⁺: 254.1909, found 254.1912.

mp: 146 °C (CHCl₃ precipitate).

Optical rotation: [α]_D²⁰ = +33.97 (MeOH, c = 1.12).

IR (max/cm⁻¹): 3104br, 1621w, 1500w, 1427w, 1336m, 1271s, 965w, 814s, 749s, 686s, 562w,.

XRD: A portion of the complex was crystallised in EtOH to give clear colourless blocks. Crystal data for C₃₈H₃₈BrNO₂ (m = 620.60 g/mol): Orthorhombic, space group *P*2₁2₁2₁ (no. 19).

(R)-N-allyl, N-methyl, N-isobutyl anilinium bromide · (R)-1,1'-bi-2-naphthol

Following the general procedure outlined in 9.8.1, **174** (0.165 g, 1.01 mmol) was dissolved in CHCl_3 (1.67 mL, 0.6 M) and allyl bromide (0.17 mL, 2.00 mmol) was added and stirred for 10 minutes at 50 °C. (*R*)-BINOL (0.286 g, 1.00 mmol) was added, and the mixture was stirred at 50 °C for 48 hours.

A white precipitate formed which was isolated by vacuum filtration to yield **221** (0.512 g, 90% yield).

Enantioenrichment of the ammonium salt measured by ^1H NMR spectroscopy using (Δ ,*R*)-BINPHAT as a chiral shift reagent: er 91:9 (*R*:*S*).

^1H NMR (599 MHz, CD_3OD) δ 7.87 (2H, d, $J = 8.9$ Hz, H_d), 7.82 (4H, apt. t, $J = 8.9$ Hz, H_{3+f}), 7.65 (2H, dd, $J = 7.4, 1.3$ Hz, H_2), 7.60 (1H, t, $J = 7.3$ Hz, H_1), 7.29 (2H, d, $J = 8.8$ Hz, H_i), 7.24 (2H, ddd, $J = 8.1, 6.7, 1.3$ Hz, H_g), 7.16 (2H, ddd, $J = 8.2, 6.8, 1.4$ Hz, H_h), 7.02 (2H, d, $J = 8.5$ Hz, H_c), 5.60 – 5.55 (2H, m, H_{11}), 5.55 – 5.51 (1H, m, H_{10}), 4.64 (1H, dd, $J = 13.2, 6.1$ Hz, H_9), 4.36 (1H, dd, $J = 12.9, 4.1$ Hz, H_9'), 3.98 (1H, dd, $J = 13.5, 6.1$ Hz, H_6), 3.69 (1H, dd, $J = 13.5, 4.6$ Hz, H_6'), 3.54 (3H, s, H_5), 1.98 – 1.94 (1H, m, H_7), 1.02 (3H, d, $J = 6.8$ Hz, H_8), 0.61 (3H, d, $J = 6.7$ Hz, H_8').

^{13}C NMR (151 MHz, CD_3OD) δ 154.2 (C_b), 143.5 (C_4), 135.8 (C_j), 131.7 (C_2), 131.7 (C_1), 130.6 (C_d), 130.5 (C_e), 129.35 (C_{10}), 129.0 (C_f), 127.1 (C_h), 126.0 (C_{11}), 125.8 (C_c), 123.8 (C_g), 123.2 (C_3), 119.3 (C_i), 116.2 (C_k), 76.6 (C_9), 73.4 (C_6), 47.7 (C_5), 25.5 (C_7), 22.8 (C_8), 22.0 (C_8').

LRMS (ESI-TOF, EI^+) m/z : 204.5 ($[\text{M}]^+$, 100%).

LRMS (ESI-TOF, EI^-) m/z : 285.4 ($[\text{M}-\text{H}]^-$, 100%).

HRMS (ESI-TOF) m/z : $[\text{M}]^+$ calculated for $\text{C}_{14}\text{H}_{22}\text{N}^+$: 204.1752, found 204.1743. $[\text{M}-\text{H}]^-$ calculated for $\text{C}_{20}\text{H}_{13}\text{O}_2^-$: 285.0916, found 285.0911.

mp: 164 °C (CHCl_3 precipitate).

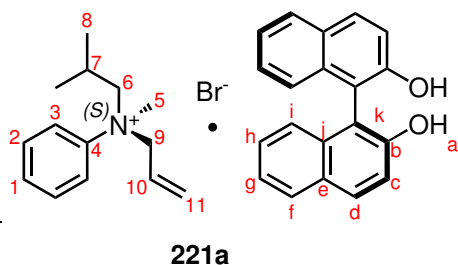
Optical rotation: $[\alpha]_D^{20} = +3.14$ (MeOH, $c = 1.08$).

IR ($\text{max}/\text{cm}^{-1}$): 3149br, 1623m, 1504m, 1430m, 1329m, 1272s, 954m, 815s, 751s, 686m, 422w.

XRD: A portion of the complex was crystallised in EtOH to give clear colourless blocks. Crystal data for $\text{C}_{34}\text{H}_{36}\text{BrNO}_2$ ($m = 570.55$ g/mol): Orthorhombic, space group

$P2_12_12_1$ (no. 19).

(S)-N-allyl, N-methyl, N-isobutyl anilinium bromide · (S)-1,1'-bi-2-naphthol



Following the general procedure outlined in 9.8.1, **174** (0.155 g, 0.95 mmol) was dissolved in CHCl_3 (1.67 mL, 0.6 M) and allyl bromide (0.17 mL, 2.00 mmol) was added and stirred for 10 minutes at 50 °C. (S)-BINOL (0.282 g, 0.99 mmol) was added, and the mixture was stirred at 50 °C for 48 hours.

A white precipitate formed which was isolated by vacuum filtration to yield **221a** (0.486 g, 90% yield).

Enantioenrichment of the ammonium salt measured by ^1H NMR spectroscopy using (Δ,R)-BINPHAT as a chiral shift reagent: er 5:95 ($R:S$).

^1H NMR (599 MHz, CD_3OD) *identical to that of 221*.

^{13}C NMR (151 MHz, CD_3OD) *identical to that of 221*.

LRMS (ESI-TOF, EI^+) m/z : 204.2 ($[\text{M}]^+$, 100%).

LRMS (ESI-TOF, EI^-) m/z : 285.4 ($[\text{M}-\text{H}]^-$, 100%).

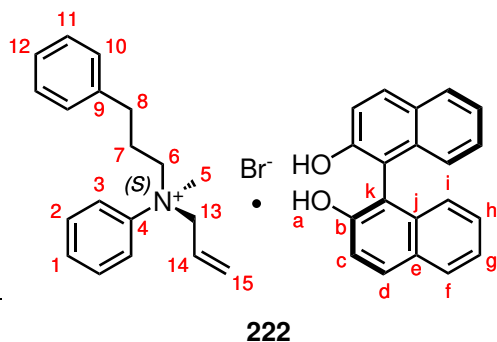
HRMS (ESI-TOF) m/z : $[\text{M}]^+$ calculated for $\text{C}_{14}\text{H}_{22}\text{N}^+$: 204.1752, found 204.1756.

mp: 163 °C (CHCl_3 precipitate).

Optical rotation: $[\alpha]_{\text{D}}^{20} = -2.64$ (MeOH, $c = 1.01$).

IR ($\text{max}/\text{cm}^{-1}$): 3150br, 1623w, 1430w, 1336m, 1271s, 954w, 815s, 752s, 688m.

XRD: A portion of the complex was crystallised in EtOH to give clear colourless blocks. Crystal data for $\text{C}_{34}\text{H}_{36}\text{BrNO}_2$ ($m = 570.55$ g/mol): Orthorhombic, space group $P2_12_12_1$ (no. 19).

(S)-N-allyl, N-methyl, N-hydrocinnamyl anilinium bromide · (R)-1,1'-bi-2-naphthol

Following the general procedure outlined in 9.8.1, **178** (0.224 g, 0.99 mmol) was dissolved in MeCN (0.50 mL, 2.0 M) and allyl bromide (0.17 mL, 2.00 mmol) was added and stirred for 10 minutes at 50 °C. (*R*)-BINOL (0.289 g, 1.00 mmol) was added, and the mixture was stirred at 50 °C for 48 hours.

A white precipitate formed which was isolated by vacuum filtration to yield **222** (0.499 g, 67% yield).

Enantioenrichment of the ammonium salt measured by ¹H NMR spectroscopy using (Λ,*R*)-BINPHAT as a chiral shift reagent: er 23:77 (*R*:*S*).

¹H NMR (599 MHz, CD₃OD) δ 7.87 (2H, d, *J* = 8.9 Hz, H_d), 7.83 (2H, d, *J* = 8.1 Hz, H_f), 7.67 (2H, d, *J* = 8.1, H₃), 7.65 – 7.55 (3H, m, H₁₊₂), 7.29 (2H, d, *J* = 8.9 Hz, H_i), 7.27 – 7.22 (4H, m, H_{11+g}), 7.21 – 7.16 (1H, m, H₁₂) 7.15 (2H, ddd, *J* = 8.1, 6.7, 1.4 Hz, H_h), 7.10 (2H, dd, *J* = 8.1, 1.2 Hz, H₁₀), 7.02 (2H, d, *J* = 8.5 Hz, H_c), 5.63 – 5.49 (3H, m, H₁₄₊₁₅), 4.58 (1H, dd, *J* = 13.2, 5.7 Hz, H₁₃), 4.35 (1H, dd, *J* = 13.2, 7.0 Hz, H_{13'}), 3.99 (1H, td, *J* = 12.6, 4.1 Hz, H₆), 3.78 (1H, td, *J* = 12.8, 5.1 Hz, H_{6'}), 3.49 (3H, s, H₅), 2.66 (1H, dt, *J* = 14.4, 7.3 Hz, H₈), 2.58 (1H, dt, *J* = 14.3, 7.5 Hz, H_{8'}), 2.07 – 1.96 (1H, m, H₇), 1.51 (1H, ttd, *J* = 12.0, 7.5, 4.1 Hz, H_{7'}).

¹³C NMR (151 MHz, CD₃OD) δ 154.2 (C_b), 143.2 (C₄), 140.9 (C₉), 135.8 (C_j), 131.8 (C₂), 131.7 (C₁), 130.6 (C_d), 130.5 (C_e), 129.7 (C₁₀), 129.4 (C₁₁), 129.3 (C₁₄), 129.0 (C_f), 127.6 (C₁₂), 127.1 (C_h), 126.0 (C₁₅), 125.8 (C_c), 123.8 (C_g), 122.8 (C₃), 119.3 (C_i), 116.2 (C_k), 72.5 (C₁₃), 68.3 (C₆), 48.0 (C₅), 32.8 (C₇), 25.7 (C₈).

LRMS (ESI-TOF, EI⁺) *m/z*: 266.8 ([M]⁺, 100%).

LRMS (ESI-TOF, EI⁻) *m/z*: 285.4 ([M-H]⁻, 100%).

HRMS (ESI-TOF) *m/z*: [M]⁺ calculated for C₁₉H₂₄N⁺: 266.1909, found 266.1918. [M-H]⁻ calculated for C₂₀H₁₃O₂⁻: 285.0916, found 285.0911.

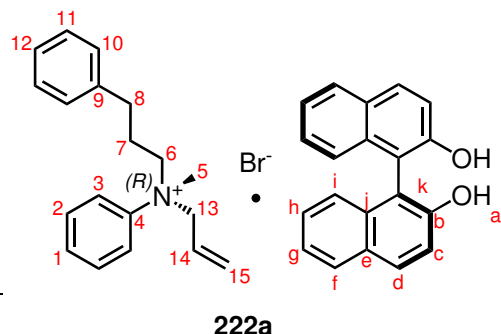
mp: 107 °C (MeCN precipitate).

Optical rotation: [α]_D²⁰ = +23.19 (MeOH, *c* = 1.44).

IR (max/cm⁻¹): 3171br, 1625m, 1505m, 1431m, 1269s, 815m, 752m, 690m.

XRD: A portion of the complex was crystallised in EtOH to give clear colourless prisms.

Crystal data for C₃₉H₃₈BrNO₂ (*m* = 632.61 g/mol): Triclinic, space group *P1* (no. 2).

(R)-N-allyl, N-methyl, N-hydrocinnamyl anilinium bromide · (S)-1,1'-bi-2-naphthol

Following the general procedure outlined in 9.8.1, **178** (0.228 g, 1.01 mmol) was dissolved in MeCN (0.50 mL, 2.0 M) and allyl bromide (0.17 mL, 2.00 mmol) was added and stirred for 10 minutes at 50 °C. (S)-BINOL (0.283 g, 0.99 mmol) was added, and the mixture was stirred at 50 °C for 48 hours. A white precipitate formed which was isolated

by vacuum filtration to yield **222a** (0.435 g, 67% yield).

Enantioenrichment of the ammonium salt measured by ^1H NMR spectroscopy using (Δ ,*R*)-BINPHAT as a chiral shift reagent: er 74:26 (*R*:*S*).

^1H NMR (599 MHz, CD_3OD) identical to that of **222**.

^{13}C NMR (151 MHz, CD_3OD) identical to that of **222**.

LRMS (ESI-TOF, EI^+) m/z : 266.2 ($[\text{M}]^+$, 100%).

LRMS (ESI-TOF, EI^-) m/z : 285.4 ($[\text{M}-\text{H}]^-$, 100%).

HRMS (ESI-TOF) m/z : $[\text{M}]^+$ calculated for $\text{C}_{19}\text{H}_{24}\text{N}^+$: 266.1909, found 266.1921.

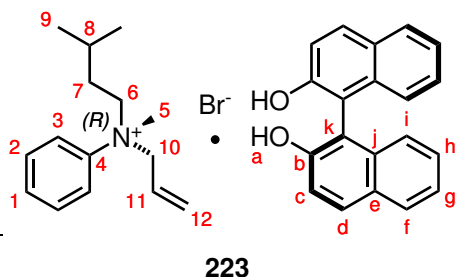
mp: 109 °C (CHCl_3 precipitate).

Optical rotation: $[\alpha]_{\text{D}}^{20} = -20.59$ (MeOH, $c = 1.25$).

IR ($\text{max}/\text{cm}^{-1}$): 3178br, 1620m, 1505m, 1430m, 1271s, 966m, 815s, 748s, 686s.

XRD: A portion of the complex was crystallised in EtOH to give clear colourless prisms.

Crystal data for $\text{C}_{39}\text{H}_{38}\text{BrNO}_2$ ($m = 632.61$ g/mol): Triclinic, space group *P*1 (no. 2).

(R)-N-allyl, N-methyl, N-isovaleryl anilinium bromide · (R)-1,1'-bi-2-naphthol

Following the general procedure outlined in 9.8.1, **175** (0.178 g, 1.00 mmol) was dissolved in CHCl_3 (1.67 mL, 0.6 M) and allyl bromide (0.17 mL, 2.00 mmol) was added and stirred for 10 minutes at 50 °C. (*R*)-BINOL (0.285 g, 0.99 mmol) was added, and the mixture was stirred at 50 °C for 48 hours.

A white precipitate formed which was isolated by vacuum filtration to yield **223** (0.449 g, 77% yield).

Enantioenrichment of the ammonium salt measured by chiral HPLC: er 75:25 (*R*:*S*).

^1H NMR (599 MHz, CD_3OD) δ 7.87 (2H, d, $J = 8.9$ Hz, H_d), 7.83 (2H, d, $J = 8.2$ Hz, H_f), 7.77 (2H, d, $J = 8.1$, H_3), 7.65 (2H, t, $J = 7.4$ Hz, H_2), 7.60 (1H, t, $J = 7.3$ Hz, H_1), 7.29 (2H, d, $J = 8.9$ Hz, H_i), 7.24 (2H, ddd, $J = 8.1$, 6.7, 1.2 Hz, H_g), 7.16 (2H, ddd, $J = 8.2$, 6.7, 1.3 Hz, H_h), 7.02 (2H, dd, $J = 8.4$, 1.2 Hz, H_c), 5.64 – 6.59 (1H, m, H_{11}), 5.58 – 5.52 (2H, m, H_{12}), 4.63 (1H, dd, $J = 13.2$, 5.7 Hz, H_{10}), 4.39 (1H, dd, $J = 13.2$, 7.1 Hz, $\text{H}_{10'}$), 4.07 (1H, td, $J = 12.5$, 4.3 Hz, H_6), 3.81 (1H, td, $J = 12.5$, 4.7 Hz, H_6'), 3.50 (3H, s, H_5), 1.69 – 1.49 (2H, m, H_7), 1.09 – 1.03 (1H, m, H_8), 0.91 (3H, d, $J = 6.4$ Hz, H_9), 0.86 (3H, d, $J = 6.4$ Hz, H_9').

^{13}C NMR (151 MHz, CD_3OD) δ 154.2 (C_b), 143.3 (C_4), 135.8 (C_j), 131.8 (C_2), 131.7 (C_1), 130.6 (C_d), 130.5 (C_e), 129.2 (C_{11}), 129.0 (C_f), 127.1 (C_h), 126.1 (C_{12}), 125.8 (C_c), 123.8 (C_g), 122.9 (C_3), 119.3 (C_i), 116.2 (C_k), 72.6 (C_{10}), 68.1 (C_6), 47.7 (C_5), 32.3 (C_7), 27.3 (C_8), 22.54 (C_9), 22.48 (C_9').

LRMS (ESI-TOF, EI^+) m/z : 218.6 ($[\text{M}]^+$, 100%).

LRMS (ESI-TOF, EI^-) m/z : 285.4 ($[\text{M}-\text{H}]^-$, 100%).

HRMS (ESI-TOF) m/z : $[\text{M}]^+$ calculated for $\text{C}_{15}\text{H}_{24}\text{N}^+$: 218.1909, found 218.1919. $[\text{M}-\text{H}]^-$ calculated for $\text{C}_{20}\text{H}_{13}\text{O}_2^-$: 285.0916, found 285.0930.

mp: 159 °C (CHCl_3 precipitate).

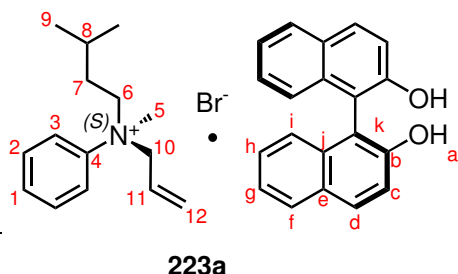
Optical rotation: $[\alpha]_D^{20} = +14.58$ (MeOH, $c = 1.14$).

IR ($\text{max}/\text{cm}^{-1}$): 3148br, 1624m, 1503m, 1431m, 1328m, 1271s, 956m, 815m, 744m, 687m, 422m.

XRD: A portion of the complex was crystallised in EtOH to give clear colourless prisms. Crystal data for $\text{C}_{35}\text{H}_{38}\text{BrNO}_2$ ($m = 584.57$ g/mol): Orthorhombic, space group

$P2_12_12_1$ (no. 19).

(S)-N-allyl, N-methyl, N-isovaleryl anilinium bromide · (S)-1,1'-bi-2-naphthol



Following the general procedure outlined in 9.8.1, **175** (0.178 g, 1.00 mmol) was dissolved in CHCl_3 (1.67 mL, 0.6 M) and allyl bromide (0.17 mL, 2.00 mmol) was added and stirred for 10 minutes at 50 °C. (S)-BINOL (0.286 g, 1.00 mmol) was added, and the mixture was stirred at 50 °C for 48 hours.

A white precipitate formed which was isolated by vacuum filtration to yield **223a** (0.464 g, 80% yield).

Enantioenrichment of the ammonium salt measured by chiral HPLC: er 28:72 (*R*:*S*).

^1H NMR (599 MHz, CD_3OD) identical to that of **223**.

^{13}C NMR (151 MHz, CD_3OD) identical to that of **223**.

LRMS (ESI-TOF, EI^+) m/z : 218.2 ($[\text{M}]^+$, 100%).

LRMS (ESI-TOF, EI^-) m/z : 285.4 ($[\text{M}-\text{H}]^-$, 100%).

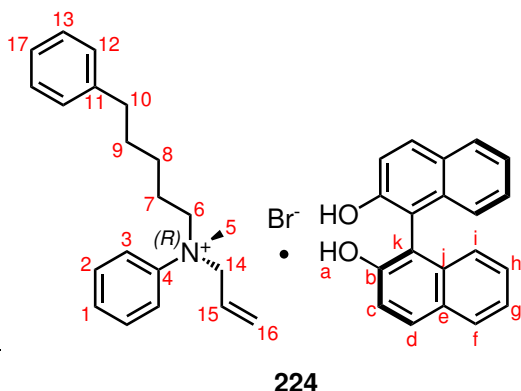
HRMS (ESI-TOF) m/z : $[\text{M}]^+$ calculated for $\text{C}_{15}\text{H}_{24}\text{N}^+$: 218.1909, found 218.1913.

mp: 166 – 167 °C (CHCl_3 precipitate).

Optical rotation: $[\alpha]_{\text{D}}^{20} = -14.42$ (MeOH, $c = 1.18$).

IR ($\text{max}/\text{cm}^{-1}$): 3150br, 1625w, 1503w, 1431w, 1329m, 1271s, 956m, 816s, 744m, 688m.

XRD: A portion of the complex was crystallised in EtOH to give clear colourless prisms. Crystal data for $\text{C}_{35}\text{H}_{38}\text{BrNO}_2$ ($m = 584.57$ g/mol): Orthorhombic, space group $P2_12_12_1$ (no. 19).

(R)-N-allyl, N-methyl, N-5-phenylvaleryl anilinium bromide · (R)-1,1'-bi-2-naphthol

Following the general procedure outlined in 9.8.1, **185** (0.256 g, 1.01 mmol) was dissolved in CHCl_3 (1.00 mL, 1.0 M) and allyl bromide (0.17 mL, 2.00 mmol) was added and stirred for 10 minutes at 50 °C. (R)-BINOL (0.287 g, 1.00 mmol) was added, and the mixture was stirred at 50 °C for 48 hours. A white precipitate formed which was isolated by vacuum fil-

tration to yield **224** (0.326 g, 49% yield).

Enantioenrichment of the ammonium salt measured by ^1H NMR spectroscopy using (Δ ,R)-BINPHAT as a chiral shift reagent: er 67:33 (R:S). Assignment of absolute configuration derived from the empirical selectivity model based on other ammonium cations synthesised by the same methodology.

^1H NMR (599 MHz, CD_3OD) δ 7.87 (2H, d, $J = 8.9$ Hz, H_d), 7.83 (2H, d, $J = 8.2$ Hz, H_f), 7.75 – 7.71 (2H, m, H_3), 7.64 (2H, t, $J = 7.8$ Hz, H_2), 7.59 (1H, t, $J = 7.3$ Hz, H_1), 7.30 (2H, d, $J = 8.9$ Hz, H_i), 7.26 – 7.19 (4H, m, 4H_{g+12}), 7.18 – 7.11 (3H, m, H_{h+17}), 7.11 – 7.07 (2H, m, H_{13}), 7.02 (2H, d, $J = 8.5$ Hz, H_c), 5.63 – 5.55 (2H, m, H_{15+16}), 5.55 – 5.50 (1H, m, H_{15}), 4.57 (1H, dd, $J = 13.2, 5.8$ Hz, H_{14}), 4.34 (1H, dd, $J = 13.2, 7.2$ Hz, H_{14}), 3.96 (1H, tt, $J = 12.6, 3.7$ Hz, H_6), 3.72 (1H, td, $J = 12.4, 5.0$ Hz, H_6), 3.47 (3H, s, H_5), 2.53 (2H, t, $J = 7.5$ Hz, H_{10}), 1.69 – 1.61 (1H, m, H_7), 1.57 (2H, p, $J = 7.6$ Hz, H_9), 1.36 – 1.23 (2H, m, H_8), 1.23 – 1.19 (1H, m, H_7).

^{13}C NMR (151 MHz, CD_3OD) δ 154.2 (C_b), 143.3 (C_4), 142.1 (C_{11}), 135.8 (C_j), 131.8 (C_2), 131.6 (C_1), 130.6 (C_d), 130.4 (C_e), 129.4 (C_{12}), 129.3 (C_{15}), 129.2 (C_{17}), 129.0 (C_f), 127.1 (C_h), 126.8 (C_{12}), 126.1 (C_{16}), 125.8 (C_c), 123.8 (C_g), 122.8 (C_3), 119.3 (C_i), 116.2 (C_k), 72.5 (C_6), 69.0 (C_7), 47.7 (C_5), 36.3 (C_{10}), 31.7 (C_9), 26.5 (C_8), 23.7 (C_7).

LRMS (ESI-TOF, EI^+) m/z : 294.2 ($[\text{M}]^+$, 100%).

LRMS (ESI-TOF, EI^-) m/z : 285.4 ($[\text{M}-\text{H}]^-$, 100%).

HRMS (ESI-TOF) m/z : $[\text{M}]^+$ calculated for $\text{C}_{21}\text{H}_{28}\text{N}^+$: 294.2222, found 294.2236.

mp: 156 – 157 °C (MeCN precipitate).

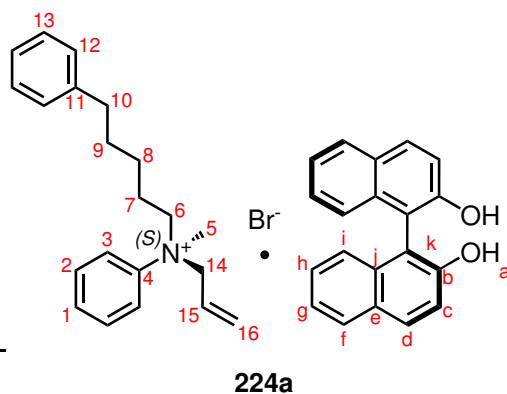
Optical rotation: $[\alpha]_D^{20} = +10.15$ (MeOH, $c = 0.96$).

9.8. CIAT OF AMMONIUM SALTS

IR (max/cm⁻¹): 3150br, 1623w, 1504m, 1431m, 1271s, 951m, 822s, 688s.

XRD: *SCXRD quality single crystals could not be recrystallised for this complex.*

(*S*)-*N*-allyl, *N*-methyl, *N*-5-phenylvaleryl anilinium bromide · (*S*)-1,1'-bi-2-naphthol



Following the general procedure outlined in 9.8.1, **185** (0.250 g, 0.99 mmol) was dissolved in CHCl₃ (1.00 mL, 1.0 M) and allyl bromide (0.17 mL, 2.00 mmol) was added and stirred for 10 minutes at 50 °C. (*S*)-BINOL (0.287 g, 1.00 mmol) was added, and the mixture was stirred at 50 °C for 48 hours. A white precipitate formed which was isolated by vacuum fil-

tration to yield **224a** (0.349 g, 54% yield).

Enantioenrichment of the ammonium salt measured by ¹H NMR spectroscopy using (Δ,*R*)-BINPHAT as a chiral shift reagent: er 38:62 (*R*:*S*). *Assignment of absolute configuration derived from the empirical selectivity model based on other ammonium cations synthesised by the same methodology.*

¹H NMR (599 MHz, CD₃OD) *identical to that of 224.*

¹³C NMR (151 MHz, CD₃OD) *identical to that of 224.*

LRMS (ESI-TOF, EI⁺) *m/z*: 294.2 ([M]⁺, 100%).

LRMS (ESI-TOF, EI⁻) *m/z*: 285.4 ([M-H]⁻, 100%).

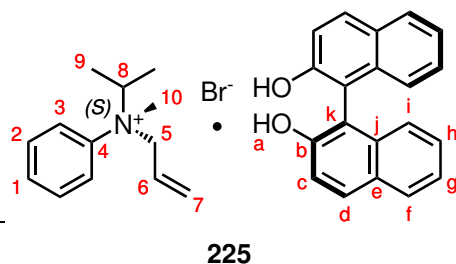
HRMS (ESI-TOF) *m/z*: [M]⁺ calculated for C₂₁H₂₈N⁺: 294.2222, found 294.2233.

mp: 152 – 154 °C (CHCl₃ precipitate).

Optical rotation: [α]_D²⁰ = -7.84 (MeOH, c = 1.00).

IR (max/cm⁻¹): 3227br, 1624w, 1507w, 1323m, 1268s, 980m, 816s, 749s, 700s.

XRD: *SCXRD quality single crystals could not be recrystallised for this complex.*

(S)-N-allyl, N-methyl, N-isopropyl anilinium bromide · (R)-1,1'-bi-2-naphthol

Following the general procedure outlined in 9.8.1, **183** (0.150 g, 1.00 mmol) was dissolved in CHCl_3 (1.67 mL, 0.6 M) and allyl bromide (0.17 mL, 2.00 mmol) was added and stirred for 10 minutes at 50 °C. (*R*)-BINOL (0.287 g, 1.00 mmol) was added, and the mixture was stirred at 50 °C for 48 hours.

A white precipitate formed which was isolated by vacuum filtration to yield **225** (0.398 g, 71% yield).

Enantioenrichment of the ammonium salt measured by ^1H NMR spectroscopy using (Δ ,*R*)-BINPHAT as a chiral shift reagent: er 34:66 (*R*:*S*).

^1H NMR (599 MHz, CD_3OD) δ 7.87 (2H, d, $J = 8.9$ Hz, H_d), 7.83 (2H, d, $J = 8.2$, 1.3 Hz, H_f), 7.73 – 7.69 (2H, m, H_3), 7.64 – 7.58 (2H, m, H_2), 7.58 – 7.54 (1H, m, H_1), 7.30 (2H, d, $J = 8.9$ Hz, H_i), 7.24 (2H, ddd, $J = 8.1$, 6.6, 1.2 Hz, H_g), 7.15 (2H, ddd, $J = 8.2$, 6.7, 1.3 Hz, H_h), 7.02 (2H, dd, $J = 8.5$, 1.3 Hz, H_c), 5.60 – 5.34 (3H, m, H_{6+7}), 4.68 (1H, dd, $J = 13.3$, 5.1 Hz, H_5), 4.43– 4.31 (2H, m, $\text{H}_{5'+8}$), 3.30 (3H, s, H_{10}), 1.54 (3H, d, $J = 6.4$ Hz, H_9), 1.03 (3H, d, $J = 6.6$ Hz, $\text{H}_{9'}$).

^{13}C NMR (151 MHz, CD_3OD) δ 154.2 (C_b), 143.8 (C_4), 135.8 (C_j), 131.6 (C_2), 131.5 (C_1), 130.6 (C_d), 130.5 (C_e), 129.0 (C_f), 128.5 (C_7), 127.1 (C_h), 126.6 (C_6), 125.8 (C_c), 123.8 (C_g), 123.3 (C_3), 119.3 (C_i), 116.2 (C_k), 73.2 (C_8), 68.6 (C_5), 41.5 (C_{10}), 17.3 (C_9), 17.1 ($\text{C}_{9'}$).

LRMS (ESI-TOF, EI^+) m/z : 190.2 ($[\text{M}]^+$, 100%).

LRMS (ESI-TOF, EI^-) m/z : 285.4 ($[\text{M}-\text{H}]^-$, 100%).

HRMS (ESI-TOF) m/z : $[\text{M}]^+$ calculated for $\text{C}_{13}\text{H}_{20}\text{N}^+$: 190.1596, found 190.1600. $[\text{M}-\text{H}]^-$ calculated for $\text{C}_{20}\text{H}_{13}\text{O}_2^-$: 285.0916, found 285.0915.

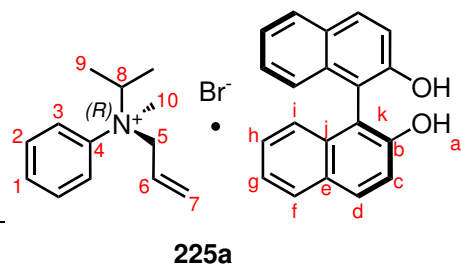
mp: 151 – 152 °C (CHCl_3 precipitate).

Optical rotation: $[\alpha]_D^{20} = +4.75$ (MeOH, $c = 0.50$).

IR ($\text{max}/\text{cm}^{-1}$): 3121br, 1623w, 1506w, 1273m, 950w, 813m, 688m.

XRD: A portion of the complex was crystallised in EtOH to give clear colourless plates.

Crystal data for $\text{C}_{32}\text{H}_{35}\text{BrNO}_2$ ($m = 542.52$ g/mol): Tetragonal, space group $P4_3$ (no. 78).

(R)-N-allyl, N-methyl, N-isopropyl anilinium bromide · (S)-1,1'-bi-2-naphthol

Following the general procedure outlined in 9.8.1, **183** (0.148 g, 1.00 mmol) was dissolved in CHCl_3 (1.67 mL, 0.6 M) and allyl bromide (0.17 mL, 2.00 mmol) was added and stirred for 10 minutes at 50 °C. (S)-BINOL (0.285 g, 1.00 mmol) was added, and the mixture was stirred at 50 °C for 48 hours.

A white precipitate formed which was isolated by vacuum filtration to yield **225a** (0.357 g, 65% yield).

Enantioenrichment of the ammonium salt measured by ^1H NMR spectroscopy using (Δ ,*R*)-BINPHAT as a chiral shift reagent: er 67:33 (*R*:*S*).

^1H NMR (599 MHz, CD_3OD) *identical to that of 225*.

^{13}C NMR (151 MHz, CD_3OD) *identical to that of 225*.

LRMS (ESI-TOF, EI^+) m/z : 190.1598 ($[\text{M}]^+$, 100%).

LRMS (ESI-TOF, EI^-) m/z : 285.4 ($[\text{M}-\text{H}]^-$, 100%).

HRMS (ESI-TOF) m/z : $[\text{M}]^+$ calculated for $\text{C}_{13}\text{H}_{20}\text{N}^+$: 190.1596, found 190.1598.

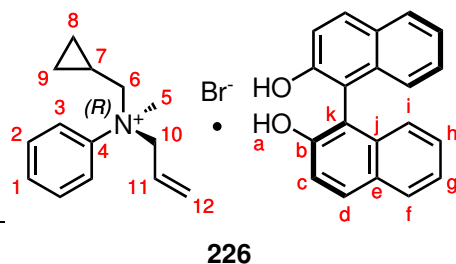
mp: 151 – 152 °C (CHCl_3 precipitate).

Optical rotation: $[\alpha]_{\text{D}}^{20} = -5.33$ (MeOH, $c = 1.00$).

IR ($\text{max}/\text{cm}^{-1}$): 3164br, 1620w, 1505w, 1277m, 984w, 812s, 680m.

XRD: A portion of the complex was crystallised in EtOH to give clear colourless plates.

Crystal data for $\text{C}_{32}\text{H}_{35}\text{BrNO}_2$ ($m = 542.52$ g/mol): Tetragonal, space group $P4_3$ (no. 78).

(R)-N-allyl, N-methyl, N-homocyclopropyl anilinium bromide · (R)-1,1'-bi-2-naphthol

Following the general procedure outlined in 9.8.1, **172** (0.159 g, 0.99 mmol) was dissolved in CHCl_3 (1.67 mL, 0.6 M) and allyl bromide (0.17 mL, 2.00 mmol) was added and stirred for 10 minutes at 50 °C. (*R*)-BINOL (0.287 g, 1.00 mmol) was added, and the mixture was stirred at 50 °C for 48 hours.

A white precipitate formed which was isolated by vacuum filtration to yield **226** (0.529 g, 93% yield).

Enantioenrichment of the ammonium salt measured by ^1H NMR spectroscopy using (Δ ,*R*)-BINPHAT as a chiral shift reagent: er 62:38 (*R*:*S*).

^1H NMR (599 MHz, CD_3OD) δ 7.87 (2H, d, $J = 8.9$ Hz, H_d), 7.83 (2H, d, $J = 8.1$ Hz, H_f), 7.79 (2H, d, $J = 8.1$, H_3), 7.64 (2H, td, $J = 7.4, 1.5$ Hz, H_2), 7.59 (1H, t, $J = 7.3$ Hz, H_1), 7.30 (2H, d, $J = 8.9$ Hz, H_i), 7.24 (2H, ddd, $J = 8.0, 6.7, 1.2$ Hz, H_g), 7.16 (2H, ddd, $J = 8.2, 6.7, 1.3$ Hz, H_h), 7.02 (2H, d, $J = 8.5$ Hz, H_c), 5.63 – 5.53 (2H, m, H_{12}), 5.53 – 5.49 (1H, m, H_{11}), 4.67 (1H, dd, $J = 13.1, 4.5$ Hz, H_{10}), 4.35 (1H, dd, $J = 13.1, 4.3$ Hz, $\text{H}_{10'}$), 4.02 (1H, dd, $J = 13.3, 6.2$ Hz, H_6), 3.61 (1H, dd, $J = 13.4, 7.9$ Hz, H_6'), 3.58 (3H, s, H_5), 0.83 – 0.79 (1H, m, H_7), 0.70 (1H, ddt, $J = 13.7, 8.5, 5.5$ Hz, H_8), 0.53 (1H, ddt, $J = 14.0, 8.7, 5.5$ Hz, H_9), 0.44 (1H, ddt, $J = 9.6, 6.2, 4.9$ Hz, H_9), 0.14 (1H, dtd, $J = 11.4, 5.6, 4.2$ Hz, H_8).

^{13}C NMR (151 MHz, CD_3OD) δ 154.2 (C_b), 143.9 (C_4), 135.8 (C_j), 131.64 (C_2), 131.57 (C_1), 130.6 (C_d), 130.4 (C_e), 129.03 (C_f), 129.01 (C_{12}), 127.1 (C_h), 126.1 (C_3), 125.8 (C_c), 123.8 (C_g), 123.1 (C_{11}), 119.3 (C_i), 116.2 (C_k), 74.7 (C_{10}), 71.2 (C_6), 47.9 (C_5), 5.9 (C_8), 5.8 (C_9), 4.1 (C_7).

LRMS (ESI-TOF, EI^+) m/z : 202.7 ($[\text{M}]^+$, 100%).

LRMS (ESI-TOF, EI^-) m/z : 285.4 ($[\text{M}-\text{H}]^-$, 100%).

HRMS (ESI-TOF) m/z : $[\text{M}]^+$ calculated for $\text{C}_{14}\text{H}_{20}\text{N}^+$: 202.1596, found 202.1598. $[\text{M}-\text{H}]^-$ calculated for $\text{C}_{20}\text{H}_{13}\text{O}_2^-$: 285.0916, found 285.0927.

mp: 171 °C (MeCN precipitate).

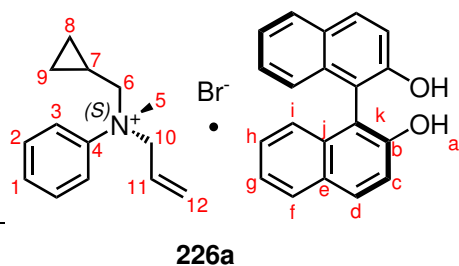
Optical rotation: $[\alpha]_D^{20} = +19.25$ (MeOH, $c = 1.04$).

IR ($\text{max}/\text{cm}^{-1}$): 3178br, 1623m, 1505m, 1431m, 1330m, 1274s, 931m, 822s, 694m, 439m.

9.8. CIAT OF AMMONIUM SALTS

XRD: A portion of the complex was crystallised in EtOH to give clear colourless plates. Crystal data for $C_{34}H_{34}BrNO_2$ ($m = 568.56$ g/mol): Tetragonal, space group $P4_1$ (no. 76).

(S)-N-allyl, N-methyl, N-homocyclopropyl anilinium bromide · (S)-1,1'-bi-2-naphthol



Following the general procedure outlined in 9.8.1, **172** (0.167 g, 1.04 mmol) was dissolved in $CHCl_3$ (1.67 mL, 0.6 M) and allyl bromide (0.17 mL, 2.00 mmol) was added and stirred for 10 minutes at 50 °C. (S)-BINOL (0.287 g, 1.00 mmol) was added, and the mixture was stirred at 50 °C for 48 hours.

A white precipitate formed which was isolated by vacuum filtration to yield **226a** (0.543 g, 96% yield).

Enantioenrichment of the ammonium salt measured by 1H NMR spectroscopy using (Δ,R)-BINPHAT as a chiral shift reagent: er 38:62 ($R:S$).

1H NMR (599 MHz, CD_3OD) identical to that of **226**.

^{13}C NMR (151 MHz, CD_3OD) identical to that of **226**.

LRMS (ESI-TOF, EI^+) m/z : 202.2 ($[M]^+$, 100%).

LRMS (ESI-TOF, EI^-) m/z : 285.4 ($[M-H]^-$, 100%).

HRMS (ESI-TOF) m/z : $[M]^+$ calculated for $C_{14}H_{20}N^+$: 202.1596, found 202.1606.

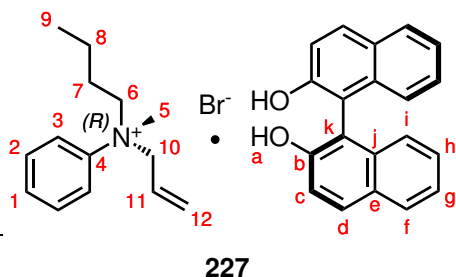
mp: 179 – 180 °C ($CHCl_3$ precipitate).

Optical rotation: $[\alpha]_D^{20} = -20.23$ (MeOH, $c = 1.00$).

IR (max/cm^{-1}): 3180br, 1623w, 1505w, 1433w, 1326m, 1274s, 823s, 755m, 694m.

XRD: A portion of the complex was crystallised in EtOH to give clear colourless plates.

Crystal data for $C_{34}H_{34}BrNO_2$ ($m = 568.56$ g/mol): Tetragonal, space group $P4_1$ (no. 76).

(R)-N-allyl, N-methyl, N-butyl anilinium bromide · (R)-1,1'-bi-2-naphthol

Following the general procedure outlined in 9.8.1, **173** (0.167 g, 1.02 mmol) was dissolved in CHCl_3 (1.67 mL, 0.6 M) and allyl bromide (0.17 mL, 2.00 mmol) was added and stirred for 10 minutes at 50 °C. (*R*)-BINOL (0.286 g, 1.00 mmol) was added, and the mixture was stirred at 50 °C for 48 hours.

A white precipitate formed which was isolated by vacuum filtration to yield **227** (0.482 g, 85% yield).

Enantioenrichment of the ammonium salt measured by chiral HPLC: er 59:41 (*R*:*S*).

^1H NMR (599 MHz, CD_3OD) δ 7.87 (2H, d, $J = 8.9$ Hz, H_d), 7.83 (2H, d, $J = 8.1$ Hz, H_f), 7.78 (2H, d, $J = 8.1$ Hz, H_3), 7.66 (2H, apt. t, $J = 8.9$ Hz, H_2), 7.60 (1H, t, $J = 7.3$ Hz, H_1), 7.29 (2H, d, $J = 8.9$ Hz, H_i), 7.24 (2H, ddd, $J = 8.1, 6.7, 1.3$ Hz, H_g), 7.16 (2H, ddd, $J = 8.3, 6.8, 1.4$ Hz, H_h), 7.02 (2H, d, $J = 8.5$ Hz, H_c), 5.67 – 5.60 (1H, m, H_{12}), 5.60 – 5.52 (2H, m, $\text{H}_{11+12'}$), 4.62 (1H, dd, $J = 13.2, 5.9$ Hz, H_{10}), 4.38 (1H, dd, $J = 13.2, 7.4$ Hz, $\text{H}_{10'}$), 4.02 (1H, td, $J = 12.6, 4.4$ Hz, H_6), 3.78 (1H, td, $J = 12.4, 5.0$ Hz, H_6'), 3.52 (3H, s, H_5), 1.70 – 1.60 (1H, m, H_7), 1.40 – 1.27 (2H, m, H_8), 1.23 – 1.13 (1H, m, H_7'), 0.90 (3H, t, $J = 7.4$ Hz, H_9).

^{13}C NMR (151 MHz, CD_3OD) δ 154.2 (C_b), 143.4 (C_4), 135.8 (C_j), 131.8 (C_2), 131.7 (C_1), 130.6 (C_d), 130.5 (C_e), 129.2 (C_{12}), 129.0 (C_f), 127.1 (C_h), 126.1 (C_{11}), 125.8 (C_c), 123.8 (C_g), 122.8 (C_3), 119.3 (C_i), 116.2 (C_k), 72.5 (C_{10}), 68.9 (C_6), 47.9 (C_5), 25.9 (C_7), 20.5 (C_8), 13.8 (C_9).

LRMS (ESI-TOF, EI^+) m/z : 204.6 ($[\text{M}]^+$, 100%).

LRMS (ESI-TOF, EI^-) m/z : 285.4 ($[\text{M}-\text{H}]^-$, 100%).

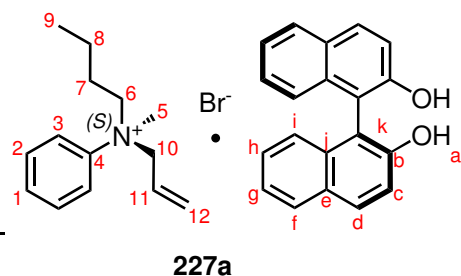
HRMS (ESI-TOF) m/z : $[\text{M}]^+$ calculated for $\text{C}_{14}\text{H}_{22}\text{N}^+$: 204.1752, found 204.1762. $[\text{M}-\text{H}]^-$ calculated for $\text{C}_{20}\text{H}_{13}\text{O}_2^-$: 285.0916, found 285.0905.

mp: 158 – 160 °C (CHCl_3 precipitate).

Optical rotation: $[\alpha]_D^{20} = +15.88$ (MeOH, $c = 1.73$).

IR ($\text{max}/\text{cm}^{-1}$): 3154br, 1623m, 1504m, 1431m, 1329m, 1272s, 815s, 752m, 687m.

XRD: A portion of the complex was crystallised in EtOH to give clear colourless blocks. Crystal data for $\text{C}_{34}\text{H}_{36}\text{BrNO}_2$ ($m = 570.55$ g/mol): Orthorhombic, space group $P2_12_12_1$ (no. 19).

(S)-N-allyl, N-methyl, N-butyl anilinium bromide · (S)-1,1'-bi-2-naphthol

Following the general procedure outlined in 9.8.1, **173** (0.158 g, 1.00 mmol) was dissolved in CHCl_3 (1.67 mL, 0.6 M) and allyl bromide (0.17 mL, 2.00 mmol) was added and stirred for 10 minutes at 50 °C. (S)-BINOL (0.284 g, 0.99 mmol) was added, and the mixture was stirred at 50 °C for 48 hours.

A white precipitate formed which was isolated by vacuum filtration to yield **227a** (0.442 g, 80% yield).

Enantioenrichment of the ammonium salt measured by chiral HPLC: er 43:57 (*R*:*S*).

^1H NMR (599 MHz, CD_3OD) identical to that of **227**.

^{13}C NMR (151 MHz, CD_3OD) identical to that of **227**.

LRMS (ESI-TOF, EI^+) m/z : 218.2 ($[\text{M}]^+$, 100%).

LRMS (ESI-TOF, EI^-) m/z : 285.4 ($[\text{M}-\text{H}]^-$, 100%).

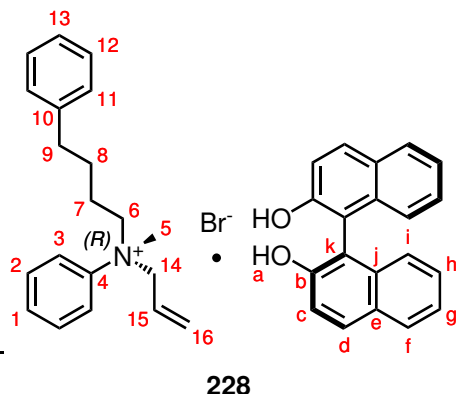
HRMS (ESI-TOF) m/z : $[\text{M}]^+$ calculated for $\text{C}_{15}\text{H}_{24}\text{N}^+$: 218.1909, found 218.1910.

mp: 169 °C (CHCl_3 precipitate).

Optical rotation: $[\alpha]_{\text{D}}^{20} = -15.12$ (MeOH, $c = 1.01$).

IR ($\text{max}/\text{cm}^{-1}$): 3151br, 1624w, 1502w, 1431m, 1332m, 1271s, 816m, 744m, 688m.

XRD: A portion of the complex was crystallised in EtOH to give clear colourless blocks. Crystal data for $\text{C}_{34}\text{H}_{36}\text{BrNO}_2$ ($m = 570.55$ g/mol): Orthorhombic, space group $P2_12_12_1$ (no. 19).

(R)-N-allyl, N-methyl, N-4-phenylbutyl anilinium bromide · (R)-1,1'-bi-2-naphthol

Following the general procedure outlined in 9.8.1, **179** (0.241 g, 1.00 mmol) was dissolved in CHCl_3 (1.00 mL, 1.0 M) and allyl bromide (0.17 mL, 2.00 mmol) was added and stirred for 10 minutes at 50 °C. (*R*)-BINOL (0.283 g, 0.99 mmol) was added, and the mixture was stirred at 50 °C for 48 hours. A white precipitate formed which was isolated by vacuum filtration to yield **228** (0.498 g,

78% yield).

Enantioenrichment of the ammonium salt measured by chiral HPLC: er 58:42 (*R*:*S*).

^1H NMR (599 MHz, CD_3OD) δ 7.87 (2H, d, $J = 9.0$ Hz, H_d), 7.83 (2H, d, $J = 8.2$ Hz, H_f), 7.74 – 7.68 (2H, m, H_3), 7.64 – 7.57 (2H, m, H_2), 7.59 – 7.53 (1H, m, H_1), 7.30 (2H, d, $J = 8.8$ Hz, H_i), 7.24 (2H, ddd, $J = 8.1, 6.7, 1.3$ Hz, H_g), 7.21 (2H, m, H_{11}), 7.19 – 7.11 (4H, m, H_{12+h}), 7.10 – 7.04 (1H, m, H_{13}), 7.02 (2H, dt, $J = 8.5, 1.0$ Hz, H_c), 5.63 – 5.49 (3H, m, H_{15+16}), 4.57 (1H, dd, $J = 13.2, 5.5$ Hz, H_{14}), 4.34 (1H, ddd, $J = 12.9, 6.9, 1.1$ Hz, $\text{H}_{14'}$), 4.00 (1H, td, $J = 12.3, 4.1$ Hz, H_6), 3.76 (1H, ddd, $J = 13.0, 11.8, 4.8$ Hz, H_6'), 3.44 (3H, s, H_5), 2.55 (2H, t, $J = 7.4$ Hz, H_7), 1.70 – 1.52 (3H, m, H_{9+8}), 1.25 – 1.16 (1H, m, H_8').

^{13}C NMR (151 MHz, CD_3OD) δ 154.2 (C_b), 143.3 (C_4), 142.4 (C_{10}), 135.8 (C_j), 131.7 (C_2), 131.6 (C_1), 130.6 (C_d), 130.4 (C_e), 129.42 (C_{12}), 129.35 (C_{15}), 129.3 (C_{13}), 129.0 (C_f), 127.12 (C_h), 127.05 (C_{11}), 126.0 (C_{16}), 125.8 (C_c), 123.8 (C_g), 122.8 (C_3), 119.3 (C_i), 116.2 (C_k), 72.5 (C_{14}), 68.8 (C_6), 47.7 (C_5), 35.8 (C_7), 28.8 (C_9), 23.3 (C_8).

LRMS (ESI-TOF, EI^+) m/z : 280.2 ($[\text{M}]^+$, 100%).

LRMS (ESI-TOF, EI^-) m/z : 285.4 ($[\text{M}-\text{H}]^-$, 100%).

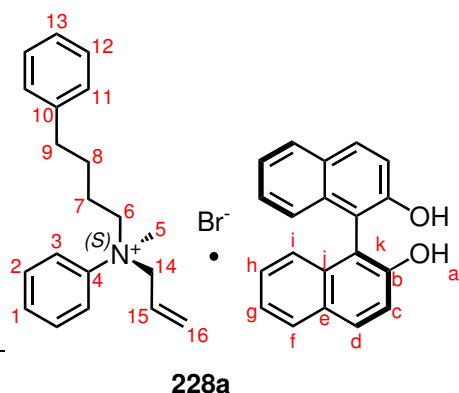
HRMS (ESI-TOF) m/z : $[\text{M}]^+$ calculated for $\text{C}_{20}\text{H}_{26}\text{N}^+$: 280.2065, found 280.2076.

mp: 160 °C (CHCl_3 precipitate).

Optical rotation: $[\alpha]_D^{20} = +15.39$ (MeOH, $c = 0.58$).

IR ($\text{max}/\text{cm}^{-1}$): 3159br, 1621w, 1431m, 1270s, 953m, 817s, 750s, 686s.

XRD: A portion of the complex was crystallised in EtOH to give clear colourless blocks. Crystal data for $\text{C}_{40}\text{H}_{40}\text{BrNO}_2$ ($m = 646.64$ g/mol): Orthorhombic, space group $P2_12_12_1$ (no. 19).

(S)-N-allyl, N-methyl, N-4-phenylbutyl anilinium bromide · (S)-1,1'-bi-2-naphthol

Following the general procedure outlined in 9.8.1, **179** (0.244 g, 1.02 mmol) was dissolved in CHCl_3 (1.00 mL, 1.0 M) and allyl bromide (0.17 mL, 2.00 mmol) was added and stirred for 10 minutes at 50 °C. (S)-BINOL (0.285 g, 1.00 mmol) was added, and the mixture was stirred at 50 °C for 48 hours. A white precipitate formed which was isolated by vacuum filtration to yield **228a** (0.416 g,

65% yield).

Enantioenrichment of the ammonium salt measured by chiral HPLC: er 45:55 (*R*:*S*).

^1H NMR (599 MHz, CD_3OD) identical to that of **228**.

^{13}C NMR (151 MHz, CD_3OD) identical to that of **228**.

LRMS (ESI-TOF, EI^+) m/z : 280.2 ($[\text{M}]^+$, 100%).

LRMS (ESI-TOF, EI^-) m/z : 285.4 ($[\text{M}-\text{H}]^-$, 100%).

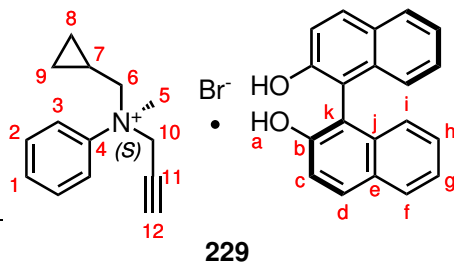
HRMS (ESI-TOF) m/z : $[\text{M}]^+$ calculated for $\text{C}_{20}\text{H}_{26}\text{N}^+$: 280.2065, found 280.2086.

mp: 161 – 163 °C (CHCl_3 precipitate).

Optical rotation: $[\alpha]_{\text{D}}^{20} = -16.88$ (MeOH, $c = 0.60$).

IR ($\text{max}/\text{cm}^{-1}$): 3161br, 1622w, 1431w, 1326m, 1271s, 952m, 818s, 751m, 685s.

XRD: A portion of the complex was crystallised in EtOH to give clear colourless blocks. Crystal data for $\text{C}_{40}\text{H}_{40}\text{BrNO}_2$ ($m = 646.64$ g/mol): Orthorhombic, space group $P2_12_12_1$ (no. 19).

(S)-N-propargyl, N-methyl, N-homocyclopropyl anilinium bromide · (R)-1,1'-bi-2-naphthol

Following the general procedure outlined in 9.8.1, **172** (0.156 g, 0.96 mmol) was dissolved in CHCl_3 (1.67 mL, 0.6 M) and 80% propargyl bromide solution (0.24 mL, 2.00 mmol) was added and stirred for 10 minutes at 50 °C. (*R*)-BINOL (0.283 g, 0.99 mmol) was added, and the mixture was stirred at 50

°C for 48 hours. A white precipitate formed which was isolated by vacuum filtration to yield **229** (0.471 g, 84% yield).

Enantioenrichment of the ammonium salt measured by ^1H NMR spectroscopy using (Λ ,*R*)-BINPHAT as a chiral shift reagent: er 45:55 (*R*:*S*).

^1H NMR (599 MHz, $\text{DMSO}-d_6$) δ 9.21 (2H, s, H_a), 7.95 (2H, dd, $J = 8.1, 1.6$ Hz, H_d), 7.87 – 7.82 (4H, m, H_{3+f}), 7.65 (2H, t, $J = 8.8$ Hz, H_2), 7.59 (1H, t, $J = 7.3$ Hz, H_1), 7.36 (2H, d, $J = 8.9$ Hz, H_i), 7.22 (2H, ddd, $J = 8.0, 6.5, 1.2$ Hz, H_g), 7.16 (2H, ddd, $J = 8.2, 6.7, 1.4$ Hz, H_h), 6.95 (2H, dd, $J = 8.4, 1.1$ Hz, H_c), 5.17 (1H, dd, $J = 16.5, 2.5$ Hz, H_{10}), 5.01 (1H, dd, $J = 16.4, 2.5$ Hz, $\text{H}_{10'}$), 4.06 (1H, td, $J = 12.5, 4.5$ Hz, H_6), 3.92 (1H, dt, $J = 12.3, 6.1$ Hz, $\text{H}_{6'}$), 3.88 (t, $J = 2.5$ Hz, H_{12}), 3.66 (3H, s, H_5), 0.84 – 0.76 (1H, m, H_7), 0.61 – 0.55 (1H, m, H_8), 0.50 – 0.45 (1H, m, H_9), 0.33 (1H, ddt, $J = 9.4, 6.0, 4.6$ Hz, $\text{H}_{8'}$), 0.13 (1H, ddt, $J = 9.4, 6.1, 4.6$ Hz, $\text{H}_{9'}$).

^{13}C NMR (151 MHz, $\text{DMSO}-d_6$) δ 153.0 (C_b), 143.0 (C_4), 134.1 (C_j), 130.3 (C_1), 130.1 (C_2), 128.6 (C_3), 128.1 (C_e), 127.8 (C_f), 125.8 (C_h), 124.4 (C_c), 122.2 (C_g), 122.0 (C_d), 118.5 (C_i), 115.4 (C_k), 82.9 (C_{12}), 72.7 (C_{11}), 72.3 (C_6), 56.0 (C_{10}), 48.6 (C_5), 4.9 (C_7), 4.4 (C_8), 3.6 (C_9).

LRMS (ESI-TOF, EI^+) m/z : 200.7 ($[\text{M}]^+$, 100%).

LRMS (ESI-TOF, EI^-) m/z : 285.4 ($[\text{M}-\text{H}]^-$, 100%).

HRMS (ESI-TOF) m/z : $[\text{M}]^+$ calculated for $\text{C}_{14}\text{H}_{18}\text{N}^+$: 200.1439, found 200.1432. $[\text{M}-\text{H}]^-$ calculated for $\text{C}_{20}\text{H}_{13}\text{O}_2^-$: 285.0916, found 285.0918.

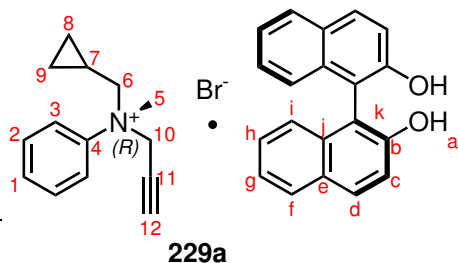
mp: 166 °C (CHCl_3 precipitate).

Optical rotation: $[\alpha]_D^{20} = +15.24$ (MeOH, $c = 1.36$).

IR ($\text{max}/\text{cm}^{-1}$): 3180br, 1622w, 1505m, 1432m, 1274s, 981m, 822m, 692m.

XRD: A portion of the complex was crystallised in EtOH to give clear colourless needles. Crystal data for $\text{C}_{34}\text{H}_{32}\text{BrNO}_2$ ($m = 566.51$ g/mol): Tetragonal, space group $P4_1$

(no. 76).

(R)-N-propargyl, N-methyl, N-homocyclopropyl anilinium bromide · (S)-1,1'-bi-2-naphthol

Following the general procedure outlined in 9.8.1, **172** (0.157 g, 0.97 mmol) was dissolved in CHCl_3 (1.67 mL, 0.6 M) and 80% propargyl bromide solution (0.24 mL, 2.00 mmol) was added and stirred for 10 minutes at 50 °C. (S)-BINOL (0.285 g, 1.00 mmol) was added, and the mixture was stirred at 50

°C for 48 hours. A white precipitate formed which was isolated by vacuum filtration to yield **229a** (0.401 g, 73% yield).

Enantioenrichment of the ammonium salt measured by ^1H NMR spectroscopy using (Δ ,*R*)-BINPHAT as a chiral shift reagent: er 57:43 (*R*:*S*).

^1H NMR (599 MHz, $\text{DMSO}-d_6$) identical to that of **229**.

^{13}C NMR (151 MHz, $\text{DMSO}-d_6$) identical to that of **229**.

LRMS (ESI-TOF, EI^+) m/z : 200.1 ($[\text{M}]^+$, 100%).

LRMS (ESI-TOF, EI^-) m/z : 285.4 ($[\text{M}-\text{H}]^-$, 100%).

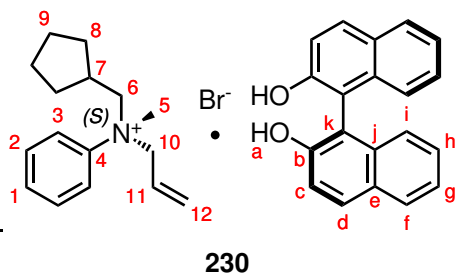
HRMS (ESI-TOF) m/z : $[\text{M}]^+$ calculated for $\text{C}_{14}\text{H}_{18}\text{N}^+$: 200.1439, found 200.1441.

mp: 174 – 175 °C (CHCl_3 precipitate).

Optical rotation: $[\alpha]_D^{20} = -16.12$ (MeOH, $c = 0.99$).

IR ($\text{max}/\text{cm}^{-1}$): 3174br, 1622w, 1505w, 1327m, 1276s, 814m, 691m.

XRD: A portion of the complex was crystallised in EtOH to give clear colourless needles. Crystal data for $\text{C}_{34}\text{H}_{32}\text{BrNO}_2$ ($m = 566.51$ g/mol): Tetragonal, space group $P4_1$ (no. 76).

(S)-N-allyl, N-methyl, N-homocyclopentyl anilinium bromide · (R)-1,1'-bi-2-naphthol

Following the general procedure outlined in 9.8.1, **171** (0.187 g, 0.99 mmol) was dissolved in CHCl_3 (1.67 mL, 0.6 M) and allyl bromide (0.17 mL, 2.00 mmol) was added and stirred for 10 minutes at 50 °C. (*R*)-BINOL (0.285 g, 1.00 mmol) was added, and the mixture was stirred at 50 °C for 48 hours.

A white precipitate formed which was isolated by vacuum filtration to yield **230** (0.501 g, 85% yield).

Enantioenrichment of the ammonium salt measured by chiral HPLC: er 47:53 (*R*:*S*).

^1H NMR (599 MHz, CD_3OD) δ 7.87 (2H, d, $J = 8.9$ Hz, H_d), 7.83 (2H, d, $J = 8.1$ Hz, H_f), 7.77 (2H, d, $J = 8.1$, H_3), 7.62 (2H, apt. t, $J = 8.9$ Hz, H_2), 7.55 (1H, t, $J = 7.3$ Hz, H_1), 7.31 (2H, d, $J = 8.9$ Hz, H_i), 7.24 (2H, ddd, $J = 8.1, 6.7, 1.2$ Hz, H_g), 7.15 (2H, ddd, $J = 8.3, 6.7, 1.4$ Hz, H_h), 7.03 (2H, d, $J = 8.6$ Hz, H_c), 5.57 – 5.52 (2H, m, H_{12}), 5.52 – 5.48 (1H, m, H_{11}), 4.66 – 4.59 (1H, m, H_{10}), 4.34 (1H, dd, $J = 13.6, 4.3$ Hz, $\text{H}_{10'}$), 4.09 (1H, dd, $J = 13.3, 6.3$ Hz, H_6), 3.83 (1H, dd, $J = 13.4, 5.6$ Hz, $\text{H}_{6'}$), 3.49 (3H, s, H_5), 2.00 – 1.92 (1H, m, H_7), 1.88 – 1.81 (1H, m, H_8), 1.64 – 1.56 (1H, m, H_9), 1.53 – 1.47 (2H, m, $\text{H}_{9+9'}$), 1.40 – 1.31 (1H, m, H_9), 1.30 – 1.19 (2H, m, H_8), 0.88 (1H, dq, $J = 12.5, 9.0$ Hz, H_8').

^{13}C NMR (151 MHz, CD_3OD) δ 154.2 (C_b), 143.6 (C_4), 135.8 (C_j), 131.6 (C_1), 130.6 (C_2), 130.6 (C_d), 130.4 (C_e), 129.2 (C_{12}), 129.0 (C_f), 127.1 (C_h), 126.1 (C_{11}), 125.8 (C_c), 123.9 (C_g), 123.2 (C_3), 119.3 (C_i), 116.2 (C_k), 75.0 (C_6), 72.9 (C_{10}), 48.0 (C_5), 36.6 (C_7), 33.3 (C_8), 32.9 ($\text{C}_{8'}$), 25.7 ($\text{C}_{9'}$), 25.4 (C_9).

LRMS (ESI-TOF, EI^+) m/z : 230.7 ($[\text{M}]^+$, 100%).

LRMS (ESI-TOF, EI^-) m/z : 285.4 ($[\text{M}-\text{H}]^-$, 100%).

HRMS (ESI-TOF) m/z : $[\text{M}]^+$ calculated for $\text{C}_{16}\text{H}_{24}\text{N}^+$: 230.1909, found 230.1914. $[\text{M}-\text{H}]^-$ calculated for $\text{C}_{20}\text{H}_{13}\text{O}_2^-$: 285.0916, found 285.0929.

mp: 160 – 161 °C (CHCl_3 precipitate).

Optical rotation: $[\alpha]_D^{20} = +16.55$ (MeOH, $c = 1.16$).

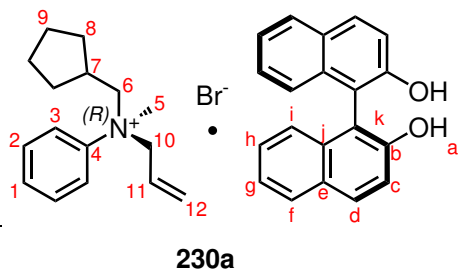
IR ($\text{max}/\text{cm}^{-1}$): 3142br, 1623m, 1504m, 1328m, 1271s, 957m, 816s, 745s, 689m, 422w.

XRD: A portion of the complex was crystallised in EtOH to give clear colourless

9.8. CIAT OF AMMONIUM SALTS

plates. Crystal data for $C_{36}H_{38}BrNO_2$ ($m = 596.58$ g/mol): Orthorhombic, space group $P2_12_12_1$ (no. 19).

(*R*)-*N*-allyl, *N*-methyl, *N*-homocyclopentyl anilinium bromide · (*S*)-1,1'-bi-2-naphthol



Following the general procedure outlined in 9.8.1, **171** (0.145 g, 0.77 mmol) was dissolved in $CHCl_3$ (1.28 mL, 0.6 M) and allyl bromide (0.13 mL, 1.54 mmol) was added and stirred for 10 minutes at 50 °C. (*S*)-BINOL (0.220 g, 0.77 mmol) was added, and the mixture was stirred at 50 °C for 48 hours.

A white precipitate formed which was isolated by vacuum filtration to yield **230a** (0.367 g, 80% yield).

Enantioenrichment of the ammonium salt measured by chiral HPLC: er 50:50 (*R*:*S*).

1H NMR (599 MHz, CD_3OD) identical to that of **230**.

^{13}C NMR (151 MHz, CD_3OD) identical to that of **230**.

LRMS (ESI-TOF, EI^+) m/z : 230.2 ($[M]^+$, 100%).

LRMS (ESI-TOF, EI^-) m/z : 285.4 ($[M-H]^-$, 100%).

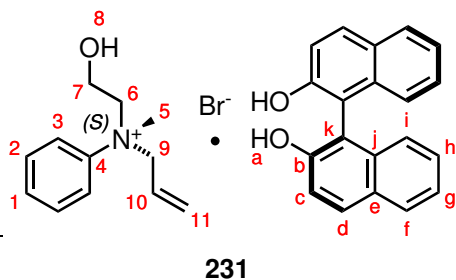
HRMS (ESI-TOF) m/z : $[M]^+$ calculated for $C_{16}H_{24}N^+$: 230.1909, found 230.1898.

mp: 168 – 169 °C ($CHCl_3$ precipitate).

Optical rotation: $[\alpha]_D^{20} = -16.85$ (MeOH, $c = 1.03$).

IR (max/cm^{-1}): 3145br, 1624w, 1431w, 1271s, 817m, 745m, 689m.

XRD: A portion of the complex was crystallised in EtOH to give clear colourless plates. Crystal data for $C_{36}H_{38}BrNO_2$ ($m = 596.58$ g/mol): Orthorhombic, space group $P2_12_12_1$ (no. 19).

(S)-N-allyl, N-methyl, N-2-hydroxyethyl anilinium bromide · (R)-1,1'-bi-2-naphthol

Following the general procedure outlined in 9.8.1, *N*-methyl, *N*-2-hydroxyethyl aniline (0.158 g, 1.05 mmol) was dissolved in CHCl_3 (1.67 mL, 0.6 M) and allyl bromide (0.17 mL, 2.00 mmol) was added and stirred for 10 minutes at 50 °C. (*R*)-BINOL (0.289 g, 1.01 mmol) was added, and the mixture was

stirred at 50 °C for 48 hours. A white precipitate formed which was isolated by vacuum filtration to yield **231** (0.449 g, 65% yield).

Enantioenrichment of the ammonium salt measured by ^1H NMR spectroscopy using (Δ ,*R*)-BINPHAT as a chiral shift reagent: er 47:53 (*R*:*S*).

^1H NMR (599 MHz, CD_3OD) δ 7.87 (2H, d, $J = 8.9$ Hz, H_d), 7.83 (2H, d, $J = 8.1$ Hz, H_f), 7.75 (2H, d, $J = 8.1$, H_3), 7.62 (2H, t, $J = 7.4$ Hz, H_2), 7.57 (1H, t, $J = 7.2$ Hz, H_1), 7.31 (2H, d, $J = 8.9$ Hz, H_i), 7.24 (2H, ddd, $J = 8.2$, 6.8, 1.3 Hz, H_g), 7.15 (2H, ddd, $J = 8.4$, 6.8, 1.4 Hz, H_h), 7.03 (2H, d, $J = 8.5$ Hz, H_c), 5.58 – 5.55 (2H, m, H_{11}), 5.53 – 5.49 (1H, m, H_{10}), 4.63 (1H, dd, $J = 13.0$, 4.2 Hz, H_9), 4.44 (1H, dd, $J = 13.0$, 4.4 Hz, H_9), 4.08 (1H, td, $J = 12.4$, 4.0 Hz, H_6), 3.94 (1H, td, $J = 14.4$, 3.3 Hz, H_6), 3.70 (1H, dt, $J = 13.8$, 4.1 Hz, H_7), 3.62 (3H, s, H_5), 3.53 (1H dt, $J = 13.6$, 2.8 Hz, H_7).

^{13}C NMR (151 MHz, CD_3OD) δ 154.2 (C_b), 143.4 (C_4), 135.8 (C_j), 131.7 (C_2), 131.6 (C_1), 130.6 (C_d), 130.4 (C_e), 129.4 (C_{10}), 129.0 (C_f), 127.1 (C_h), 126.0 (C_{11}), 125.8 (C_c), 123.9 (C_g), 123.0 (C_3), 119.3 (C_i), 116.2 (C_k), 72.91 (C_9), 70.68 (C_7), 57.11 (C_6), 49.74 (C_5).

LRMS (ESI-TOF, EI^+) m/z : 192.7 ($[\text{M}]^+$, 100%).

LRMS (ESI-TOF, EI^-) m/z : 285.4 ($[\text{M}-\text{H}]^-$, 100%).

HRMS (ESI-TOF) m/z : $[\text{M}]^+$ calculated for $\text{C}_{12}\text{H}_{18}\text{NO}^+$: 192.1388, found 192.1386.

$[\text{M}-\text{H}]^-$ calculated for $\text{C}_{20}\text{H}_{13}\text{O}_2^-$: 285.0916, found 285.0930.

mp: 146 °C (CHCl_3 precipitate).

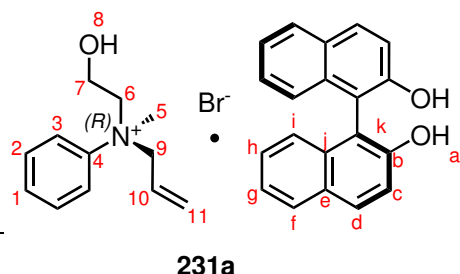
Optical rotation: $[\alpha]_D^{20} = +16.18$ (MeOH, $c = 1.03$).

IR ($\text{max}/\text{cm}^{-1}$): 3161br, 1622m, 1504m, 1430m, 1328m, 1269s, 930m, 815s, 753s, 689m, 420m.

XRD: A portion of the complex was crystallised in EtOH to give clear colourless prisms. Crystal data for $\text{C}_{32}\text{H}_{32}\text{BrNO}_3$ ($m = 558.49$ g/mol): Orthorhombic, space group

$P2_12_12_1$ (no. 19).

(*R*)-*N*-allyl, *N*-methyl, *N*-2-hydroxyethyl anilinium bromide · (*S*)-1,1'-bi-2-naphthol



Following the general procedure outlined in 9.8.1, *N*-methyl, *N*-2-hydroxyethyl aniline (0.154 g, 1.02 mmol) was dissolved in CHCl_3 (1.67 mL, 0.6 M) and allyl bromide (0.17 mL, 2.00 mmol) was added and stirred for 10 minutes at 50 °C. (*S*)-BINOL (0.288 g, 1.01 mmol) was added, and the mixture was

stirred at 50 °C for 48 hours. A white precipitate formed which was isolated by vacuum filtration to yield **231a** (0.406 g, 72% yield).

Enantioenrichment of the ammonium salt measured by ^1H NMR spectroscopy using (Δ ,*R*)-BINPHAT as a chiral shift reagent: er 52:48 (*R*:*S*).

^1H NMR (599 MHz, CD_3OD) *identical to that of 231*.

^{13}C NMR (151 MHz, CD_3OD) *identical to that of 231*.

LRMS (ESI-TOF, EI^+) m/z : 192.1 ($[\text{M}]^+$, 100%).

LRMS (ESI-TOF, EI^-) m/z : 285.4 ($[\text{M}-\text{H}]^-$, 100%).

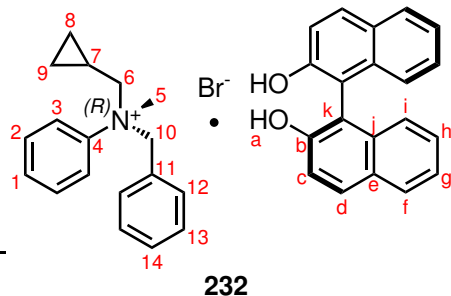
HRMS (ESI-TOF) m/z : $[\text{M}]^+$ calculated for $\text{C}_{12}\text{H}_{18}\text{NO}^+$: 192.1388, found 192.1397.

mp: 151 – 152 °C (CHCl_3 precipitate).

Optical rotation: $[\alpha]_D^{20} = -17.00$ (MeOH, $c = 0.99$).

IR ($\text{max}/\text{cm}^{-1}$): 3144br, 1622m, 1504m, 1430m, 1269s, 962w, 816s.

XRD: A portion of the complex was crystallised in EtOH to give clear colourless prisms. Crystal data for $\text{C}_{32}\text{H}_{32}\text{BrNO}_3$ ($m = 558.49$ g/mol): Orthorhombic, space group $P2_12_12_1$ (no. 19).

(S)-N-benzyl, N-methyl, N-homocyclopropyl anilinium bromide · (R)-1,1'-bi-2-naphthol

Following the general procedure outlined in 9.8.1, **172** (0.160 g, 0.99 mmol) was dissolved in MeCN (1.67 mL, 0.6 M) and benzyl bromide (0.22 mL, 2.00 mmol) was added and stirred for 10 minutes at 50 °C. (*R*)-BINOL (0.287 g, 1.00 mmol) was added, and the mixture was stirred at 50 °C for 48 hours.

A white precipitate formed which was isolated by vacuum filtration to yield **232** (0.199 g, 32% yield).

Enantioenrichment of the ammonium salt measured by ^1H NMR spectroscopy using (Δ ,*R*)-BINPHAT as a chiral shift reagent: er 50:50 (*R*:*S*).

^1H NMR (599 MHz, CD_3OD) δ 7.87 (2H, d, $J = 8.9$ Hz, H_d), 7.83 (2H, d, $J = 8.2$ Hz, H_f), 7.76 – 7.71 (2H, m, H_3), 7.65 – 7.59 (3H, m, H_{1+2}), 7.44 – 7.39 (1H, apt. t, $J = 7.5$ Hz, H_{14}), 7.31 – 7.26 (6H, m, $\text{H}_{12+13+i}$), 7.26 – 7.22 (m, 2H, H_g), 7.16 (2H, ddd, $J = 8.2, 6.7, 1.3$ Hz, H_h), 7.02 (2H, d, $J = 8.5$ Hz, H_c), 5.12 (1H, d, $J = 12.9$ Hz, H_{10}), 4.88 (1H, d, $J = 12.9$ Hz, $\text{H}_{10'}$), 4.40 (1H, dd, $J = 13.4, 5.6$ Hz, H_6), 3.66 (1H, dd, $J = 13.4, 8.4$ Hz, H_6'), 3.53 (3H, s, H_5), 0.82 (1H, dtt, $J = 10.6, 5.1, 2.6$ Hz, H_7), 0.77 – 0.71 (1H, m, H_8), 0.60 – 0.50 (2H, m, H_{8+9}), 0.27 – 0.20 (1H, m, H_9).

^{13}C NMR (151 MHz, CD_3OD) δ 154.2 (C_b), 143.5 (C_4), 135.9 (C_j), 133.8 (C_{13}), 131.8 (C_{14}), 131.7 (C_1), 131.5 (C_2), 130.6 (C_d), 130.4 (C_e), 129.8 (C_{12}), 129.0 (C_f), 128.6 (C_{11}), 127.1 (C_h), 125.8 (C_c), 123.8 (C_g), 123.6 (C_3), 119.3 (C_i), 116.2 (C_k), 79.5 (C_{10}), 74.0 (C_6), 47.1 (C_5), 6.4 (C_8), 6.1 (C_7), 3.9 (C_9).

LRMS (ESI-TOF, EI^+) m/z : 252.2 ($[\text{M}]^+$, 100%).

LRMS (ESI-TOF, EI^+) m/z : 287.1 ($[\text{M}+\text{H}]^+$, 100%).

HRMS (ESI-TOF) m/z : $[\text{M}]^+$ calculated for $\text{C}_{18}\text{H}_{22}\text{N}^+$: 252.1752, found 252.1767.

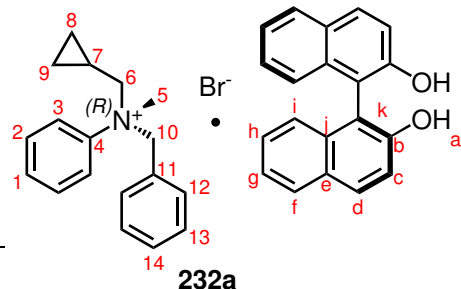
mp: 140 °C (MeCN precipitate).

Optical rotation: $[\alpha]_D^{20} = -1.11$ (MeOH, $c = 1.33$).

IR ($\text{max}/\text{cm}^{-1}$): 3037br, 1620w, 1503m, 1271s, 751s.

XRD: A portion of the complex was crystallised in EtOH to give clear colourless plates.

Crystal data for $\text{C}_{34}\text{H}_{34}\text{BrNO}_2$ ($m = 568.56$ g/mol): Tetragonal, space group $P4_1$ (no. 76).

(R)-N-benzyl, N-methyl, N-homocyclopropyl anilinium bromide · (S)-1,1'-bi-2-naphthol

Following the general procedure outlined in 9.8.1, **172** (0.160 g, 0.99 mmol) was dissolved in MeCN (1.00 mL, 1.00 M) and benzyl bromide (0.22 mL, 2.00 mmol) was added and stirred for 10 minutes at 50 °C. (S)-BINOL (0.285 g, 1.00 mmol) was added, and the mixture was stirred at 50 °C for 48 hours.

A white precipitate formed which was isolated by vacuum filtration to yield **232a** (0.401 g, 71% yield).

Enantioenrichment of the ammonium salt measured by ^1H NMR spectroscopy using (Δ ,*R*)-BINPHAT as a chiral shift reagent: er 50:50 (*R*:*S*).

^1H NMR (599 MHz, CD_3OD) *identical to that of 232*.

^{13}C NMR (151 MHz, CD_3OD) *identical to that of 232*.

LRMS (ESI-TOF, EI^+) m/z : 287.1 ($[\text{M}+\text{H}]^+$, 100%).

HRMS (ESI-TOF) m/z : $[\text{M}]^+$ calculated for $\text{C}_{15}\text{H}_{22}\text{N}^+$: 252.1752, found 252.1759.

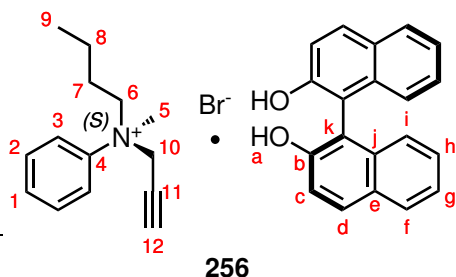
mp: 144 °C (MeCN precipitate).

Optical rotation: $[\alpha]_{\text{D}}^{20} = +0.40$ (MeOH, $c = 1.49$).

IR ($\text{max}/\text{cm}^{-1}$): 3113br, 1619w, 1501w, 1334m, 1271s, 978w, 818m, 750s, 701m.

XRD: A portion of the complex was crystallised in EtOH to give clear colourless plates.

Crystal data for $\text{C}_{34}\text{H}_{34}\text{BrNO}_2$ ($m = 568.56$ g/mol): Tetragonal, space group $P4_1$ (no. 76).

(S)-N-propargyl, N-methyl, N-butyl anilinium bromide · (R)-1,1'-bi-2-naphthol

Following the general procedure outlined in 9.8.1, **173** (0.162 g, 0.99 mmol) was dissolved in CHCl_3 (0.50 mL, 2.0 M) and 80% propargyl bromide solution (0.24 mL, 2.00 mmol) was added and stirred for 10 minutes at 50 °C. (*R*)-BINOL (0.286 g, 1.00 mmol) was added, and the mixture was stirred at 50

°C for 48 hours. A white precipitate formed which was isolated by vacuum filtration to yield **256** (0.529 g, 94% yield).

Enantioenrichment of the ammonium salt measured by ^1H NMR spectroscopy using (Δ ,*R*)-BINPHAT as a chiral shift reagent: er 34:66 (*R*:*S*). *The salt forms a complex with (Δ ,*R*)-BINPHAT and precipitates out of solution in CD_2Cl_2 , therefore the enantioenrichment is likely underestimated.*

^1H NMR (599 MHz, $\text{DMSO}-d_6$) δ 9.21 (2H, s, H_a), 7.95 (2H, dd, $J = 8.1, 1.6$ Hz, H_d), 7.87 – 7.82 (4H, m, H_{3+f}), 7.65 (2H, t, $J = 7.1$ Hz, H_2), 7.59 (1H, t, $J = 7.3$ Hz, H_1), 7.36 (2H, d, $J = 8.9$ Hz, H_i), 7.22 (2H, ddd, $J = 8.0, 6.5, 1.2$ Hz, H_g), 7.16 (2H, ddd, $J = 8.2, 6.7, 1.4$ Hz, H_h), 6.95 (2H, dd, $J = 8.4, 1.1$ Hz, H_c), 5.17 (1H, dd, $J = 16.5, 2.5$ Hz, H_{10}), 5.01 (1H, dd, $J = 16.4, 2.5$ Hz, $\text{H}_{10'}$), 4.06 (1H, td, $J = 12.5, 4.5$ Hz, H_6), 3.92 (1H, td, $J = 12.3, 6.1$ Hz, $\text{H}_{6'}$), 3.88 (1H, t, $J = 2.5$ Hz, H_{12}), 3.66 (3H, s, H_5), 1.52 (1H, apt. dq, $J = 12.5, 6.6$ Hz, H_7), 1.21 (2H, apt. dp, $J = 14.0, 6.6$ Hz, H_8), 1.10 (1H, apt. dq, $J = 17.8, 6.8$ Hz, H_7), 0.79 (3H, t, $J = 7.4$ Hz, H_9).

^{13}C NMR (151 MHz, $\text{DMSO}-d_6$) δ 153.0 (C_b), 142.3 (C_4), 134.1 (C_j), 130.3 (C_1), 130.2 (C_2), 128.6 (C_d), 128.1 (C_e), 127.8 (C_f), 125.8 (C_h), 124.4 (C_c), 122.2 (C_g), 121.9 (C_3), 118.5 (C_i), 115.4 (C_k), 82.9 (C_{12}), 72.5 (C_{11}), 68.7 (C_6), 57.4 (C_{10}), 48.6 (C_5), 24.5 (C_8), 18.8 (C_7), 13.3 (C_9).

LRMS (ESI-TOF, EI^+) m/z : 202.7 ($[\text{M}]^+$, 100%).

LRMS (ESI-TOF, EI^-) m/z : 285.4 ($[\text{M}-\text{H}]^-$, 100%).

HRMS (ESI-TOF) m/z : $[\text{M}]^+$ calculated for $\text{C}_{14}\text{H}_{20}\text{N}^+$: 202.1596, found 202.1605. $[\text{M}-\text{H}]^-$ calculated for $\text{C}_{20}\text{H}_{13}\text{O}_2^-$: 285.0916, found 285.0923.

mp: 145 °C (MeCN precipitate).

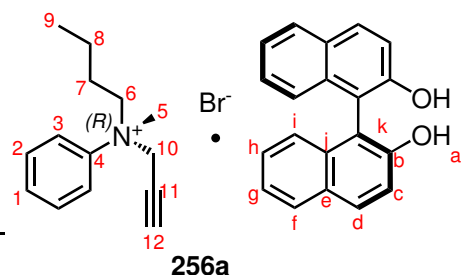
Optical rotation: $[\alpha]_D^{20} = +11.52$ (MeOH, $c = 1.01$).

IR ($\text{max}/\text{cm}^{-1}$): 3159br, 1622m, 1505m, 1432m, 1274s, 823s, 691s.

9.8. CIAT OF AMMONIUM SALTS

XRD: A portion of the complex was crystallised in MeOH to give clear colourless planks. Crystal data for $C_{34}H_{34}BrNO_2$ ($m = 568.53$ g/mol): Tetragonal, space group $P4_1$ (no. 76).

(*R*)-*N*-propargyl, *N*-methyl, *N*-butyl anilinium bromide · (*S*)-1,1'-bi-2-naphthol



Following the general procedure outlined in 9.8.1, **173** (0.163 g, 1.00 mmol) was dissolved in $CHCl_3$ (0.50 mL, 2.0 M) and 80% propargyl bromide solution (0.24 mL, 2.00 mmol) was added and stirred for 10 minutes at 50 °C. (*S*)-BINOL (0.283 g, 0.99 mmol) was added, and the mixture was stirred at 50

°C for 48 hours. A white precipitate formed which was isolated by vacuum filtration to yield **256a** (0.471 g, 86% yield).

Enantioenrichment of the ammonium salt measured by 1H NMR spectroscopy using (Δ ,*R*)-BINPHAT as a chiral shift reagent: er 76:24 (*R*:*S*).

1H NMR (599 MHz, $DMSO-d_6$) identical to that of **256**.

^{13}C NMR (151 MHz, $DMSO-d_6$) identical to that of **256**.

LRMS (ESI-TOF, EI^+) m/z : 216.2 ($[M]^+$, 100%).

LRMS (ESI-TOF, EI^-) m/z : 285.2 ($[M-H]^-$, 100%).

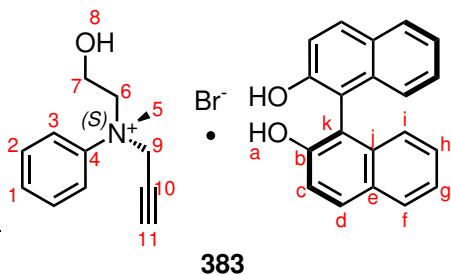
HRMS (ESI-TOF) m/z : $[M]^+$ calculated for $C_{15}H_{22}N^+$: 216.1752, found 216.1763.

mp: 145 °C ($CHCl_3$ precipitate).

Optical rotation: $[\alpha]_D^{20} = -10.91$ (MeOH, $c = 1.15$).

IR (max/cm^{-1}): 3184, 1621w, 1431m, 1272m, 868m, 696s.

XRD: A portion of the complex was crystallised in MeOH to give clear colourless planks. Crystal data for $C_{34}H_{34}BrNO_2$ ($m = 568.53$ g/mol): Tetragonal, space group $P4_1$ (no. 76).

(S)-N-propargyl, N-methyl, N-2-hydroxyethyl anilinium bromide · (R)-1,1'-bi-2-naphthol

Following the general procedure outlined in 9.8.1, *N*-methyl, *N*-2-hydroxyethyl aniline (0.152 g, 1.01 mmol) was dissolved in MeCN (0.50 mL, 2.0 M) and 80% propargyl bromide solution (0.24 mL, 2.00 mmol) was added and stirred for 10 minutes at 50 °C. (*R*)-BINOL (0.286 g, 1.00 mmol) was added, and

the mixture was stirred at 50 °C for 48 hours. A white precipitate formed which was isolated by vacuum filtration to yield **383** (0.294 g, 53% yield).

^1H NMR (599 MHz, DMSO- d_6) δ 9.19 (2H, s, H_a), 7.93 (2H, dd, J = 8.1, 1.6 Hz, H_d), 7.87 – 7.82 (4H, m, H_{3+f}), 7.66 (2H, t, J = 8.8 Hz, H₂), 7.60 (1H, t, J = 7.3 Hz, H₁), 7.33 (2H, d, J = 8.9 Hz, H_i), 7.23 (2H, ddd, J = 8.0, 6.7, 1.3 Hz, H_g), 7.16 (2H, ddd, J = 8.2, 6.6, 1.4 Hz, H_h), 6.93 (2H, dd, J = 8.4, 1.1 Hz, H_c), 5.27 (1H, t, J = 4.9 Hz, H₈), 5.15 (1H, dd, J = 16.4, 2.5 Hz, H₉), 5.00 (1H, dd, J = 16.4, 2.5 Hz, H_{9'}), 4.10 (1H, dt, J = 13.7, 4.6 Hz, H₇), 3.99 (dt, J = 13.5, 4.0 Hz, H_{7'}), 3.86 (1H, d, J = 2.4 Hz, H₁₁), 3.74 (3H, s, H₅), 3.55 – 3.51 (1H, m, H₆), 3.44 – 3.33 (1H, m, H_{6'}).

^{13}C NMR (151 MHz, DMSO- d_6) δ 153.0 (C_b), 142.3 (C₄), 134.1 (C_j), 130.4 (C₁), 130.1 (C₂), 128.6 (C₃), 128.1 (C_e), 127.8 (C_f), 125.8 (C_h), 124.4 (C_c), 122.2 (C_g), 122.0 (C_d), 118.5 (C_i), 115.4 (C_k), 83.0 (C₁₁), 72.6 (C₁₀), 68.7 (C₇), 58.1 (C₉), 55.3 (C₆), 49.9 (C₅).

LRMS (ESI-TOF, EI⁺) m/z : 190.5 ([M]⁺, 100%).

LRMS (ESI-TOF, EI⁻) m/z : 285.4 ([M-H]⁻, 100%).

HRMS (ESI-TOF) m/z : [M]⁺ calculated for C₁₂H₁₆NO⁺: 190.1232, found 190.1226.

[M-H]⁻ calculated for C₂₀H₁₃O₂⁻: 285.0916, found 285.0920.

mp: 149 – 151 °C (MeCN precipitate).

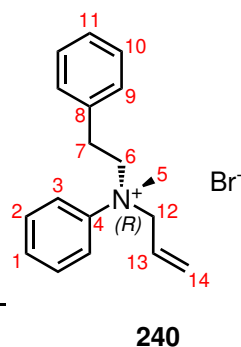
Optical rotation: $[\alpha]_D^{20} = +13.95$ (MeOH, $c = 1.27$).

XRD: A portion of the complex was crystallised in EtOH to give clean irregular crystals.

Crystal data for C₃₂H₃₀BrNO₃ ($m = 556.48$ g/mol): Monoclinic, space group $P2_1$ (no. 3).

9.9 Isolation of enantioenriched ammonium salt

(*R*)-*N*-allyl, *N*-methyl, *N*-phenylacetyl anilinium bromide



215 (4.520 g, 7.31 mmol) was dissolved into the minimum volume of MeOH and the resulting solution was partitioned between Et₂O and H₂O in a separating funnel. The aqueous layer was extracted with H₂O and the solvent removed *in vacuo* to produce a hygroscopic white solid. The resulting solid was recrystallised from MeOH/Et₂O to yield large colourless crystals of **240** (2.325 g, 96% yield). Enantioenrichment of the ammonium salt measured by chiral HPLC: er 99:1 (*R*:*S*).

¹H NMR (400 MHz, CD₃OD) δ 7.94 – 7.85 (2H, m, H₃), 7.77 – 7.68 (2H, m, H₂), 7.68 – 7.60 (1H, m, H₁), 7.30 (2H, ddt, *J* = 8.0, 6.6, 1.2 Hz, H₁₀), 7.28 – 7.20 (1H, m, H₁₁), 7.20 – 7.13 (2H, m, H₉), 5.74 – 5.52 (3H, m, H₁₃₊₁₄), 4.71 (1H, dd, *J* = 13.1, 5.7 Hz, H₁₂), 4.49 (1H, dd, *J* = 12.7, 5.7 Hz, H₁₂), 4.29 (1H, td, *J* = 12.5, 4.7 Hz, H₆), 4.09 (1H, ddd, *J* = 13.0, 11.6, 5.6 Hz, H_{6'}), 3.67 (3H, s, H₅), 3.04 (1H, td, *J* = 12.5, 5.6 Hz, H₇), 2.54 (1H, ddd, *J* = 13.0, 11.6, 4.7 Hz, H₇).

¹³C NMR (101 MHz, CD₃OD) δ 143.2 (C₄), 136.7 (C₈), 131.9 (C₂), 131.8 (C₁), 130.02 (C₉), 129.95 (C₁₀), 129.4 (C₁₄), 128.4 (C₁₁), 126.1 (C₁₃), 123.0 (C₃), 72.7 (C₁₂), 69.7 (C₆), 48.0 (C₅), 30.3 (C₇).

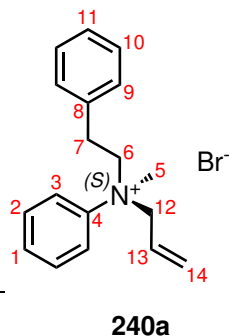
LRMS (ESI-TOF, EI⁺) *m/z*: 252.3 ([M]⁺, 100%).

mp: 106 °C (EtOH precipitate).

IR (max/cm⁻¹): 3336br, 2981br(w), 1595w, 1494w, 1020m, 863m, 700s, 549m.

Optical rotation: [α]_D²⁰ = -57.58 (MeOH, *c* = 0.55).

XRD: Crystallised in MeOH/Et₂O to give clear colourless blocks. Crystal data for C₁₉H₂₆BrNO (*m* = 364.32 g/mol): Orthorhombic, space group *P*2₁2₁2₁ (no. 19).

(S)-N-allyl, N-methyl, N-phenylacetyl anilinium bromide

215a (3.000 g, 4.85 mmol) was dissolved into the minimum volume of MeOH and the resulting solution was partitioned between Et₂O and H₂O in a separating funnel. The aqueous layer was extracted with H₂O and the solvent removed *in vacuo* to produce a hygroscopic white solid. The resulting solid was recrystallised from MeOH/Et₂O to yield large colourless crystals of **240a** (1.433 g, 89% yield). Enantioenrichment of the ammonium salt measured by chiral HPLC: er 1:99 (*R*:*S*).

¹H NMR (400 MHz, CD₃OD) *identical to that of 240*.

¹³C NMR (101 MHz, CD₃OD) *identical to that of 240*.

LRMS (ESI-TOF, EI⁺) *m/z*: 252.3 ([M]⁺, 100%).

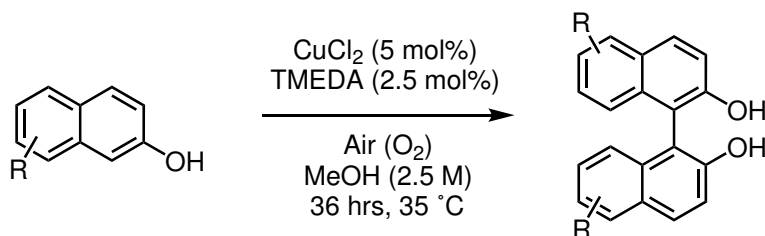
mp: 108 °C (EtOH precipitate).

IR (max/cm⁻¹): 3340br, 2981br(w), 1596w, 1497m, 998m, 864m, 698s, 550m.

Optical rotation: [α]_D²⁰ = +55.44 (MeOH, c = 0.62).

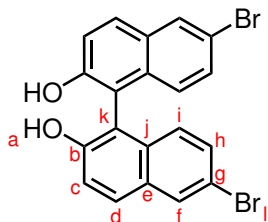
9.10 Synthesis of substituted BINOLs

9.10.1 General procedure for the synthesis of substituted BINOLs



Scheme 9.34: The synthesis of racemic substituted 1,1'-bi-2-naphthols.

Adapted from Munenori *et al.*³²³ The selected substituted naphthol (1.0 equiv.) was dissolved into MeOH (2.5 M) and CuCl_2 (5 mol%) and TMEDA (2.5 mol%) were added. With stirring, the reaction mixture was heated to 35 °C and a stream of air was passed through the mixture for 36 hours. MeOH was added at intervals to ensure the solvent did not fully evaporate. The mixture was cooled to rt and conc. HCl added until the black residue was fully destroyed. H_2O was then added to the mixture to precipitate the desired substituted 1,1'-bi-2-naphthol and the solid product was filtered off, washed with MeOH and dried. Purification could be achieved by recrystallisation from various solvents (toluene, MeOH, MeCN).

***rac*-6,6'-dibromo, 1,1'-bi-2-naphthol****246**

Following the general procedure outlined in 9.10.1, 6-bromo-2-naphthol (3.000 g, 13.4 mmol) was dissolved into MeOH (5.0 mL, 2.5 M) and CuCl₂ (0.0711 g, 0.7 mmol) and TMEDA (0.05 mL, 0.35 mmol) were added. Air was bubbled through the solution and the reaction mixture was heated for 36 h. After addition of conc. HCl (37%) to destroy the black residue, H₂O was added and the brown

precipitate filtered to yield the crude product. Recrystallisation of the brown precipitate from toluene produced **246** (1.015 g, 34% yield).

¹H NMR (400 MHz, CD₃OD) δ 8.00 (2H, d, *J* = 2.1 Hz, H_f), 7.81 (2H, d, *J* = 8.9 Hz, H_d), 7.31 (2H, d, *J* = 8.9 Hz, H_i), 7.25 (2H, dd, *J* = 9.0, 2.1 Hz, H_h), 6.91 (2H, d, *J* = 9.0 Hz, H_c).

¹³C NMR (101 MHz, CD₃OD) δ 154.8, 134.3, 131.5, 131.0, 130.3, 129.9, 127.7, 120.5, 117.3, 116.1.

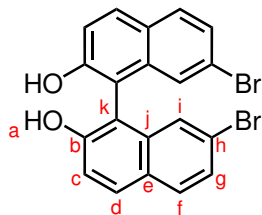
LRMS (ESI-TOF, EI⁻) *m/z*: 443.2 ([M-H]⁻, 100%).

HRMS (ESI-TOF) *m/z*: [M-H]⁻ calculated for C₂₀H₁₁Br₂O₂⁻: 440.9126, found 440.9139.

IR (max/cm⁻¹): 3332br, 2981m, 1584m, 1492m, 1333m, 1144m, 930s, 877s, 804s, 484m.

mp: 205 °C (MeOH precipitate).

XRD: Crystallised in toluene to give clear colourless blocks. Crystal data for C₂₀H₁₂Br₂O₂ (*m* = 444.12 g/mol): Monoclinic, space group *P*2₁/*n* (no. 14).

***rac*-7,7'-dibromo, 1,1'-bi-2-naphthol****244**

Following the general procedure outlined in 9.10.1, 7-bromo-2-naphthol (3.274 g, 14.7 mmol) was dissolved into MeOH (5.0 mL, 2.5 M) and CuCl₂ (0.0715 g, 0.7 mmol) and TMEDA (0.05 mL, 0.35 mmol) were added. Air was bubbled through the solution and the reaction mixture was heated for 36 h. After addition of conc. HCl (37%) to destroy the black residue, H₂O was added and the brown

precipitate filtered to yield the crude product. Recrystallisation of the brown precipitate from toluene produced **244** (2.166 g, 67% yield).

¹H NMR (400 MHz, CD₃OD) δ 7.88 (2H, dd, *J* = 9.0, 0.8 Hz, H_d), 7.75 (2H, d, *J* = 8.7 Hz, H_f), 7.38 – 7.29 (4H, m, H_{i+g}), 7.13 (2H, d, *J* = 1.9 Hz, H_c).

¹³C NMR (101 MHz, CD₃OD) δ 155.4, 137.0, 131.1, 130.9, 128.8, 127.5, 127.1, 121.8, 119.9, 115.1.

LRMS (ESI-TOF, EI⁻) *m/z*: 443.2 ([M-H]⁻, 100%).

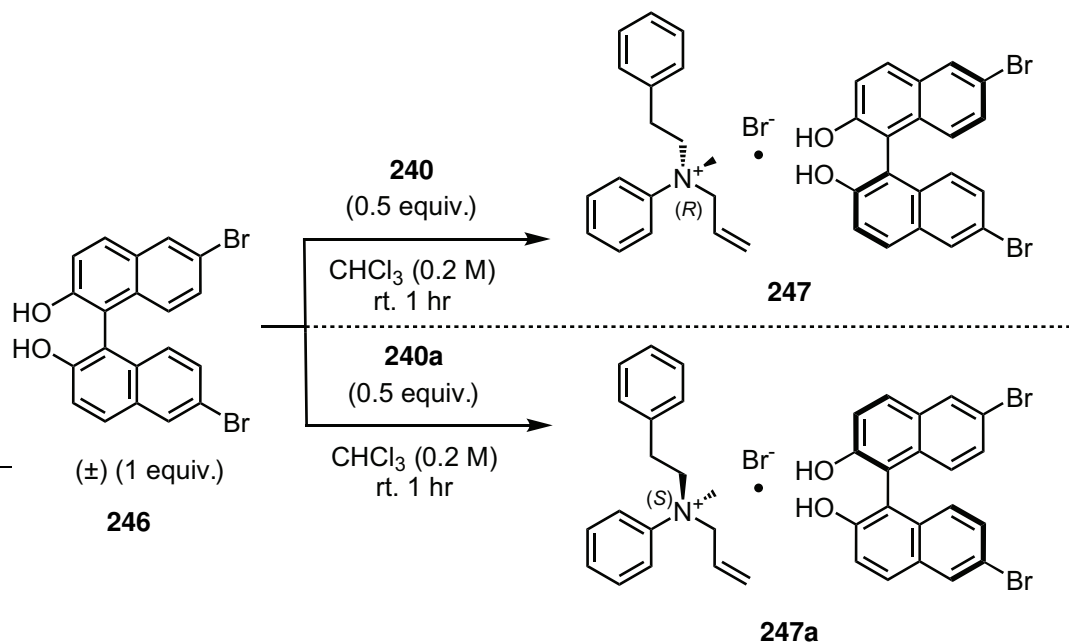
HRMS (ESI-TOF) *m/z*: [M-H]⁻ calculated for C₂₀H₁₁Br₂O₂⁻: 440.9126, found 440.9144.

IR (max/cm⁻¹): 3465br(m), 1608m, 1495m, 1351w, 842s, 557m, 425s.

mp: 197 – 198 °C (MeOH precipitate).

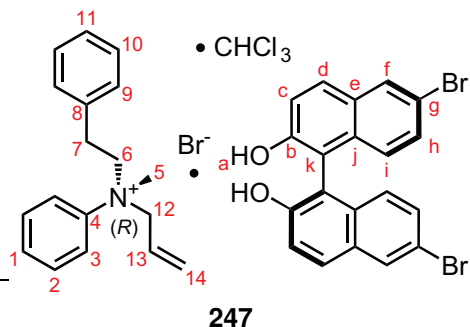
XRD: Crystallised in toluene to give clear colourless blocks. Crystal data for C₂₀H₁₂Br₂O₂ (*m* = 444.12 g/mol): Monoclinic space group *I*4₁/*a* (no. 88).

9.10.2 Resolution of 6,6'-dibromo, 1,1'-bi-2-naphthol



Scheme 9.35: The resolution of 6,6'-dibromo, 1,1'-bi-2-naphthol using an ammonium salt.

6,6'-dibromo, 1,1'-bi-2-naphthol (1.0 equiv.) was dissolved into CHCl_3 (0.2 M) and either **240** or **240a** (0.5 equiv.) were added to the solution. The reaction mixture was stirred vigorously for 1 hour. The resulting precipitate was then filtered, washed with CHCl_3 and dried *in vacuo*. Analysis by ^1H NMR ensured that a 1:1 complex had formed.

(R)-6,6'-dibromo, 1,1'-bi-2-naphthol : (R)-N-allyl, N-methyl, N-phenylacetyl anilinium bromide

Following the general procedure outlined in 9.10.2, *rac*-6,6'-dibromo, 1,1'-bi-2-naphthol (0.118 g, 0.27 mmol) was dissolved into CHCl_3 (1.35 mL, 0.2 M), **240** (0.043 g, 0.5 equiv.) was added and the mixture stirred for 1 hour. A white precipitate formed which was isolated by vacuum filtration to yield **247** (0.040 g, 38%

yield).

Enantioenrichment of the 6,6'-dibromo, 1,1'-bi-2-naphthol measured by chiral HPLC: er 78:22 (*R:S*).

^1H NMR (400 MHz, CD_3OD) δ 8.01 (2H, d, $J = 2.0$ Hz, H_d), 7.90 (1H, s, CHCl_3), 7.88 – 7.84 (2H, m, H_3), 7.81 (2H, d, $J = 8.9$ Hz, H_d), 7.70 (2H, t, $J = 7.1$ Hz, H_2), 7.64 (1H, t, $J = 7.5$ Hz, H_1), 7.31 (2H, d, $J = 8.9$ Hz, H_i), 7.32 – 7.20 (5H, m, H_{9+11+h}), 7.15 (2H, dd, $J = 6.9, 1.9$ Hz, H_{10}), 6.92 (2H, d, $J = 9.0$ Hz, H_c), 5.71 – 5.54 (3H, m, H_{13+14}), 4.67 (1H, dd, $J = 13.1, 5.7$ Hz, H_{12}), 4.43 (1H, dd, $J = 13.1, 7.1$ Hz, H_{12}), 4.26 (1H, td, $J = 12.4, 4.7$ Hz, H_6), 4.04 (1H, ddd, $J = 13.1, 11.6, 5.6$ Hz, H_6), 3.64 (3H, s, H_5), 3.01 (1H, td, $J = 12.5, 5.6$ Hz, H_7), 2.54 (1H, td, $J = 12.4, 4.7$ Hz, H_7).

^{13}C NMR (101 MHz, CD_3OD) δ 154.9, 143.2, 136.6, 134.3, 131.93, 131.85, 131.5, 131.0, 130.3, 130.0, 129.91, 129.87, 129.4, 128.4, 127.7, 126.0, 122.9, 120.5, 117.3, 116.2, 79.5 (CHCl_3), 72.7, 69.7, 47.9, 30.3.

LRMS (ESI-TOF, EI^+) m/z : 252.3 ($[\text{M}]^+$, 100%).

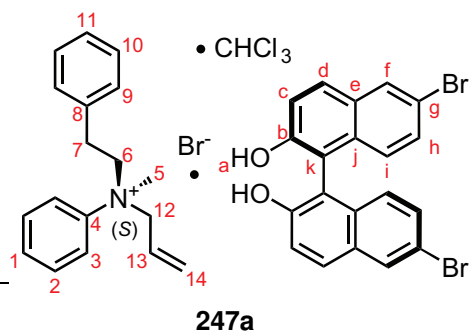
LRMS (ESI-TOF, EI^-) m/z : 443.2 ($[\text{M}-\text{H}]^-$, 100%).

IR ($\text{max}/\text{cm}^{-1}$): 3193br, 1619w, 1582w, 1491m, 1312m, 1271s, 929s, 813s, 753s, 680m, 485m, 421m.

mp: 150 °C (CHCl_3 precipitate).

Optical rotation: $[\alpha]_D^{20} = +35.68$ (MeOH, $c = 0.08$).

XRD: Crystallised in CHCl_3 to give clear colourless blocks. Crystal data for $\text{C}_{39}\text{H}_{35}\text{Br}_3\text{Cl}_3\text{NO}_2$ ($m = 895.76$ g/mol): Monoclinic, space group $P2_1/n$ (no. 14).

(S)-6,6'-dibromo, 1,1'-bi-2-naphthol · (S)-N-allyl, N-methyl, N-phenylacetyl anilinium bromide

Following the general procedure outlined in 9.10.2, *rac*-6,6'-dibromo, 1,1'-bi-2-naphthol (0.122 g, 0.27 mmol) was dissolved into CHCl₃ (1.35 mL, 0.2 M), **240** (0.043 g, 0.5 equiv.) was added and the mixture stirred for 1 hour. A white precipitate formed which was isolated by vacuum filtration to yield **247a** (0.043 g, 41%

yield).

Enantioenrichment of the 6,6'-dibromo, 1,1'-bi-2-naphthol measured by chiral HPLC: er 28:72 (*R*:*S*).

¹H NMR (400 MHz, CD₃OD) *identical to that of 247*.

¹³C NMR (101 MHz, CD₃OD) *identical to that of 247*.

LRMS (ESI-TOF, EI⁺) *m/z*: 252.3 ([M]⁺, 100%).

LRMS (ESI-TOF, EI⁻) *m/z*: 443.2 ([M-H]⁻, 100%).

IR (max/cm⁻¹): 3197br, 1584w, 1492m, 1314m, 1271s, 929s, 812s, 751s, 680m, 485m, 421m.

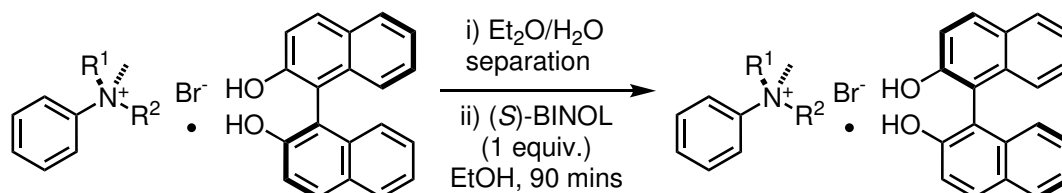
mp: 147 °C (CHCl₃ precipitate).

Optical rotation: [α]_D²⁰ = -32.24 (MeOH, c = 0.10).

XRD: Crystallised in CHCl₃ to give clear colourless plates. Crystal data for C₃₉H₃₅Br₃Cl₃NO₂ (m = 895.76 g/mol): Monoclinic, space group *P*2₁/*n* (no. 14).

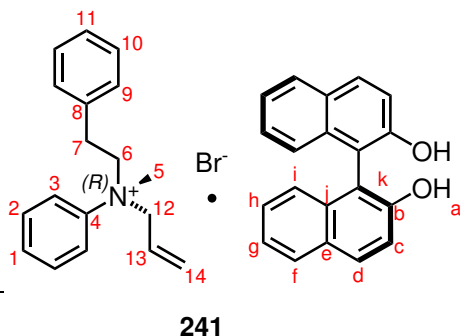
9.11 Mismatched diastereomeric complexes

9.11.1 General procedure for mismatched complex synthesis



Scheme 9.36: Mismatched diastereomeric complex synthesis and single crystal growth.

The matched diastereomeric complex with (*R*)-BINOL (1 equiv.) was dissolved into the minimum volume of MeOH (approx. 1 mg mL⁻¹). This solution was extracted by partition between Et₂O/H₂O and the aqueous layer concentrated under reduced pressure to yield the corresponding enriched quaternary ammonium salt. The quaternary ammonium salt (1 equiv.) was dissolved into EtOH (0.5 M) in a 10 mL vial. (*S*)-BINOL (1 equiv.) was dissolved into a separate solution in EtOH (0.5 M) before being added to the solution of quaternary ammonium salt. The mixture was stirred vigorously at rt for 90 minutes, after which a precipitate was observed. After vacuum filtration, a white precipitate was isolated which can be recrystallised from EtOH to produce single crystals suitable for SCXRD.

(R)-N-allyl, N-methyl, N-phenylacetyl anilinium bromide · (S)-1,1'-bi-2-naphthol

Following the general procedure in 9.11.1 using **215** (119.8 mg, 0.19 mmol), yielded **241** (62.8 mg, 52% yield) as a white solid. Single crystals of **241** were obtained via crystallisation from EtOH.

^1H NMR (599 MHz, CD_3OD) *identical to that of 215.*

^{13}C NMR (151 MHz, CD_3OD) *identical to that*

of 215.

LRMS (ESI-TOF, EI^+) m/z : 252.2 ($[\text{M}]^+$, 100%).

LRMS (ESI-TOF, EI^+) m/z : 287.1 ($[\text{M}+\text{H}]^+$, 100%).

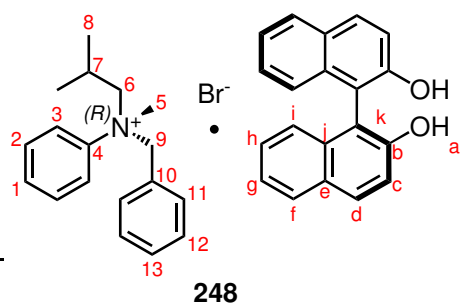
HRMS (ESI-TOF) m/z : $[\text{M}]^+$ calculated for $\text{C}_{18}\text{H}_{22}\text{N}^+$: 252.1752, found 252.1760.

mp: 152 °C (EtOH precipitate).

Optical rotation: $[\alpha]_{\text{D}}^{20} = -32.97$ (MeOH, $c = 0.75$).

IR ($\text{max}/\text{cm}^{-1}$): 3202br, 1620m, 1505m, 1271s, 1143s, 952m, 815s, 747s, 421m.

XRD: Crystallised in EtOH to give clear colourless blocks. Crystal data for $\text{C}_{38}\text{H}_{36}\text{BrNO}_2$ ($m = 618.59$ g/mol): Orthorhombic, space group $P2_12_12_1$ (no. 19).

(R)-N-benzyl, N-methyl, N-isobutyl anilinium bromide · (S)-1,1'-bi-2-naphthol

Following the general procedure in 9.11.1 using **220** (118.8 mg, 0.19 mmol), yielded **248** (46.5 mg, 39% yield). Single crystals of **248** were obtained via crystallisation from EtOH.

^1H NMR (599 MHz, CD_3OD) *identical to that of 220.*

^{13}C NMR (151 MHz, CD_3OD) *identical to that of 220.*

LRMS (ESI-TOF, EI^+) m/z : 254.2 ($[\text{M}]^+$, 100%).

LRMS (ESI-TOF, EI^+) m/z : 287.1 ($[\text{M}+\text{H}]^+$, 100%).

HRMS (ESI-TOF) m/z : $[\text{M}]^+$ calculated for $\text{C}_{18}\text{H}_{24}\text{N}^+$: 254.1909, found 254.1925.

mp: 182 °C (EtOH precipitate).

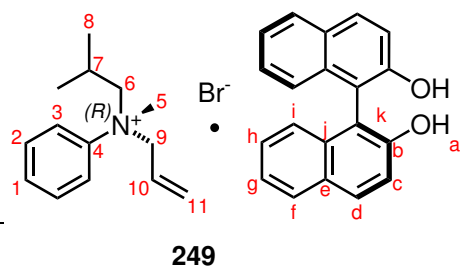
Optical rotation: $[\alpha]_{\text{D}}^{20} = -27.89$ (MeOH, $c = 0.36$).

9.11. MISMATCHED DIASTEREOMERIC COMPLEXES

IR (max/cm⁻¹): 3071br, 1621m, 1431m, 1271s, 818s, 750m.

XRD: Crystallised in EtOH to give clear irregular crystals. Crystal data for C₃₈H₃₈BrNO₂ (m = 620.60 g/mol): Orthorhombic, space group *P*2₁2₁2₁ (no. 19).

(*R*)-*N*-allyl, *N*-methyl, *N*-isobutyl anilinium bromide · (*S*)-1,1'-bi-2-naphthol



Following the general procedure in 9.11.1 using **221** (120.1 mg, 0.21 mmol), yielded **249** (48.4 mg, 40% yield) as a white solid. Single crystals of **249** were obtained via crystallisation from EtOH.

¹H NMR (599 MHz, CD₃OD) *identical to that of 221*.

¹³C NMR (151 MHz, CD₃OD) *identical to that of 221*.

LRMS (ESI-TOF, EI⁺) m/z: 204.2 ([M]⁺, 100%).

LRMS (ESI-TOF, EI⁺) m/z: 286.1 ([M], 100%), 287.1 ([M+H]⁺, 77%).

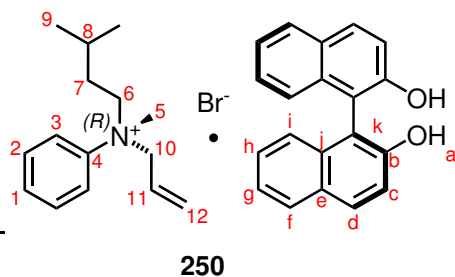
HRMS (ESI-TOF) m/z: [M]⁺ calculated for C₁₄H₂₂N⁺: 204.1752, found 204.1759.

mp: 144 °C (EtOH precipitate).

Optical rotation: [α]_D²⁰ = -12.82 (MeOH, c = 0.22).

IR (max/cm⁻¹): 3476br, 3056br, 1620m, 1507m, 1229m, 872s, 817s, 752s, 688s.

XRD: Crystallised in EtOH to give clear colourless prisms. Crystal data for C₃₄H₃₆BrNO₂ (m = 570.55 g/mol): Orthorhombic, space group *P*2₁2₁2₁ (no. 19).

(R)-N-allyl, N-isovaleryl, N-methyl anilinium bromide · (S)-1,1'-bi-2-naphthol

Following the general procedure in 9.11.1 using **223** (122.6 mg, 0.21 mmol), yielded **250** (49.3 mg, 40% yield) as a white solid. Single crystals of **250** were obtained via crystallisation from EtOH.

^1H NMR (599 MHz, CD_3OD) *identical to that of 223*.

^{13}C NMR (151 MHz, CD_3OD) *identical to that of 223*.

LRMS (ESI-TOF, EI^+) m/z : 218.2 ($[\text{M}]^+$, 100%).

LRMS (ESI-TOF, EI^+) m/z : 287.1 ($[\text{M}+\text{H}]^+$, 100%).

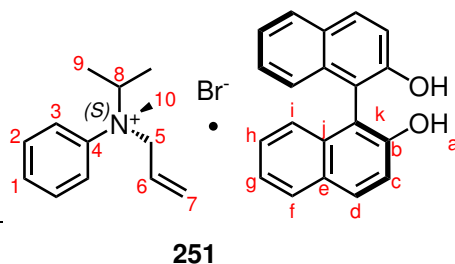
HRMS (ESI-TOF) m/z : $[\text{M}]^+$ calculated for $\text{C}_{15}\text{H}_{24}\text{N}^+$: 218.1909, found 218.1921.

mp: 148 °C (EtOH precipitate).

Optical rotation: $[\alpha]_{\text{D}}^{20} = -9.12$ (MeOH, $c = 0.15$).

IR ($\text{max}/\text{cm}^{-1}$): 3153br, 1621m, 1431m, 1324m, 1271s, 955m, 814s, 745s, 422w.

XRD: Crystallised in EtOH to give clear colourless blocks. Crystal data for $\text{C}_{35}\text{H}_{38}\text{BrNO}_2$ ($m = 584.57$ g/mol): Orthorhombic, space group $P2_12_12_1$ (no. 19).

(S)-N-allyl, N-methyl, N-isopropyl anilinium bromide · (S)-1,1'-bi-2-naphthol

Following the general procedure in 9.11.1 using **225** (102.1 mg, 0.18 mmol), yielded **251** (32.4 mg, 32% yield) as a white solid. Single crystals of **251** were obtained via crystallisation from EtOH.

^1H NMR (599 MHz, CD_3OD) *identical to that of 225*.

^{13}C NMR (151 MHz, CD_3OD) *identical to that of 225*.

LRMS (ESI-TOF, EI^+) m/z : 190.2 ($[\text{M}]^+$, 100%).

LRMS (ESI-TOF, EI^+) m/z : 287.1 ($[\text{M}+\text{H}]^+$, 100%).

HRMS (ESI-TOF) m/z : $[\text{M}]^+$ calculated for $\text{C}_{13}\text{H}_{20}\text{N}^+$: 190.1596, found 191.1605.

mp: 146 °C (EtOH precipitate).

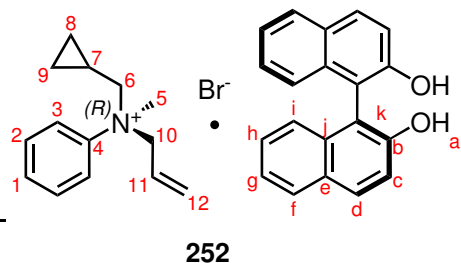
Optical rotation: $[\alpha]_{\text{D}}^{20} = -11.57$ (MeOH, $c = 0.14$).

IR ($\text{max}/\text{cm}^{-1}$): 3137br, 1622m, 1504m, 1430m, 1272s, 952m, 815s, 752s, 690m.

9.11. MISMATCHED DIASTEREOMERIC COMPLEXES

XRD: Crystallised in EtOH to give clear colourless prisms. Crystal data for $C_{33}H_{34}BrNO_2$ ($m = 556.52$ g/mol): Orthorhombic, space group $P2_12_12_1$ (no. 19).

(*R*)-*N*-allyl, *N*-methyl, *N*-homocyclopropyl anilinium bromide · (*S*)-1,1'-bi-2-naphthol



Following the general procedure in 9.11.1 using **226** (148.9 mg, 0.26 mmol), yielded **252** (65.4 mg, 44% yield) as a white solid. Single crystals of **252** were obtained via crystallisation from EtOH.

1H NMR (599 MHz, CD_3OD) *identical to that of 226*.

^{13}C NMR (151 MHz, CD_3OD) *identical to that of 226*.

LRMS (ESI-TOF, EI^+) m/z : 202.2 ($[M]^+$, 100%).

LRMS (ESI-TOF, EI^+) m/z : 287.1 ($[M+H]^+$, 100%).

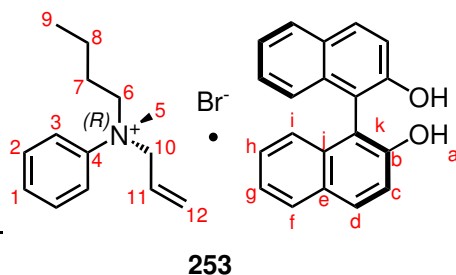
HRMS (ESI-TOF) m/z : $[M]^+$ calculated for $C_{14}H_{20}N^+$: 202.1596, found 202.1601.

mp: 182 °C (EtOH precipitate).

Optical rotation: $[\alpha]_D^{20} = -5.54$ (MeOH, $c = 0.31$).

IR (max/cm^{-1}): 3180br, 1622m, 1504m, 1339m, 1274s, 962w, 815s, 686m.

XRD: Crystallised in EtOH to give clear colourless prisms. Crystal data for $C_{34}H_{34}BrNO_2$ ($m = 568.53$ g/mol): Tetragonal, space group $P4_3$ (no. 78).

(R)-N-allyl, N-methyl, N-butyl anilinium bromide · (S)-1,1'-bi-2-naphthol

Following the general procedure in 9.11.1 using **227** (132.5 mg, 0.23 mmol), yielded **253** (12.2 mg, 9% yield) as a white solid. Single crystals of **253** were obtained via crystallisation from EtOH.

$^1\text{H NMR}$ (599 MHz, CD_3OD) *identical to that of 227.*

$^{13}\text{C NMR}$ (151 MHz, CD_3OD) *identical to that of 227.*

LRMS (ESI-TOF, EI^+) m/z : 218.2 ($[\text{M}]^+$, 100%).

LRMS (ESI-TOF, EI^+) m/z : 287.1 ($[\text{M}+\text{H}]^+$, 100%).

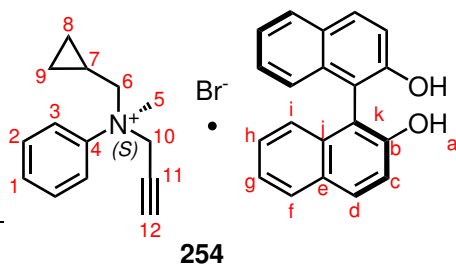
HRMS (ESI-TOF) m/z : $[\text{M}]^+$ calculated for $\text{C}_{15}\text{H}_{24}\text{N}^+$: 218.1909, found 218.1918.

mp: 148 °C (EtOH precipitate).

Optical rotation: $[\alpha]_{\text{D}}^{20} = -12.82$ (MeOH, $c = 0.17$).

IR (max/cm^{-1}): 3155br, 1624m, 1431m, 1271s, 975m, 815s, 744s, 687m.

XRD: Crystallised in EtOH to give clear colourless prisms. Crystal data for $\text{C}_{34}\text{H}_{36}\text{BrNO}_2$ ($m = 570.57$ g/mol): Tetragonal, space group $P4_3$ (no. 78).

(S)-N-propargyl, N-methyl, N-homocyclopropyl anilinium bromide · (S)-1,1'-bi-2-naphthol

Following the general procedure in 9.11.1 using **229** (125.3 mg, 0.07 mmol), yielded **254** (63.3 g, 37% yield) as a white solid. Single crystals of **254** were obtained via crystallisation from EtOH.

$^1\text{H NMR}$ (599 MHz, CD_3OD) *identical to that of 229.*

$^{13}\text{C NMR}$ (151 MHz, CD_3OD) *identical to that of 229.*

LRMS (ESI-TOF, EI^+) m/z : 200.1 ($[\text{M}]^+$, 100%).

LRMS (ESI-TOF, EI^+) m/z : 287.1 ($[\text{M}+\text{H}]^+$, 100%).

HRMS (ESI-TOF) m/z : $[\text{M}]^+$ calculated for $\text{C}_{14}\text{H}_{18}\text{N}^+$: 200.1439, found 200.1440.

mp: 167 °C (EtOH precipitate).

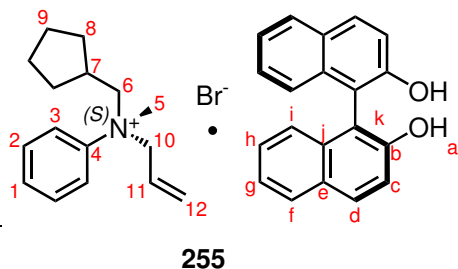
Optical rotation: $[\alpha]_{\text{D}}^{20} = +4.71$ (MeOH, $c = 0.20$).

IR (max/cm^{-1}): 3182br, 1621m, 1505m, 1430m, 1272s, 966m, 814s, 749s, 685s.

9.11. MISMATCHED DIASTEREOMERIC COMPLEXES

XRD: Crystallised in EtOH to give clear colourless plates. Crystal data for $C_{34}H_{32}BrNO_2$ ($m = 566.51$ g/mol): Tetragonal, space group $P4_3$ (no. 78).

(S)-N-allyl, N-methyl, N-homocyclopentyl anilinium bromide · (S)-1,1'-bi-2-naphthol



Following the general procedure in 9.11.1 using **230** (118.0 mg, 0.20 mmol), yielded **255** (37.6 mg, 32% yield) as a white solid. Single crystals of **255** were obtained via crystallisation from EtOH.

1H NMR (599 MHz, CD_3OD) *identical to that of 230*.

^{13}C NMR (151 MHz, CD_3OD) *identical to that of 230*.

LRMS (ESI-TOF, EI^+) m/z : 230.2 ($[M]^+$, 100%).

LRMS (ESI-TOF, EI^+) m/z : 287.1 ($[M+H]^+$, 100%).

HRMS (ESI-TOF) m/z : $[M]^+$ calculated for $C_{16}H_{24}N^+$: 230.1909, found 230.1920.

mp: 175 °C (EtOH precipitate).

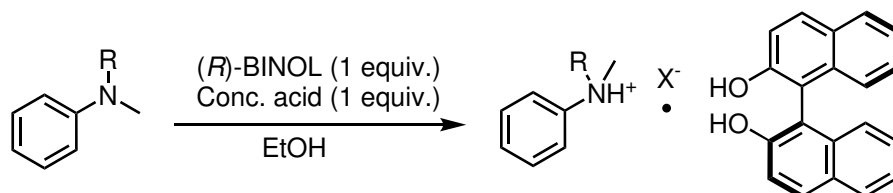
Optical rotation: $[\alpha]_D^{20} = -15.45$ (MeOH, $c = 0.50$).

IR (max/cm^{-1}): 3136br, 1624m, 1431m, 1271s, 957m, 817m, 745m, 689m.

XRD: Crystallised in EtOH to give clear colourless blocks. Crystal data for $C_{36}H_{37}BrNO_2$ ($m = 595.57$ g/mol): Orthorhombic, space group $P2_12_12_1$ (no. 19).

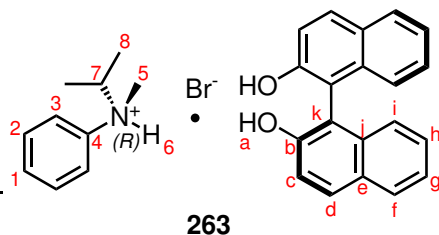
9.12 Chiral tertiary ammonium salt complexes

9.12.1 General procedure tertiary ammonium salt complex synthesis



Scheme 9.37: General procedure for recognition of chiral tertiary ammonium salts by (*R*)-BINOL.

The selected aniline (1.0 equiv.) was dissolved into EtOH (0.9 – 2.0 M), solid (*R*)-BINOL (1.0 equiv.) and conc. acid (1.5 equiv.) was added to the solution and the reaction mixture was stirred vigorously at room temperature. A white precipitate is generally observed 5 – 30 minutes after (*R*)-BINOL addition. After 24 hours the reaction is filtered and washed with reaction solvent to yield a white solid precipitate which can be recrystallised (MeOH, CHCl₃, EtOH) to yield SCXRD quality crystals.

(*R*)-*N*-methyl, *N*-isopropyl anilinium hydrobromide · (*R*)-1,1'-bi-2-naphthol

Following the general procedure outlined in 9.12.1, **183** (0.119 g, 0.91 mmol) was dissolved in EtOH (1.00 mL, 0.9 M) and HBr (48%, 0.20 mL, 1.50 mmol) was added. (*R*)-BINOL (0.279 g, 0.97 mmol) was added, and the mixture was stirred at 1500 rpm for 24

hours. A white precipitate formed which was isolated by vacuum filtration to yield **263** (0.214 g, 47% yield).

¹H NMR (599 MHz, CDCl₃) δ 12.69 (1H, s, H₆), 7.95 (2H, d, *J* = 8.9 Hz, H_d), 7.88 (2H, d, *J* = 8.1 Hz, H_f), 7.78 – 7.72 (2H, m, H₃), 7.53 – 7.46 (2H, m, H₁₊₂), 7.40 (2H, apt. d, H_i), 7.36 (2H, ddd, *J* = 8.2, 6.8, 1.1 Hz, H_g), 7.29 (2H, ddd, *J* = 8.2, 6.8, 1.3 Hz, H_h), 7.14 (2H, dq, *J* = 8.5, 0.9 Hz, H_c), 5.29 (2H, s, H_a), 3.74 (1H, sept., *J* = 4.4 Hz, H₇), 3.11 (3H, s, H₅), 1.52 (3H, dd, *J* = 6.6, 2.2 Hz, H₈), 1.33 (3H, d, *J* = 6.5 Hz, H₈).

¹³C NMR (151 MHz, CDCl₃) δ 152.7 (C_b), 139.5 (C₄), 133.5 (C_j), 131.3 (C_d), 130.24 (C₁), 130.18 (C₂), 129.4 (C_e), 128.4 (C_f), 127.4 (C_h), 124.3 (C_c), 123.9 (C_g), 122.6 (C₃), 117.8 (C_i), 111.1 (C_k), 62.1 (C₇), 41.5 (C₅), 18.2 (C₈), 17.8 (C₈).

LRMS (ESI-TOF, EI⁺) *m/z*: 150.2 ([M]⁺, 100%).

LRMS (ESI-TOF, EI⁻) *m/z*: 285.4 ([M-H]⁻, 100%).

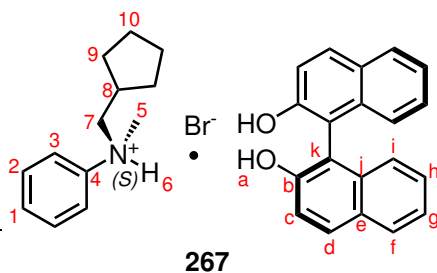
HRMS (ESI-TOF) *m/z*: [M]⁺ calculated for C₁₀H₁₆N⁺: 150.1283, found 150.1276. [M-H]⁻ calculated for C₂₀H₁₃O₂⁻: 285.0916, found 285.0920.

mp: 160 – 162 °C (EtOH).

Optical rotation: [α]_D²⁰ = +21.04 (MeOH, *c* = 1.00).

IR (max/cm⁻¹): 3226br(s), 2692br(w), 1619w, 1430m, 1267s, 962m, 817s, 749s, 548m.

XRD: A portion of the complex was crystallised in EtOH to give clear colourless blocks. Crystal data for C₃₀H₃₀BrNO₂ (*m* = 516.46 g/mol): Monoclinic, space group *P*2₁ (no. 4).

(S)-N-methyl, N-homocyclopentyl anilinium hydrobromide · (R)-1,1'-bi-2-naphthol

Following the general procedure outlined in 9.12.1, **188** (0.193 g, 1.02 mmol) was dissolved in EtOH (1.00 mL, 1.0 M) and HBr (48%, 0.20 mL, 1.50 mmol) was added. (*R*)-BINOL (0.289 g, 1.01 mmol) was added, and the mixture was stirred at 1500 rpm for 24 hours. A white precipitate formed which was

isolated by vacuum filtration to yield **267** (0.312 g, 55% yield).

^1H NMR (599 MHz, CDCl_3) δ 12.65 (1H, s, H_6), 7.96 (2H, d, $J = 8.9$ Hz, H_d), 7.88 (2H, dd, $J = 8.2, 1.0$ Hz, H_f), 7.83 – 7.77 (2H, m, H_3), 7.54 – 7.46 (3H, m, H_{1+2}), 7.40 (2H, d, $J = 8.9$ Hz, H_i), 7.36 (2H, ddd, $J = 8.1, 6.8, 1.2$ Hz, H_g), 7.29 (2H, ddd, $J = 8.2, 6.8, 1.3$ Hz, H_h), 7.14 (2H, dq, $J = 8.5, 0.9$ Hz, H_c), 5.29 (2H, s, H_a), 3.48 – 3.40 (1H, m, H_7), 3.35 – 3.24 (1H, m, $\text{H}_{7'}$), 3.13 (3H, dd, $J = 20.7, 4.8$ Hz, H_5), 2.04 (1H, p, $J = 7.6$ Hz, H_8), 1.86 (1H, dh, $J = 11.6, 3.6$ Hz, H_9), 1.65 – 1.36 (2H, m, $\text{H}_{10'}$), 1.57 – 1.48 (2H, m, H_{9+10}), 1.48 – 1.36 (2H, m, H_{9+10}), 0.91 (1H, ddd, $J = 21.8, 14.7, 8.6$ Hz, H_9).

^{13}C NMR (151 MHz, CDCl_3) δ 152.8 (C_b), 140.6 (C_4), 133.6 (C_j), 131.4 (C_d), 130.6 (C_2), 130.5 (C_1), 129.5 (C_e), 128.5 (C_f), 127.5 (C_h), 124.4 (C_c), 124.1 (C_g), 121.8 (C_3), 117.9 (C_i), 111.3 (C_k), 65.0 (d, $J = 5.6$ Hz, C_7), 47.6 (d, $J = 3.3$ Hz, C_5), 36.3 (C_8), 31.6 (C_9), 31.35 (C_9), 25.1 (C_{10}), 25.01 ($\text{C}_{10'}$).

LRMS (ESI-TOF, EI^+) m/z : 190.2 ($[\text{M}]^+$, 100%).

LRMS (ESI-TOF, EI^-) m/z : 285.4 ($[\text{M}-\text{H}]^-$, 100%).

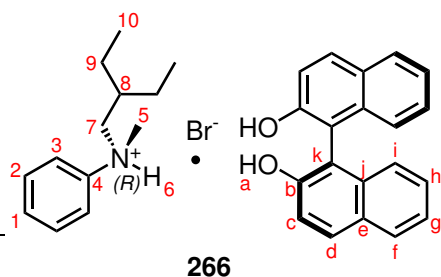
HRMS (ESI-TOF) m/z : $[\text{M}]^+$ calculated for $\text{C}_{13}\text{H}_{20}\text{N}^+$: 190.1596, found 190.1588. $[\text{M}-\text{H}]^-$ calculated for $\text{C}_{20}\text{H}_{13}\text{O}_2^-$: 285.0916, found 285.0924.

mp: 172 °C (EtOH).

Optical rotation: $[\alpha]_D^{20} = +15.51$ (MeOH, $c = 1.00$).

IR (max/cm $^{-1}$): 3308br, 1622m, 1272s, 979m, 818s, 747s, 691m, 552m.

XRD: A portion of the complex was crystallised in EtOH to give clear colourless prisms. Crystal data for $\text{C}_{33}\text{H}_{34}\text{BrNO}_2$ ($m = 556.52$ g/mol): Orthorhombic, space group $P2_12_12_1$ (no. 19).

(*R*)-*N*-methyl, *N*-2-ethylbutyl anilinium hydrobromide · (*R*)-1,1'-bi-2-naphthol

Following the general procedure outlined in 9.12.1, **349** (0.194 g, 1.01 mmol) was dissolved in EtOH (1.00 mL, 1.0 M) and HBr (48%, 0.20 mL, 1.50 mmol) was added. (*R*)-BINOL (0.287 g, 1.00 mmol) was added, and the mixture was stirred at 1500 rpm for 24 hours. A white precipitate formed which was

isolated by vacuum filtration to yield **266** (0.351 g, 63% yield).

^1H NMR (599 MHz, CDCl_3) δ 12.54 (1H, s, H_6), 7.96 (2H, d, $J = 8.9$ Hz, H_d), 7.91 – 7.87 (2H, m, H_f), 7.80 (2H, dt, $J = 6.6, 1.5$ Hz, H_3), 7.56 – 7.46 (3H, m, H_{1+2}), 7.40 (2H, d, $J = 8.9$ Hz, H_i), 7.36 (2H, ddd, $J = 8.1, 6.8, 1.2$ Hz, H_g), 7.29 (2H, ddd, $J = 8.3, 6.8, 1.3$ Hz, H_h), 7.14 (2H, dt, $J = 8.4, 1.0$ Hz, H_c), 5.29 (2H, s, H_a), 3.32 (1H, ddt, $J = 12.6, 8.8, 3.7$ Hz, H_7), 3.21 (1H, ddt, $J = 12.7, 8.0, 4.0$ Hz, H_7), 3.15 (3H, dd, $J = 20.5, 5.0$ Hz, H_5), 1.77 (1H, ddq, $J = 17.8, 7.5, 3.8$ Hz, H_9), 1.48 (1H, dpd, $J = 14.7, 7.4, 5.2$ Hz, H_9), 1.39 – 1.32 (1H, m, H_8), 1.29 (1H, ddd, $J = 13.1, 10.3, 6.4$ Hz, H_9), 1.15 (1H, tp, $J = 14.4, 7.1$ Hz, H_9), 0.79 (3H, td, $J = 7.4, 5.4$ Hz, H_{10}), 0.75 (3H, td, $J = 7.4, 5.4$ Hz, H_{10}).

^{13}C NMR (151 MHz, CDCl_3) δ 152.8 (C_b), 140.4 (C_4), 133.6 (C_j), 131.4 (C_d), 130.6 (C_2), 130.5 (C_1), 129.5 (C_e), 128.5 (C_f), 127.5 (C_h), 124.4 (C_c), 124.1 (C_g), 121.7 (C_3), 117.9 (C_i), 111.3 (C_k), 63.0 (d, $J = 4.0$ Hz, C_7), 48.1 (d, $J = \text{Hz}$, C_5), 36.8 (C_8), 23.5 (C_9), 23.4 (d, $J = 2.0$ Hz, C_9), 10.5 (d, $J = 2.2$ Hz, C_{10}), 10.1 (C_{10}).

LRMS (ESI-TOF, EI^+) m/z : 192.2 ($[\text{M}]^+$, 100%).

LRMS (ESI-TOF, EI^-) m/z : 285.4 ($[\text{M}-\text{H}]^-$, 100%).

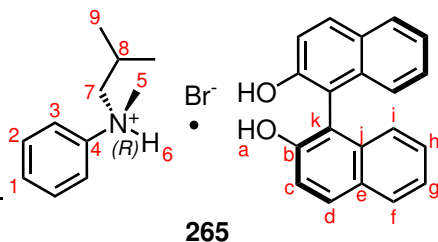
HRMS (ESI-TOF) m/z : $[\text{M}]^+$ calculated for $\text{C}_{13}\text{H}_{22}\text{N}^+$: 192.1752, found 192.1746. $[\text{M}-\text{H}]^-$ calculated for $\text{C}_{20}\text{H}_{13}\text{O}_2^-$: 285.0916, found 285.0908.

mp: 159 °C (EtOH).

Optical rotation: $[\alpha]_D^{20} = +21.67$ (MeOH, $c = 1.00$).

IR ($\text{max}/\text{cm}^{-1}$): 3216br(s), 1624m, 1432m, 1268s, 981m, 814s, 747s, 697m, 566m.

XRD: A portion of the complex was crystallised in EtOH to give clear colourless prisms. Crystal data for $\text{C}_{33}\text{H}_{33}\text{BrNO}_2$ ($m = 555.51$ g/mol): Orthorhombic, space group $P2_12_12_1$ (no. 19).

(R)-N-methyl, N-isobutyl anilinium hydrobromide · (R)-1,1'-bi-2-naphthol

Following the general procedure outlined in 9.12.1, **174** (0.161 g, 0.98 mmol) was dissolved in EtOH (1.00 mL, 1.0 M) and HBr (48%, 0.20 mL, 1.50 mmol) was added. (*R*)-BINOL (0.286 g, 0.99 mmol) was added, and the mixture was stirred at 1500 rpm for 24 hours. A white precipitate formed which was

isolated by vacuum filtration to yield **265** (0.330 g, 63% yield).

^1H NMR (599 MHz, CDCl_3) δ 12.72 (1H, s, H_6), 7.97 (2H, d, $J = 8.9$ Hz, H_d), 7.89 (2H, d, $J = 8.2$ Hz, H_f), 7.85 – 7.80 (2H, m, H_3), 7.56 – 7.47 (3H, m, H_{1+2}), 7.40 (2H, d, $J = 8.9$ Hz, H_i), 7.37 (2H, ddd, $J = 8.1, 6.8, 1.2$ Hz, H_g), 7.30 (2H, ddd, $J = 8.2, 6.8, 1.3$ Hz, H_h), 7.15 (2H, apt. d, $J = 8.5$ Hz, H_c), 5.17 (2H, s, H_a), 3.29 (1H, ddd, $J = 12.8, 8.9, 4.2$ Hz, H_7), 3.22 (1H, ddd, $J = 12.8, 8.9, 4.2$ Hz, H_7), 3.16 (3H, dd, $J = 12.8, 5.0$ Hz, H_5), 1.84 – 1.76 (1H, m, H_8), 1.17 (3H, dd, $J = 6.7, 2.4$ Hz, H_9), 0.84 (3H, dd, $J = 6.8, 5.0$ Hz, H_9).

^{13}C NMR (151 MHz, CDCl_3) δ 152.9 (C_b), 140.4 (C_4), 133.6 (C_j), 131.5 (C_d), 130.7 (C_2), 130.6 (C_1), 129.6 (C_e), 128.5 (C_f), 127.6 (C_h), 124.4 (C_c), 124.1 (C_g), 121.7 (C_3), 117.9 (C_i), 111.1 (C_k), 66.4 (d, $J = 4.5$ Hz, C_7), 48.4 (C_5), 25.3 (C_8), 21.2 (C_9), 20.9 (d, $J = 2.0$ Hz, C_9).

LRMS (ESI-TOF, EI^+) m/z : 164.2 ($[\text{M}]^+$, 100%).

LRMS (ESI-TOF, EI^-) m/z : 285.4 ($[\text{M}-\text{H}]^-$, 100%).

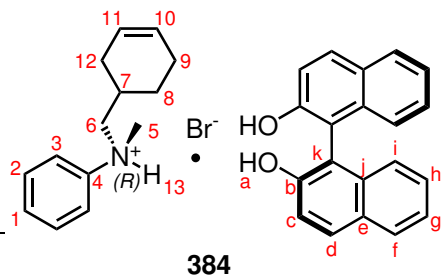
HRMS (ESI-TOF) m/z : $[\text{M}]^+$ calculated for $\text{C}_{11}\text{H}_{18}\text{N}^+$: 164.1439, found 164.1437. $[\text{M}-\text{H}]^-$ calculated for $\text{C}_{20}\text{H}_{13}\text{O}_2^-$: 285.0916, found 285.0925.

mp: 174 °C (EtOH).

Optical rotation: $[\alpha]_D^{20} = +18.98$ (MeOH, $c = 1.00$).

IR (max/ cm^{-1}): 3182br(s), 1624m, 1270s, 982m, 813s, 749s, 698m, 560m..

XRD: A portion of the complex was crystallised in EtOH to give clear colourless prisms. Crystal data for $\text{C}_{31}\text{H}_{32}\text{BrNO}_2$ ($m = 530.48$ g/mol): Orthorhombic, space group $P2_12_12_1$ (no. 19).

(R)-N-methyl, N-homocyclohex-2-ene anilinium hydrobromide · (R)-1,1'-bi-2-naphthol

Following the general procedure outlined in 9.12.1, **350** (0.197 g, 1.01 mmol) was dissolved in EtOH (0.50 mL, 2.0 M) and HBr (48%, 0.20 mL, 1.50 mmol) was added. (*R*)-BINOL (0.286 g, 1.00 mmol) was added, and the mixture was stirred at 1500 rpm for 24 hours. A white precipitate formed which was

isolated by vacuum filtration to yield **384** (0.294 g, 53% yield). The product was isolated as a single diastereomer.

^1H NMR (599 MHz, CD_3OD) δ 7.86 (2H, d, $J = 8.9$ Hz, H_d), 7.82 (2H, dd, $J = 8.2, 1.3$ Hz, H_f), 7.64 (2H, dd, $J = 7.6, 1.9$ Hz, H_3), 7.59 – 7.53 (2H, m, H_2), 7.56 – 7.49 (1H, m, H_1), 7.31 (2H, d, $J = 8.9$ Hz, H_i), 7.23 (2H, ddd, $J = 8.0, 6.7, 1.2$ Hz, H_g), 7.13 (2H, ddd, $J = 8.2, 6.7, 1.3$ Hz, H_h), 7.03 (2H, d, $J = 8.3$ Hz, H_c), 5.62 – 5.51 (1H, m, H_{10}), 5.56 – 5.52 (1H, m, H_{11}), 4.87 (1H, s, H_{13}), 3.63 – 3.45 (2H, m, H_6), 3.20 (3H, s, H_5), 2.06 – 1.95 (2H, m, H_{12}), 1.91 – 1.83 (2H, m, H_8), 1.62 – 1.53 (2H, m, H_9), 1.35 – 1.25 (1H, m, H_7). ^{13}C NMR (151 MHz, CD_3OD) δ 154.1 (C_b), 141.5 (C_4), 135.8 (C_j), 131.9 (C_2), 131.7 (C_1), 130.5 (C_d), 130.4 (C_e), 129.0 (C_f), 127.8 (C_{10}), 127.1 (C_h), 125.8 (C_c), 125.3 (C_{11}), 123.8 (C_g), 122.3 (C_3), 119.3 (C_i), 116.2 (C_k), 65.5 (C_6), 47.9 (C_5), 31.3 (C_9), 29.9 (C_8), 26.9 (C_7), 24.9 (C_{12}). LRMS (ESI-TOF, EI^+) m/z : 202.2 ($[\text{M}]^+$, 100%).

LRMS (ESI-TOF, EI^-) m/z : 285.4 ($[\text{M}-\text{H}]^-$, 100%).

HRMS (ESI-TOF) m/z : $[\text{M}]^+$ calculated for $\text{C}_{11}\text{H}_{18}\text{N}^+$: 202.1596, found 202.1589. $[\text{M}-\text{H}]^-$ calculated for $\text{C}_{20}\text{H}_{13}\text{O}_2^-$: 285.0916, found 285.0901.

mp: 149 – 150 °C (EtOH).

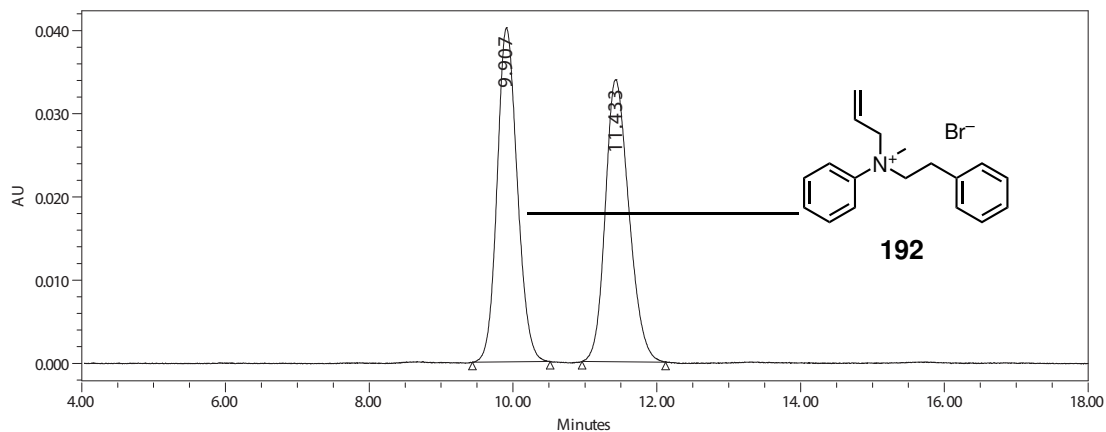
Optical rotation: $[\alpha]_D^{20} = +14.70$ (MeOH, $c = 1.00$).

IR ($\text{max}/\text{cm}^{-1}$): 3306br, 2653br, 1623m, 1432m, 1272s, 980m, 816s, 749s, 556m.

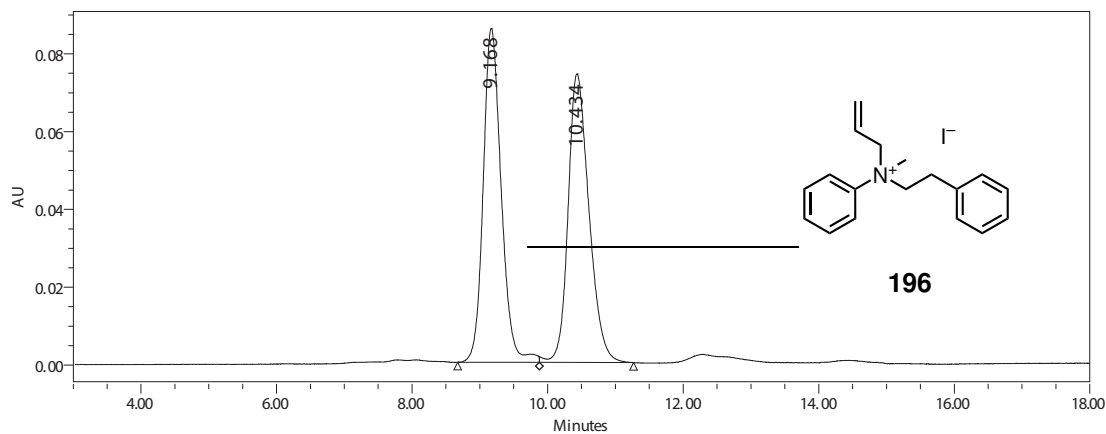
9.13 Enantioenrichment determination

9.13.1 Racemic ammonium salt HPLC traces

N-allyl, *N*-phenylacetyl, *N*-methyl anilinium bromide

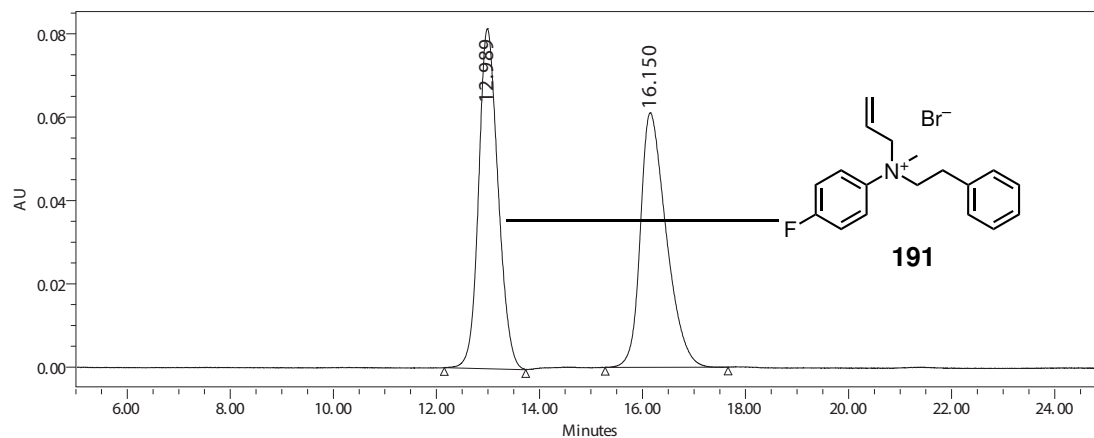


N-allyl, *N*-phenylacetyl, *N*-methyl anilinium iodide



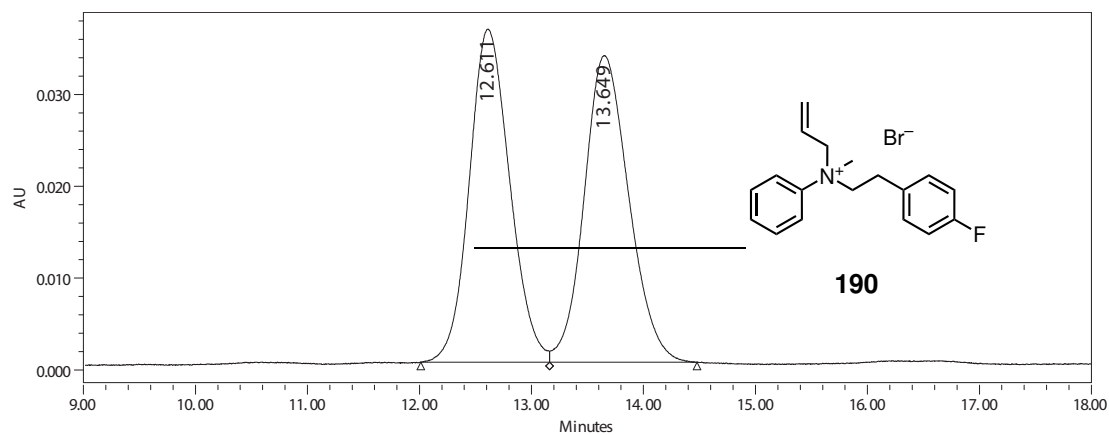
9.13. ENANTIOENRICHMENT DETERMINATION

N-allyl, *N*-phenylacetyl, *N*-methyl-4-fluoroanilinium bromide

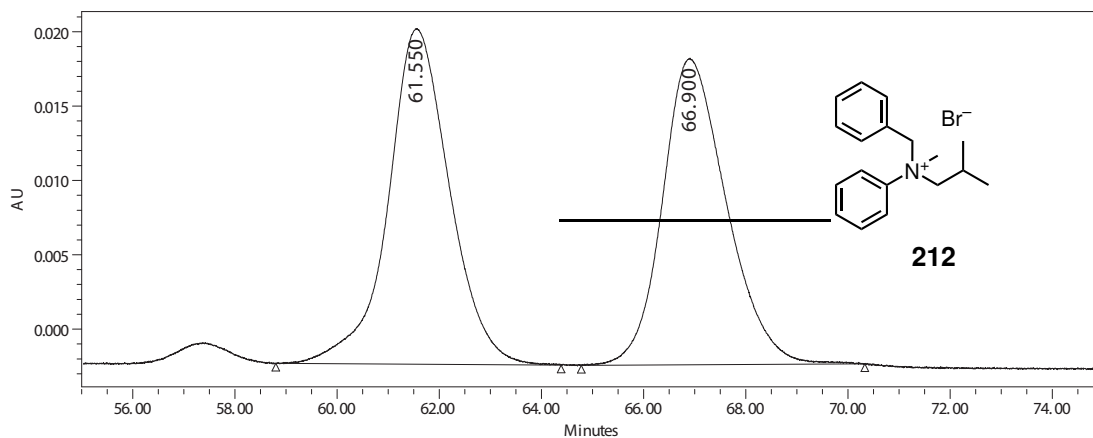


Flow Rate (mL min ⁻¹)	0.5
Retention Time (min)	12.989 16.150
Peak Area (%)	50.00 50.00

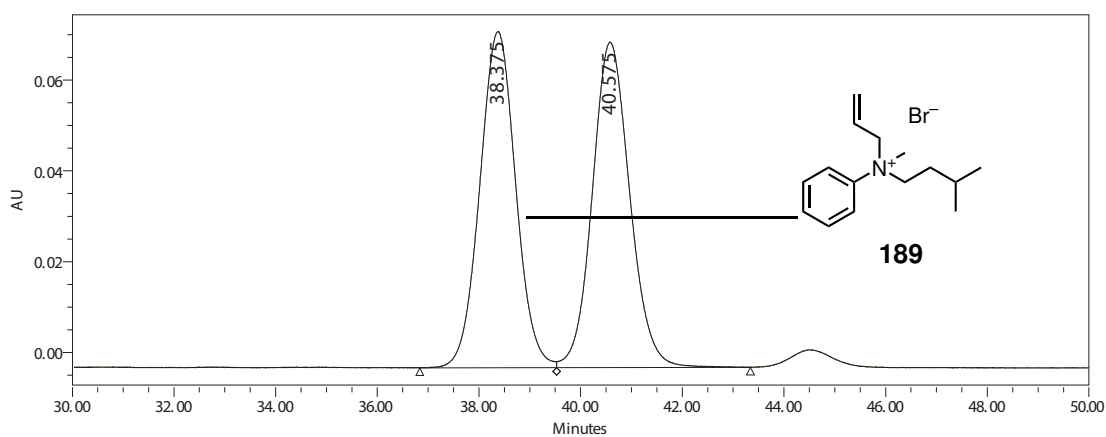
N-allyl, *N*-4-fluorophenylacetyl, *N*-methyl anilinium bromide



Flow Rate (mL min ⁻¹)	0.5
Retention Time (min)	12.611 13.649
Peak Area (%)	49.60 50.40

***N*-benzyl, *N*-isobutyl, *N*-methyl anilinium bromide**

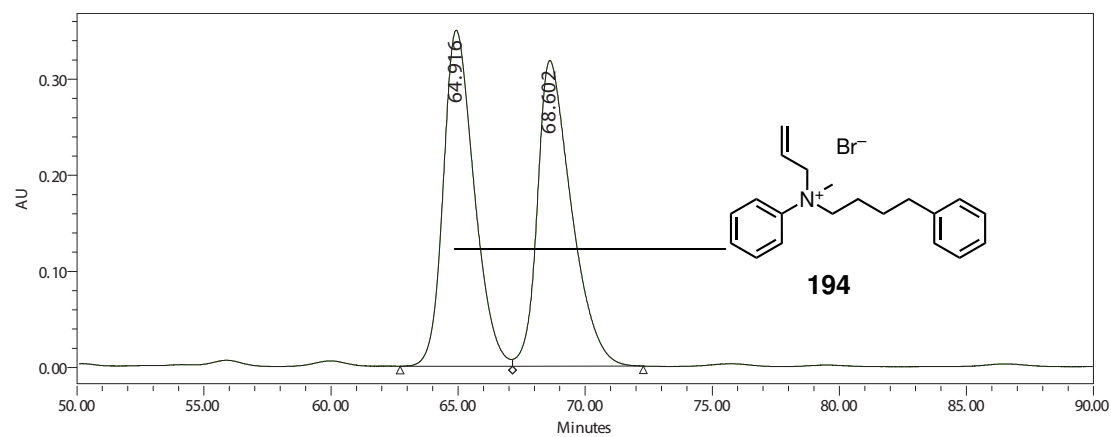
Flow Rate (mL min⁻¹) **0.1**
Retention Time (min) **61.550 66.900**
Peak Area (%) **51.28 48.72**

***N*-allyl, *N*-isovaleryl, *N*-methyl anilinium bromide**

Flow Rate (mL min⁻¹) **0.1**
Retention Time (min) **38.375 40.575**
Peak Area (%) **49.98 50.02**

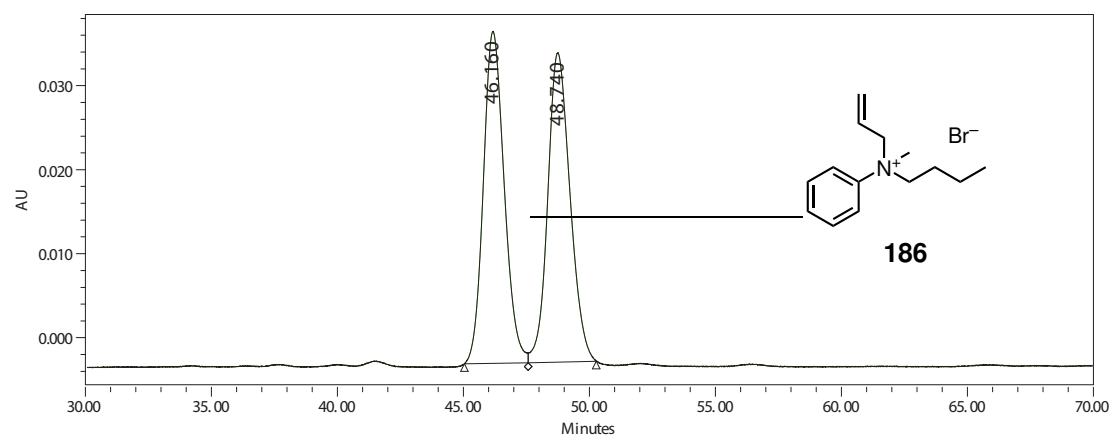
9.13. ENANTIOENRICHMENT DETERMINATION

N-allyl, *N*-4-phenylbutyl, *N*-methyl anilinium bromide

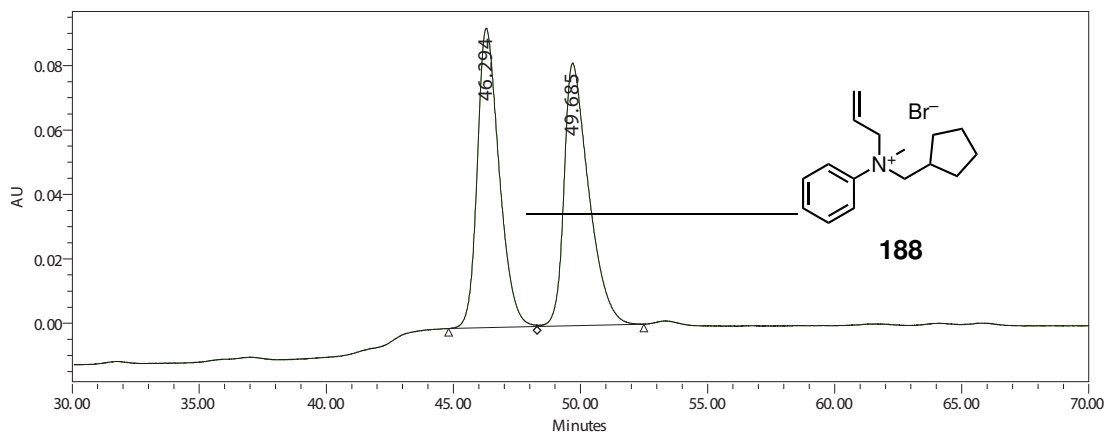


Flow Rate (mL min ⁻¹)	0.1	
Retention Time (min)	64.916	68.602
Peak Area (%)	49.93	50.07

N-allyl, *N*-butyl, *N*-methyl anilinium bromide



Flow Rate (mL min ⁻¹)	0.1	
Retention Time (min)	46.160	48.740
Peak Area (%)	50.08	49.92

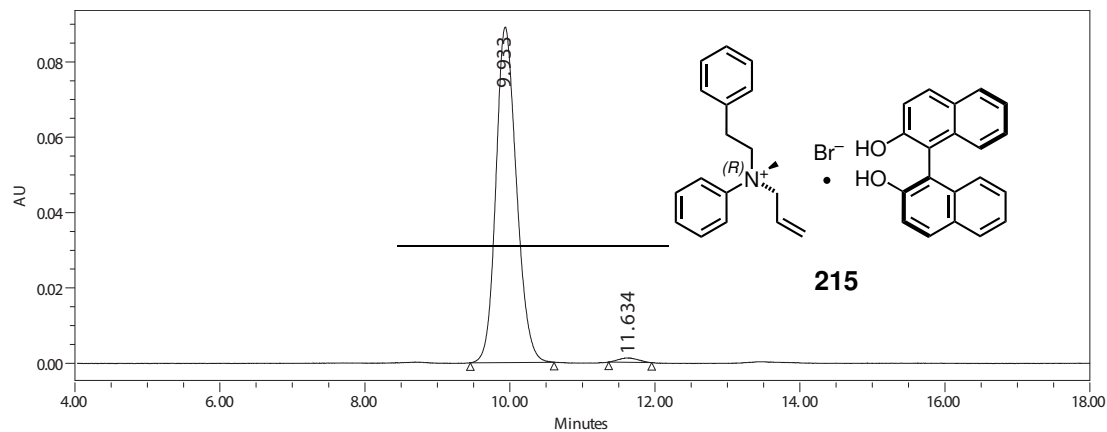
***N*-allyl, *N*-homocyclopentyl, *N*-methyl anilinium bromide**

Flow Rate (mL min ⁻¹)	0.1
Retention Time (min)	46.294 49.685
Peak Area (%)	53.77 46.23

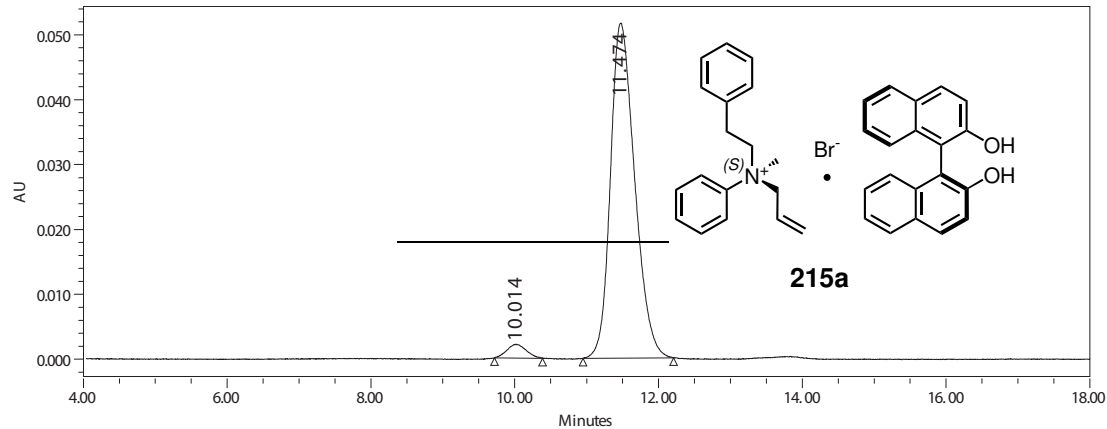
9.13. ENANTIOENRICHMENT DETERMINATION

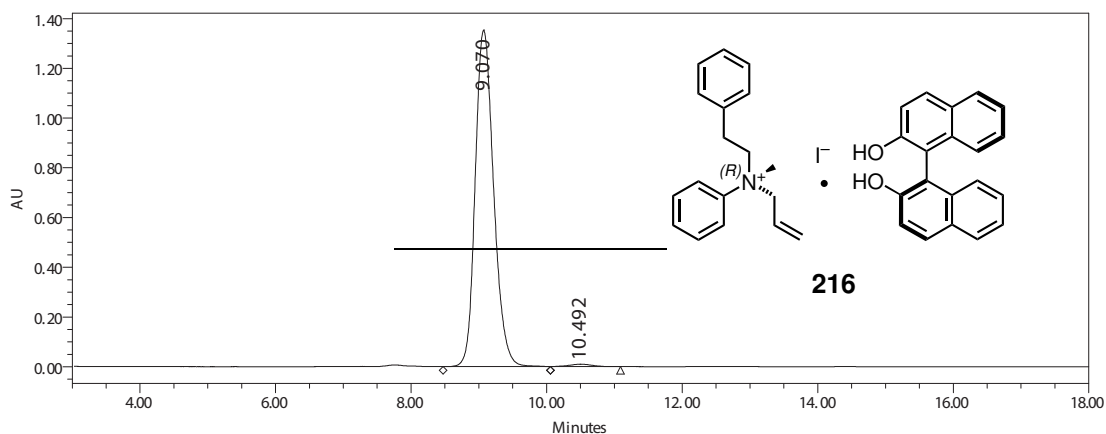
9.13.2 (*R*)-BINOL and (*S*)-BINOL complex HPLC traces

N-allyl, *N*-phenylacetyl, *N*-methyl anilinium bromide · (*R*)-1,1'-bi-2-naphthol

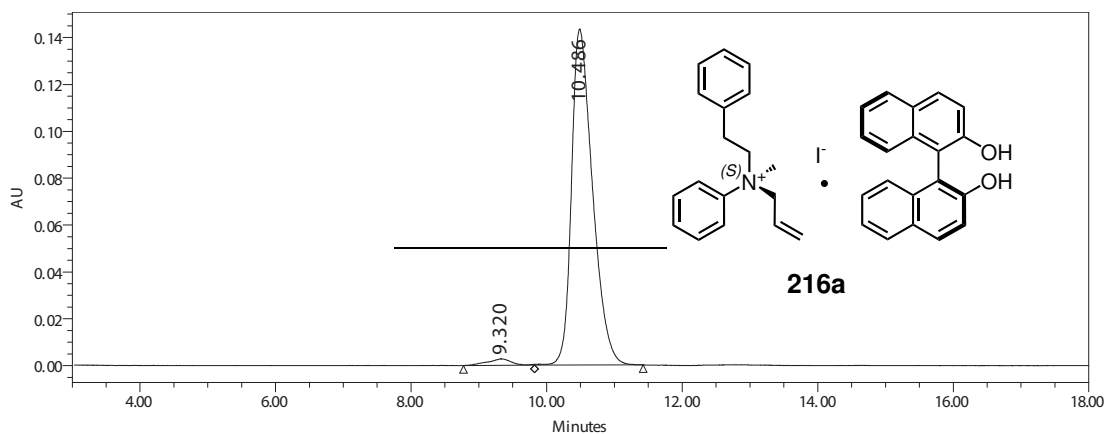


N-allyl, *N*-phenylacetyl, *N*-methyl anilinium bromide · (*S*)-1,1'-bi-2-naphthol



***N*-allyl, *N*-phenylacetyl, *N*-methyl anilinium iodide · (*R*)-1,1'-bi-2-naphthol**

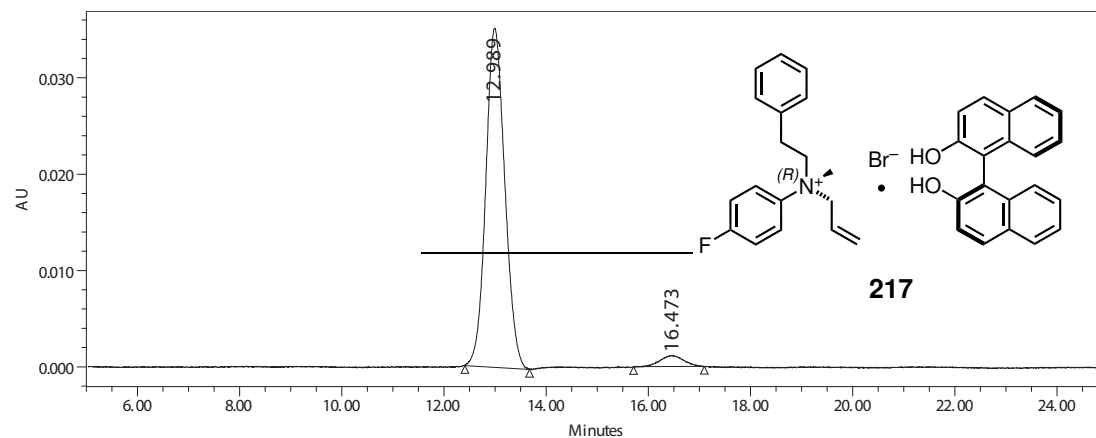
Flow Rate (mL min ⁻¹)	0.5	
Retention Time (min)	9.070	10.492
Peak Area (%)	99.12	0.88

***N*-allyl, *N*-phenylacetyl, *N*-methyl anilinium iodide · (*S*)-1,1'-bi-2-naphthol**

Flow Rate (mL min ⁻¹)	0.5	
Retention Time (min)	9.320	10.486
Peak Area (%)	2.17	97.83

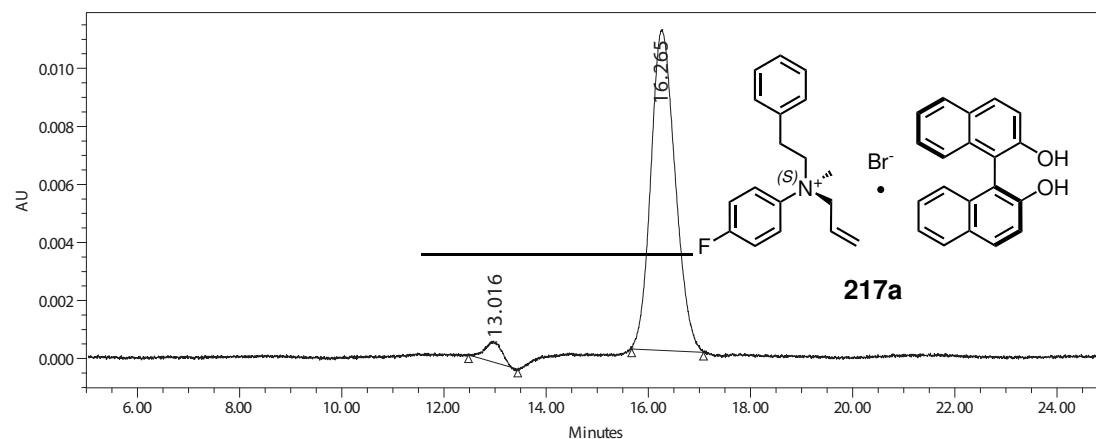
9.13. ENANTIOENRICHMENT DETERMINATION

N-allyl, *N*-phenylacetyl, *N*-methyl-4-fluoroanilinium bromide · (*R*)-1,1'-bi-2-naphthol

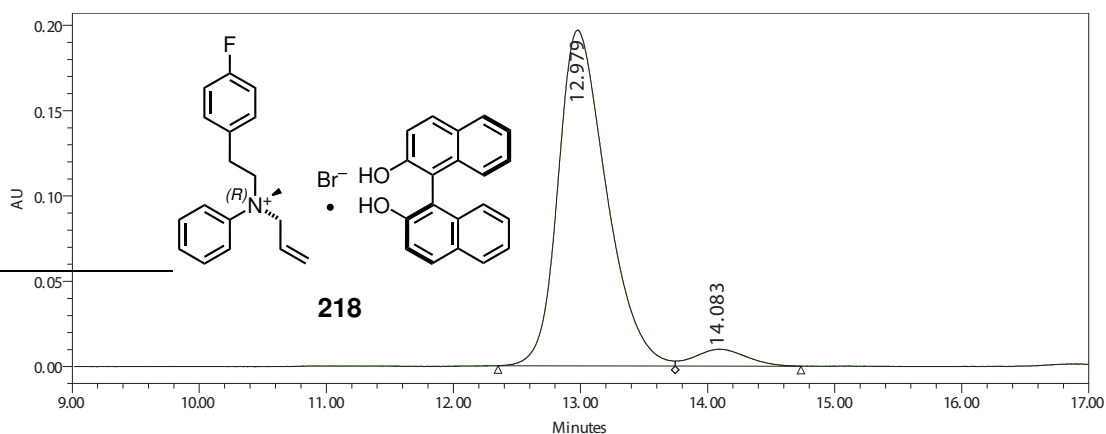


Flow Rate (mL min ⁻¹)	0.5	
Retention Time (min)	12.989	16.473
Peak Area (%)	96.15	3.85

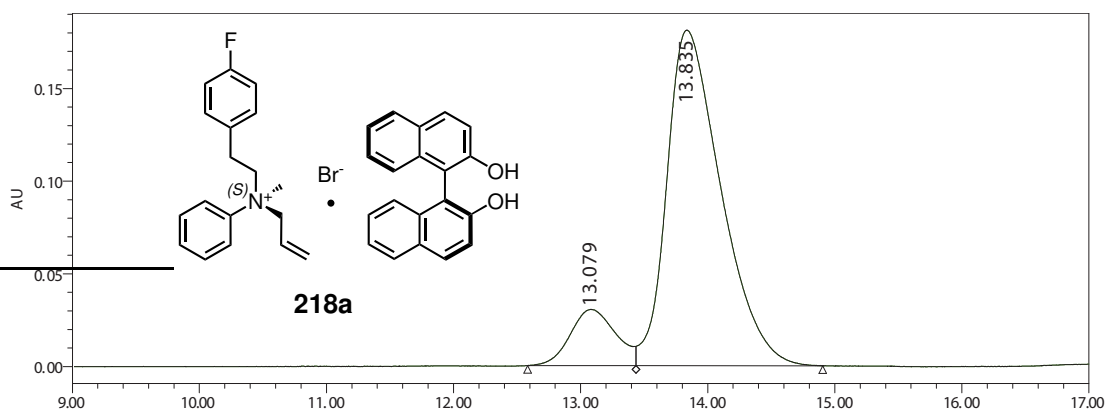
N-allyl, *N*-phenylacetyl, *N*-methyl-4-fluoroanilinium bromide · (*S*)-1,1'-bi-2-naphthol



Flow Rate (mL min ⁻¹)	0.5	
Retention Time (min)	13.016	16.265
Peak Area (%)	4.37	95.93

***N*-allyl, *N*-4-fluorophenylacetyl, *N*-methyl anilinium bromide · (*R*)-1,1'-bi-2-naphthol**

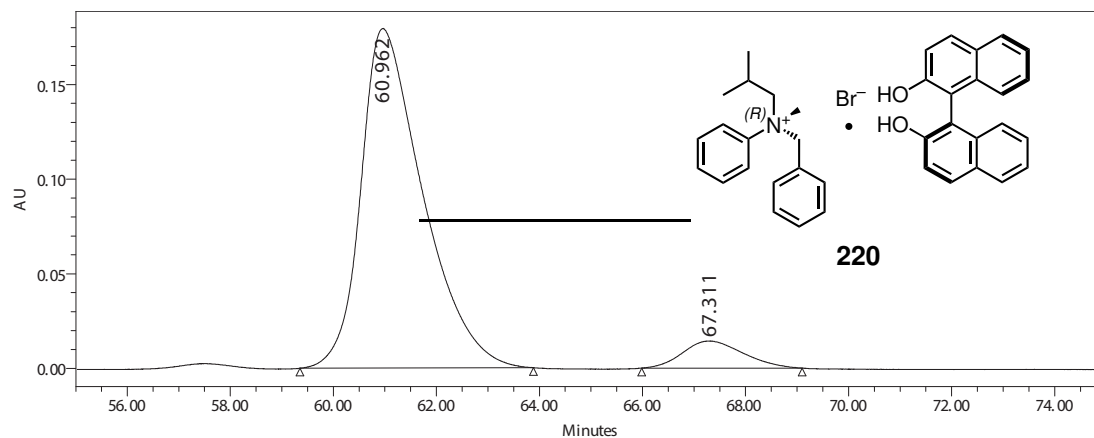
Flow Rate (mL min ⁻¹)	0.5	
Retention Time (min)	12.979	14.083
Peak Area (%)	94.87	5.13

***N*-allyl, *N*-4-fluorophenylacetyl, *N*-methyl anilinium bromide · (*S*)-1,1'-bi-2-naphthol**

Flow Rate (mL min ⁻¹)	0.5	
Retention Time (min)	13.079	13.835
Peak Area (%)	12.19	87.81

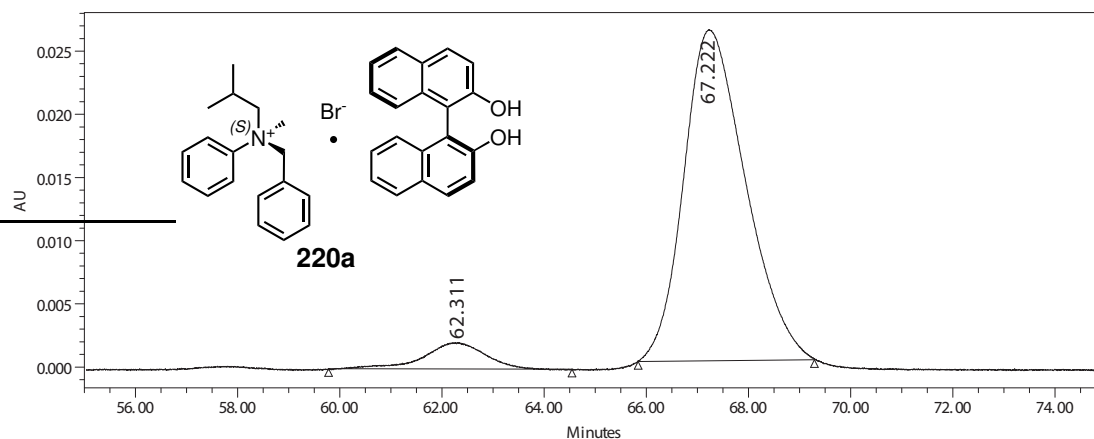
9.13. ENANTIOENRICHMENT DETERMINATION

N-benzyl, *N*-isobutyl, *N*-methyl anilinium bromide · (*R*)-1,1'-bi-2-naphthol

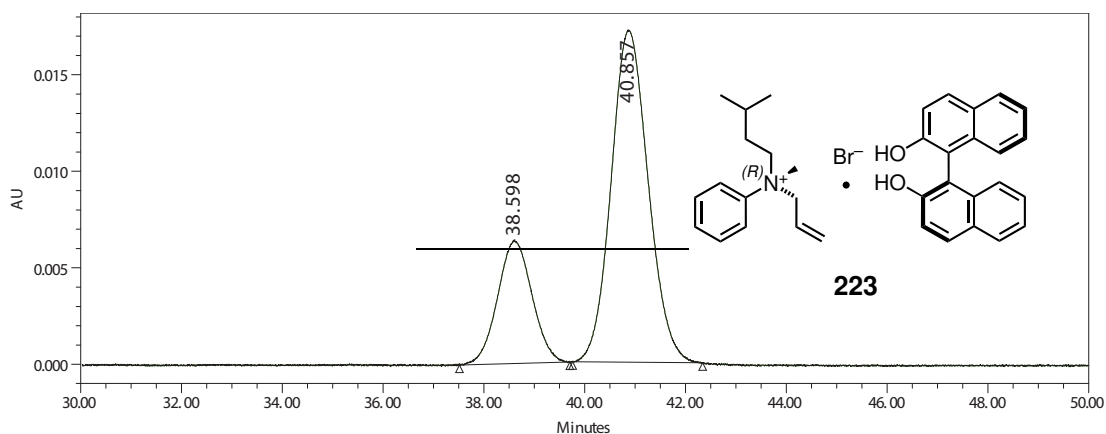
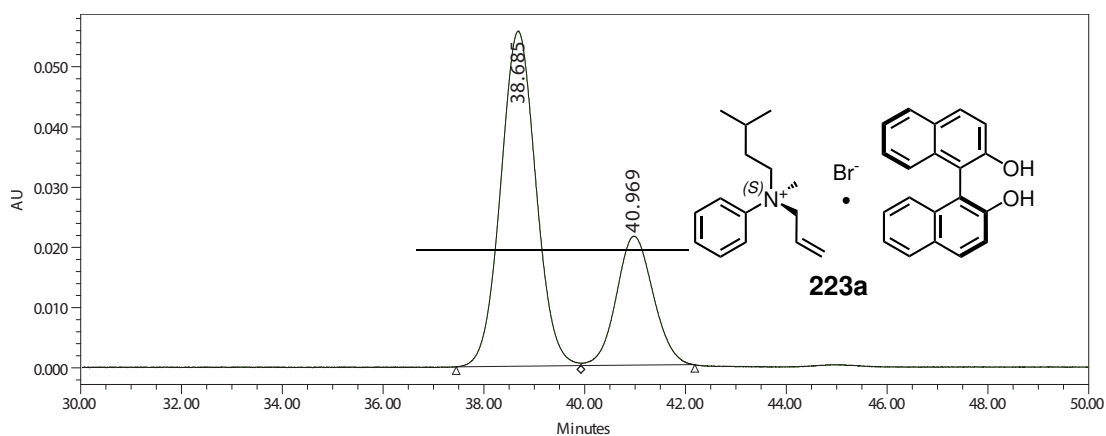


Flow Rate (mL min ⁻¹)	0.1
Retention Time (min)	60.962 67.311
Peak Area (%)	92.73 7.27

N-benzyl, *N*-isobutyl, *N*-methyl anilinium bromide · (*S*)-1,1'-bi-2-naphthol

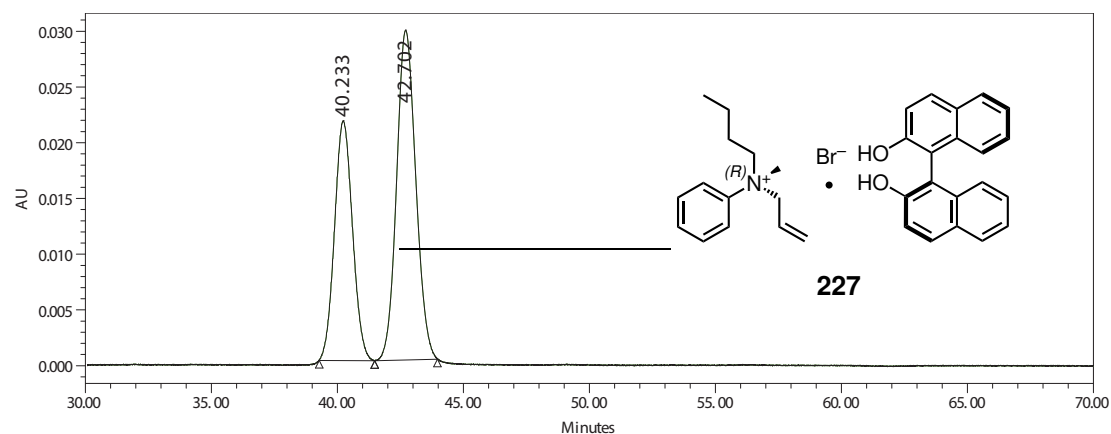


Flow Rate (mL min ⁻¹)	0.1
Retention Time (min)	62.311 67.222
Peak Area (%)	7.25 92.75

N*-allyl, *N*-isovaleryl, *N*-methyl anilinium bromide · (*R*)-1,1'-bi-2-naphthol**Flow Rate (mL min⁻¹) **0.1**Retention Time (min) **38.598 40.857**Peak Area (%) **24.77 75.23**N*-allyl, *N*-isovaleryl, *N*-methyl anilinium bromide · (*S*)-1,1'-bi-2-naphthol**Flow Rate (mL min⁻¹) **0.1**Retention Time (min) **38.685 40.969**Peak Area (%) **71.35 28.65**

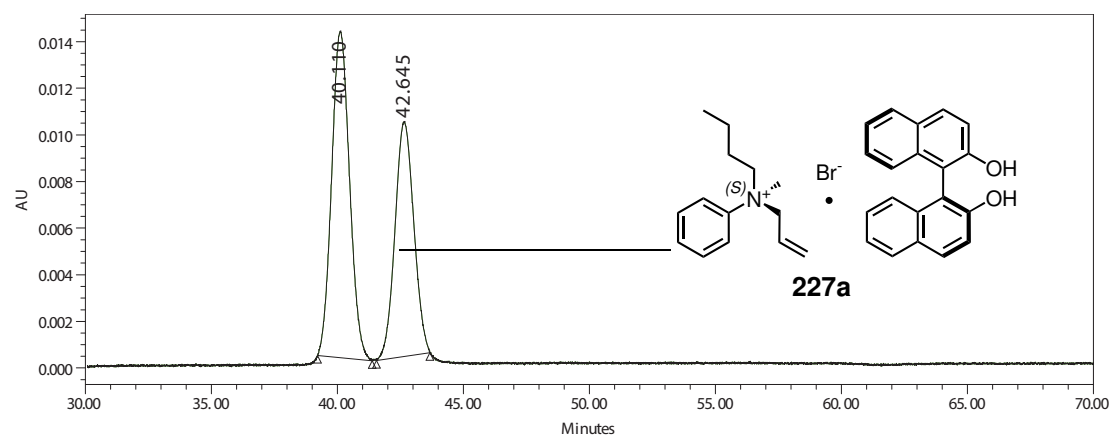
9.13. ENANTIOENRICHMENT DETERMINATION

N-allyl, *N*-butyl, *N*-methyl anilinium bromide · (*R*)-1,1'-bi-2-naphthol

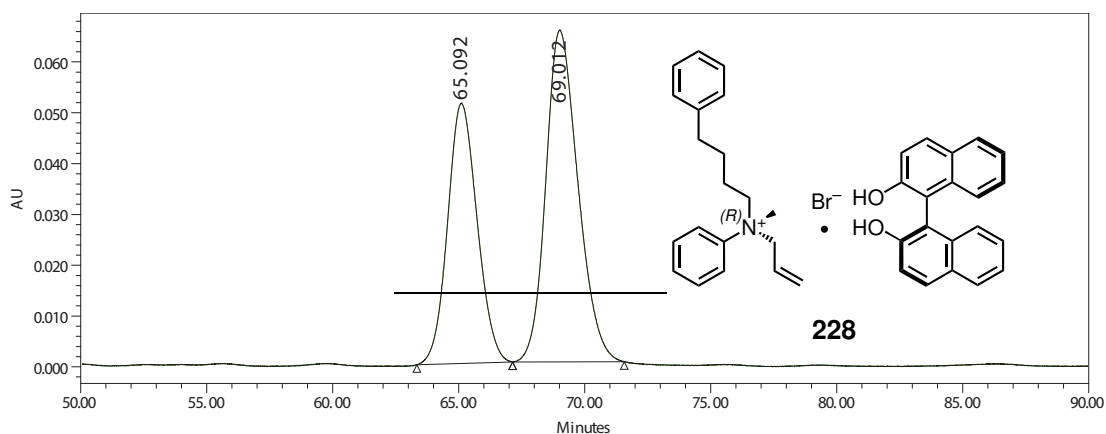


Flow Rate (mL min ⁻¹)	0.1
Retention Time (min)	40.233 42.702
Peak Area (%)	40.57 59.43

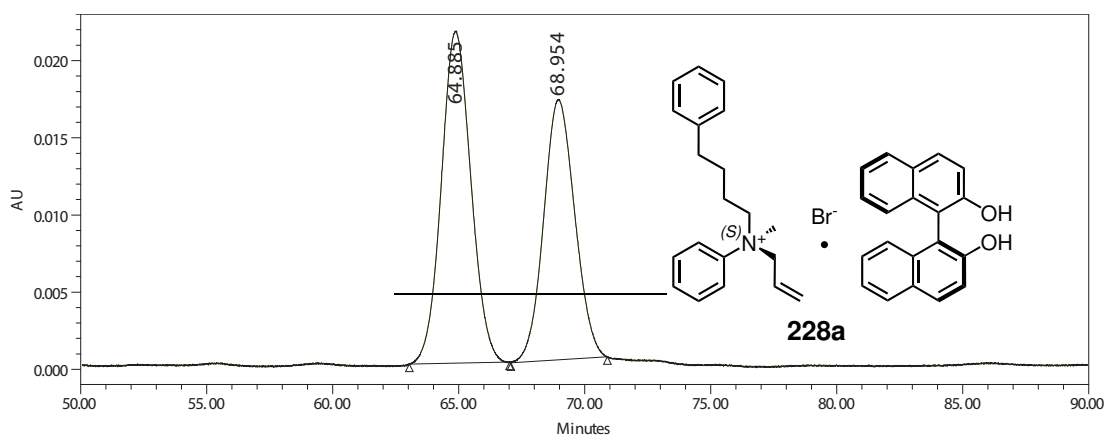
N-allyl, *N*-butyl, *N*-methyl anilinium bromide · (*S*)-1,1'-bi-2-naphthol



Flow Rate (mL min ⁻¹)	0.1
Retention Time (min)	40.110 42.645
Peak Area (%)	56.50 43.50

***N*-allyl, *N*-4-phenylbutyl, *N*-methyl anilinium bromide · (*R*)-1,1'-bi-2-naphthol**

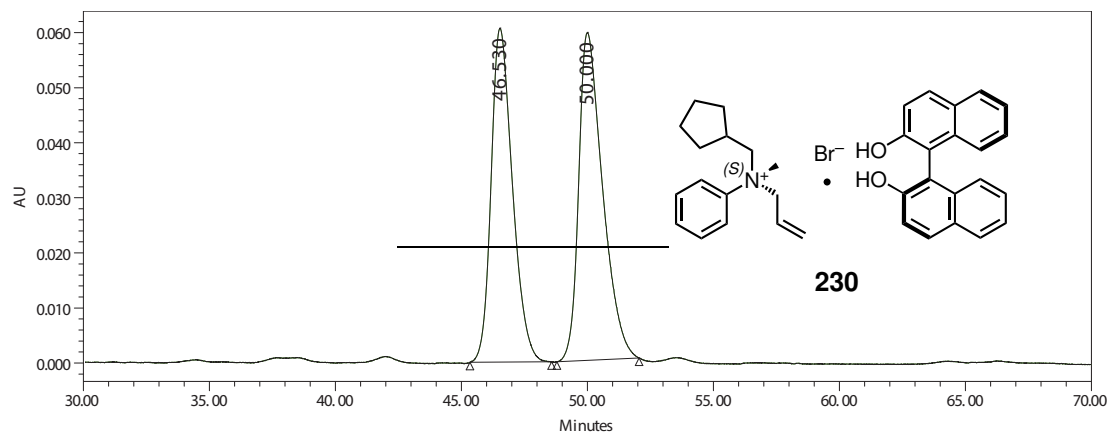
Flow Rate (mL min ⁻¹)	0.1	
Retention Time (min)	65.092	69.012
Peak Area (%)	41.85	58.15

***N*-allyl, *N*-4-phenylbutyl, *N*-methyl anilinium bromide · (*S*)-1,1'-bi-2-naphthol**

Flow Rate (mL min ⁻¹)	0.1	
Retention Time (min)	64.885	68.954
Peak Area (%)	54.72	45.28

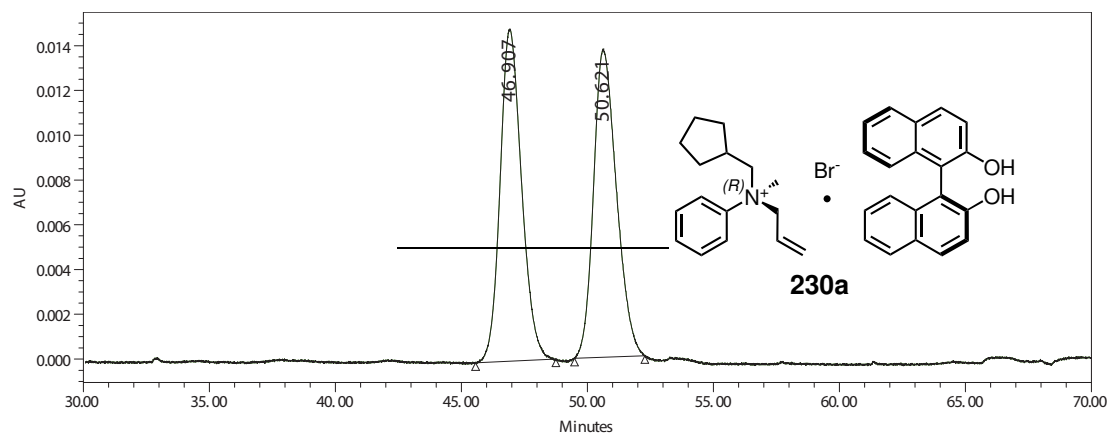
9.13. ENANTIOENRICHMENT DETERMINATION

N-allyl, *N*-homocyclopentyl, *N*-methyl anilinium bromide · (*R*)-1,1'-bi-2-naphthol



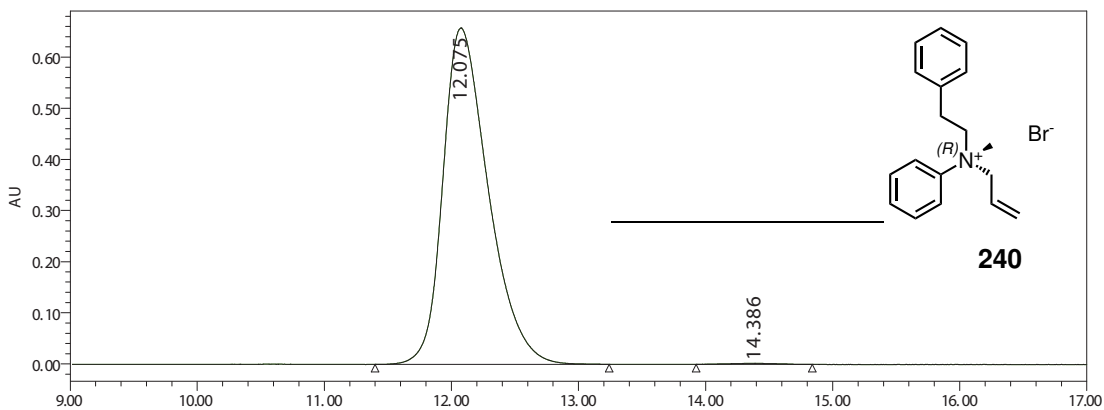
Flow Rate (mL min ⁻¹)	0.1	
Retention Time (min)	46.530	50.000
Peak Area (%)	47.42	52.58

N-allyl, *N*-homocyclopentyl, *N*-methyl anilinium bromide · (*S*)-1,1'-bi-2-naphthol

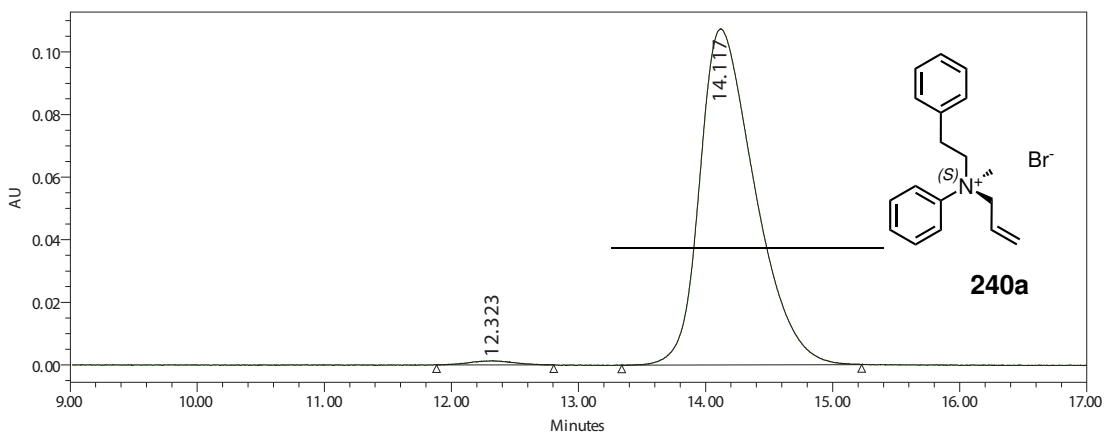


Flow Rate (mL min ⁻¹)	0.1	
Retention Time (min)	46.907	50.621
Peak Area (%)	49.75	50.25

9.13.3 Liberated salts HPLC traces

(R)-N-allyl, N-phenylacetyl, N-methyl anilinium bromide

Flow Rate (mL min ⁻¹)	0.5
Retention Time (min)	12.075 14.386
Peak Area (%)	99.72 0.28

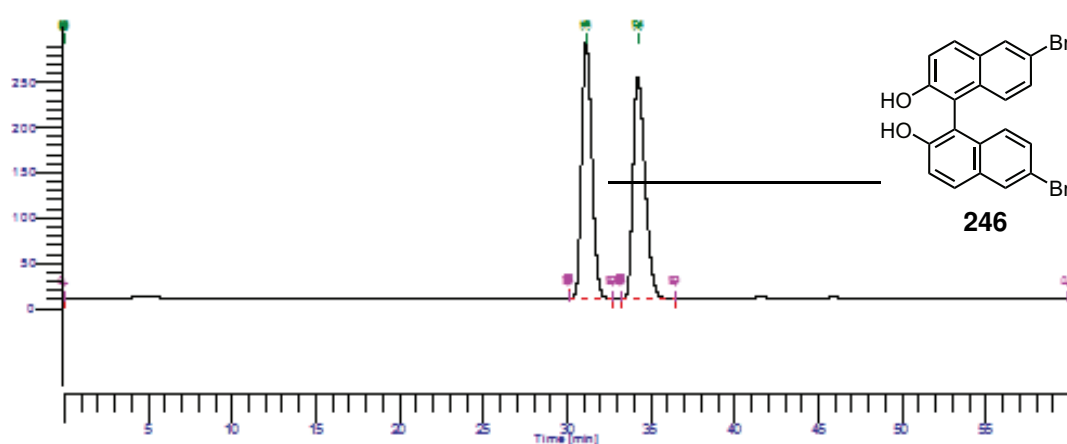
(S)-N-allyl, N-phenylacetyl, N-methyl anilinium bromide

Flow Rate (mL min ⁻¹)	0.5
Retention Time (min)	12.323 14.117
Peak Area (%)	0.64 99.36

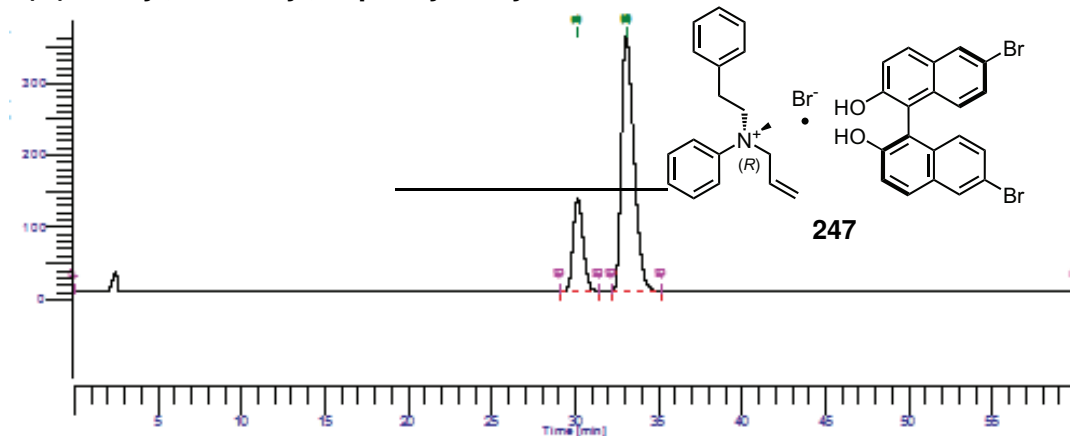
9.13.4 Substituted BINOL HPLC traces

Chiral HPLC for the separation of 6,6'-dibromo, 1,1'-bi-2-naphthol enantiomers was performed with a *Sunfire* C18 column on a *Perkin Elmer* Series 200 HPLC Apparatus with Autosampler, Pump, UV-Vis Detector and Chromatography Interface. The 6,6'-dibromo, 1,1'-bi-2-naphthol enantiomers were isolated using MeCN in an isocratic and isothermal manner with flow rate of 1 mL min⁻¹.

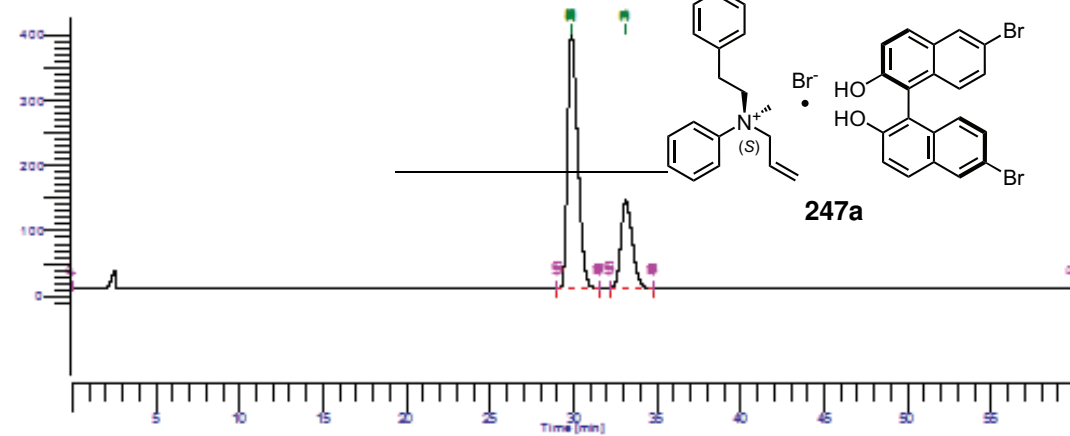
rac-6,6'-dibromo, 1,1'-bi-2-naphthol



Flow Rate (mL min ⁻¹)	0.5
Retention Time (min)	31.147 34.223
Peak Area (%)	49.62 50.38

(R)-6,6'-dibromo, 1,1'-bi-2-naphthol**(R)-N-allyl, N-methyl, N-phenylacetyl anilinium bromide**

Flow Rate (mL min ⁻¹)	0.5	
Retention Time (min)	30.140	33.055
Peak Area (%)	22.17	77.83

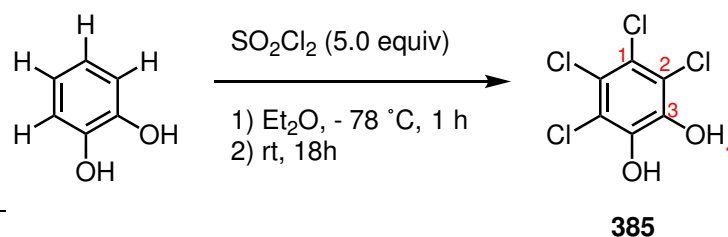
(S)-6,6'-dibromo, 1,1'-bi-2-naphthol**(S)-N-allyl, N-methyl, N-phenylacetyl anilinium bromide**

Flow Rate (mL min ⁻¹)	0.5	
Retention Time (min)	29.880	33.135
Peak Area (%)	71.99	28.01

9.14 Chiral shift NMR spectroscopy

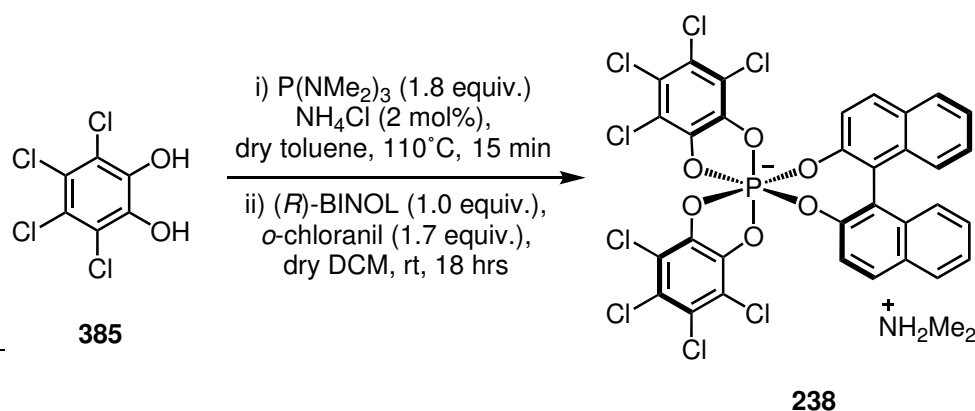
9.14.1 Procedure for the synthesis of $[(\Lambda,R)\text{-BINPHAT}][\text{NH}_2\text{Me}_2^+]$

Tetrachlorocatechol Synthesis



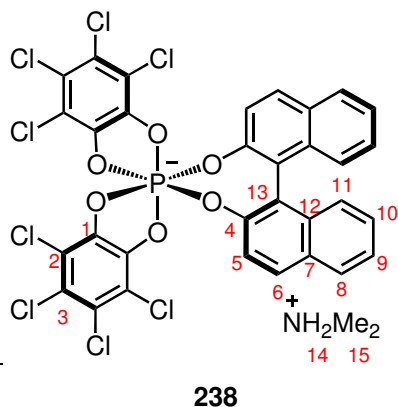
Scheme 9.38: General procedure for the synthesis of tetrachlorocatechol.

Followed procedure outline by Ingleson et al.³²⁴ An oven dried two-necked round bottom flask was flushed with argon and charged with catechol (3.99 g, 36.2 mmol, 1.0 equiv.), which was subsequently dissolved into anhydrous diethyl ether (0.9 M). This solution was cooled to $-78\text{ }^\circ\text{C}$. SO_2Cl_2 (14.8 mL, 182.6 mmol, 5.0 equiv.) was added neat, dropwise over 60 minutes. The mixture was stirred at $-78\text{ }^\circ\text{C}$ for a further 60 minutes before being allowed to warm to room temperature and stirred overnight. The mixture was then placed under vacuum to remove the volatile compounds to yield a red solid (4.84 g, 19.5 mmol, 54% yield). The crude material was recrystallised in CH_2Cl_2 to yield the anhydrous form as pale red prisms/needles, **385**.

Procedure for $[(\Lambda,R)\text{-BINPHAT}][\text{NH}_2\text{Me}_2^+]$ synthesis


Scheme 9.39: General procedure for the synthesis of (Λ,R) -bis(tetrachlorobenzenediolato)mono([1,1']-binaphthalenyl-2,2'-diolato) phosphate (V) dimethylammonium.

Followed procedure outlined by Lacour *et al.*³²⁵ An oven dried three-necked round bottom flask was flushed with argon and charged with anhydrous **385** (0.84 g, 3.39 mmol, 1.7 equiv.) and NH_4Cl (0.004 g, 2 mol%). Dry toluene (10 mL, 0.2 M) was added and allowed stir until fully dissolved. Freshly purchased tris(dimethylamino)phosphine (0.70 mL, 3.85 mmol, 1.9 equiv.) was added dropwise, which evolved dimethylamine upon addition. The solution was then refluxed for 15 minutes at 110°C . Upon heating the solution turned clear with a purple solid residue. The toluene and excess tris(dimethylamino)phosphine was then removed under vacuum, to give a white solid (kept on Schlenk line for a minimum of 2 hours). The flask was re-flushed with argon and $(R)\text{-BINOL}$ (0.58 g, 2.01 mmol, 1.0 equiv.) and 3,4,5,6-Tetrachloro-1,2-benzoquinone (*o*-chloranil, 0.84 g, 1.70 equiv.) were added. The mixture is dissolved into anhydrous CH_2Cl_2 (20 mL, 0.1 M) and allowed to stir at room temperature. Over the course of 3 hours, the dark red/brown solution begins to form a white precipitate while paling in colour to an orange/yellow colour. After 18 hours, the precipitate was isolated using vacuum filtration and was subsequently washed with CH_2Cl_2 , Et_2O , CH_2Cl_2 , and then hexanes to yield **238** as a white solid (1.42 g, 1.66 mmol, 82% yield). **238** was isolated as a single diastereomer. *Data consistent with Walsh et al.*³⁷ *Caution must be exercised when using tris(dimethylamino)phosphine as the oxidation product (hexamethylphosphoramide) is a human carcinogen.*

[(Δ ,*R*)-BINPHAT][NH₂Me₂⁺]

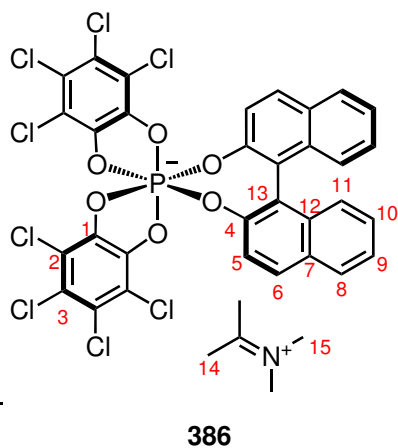
Following the procedure described above, **238** was isolated in 82% yield.

¹H NMR (400 MHz, DMSO-*d*₆) δ 8.24 (2H, s, H₁₄), 7.96 (2H, d, *J* = 8.1 Hz, H₁₁), 7.84 (2H, dd, *J* = 9.0, 1.1 Hz, H₆), 7.40 (2H, ddd, *J* = 7.9, 5.1, 2.7 Hz, H₈), 7.33 – 7.25 (4H, m, H₉₊₁₀), 6.57 (2H, dd, *J* = 8.9, 1.2 Hz, H₅), 2.54 (6H, s, H₁₅).

¹³C NMR (101 MHz, DMSO-*d*₆) δ 151.8 (d, *J* = 12.4 Hz), 142.7 (d, *J* = 5.5 Hz),

142.1 (d, *J* = 8.8 Hz), 131.8 (d, *J* = 1.7 Hz), 130.0 (d, *J* = 2.2 Hz), 129.2, 128.3, 126.3, 125.7, 124.2, 122.6, 122.4 (d, *J* = 3.3 Hz), 121.4, 120.0, 112.9 (d, *J* = 15.5 Hz), 112.7 (d, *J* = 14.4 Hz), 34.4.

³¹P NMR (162 MHz, DMSO-*d*₆) δ -82.65.

[(Δ ,*R*)-BINPHAT][Me₂N=C(Me)₂]

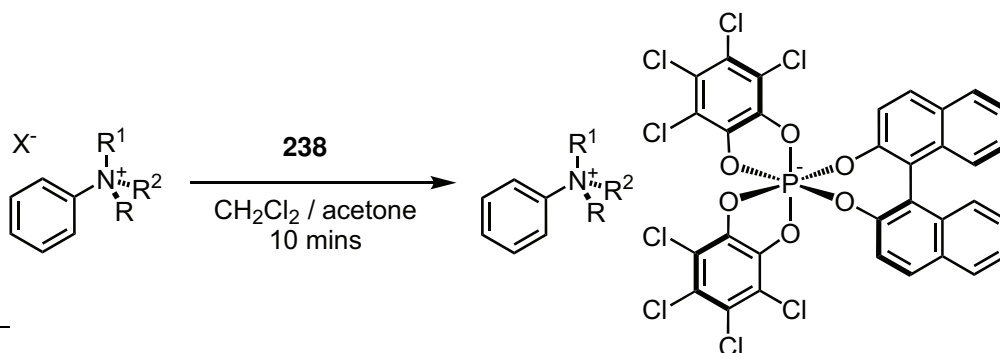
If **238** is recrystallised from acetone the H₂NMe₂⁺ counterion reacts to produce the iminium species (Me₂N=C(Me)₂)⁺. This recrystallised product **386** is insoluble in acetone and CH₂Cl₂ and as such is unsuitable for counterion exchange with chiral ammonium salts.

¹H NMR (400 MHz, DMSO-*d*₆) δ 7.96 (2H, d, *J* = 8.2 Hz, H₁₁), 7.84 (2H, dd, *J* = 9.0, 1.1 Hz, H₁₁), 7.45 – 7.35 (2H, m,

H₈), 7.33 – 7.24 (4H, m, H₉₊₁₀), 6.57 (2H, dd, *J* = 8.8, 1.1 Hz, H₅), 3.49 (6H, p, *J* = 1.1 Hz, H₁₅), 2.43 (6H p, *J* = 1.0 Hz, H₁₄).

³¹P NMR (162 MHz, DMSO-*d*₆) δ -82.59.

9.14.2 Counterion exchange for chiral shift NMR experiments

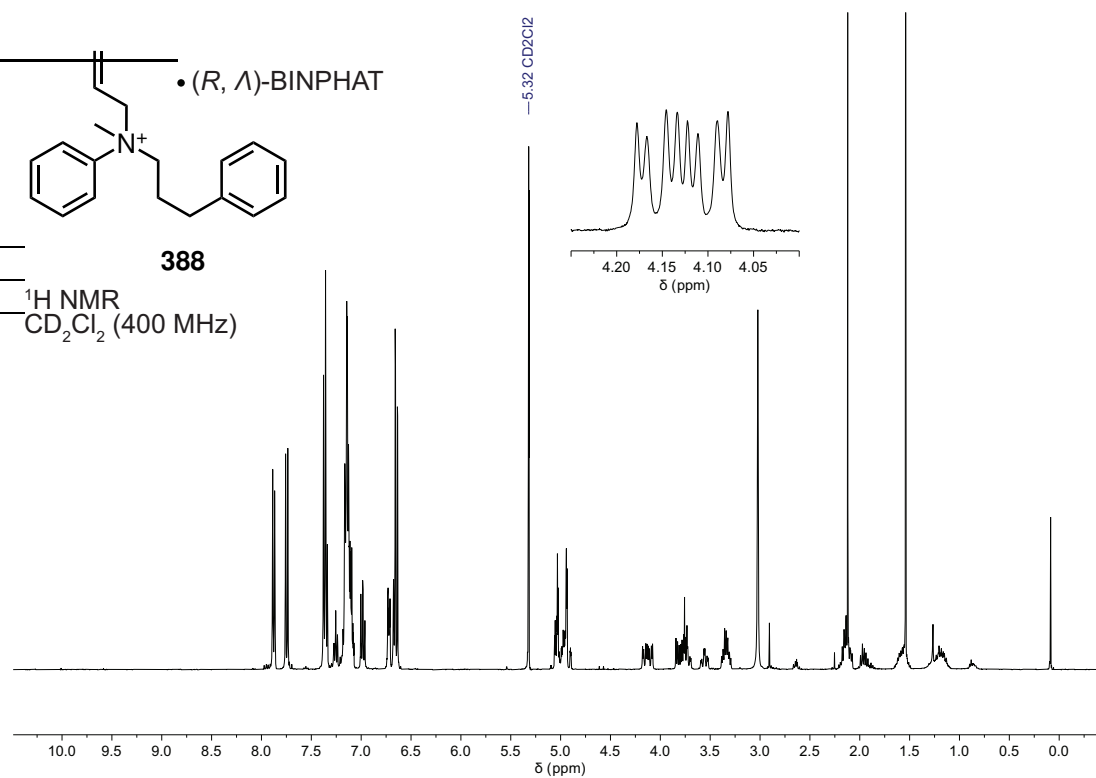
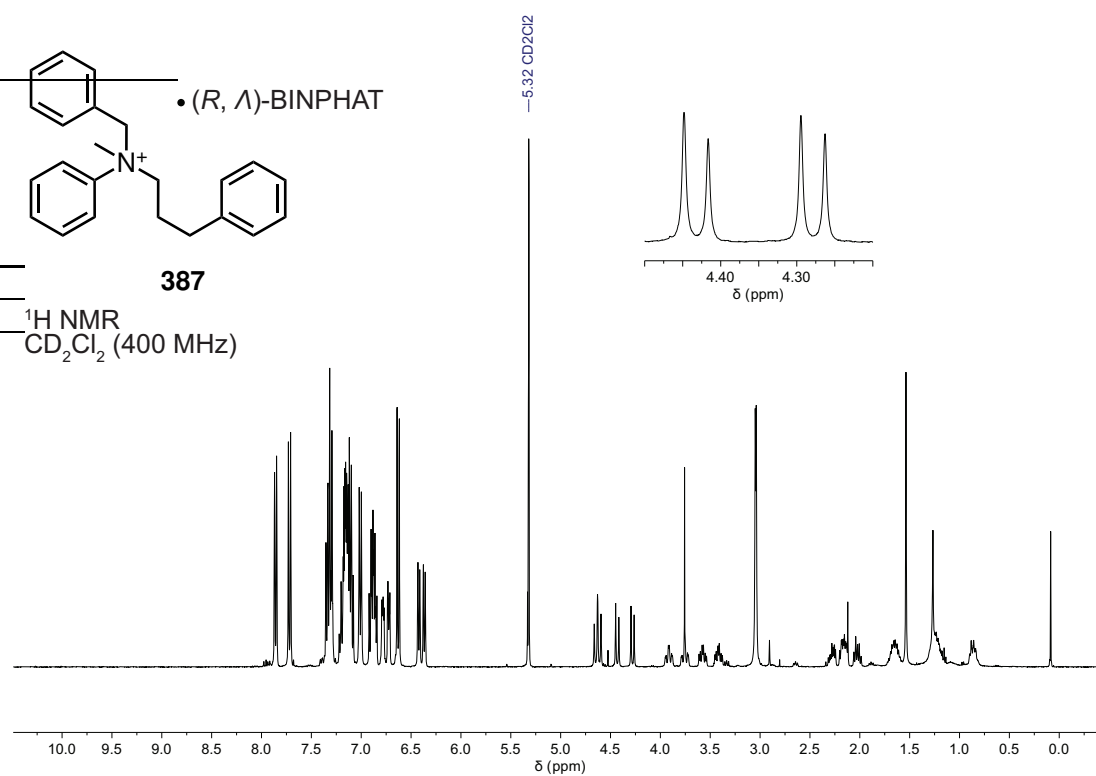


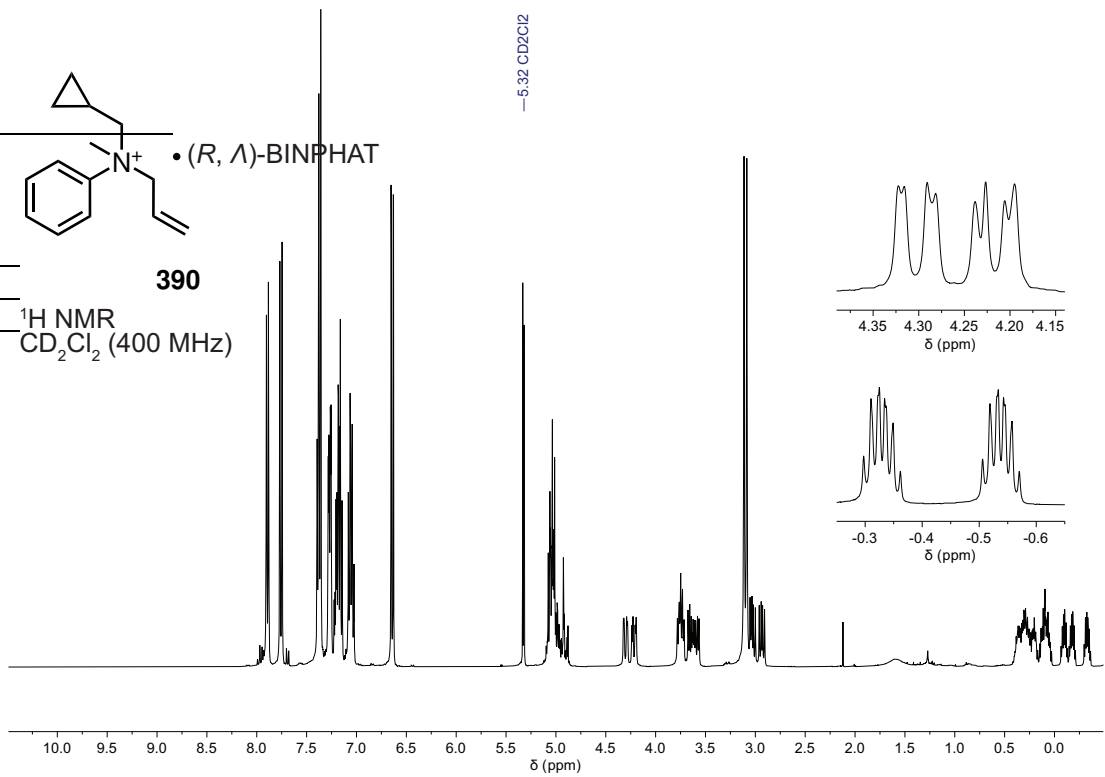
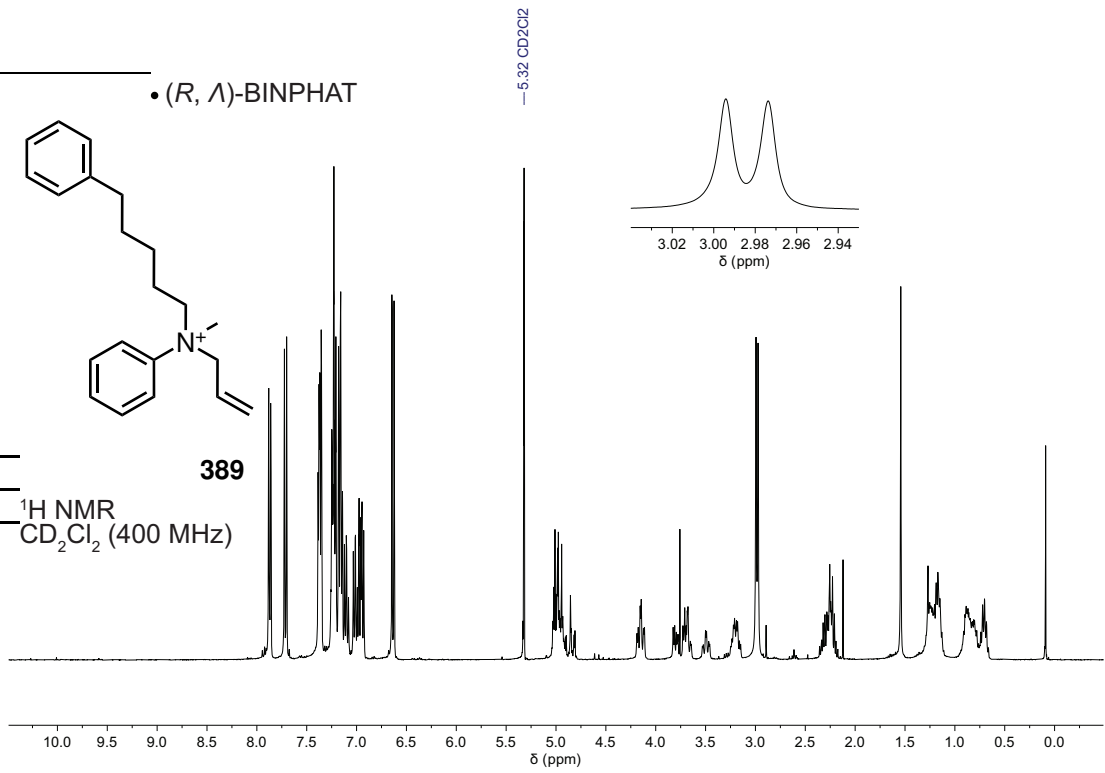
Scheme 9.40: General procedure for the counterion exchange to produce the chiral shift salt to be analysed by ¹H NMR Experiments.

Procedure adapted from Walsh *et al.*² The selected ammonium salt · BINOL complex (1.0 equiv.) is dissolved into the minimum volume of MeOH (approx. 1 mg mL⁻¹). This solution was extracted by partition between Et₂O/H₂O and the aqueous layer concentrated under reduced pressure to yield the corresponding enriched quaternary ammonium salt. This ammonium salt is dissolved into CH₂Cl₂ (0.03 M). A solution of [(Λ,*R*)-BINPHAT][NH₂Me₂⁺] salt (1.0 equiv.) is prepared in acetone (0.03 M) and is then added with stirring to the ammonium halide solution. Once added, the solution is concentrated, then re-dissolved into CH₂Cl₂ (0.03 M) and is allowed to stir for 10 min at room temperature. The mixture is then purified by flash chromatography using Al₂O₃ (basic) and a 100% CH₂Cl₂ eluent. The resulting salt is analysed by ¹H NMR spectroscopy using CD₂Cl₂.

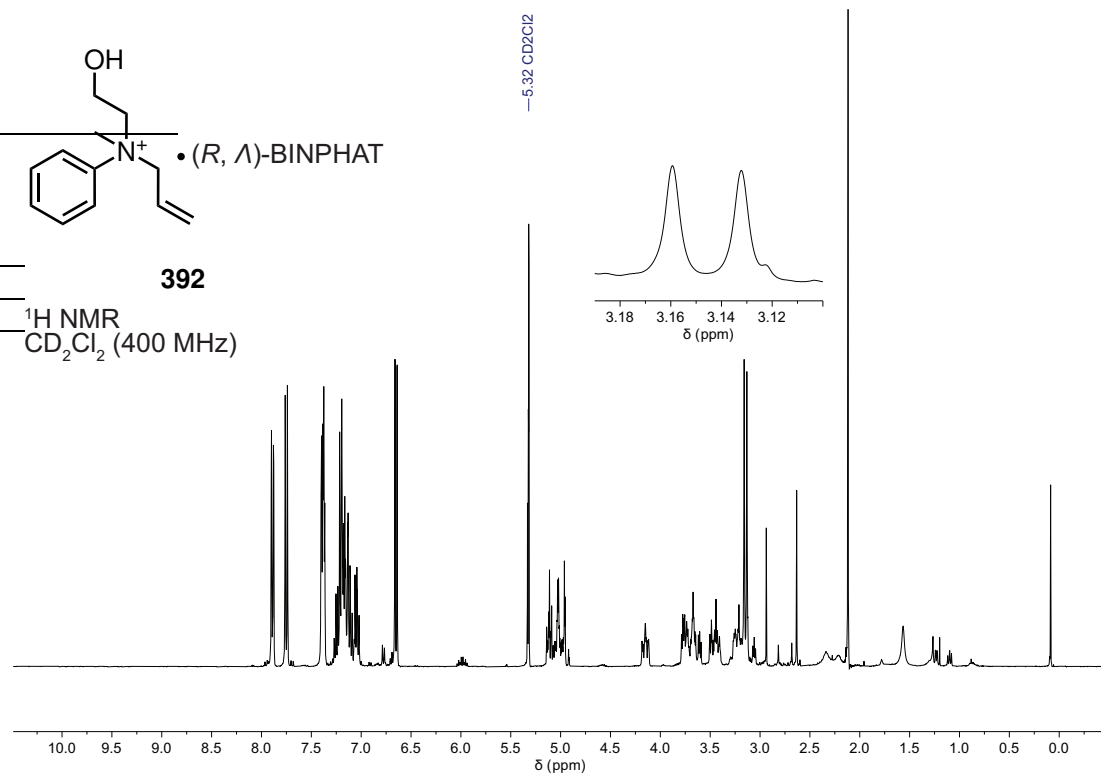
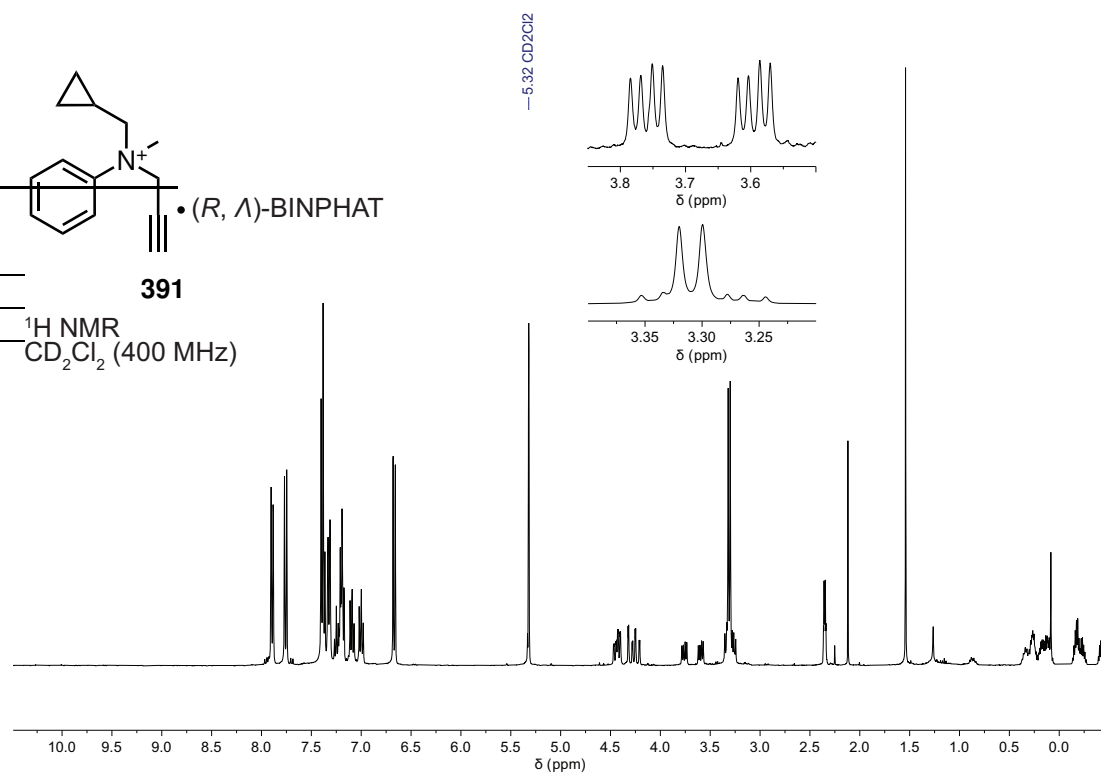
Each enriched ammonium halide sample was compared to a standard prepared from a racemic ammonium halide which showed a 50:50 ratio (*S*:*R*) for the ammonium cation to ensure accurate assignment of peaks and to rule out the possibility of resolution by ion-exchange with [(Λ,*R*)-BINPHAT].

Enantioenrichment values for *N*-allyl, *N*-methyl, *N*-isobutyl anilinium bromide salts (**221** and **221a**) and *N*-allyl, *N*-methyl, *N*-isopropyl anilinium bromide salts (**225** and **225a**) are taken from Walsh *et al.*²

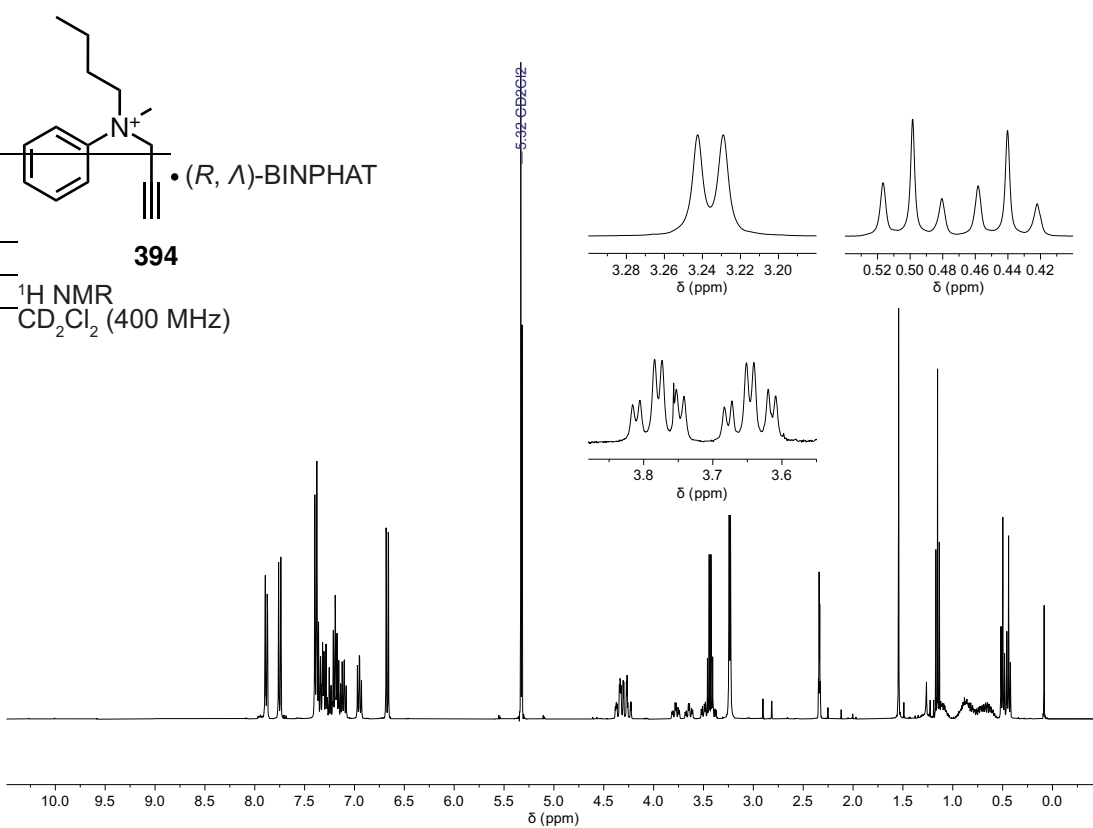
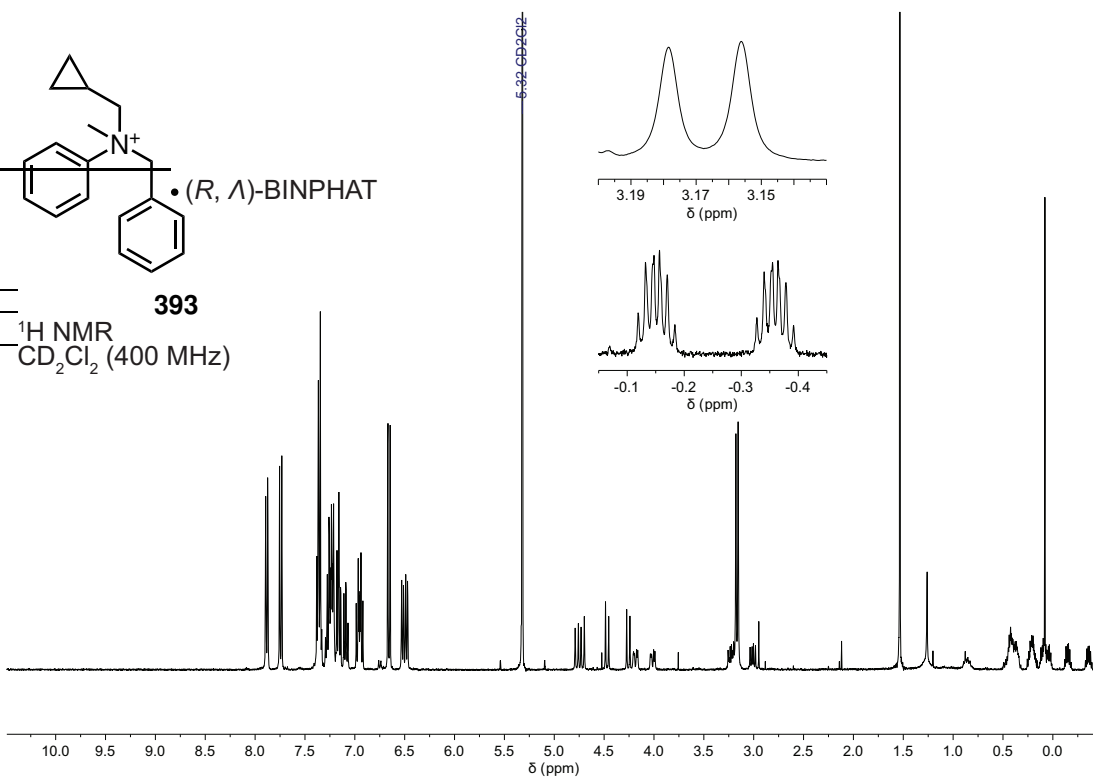
9.14.3 ^1H NMR spectra of ammonium cations · [(Δ , R)-BINPHAT]



9.14. CHIRAL SHIFT NMR SPECTROSCOPY

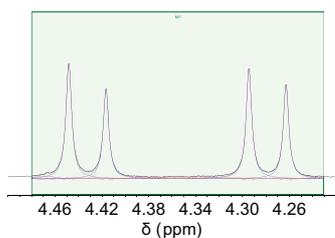


9.14. CHIRAL SHIFT NMR SPECTROSCOPY

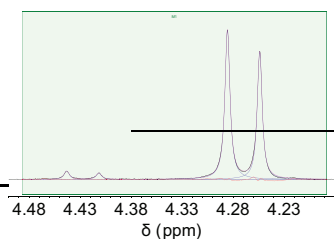
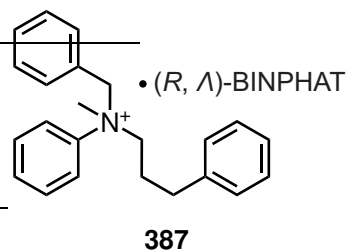


***N*-benzyl, *N*-hydrocinnamyl, *N*-methyl anilinium bromide salts · [(Λ ,*R*)-BINPHAT]**

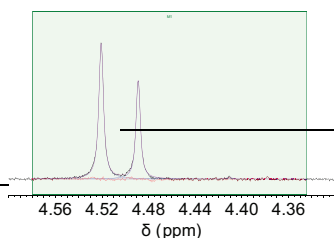
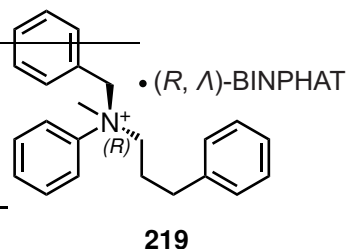
	dr (<i>R</i>:<i>S</i>)
<i>rac</i> -salt, 211	50:50
salt from (<i>R</i>)-BINOL complex, 219	95:5
salt from (<i>S</i>)-BINOL complex, 219a	3:97



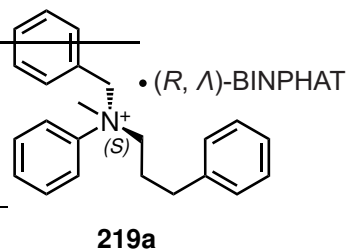
#	ppm	Area
1	4.2629	155163.97
2	4.2945	185930.49
3	4.4165	148802.57
4	4.4482	195417.62



#	ppm	Area
1	4.2539	369497.80
2	4.2856	450326.92
3	4.4117	20636.36
4	4.4432	25722.15

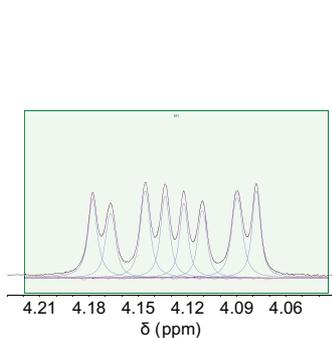


#	ppm	Area
1	4.4108	577.18
2	4.4889	42145.65
3	4.5207	62941.10

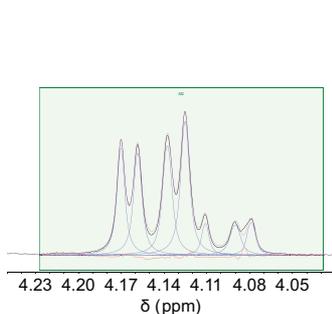
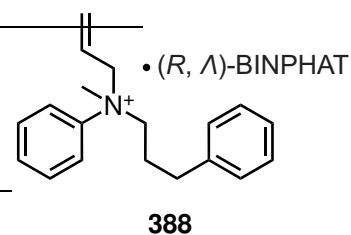


N*-allyl, *N*-hydrocinnamyl, *N*-methyl anilinium bromide salts · [(*Λ*,*R*)-BINPHAT]*dr *R*:*S***

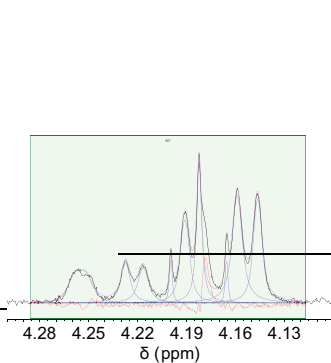
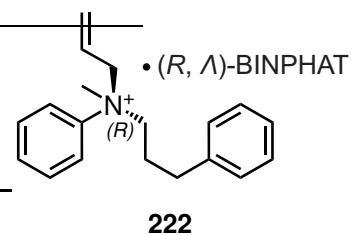
<i>rac</i> -salt, 193	50:50
salt from (<i>R</i>)-BINOL complex, 222	23:77
salt from (<i>S</i>)-BINOL complex, 222a	74:26



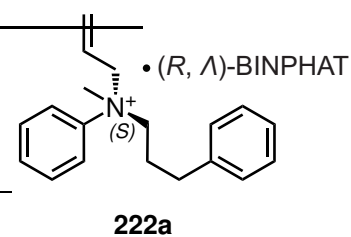
#	ppm	Area
1	4.0781	97951.38
2	4.0898	111287.81
3	4.1110	79317.07
4	4.1223	83883.20
5	4.1337	98600.87
6	4.1458	111080.26
7	4.1669	83066.61
8	4.1778	101169.97



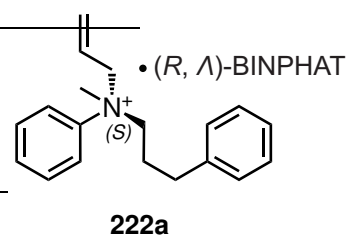
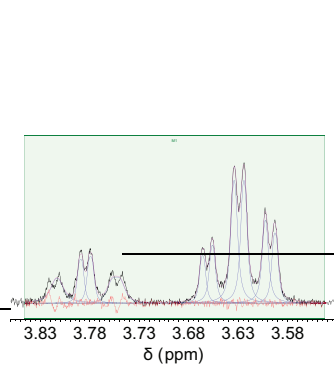
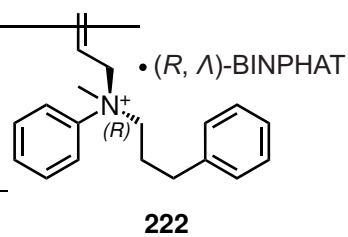
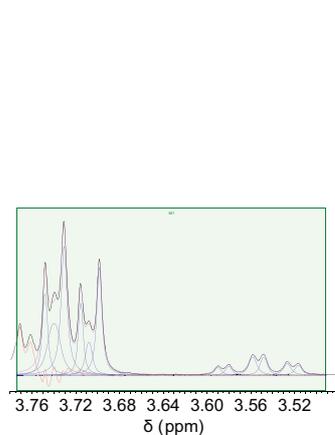
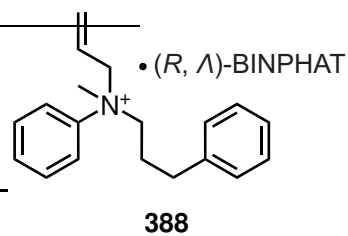
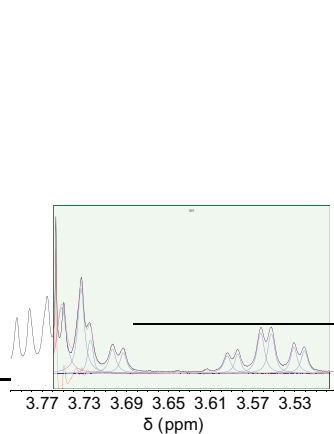
#	ppm	Area
1	4.0789	55676.89
2	4.0901	68295.27
3	4.1110	50409.22
4	4.1252	262241.92
5	4.1377	220806.85
6	4.1584	187238.06
7	4.1702	184974.30



#	ppm	Area
1	4.1464	34728.66
2	4.1590	43881.60
3	4.1655	4359.38
4	4.1823	29812.60
5	4.1910	28939.57
6	4.1996	5020.72
7	4.2166	14532.94
8	4.2274	15120.43
9	4.2550	21544.40

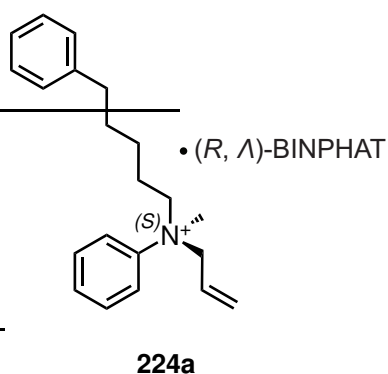
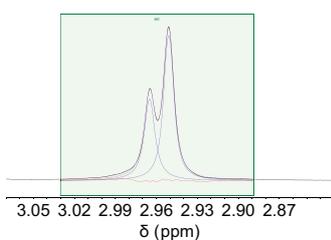
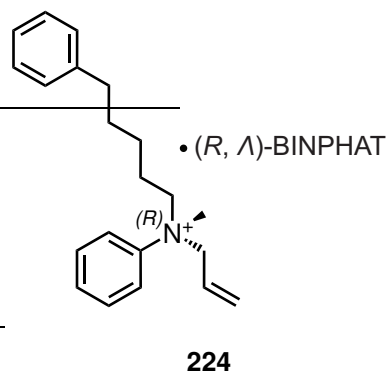
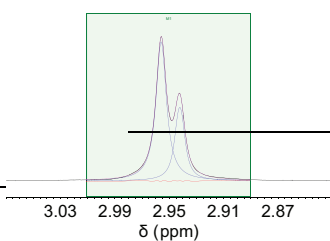
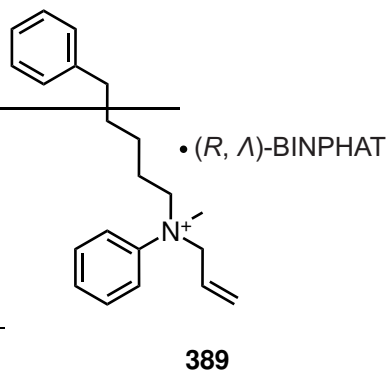
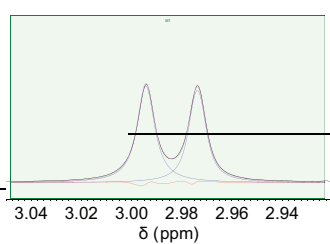


9.14. CHIRAL SHIFT NMR SPECTROSCOPY



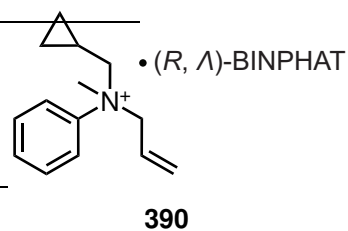
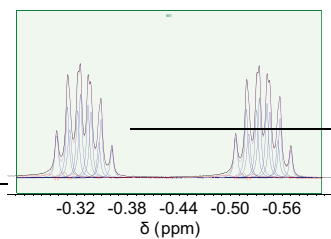
***N*-allyl, *N*-5-phenylvaleryl, *N*-methyl anilinium bromide salts · [(Λ),*R*]-BINPHAT]**

	dr (<i>R</i>:<i>S</i>)
<i>rac</i> -salt, 195	52:48
salt from (<i>R</i>)-BINOL complex, 224	67:33
salt from (<i>S</i>)-BINOL complex, 224a	38:62

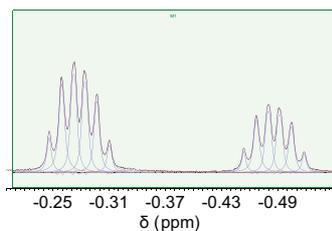


***N*-allyl, *N*-homocyclopropyl, *N*-methyl anilinium bromide salts · [(Λ ,*R*)-BINPHAT]**

	dr (<i>R</i>:<i>S</i>)
<i>rac</i> -salt, 187	50:50
salt from (<i>R</i>)-BINOL complex, 226	62:38
salt from (<i>S</i>)-BINOL complex, 226a	38:62

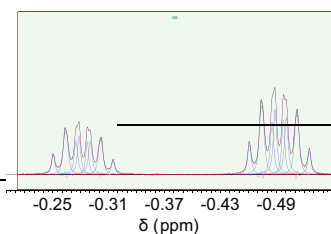
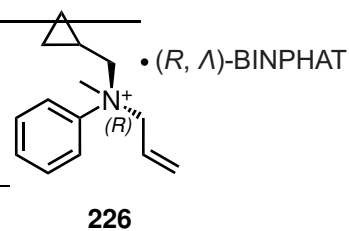


9.14. CHIRAL SHIFT NMR SPECTROSCOPY



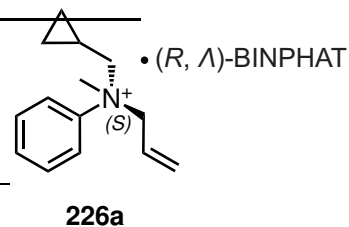
From: -0.560 ppm
To: -0.207 ppm
Residual Error: 3e+03

#	ppm	Area
1	-0.5180	20057.81
2	-0.5044	58403.95
3	-0.4917	75580.96
4	-0.4798	78958.27
5	-0.4670	71437.20
6	-0.4536	21662.65
7	-0.3103	31148.30
8	-0.2968	88792.54
9	-0.2841	120329.68
10	-0.2722	129081.62
11	-0.2594	119381.72
12	-0.2459	38781.48



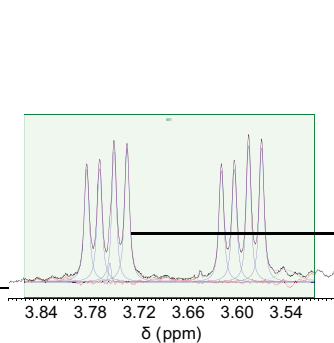
From: -0.572 ppm
To: -0.212 ppm
Residual Error: 5.93e+03

#	ppm	Area
1	-0.5253	28825.73
2	-0.5118	96701.09
3	-0.5007	80611.26
4	-0.4973	64191.68
5	-0.4885	88840.95
6	-0.4852	70498.28
7	-0.4742	116006.93
8	-0.4609	39077.93
9	-0.3148	18264.70
10	-0.3015	55364.44
11	-0.2904	47048.47
12	-0.2870	37832.74
13	-0.2783	49977.43
14	-0.2750	47276.95
15	-0.2640	72082.73
16	-0.2506	25688.92

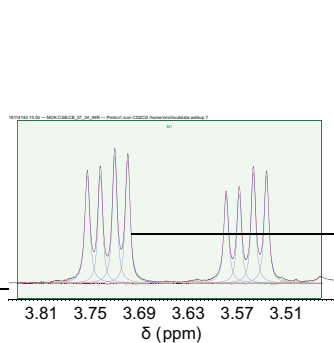
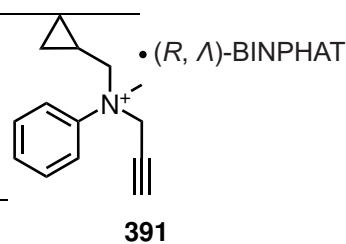


***N*-homocyclopropyl, *N*-propargyl, *N*-methyl anilinium bromide salts · [(Δ ,*R*)-BINPHAT]**

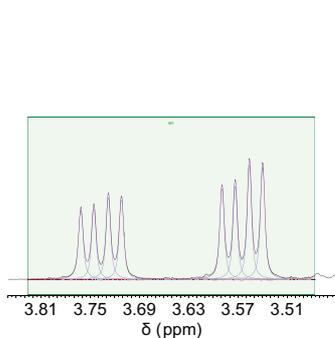
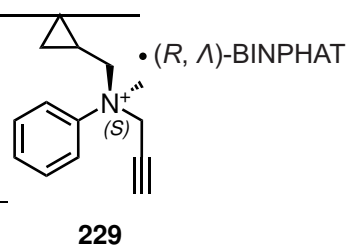
	dr <i>R</i>:<i>S</i>
<i>rac</i> -salt, 200	50:50
salt from (<i>R</i>)-BINOL complex, 229	45:55
salt from (<i>S</i>)-BINOL complex, 229a	57:43



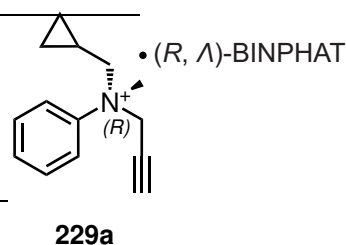
#	ppm	Area
1	3.5701	93821.12
2	3.5860	93439.15
3	3.6035	80468.92
4	3.6194	79104.79
5	3.7351	98187.95
6	3.7509	87978.67
7	3.7687	82611.02
8	3.7845	83191.89



#	ppm	Area
1	3.5340	161432.27
2	3.5502	164550.41
3	3.5675	130583.37
4	3.5835	139215.69
5	3.7042	181709.59
6	3.7201	192906.99
7	3.7378	160121.57
8	3.7537	174630.16

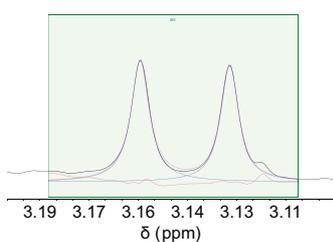


#	ppm	Area
1	3.5398	196411.45
2	3.5559	197543.09
3	3.5732	159677.42
4	3.5893	159113.94
5	3.7118	140503.26
6	3.7278	145031.63
7	3.7455	123310.86
8	3.7613	127260.10



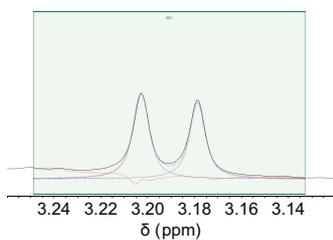
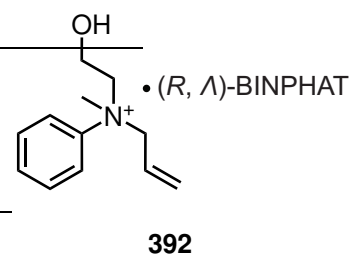
***N*-allyl, *N*-2-hydroxyethyl, *N*-methyl anilinium bromide salts · [(Λ),*R*]-BINPHAT]**

	dr (<i>R</i>:<i>S</i>)
<i>rac</i> -salt, 198	48:52
salt from (<i>R</i>)-BINOL complex, 231	47:53
salt from (<i>S</i>)-BINOL complex, 231a	48:52



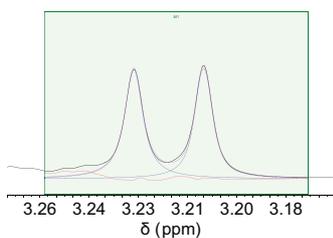
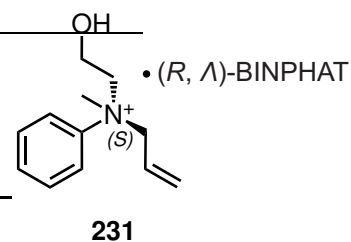
From: 3.111 ppm
To: 3.187 ppm
Residual Error:1.84e+06

#	ppm	Area
1	3.1322	1225934.21
2	3.1594	1339418.35



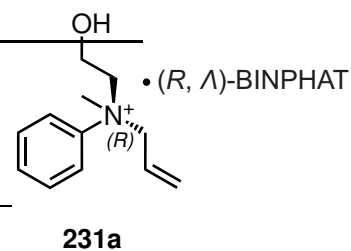
From: 3.133 ppm
To: 3.249 ppm
Residual Error:7.04e+05

#	ppm	Area
1	3.1788	505985.21
2	3.2028	579336.52



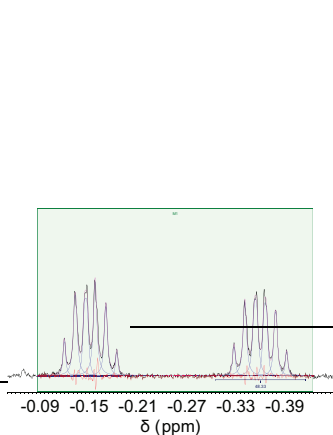
From: 3.178 ppm
To: 3.259 ppm
Residual Error:6.6e+05

#	ppm	Area
1	3.2101	818518.40
2	3.2314	874734.93



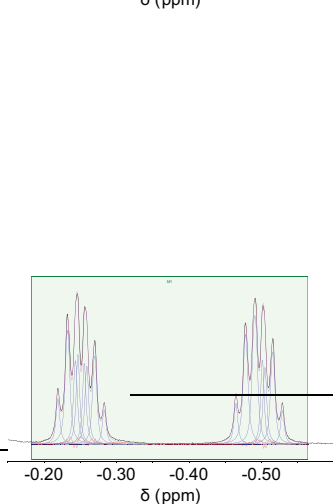
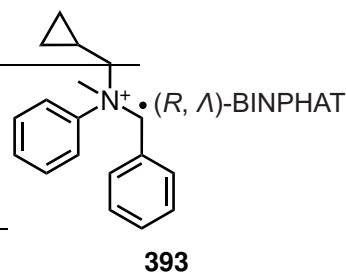
N*-benzyl, *N*-homocyclopropyl, *N*-methyl anilinium bromide salts · [(Λ ,*R*)-BINPHAT]*dr *R*:*S***

<i>rac</i> -salt, 207	51:49
salt from (<i>R</i>)-BINOL, 232	50:50
salt from (<i>S</i>)-BINOL, 232a	50:50



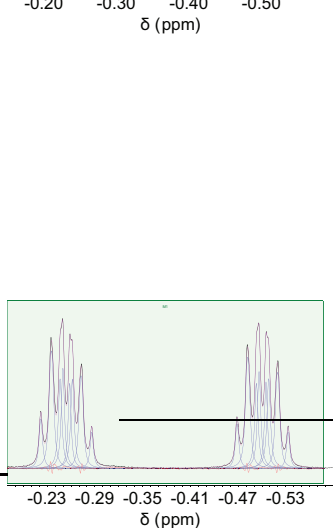
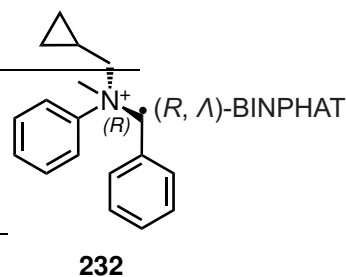
From: -0.424 ppm
To: -0.087 ppm
Residual Error: 1.06e+03

#	ppm	Area
1	-0.3917	5156.26
2	-0.3783	19283.55
3	-0.3656	22782.67
4	-0.3536	30117.46
5	-0.3406	23446.87
6	-0.3273	6867.96
7	-0.1836	4760.69
8	-0.1702	20375.71
9	-0.1571	31126.75
10	-0.1456	25958.08
11	-0.1328	27243.45
12	-0.1194	7959.87



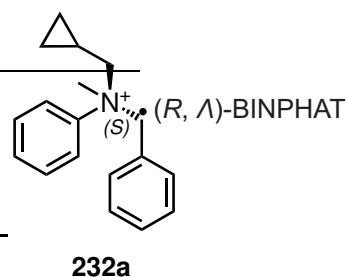
From: -0.563 ppm
To: -0.183 ppm
Residual Error: 1.28e+04

#	ppm	Area
1	-0.5287	49682.60
2	-0.5154	156241.41
3	-0.5046	113346.68
4	-0.5011	113882.14
5	-0.4907	242197.30
6	-0.4779	204123.59
7	-0.4645	63296.76
8	-0.2831	51703.70
9	-0.2698	144656.39
10	-0.2590	117754.52
11	-0.2555	115984.59
12	-0.2467	125469.08
13	-0.2432	128570.83
14	-0.2324	201760.57
15	-0.2191	70869.27



From: -0.577 ppm
To: -0.179 ppm
Residual Error: 8.05e+03

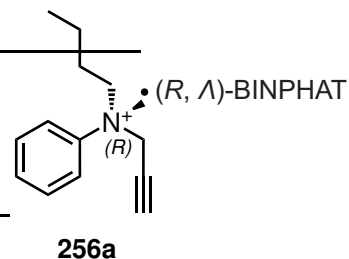
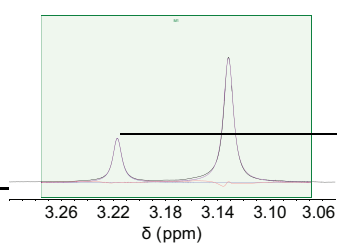
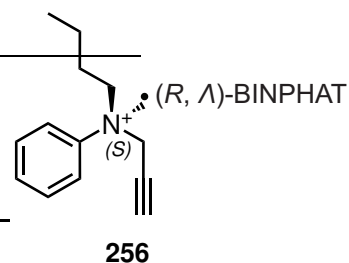
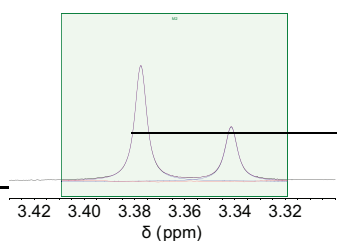
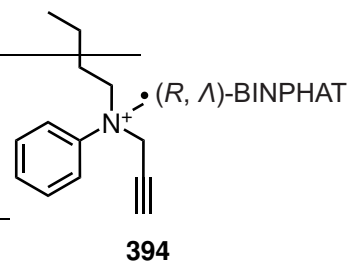
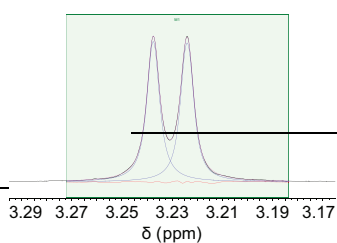
#	ppm	Area
1	-0.5329	46703.42
2	-0.5195	153734.44
3	-0.5084	128378.80
4	-0.5050	105604.93
5	-0.4963	131493.13
6	-0.4930	118848.95
7	-0.4820	183692.02
8	-0.4687	61165.42
9	-0.2859	48885.56
10	-0.2727	148260.96
11	-0.2617	125892.53
12	-0.2582	103092.44
13	-0.2497	132373.68
14	-0.2462	126383.44
15	-0.2353	196840.41
16	-0.2219	67944.37



***N*-butyl, *N*-propargyl, *N*-methyl anilinium bromide salts · [(Λ),*R*]-BINPHAT]**

	dr (<i>R</i>:<i>S</i>)
<i>rac</i> -salt, 199	50:50
salt from (<i>R</i>)-BINOL complex, 256	34:66
salt from (<i>S</i>)-BINOL complex, 256a	76:24

Note: (*S*)-salt forms a complex with (Λ),*R*-BINPHAT and crashes out of solution in CD_2Cl_2 , therefore the enantioenrichment is likely underestimated.



Bibliography

- [1] Pope, W. J.; Peachey, S. J. *J. Chem. Soc.* **1899**, 75, 1127–1131.
- [2] Walsh, M. P.; Phelps, J. M.; Lennon, M. E.; Yufit, D. S.; Kitching, M. O. *Nature* **2021**, 597, 70–76.
- [3] Kelvin, W. T. B. *Baltimore lectures on molecular dynamics and the wave theory of light* **1904**,
- [4] Pasteur, L. *Annales Chimie Phys.* **1848**, 24, 442–459.
- [5] van't Hoff, J. H. *Arch. neer.* **1874**, 9, 445–454.
- [6] Le Bel, J. A. *Bull. Soc. Chim. Fr.* **1874**, 22, 337–347.
- [7] van't Hoff, J. H. *Bull. Soc. Chim. Fr.* **1875**, 23, 295.
- [8] Bunnenberg, E.; Djerassi, C.; Mislow, K.; Moscovitz, A. *J. Am. Chem. Soc.* **1962**, 84, 2823–2826.
- [9] Mislow, K. *Molecular Chirality*, Wiley. **1999**, 22, 1–82.
- [10] Prelog, V. *Science* **1976**, 193, 17–24.
- [11] Marckwald, W. *Chem. Ber.* **1904**, 37, 349.
- [12] Kagan, H. B.; Gopalaiah, K. *New J. Chem.* **2011**, 35, 1933–1937.
- [13] Bredig, G.; Fiske, P. *Biochem. Z* **1913**, 46, 7–23.
- [14] Akabori, S.; Sakurai, S.; Izumi, Y.; Fujii, Y. *Nature* **1956**, 178.
- [15] *Advanced information on the Nobel Prize in Chemistry 2001*, The Royal Swedish Academy of Sciences **2001**, 1–12.
- [16] Knowles, W. S. *Acc. Chem. Res.* **1983**, 106.
- [17] Knowles, W. S.; Sabacky, M. J. *ChemComm.* **1968**, 1445–1446.
- [18] Vineyard, B. D.; Knowles, W. S.; Sabacky, M. J.; Bachman, G. L.; Weinkauff, D. J. *J. Am. Chem. Soc.* **1977**, 99, 5946–5952.
- [19] Miyashita, A.; Yasuda, A.; Takaya, H.; Toriumi, K.; Ito, T.; Souchi, T.; Noyori, R. *J. Am. Chem. Soc.* **1980**, 102, 7932–7934.
- [20] Ohta, T.; Takaya, H.; Kitamura, M.; Nagai, K.; Noyori, R. *J. Org. Chem.* **1987**, 52, 3174–3176.
- [21] Douglas, C. J.; Overman, L. E. *Proc. Natl. Acad. Sci.* **2003**, 101, 5363–5367.

- [22] Aupic, C.; Mohamed, A. A.; Figliola, C.; Nava, P.; Tuccio, B.; Chouraqui, G.; Parrain, J.-L.; Chuzel, O. *Chem. Sci.* **2019**, *10*, 6524–6530.
- [23] Oestreich, M. *Synlett.* **2007**, *11*, 1629–1643.
- [24] Korpiun, O.; Mislow, K. *J. Am. Chem. Soc.* **1967**, *89*, 4784–4786.
- [25] Meisenheimer, J.; Lichtenstadt, L. *Chem. Ber.* **1911**, *44*, 356–359.
- [26] Pope, W. J.; Peachey, S. J. *J. Chem. Soc.* **1900**, *77*, 1072–1075.
- [27] Smith, O.; Popescu, M. V.; Hindson, M. J.; Paton, R. S.; Burton, J. W.; Smith, M. D. *Nature* **2023**, *615*, 430–435.
- [28] van 't Hoff, J. H. *The Arrangement of Atoms in Space, Stereochemistry of Nitrogen Compounds*, Cambridge University Press **1898**, 169–184.
- [29] Lehn, J.-M. *Fortschr. Chem. Forsch.* **1970**, *15*, 311–371.
- [30] Bosmani, A.; Guarnieri-Ibáñez, A.; Lacour, J. *Helv. Chim. Acta.* **2019**, *102*, e1900021.
- [31] Mocquet, C.; Salaün, A.; Claudon, P.; Grel, B. L.; Potel, M.; Guichard, G.; Jamart-Grégoire, B.; Grel, P. L. *J. Am. Chem. Soc.* **2009**, *131*, 14521–14525.
- [32] Chai, Z. *Synthesis* **2020**, *52*, 1738–1750.
- [33] Feng, G.; Xu, H.; Li, W.; Zhang, J. *Inorg. Chem. Commun.* **2018**, *96*, 81–85.
- [34] Bedford, R. B.; Brenner, P. B.; Elorriaga, D.; Harvey, J. N.; Nunn, J. *Dalton Trans.* **2016**, *45*, 15811–15817.
- [35] Toda, F.; Mori, K. *Tetrahedron Lett.* **1989**, *30*, 1841–1844.
- [36] Wedekind, E. *J. Chem. Soc.* **1899**, *32*, 3561–3569.
- [37] Walsh, M. P. *PhD Thesis, University of Durham: Enantioselective Synthesis of Chiral Ammonium Cations* **2020**,
- [38] Jacobsen, E. N.; Marko, I.; Mungall, W. S.; Schroeder, G.; Sharpless, K. B. *J. Am. Chem. Soc.* **1988**, *110*, 1968–1970.
- [39] Bart, S. C.; Hawrelak, E. J.; Schmisser, A. K.; Lobkovsky, E.; Chirik, P. J. *Organometallics* **2004**, *23*, 237–246.
- [40] Arava, S.; Diesendruck, C. E. *Synthesis* **2017**, *49*, 3535–3545.
- [41] Gabriel, S. *Ber. Dtsch. Chem. Ges.* **1888**, *21*, 1049–1057.
- [42] Gabriel, S. *Ber. Dtsch. Chem. Ges.* **1891**, *24*, 1110–1121.

- [43] Wenker, H. *J. Am. Chem. Soc.* **1935**, *57*, 2328.
- [44] Tanner, D. *Angew. Chem. Int. Ed.* **1994**, *33*, 599–619.
- [45] Osborn, H. M.; Sweeney, J. *Tetrahedron Asymm.* **1997**, *8*, 1693–1715.
- [46] Gutowsky, H. S. *Ann. N. Y. Acad. Sci.* **1958**, *70*.
- [47] Lehn, J. M.; Wagner, J. *Tetrahedron* **1970**, *26*, 4227–4240.
- [48] Lehn, J. M.; Wagner, J. *J. Chem. Soc. D* **1970**, 414–415.
- [49] Lambert, J. B.; Oliver, W. L. *J. Am. Chem. Soc.* **1969**, *91*, 7774–7775.
- [50] Saunders, M.; Yamada, F. *J. Am. Chem. Soc.* **1963**, *85*, 1882.
- [51] Jautelat, M.; Roberts, J. D. *J. Am. Chem. Soc.* **1969**, *91*, 642–645.
- [52] Brois, S. J. *Tetrahedron Lett.* **1968**, *9*, 5997–6000.
- [53] Brois, S. J. *J. Am. Chem. Soc.* **1970**, *92*, 1079–1080.
- [54] Kostyanovsky, R. G.; Gella, I. M.; Markov, V. I.; Samojlova, Z. E. *Tetrahedron* **1974**, *30*, 39–45.
- [55] A. Müller, E., K. *Helv. Chim. Acta.* **1969**, *52*, 1823–1830.
- [56] Montanari, F.; Moretti, I.; Torre, G. *ChemComm.* **1968**, 1694–1695.
- [57] Brois, S. J. *J. Am. Chem. Soc.* **1967**, *89*, 4242–4243.
- [58] Pinner, A.; Wolfenstein, R. *Ber. Dtsch. Chem. Ges.* **1892**, *25*, 1428–1433.
- [59] Lister, M. W.; Sutton, L. E. *Trans. Faraday Soc.* **1939**, *35*, 495–505.
- [60] Richards, S. P. *PhD Thesis, University of Liverpool: The Synthesis of Chiral N-Oxides and Their Applications to β -Turn Mimetic Design* **2019**,
- [61] Oswald, A. A.; Griesbaum, K.; Hudson, B. E. *J. Org. Chem.* **1963**, *28*, 2351–2354.
- [62] Miyano, S.; Lu, L. D. L.; Viti, S. M.; Sharpless, K. B. *J. Org. Chem.* **1985**, *50*, 4350–4360.
- [63] Craig, J. C.; Purushothaman, K. K. *J. Org. Chem.* **1970**, *35*, 1721–1722.
- [64] He, B.; Chen, F.-X.; Li, Y.; Feng, X.; Zhang, G. *Tetrahedron Lett.* **2004**, *45*, 5465–5467.
- [65] Riley, D. P. *ChemComm.* **1983**, 1530–1532.
- [66] Zajac, W. W.; Walters, T. R.; Darcy, M. G. *J. Org. Chem.* **1988**, *53*, 5856–5860.

- [67] Cope, A. C.; LeBel, N. A. *J. Am. Chem. Soc.* **1960**, *82*, 4656–4662.
- [68] Dunstan, W. R.; Goulding, E. *J. Chem. Soc. Trans.* **1899**, *75*, 792–807.
- [69] Meisenheimer, J. *Ber. Dtsch. Chem. Ges.* **1908**, *41*, 3966–3976.
- [70] Drabowicz, J.; Dudziński, B.; Mikołajczyk, M.; Colonna, S.; Gaggero, N. *Tetrahedron Asymm.* **1997**, *8*, 2267–2270.
- [71] Toda, F.; Mori, K.; Stein, Z.; Goldberg, I. *Tetrahedron Lett.* **1989**, *30*, 1841–1844.
- [72] O’Neil, I. A.; Miller, N. D.; Peake, J.; Barkley, J. V.; Low, C. M.; Kalindjian, S. B. *Synlett.* **1993**, *1993*, 515–518.
- [73] O’Neil, I. A.; Miller, N. D.; Barkley, J. V.; Low, C. M.; Kalindjian, S. B. *Synlett.* **1995**, *1995*, 619–621.
- [74] Meisenheimer, J. *Ber. Dtsch. Chem. Ges.* **1919**, *52*, 1667–1677.
- [75] Xie, Y.; Sun, M.; Zhou, H.; Cao, Q.; Gao, K.; Niu, C.; Yang, H. *J. Org. Chem.* **2013**, *78*, 10251–10263.
- [76] O’Neil, I. A.; Turner, C. D.; Kalindjian, S. B. *Synlett.* **1997**, *1997*, 777–780.
- [77] Bel, J. A. L. *Compt. Rend.* **1891**, *112*, 724–726.
- [78] Marckwald, W.; v. Droste-Huelshoff, A. F. *Chem. Ber.* **1899**, *32*, 560–564.
- [79] Bel, J. A. L. *Compt. Rend.* **1899**, *129*, 548–550.
- [80] Pope, W. J.; Read, J. *J. Chem. Soc., Trans.* **1912**, *101*, 519–529.
- [81] Jones, H. O. *J. Chem. Soc.* **1903**, *83*, 1400–1421.
- [82] Kauffman, G. B. *Isis* **1973**, *64*, 78–95.
- [83] Wedekind, E. *Chem. Ber.* **1902**, *35*, 766–776.
- [84] Jones, H. O.; Hill, J. R. *J. Chem. Soc.* **1907**, *91*, 2083–2089.
- [85] El Gihani, M. T.; Williams, J. M. *Curr. Opin. Chem. Biol.* **1999**, *3*, 11–15.
- [86] Jacques, J.; Collet, A.; Wilen, S. H. *Enantiomers, racemates, and resolutions* **1981**, Wiley New York.
- [87] Carvalho, P. O.; Cass, Q. B.; Calafatti, S. A.; Contesini, F. J.; Bizaco, R. *Braz. J. Chem. Eng.* **2006**, *23*, 291–300.
- [88] Fogassy, E.; Nógrádi, M.; Kozma, D.; Egri, G.; Pálovics, E.; Kiss, V. *Org. Biomol. Chem.* **2006**, *4*, 3011–3030.

- [89] Levilain, G.; Coquerel, G. *CrystEngComm*. **2010**, *12*, 1983–1992.
- [90] Wang, Y.; Chen, A. *Stereoselective synthesis of drugs and natural products*, Wiley. **2013**, 1–20.
- [91] Kamiyama, T.; Ozer, M. S.; Otth, E.; Deska, J.; Cvengros, J. *ChemPlusChem* **2013**, *78*, 1510–1516.
- [92] Siedlecka, R. *Tetrahedron* **2013**, *69*, 6331–6363.
- [93] Chakraborty, S.; Saha, C. *Resonance* **2016**, *21*, 151–171.
- [94] Wilen, S. H.; Qi, J. Z.; Williard, P. G. *J. Org. Chem.* **1991**, *56*, 485–487.
- [95] Jameson, D. L.; Field, T.; Schmidt, M. R.; Destefano, A. K.; Stiteler, C. J.; Venditto, V. J.; Krovic, B.; Hoffman, C. M.; Ondisco, M. T.; Belowich, M. E. *J. Org. Chem.* **2013**, *78*, 11590–11596.
- [96] Hughes, D. L.; Cai, D.; Verhoeven, T. R.; Reider, P. J. *Org. Synth.* **1999**, *76*, 1.
- [97] Toda, F.; Tanaka, K.; Stein, Z.; Goldberg, I. *J. Org. Chem.* **1994**, *59*, 5748–5751.
- [98] Tayama, E.; Kimura, H. *Angew. Chem. Int. Ed.* **2007**, *46*, 8869–8871.
- [99] Tayama, E.; Otoyama, S.; Tanaka, H. *Tetrahedron Asymm.* **2009**, *20*, 2600–2608.
- [100] Tayama, E.; Tanaka, H. *Tetrahedron Lett.* **2007**, *48*, 4183–4185.
- [101] Wu, H.-F.; Lin, W.-B.; Xia, L.-Z.; Luo, Y.-G.; Chen, X.-Z.; Li, G.-Y.; Zhang, G.-L.; Pan, X.-F. *Helv. Chim. Acta.* **2009**, *92*, 677–688.
- [102] Wang, Y.; Chen, A. M. *Org. Process Res. Dev.* **2008**, *12*, 282–290.
- [103] Walsh, M. P.; Barclay, J. A.; Begg, C. S.; Xuan, J.; Johnson, N. T.; Cole, J. C.; Kitching, M. O. *J. Am. Chem. Soc.* **2022**, *2*, 2235–2250.
- [104] Walsh, M. P.; Barclay, J. A.; Begg, C. S.; Xuan, J.; Kitching, M. O. *Cryst. Growth Des.* **2023**, *23*, 2837–2844.
- [105] He, Q.; Rohani, S.; Zhu, J.; Gomaa, H. *Cryst. Growth Des.* **2010**, *10*, 5136–5145.
- [106] Havinga, E. *Biochimica et Biophysica Acta* **1954**, *13*, 171–174.
- [107] Kostyanovsky, R. G.; Kostyanovsky, V. R.; Kadorkina, G. K.; Lyssenko, K. A. *Mendeleev Commun.* **2001**, *11*, 1–6.
- [108] Wang, Y.; Sun, J.; Ding, K. *Tetrahedron* **2000**, *56*, 4447–4451.

BIBLIOGRAPHY

- [109] Denmark, S. E.; Gould, N. D.; Wolf, L. M. *J. Org. Chem.* **2011**, *76*, 4337–4357.
- [110] Holbrey, J. D.; Seddon, K. *Clean Prod. Process* **1999**, *1*, 223–236.
- [111] Han, J.; Varzi, A.; Passerini, S. *Angew. Chem. Int. Ed.* **2022**, *134*, e202115046.
- [112] In, M.; Bec, V.; Aguerre-Chariol, O.; Zana, R. *Langmuir* **2000**, *16*, 141–148.
- [113] Su, G.; Geng, T.; Jiang, Y.-J.; Ju, H.-B.; Wang, Y.-K. *Tens. Surf. Det.* **2020**, *57*, 318–325.
- [114] Jackowski, A.; Zones, S. I.; Hwang, S.-J.; Burton, A. W. *J. Am. Chem. Soc.* **2009**, *131*, 1092–1100.
- [115] Bureš, F. *Top. Curr. Chem.* **2019**, *377*, 14.
- [116] Dan, W.; Gao, J.; Qi, X.; Wang, J.; Dai, J. *Eur. J. Med. Chem.* **2022**, *243*, 114765.
- [117] Hofmann, A. W. *Phil. Trans. R. Soc. Lond.* **1850**, *140*, 93–131.
- [118] Menshutkin, N. *Z. Phys. Chem.* **1890**, *5*, 589–600.
- [119] Menshutkin, N. *Z. Phys. Chem.* **1890**, *6*, 41–57.
- [120] Sikora, K.; Nowacki, A.; Liberek, B.; Dmochowska, B. *J. Mol. Struct.* **2020**, *1206*, 127701.
- [121] Gordon, J. E. *J. Org. Chem.* **1965**, *30*, 2760–2763.
- [122] Shamma, M.; Deno, N. C.; Remar, J. F. *Tetrahedron Lett.* **1966**, *7*, 1375–1379.
- [123] von Hofmann, A. W. *Liebigs Ann. Chem.* **1851**, *78*, 253–286.
- [124] Brown, D. R.; Lygo, R.; McKenna, J.; McKenna, J. M.; Hutley, B. G. *J. Chem. Soc.* **1967**, 1184–1194.
- [125] Tayama, E.; Watanabe, K.; Matano, Y. *Eur. J. Org. Chem.* **2016**, 3631–3641.
- [126] Tayama, E.; Nanbara, S.; Nakai, T. *Chem. Lett.* **2006**, *35*, 478–479.
- [127] Tayama, E. *Chem. Rec.* **2015**, *15*, 789–800.
- [128] Glaeske, K. W.; West, F. *Org. Lett.* **1999**, *1*, 31–34.
- [129] Nubbemeyer, U. *Natural Products Synthesis II: Targets, Methods, Concepts* **2005**, 149–213.
- [130] Diederich, M.; Nubbemeyer, U. *Chem. Eur. J.* **1996**, *2*, 894–900.
- [131] McComsey, D. F.; Maryanoff, B. E. *J. Org. Chem.* **2000**, *65*, 4938–4943.
- [132] Meyers, A. I.; Sielecki, T. M. *J. Am. Chem. Soc.* **1991**, *113*, 2790–2791.

- [133] Kyba, E. B.; Koga, K.; Sousa, L. R.; Siegel, M. G.; Cram, D. J. *J. Am. Chem. Soc.* **1973**, *95*, 2692–2693.
- [134] Kyba, E. P.; Helgeson, R. C.; Madan, K.; Gokel, G. W.; Tarnowski, T. L.; Moore, S. S.; Cram, D. J. *J. Am. Chem. Soc.* **1977**, *99*, 2564–2571.
- [135] Goldberg, I. *J. Am. Chem. Soc.* **1977**, *99*, 6049–6057.
- [136] Shinkai, S. *Tetrahedron* **1993**, *49*, 8933–8968.
- [137] Beer, P. D.; Chen, Z.; Gale, P. A. *Tetrahedron* **1994**, *50*, 931–940.
- [138] Beer, P. D.; Chen, Z.; Michael, G. B.; Gale, P. A. *ChemComm.* **1994**, *19*, 2207–2208.
- [139] Lehn, J.-M.; Meric, R.; Vigneron, J.-P.; Cesario, M.; Guilhem, J.; Pascard, C.; Asfari, Z.; Vicens, J. *Supramol. Chem.* **1995**, *5*, 97–103.
- [140] Meyer, E. A.; Castellano, R. K.; Diederich, F. *Angew. Chem. Int. Ed.* **2003**, *42*, 1210–1250.
- [141] Freeman, W. A.; Mock, W. L.; Shih, N. Y. *J. Am. Chem. Soc.* **1981**, *103*, 7367–7368.
- [142] Freeman, W. A. *Acta Cryst.* **1984**, *B40*, 382–387.
- [143] Márquez, C.; Hudgins, R. R.; Nau, W. M. *J. Am. Chem. Soc.* **2004**, *126*, 5806–5816.
- [144] Datta, B.; Roy, A.; Roy, M. N. *J. Chem. Sci.* **2017**, *129*, 579–587.
- [145] Gelb, R. I.; Schwartz, L. M. *J. Incl. Phenom. Macrocycl. Chem.* **1989**, *7*, 537–543.
- [146] Iglesias, E. *J. Org. Chem.* **2006**, *71*, 4383–4392.
- [147] Cramer, F.; Hettler, H. *Die Naturwissenschaften* **1967**, *54*, 625–632.
- [148] Ogoshi, T.; Yamagishi, T.; Nakamoto, Y. *Chem. Rev.* **2016**, *116*, 7937–8002.
- [149] Ogoshi, T.; Kanai, S.; Fujinami, S.; Yamagishi, T.; Nakamoto, Y. *J. Am. Chem. Soc.* **2008**, *130*, 5022–5023.
- [150] Ashton, P. R.; Campbell, P. J.; Glink, P. T.; Philp, D.; Spencer, N.; Stoddart, J. F.; Chrystal, E. J.; Menzer, S.; Williams, D. J.; Tasker, P. A. *Angew. Chem. Int. Ed.* **1995**, *34*, 1865–1869.
- [151] Leigh, D. A.; Thomson, A. R. *Tetrahedron* **2008**, *64*, 8411–8416.
- [152] McEnery, M.; Siegel, R. *Encycl. Neurol. Sci.* **2014**, *65*, 552–564.

BIBLIOGRAPHY

- [153] Wang, K. H.; Penmatsa, A.; Gouaux, E. *Nature* **2015**, *521*, 322–327.
- [154] Pramod, A. B.; Foster, J.; Carvelli, L.; Henry, L. K. *Mol. Aspects Med.* **2013**, *34*, 197–219.
- [155] Kilty, J. E.; Lorang, D.; Amara, S. G. *Science* **1991**, *254*, 578–579.
- [156] Wise, R. A. *NIDA Res. Monogr.* **1976**, *50*, 15.
- [157] Penmatsa, A.; Wang, K. H.; Gouaux, E. *Nature* **2013**, *503*, 85–90.
- [158] Wang, K. H.; Penmatsa, A.; Gouaux, E. *Nature* **2015**, *521*, 322–327.
- [159] Absollhi, M. *Acetylcholine. Encycl. Toxicol.* **2014**,
- [160] Sussman, J. L.; Harel, M.; Frolow, F.; Oefner, C.; Goldman, A.; Toker, L.; Silman, I. *Science* **1991**, *253*, 872–879.
- [161] Park, Y. S.; Kim, Y.; Paek, K. *Org. Lett.* **2019**, *21*, 8300–8303.
- [162] Unwin, N. *J. Mol. Biol.* **2005**, *346*, 967–989.
- [163] Karlin, A. *Nat. Rev. Neurosci.* **2002**, *3*, 102–114.
- [164] Karlin, A. *J. Gen. Physiol.* **1969**, *54*, 245–264.
- [165] Tsyskovskaia, I.; Kandil, M.; Beaumier, Y. *Synth. Commun.* **2007**, *37*, 439–446.
- [166] Banholzer, R.; Reichl, R.; Disse, B.; Speck, G. *CIPO* **1996**, *C07D 451/1*.
- [167] Kobylecki, R. J.; Lane, A. C.; Smith, C. F. C.; Wakelin, L. P. G.; Cruse, W. B. T.; Egert, E.; Kennard, O. *J. Med. Chem.* **1982**, *25*, 1280–1286.
- [168] Doshan, H. D.; Perez, J. *EPO* **2008**, *PCT/US2006*.
- [169] Boyd, T. A.; Wagoner, H.; Sanghvi, S. P.; Verbicky, C.; Andruski, S. *USPTO* **2009**, *US 7,563,8*.
- [170] Cho, H.; Jeon, H.; Shin, J. E.; Lee, S.; Park, S.; Kim, S. *Chem. Eur. J.* **2019**, *25*, 2447–2451.
- [171] Zaitseva, S.; Prescimone, A.; Köhler, V. *Org. Lett.* **2023**, *25*, 1649–1654.
- [172] Zhou, H.-C.; Long, J. R.; Yaghi, O. M. *Chem. Rev.* **2012**, *112*, 673–674.
- [173] Li, H.; Eddaoudi, M.; O’Keeffe, M.; Yaghi, O. M. *Nature* **1999**, *402*, 276–279.
- [174] Chang, Z.; Yang, D.-H.; Xu, J.; Hu, T.-L.; Bu, X.-H. *Adv. Mater.* **2015**, *27*, 5432–5441.
- [175] Lin, R.-B.; He, Y.; Li, P.; Wang, H.; Zhou, W.; Chen, B. *Chem. Soc. Rev.* **2019**, *48*, 1362–1389.

- [176] Huang, Q.; Li, W.; Mao, Z.; Qu, L.; Li, Y.; Zhang, H.; Yu, T.; Yang, Z.; Zhao, J.; Zhang, M. P., Yi Aldred; Zhengu, C. *Nat. Commun.* **2019**, *10*, 3074.
- [177] Rademacher, W. *Annu. Rev. Plant Biol.* **2000**, *51*, 501–531.
- [178] Raine, A. R.; Yang, C.-C.; Packman, L. C.; White, S. A.; Mathews, F. S.; Scrutton, N. S. *Protein Sci.* **1995**, *4*, 2625–2628.
- [179] Steidl, J. V.; Yool, A. J. *Biophys. J.* **2001**, *81*, 2606–2613.
- [180] Pike, S. J.; Lavagnini, E.; Varley, L. M.; Cook, J. L.; Hunter, C. A. *Chem. Sci.* **2019**, *10*, 5943–5951.
- [181] Dougherty, D. A. *Acc. Chem. Res.* **2013**, *46*, 885–893.
- [182] Moerkerke, S.; Ménand, M.; Jabin, I. *Chem. Eur. J.* **2010**, *16*, 11712–11719.
- [183] Moerkerke, S.; Malytskyi, V.; Marcélis, L.; Wouters, J.; Jabin, I. *Org. Biomol. Chem.* **2017**, *15*, 8967–8974.
- [184] Späth, A.; König, B. *Beilstein J. Org. Chem.* **2010**, *6*, 32.
- [185] Beyeh, N. K.; Weimann, D. P.; Kaufmann, L.; Schalley, C. A.; Rissanen, K. *Chem. Eur. J.* **2012**, *18*, 5552–5557.
- [186] Beyeh, N. K.; Pan, F.; Valkonen, A.; Rissanen, K. *CrystEngComm.* **2015**, *17*, 1182–1188.
- [187] Tanaka, K.; Okada, T.; Toda, F. *Angew. Chem. Int. Ed.* **1993**, *32*, 1147–1148.
- [188] Rozhenko, A. B.; Schoeller, W. W.; Letzel, M. C.; Decker, B.; Agena, C.; Matay, J. *Chem. Eur. J.* **2006**, *12*, 8995–9000.
- [189] Mock, W. L.; Shih, N. Y. *J. Org. Chem.* **1986**, *51*, 4440–4446.
- [190] Xue, M.; Yang, Y.; Chi, X.; Zhang, Z.; Huang, F. *Acc. Chem. Res.* **2012**, *45*, 1294–1308.
- [191] Rüdiger, V.; Schneider, H. J.; Solov'ev, V. P.; Kazachenko, V. P.; Raevsky, O. A. *Eur. J. Org. Chem.* **1999**, 1847–1856.
- [192] Etter, M. C.; MacDonald, J. C.; Bernstein, J. *Acta Cryst.* **1990**, *B46*, 256–262.
- [193] Chisholm, J. A.; Motherwell, S. *Appl. Crystallogr.* **2005**, *38*, 228–231.
- [194] *The CP2K developers group*, <http://cp2k.berlios.de/>
- [195] Vandevondele, J.; Hutter, J. *J. Chem. Phys.* **2007**, *127*.
- [196] Vandevondele, J.; Krack, M.; Mohamed, F.; Parrinello, M.; Chassaing, T.; Hutter, J. *Comput. Phys. Commun.* **2005**, *167*, 103–128.

BIBLIOGRAPHY

- [197] Perdew, J. P.; Burke, K.; Ernzerhof, M. *Phys. Rev. Lett.* **1997**, *78*, 1396.
- [198] Goedecker, S.; Teter, M. *Phys. Rev. B* **1996**, *54*, 1703.
- [199] Grimme, S.; Antony, J.; Ehrlich, S.; Krieg, H. *J. Chem. Phys.* **2010**, *132*, 154104.
- [200] Gavezzotti, A. *Acc. Chem. Res.* **1994**, *27*, 309–314.
- [201] Gavezzotti, A.; Filippini, G. *Journal of Physical Chemistry* **1994**, *98*, 4831–4837.
- [202] Gavezzotti, A.; Filippini, G. *J. Am. Chem. Soc.* **1995**, *117*, 12299–12305.
- [203] Cruz-Cabeza, A. J.; Reutzel-Edens, S. M.; Bernstein, J. *Chem. Soc. Rev.* **2015**, *44*, 8619–8635.
- [204] Liebig, J.; Wöhler, F. *Ann. Pharm.* **1832**, *3*, 249–282.
- [205] Kras, W.; Carletta, A.; Montis, R.; Sullivan, R. A.; Cruz-Cabeza, A. J. *Nat. Commun. Chem.* **2021**, *4*, 38.
- [206] Penfold, B.; White, J. C. *Acta Cryst.* **1959**, *12*, 130–135.
- [207] David, W.; Shankland, K.; Pulham, C.; Blagden, N.; Davey, R.; Song, M. *Angew. Chem. Int. Ed.* **2005**, *117*, 7194–7197.
- [208] Thun, J.; Seyfarth, L.; Senker, J.; Dinnebier, R. E.; Breu, J. *Angew. Chem. Int. Ed.* **2007**, *46*, 6729–6731.
- [209] Bauer, J.; Spanton, S.; Henry, R.; Quick, J.; Dziki, W.; Porter, W.; Morris, J. *Pharm. Res.* **2001**, *18*, 859–866.
- [210] Vishweshwar, P.; McMahon, J. A.; Oliveira, M.; Peterson, M. L.; Zaworotko, M. J. *J. Am. Chem. Soc.* **2005**, *127*, 16802–16803.
- [211] Bond, A. D.; Boese, R.; Desiraju, G. R. *Angew. Chem. Int. Ed.* **2007**, *46*, 615–617.
- [212] Agnew, L. R.; Cruickshank, D. L.; McGlone, T.; Wilson, C. C. *ChemComm.* **2016**, *52*, 7368–7371.
- [213] Sacchi, P.; Wright, S.; Neoptolemu, P.; Lampronti, G.; Rajagopalan, A.; Kras, W.; Evans, C.; Hodgkinson, P.; Cruz-Cabeza, A. *ChemRxiv* **2023**,
- [214] Yoshizawa, K.; Toyota, S.; Toda, F. *ChemComm.* **2004**, 1844–1845.
- [215] Wedekind, E.; Wedekind, O. *Chem. Ber.* **1907**, 4450–4456.
- [216] Fröhlich, E.; Wedekind, E. *Chem. Ber.* **1907**, 1009–1013.
- [217] Menshutkin, N. *Z. Phys. Chem.* **1890**, 589–600.

- [218] Brands, K. M. J.; Davies, A. J. *Chem. Rev.* **2006**, *106*, 2711–2733.
- [219] Horeau, A. *Tetrahedron Lett.* **1969**, *10*, 3121–3124.
- [220] Harned, A. M. *Tetrahedron* **2018**, *74*, 3797–3841.
- [221] Favarger, F.; Goujon-Ginglinger, C.; Monchaud, D.; Lacour, J. *J. Org. Chem.* **2004**, *69*, 8521–8524.
- [222] Spackman, M. A.; Jayatilaka, D. *CrystEngComm*. **2009**, *11*, 19–32.
- [223] Maggioni, G. M.; Mazzotti, M. *Faraday Discuss.* **2015**, *179*, 359–382.
- [224] Tang, S.; Zhao, Z.; Chen, J.; Yang, T.; Wang, Y.; Chen, X.; Lv, M.; Yuan, W. Z. *Angew. Chem. Int. Ed.* **2022**, *134*, e202117368.
- [225] Klimash, A.; Prlj, A.; Yufit, D. S.; Mallick, A.; Curchod, B. F.; McGonigal, P. R.; Skabara, P. J.; Etherington, M. K. *J. Mater. Chem.* **2022**, *C10*, 9484–9491.
- [226] Liu, Y.; Li, C.; Ren, Z.; Yan, S.; Bryce, M. R. *Nat. Rev. Mater.* **2018**, *3*, 1–20.
- [227] Guo, Y.; Apergi, S.; Li, N.; Chen, M.; Yin, C.; Yuan, Z.; Gao, F.; Xie, F.; Brocks, G.; Tao, S.; Zhao, N. *Nat. Commun.* **2021**, *12*, 644.
- [228] Wang, M.; Shi, Z.; Fei, C.; Deng, Z. J. D.; Yang, G.; Dunfield, S. P.; Fenning, D. P.; Huang, J. *Nat. Energy* **2023**, 1–11.
- [229] Ye, H.-Y.; Tang, Y.-Y.; Li, P.-F.; Liao, W.-Q.; Gao, J.-X.; Hua, X.-N.; Cai, H.; Shi, P.-P.; You, Y.-M.; Xiong, R.-G. *Science* **2018**, *361*, 151–155.
- [230] von Richter, V. *Chem. Ber.* **1873**, *6*.
- [231] Brunel, J. M. *Chem. Rev.* **2005**, *105*, 857–898.
- [232] Krajnc, M.; Niemeyer, J. *Beilstein J. Org. Chem.* **2022**, *18*, 508–523.
- [233] Zhang, S.-Y.; Lan, J.-B.; Su, X.-Y.; Guo, S.-J.; Chen, L.; You, J.-S.; Xie, R.-G. *J. Chem. Res.* **2005**, *2005*, 418–419.
- [234] Rekis, T. *Acta Cryst.* **2020**, *B76*, 307–315.
- [235] Flack, H. D. *Helv. Chim. Acta.* **2003**, *86*, 905–921.
- [236] Pidcock, E. *ChemComm.* **2005**, *27*, 3457–3459.
- [237] Wallach, O. *Liebigs Ann. Chem.* **1895**, *286*, 90–118.
- [238] Brock, C. P.; Schweizer, W. B.; Dunitz, J. D. *J. Am. Chem. Soc.* **1991**, *113*, 9811–9820.

BIBLIOGRAPHY

- [239] Laubenstein, R.; Šerb, M.-D.; Englert, U.; Raabe, G.; Braun, T.; Braun, B. *ChemComm*. **2016**, *52*, 1214–1217.
- [240] Kramer, P.; Bolte, M. *Acta Cryst.* **2017**, *C73*, 575–581.
- [241] Fábíán, L.; Brock, C. P. *Acta Cryst.* **2010**, *B66*, 94–103.
- [242] Lineberry, A. M.; Benjamin, E. T.; Davis, R. E.; Kassel, W. S.; Wheeler, K. A. *Cryst. Growth Des.* **2008**, *8*, 612–619.
- [243] Rekiš, T.; Bērziņš, A. *CrystEngComm*. **2018**, *20*, 6909–6918.
- [244] Chion, B.; Lajzerowicz, J.; Bordeaux, D.; Collet, A.; Jacques, J. *J. Phys. Chem.* **1978**, *82*, 2682–2688.
- [245] Blaser, H. U. *Chem. Rev.* **1992**, *92*, 935–952.
- [246] Bredikhin, A. A.; Eliseenkova, R. M.; Bredikhina, Z. A.; Dobrynin, A. B.; Kostyanovsky, R. G. *Chirality* **2009**, *21*, 637–641.
- [247] Sogutoglu, L.-C.; Steendam, R. R. E.; Meekes, H.; Vlieg, E.; Rutjes, F. P. J. T. *Chem. Soc. Rev.* **2015**, *44*, 6723–6732.
- [248] Viedma, C. *Astrobiology* **2007**, *7*, 312–319.
- [249] Engwerda, A. H. J.; Koning, N.; Tinnemans, P.; Meekes, H.; Bickelhaupt, F. M.; Rutjes, F. P. J. T.; Vlieg, E. *Cryst. Growth Des.* **2017**, *17*, 4454–4457.
- [250] Viedma, C. *Phys. Rev. Lett.* **2005**, *94*, 65504.
- [251] Noorduin, W. L.; Meekes, H.; Bode, A. A. C.; van Enkevort, W. J. P.; Kaptein, B.; Kellogg, R. M.; Vlieg, E. *Cryst. Growth Des.* **2008**, *8*, 1675–1681.
- [252] Belletti, G.; Tortora, C.; Mellema, I. D.; Tinnemans, P.; Meekes, H.; Rutjes, F. P. J. T.; Tsogoeva, S. B.; Vlieg, E. *Chem. Eur. J.* **2020**, *26*, 839–844.
- [253] Viedma, C.; Ortiz, J. E.; de Torres, T.; Izumi, T.; Blackmond, D. G. *J. Am. Chem. Soc.* **2008**, *130*, 15274–15275.
- [254] IUCr *International Union of Crystallography*, <https://www.iucr.org/> **2023**, accessed 04/10/2023.
- [255] Steed, K. M.; Steed, J. W. *Chem. Rev.* **2015**, *115*, 2895–2933.
- [256] Steed, J. W. *What is Z'?*, <https://zprime.co.uk/introduction> **2006**, accessed 15/09/2023.
- [257] Anderson, K. M.; Goeta, A. E.; Hancock, K. S.; Steed, J. W. *ChemComm*. **2006**, 2138–2140.

- [258] Steiner, T. *Acta Cryst.* **2000**, *B56*, 673–676.
- [259] Anderson, K. M.; Afarinkia, K.; Yu, H.-w.; Goeta, A. E.; Steed, J. W. *Cryst. Growth Des.* **2006**, *6*, 2109–2113.
- [260] Nichol, G. S.; Clegg, W. *CrystEngComm.* **2007**, *9*, 959–960.
- [261] Desiraju, G. R. *CrystEngComm.* **2007**, *9*, 91–92.
- [262] Bernstein, J.; Dunitz, J.; Gavezzotti, A. *Cryst. Growth Des.* **2008**, *8*, 2011–2018.
- [263] Plass, K. E.; Kim, K.; Matzger, A. J. *J. Am. Chem. Soc.* **2004**, *126*, 9042–9053.
- [264] Steed, J. W. *CrystEngComm.* **2003**, *5*, 169–179.
- [265] Bishop, R.; Scudder, M. L. *Cryst. Growth Des.* **2009**, *9*, 2890–2894.
- [266] Pidcock, E.; Motherwell, W. S.; Cole, J. C. *Acta Cryst.* **2003**, *B59*, 634–640.
- [267] Marsh, R. E. *Acta Cryst.* **1999**, *B55*, 931–936.
- [268] Marsh, R. E.; Spek, A. L. *Acta Cryst.* **2001**, *B57*, 800–805.
- [269] Walker, M.; Pohl, E.; Herbst-Irmer, R.; Gerlitz, M.; Rohr, J.; Sheldrick, G. M. *Acta Cryst.* **1999**, *B55*, 607–616.
- [270] Craddock, D. E.; Parks, M. J.; Taylor, L. A.; Wagner, B. L.; Ruf, M.; Wheeler, K. A. *CrystEngComm.* **2021**, *23*, 210–215.
- [271] Xu, L.; Liu, F.-Y.; Zhang, Q.; Chang, W.-J.; Liu, Z.-L.; Lv, Y.; Yu, H.-Z.; Xu, J.; Dai, J.-J.; Xu, H.-J. *Nat. Catal.* **2021**, *4*, 71–78.
- [272] Avanthay, M.; Bedford, R. B.; Begg, C. S.; Böse, D.; Clayden, J.; Davis, S. A.; Eloi, J. C.; Goryunov, G. P.; Hartung, I. V.; Heeley, J.; Khaikin, K. A.; Kitching, M. O.; Krieger, J.; Kulyabin, P. S.; Lennox, A. J.; Nolla-Saltiel, R.; Pridmore, N. E.; Rowsell, B. J.; Sparkes, H. A.; Uborsky, D. V.; Voskoboinikov, A. Z.; Walsh, M. P.; Wilkinson, H. J. *Nat. Catal.* **2021**, *4*, 994–998.
- [273] Novák, Z.; Adamik, R.; Csenki, J. T.; Béke, F.; Gavaldik, R.; Varga, B.; Nagy, B.; May, Z.; Daru, J.; Gonda, Z.; Tolnai, G. L. *Nat. Catal.* **2021**, *4*, 991–993.
- [274] Vinod, J. K.; Wanner, A. K.; James, E. I.; Koide, K. *Nat. Catal.* **2021**, *4*, 999–1001.
- [275] *World Health Organization, Global tuberculosis report 2022*, 1–68.
- [276] Frénois, F.; Engohang-Ndong, J.; Locht, C.; Baulard, A. R.; Villeret, V. *Mol. Cell* **2004**, *16*, 301–307.

BIBLIOGRAPHY

- [277] Engohang-Ndong, J.; Baillat, D.; Aumercier, M.; Bellefontaine, F.; Besra, G. S.; Locht, C.; Baulard, A. R. *Mol. Microbiol.* **2004**, *51*, 175–188.
- [278] Willand, N.; Dirié, B.; Carette, X.; Bifani, P.; Singhal, A.; Desroses, M.; Leroux, F.; Willery, E.; Mathys, V.; Déprez-Poulain, R.; Delcroix, G.; Frénois, F.; Aumercier, M.; Locht, C.; Villeret, V.; Déprez, B.; Baulard, A. R. *Nat. Med.* **2009**, *15*, 537–544.
- [279] Flipo, M.; Desroses, M.; Lecat-Guillet, N.; Dirié, B.; Carette, X.; Leroux, F.; Piveteau, C.; Demirkaya, F.; Lens, Z.; Rucktooa, P.; Villeret, V.; Christophe, T.; Jeon, H. K.; Locht, C.; Brodin, P.; Déprez, B.; Baulard, A. R.; Willand, N. *J. Med. Chem.* **2011**, *54*, 2994–3010.
- [280] Flipo, M.; Desroses, M.; Lecat-Guillet, N.; Villemagne, B.; Blondiaux, N.; Leroux, F.; Piveteau, C.; Mathys, V.; Flament, M. P.; Siepmann, J.; Villeret, V.; Wohlkönig, A.; Wintjens, R.; Soror, S. H.; Christophe, T.; Jeon, H. K.; Locht, C.; Brodin, P.; Déprez, B.; Baulard, A. R.; Willand, N. *J. Med. Chem.* **2012**, *55*, 68–83.
- [281] Flipo, M.; Willand, N.; Lecat-Guillet, N.; Hounsou, C.; Desroses, M.; Leroux, F.; Lens, Z.; Villeret, V.; Wohlkönig, A.; Wintjens, R.; Christophe, T.; Jeon, H. K.; Locht, C.; Brodin, P.; Baulard, A. R.; Déprez, B. *J. Med. Chem.* **2012**, *55*, 6391–6402.
- [282] Tatum, N. J.; Duarte, F.; Kamerlin, S. C.; Pohl, E. *J. Phys. Chem. Lett.* **2019**, *10*, 2244–2249.
- [283] Brittain, W. D.; Cobb, S. L. *Org. Lett.* **2021**, *23*, 5793–5798.
- [284] Gillis, E. P.; Eastman, K. J.; Hill, M. D.; Donnelly, D. J.; Meanwell, N. A. *J. Med. Chem.* **2015**, *58*, 8315–8359.
- [285] Purser, S.; Moore, P. R.; Swallow, S.; Gouverneur, V. *Chem. Soc. Rev.* **2008**, *37*, 320–330.
- [286] Shah, P.; Westwell, A. D. *J. Enzyme Inhib. Med. Chem.* **2007**, *22*, 527–540.
- [287] Hagmann, W. K. *J. Med. Chem.* **2008**, *51*, 4359–4369.
- [288] Inoue, M.; Sumii, Y.; Shibata, N. *ACS Omega* **2020**, *5*.
- [289] Lemoine, K.; Hémon-Ribaud, A.; Leblanc, M.; Lhoste, J.; Tarascon, J. M.; Maisonneuve, V. *Chem. Rev.* **2022**, *122*, 14405–14439.
- [290] Babudri, F.; Farinola, G. M.; Naso, F.; Ragni, R. *ChemComm.* **2007**, 1003–1022.
- [291] Cardoso, V. F.; Correia, D. M.; Ribeiro, C.; Fernandes, M. M.; Lanceros-Méndez, S. *Polymers* **2018**, *10*, 161.

- [292] Lv, J.; Cheng, Y. *Chem. Soc. Rev.* **2021**, *50*, 5435–5467.
- [293] Lamotte, J.; Dupont, L.; Dideberg, O.; Campsteyn, H.; Vermeire, M.; De-laude, C.; Huls, R. *Acta Cryst.* **1977**, *B33*, 2392–2398.
- [294] Kettmann, V.; Mašterová, I.; Tomko, J.; *IUCr Acta Cryst.* **1982**, *B38*, 978–980.
- [295] Sakai, R.; Higa, T.; Jefford, C. W.; Bernardinelli, G. *J. Am. Chem. Soc.* **1986**, *108*, 6404–6405.
- [296] Ou, G. C.; Chen, H. Y.; Wang, Q.; Zhou, Q.; Zeng, F. *RSC Advances* **2022**, *12*, 6459–6462.
- [297] Rodeschini, V.; Simpkins, N. S.; Wilson, C. *J. Org. Chem.* **2007**, *72*, 4265–4267.
- [298] Sugawara, K.; Sugawara, F.; Strobel, G. A.; Fu, Y.; Cun-Heng, H.; Clardy, J. *J. Org. Chem.* **1985**, *50*, 5631–5633.
- [299] Usuki, T.; Yoshimoto, Y.; Sato, M.; Takenaka, T.; Takezawa, R.; Yoshida, Y.; Satake, M.; Suzuki, N.; Hashizume, D.; Dzyuba, S. V. *Bioorg. Med. Chem.* **2020**, *28*, 115251.
- [300] Kashiwada, Y.; Yamazaki, K.; Ikeshiro, Y.; Yamagishi, T.; Fujioka, T.; Mihashi, K.; Mizuki, K.; Cosentino, L. M.; Fowke, K.; Morris-Natschke, S. L.; Lee, K. H. *Tetrahedron* **2001**, *57*, 1559–1563.
- [301] Inokuma, Y.; Yoshioka, S.; Ariyoshi, J.; Arai, T.; Hitora, Y.; Takada, K.; Matsunaga, S.; Rissanen, K.; Fujita, M. *Nature* **2013**, *495*, 461–466.
- [302] Liebing, P.; Pitts, C. R.; Reimann, M.; Trapp, N.; Rombach, D.; Bornemann, D.; Kaupp, M.; Togni, A. *Chem. Eur. J.* **2021**, *27*, 6086–6093.
- [303] Heo, Y.-A. *CNS Drugs* **2022**, *36*, 1007–1013.
- [304] Walsh, M. P.; Kitching, M. O. *Cryst. Growth Des.* **2021**, *22*, 251–258.
- [305] Tyler, A. R.; Ragbirsingh, R.; McMonagle, C. J.; Waddell, P. G.; Heaps, S. E.; Steed, J. W.; Thaw, P.; Hall, M. J.; Probert, M. R. *Chem* **2020**, *6*, 1755–1765.
- [306] Gottlieb, H. E.; Kotlyar, V.; Nudelman, A. *J. Org. Chem.* **1997**, *62*, 7512–7515.
- [307] Dolomanov, O. V.; Bourhis, L. J.; Howard, J. A.; Puschmann, H. *J. Appl. Cryst.* **2009**, *42*, 339–341.
- [308] Sheldrick, G. M. *Acta Cryst.* **2015**, *A71*, 3–8.
- [309] Hübschle, C. B.; Sheldrick, G. M.; Dittrich, B. *J. Appl. Cryst.* **2011**, *44*, 1281–1284.

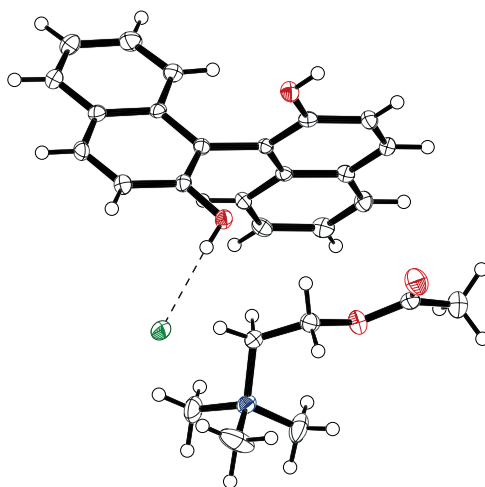
BIBLIOGRAPHY

- [310] Fournier, A. M.; Clayden, J. *Org. Lett.* **2012**, *14*, 142–145.
- [311] Giumanini, A. G.; Chiavari, G.; Musiani, M. M.; Rossi, P. *Synth. Commun.* **1980**, 743–746.
- [312] Parikh, J. R.; Doering, W. v. E. *J. Am. Chem. Soc.* **1967**, *89*, 5505–5507.
- [313] Chen, D.; Xu, L.; Yu, Y.; Mo, Q.; Qi, X.; Liu, C. *Angew. Chem. Int. Ed.* **2023**, *62*, e202215168.
- [314] Kulchat, S.; Lehn, J.-M. *Chem. Asian. J.* **2015**, *10*, 2484–2496.
- [315] Gan, B.; Jiang, X.; Mi, Z.; Zhang, C.; Bai, R.; Shuai, Q.; Xie, Y. *Synth. Commun.* **2019**, *49*, 73–79.
- [316] Walden, P. *J. Am. Chem. Soc.* **1913**, *35*, 1649–1664.
- [317] Chenon, B.; Sandorfy, C. *Can. J. Chem.* **1958**, *36*, 1181–1206.
- [318] Chen, F.; Topf, C.; Radnik, J.; Kreyenschulte, C.; Lund, H.; Schneider, M.; Surkus, A.-E.; He, L.; Junge, K.; Beller, M. *J. Am. Chem. Soc.* **2016**, *138*, 8781–8788.
- [319] Zhang, G.; Wu, J.; Zheng, S.; Neary, M. C.; Mao, J.; Flores, M.; Trovitch, R. J.; Dub, P. A. *J. Am. Chem. Soc.* **2020**, *142*, 16507–16509.
- [320] Ramalingam, K.; Rajaraman, T. *J. Mol. Struct.* **2020**, *1218*, 128489.
- [321] Xu, C.-R.; Zhang, Z.; Pan, C.-Y.; Hong, C.-Y. *Polymer* **2019**, *172*, 294–304.
- [322] Chang, C.-L.; Leung, M.; Yang, M.-H. *Tetrahedron* **2004**, *60*, 9205–9212.
- [323] Munenori, S.; Kentaro, I.; Koji, H.; Shinya, I.; Noriyuki, K.; Mitsuteru, K.; Shoko, S.; Kensuke, O.; Florian, S. *Polycyclic Compounds, Patent no. WO2020080558A1* **2020**,
- [324] Grosso, A. D.; Singleton, P. J.; Muryn, C. A.; Ingleson, M. J. *Angew. Chem. Int. Ed.* **2011**, *50*, 2102–2106.
- [325] Lacour, J.; Londez, A.; Goujon-Ginglinger, C.; Buss, V.; Bernardinelli, G. *Org. Lett.* **2000**, *2*, 4185–4188.

Appendix A

Crystallographic data

Crystal Structure: 133



Crystal data for $C_{27}H_{30}ClNO_4$ ($m = 467.97$ g/mol);

Orthorhombic, space group $P2_12_12_1$ (no. 19)

$a = 10.9188(4)$ Å

$b = 11.1913(4)$ Å

$c = 19.7175(6)$ Å

$\alpha = 90^\circ$

$\beta = 90^\circ$

$\gamma = 90^\circ$

$V = 2409.39(14)$ Å³

$Z = 4$

$T = 120.0$ K

Radiation: MoK α ($\lambda = 0.71073$ Å)

$\mu(\text{MoK}\alpha) = 0.192$ mm⁻¹

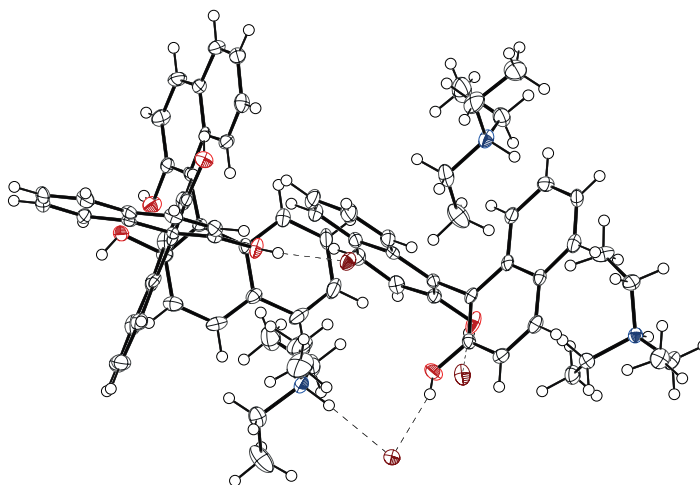
$D_{\text{calc}} = 1.460$ g/cm³

31447 reflections measured ($4.132^\circ \leq 2\theta \leq 59.986^\circ$), 7007 unique ($R_{\text{int}} = 0.0614$, $R_{\text{sigma}} = 0.0657$) which were used in all calculations.

The final $R1$ was 0.0483 ($I > 2\sigma(I)$) and $wR2$ was 0.1215 (all data).

Flack parameter = 0.01(3).

Crystal Structure: 135



Crystal data for 3 (C₂₆H₃₀BrNO₂) (m = 1405.25 g/mol);

Orthorhombic, space group *P*2₁2₁2₁ (no. 19)

a = 14.8884(7) Å

b = 16.3656(8) Å

c = 28.2957(14) Å

α = 90°

β = 90°

γ = 90°

V = 6894.5(6) Å³

Z = 4

T = 120.0 K

Radiation: MoKα (λ = 0.71073 Å)

μ(MoKα) = 1.811 mm⁻¹

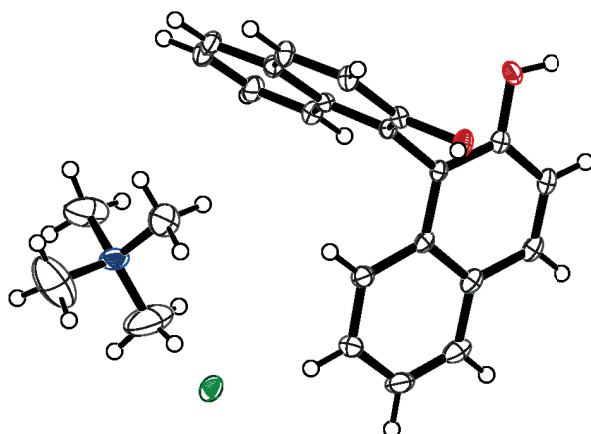
*D*_{calc} = 1.354 g/cm³

120251 reflections measured (3.092° ≤ 2θ ≤ 60°), 20088 unique (*R*_{int} = 0.0830, *R*_{sigma} = 0.0744) which were used in all calculations.

The final *R*1 was 0.0443 (*I* > 2σ(*I*)) and *wR*2 was 0.0588 (all data).

Flack parameter = 0.004(3).

Crystal Structure: 138



Crystal data for $C_{24}H_{26}ClNO_2$ ($m = 395.91$ g/mol);

Orthorhombic, space group $P2_12_12_1$ (no. 19).

$a = 9.0063(3)$ Å

$b = 14.1387(4)$ Å

$c = 16.6389(5)$ Å

$\alpha = 90^\circ$

$\beta = 90^\circ$

$\gamma = 90^\circ$

$V = 2124.48(11)$ Å³

$Z = 4$

$T = 120.0$ K

Radiation: MoK α ($\lambda = 0.71073$ Å)

$\mu(\text{MoK}\alpha) = 0.199$ mm⁻¹

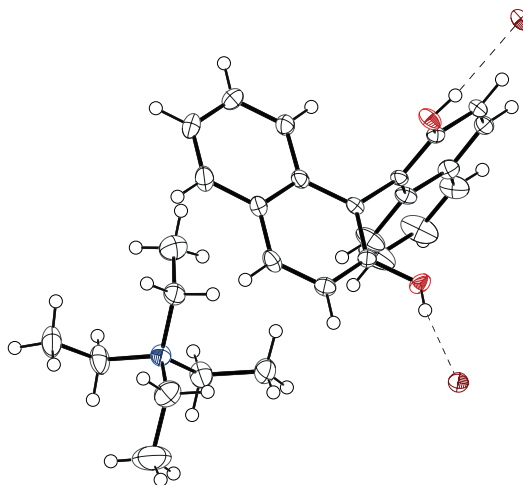
$D_{\text{calc}} = 1.238$ g/cm³

27409 reflections measured ($3.776^\circ \leq 2\theta \leq 59.994^\circ$), 6169 unique ($R_{\text{int}} = 0.0378$, $R_{\text{sigma}} = 0.0341$) which were used in all calculations.

The final $R1$ was 0.0487 ($I > 2\sigma(I)$) and $wR2$ was 0.1518 (all data).

Flack parameter = 0.038(17).

Crystal Structure: 149



Crystal data for $C_{28}H_{34}BrNO_2$ ($m = 496.47$ g/mol);

Tetragonal, space group $P4_32_12$ (no. 96)

$a = 12.1968(3)$ Å

$b = 12.1968(3)$ Å

$c = 33.8960(11)$ Å

$\alpha = 90^\circ$

$\beta = 90^\circ$

$\gamma = 90^\circ$

$V = 5042.4(4)$ Å³

$Z = 8$

$T = 120.0$ K

Radiation: MoK α ($\lambda = 0.71073$ Å)

$\mu(\text{MoK}\alpha) = 1.654$ mm⁻¹

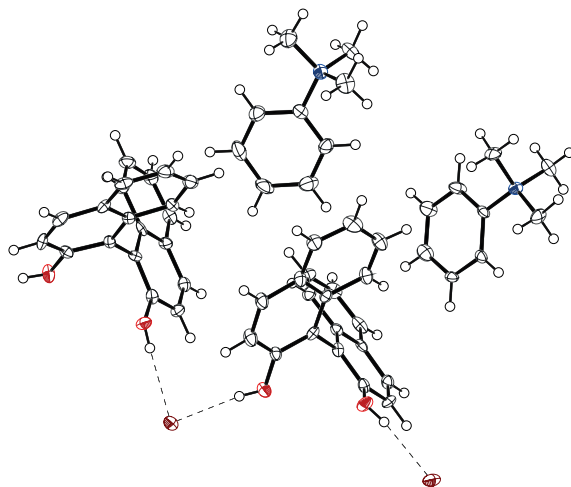
$D_{calc} = 1.308$ g/cm³

87957 reflections measured ($3.548^\circ \leq 2\theta \leq 60^\circ$), 7361 unique ($R_{int} = 0.0549$, $R_{sigma} = 0.0287$) which were used in all calculations.

The final $R1$ was 0.0290 ($I > 2\sigma(I)$) and $wR2$ was 0.0960 (all data).

Flack parameter = 0.006(2).

Crystal Structure: 153



Crystal data for $C_{46}H_{43}NO_6$ ($m = 387.50$ g/mol);

Monoclinic, space group $P2_1$ (no. 4)

$a = 11.2619(4)$ Å

$b = 19.5062(7)$ Å

$c = 11.8894(4)$ Å

$\alpha = 90^\circ$

$\beta = 111.1800(10)^\circ$

$\gamma = 90^\circ$

$V = 2435.40(15)$ Å³

$Z = 4$

$T = 120.0$ K

Radiation: MoK α ($\lambda = 0.71073$ Å)

$\mu(\text{MoK}\alpha) = 0.087$ mm⁻¹

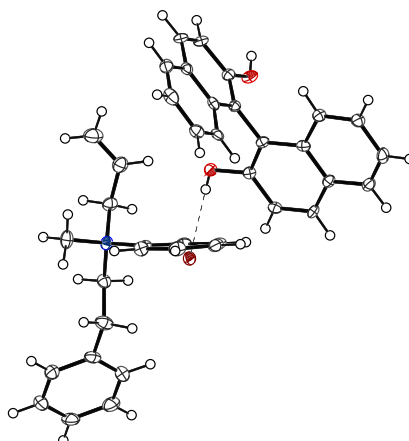
$D_{calc} = 1.370$ g/cm³

42106 reflections measured ($3.878^\circ \leq 2\theta \leq 60^\circ$), 14109 unique ($R_{int} = 0.0816$, $R_{sigma} = 0.1401$) which were used in all calculations.

The final $R1$ was 0.0547 ($I > 2\sigma(I)$) and $wR2$ was 0.0774 (all data).

Flack parameter = 0.024(6).

Crystal Structure: 215



Crystal data for $C_{38}H_{36}BrNO_2$ ($m = 618.59$ g/mol);

Orthorhombic, space group $P2_12_12$ (no. 18)

$a = 22.8789(12)$ Å

$b = 10.7729(7)$ Å

$c = 12.3333(7)$ Å

$\alpha = 90^\circ$

$\beta = 90^\circ$

$\gamma = 90^\circ$

$V = 3039.8(3)$ Å³

$Z = 4$

$T = 120.0$ K

Radiation: MoK α ($\lambda = 0.71073$ Å)

$\mu(\text{MoK}\alpha) = 1.387$ mm⁻¹

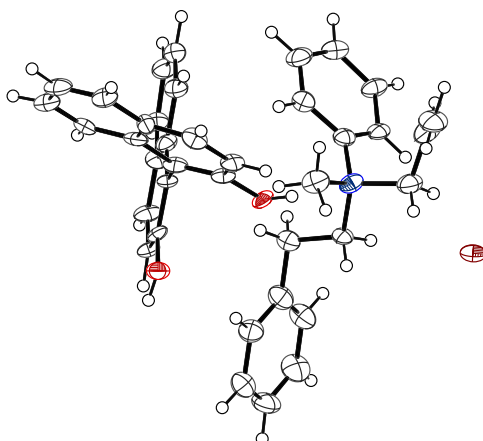
$D_{\text{calc}} = 1.352$ g cm⁻³

44262 reflections measured ($4.18 \leq 2\theta \leq 54.994^\circ$), 6765 unique ($R_{\text{int}} = 0.0891$, $R_{\text{sigma}} = 0.0616$) which were used in all calculations.

The final $R1$ was 0.0450 ($I > 2\sigma(I)$) and $wR2$ was 0.0889 (all data)

Flack parameter = 0.004(6)

Crystal Structure: 215a



Crystal data for $C_{38}H_{36}BrNO_2$ ($m = 618.59$ g/mol);

Orthorhombic, space group $P2_12_12$ (no. 18)

$a = 22.918(8)$ Å

$b = 10.832(4)$ Å

$c = 12.374(4)$ Å

$\alpha = 90^\circ$

$\beta = 90^\circ$

$\gamma = 90^\circ$

$V = 3071.9(19)$ Å³

$Z = 4$

$T = 120.00$ K

Radiation: MoK α ($\lambda = 0.71073$ Å)

$\mu(\text{MoK}\alpha) = 1.373$ mm⁻¹

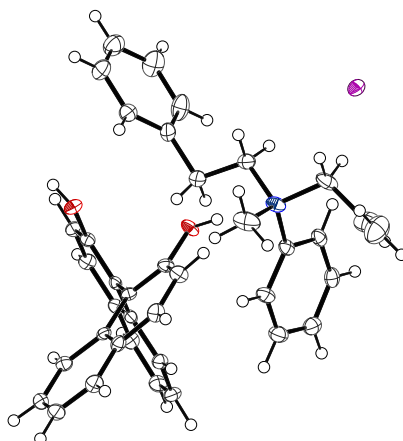
$D_{\text{calc}} = 1.338$ g cm⁻³

47465 reflections measured ($3.74 \leq 2\theta \leq 56.99^\circ$), 7801 unique ($R_{\text{int}} = 0.2453$, $R_{\text{sigma}} = 0.2167$) which were used in all calculations.

The final R_1 was 0.0898 ($I > 2\sigma(I)$) and wR_2 was 0.1736 (all data)

Flack parameter = 0.013(13)

Crystal Structure: 216



Crystal data for $C_{38}H_{36}INO_2$ ($m = 665.58$ g/mol);

Orthorhombic, space group $P2_12_12$ (no. 18)

$a = 23.3017(8)$ Å

$b = 10.8122(4)$ Å

$c = 12.4560(4)$ Å

$\alpha = 90^\circ$

$\beta = 90^\circ$

$\gamma = 90^\circ$

$V = 3138.20(19)$ Å³

$Z = 4$

$T = 120.0$ K

Radiation: MoK α ($\lambda = 0.71073$ Å)

$\mu(\text{MoK}\alpha) = 1.055$ mm⁻¹

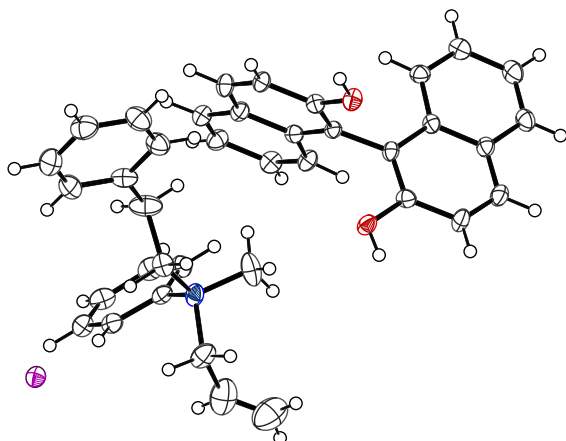
$D_{\text{calc}} = 1.409$ g cm⁻³

56442 reflections measured ($3.708 \leq 2\theta \leq 59.996^\circ$), 9128 unique ($R_{\text{int}} = 0.0530$, $R_{\text{sigma}} = 0.0399$) which were used in all calculations.

The final $R1$ was 0.0361 ($I > 2\sigma(I)$) and $wR2$ was 0.0907 (all data)

Flack parameter = $-0.024(9)$

Crystal Structure: 216a



Crystal data for $C_{38}H_{36}INO_2$ ($m = 665.58$ g/mol);

Orthorhombic, space group $P2_12_12$ (no. 18)

$a = 23.3663(16)$ Å

$b = 10.8397(7)$ Å

$c = 12.4894(9)$ Å

$\alpha = 90^\circ$

$\beta = 90^\circ$

$\gamma = 90^\circ$

$V = 3163.4(4)$ Å³

$Z = 4$

$T = 120.00$ K

Radiation: MoK α ($\lambda = 0.71073$ Å)

$\mu(\text{MoK}\alpha) = 1.046$ mm⁻¹

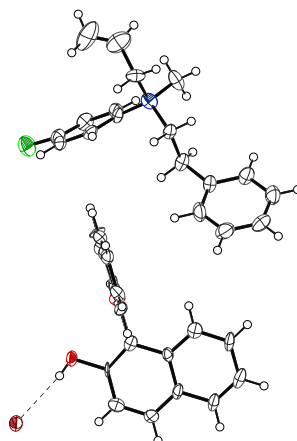
$D_{\text{calc}} = 1.398$ g cm⁻³

54757 reflections measured ($3.698 \leq 2\theta \leq 59.994^\circ$), 9227 unique ($R_{\text{int}} = 0.0645$, $R_{\text{sigma}} = 0.0521$) which were used in all calculations.

The final $R1$ was 0.0429 ($I > 2\sigma(I)$) and $wR2$ was 0.0946 (all data)

Flack parameter = $-0.008(8)$

Crystal Structure: 217



Crystal data for $C_{38}H_{35}BrFNO_2$ ($m = 636.58$ g/mol);

Orthorhombic, space group $P2_12_12$ (no. 18)

$a = 23.141(4)$ Å

$b = 10.9188(19)$ Å

$c = 12.493(2)$ Å

$\alpha = 90^\circ$

$\beta = 90^\circ$

$\gamma = 90^\circ$

$V = 3156.7(9)$ Å³

$Z = 4$

$T = 120.00$ K

Radiation: MoK α ($\lambda = 0.71073$ Å)

$\mu(\text{MoK}\alpha) = 1.343$ mm⁻¹

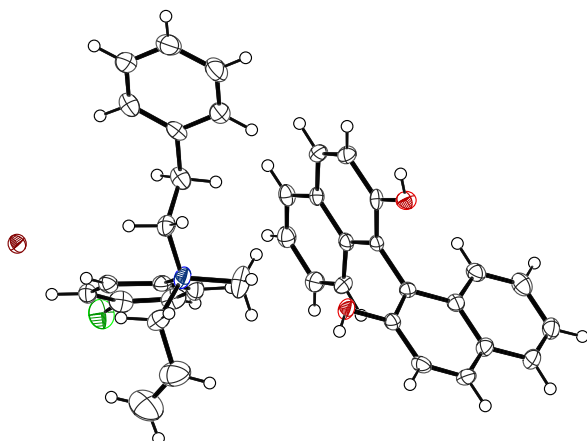
$D_{\text{calc}} = 1.339$ g cm⁻³

39515 reflections measured ($4.798 \leq 2\theta \leq 49.99^\circ$), 5554 unique ($R_{\text{int}} = 0.1847$, $R_{\text{sigma}} = 0.1388$) which were used in all calculations.

The final $R1$ was 0.0727 ($I > 2\sigma(I)$) and $wR2$ was 0.1517 (all data)

Flack parameter = 0.035(10)

Crystal Structure: 217a



Crystal data for $C_{38}H_{35}BrFNO_2$ ($m = 636.58$ g/mol);

Orthorhombic, space group $P2_12_12$ (no. 18)

$a = 23.1555(16)$ Å

$b = 10.9115(8)$ Å

$c = 12.4884(9)$ Å

$\alpha = 90^\circ$

$\beta = 90^\circ$

$\gamma = 90^\circ$

$V = 3155.3(4)$ Å³

$Z = 4$

$T = 120.00$ K

Radiation: MoK α ($\lambda = 0.71073$ Å)

$\mu(\text{MoK}\alpha) = 1.343$ mm⁻¹

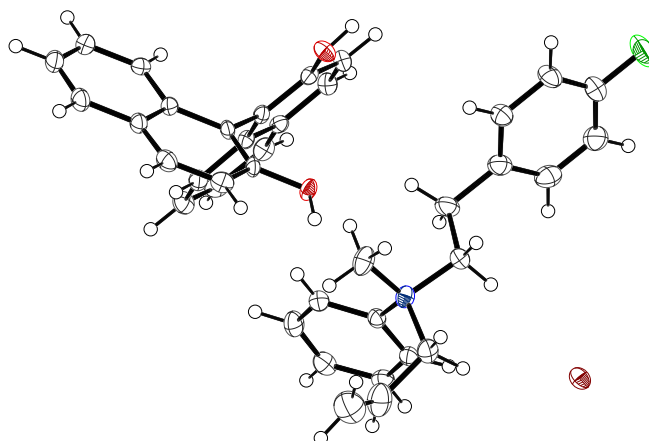
$D_{calc} = 1.340$ g cm⁻³

53334 reflections measured ($4.126 \leq 2\theta \leq 58.992^\circ$), 8786 unique ($R_{int} = 0.1441$, $R_{sigma} = 0.1329$) which were used in all calculations.

The final $R1$ was 0.0640 ($I > 2\sigma(I)$) and $wR2$ was 0.1154 (all data)

Flack parameter = 0.004(6)

Crystal Structure: 218



Crystal data for $C_{38}H_{35}BrFNO_2$ ($m = 636.58$ g/mol);

Orthorhombic, space group $P2_12_12$ (no. 18)

$a = 23.5398(9)$ Å

$b = 10.8657(4)$ Å

$c = 12.1941(5)$ Å

$\alpha = 90^\circ$

$\beta = 90^\circ$

$\gamma = 90^\circ$

$V = 3119.0(2)$ Å³

$Z = 4$

$T = 120.0$ K

Radiation: MoK α ($\lambda = 0.71073$ Å)

$\mu(\text{MoK}\alpha) = 1.359$ mm⁻¹

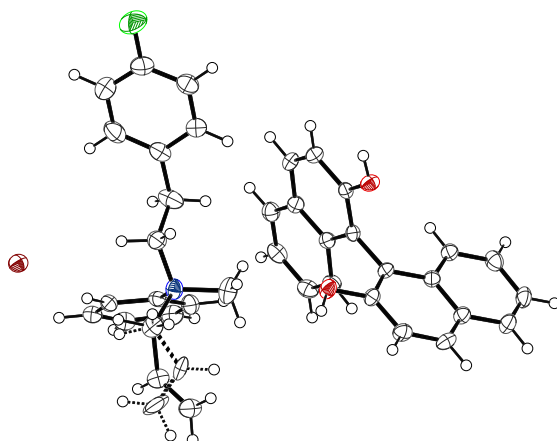
$D_{\text{calc}} = 1.356$ g cm⁻³

57065 reflections measured ($4.128 \leq 2\theta \leq 59.998^\circ$), 9102 unique ($R_{\text{int}} = 0.1003$, $R_{\text{sigma}} = 0.0763$) which were used in all calculations.

The final $R1$ was 0.0550 ($I > 2\sigma(I)$) and $wR2$ was 0.1001 (all data)

Flack parameter = 0.013(4)

Crystal Structure: 218a



Crystal data for $C_{38}H_{35}BrFNO_2$ ($m = 636.58$ g/mol);

Orthorhombic, space group $P2_12_12$ (no. 18)

$a = 23.5700(14)$ Å

$b = 10.8918(7)$ Å

$c = 12.2051(7)$ Å

$\alpha = 90^\circ$

$\beta = 90^\circ$

$\gamma = 90^\circ$

$V = 3133.3(3)$ Å³

$Z = 4$

$T = 120.00$ K

Radiation: MoK α ($\lambda = 0.71073$ Å)

$\mu(\text{MoK}\alpha) = 1.353$ mm⁻¹

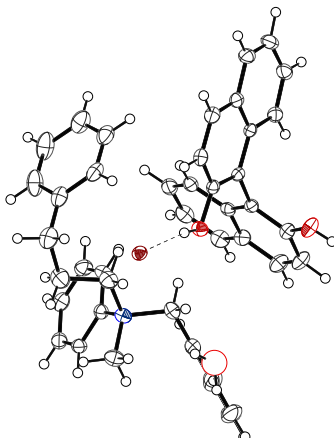
$D_{\text{calc}} = 1.349$ g cm⁻³

51611 reflections measured ($4.12 \leq 2\theta \leq 57.998^\circ$), 8335 unique ($R_{\text{int}} = 0.0934$, $R_{\text{sigma}} = 0.0791$) which were used in all calculations.

The final $R1$ was 0.0491 ($I > 2\sigma(I)$) and $wR2$ was 0.1108 (all data)

Flack parameter = $-0.005(5)$

Crystal Structure: 219



Crystal data for $C_{43}H_{40}BrNO_2 \cdot 0.2(H_2O)$ ($m = 686.27$ g/mol);

Orthorhombic, space group $P2_12_12_1$ (no. 19)

$a = 11.8410(3)$ Å

$b = 12.5268(3)$ Å

$c = 23.6549(5)$ Å

$\alpha = 90^\circ$

$\beta = 90^\circ$

$\gamma = 90^\circ$

$V = 3508.73(14)$ Å³

$Z = 4$

$T = 120.0$ K

Radiation: MoK α ($\lambda = 0.71073$ Å)

$\mu(\text{MoK}\alpha) = 1.210$ mm⁻¹

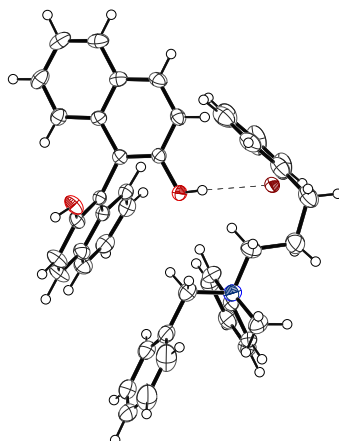
$D_{\text{calc}} = 1.299$ g cm⁻³

63963 reflections measured ($3.846 \leq 2\theta \leq 59.992^\circ$), 10197 unique ($R_{\text{int}} = 0.0405$, $R_{\text{sigma}} = 0.0293$) which were used in all calculations.

The final $R1$ was 0.0268 ($I > 2\sigma(I)$) and $wR2$ was 0.0568 (all data)

Flack parameter = $-0.0047(19)$

Crystal Structure: 219a



Crystal data for $C_{43}H_{40}BrNO_2$ ($m = 682.67$ g/mol);

Orthorhombic, space group $P2_12_12_1$ (no. 19)

$a = 11.8735(3)$ Å

$b = 12.4993(4)$ Å

$c = 23.6477(7)$ Å

$\alpha = 90^\circ$

$\beta = 90^\circ$

$\gamma = 90^\circ$

$V = 3509.57(18)$ Å³

$Z = 4$

$T = 120.00$ K

Radiation: MoK α ($\lambda = 0.71073$ Å)

$\mu(\text{MoK}\alpha) = 1.209$ mm⁻¹

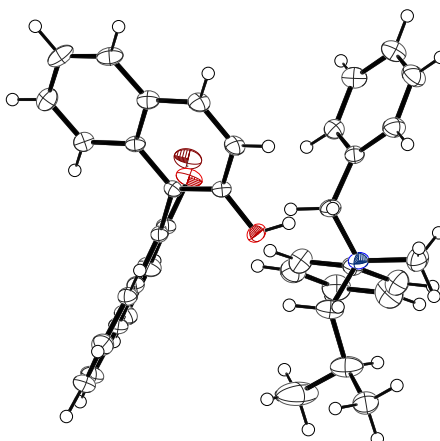
$D_{calc} = 1.292$ g cm⁻³

86166 reflections measured ($4.732 \leq 2\theta \leq 59.996^\circ$), 10226 unique ($R_{int} = 0.0688$, $R_{sigma} = 0.0442$) which were used in all calculations.

The final $R1$ was 0.0363 ($I > 2\sigma(I)$) and $wR2$ was 0.0769 (all data)

Flack parameter = 0.004(3)

Crystal Structure: 220



Crystal data for $C_{38}H_{38}BrNO_2$ ($m = 620.60$ g/mol);

Orthorhombic, space group $P2_12_12_1$ (no. 19)

$a = 10.3270(7)$ Å

$b = 14.3332(10)$ Å

$c = 20.8734(14)$ Å

$\alpha = 90^\circ$

$\beta = 90^\circ$

$\gamma = 90^\circ$

$V = 3089.7(4)$ Å³

$Z = 4$

$T = 273.15$ K

Radiation: MoK α ($\lambda = 0.71073$ Å)

$\mu(\text{MoK}\alpha) = 1.365$ mm⁻¹

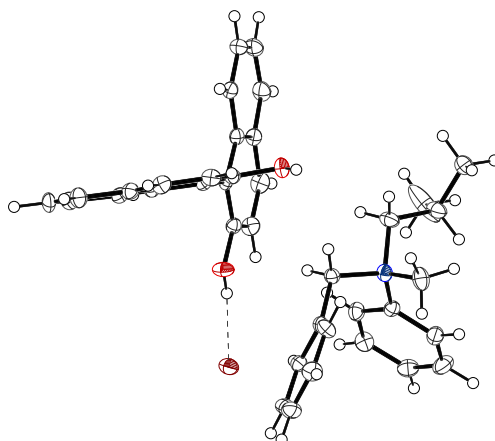
$D_{\text{calc}} = 1.334$ g cm⁻³

50103 reflections measured ($3.446 \leq 2\theta \leq 57.99^\circ$), 8203 unique ($R_{\text{int}} = 0.0454$, $R_{\text{sigma}} = 0.0364$) which were used in all calculations.

The final $R1$ was 0.0434 ($I > 2\sigma(I)$) and $wR2$ was 0.1070 (all data)

Flack parameter = $-0.001(3)$

Crystal Structure: 220a



Crystal data for $C_{38}H_{38}BrNO_2$ ($m = 620.60$ g/mol);

Orthorhombic, space group $P2_12_12_1$ (no. 19)

$a = 10.3490(4)$ Å

$b = 14.3961(5)$ Å

$c = 20.7363(8)$ Å

$\alpha = 90^\circ$

$\beta = 90^\circ$

$\gamma = 90^\circ$

$V = 3089.4(2)$ Å³

$Z = 4$

$T = 120.00$ K

Radiation: MoK α ($\lambda = 0.71073$ Å)

$\mu(\text{MoK}\alpha) = 1.365$ mm⁻¹

$D_{\text{calc}} = 1.334$ g cm⁻³

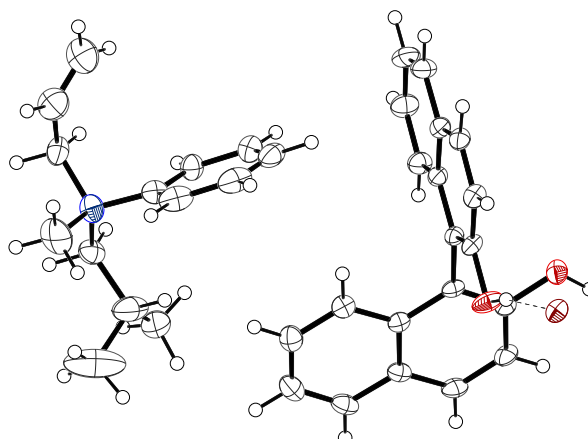
8999 reflections measured ($3.444 \leq 2\theta \leq 59.994^\circ$), 8999 unique ($R_{\text{int}} = 0.0540$, $R_{\text{sigma}} = 0.0484$) which were used in all calculations.

The final R_1 was 0.0423 ($I > 2\sigma(I)$) and wR_2 was 0.1124 (all data)

Largest diff. peak/hole / e Å⁻³ 0.48/-1.15

Flack parameter = 0.000(3)

Crystal Structure: 221



Crystal data for $C_{34}H_{36}BrNO_2$ ($m = 570.55$ g/mol);

Orthorhombic, space group $P2_12_12_1$ (no. 19)

$a = 10.1979(3)$ Å

$b = 11.1421(4)$ Å

$c = 25.5951(8)$ Å

$\alpha = 90^\circ$

$\beta = 90^\circ$

$\gamma = 90^\circ$

$V = 2908.27(16)$ Å³

$Z = 4$

$T = 120.0$ K

Radiation: MoK α ($\lambda = 0.71073$ Å)

$\mu(\text{MoK}\alpha) = 1.444$ mm⁻¹

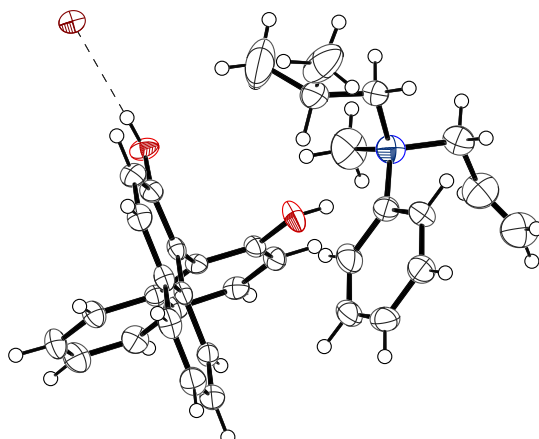
$D_{\text{calc}} = 1.303$ g cm⁻³

51383 reflections measured ($3.986 \leq 2\theta \leq 58.996^\circ$), 8081 unique ($R_{\text{int}} = 0.0545$, $R_{\text{sigma}} = 0.0388$) which were used in all calculations.

The final $R1$ was 0.0377 ($I > 2\sigma(I)$) and $wR2$ was 0.0771 (all data)

Flack parameter = 0.009(3)

Crystal Structure: 221a



Crystal data for $C_{34}H_{36}BrNO_2$ ($m = 570.55$ g/mol);

Orthorhombic, space group $P2_12_12_1$ (no. 19)

$a = 10.2187(2)$ Å

$b = 11.1423(2)$ Å

$c = 25.6625(6)$ Å

$\alpha = 90^\circ$

$\beta = 90^\circ$

$\gamma = 90^\circ$

$V = 2921.93(10)$ Å³

$Z = 4$

$T = 120.00$ K

Radiation: MoK α ($\lambda = 0.71073$ Å)

$\mu(\text{MoK}\alpha) = 1.437$ mm⁻¹

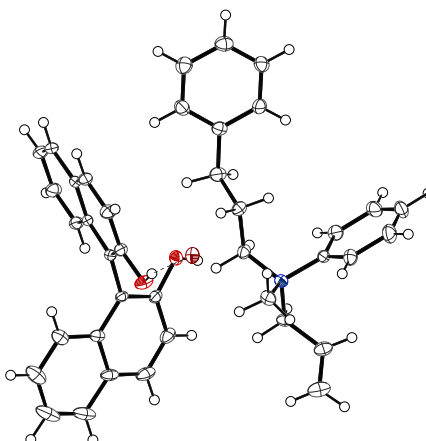
$D_{\text{calc}} = 1.297$ g cm⁻³

38043 reflections measured ($3.986 \leq 2\theta \leq 59.998^\circ$), 8525 unique ($R_{\text{int}} = 0.0439$, $R_{\text{sigma}} = 0.0453$) which were used in all calculations.

The final $R1$ was 0.0370 ($I > 2\sigma(I)$) and $wR2$ was 0.0773 (all data)

Flack parameter = 0.001(3)

Crystal Structure: 222



Crystal data for $C_{39}H_{38}BrNO_2$ ($m = 632.61$ g/mol);

Orthorhombic, space group $P1$ (no. 1)

$a = 8.4789(3)$ Å

$b = 9.0231(3)$ Å

$c = 11.6960(4)$ Å

$\alpha = 96.0906(12)^\circ$

$\beta = 106.5936(12)^\circ$

$\gamma = 104.9088(12)^\circ$

$V = 812.95(5)$ Å³

$Z = 1$

$T = 120.0$ K

Radiation: MoK α ($\lambda = 0.71073$ Å)

$\mu(\text{MoK}\alpha) = 0.71073$ mm⁻¹

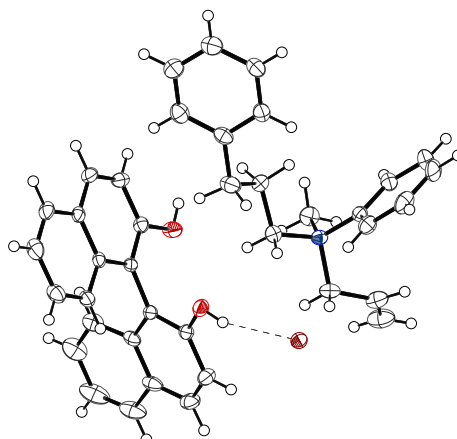
$D_{\text{calc}} = 1.292$ g cm⁻³

18764 reflections measured ($6.578^\circ \leq 2\theta \leq 59.998^\circ$), 9037 unique ($R_{\text{int}} = 0.0232$, $R_{\text{sigma}} = 0.0336$) which were used in all calculations.

The final $R1$ was 0.0220 ($I > 2\sigma(I)$) and $wR2$ was 0.0514 (all data)

Flack parameter = $-0.009(2)$

Crystal Structure: 222a



Crystal data for $C_{39}H_{38}BrNO_2$ ($m = 632.61$ g/mol);

Triclinic, space group $P1$ (no. 1)

$a = 8.5068(4)$ Å

$b = 9.0303(4)$ Å

$c = 11.7205(6)$ Å

$\alpha = 95.944(2)^\circ$

$\beta = 106.769(2)^\circ$

$\gamma = 104.9100(10)^\circ$

$V = 817.52(7)$ Å³

$Z = 1$

$T = 130.00$ K

Radiation: MoK α ($\lambda = 0.71073$ Å)

$\mu(\text{MoK}\alpha) = 1.291$ mm⁻¹

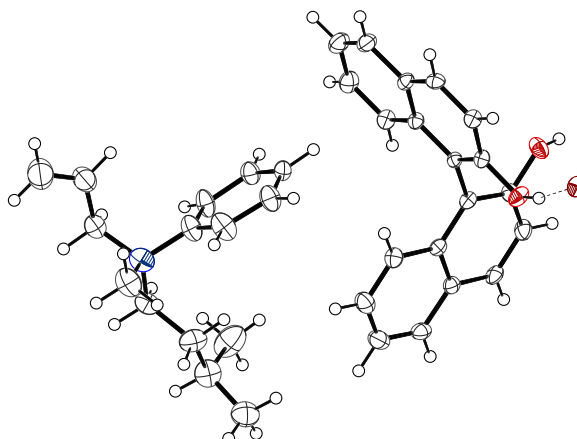
$D_{calc} = 1.285$ g cm⁻³

14222 reflections measured ($3.698^\circ \leq 2\theta \leq 60^\circ$), 9181 unique ($R_{int} = 0.0237$, $R_{sigma} = 0.0528$) which were used in all calculations.

The final $R1$ was 0.0364 ($I > 2\sigma(I)$) and $wR2$ was 0.0790 (all data)

Flack parameter = $-0.010(3)$

Crystal Structure: 223



Crystal data for $C_{35}H_{38}BrNO_2$ ($m = 584.57$ g/mol);

Orthorhombic, space group $P2_12_12_1$ (no. 19)

$a = 10.1986(5)$ Å

$b = 11.4846(6)$ Å

$c = 25.7574(13)$ Å

$\alpha = 90^\circ$

$\beta = 90^\circ$

$\gamma = 90^\circ$

$V = 3016.9(3)$ Å³

$Z = 4$

$T = 120.0$ K

Radiation: MoK α ($\lambda = 0.71073$ Å)

$\mu(\text{MoK}\alpha) = 1.394$ mm⁻¹

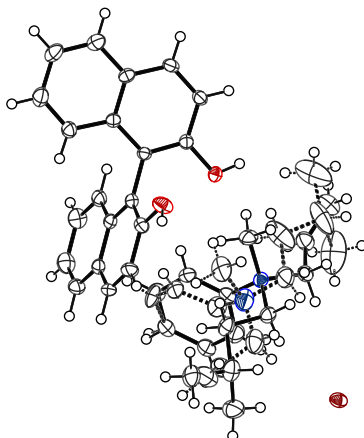
$D_{\text{calc}} = 1.287$ g cm⁻³

70531 reflections measured ($3.884 \leq 2\theta \leq 59.996^\circ$), 8806 unique ($R_{\text{int}} = 0.0763$, $R_{\text{sigma}} = 0.0482$) which were used in all calculations.

The final $R1$ was 0.0490 ($I > 2\sigma(I)$) and $wR2$ was 0.1214 (all data)

Flack parameter = 0.031(4)

Crystal Structure: 223a



Crystal data for $C_{35}H_{38}BrNO_2$ ($m = 584.57$ g/mol);

Orthorhombic, space group $P2_12_12_1$ (no. 19)

$a = 10.1794(3)$ Å

$b = 11.5272(3)$ Å

$c = 25.8005(8)$ Å

$\alpha = 90^\circ$

$\beta = 90^\circ$

$\gamma = 90^\circ$

$V = 3027.43(15)$ Å³

$Z = 4$

$T = 120.00$ K

Radiation: MoK α ($\lambda = 0.71073$ Å)

$\mu(\text{MoK}\alpha) = 1.389$ mm⁻¹

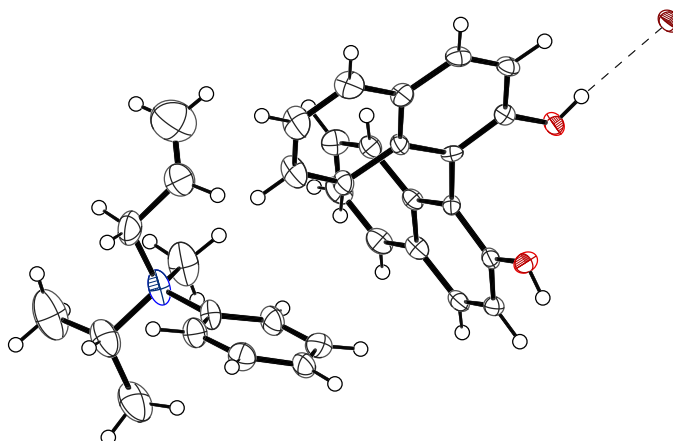
$D_{\text{calc}} = 1.283$ g cm⁻³

52681 reflections measured ($3.87 \leq 2\theta \leq 59.998^\circ$), 8838 unique ($R_{\text{int}} = 0.0766$, $R_{\text{sigma}} = 0.0674$) which were used in all calculations.

The final $R1$ was 0.0477 ($I > 2\sigma(I)$) and $wR2$ was 0.0975 (all data)

Flack parameter = 0.021(4)

Crystal Structure: 225a



Crystal data for $C_{33}H_{34}BrNO_2$ ($m = 556.52$ g/mol);

Tetragonal, space group $P4_1$ (no. 76)

$a = 9.1851(3)$ Å

$b = 9.1851(3)$ Å

$c = 32.7483(14)$ Å

$\alpha = 90^\circ$

$\beta = 90^\circ$

$\gamma = 90^\circ$

$V = 2762.8(2)$ Å³

$Z = 4$

$T = 120.00$ K

Radiation: MoK α ($\lambda = 0.71073$ Å)

$\mu(\text{MoK}\alpha) = 1.518$ mm⁻¹

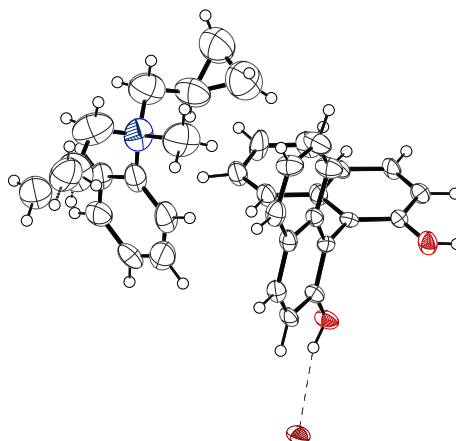
$D_{\text{calc}} = 1.338$ g cm⁻³

48052 reflections measured ($4.434 \leq 2\theta \leq 59.988^\circ$), 8054 unique ($R_{\text{int}} = 0.0675$, $R_{\text{sigma}} = 0.0598$) which were used in all calculations.

The final $R1$ was 0.0610 ($I > 2\sigma(I)$) and $wR2$ was 0.1495 (all data)

Flack parameter = 0.046(4)

Crystal Structure: 226



Crystal data for $C_{34}H_{34}BrNO_2$ ($m = 568.53$ g/mol);

Tetragonal, space group $P4_1$ (no. 76)

$a = 8.9668(3)$ Å

$b = 8.9668(3)$ Å

$c = 34.477(2)$ Å

$\alpha = 90^\circ$

$\beta = 90^\circ$

$\gamma = 90^\circ$

$V = 2772.1(2)$ Å³

$Z = 4$

$T = 120.0$ K

Radiation: $MoK\alpha$ ($\lambda = 0.71073$ Å)

$\mu(MoK\alpha) = 1.515$ mm⁻¹

$D_{calc} = 1.362$ g cm⁻³

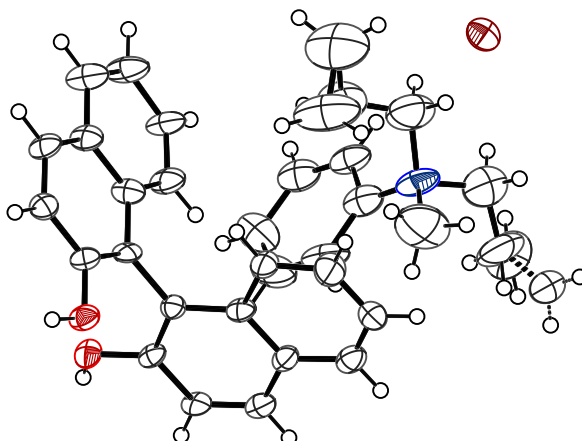
37334 reflections measured ($4.542 \leq 2\theta \leq 54.994^\circ$), 6359 unique ($R_{int} = 0.0679$,

$R_{sigma} = 0.0571$) which were used in all calculations.

The final $R1$ was 0.0625 ($I > 2\sigma(I)$) and $wR2$ was 0.1405 (all data)

Flack parameter = 0.092(6)

Crystal Structure: 226a



Crystal data for $C_{34}H_{34}BrNO_2$ ($m = 568.18$ g/mol);

Tetragonal, space group $P4_3$ (no. 81)

$a = 8.9823(5)$ Å

$b = 8.9823(5)$ Å

$c = 34.550(3)$ Å

$\alpha = 90^\circ$

$\beta = 90^\circ$

$\gamma = 90^\circ$

$V = 2787.5(4)$ Å³

$Z = 4$

$T = 120.00$ K

Radiation: $MoK\alpha$ ($\lambda = 0.71073$ Å)

$\mu(MoK\alpha) = 1.506$ mm⁻¹

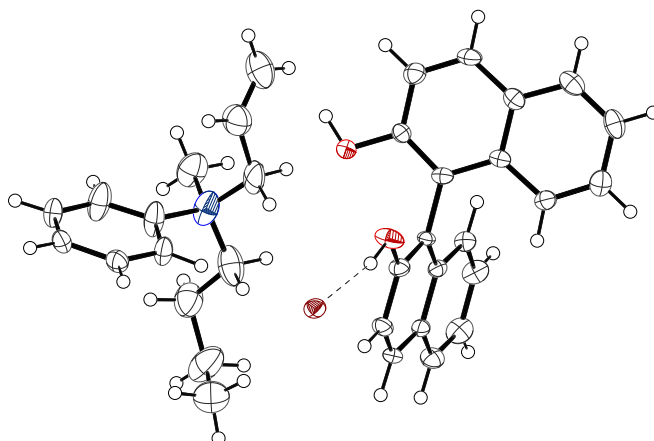
$D_{calc} = 1.354$ g cm⁻³

46860 reflections measured ($4.534 \leq 2\theta \leq 59.974^\circ$), 8120 unique ($R_{int} = 0.1702$, $R_{sigma} = 0.1823$) which were used in all calculations.

The final $R1$ was 0.0830 ($I > 2\sigma(I)$) and $wR2$ was 0.1622 (all data)

Flack parameter = 0.023(13)

Crystal Structure: 227



Crystal data for $C_{34}H_{36}BrNO_2$ ($m = 570.55$ g/mol);

Orthorhombic, space group $P2_12_12_1$ (no. 19)

$a = 10.2261(3)$ Å

$b = 11.1111(4)$ Å

$c = 25.8161(9)$ Å

$\alpha = 90^\circ$

$\beta = 90^\circ$

$\gamma = 90^\circ$

$V = 2933.31(17)$ Å³

$Z = 4$

$T = 120.0$ K

Radiation: MoK α ($\lambda = 0.71073$ Å)

$\mu(\text{MoK}\alpha) = 1.432$ mm⁻¹

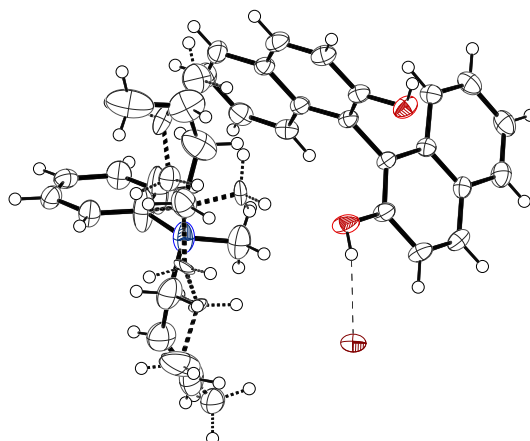
$D_{\text{calc}} = 1.292$ g cm⁻³

49896 reflections measured ($3.99 \leq 2\theta \leq 57.998^\circ$), 7794 unique ($R_{\text{int}} = 0.0668$, $R_{\text{sigma}} = 0.0515$) which were used in all calculations.

The final $R1$ was 0.0523 ($I > 2\sigma(I)$) and $wR2$ was 0.1197 (all data)

Flack parameter = 0.013(4)

Crystal Structure: 227a



Crystal data for $C_{34}H_{36}BrNO_2$ ($m = 570.55$ g/mol);

Orthorhombic, space group $P2_12_12_1$ (no. 19)

$a = 10.1936(4)$ Å

$b = 11.1597(4)$ Å

$c = 25.9277(10)$ Å

$\alpha = 90^\circ$

$\beta = 90^\circ$

$\gamma = 90^\circ$

$V = 2949.47(19)$ Å³

$Z = 4$

$T = 120.00$ K

Radiation: MoK α ($\lambda = 0.71073$ Å)

$\mu(\text{MoK}\alpha) = 1.424$ mm⁻¹

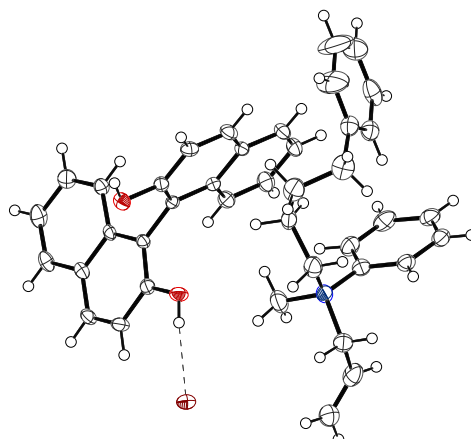
$D_{\text{calc}} = 1.285$ g cm⁻³

50892 reflections measured ($5.412 \leq 2\theta \leq 59.998^\circ$), 8602 unique ($R_{\text{int}} = 0.0463$, $R_{\text{sigma}} = 0.0383$) which were used in all calculations.

The final $R1$ was 0.0353 ($I > 2\sigma(I)$) and $wR2$ was 0.1026 (all data)

Flack parameter = 0.006(3)

Crystal Structure: 228



Crystal data for $C_{40}H_{40}BrNO_2$ ($m = 646.64$ g/mol);

Orthorhombic, space group $P2_12_12_1$ (no. 19)

$a = 10.3478(3)$ Å

$b = 10.9076(3)$ Å

$c = 28.9602(8)$ Å

$\alpha = 90^\circ$

$\beta = 90^\circ$

$\gamma = 90^\circ$

$V = 3268.73(16)$ Å³

$Z = 4$

$T = 120.00$ K

Radiation: MoK α ($\lambda = 0.71073$ Å)

$\mu(\text{MoK}\alpha) = 1.293$ mm⁻¹

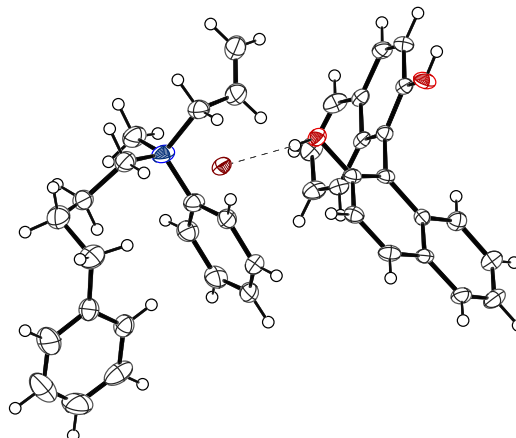
$D_{\text{calc}} = 1.314$ g cm⁻³

35555 reflections measured ($3.99 \leq 2\theta \leq 54.294^\circ$), 7224 unique ($R_{\text{int}} = 0.0458$, $R_{\text{sigma}} = 0.0524$) which were used in all calculations.

The final $R1$ was 0.0316 ($I > 2\sigma(I)$) and $wR2$ was 0.0600 (all data)

Flack parameter = 0.009(4)

Crystal Structure: 228a



Crystal data for $C_{40}H_{40}BrNO_2$ ($m = 646.64$ g/mol);

Orthorhombic, space group $P2_12_12_1$ (no. 19)

$a = 10.3602(8)$ Å

$b = 10.9010(8)$ Å

$c = 28.977(2)$ Å

$\alpha = 90^\circ$

$\beta = 90^\circ$

$\gamma = 90^\circ$

$V = 3272.6(4)$ Å³

$Z = 4$

$T = 120.00$ K

Radiation: MoK α ($\lambda = 0.71073$ Å)

$\mu(\text{MoK}\alpha) = 1.292$ mm⁻¹

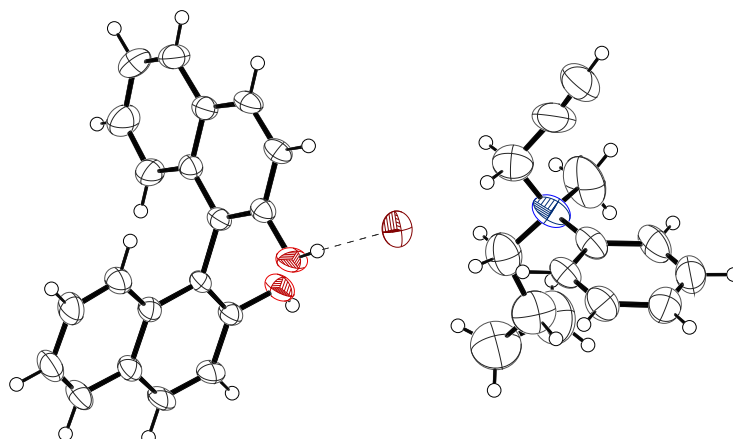
$D_{calc} = 1.312$ g cm⁻³

57132 reflections measured ($4.176 \leq 2\theta \leq 59.998^\circ$), 9545 unique ($R_{int} = 0.0728$, $R_{sigma} = 0.0643$) which were used in all calculations.

The final $R1$ was 0.0501 ($I > 2\sigma(I)$) and $wR2$ was 0.1299 (all data)

Flack parameter = 0.015(4)

Crystal Structure: 229



Crystal data for $C_{34}H_{32}BrNO_2$ ($m = 566.51$ g/mol);

Tetragonal, space group $P4_1$ (no. 76)

$a = 9.0094(2)$ Å

$b = 9.0094(2)$ Å

$c = 34.5061(13)$ Å

$\alpha = 90^\circ$

$\beta = 90^\circ$

$\gamma = 90^\circ$

$V = 2800.84(16)$ Å³

$Z = 4$

$T = 200.0$ K

Radiation: $MoK\alpha$ ($\lambda = 0.71073$ Å)

$\mu(MoK\alpha) = 1.499$ mm⁻¹

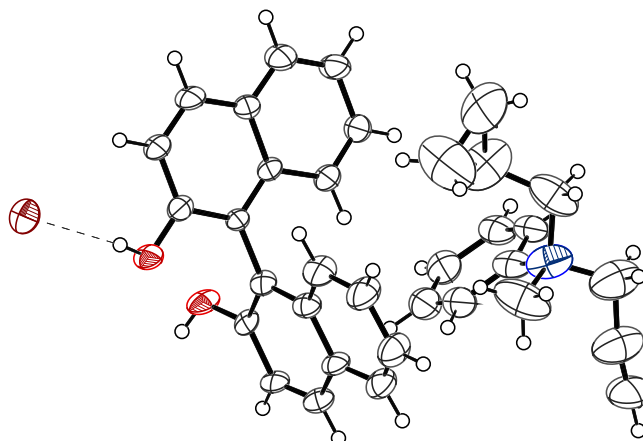
$D_{calc} = 1.343$ g cm⁻³

40539 reflections measured ($4.522 \leq 2\theta \leq 55.988^\circ$), 6736 unique ($R_{int} = 0.0628$, $R_{sigma} = 0.0494$) which were used in all calculations.

The final $R1$ was 0.0501 ($I > 2\sigma(I)$) and $wR2$ was 0.1138 (all data)

Flack parameter = 0.032(7)

Crystal Structure: 229a



Crystal data for $C_{34}H_{31} \cdot 7 BrNO_2$ ($m = 566.21$ g/mol);

Tetragonal, space group $P4_3$ (no. 81)

$a = 9.0006(8)$ Å

$b = 9.0006(8)$ Å

$c = 34.405(4)$ Å

$\alpha = 90^\circ$

$\beta = 90^\circ$

$\gamma = 90^\circ$

$V = 2787.2(6)$ Å³

$Z = 4$

$T = 120.00$ K

Radiation: $MoK\alpha$ ($\lambda = 0.71073$ Å)

$\mu(MoK\alpha) = 1.506$ mm⁻¹

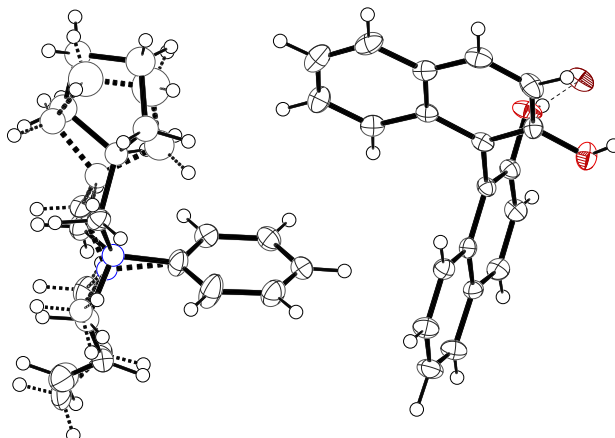
$D_{calc} = 1.349$ g cm⁻³

40647 reflections measured ($4.526 \leq 2\theta \leq 57.998^\circ$), 7421 unique ($R_{int} = 0.1245$, $R_{sigma} = 0.1189$) which were used in all calculations.

The final $R1$ was 0.0793 ($I > 2\sigma(I)$) and $wR2$ was 0.1833 (all data)

Flack parameter = 0.045(9)

Crystal Structure: 230



Crystal data for $C_{36}H_{38}BrNO_2$ ($m = 596.58$ g/mol);

Orthorhombic, space group $P2_12_12_1$ (no. 19)

$a = 10.2431(3)$ Å

$b = 11.4429(4)$ Å

$c = 25.8263(8)$ Å

$\alpha = 90^\circ$

$\beta = 90^\circ$

$\gamma = 90^\circ$

$V = 3027.12(17)$ Å³

$Z = 4$

$T = 120.0$ K

Radiation: MoK α ($\lambda = 0.71073$ Å)

$\mu(\text{MoK}\alpha) = 1.390$ mm⁻¹

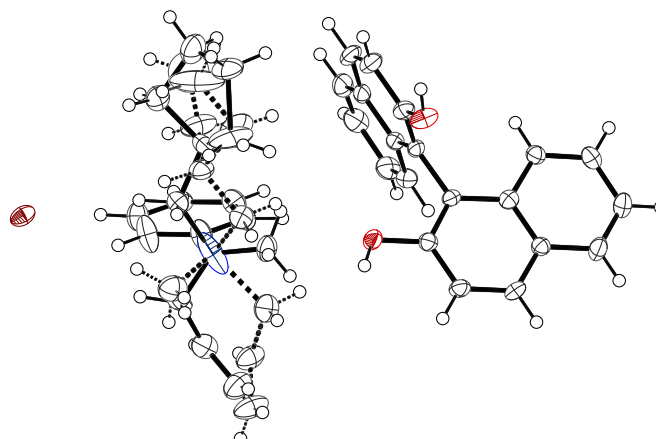
$D_{\text{calc}} = 1.309$ g cm⁻³

50726 reflections measured ($3.894 \leq 2\theta \leq 58.998^\circ$), 8419 unique ($R_{\text{int}} = 0.0832$, $R_{\text{sigma}} = 0.0573$) which were used in all calculations.

The final $R1$ was 0.0471 ($I > 2\sigma(I)$) and $wR2$ was 0.1164 (all data)

Flack parameter = 0.014(9)

Crystal Structure: 230a



Crystal data for $C_{36}H_{38}BrNO_2$ ($m = 596.58$ g/mol);

Orthorhombic, space group $P2_12_12_1$ (no. 19)

$a = 10.2573(6)$ Å

$b = 11.4415(7)$ Å

$c = 25.9264(16)$ Å

$\alpha = 90^\circ$

$\beta = 90^\circ$

$\gamma = 90^\circ$

$V = 3042.7(3)$ Å³

$Z = 4$

$T = 120.00$ K

Radiation: MoK α ($\lambda = 0.71073$ Å)

$\mu(\text{MoK}\alpha) = 1.383$ mm⁻¹

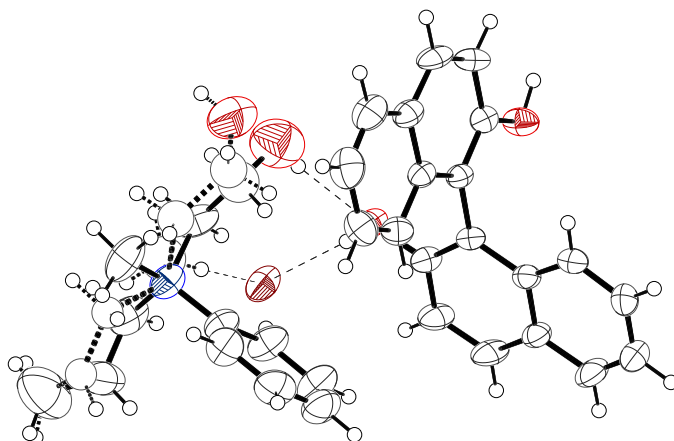
$D_{\text{calc}} = 1.302$ g cm⁻³

53028 reflections measured ($4.27 \leq 2\theta \leq 59.996^\circ$), 8875 unique ($R_{\text{int}} = 0.0675$, $R_{\text{sigma}} = 0.0591$) which were used in all calculations.

The final $R1$ was 0.0497 ($I > 2\sigma(I)$) and $wR2$ was 0.1256 (all data)

Flack parameter = 0.008(4)

Crystal Structure: 231



Crystal data for $C_{32}H_{32}BrNO_3$ ($m = 558.49$ g/mol);

Orthorhombic, space group $P2_12_12_1$ (no. 19)

$a = 10.4459(3)$ Å

$b = 11.0379(3)$ Å

$c = 24.1519(7)$ Å

$\alpha = 90^\circ$

$\beta = 90^\circ$

$\gamma = 90^\circ$

$V = 2784.73(14)$ Å³

$Z = 4$

$T = 250.0$ K

Radiation: MoK α ($\lambda = 0.71073$ Å)

$\mu(\text{MoK}\alpha) = 1.509$ mm⁻¹

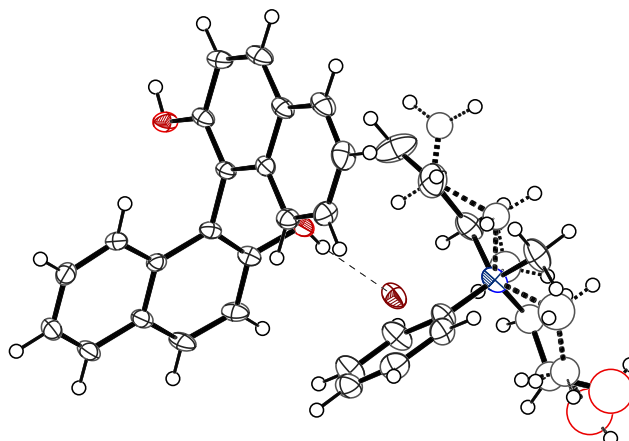
$D_{\text{calc}} = 1.332$ g cm⁻³

31969 reflections measured ($5.156 \leq 2\theta \leq 55.99^\circ$), 6628 unique ($R_{\text{int}} = 0.0529$, $R_{\text{sigma}} = 0.0573$) which were used in all calculations.

The final R_1 was 0.0448 ($I > 2\sigma(I)$) and wR_2 was 0.0826 (all data)

Flack parameter = $-0.011(4)$

Crystal Structure: 231a



Crystal data for $C_{32}H_{32}BrNO_3$ ($m = 558.49$ g/mol);

Orthorhombic, space group $P2_12_12_1$ (no. 19)

$a = 10.3908(7)$ Å

$b = 11.0388(8)$ Å

$c = 23.8811(17)$ Å

$\alpha = 90^\circ$

$\beta = 90^\circ$

$\gamma = 90^\circ$

$V = 2739.2(3)$ Å³

$Z = 4$

$T = 120.00$ K

Radiation: MoK α ($\lambda = 0.71073$ Å)

$\mu(\text{MoK}\alpha) = 1.534$ mm⁻¹

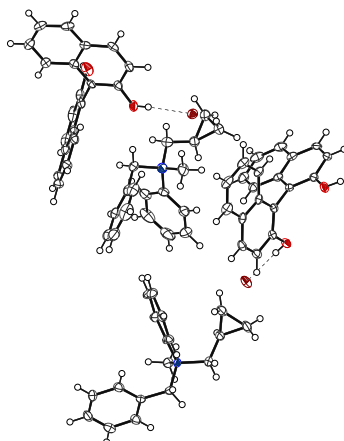
$D_{\text{calc}} = 1.354$ g cm⁻³

45377 reflections measured ($4.064 \leq 2\theta \leq 58.998^\circ$), 7632 unique ($R_{\text{int}} = 0.0765$, $R_{\text{sigma}} = 0.0573$) which were used in all calculations.

The final $R1$ was 0.0448 ($I > 2\sigma(I)$) and $wR2$ was 0.1062 (all data)

Flack parameter = 0.015(5)

Crystal Structure: 232



Crystal data for $C_{38}H_{36}BrNO_2$ ($m = 618.59$ g/mol);

Orthorhombic, space group $P2_12_12_1$ (no. 19)

$a = 10.2148(2)$ Å

$b = 14.4301(3)$ Å

$c = 41.2731(9)$ Å

$\alpha = 90^\circ$

$\beta = 90^\circ$

$\gamma = 90^\circ$

$V = 6083.7(2)$ Å³

$Z = 8$

$T = 120.0$ K

Radiation: MoK α ($\lambda = 0.71073$ Å)

$\mu(\text{MoK}\alpha) = 1.387$ mm⁻¹

$D_{calc} = 1.351$ g cm⁻³

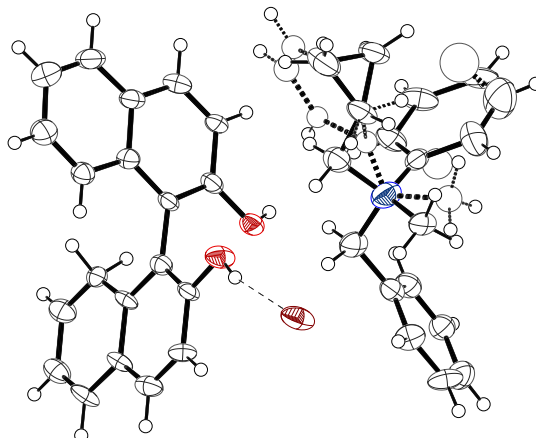
111397 reflections measured ($3.948 \leq 2\theta \leq 59.998^\circ$), 17725 unique ($R_{int} = 0.0759$,

$R_{sigma} = 0.0590$) which were used in all calculations.

The final $R1$ was 0.0450 ($I > 2\sigma(I)$) and $wR2$ was 0.0973 (all data)

Flack parameter = 0.012(3)

Crystal Structure: 232a



Crystal data for the compound (Formula weight = 618.59 g/mol);

Orthorhombic, space group $P2_12_12_1$ (no. 19)

$a = 10.3397(8) \text{ \AA}$

$b = 13.7328(11) \text{ \AA}$

$c = 21.6439(17) \text{ \AA}$

$\alpha = 90^\circ$

$\beta = 90^\circ$

$\gamma = 90^\circ$

$V = 3073.3(4) \text{ \AA}^3$

$Z = 4$

$T = 120.0 \text{ K}$

Radiation: $\text{MoK}\alpha$ ($\lambda = 0.71073 \text{ \AA}$)

$\mu(\text{MoK}\alpha) = 1.372 \text{ mm}^{-1}$

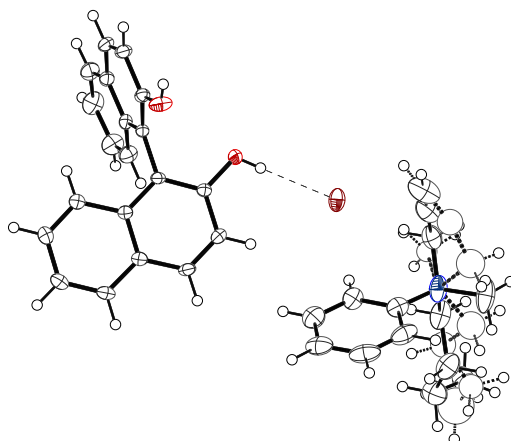
$D_{\text{calc}} = 1.337 \text{ g cm}^{-3}$

52505 reflections measured ($4.366 \leq 2\theta \leq 59.998^\circ$), 8963 unique ($R_{\text{int}} = 0.1501$, $R_{\text{sigma}} = 0.1409$) which were used in all calculations.

The final $R1$ was 0.0871 ($I > 2\sigma(I)$) and $wR2$ was 0.2030 (all data)

Flack parameter: 0.029(12)

Crystal Structure: 256



Crystal data for $C_{34}H_{34}BrNO_2$ ($m = 568.53$ g/mol);

Tetragonal space group $P4_1$ (no. 76)

$a = 8.98830(10)$ Å

$b = 8.98830(10)$ Å

$c = 34.7053(9)$ Å

$\alpha = 90^\circ$

$\beta = 90^\circ$

$\gamma = 90^\circ$

$V = 2803.83(10)$ Å³

$Z = 4$

$T = 120.0$ K

Radiation: $MoK\alpha$ ($\lambda = 0.71073$ Å)

$\mu(MoK\alpha) = 1.497$ mm⁻¹

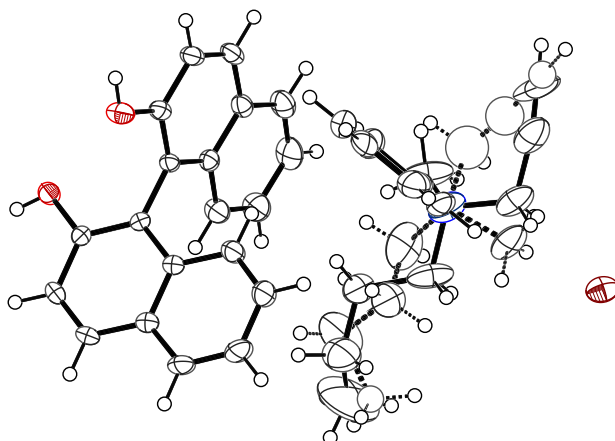
$D_{calc} = 1.347$ g cm⁻³

44287 reflections measured ($4.532^\circ \leq 2\theta \leq 57.99^\circ$), 7451 unique ($R_{int} = 0.0499$, $R_{sigma} = 0.0345$) which were used in all calculations.

The final $R1$ was 0.0404 ($I > 2\sigma(I)$) and $wR2$ was 0.0863 (all data)

Flack parameter = 0.003(4)

Crystal Structure: 256a



Crystal data for $C_{34}H_{34}BrNO_2$ ($m = 568.53$ g/mol);

Tetragonal, space group $P4_3$ (no. 81)

$a = 9.0056(3)$ Å

$b = 9.0056(3)$ Å

$c = 34.7700(18)$ Å

$\alpha = 90^\circ$

$\beta = 90^\circ$

$\gamma = 90^\circ$

$V = 2819.9(2)$ Å³

$Z = 4$

$T = 120.00$ K

Radiation: $MoK\alpha$ ($\lambda = 0.71073$ Å)

$\mu(MoK\alpha) = 1.489$ mm⁻¹

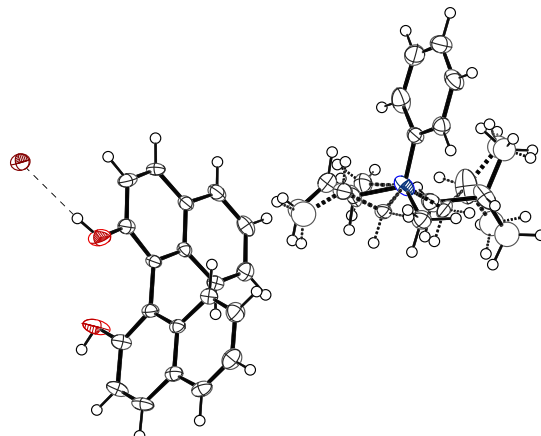
$D_{calc} = 1.339$ g cm⁻³

49071 reflections measured ($4.524 \leq 2\theta \leq 59.986^\circ$), 8229 unique ($R_{int} = 0.0474$, $R_{sigma} = 0.0430$) which were used in all calculations.

The final $R1$ was 0.0438 ($I > 2\sigma(I)$) and $wR2$ was 0.1149 (all data)

Flack parameter = 0.002(3)

Crystal Structure: 249



Crystal data for $C_{34}H_{36}BrNO_2$ ($m = 570.55$ g/mol);

Tetragonal, space group $P4_3$ (no. 81)

$a = 9.1832(3)$ Å

$b = 9.1832(3)$ Å

$c = 33.8322(15)$ Å

$\alpha = 90^\circ$

$\beta = 90^\circ$

$\gamma = 90^\circ$

$V = 2853.1(2)$ Å³

$Z = 4$

$T = 273.15$ K

Radiation: $MoK\alpha$ ($\lambda = 0.71073$ Å)

$\mu(MoK\alpha) = 1.472$ mm⁻¹

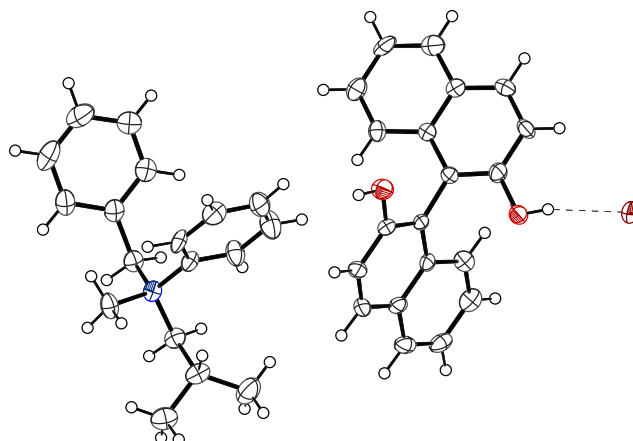
$D_{calc} = 1.328$ g cm⁻³

49545 reflections measured ($4.436 \leq 2\theta \leq 59.988^\circ$), 8296 unique ($R_{int} = 0.0608$, $R_{sigma} = 0.0705$) which were used in all calculations.

The final $R1$ was 0.0587 ($I > 2\sigma(I)$) and $wR2$ was 0.1379 (all data)

Flack parameter = 0.023(5)

Crystal Structure: 248



Crystal data for $C_{38}H_{38}BrNO_2$ ($m = 620.60$ g/mol);

Orthorhombic, space group $P2_12_12_1$ (no. 19)

$a = 9.469(2)$ Å

$b = 16.571(3)$ Å

$c = 20.670(4)$ Å

$\alpha = 90^\circ$

$\beta = 90^\circ$

$\gamma = 90^\circ$

$V = 3243.2(12)$ Å³

$Z = 4$

$T = 120.0$ K

Radiation: Mo $K\alpha$ ($\lambda = 0.71073$ Å)

$\mu(\text{Mo } K\alpha) = 1.301$ mm⁻¹

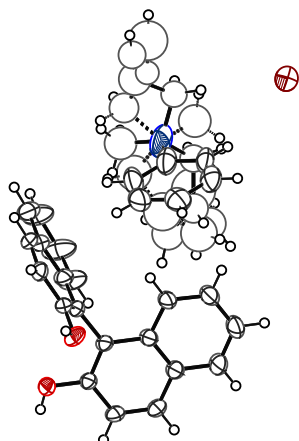
$D_{calc} = 1.271$ g cm⁻³

52041 reflections measured ($4.732 \leq 2\theta \leq 50.998^\circ$), 6028 unique ($R_{int} = 0.1575$, $R_{sigma} = 0.1104$) which were used in all calculations.

The final $R1$ was 0.0559 ($I > 2\sigma(I)$) and $wR2$ was 0.0804 (all data)

Flack parameter = 0.006(9)

Crystal Structure: 254



Crystal data for $C_{34}H_{32}BrNO_2$ ($m = 566.51$ g/mol);

Tetragonal, space group $P4_3$ (no. 81)

$a = 9.0065(2)$ Å

$b = 9.0065(2)$ Å

$c = 34.3741(10)$ Å

$\alpha = 90^\circ$

$\beta = 90^\circ$

$\gamma = 90^\circ$

$V = 2788.32(15)$ Å³

$Z = 4$

$T = 120.00$ K

Radiation: $MoK\alpha$ ($\lambda = 0.71073$ Å)

$\mu(MoK\alpha) = 1.506$ mm⁻¹

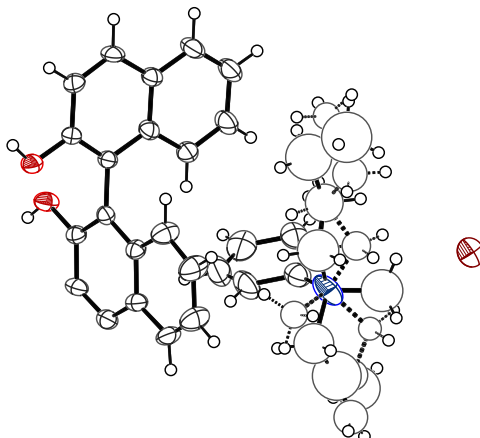
$D_{calc} = 1.350$ g cm⁻³

47966 reflections measured ($4.522 \leq 2\theta \leq 59.992^\circ$), 8129 unique ($R_{int} = 0.0715$, $R_{sigma} = 0.0669$) which were used in all calculations.

The final $R1$ was 0.0533 ($I > 2\sigma(I)$) and $wR2$ was 0.1219 (all data)

Flack parameter = 0.037(6)

Crystal Structure: 253



Crystal data for $C_{34}H_{36}BrNO_2$ ($m = 570.55$ g/mol);

Tetragonal, space group $P4_3$ (no. 81)

$a = 9.0988(3)$ Å

$b = 9.0988(3)$ Å

$c = 34.1899(18)$ Å

$\alpha = 90^\circ$

$\beta = 90^\circ$

$\gamma = 90^\circ$

$V = 2830.5(2)$ Å³

$Z = 4$

$T = 120.00$ K

Radiation: $MoK\alpha$ ($\lambda = 0.71073$ Å)

$\mu(MoK\alpha) = 1.484$ mm⁻¹

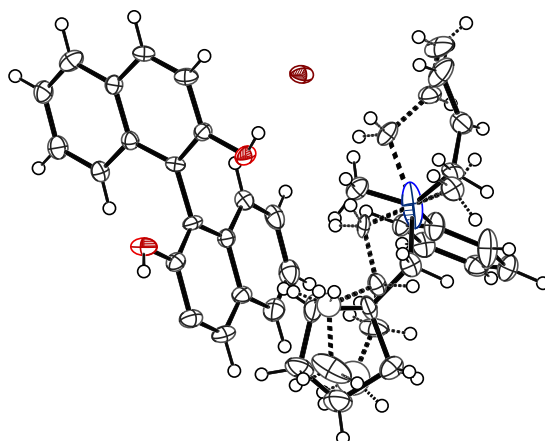
$D_{calc} = 1.339$ g cm⁻³

49063 reflections measured ($4.476 \leq 2\theta \leq 59.996^\circ$), 8239 unique ($R_{int} = 0.0588$, $R_{sigma} = 0.0609$) which were used in all calculations.

The final $R1$ was 0.0527 ($I > 2\sigma(I)$) and $wR2$ was 0.1258 (all data)

Flack parameter = 0.030(6)

Crystal Structure: 255



Crystal data for $C_{36}H_{37}BrNO_2$ ($m = 595.57$ g/mol);

Orthorhombic, space group $P2_12_12_1$ (no. 19)

$a = 11.4490(5)$ Å

$b = 25.8732(10)$ Å

$c = 10.2632(4)$ Å

$\alpha = 90^\circ$

$\beta = 90^\circ$

$\gamma = 90^\circ$

$V = 3040.2(2)$ Å³

$Z = 4$

$T = 120.00$ K

Radiation: MoK α ($\lambda = 0.71073$ Å)

$\mu(\text{MoK}\alpha) = 1.384$ mm⁻¹

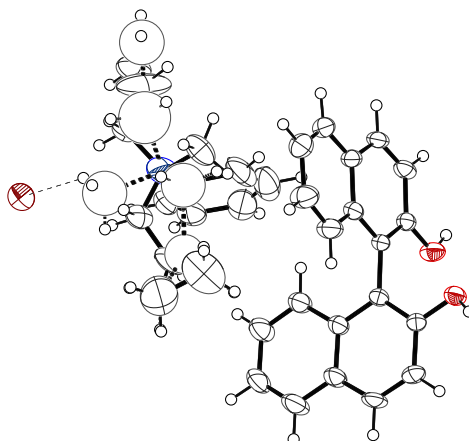
$D_{\text{calc}} = 1.301$ g cm⁻³

37068 reflections measured ($3.89 \leq 2\theta \leq 60^\circ$), 8851 unique ($R_{\text{int}} = 0.0946$, $R_{\text{sigma}} = 0.0875$) which were used in all calculations.

The final R_1 was 0.0592 ($I > 2\sigma(I)$) and wR_2 was 0.1672 (all data)

Flack parameter = 0.022(12)

Crystal Structure: 252



Crystal data for $C_{34}H_{34}BrNO_2$ ($m = 568.53$ g/mol);

Tetragonal, space group $P4_3$ (no. 81)

$a = 9.0070(2)$ Å

$b = 9.0070(2)$ Å

$c = 34.5344(14)$ Å

$\alpha = 90^\circ$

$\beta = 90^\circ$

$\gamma = 90^\circ$

$V = 2801.64(17)$ Å³

$Z = 4$

$T = 120.00$ K

Radiation: $MoK\alpha$ ($\lambda = 0.71073$ Å)

$\mu(MoK\alpha) = 1.499$ mm⁻¹

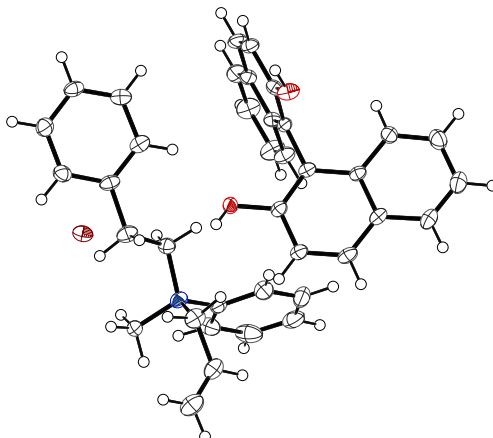
$D_{calc} = 1.348$ g cm⁻³

71404 reflections measured ($4.522 \leq 2\theta \leq 63.216^\circ$), 9379 unique ($R_{int} = 0.0837$, $R_{sigma} = 0.0676$) which were used in all calculations.

The final $R1$ was 0.0589 ($I > 2\sigma(I)$) and $wR2$ was 0.1474 (all data)

Flack parameter = 0.058(4)

Crystal Structure: 241



Crystal data for $C_{38}H_{36}BrNO_2$ ($m = 618.59$ g/mol);

Orthorhombic, space group $P2_12_12_1$ (no. 19)

$a = 10.3172(3)$ Å

$b = 12.2868(3)$ Å

$c = 24.1826(6)$ Å

$\alpha = 90^\circ$

$\beta = 90^\circ$

$\gamma = 90^\circ$

$V = 3065.52(14)$ Å³

$Z = 4$

$T = 120.00$ K

Radiation: MoK α ($\lambda = 0.71073$ Å)

$\mu(\text{MoK}\alpha) = 1.376$ mm⁻¹

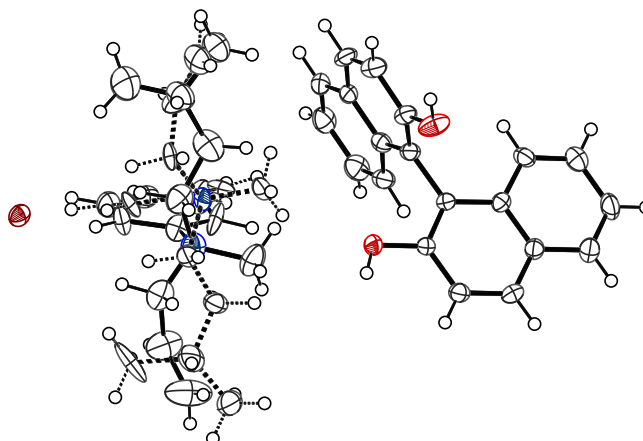
$D_{calc} = 1.340$ g cm⁻³

40036 reflections measured ($3.718 \leq 2\theta \leq 59.998^\circ$), 8922 unique ($R_{int} = 0.0486$, $R_{sigma} = 0.0504$) which were used in all calculations.

The final $R1$ was 0.0435 ($I > 2\sigma(I)$) and $wR2$ was 0.1194 (all data)

Flack parameter = 0.003(3)

Crystal Structure: 395



Crystal data for $C_{35}H_{38}BrNO_2$ ($m = 584.57$ g/mol);

Orthorhombic, space group $P2_12_12_1$ (no. 19)

$a = 10.0977(6)$ Å

$b = 11.5983(7)$ Å

$c = 25.8713(16)$ Å

$\alpha = 90^\circ$

$\beta = 90^\circ$

$\gamma = 90^\circ$

$V = 3029.9(3)$ Å³

$Z = 4$

$T = 120.00$ K

Radiation: MoK α ($\lambda = 0.71073$ Å)

$\mu(\text{MoK}\alpha) = 1.388$ mm⁻¹

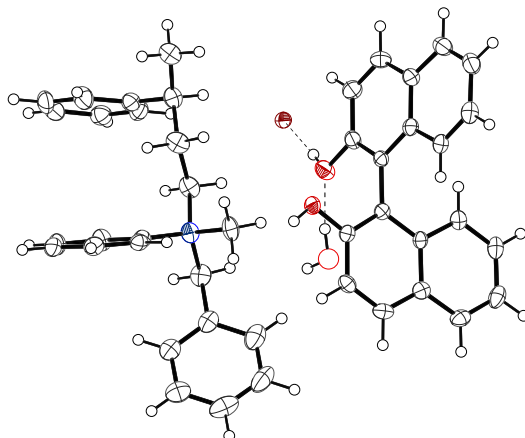
$D_{calc} = 1.281$ g cm⁻³

52898 reflections measured ($4.33 \leq 2\theta \leq 60^\circ$), 8831 unique ($R_{int} = 0.1000$, $R_{sigma} = 0.0933$) which were used in all calculations.

The final $R1$ was 0.0613 ($I > 2\sigma(I)$) and $wR2$ was 0.1374 (all data)

Flack parameter = 0.022(5)

Crystal Structure: 396



Crystal data for $C_{44}H_{42} \cdot 5 BrNO_2 \cdot 25$ ($m = 701.20$ g/mol);

Orthorhombic, space group $P2_12_12_1$ (no. 19)

$a = 11.9008(3)$ Å

$b = 12.6816(3)$ Å

$c = 23.7967(6)$ Å

$\alpha = 90^\circ$

$\beta = 90^\circ$

$\gamma = 90^\circ$

$V = 3591.43(15)$ Å³

$Z = 4$

$T = 120.0$ K

Radiation: MoK α ($\lambda = 0.71073$ Å)

$\mu(\text{MoK}\alpha) = 1.183$ mm⁻¹

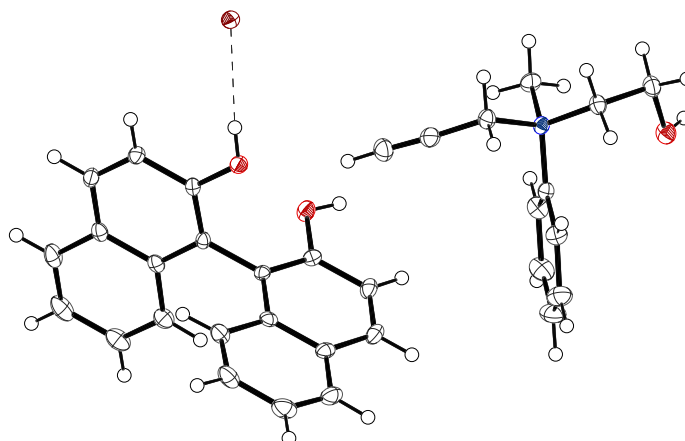
$D_{calc} = 1.297$ g cm⁻³

61973 reflections measured ($4.694 \leq 2\theta \leq 57.996^\circ$), 9536 unique ($R_{int} = 0.0573$, $R_{sigma} = 0.0413$) which were used in all calculations.

The final $R1$ was 0.0323 ($I > 2\sigma(I)$) and $wR2$ was 0.0629 (all data)

Flack parameter = 0.002(3)

Crystal Structure: 383



Crystal data for $C_{32}H_{30}BrNO_3$ ($m = 556.48$ g/mol);

Monoclinic, space group $P2_1$ (no. 4)

$a = 9.6625(2)$ Å

$b = 11.5365(3)$ Å

$c = 12.2338(3)$ Å

$\alpha = 90^\circ$

$\beta = 104.4640(10)^\circ$

$\gamma = 90^\circ$

$V = 1320.50(5)$ Å³

$Z = 2$

$T = 120.0$ K

Radiation: MoK α ($\lambda = 0.71073$ Å)

$\mu(\text{MoK}\alpha) = 1.591$ mm⁻¹

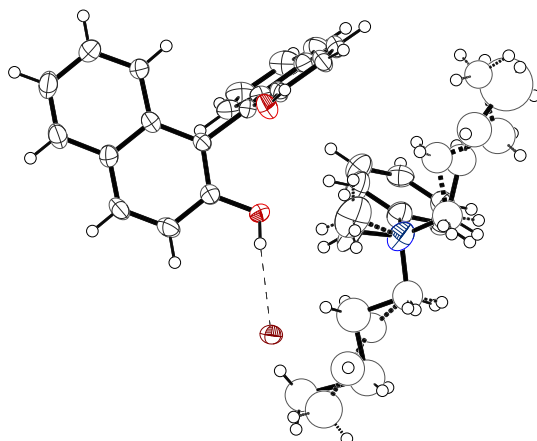
$D_{\text{calc}} = 1.400$ g cm⁻³

22593 reflections measured ($4.354 \leq 2\theta \leq 59.98^\circ$), 7646 unique ($R_{\text{int}} = 0.0243$, $R_{\text{sigma}} = 0.0281$) which were used in all calculations.

The final $R1$ was 0.0215 ($I > 2\sigma(I)$) and $wR2$ was 0.0487 (all data)

Flack parameter = -0.007(2)

Crystal Structure: 397



Crystal data for $C_{35}H_{38}BrNO_2$ ($m = 584.57$ g/mol);

Orthorhombic, space group $P2_12_12_1$ (no. 19)

$a = 10.3197(4)$ Å

$b = 11.2995(4)$ Å

$c = 26.2296(9)$ Å

$\alpha = 90^\circ$

$\beta = 90^\circ$

$\gamma = 90^\circ$

$V = 3058.57(19)$ Å³

$Z = 4$

$T = 120.0$ K

Radiation: MoK α ($\lambda = 0.71073$ Å)

$\mu(\text{MoK}\alpha) = 1.375$ mm⁻¹

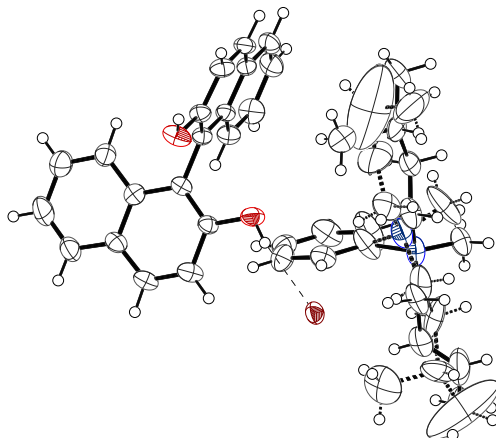
$D_{calc} = 1.269$ g cm⁻³

39777 reflections measured ($3.924 \leq 2\theta \leq 60^\circ$), 8913 unique ($R_{int} = 0.0735$, $R_{sigma} = 0.0823$) which were used in all calculations.

The final $R1$ was 0.0514 ($I > 2\sigma(I)$) and $wR2$ was 0.1120 (all data)

Flack parameter = 0.002(5)

Crystal Structure: 398



Crystal data for $C_{36}H_{40}BrNO_2$ ($m = 598.60$ g/mol);

Orthorhombic, space group $P2_12_12_1$ (no. 19)

$a = 10.1537(4)$ Å

$b = 11.8411(5)$ Å

$c = 26.0803(10)$ Å

$\alpha = 90^\circ$

$\beta = 90^\circ$

$\gamma = 90^\circ$

$V = 3135.7(2)$ Å³

$Z = 4$

$T = 120.0$ K

Radiation: MoK α ($\lambda = 0.71073$ Å)

$\mu(\text{MoK}\alpha) = 1.342$ mm⁻¹

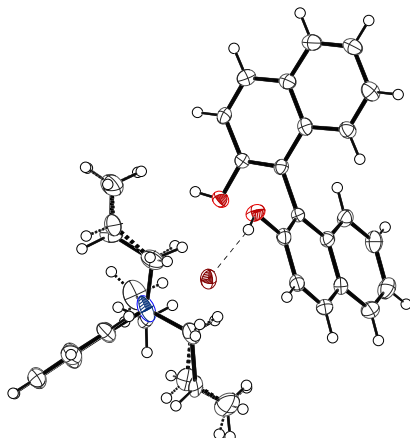
$D_{\text{calc}} = 1.268$ g cm⁻³

39774 reflections measured ($3.778 \leq 2\theta \leq 59.996^\circ$), 9144 unique ($R_{\text{int}} = 0.0804$, $R_{\text{sigma}} = 0.0827$) which were used in all calculations.

The final $R1$ was 0.0509 ($I > 2\sigma(I)$) and $wR2$ was 0.1254 (all data)

Flack parameter = $-0.002(8)$

Crystal Structure: 399



Crystal data for $C_{33}H_{34}BrNO_2$ ($m = 556.52$ g/mol);

Orthorhombic, space group $P2_12_12_1$ (no. 19)

$a = 10.6151(5)$ Å

$b = 11.0827(5)$ Å

$c = 23.7986(11)$ Å

$\alpha = 90^\circ$

$\beta = 90^\circ$

$\gamma = 90^\circ$

$V = 2799.8(2)$ Å³

$Z = 4$

$T = 120.0$ K

Radiation: MoK α ($\lambda = 0.71073$ Å)

$\mu(\text{MoK}\alpha) = 1.498$ mm⁻¹

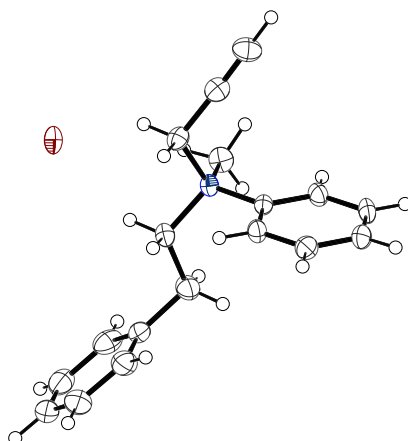
$D_{\text{calc}} = 1.320$ g cm⁻³

36349 reflections measured ($4.054 \leq 2\theta \leq 59.986^\circ$), 8148 unique ($R_{\text{int}} = 0.0814$, $R_{\text{sigma}} = 0.0928$) which were used in all calculations.

The final R_1 was 0.0552 ($I > 2\sigma(I)$) and wR_2 was 0.1256 (all data)

Flack parameter = 0.012(5)

Crystal Structure: 400



Crystal data for $C_{18}H_{20}BrN \cdot 0.25(H_2O)$ ($m = 330.26$ g/mol);

Orthorhombic, space group $Pbcn$ (no. 60)

$a = 13.3180(4)$ Å

$b = 12.3219(3)$ Å

$c = 20.5297(6)$ Å

$\alpha = 90^\circ$

$\beta = 90^\circ$

$\gamma = 90^\circ$

$V = 3368.99(16)$ Å³

$Z = 8$

$T = 120.0$ K

Radiation: $MoK\alpha$ ($\lambda = 0.71073$ Å)

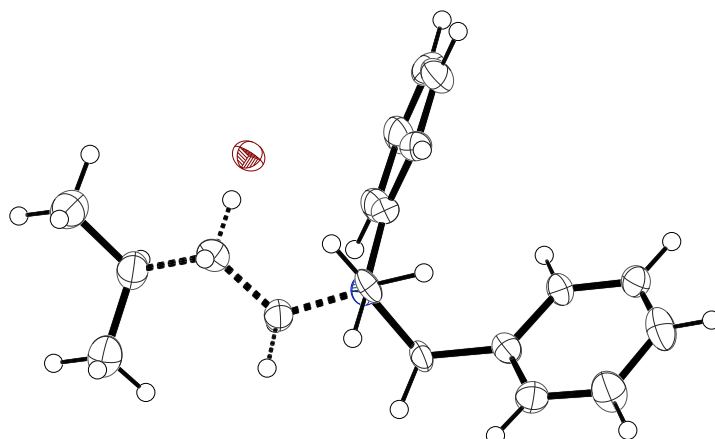
$\mu(MoK\alpha) = 2.431$ mm⁻¹

$D_{calc} = 1.302$ g cm⁻³

53941 reflections measured ($3.968 \leq 2\theta \leq 57.996^\circ$), 4476 unique ($R_{int} = 0.0441$, $R_{sigma} = 0.0216$) which were used in all calculations.

The final $R1$ was 0.0340 ($I > 2\sigma(I)$) and $wR2$ was 0.0762 (all data)

Crystal Structure: 262a



Crystal data for $C_{19}H_{26}BrN$ ($m = 348.32$ g/mol);

Monoclinic, space group $P2_1$ (no. 4)

$a = 10.3280(7)$ Å

$b = 8.7369(6)$ Å

$c = 10.5031(7)$ Å

$\alpha = 90^\circ$

$\beta = 110.545(3)^\circ$

$\gamma = 90^\circ$

$V = 887.46(11)$ Å³

$Z = 2$

$T = 120.0$ K

Radiation: MoK α ($\lambda = 0.71073$ Å)

$\mu(\text{MoK}\alpha) = 2.311$ mm⁻¹

$D_{calc} = 1.303$ g cm⁻³

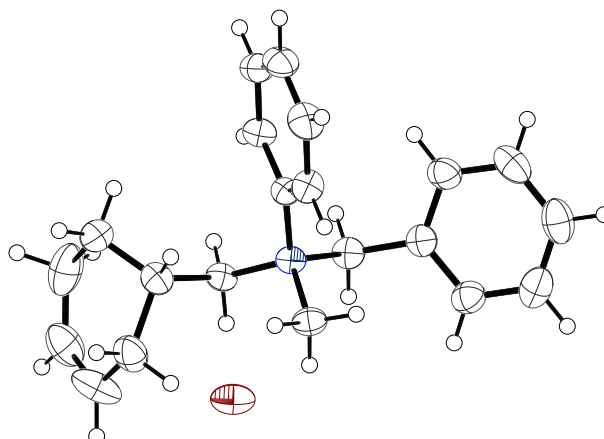
14055 reflections measured ($4.142 \leq 2\theta \leq 55.984^\circ$), 4252 unique ($R_{int} = 0.0559$, $R_{sigma} = 0.0697$) which were used in all calculations.

The final $R1$ was 0.0571 ($I > 2\sigma(I)$) and $wR2$ was 0.1379 (all data)

Largest diff. peak/hole / e Å⁻³ 1.41/-0.82

Flack parameter = 0.133(8)

Crystal Structure: 200



Crystal data for $C_{21}H_{26}BrN$ ($m = 372.34$ g/mol);

Monoclinic, space group $P2_1/n$ (no. 14)

$a = 10.7185(3)$ Å

$b = 9.0405(2)$ Å

$c = 18.9692(5)$ Å

$\alpha = 90^\circ$

$\beta = 98.1738(11)^\circ$

$\gamma = 90^\circ$

$V = 1819.45(8)$ Å³

$Z = 4$

$T = 250.0$ K

Radiation: $MoK\alpha$ ($\lambda = 0.71073$ Å)

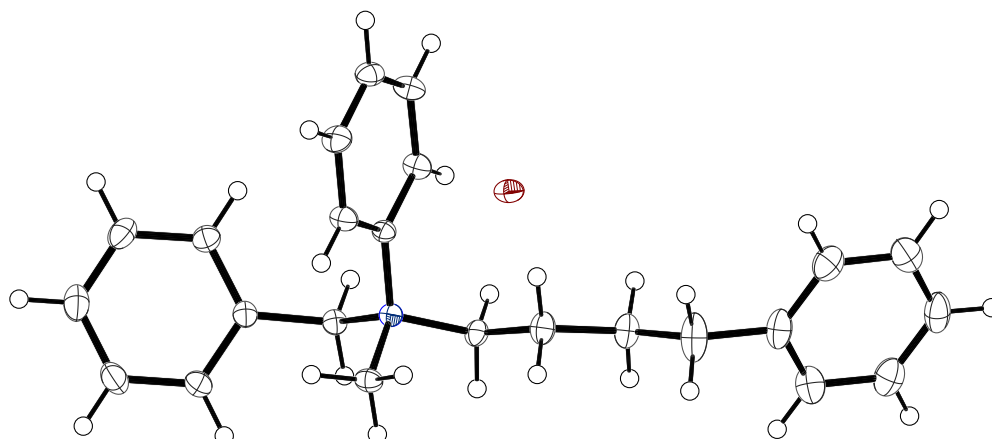
$\mu(MoK\alpha) = 2.259$ mm⁻¹

$D_{calc} = 1.359$ g cm⁻³

25210 reflections measured ($4.132 \leq 2\theta \leq 53.998^\circ$), 3961 unique ($R_{int} = 0.0404$, $R_{sigma} = 0.0298$) which were used in all calculations.

The final $R1$ was 0.0312 ($I > 2\sigma(I)$) and $wR2$ was 0.0667 (all data)

Crystal Structure: 401



Crystal data for $C_{24}H_{28}BrN$ ($m = 410.38$ g/mol);

Monoclinic, space group $P2_1/c$ (no. 14)

$a = 8.7620(3)$ Å

$b = 20.9560(7)$ Å

$c = 11.6675(4)$ Å

$\alpha = 90^\circ$

$\beta = 103.5030(10)^\circ$

$\gamma = 90^\circ$

$V = 2083.13(12)$ Å³

$Z = 4$

$T = 120.0$ K

Radiation: MoK α ($\lambda = 0.71073$ Å)

$\mu(\text{MoK}\alpha) = 1.980$ mm⁻¹

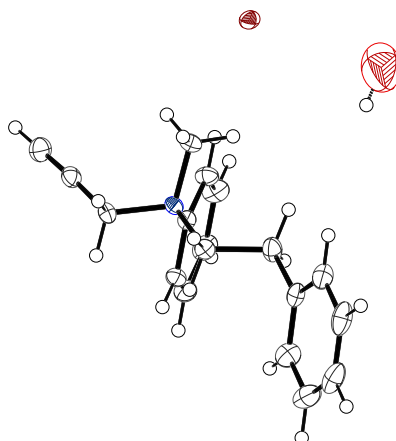
$D_{\text{calc}} = 1.309$ g cm⁻³

37667 reflections measured ($4.082 \leq 2\theta \leq 59.998^\circ$), 6067 unique ($R_{\text{int}} = 0.0466$,

$R_{\text{sigma}} = 0.0338$) which were used in all calculations.

The final $R1$ was 0.0313 ($I > 2\sigma(I)$) and $wR2$ was 0.0730 (all data)

Crystal Structure: 400



Crystal data for $C_{18}H_{20}BrN \cdot 0.5(H_2O)$ ($m = 339.27$ g/mol);

Orthorhombic, space group $Pbcn$ (no. 60)

$a = 13.3166(8)$ Å

$b = 12.3333(7)$ Å

$c = 20.5678(12)$ Å

$\alpha = 90^\circ$

$\beta = 90^\circ$

$\gamma = 90^\circ$

$V = 3378.0(3)$ Å³

$Z = 8$

$T = 120.0$ K

Radiation: $MoK\alpha$ ($\lambda = 0.71073$ Å)

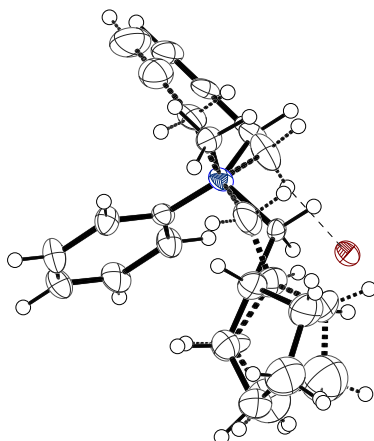
$\mu(MoK\alpha) = 2.429$ mm⁻¹

$D_{calc} = 1.334$ g cm⁻³

53476 reflections measured ($3.96 \leq 2\theta \leq 58.998^\circ$), 4701 unique ($R_{int} = 0.0442$, $R_{sigma} = 0.0243$) which were used in all calculations.

The final $R1$ was 0.0286 ($I > 2\sigma(I)$) and $wR2$ was 0.0653 (all data)

Crystal Structure: 201



Crystal data for $C_{16}H_{22}BrN$ ($m = 308.25$ g/mol);

Monoclinic, space group $C2/c$ (no. 15)

$a = 14.9074(5)$ Å

$b = 9.3034(3)$ Å

$c = 22.8105(8)$ Å

$\alpha = 90^\circ$

$\beta = 93.8000(10)^\circ$

$\gamma = 90^\circ$

$V = 3156.62(18)$ Å³

$Z = 8$

$T = 120.0$ K

Radiation: $MoK\alpha$ ($\lambda = 0.71073$ Å)

$\mu(MoK\alpha) = 2.589$ mm⁻¹

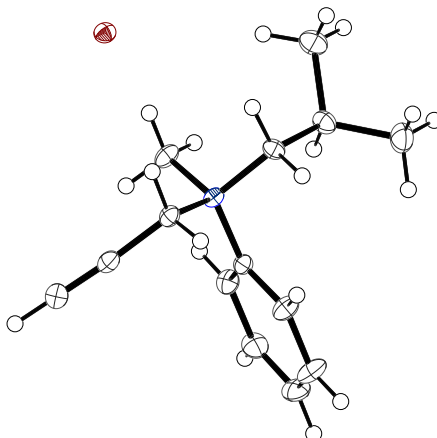
$D_{calc} = 1.297$ g cm⁻³

24568 reflections measured ($5.406 \leq 2\theta \leq 57.958^\circ$), 4158 unique ($R_{int} = 0.0385$,

$R_{sigma} = 0.0301$) which were used in all calculations.

The final $R1$ was 0.0419 ($I > 2\sigma(I)$) and $wR2$ was 0.0831 (all data)

Crystal Structure: 204



Crystal data for $C_{14}H_{20}BrN$ ($m = 282.22$ g/mol);

Orthorhombic, space group $Pna2_1$ (no. 33)

$a = 12.0935(12)$ Å

$b = 14.4582(15)$ Å

$c = 8.0596(8)$ Å

$\alpha = 90^\circ$

$\beta = 90^\circ$

$\gamma = 90^\circ$

$V = 1409.2(2)$ Å³

$Z = 4$

$T = 120.0$ K

Radiation: $MoK\alpha$ ($\lambda = 0.71073$ Å)

$\mu(MoK\alpha) = 2.893$ mm⁻¹

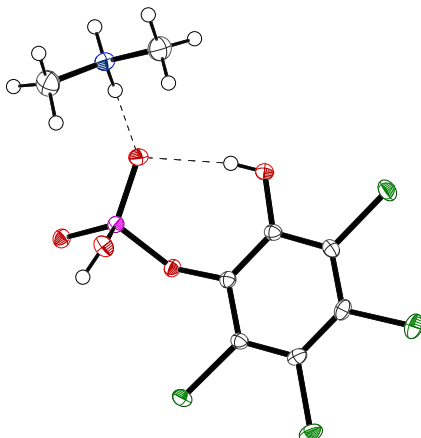
$D_{calc} = 1.330$ g cm⁻³

23292 reflections measured ($5.636 \leq 2\theta \leq 59.996^\circ$), 4102 unique ($R_{int} = 0.0325$, $R_{sigma} = 0.0250$) which were used in all calculations.

The final $R1$ was 0.0198 ($I > 2\sigma(I)$) and $wR2$ was 0.0401 (all data)

Flack parameter = 0.014(3)

Crystal Structure: 239



Crystal data for $C_8H_{10}Cl_4NO_5P$ ($m = 372.94$ g/mol);

Triclinic, space group $P\bar{1}$ (no. 2)

$a = 8.4480(7)$ Å

$b = 8.4973(7)$ Å

$c = 11.6538(10)$ Å

$\alpha = 73.687(3)^\circ$

$\beta = 89.732(3)^\circ$

$\gamma = 60.437(3)^\circ$

$V = 689.32(10)$ Å³

$Z = 2$

$T = 120.0$ K

Radiation: MoK α ($\lambda = 0.71073$ Å)

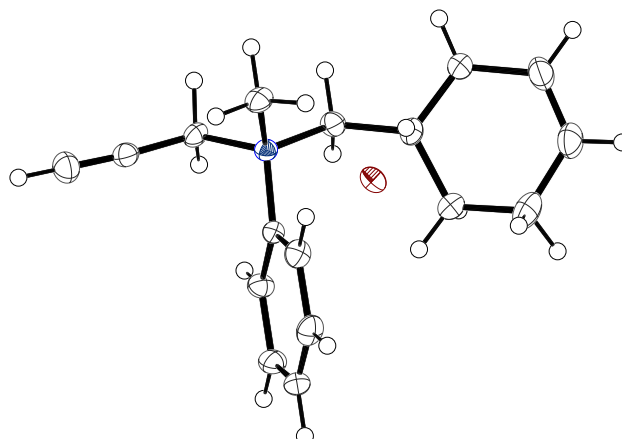
$\mu(\text{MoK}\alpha) = 0.987$ mm⁻¹

$D_{calc} = 1.797$ g cm⁻³

11686 reflections measured ($5.616 \leq 2\theta \leq 59.99^\circ$), 3974 unique ($R_{int} = 0.0363$, $R_{sigma} = 0.0386$) which were used in all calculations.

The final $R1$ was 0.0257 ($I > 2\sigma(I)$) and $wR2$ was 0.0656 (all data)

Crystal Structure: 214b



Crystal data for $C_{17}H_{22}BrN$ ($m = 320.26$ g/mol);

Orthorhombic, space group $P2_12_12_1$ (no. 19)

$a = 9.7091(7)$ Å

$b = 11.6808(9)$ Å

$c = 13.5862(10)$ Å

$\alpha = 90^\circ$

$\beta = 90^\circ$

$\gamma = 90^\circ$

$V = 1540.8(2)$ Å³

$Z = 4$

$T = 120.0$ K

Radiation: MoK α ($\lambda = 0.71073$ Å)

$\mu(\text{MoK}\alpha) = 2.655$ mm⁻¹

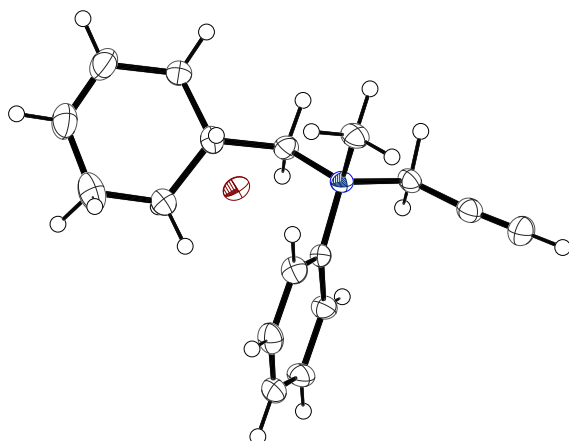
$D_{\text{calc}} = 1.381$ g cm⁻³

26605 reflections measured ($4.598 \leq 2\theta \leq 59.99^\circ$), 4498 unique ($R_{\text{int}} = 0.0488$, $R_{\text{sigma}} = 0.0383$) which were used in all calculations.

The final $R1$ was 0.0263 ($I > 2\sigma(I)$) and $wR2$ was 0.0561 (all data)

Flack parameter = $-0.010(4)$

Crystal Structure: 214a



Crystal data for $C_{17}H_{22}BrN$ ($m = 320.26$ g/mol);

Orthorhombic, space group $P2_12_12_1$ (no. 19)

$a = 9.6595(3)$ Å

$b = 11.6778(4)$ Å

$c = 13.6995(5)$ Å

$\alpha = 90^\circ$

$\beta = 90^\circ$

$\gamma = 90^\circ$

$V = 1545.33(9)$ Å³

$Z = 4$

$T = 120.0$ K

Radiation: MoK α ($\lambda = 0.71073$ Å)

$\mu(\text{MoK}\alpha) = 2.648$ mm⁻¹

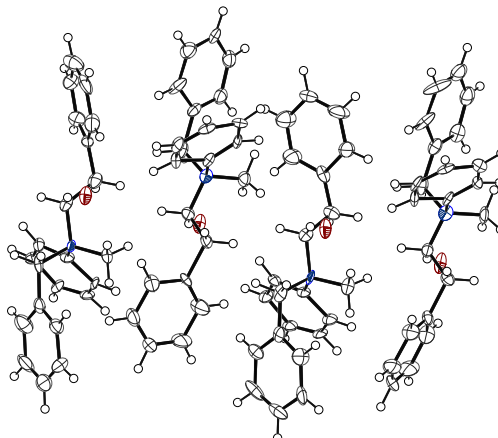
$D_{\text{calc}} = 1.377$ g cm⁻³

26818 reflections measured ($4.584 \leq 2\theta \leq 59.998^\circ$), 4518 unique ($R_{\text{int}} = 0.0513$, $R_{\text{sigma}} = 0.0410$) which were used in all calculations.

The final $R1$ was 0.0318 ($I > 2\sigma(I)$) and $wR2$ was 0.0637 (all data)

Flack parameter = 0.010(5)

Crystal Structure: 210



Crystal data for $C_{22}H_{24}BrN$ ($m = 382.33$ g/mol);

Monoclinic, space group C_c (no. 9)

$a = 24.4770(16)$ Å

$b = 17.4066(11)$ Å

$c = 20.0973(13)$ Å

$\alpha = 90^\circ$

$\beta = 118.788(2)^\circ$

$\gamma = 90^\circ$

$V = 7504.4(8)$ Å³

$Z = 16$

$T = 120.0$ K

Radiation: $MoK\alpha$ ($\lambda = 0.71073$ Å)

$\mu(MoK\alpha) = 2.193$ mm⁻¹

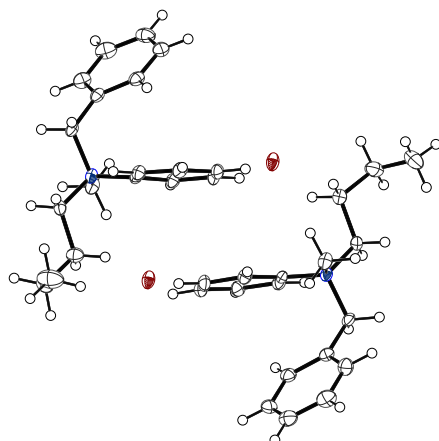
$D_{calc} = 1.354$ g cm⁻³

60229 reflections measured ($3.014 \leq 2\theta \leq 57.998^\circ$), 19890 unique ($R_{int} = 0.0639$, $R_{sigma} = 0.0932$) which were used in all calculations.

The final $R1$ was 0.0489 ($I > 2\sigma(I)$) and $wR2$ was 0.0863 (all data)

Flack parameter = 0.437(14)

Crystal Structure: 206



Crystal data for $C_{18}H_{24}BrN$ ($m = 334.29$ g/mol);

Monoclinic, space group $P2_1/n$ (no. 14)

$a = 19.7167(5)$ Å

$b = 8.7511(2)$ Å

$c = 20.6559(5)$ Å

$\alpha = 90^\circ$

$\beta = 111.7240(10)^\circ$

$\gamma = 90^\circ$

$V = 3310.90(14)$ Å³

$Z = 8$

$T = 296.15$ K

Radiation: MoK α ($\lambda = 0.71073$ Å)

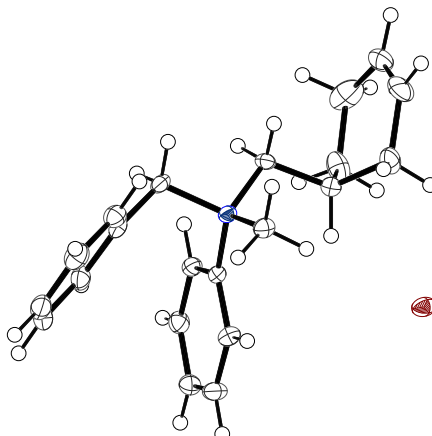
$\mu(\text{MoK}\alpha) = 2.475$ mm⁻¹

$D_{calc} = 1.341$ g cm⁻³

75161 reflections measured ($4.246 \leq 2\theta \leq 58.988^\circ$), 9199 unique ($R_{int} = 0.0468$, $R_{sigma} = 0.0285$) which were used in all calculations.

The final $R1$ was 0.0393 ($I > 2\sigma(I)$) and $wR2$ was 0.0807 (all data)

Crystal Structure: 402



Crystal data for $C_{21}H_{26}BrN$ ($m = 372.34$ g/mol);

Monoclinic, space group $P2_1/n$ (no. 14)

$a = 10.6754(3)$ Å

$b = 8.9852(3)$ Å

$c = 18.7365(6)$ Å

$\alpha = 90^\circ$

$\beta = 98.4290(10)^\circ$

$\gamma = 90^\circ$

$V = 1777.80(10)$ Å³

$Z = 4$

$T = 120.0$ K

Radiation: MoK α ($\lambda = 0.71073$ Å)

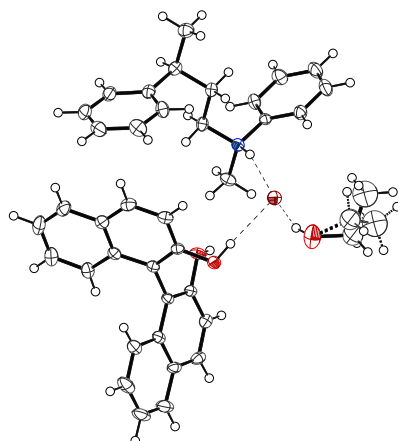
$\mu(\text{MoK}\alpha) = 2.312$ mm⁻¹

$D_{\text{calc}} = 1.391$ g cm⁻³

38551 reflections measured ($4.15 \leq 2\theta \leq 57.992^\circ$), 4720 unique ($R_{\text{int}} = 0.0417$, $R_{\text{sigma}} = 0.0262$) which were used in all calculations.

The final $R1$ was 0.0292 ($I > 2\sigma(I)$) and $wR2$ was 0.0635 (all data)

Crystal Structure: 268



Crystal data for $C_{39}H_{42}BrNO_3$ ($m = 652.64$ g/mol);

Monoclinic, space group $P2_1$ (no.4)

$a = 8.6465(2)$ Å

$b = 20.8530(5)$ Å

$c = 9.9079(4)$ Å

$\alpha = 90^\circ$

$\beta = 106.2280(10)^\circ$

$\gamma = 90^\circ$

$V = 1715.27(9)$ Å³

$Z = 2$

$T = 120.0$ K

Radiation: MoK α ($\lambda = 0.71073$ Å)

$\mu(\text{MoK}\alpha) = 1.235$ mm⁻¹

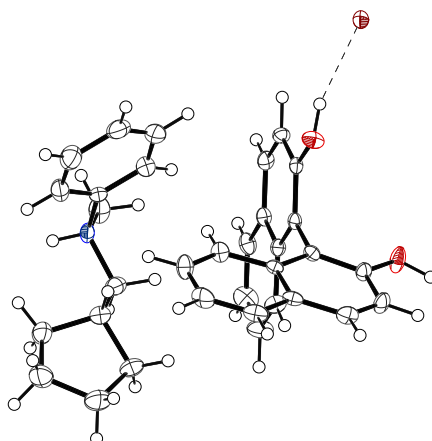
$D_{calc} = 1.264$ g cm⁻³

21625 reflections measured ($4.282 \leq 2\theta \leq 58.998^\circ$), 9383 unique ($R_{int} = 0.0318$, $R_{sigma} = 0.0509$) which were used in all calculations.

The final $R1$ was 0.0365 ($I > 2\sigma(I)$) and $wR2$ was 0.0804 (all data)

Flack parameter = $-0.011(4)$

Crystal Structure: 267



Crystal data for $C_{33}H_{34}BrNO_2$ ($m = 556.52$ g/mol);

Orthorhombic, space group $P2_12_12_1$ (no. 19)

$a = 8.3737(2)$ Å

$b = 11.5658(3)$ Å

$c = 28.5295(8)$ Å

$\alpha = 90^\circ$

$\beta = 90^\circ$

$\gamma = 90^\circ$

$V = 2763.04(12)$ Å³

$Z = 4$

$T = 120.0$ K

Radiation: MoK α ($\lambda = 0.71073$ Å)

$\mu(\text{MoK}\alpha) = 1.518$ mm⁻¹

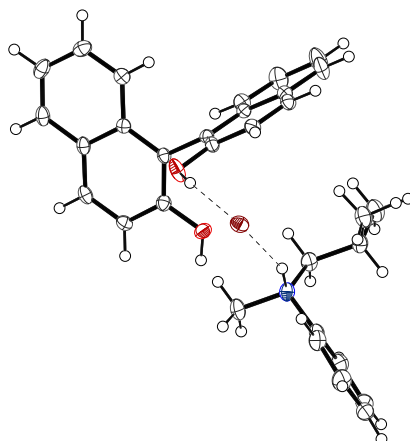
$D_{\text{calc}} = 1.338$ g cm⁻³

33919 reflections measured ($4.534 \leq 2\theta \leq 57.998^\circ$), 7351 unique ($R_{\text{int}} = 0.0606$, $R_{\text{sigma}} = 0.0603$) which were used in all calculations.

The final $R1$ was 0.0404 ($I > 2\sigma(I)$) and $wR2$ was 0.0724 (all data)

Flack parameter = $-0.003(6)$

Crystal Structure: 265



Crystal data for $C_{31}H_{32}BrNO_2$ ($m = 530.48$ g/mol);

Orthorhombic, space group $P2_12_12_1$ (no. 19)

$a = 10.0173(4)$ Å

$b = 10.2390(4)$ Å

$c = 25.9906(10)$ Å

$\alpha = 90^\circ$

$\beta = 90^\circ$

$\gamma = 90^\circ$

$V = 2665.78(18)$ Å³

$Z = 4$

$T = 120.0$ K

Radiation: MoK α ($\lambda = 0.71073$ Å)

$\mu(\text{MoK}\alpha) = 1.570$ mm⁻¹

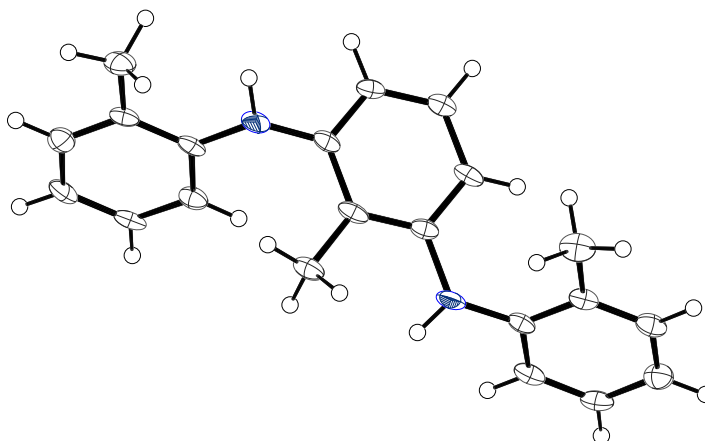
$D_{calc} = 1.322$ g cm⁻³

45929 reflections measured ($4.276 \leq 2\theta \leq 60^\circ$), 7777 unique ($R_{int} = 0.0442$, $R_{sigma} = 0.0356$) which were used in all calculations.

The final $R1$ was 0.0296 ($I > 2\sigma(I)$) and $wR2$ was 0.0554 (all data)

Flack parameter = 0.001(2)

Crystal Structure: 269



Crystal data for $C_{21}H_{22}N_2$ ($m = 302.40$ g/mol);

Monoclinic, space group $P2_1/n$ (no. 14)

$a = 9.2469(9)$ Å

$b = 6.2034(6)$ Å

$c = 28.662(3)$ Å

$\alpha = 90^\circ$

$\beta = 93.902(4)^\circ$

$\gamma = 90^\circ$

$V = 1640.3(3)$ Å³

$Z = 4$

$T = 120.0$ K

Radiation: MoK α ($\lambda = 0.71073$ Å)

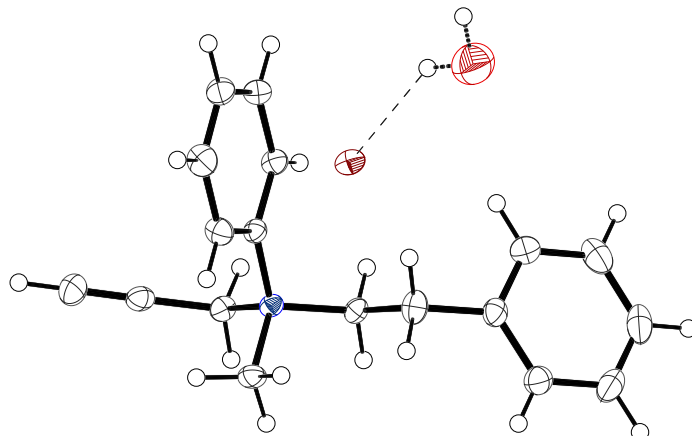
$\mu(\text{MoK}\alpha) = 0.072$ mm⁻¹

$D_{\text{calc}} = 1.225$ g cm⁻³

16824 reflections measured ($1.424 \leq 2\theta \leq 51.994^\circ$), 3226 unique ($R_{\text{int}} = 0.1128$, $R_{\text{sigma}} = 0.1046$) which were used in all calculations.

The final $R1$ was 0.0988 ($I > 2\sigma(I)$) and $wR2$ was 0.2253 (all data)

Crystal Structure: 400



Crystal data for $C_{18}H_{21}BrNO_0.5$ ($m = 339.27$ g/mol);

Orthorhombic, space group $Pbcn$ (no. 60)

$a = 13.3364(5)$ Å

$b = 12.3414(5)$ Å

$c = 20.5283(8)$ Å

$\alpha = 90^\circ$

$\beta = 90^\circ$

$\gamma = 90^\circ$

$V = 3378.7(2)$ Å³

$Z = 8$

$T = 120.0$ K

Radiation: MoK α ($\lambda = 0.71073$ Å)

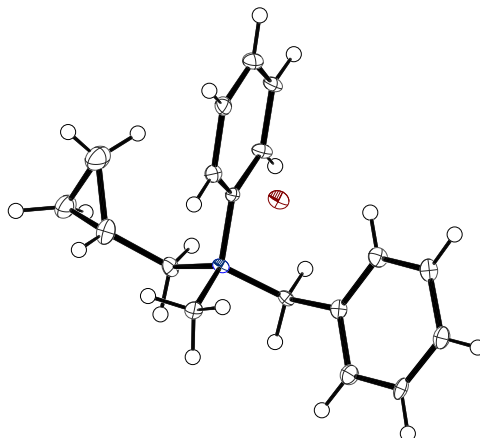
$\mu(\text{MoK}\alpha) = 2.428$ mm⁻¹

$D_{calc} = 1.334$ g cm⁻³

55070 reflections measured ($4.916 \leq 2\theta \leq 59.998^\circ$), 4927 unique ($R_{int} = 0.0408$, $R_{sigma} = 0.0226$) which were used in all calculations.

The final $R1$ was 0.0257 ($I > 2\sigma(I)$) and $wR2$ was 0.0597 (all data)

Crystal Structure: 207



Crystal data for $C_{18}H_{22}BrN$ ($m = 332.27$ g/mol);

Orthorhombic, space group $Pna2_1$ (no. 33)

$a = 12.0154(7)$ Å

$b = 8.9869(5)$ Å

$c = 14.7297(8)$ Å

$\alpha = 90^\circ$

$\beta = 90^\circ$

$\gamma = 90^\circ$

$V = 1590.53(15)$ Å³

$Z = 4$

$T = 120.00$ K

Radiation: Mo $K\alpha$ ($\lambda = 0.71073$ Å)

$\mu(\text{MoK}\alpha) = 2.575$ mm⁻¹

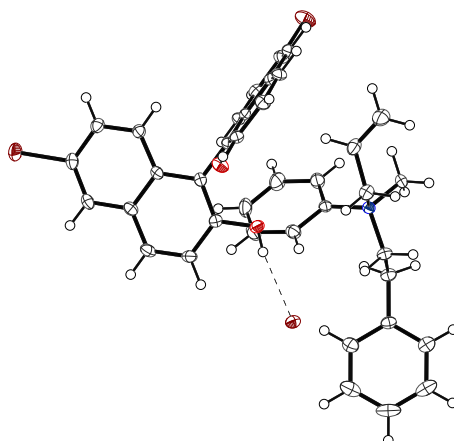
$D_{\text{calc}} = 1.388$ g cm⁻³

43862 reflections measured ($5.31 \leq 2\theta \leq 58.982^\circ$), 4433 unique ($R_{\text{int}} = 0.1150$, $R_{\text{sigma}} = 0.0633$) which were used in all calculations.

The final $R1$ was 0.0788 ($I > 2\sigma(I)$) and $wR2$ was 0.1335 (all data)

Flack parameter = 0.060(8)

Crystal Structure: 403



Crystal data for $C_{38}H_{34}Br_3NO_2$ ($m = 776.39$ g/mol);

Monoclinic, space group $P2_1$ (no. 4)

$a = 11.0954(5)$ Å

$b = 10.6208(5)$ Å

$c = 14.8901(7)$ Å

$\alpha = 90^\circ$

$\beta = 108.075(2)^\circ$

$\gamma = 90^\circ$

$V = 1668.09(14)$ Å³

$Z = 2$

$T = 120.00$ K

Radiation: Mo $K\alpha$ ($\lambda = 0.71073$ Å)

$\mu(\text{MoK}\alpha) = 3.662$ mm⁻¹

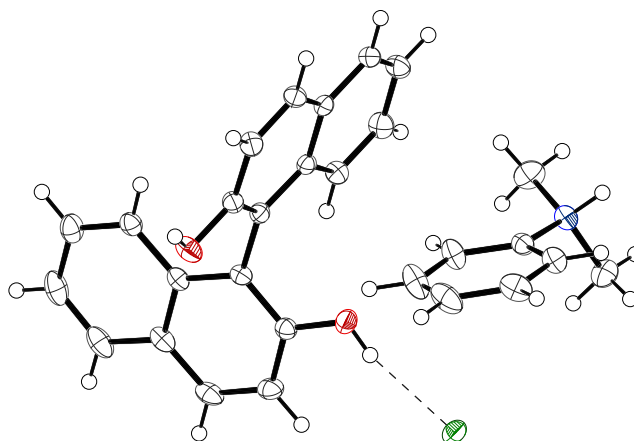
$D_{\text{calc}} = 1.546$ g cm⁻³

47617 reflections measured ($3.862 \leq 2\theta \leq 57.992^\circ$), 8854 unique ($R_{\text{int}} = 0.0438$, $R_{\text{sigma}} = 0.0344$) which were used in all calculations.

The final R_1 was 0.0265 ($I > 2\sigma(I)$) and wR_2 was 0.0500 (all data)

Flack parameter = $-0.006(3)$

Crystal Structure: 404



Crystal data for $C_{28}H_{26}ClNO_2$ ($m = 443.95$ g/mol);

Orthorhombic, space group $P2_12_12_1$

$a = 10.8134(5)$ Å

$b = 12.1073(5)$ Å

$c = 17.8461(8)$ Å

$\alpha = 90^\circ$

$\beta = 90^\circ$

$\gamma = 90^\circ$

$V = 2336.43(18)$ Å³

$Z = 4$

$T = 120.00$ K

Radiation: $MoK\alpha$ ($\lambda = 0.71073$ Å)

$\mu(MoK\alpha) = 0.188$ mm⁻¹

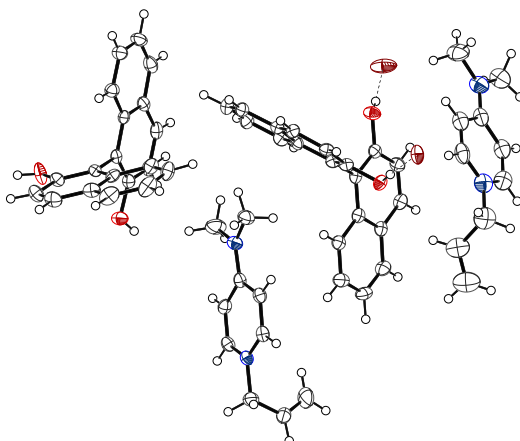
$D_{calc} = 1.262$ g cm⁻³

30340 reflections measured ($4.066 \leq 2\theta \leq 60^\circ$), 6779 unique ($R_{int} = 0.0445$, $R_{sigma} = 0.0447$) which were used in all calculations.

The final $R1$ was 0.0394 ($I > 2\sigma(I)$) and $wR2$ was 0.1097 (all data)

Flack parameter = 0.03(2)

Crystal Structure: 165b



Crystal data for $C_{60}H_{58}Br_2N_4O_4$ ($m = 1058.92$ g/mol);

Monoclinic, space group $P2_1$ (no 4.)

$a = 10.3813(5)$ Å

$b = 21.4806(10)$ Å

$c = 11.6460(5)$ Å

$\alpha = 90^\circ$

$\beta = 92.919(2)^\circ$

$\gamma = 90^\circ$

$V = 2593.6(2)$ Å³

$Z = 2$

$T = 120.00$ K

Radiation: MoK α ($\lambda = 0.71073$ Å)

$\mu(\text{MoK}\alpha) = 1.614$ mm⁻¹

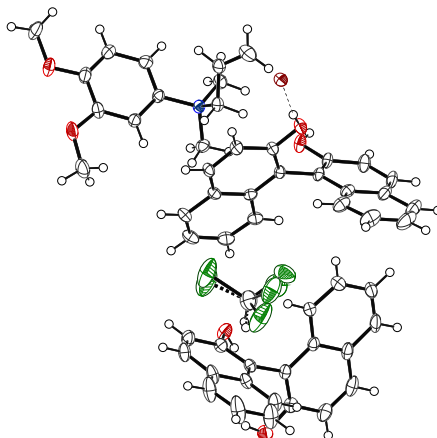
$D_{calc} = 1.356$ g cm⁻³

44805 reflections measured ($3.792 \leq 2\theta \leq 60^\circ$), 15088 unique ($R_{int} = 0.0566$, $R_{sigma} = 0.0800$) which were used in all calculations.

The final $R1$ was 0.0526 ($I > 2\sigma(I)$) and $wR2$ was 0.1287 (all data)

Flack parameter = 0.016(4)

Crystal Structure: 163b



Crystal data for $C_{27}H_{24} \cdot 5 Br_0 \cdot 5 Cl_1 \cdot 5 N_0 \cdot 5 O_3$ ($m = 497.10$ g/mol);

Monoclinic, space group $P2_1$ (no 4.)

$a = 11.6896(3)$ Å

$b = 12.3927(3)$ Å

$c = 16.6159(4)$ Å

$\alpha = 90^\circ$

$\beta = 92.5140(10)^\circ$

$\gamma = 90^\circ$

$V = 2404.76(10)$ Å³

$Z = 4$

$T = 120.00$ K

Radiation: MoK α ($\lambda = 0.71073$ Å)

$\mu(\text{MoK}\alpha) = 1.073$ mm⁻¹

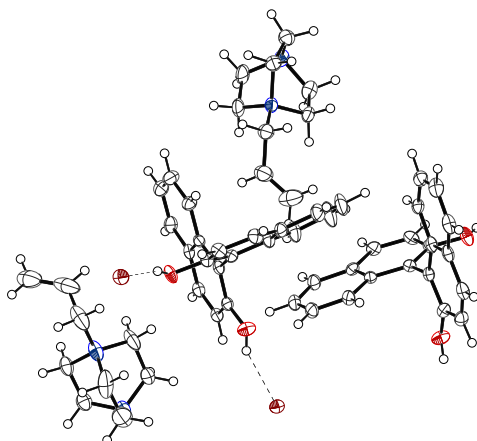
$D_{calc} = 1.373$ g cm⁻³

41892 reflections measured ($2.454 \leq 2\theta \leq 59.994^\circ$), 13920 unique ($R_{int} = 0.0339$, $R_{sigma} = 0.0462$) which were used in all calculations.

The final $R1$ was 0.0368 ($I > 2\sigma(I)$) and $wR2$ was 0.0975 (all data)

Flack parameter = 0.009(2)

Crystal Structure: 164b



Crystal data for $C_{58}H_{62}Br_2N_4O_4$ ($m = 1038.93$ g/mol);

Monoclinic, space group $P2_1$ (no. 4)

$a = 11.8812(3)$ Å

$b = 17.6104(5)$ Å

$c = 12.0372(4)$ Å

$\alpha = 90^\circ$

$\beta = 92.9140(10)^\circ$

$\gamma = 90^\circ$

$V = 2515.32(13)$ Å³

$Z = 2$

$T = 120.00$ K

Radiation: MoK α ($\lambda = 0.71073$ Å)

$\mu(\text{MoK}\alpha) = 1.663$ mm⁻¹

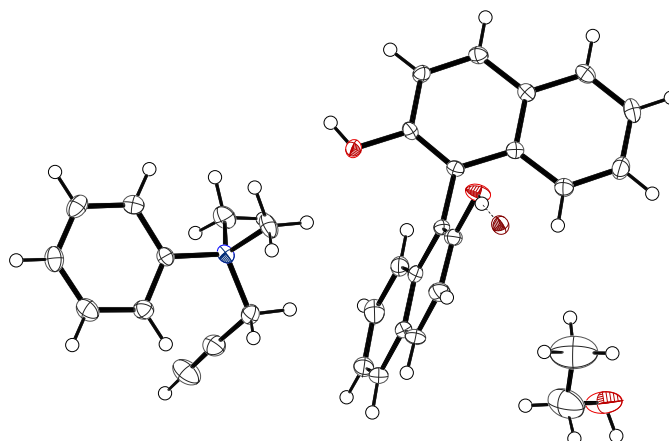
$D_{calc} = 1.372$ g cm⁻³

43472 reflections measured ($4.102 \leq 2\theta \leq 59.998^\circ$), 14569 unique ($R_{int} = 0.0343$, $R_{sigma} = 0.0438$) which were used in all calculations.

The final $R1$ was 0.0334 ($I > 2\sigma(I)$) and $wR2$ was 0.0943 (all data)

Flack parameter = $-0.002(2)$

Crystal Structure: 405



Crystal data for $C_{33}H_{34}BrNO_3$ ($m = 572.52$ g/mol);

Orthorhombic, space group $P2_12_12_1$ (no. 19)

$a = 10.3132(2)$ Å

$b = 12.4986(3)$ Å

$c = 22.1449(5)$ Å

$\alpha = 90^\circ$

$\beta = 90^\circ$

$\gamma = 90^\circ$

$V = 2854.49(11)$ Å³

$Z = 4$

$T = 120.00$ K

Radiation: MoK α ($\lambda = 0.71073$ Å)

$\mu(\text{MoK}\alpha) = 1.474$ mm⁻¹

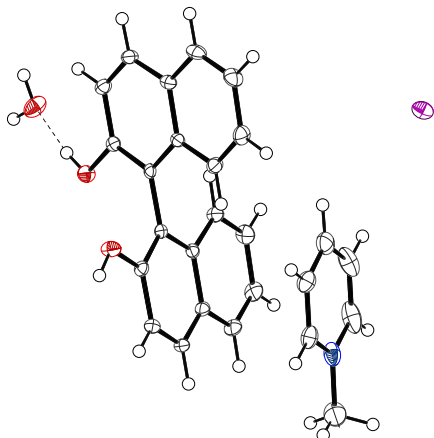
$D_{\text{calc}} = 1.332$ g cm⁻³

37371 reflections measured ($3.742 \leq 2\theta \leq 59.998^\circ$), 8316 unique ($R_{\text{int}} = 0.0414$, $R_{\text{sigma}} = 0.0407$) which were used in all calculations.

The final $R1$ was 0.0314 ($I > 2\sigma(I)$) and $wR2$ was 0.0613 (all data)

Flack parameter = $-0.002(3)$

Crystal Structure: 162a



Crystal data for $C_{26}H_{24}INO_3$ ($m = 525.36$ g/mol);

Orthorhombic, space group $P2_12_12_1$ (no. 19)

$a = 9.1389(2)$ Å

$b = 13.4774(3)$ Å

$c = 18.6368(4)$ Å

$\alpha = 90^\circ$

$\beta = 90^\circ$

$\gamma = 90^\circ$

$V = 2295.47(9)$ Å³

$Z = 4$

$T = 120.00$ K

Radiation: MoK α ($\lambda = 0.71073$ Å)

$\mu(\text{MoK}\alpha) = 1.422$ mm⁻¹

$D_{\text{calc}} = 1.520$ g cm⁻³

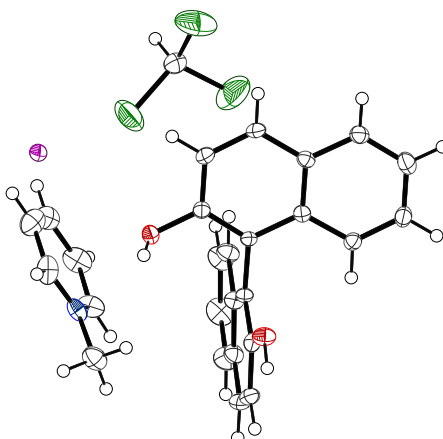
29457 reflections measured ($4.372 \leq 2\theta \leq 59.996^\circ$), 6638 unique ($R_{\text{int}} = 0.0257$,

$R_{\text{sigma}} = 0.0243$) which were used in all calculations.

The final $R1$ was 0.0209 ($I > 2\sigma(I)$) and $wR2$ was 0.0784 (all data)

Flack parameter = -0.012(6)

Crystal Structure: 162b



Crystal data for $C_{27}H_{23}Cl_3INO_2$ ($m = 626.71$ g/mol);

Orthorhombic, space group $P2_12_12_1$ (no. 19)

$a = 9.4989(5)$ Å

$b = 11.5324(6)$ Å

$c = 24.1040(13)$ Å

$\alpha = 90^\circ$

$\beta = 90^\circ$

$\gamma = 90^\circ$

$V = 2640.5(2)$ Å³

$Z = 4$

$T = 120.00$ K

Radiation: MoK α ($\lambda = 0.71073$ Å)

$\mu(\text{MoK}\alpha) = 1.541$ mm⁻¹

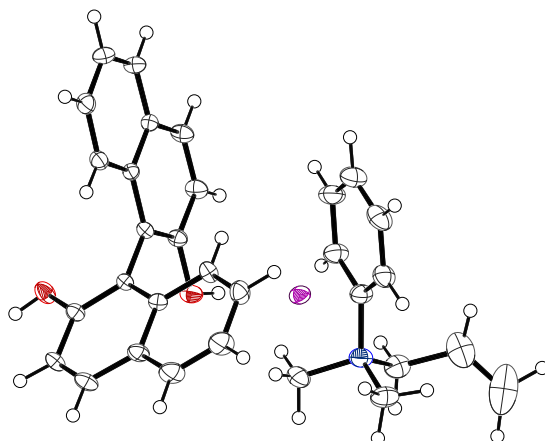
$D_{\text{calc}} = 1.577$ g cm⁻³

45332 reflections measured ($4.61 \leq 2\theta \leq 60^\circ$), 7619 unique ($R_{\text{int}} = 0.0303$, $R_{\text{sigma}} = 0.0216$) which were used in all calculations.

The final $R1$ was 0.0257 ($I > 2\sigma(I)$) and $wR2$ was 0.0898 (all data)

Flack parameter = $-0.028(4)$

Crystal Structure: 116



Crystal data for $C_{31}H_{30}INO_2$ ($m = 575.46$ g/mol);

Orthorhombic, space group $P2_12_12_1$ (no. 19)

$a = 10.3570(5)$ Å

$b = 10.4721(5)$ Å

$c = 24.5555(11)$ Å

$\alpha = 90^\circ$

$\beta = 90^\circ$

$\gamma = 90^\circ$

$V = 2663.3(2)$ Å³

$Z = 4$

$T = 120.00$ K

Radiation: MoK α ($\lambda = 0.71073$ Å)

$\mu(\text{MoK}\alpha) = 1.230$ mm⁻¹

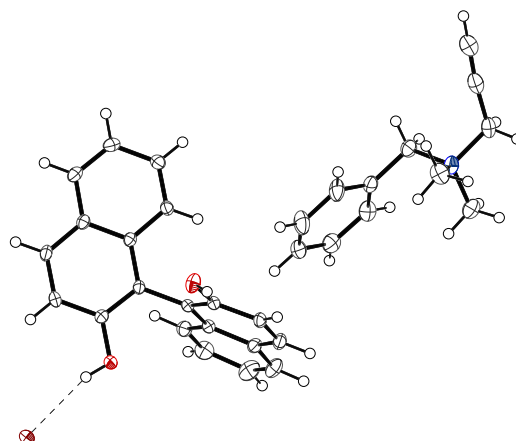
$D_{calc} = 1.435$ g cm⁻³

45654 reflections measured ($4.228 \leq 2\theta \leq 59.988^\circ$), 7752 unique ($R_{int} = 0.0295$, $R_{sigma} = 0.0201$) which were used in all calculations.

The final $R1$ was 0.0208 ($I > 2\sigma(I)$) and $wR2$ was 0.0768 (all data)

Flack parameter = $-0.020(4)$

Crystal Structure: 120



Crystal data for $C_{32}H_{30}BrNO_2$ ($m = 540.48$ g/mol);

Orthorhombic, space group $P2_12_12_1$ (no. 19)

$a = 10.3994(4)$ Å

$b = 10.4663(4)$ Å

$c = 24.2221(8)$ Å

$\alpha = 90^\circ$

$\beta = 90^\circ$

$\gamma = 90^\circ$

$V = 2636.41(17)$ Å³

$Z = 4$

$T = 120.00$ K

Radiation: MoK α ($\lambda = 0.71073$ Å)

$\mu(\text{MoK}\alpha) = 1.589$ mm⁻¹

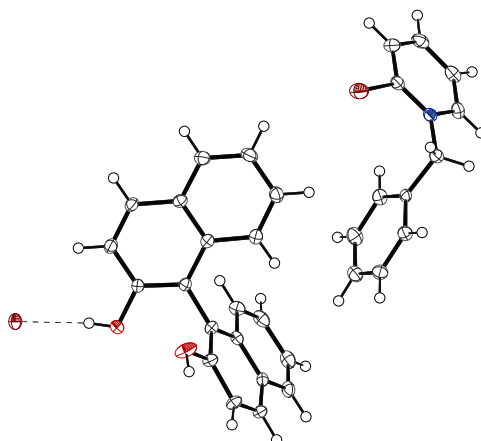
$D_{calc} = 1.362$ g cm⁻³

45492 reflections measured ($4.24 \leq 2\theta \leq 59.998^\circ$), 7668 unique ($R_{int} = 0.0360$, $R_{sigma} = 0.0286$) which were used in all calculations.

The final $R1$ was 0.0254 ($I > 2\sigma(I)$) and $wR2$ was 0.0830 (all data)

Flack parameter = $-0.003(2)$

Crystal Structure: 143



Crystal data for $C_{32}H_{25}Br_2NO_2$ ($m = 615.35$ g/mol);

Monoclinic, space group $P2_1$ (no. 4)

$a = 10.7034(3)$ Å

$b = 10.2407(2)$ Å

$c = 12.6638(3)$ Å

$\alpha = 90^\circ$

$\beta = 108.0650(10)^\circ$

$\gamma = 90^\circ$

$V = 1319.66(6)$ Å³

$Z = 2$

$T = 120.00$ K

Radiation: MoK α ($\lambda = 0.71073$ Å)

$\mu(\text{MoK}\alpha) = 3.102$ mm⁻¹

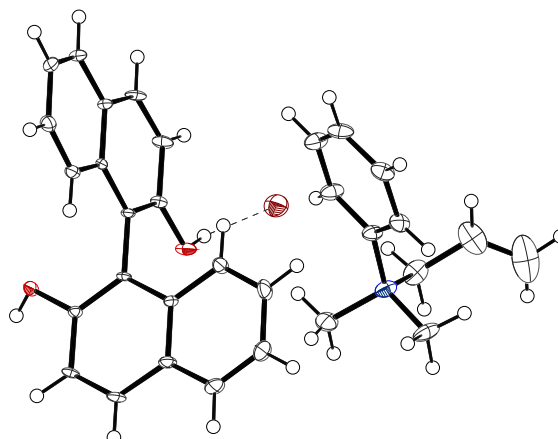
$D_{\text{calc}} = 1.549$ g cm⁻³

22643 reflections measured ($4.002 \leq 2\theta \leq 59.998^\circ$), 7646 unique ($R_{\text{int}} = 0.0283$, $R_{\text{sigma}} = 0.0337$) which were used in all calculations.

The final R_1 was 0.0242 ($I > 2\sigma(I)$) and wR_2 was 0.0781 (all data)

Flack parameter = $-0.008(2)$

Crystal Structure: 115



Crystal data for $C_{31}H_{30}BrNO_2$ ($m = 528.47$ g/mol);

Orthorhombic, space group $P2_12_12_1$ (no. 19)

$a = 10.2788(2)$ Å

$b = 10.9000(2)$ Å

$c = 23.3163(5)$ Å

$\alpha = 90^\circ$

$\beta = 90^\circ$

$\gamma = 90^\circ$

$V = 2612.33(9)$ Å³

$Z = 4$

$T = 120.0$ K

Radiation: MoK α ($\lambda = 0.71073$ Å)

$\mu(\text{MoK}\alpha) = 1.602$ mm⁻¹

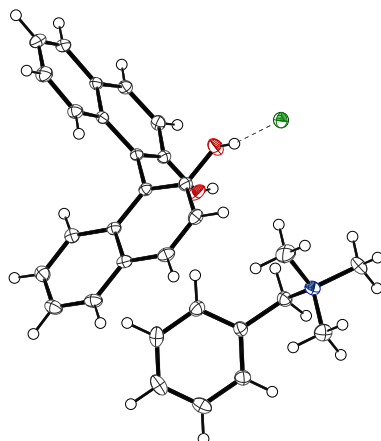
$D_{\text{calc}} = 1.344$ g cm⁻³

44929 reflections measured ($4.124 \leq 2\theta \leq 59.99^\circ$), 7591 unique ($R_{\text{int}} = 0.0409$, $R_{\text{sigma}} = 0.0325$) which were used in all calculations.

The final $R1$ was 0.0493 ($I > 2\sigma(I)$) and $wR2$ was 0.1525 (all data)

Flack parameter = 0.067(3)

Crystal Structure: 406



Crystal data for $C_{30}H_{30}ClNO_2$ ($m = 472.00$ g/mol);

Triclinic, space group $P\bar{1}$ (no. 2)

$a = 9.8918(5)$ Å

$b = 10.0667(5)$ Å

$c = 13.5065(7)$ Å

$\alpha = 78.734(2)^\circ$

$\beta = 69.632(2)^\circ$

$\gamma = 89.674(2)^\circ$

$V = 1233.72(11)$ Å³

$Z = 2$

$T = 120.0$ K

Radiation: MoK α ($\lambda = 0.71073$ Å)

$\mu(\text{MoK}\alpha) = 0.183$ mm⁻¹

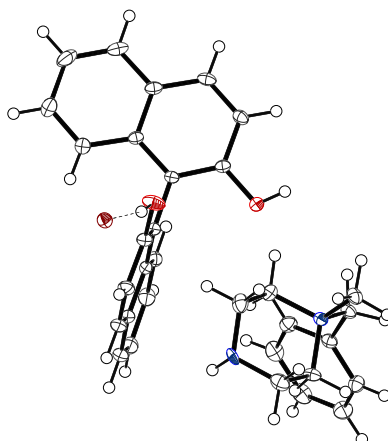
$D_{calc} = 1.271$ g cm⁻³

37569 reflections measured ($4.136 \leq 2\theta \leq 59.994^\circ$), 7168 unique ($R_{int} = 0.0446$,

$R_{sigma} = 0.0348$) which were used in all calculations.

The final $R1$ was 0.0410 ($I > 2\sigma(I)$) and $wR2$ was 0.0973 (all data)

Crystal Structure: 407



Crystal data for $C_{32}H_{33}BrN_2O_2$ ($m = 557.51$ g/mol);

Triclinic, space group $P\bar{1}$ (no. 2)

$a = 10.2400(2)$ Å

$b = 10.7027(3)$ Å

$c = 13.5673(3)$ Å

$\alpha = 73.9810(10)^\circ$

$\beta = 68.1670(10)^\circ$

$\gamma = 84.6770(10)^\circ$

$V = 1326.59(6)$ Å³

$Z = 2$

$T = 120.0$ K

Radiation: MoK α ($\lambda = 0.71073$ Å)

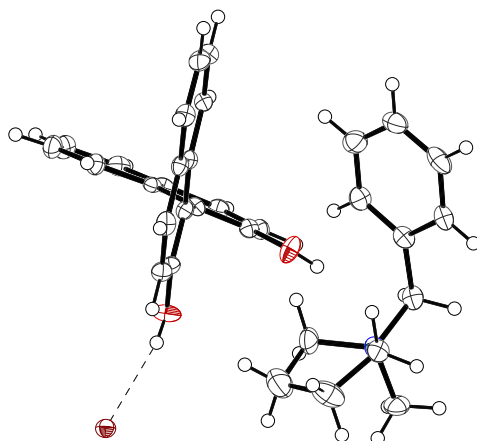
$\mu(\text{MoK}\alpha) = 1.582$ mm⁻¹

$D_{\text{calc}} = 1.396$ g cm⁻³

23679 reflections measured ($3.96 \leq 2\theta \leq 59.998^\circ$), 7698 unique ($R_{\text{int}} = 0.0282$, $R_{\text{sigma}} = 0.0321$) which were used in all calculations.

The final $R1$ was 0.0301 ($I > 2\sigma(I)$) and $wR2$ was 0.0764 (all data)

Crystal Structure: 169



Crystal data for $C_{32}H_{32}BrNO_2$ ($m = 542.49$ g/mol);

Monoclinic, space group $P2_1/c$ (no. 14)

$a = 10.0705(2)$ Å

$b = 10.1032(2)$ Å

$c = 26.3679(6)$ Å

$\alpha = 90^\circ$

$\beta = 100.4880(10)^\circ$

$\gamma = 90^\circ$

$V = 2637.96(10)$ Å³

$Z = 4$

$T = 120.0$ K

Radiation: MoK α ($\lambda = 0.71073$ Å)

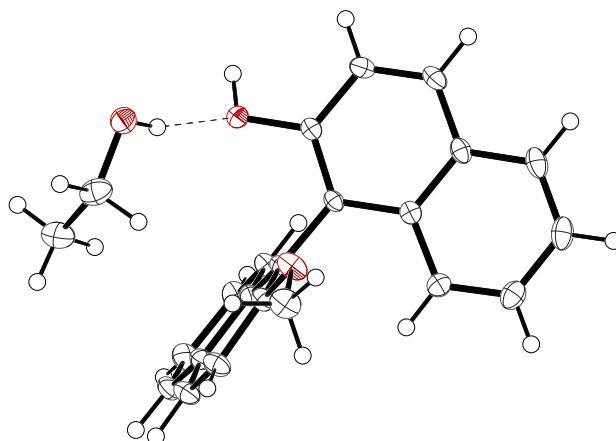
$\mu(\text{MoK}\alpha) = 1.588$ mm⁻¹

$D_{\text{calc}} = 1.366$ g cm⁻³

46104 reflections measured ($4.114 \leq 2\theta \leq 59.996^\circ$), 7678 unique ($R_{\text{int}} = 0.0613$, $R_{\text{sigma}} = 0.0499$) which were used in all calculations.

The final R_1 was 0.0451 ($I > 2\sigma(I)$) and wR_2 was 0.1317 (all data)

Crystal Structure: 408



Crystal data for $C_{23}H_{22}O_3$ ($m = 346.40$ g/mol);

Monoclinic, space group $P2_1$ (no. 4)

$a = 9.3773(2)$ Å

$b = 7.6571(2)$ Å

$c = 12.8736(3)$ Å

$\alpha = 90^\circ$

$\beta = 103.1370(10)^\circ$

$\gamma = 90^\circ$

$V = 900.17(4)$ Å³

$Z = 2$

$T = 120.0$ K

Radiation: MoK α ($\lambda = 0.71073$ Å)

$\mu(\text{MoK}\alpha) = 0.083$ mm⁻¹

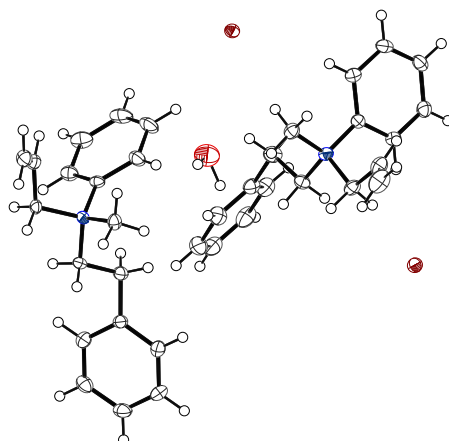
$D_{\text{calc}} = 1.278$ g cm⁻³

15216 reflections measured ($6.5 \leq 2\theta \leq 59.978^\circ$), 5188 unique ($R_{\text{int}} = 0.0252$, $R_{\text{sigma}} = 0.0289$) which were used in all calculations.

The final $R1$ was 0.0355 ($I > 2\sigma(I)$) and $wR2$ was 0.0937 (all data)

Flack parameter = $-0.1(3)$

Crystal Structure: 192



Crystal data for $C_{36}H_{46}Br_2N_2O$ ($m = 682.57$ g/mol);

Monoclinic, space group $P2_1/n$ (no. 14)

$a = 18.1894(8)$ Å

$b = 10.0428(4)$ Å

$c = 19.5856(8)$ Å

$\alpha = 90^\circ$

$\beta = 107.476(2)^\circ$

$\gamma = 90^\circ$

$V = 3412.6(2)$ Å³

$Z = 4$

$T = 120.0$ K

Radiation: MoK α ($\lambda = 0.71073$ Å)

$\mu(\text{MoK}\alpha) = 2.405$ mm⁻¹

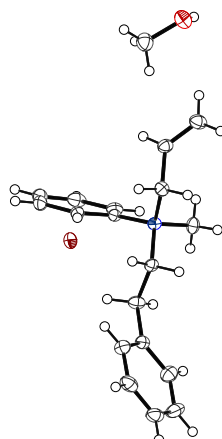
$D_{\text{calc}} = 1.329$ g cm⁻³

57668 reflections measured ($3.652 \leq 2\theta \leq 59.998^\circ$), 9933 unique ($R_{\text{int}} = 0.0344$,

$R_{\text{sigma}} = 0.0281$) which were used in all calculations.

The final R_1 was 0.0269 ($I > 2\sigma(I)$) and wR_2 was 0.0600 (all data)

Crystal Structure: 240



Crystal data for $C_{19}H_{26}BrNO$ ($m = 364.32$ g/mol);

Orthorhombic, space group $P2_12_12_1$ (no. 19)

$a = 10.0041(5)$ Å

$b = 11.5794(6)$ Å

$c = 15.6325(8)$ Å

$\alpha = 90^\circ$

$\beta = 90^\circ$

$\gamma = 90^\circ$

$V = 1810.89(16)$ Å³

$Z = 4$

$T = 120.0$ K

Radiation: $MoK\alpha$ ($\lambda = 0.71073$ Å)

$\mu(MoK\alpha) = 2.272$ mm⁻¹

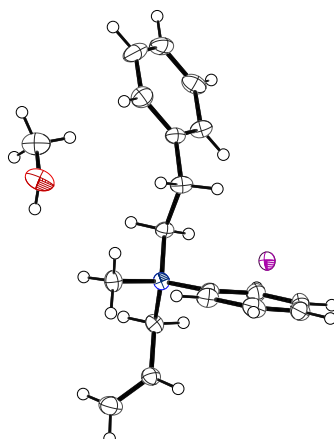
$D_{calc} = 1.336$ g cm⁻³

31805 reflections measured ($4.378 \leq 2\theta \leq 59.976^\circ$), 5287 unique ($R_{int} = 0.0545$, $R_{sigma} = 0.0453$) which were used in all calculations.

The final $R1$ was 0.0323 ($I > 2\sigma(I)$) and $wR2$ was 0.0555 (all data)

Flack parameter = 0.001(4)

Crystal Structure: 409



Crystal data for $C_{19}H_{26}INO$ ($m = 411.31$ g/mol);

Orthorhombic, space group $P2_12_12_1$ (no. 19)

$a = 10.1164(5)$ Å

$b = 11.8297(6)$ Å

$c = 15.8142(8)$ Å

$\alpha = 90^\circ$

$\beta = 90^\circ$

$\gamma = 90^\circ$

$V = 1892.55(16)$ Å³

$Z = 4$

$T = 120.0$ K

Radiation: MoK α ($\lambda = 0.71073$ Å)

$\mu(\text{MoK}\alpha) = 1.694$ mm⁻¹

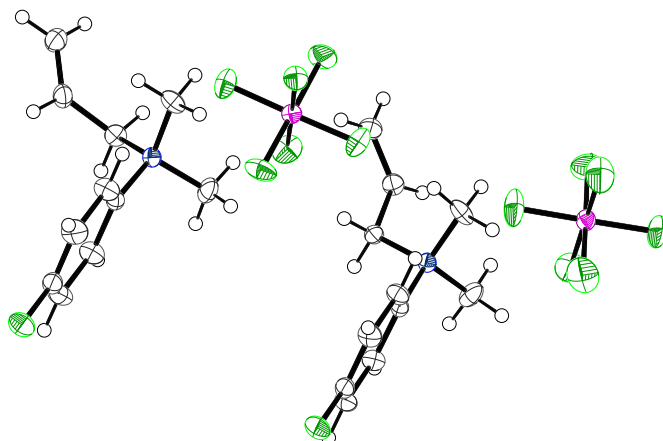
$D_{calc} = 1.444$ g cm⁻³

33093 reflections measured ($4.3 \leq 2\theta \leq 59.996^\circ$), 5518 unique ($R_{int} = 0.0647$, $R_{sigma} = 0.0536$) which were used in all calculations.

The final $R1$ was 0.0360 ($I > 2\sigma(I)$) and $wR2$ was 0.0715 (all data)

Flack parameter = $-0.015(14)$

Crystal Structure: 410



Crystal data for $C_{11}H_{15}F_7NP$ ($m = 325.21$ g/mol);

Monoclinic, space group $P2_1/n$ (no. 14)

$a = 13.8500(3)$ Å

$b = 14.9910(3)$ Å

$c = 13.8807(3)$ Å

$\alpha = 90^\circ$

$\beta = 110.3630(10)^\circ$

$\gamma = 90^\circ$

$V = 2701.88(10)$ Å³

$Z = 8$

$T = 120.0$ K

Radiation: MoK α ($\lambda = 0.71073$ Å)

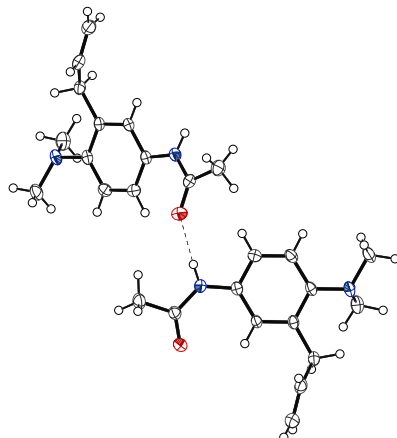
$\mu(\text{MoK}\alpha) = 0.274$ mm⁻¹

$D_{\text{calc}} = 1.599$ g cm⁻³

46340 reflections measured ($4.144 \leq 2\theta \leq 59.994^\circ$), 7887 unique ($R_{\text{int}} = 0.0494$, $R_{\text{sigma}} = 0.0334$) which were used in all calculations.

The final $R1$ was 0.0503 ($I > 2\sigma(I)$) and $wR2$ was 0.1268 (all data)

Crystal Structure: 411



Crystal data for $C_{26}H_{36}N_4O_2$ ($m = 436.59$ g/mol);

Triclinic, space group $P\bar{1}$ (no. 2)

$a = 9.2074(8)$ Å

$b = 9.5477(8)$ Å

$c = 14.1637(12)$ Å

$\alpha = 81.278(3)^\circ$

$\beta = 89.981(3)^\circ$

$\gamma = 88.692(3)^\circ$

$V = 1230.40(18)$ Å³

$Z = 2$

$T = 120.0$ K

Radiation: MoK α ($\lambda = 0.71073$ Å)

$\mu(\text{MoK}\alpha) = 0.076$ mm⁻¹

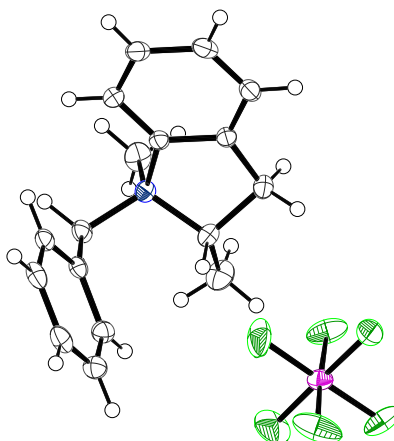
$D_{calc} = 1.178$ g cm⁻³

23133 reflections measured ($2.91 \leq 2\theta \leq 63.196^\circ$), 8147 unique ($R_{int} = 0.0625$,

$R_{sigma} = 0.0786$) which were used in all calculations.

The final $R1$ was 0.0850 ($I > 2\sigma(I)$) and $wR2$ was 0.2241 (all data)

Crystal Structure: 412



Crystal data for $C_{17}H_{20}F_6NP$ ($m = 383.31$ g/mol);

Monoclinic, space group $P2_1/n$ (no. 14)

$a = 8.8266(3)$ Å

$b = 11.6599(4)$ Å

$c = 16.8407(6)$ Å

$\alpha = 90^\circ$

$\beta = 98.7330(10)^\circ$

$\gamma = 90^\circ$

$V = 1713.11(10)$ Å³

$Z = 4$

$T = 120.0$ K

Radiation: MoK α ($\lambda = 0.71073$ Å)

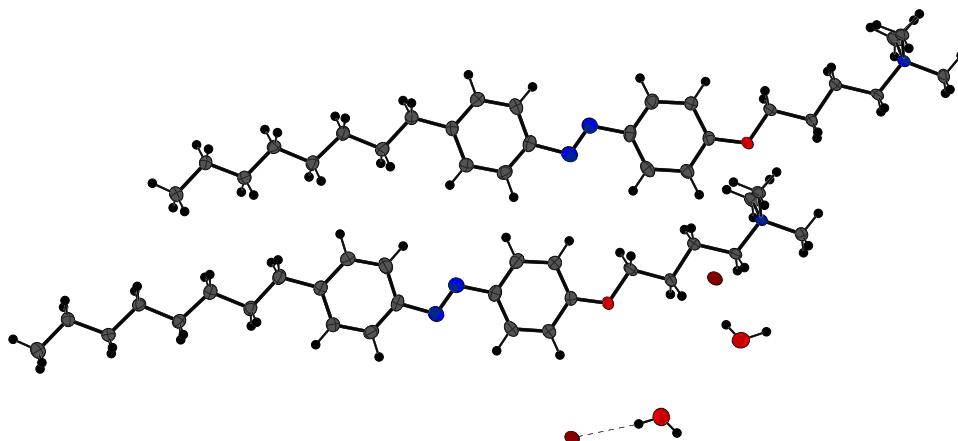
$\mu(\text{MoK}\alpha) = 0.221$ mm⁻¹

$D_{\text{calc}} = 1.486$ g cm⁻³

28694 reflections measured ($4.266 \leq 2\theta \leq 59.996^\circ$), 4992 unique ($R_{\text{int}} = 0.0343$, $R_{\text{sigma}} = 0.0253$) which were used in all calculations.

The final $R1$ was 0.0475 ($I > 2\sigma(I)$) and $wR2$ was 0.1149 (all data)

Crystal Structure: 413



Crystal data for $C_{27}H_{44}BrN_3O_2$ ($m = 522.56$ g/mol);

Triclinic, space group $P\bar{1}$

$a = 7.4326(3)$ Å

$b = 14.4112(5)$ Å

$c = 25.5652(9)$ Å

$\alpha = 89.1380(10)^\circ$

$\beta = 86.4810(10)^\circ$

$\gamma = 88.5900(10)^\circ$

$V = 2732.11(17)$ Å³

$Z = 4$

$T = 120.0$ K

Radiation: MoK α ($\lambda = 0.71073$ Å)

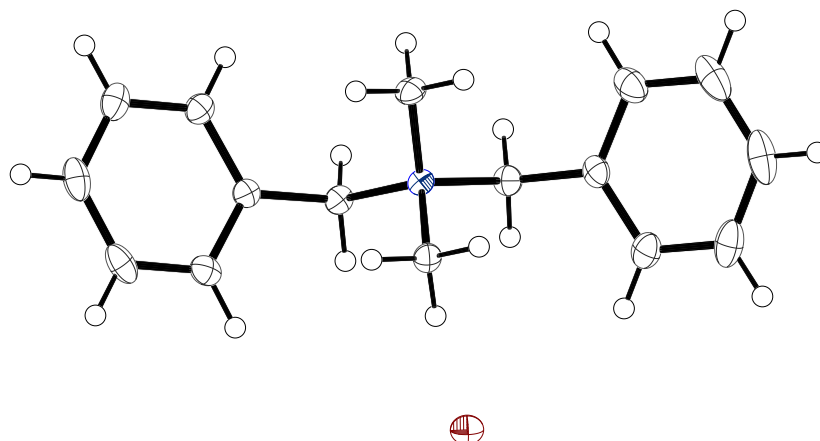
$\mu(\text{MoK}\alpha) = 1.532$ mm⁻¹

$D_{\text{calc}} = 1.270$ g cm⁻³

47408 reflections measured ($2.828 \leq 2\theta \leq 59.998^\circ$), 15867 unique ($R_{\text{int}} = 0.0526$, $R_{\text{sigma}} = 0.0762$) which were used in all calculations.

The final R_1 was 0.0481 ($I > 2\sigma(I)$) and wR_2 was 0.1007 (all data)

Crystal Structure: 414



Crystal data for $C_{16}H_{20}BrN$ ($m = 306.24$ g/mol);

Monoclinic, space group $P2_1/c$

$a = 12.9898(3)$ Å

$b = 10.2487(2)$ Å

$c = 10.8155(2)$ Å

$\alpha = 90^\circ$

$\beta = 91.5570(10)^\circ$

$\gamma = 90^\circ$

$V = 1439.32(5)$ Å³

$Z = 4$

$T = 120.0$ K

Radiation: $MoK\alpha$ ($\lambda = 0.71073$ Å)

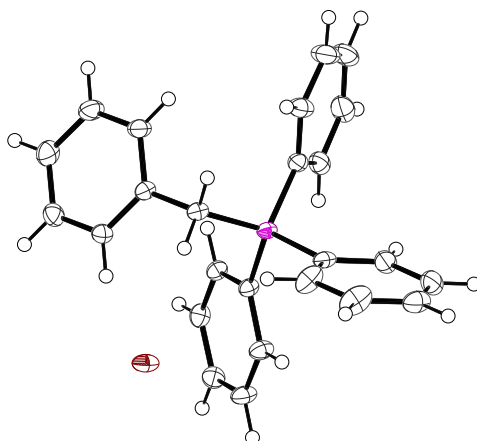
$\mu(MoK\alpha) = 2.839$ mm⁻¹

$D_{calc} = 1.413$ g cm⁻³

24044 reflections measured ($5.064 \leq 2\theta \leq 59.994^\circ$), 4185 unique ($R_{int} = 0.0326$, $R_{sigma} = 0.0230$) which were used in all calculations.

The final $R1$ was 0.0219 ($I > 2\sigma(I)$) and $wR2$ was 0.0537 (all data)

Crystal Structure: 415



Crystal data for $C_{25}H_{22}BrP$ ($m = 433.30$ g/mol);

Monoclinic, space group $P2_1/c$ (no. 14)

$a = 9.7108(3)$ Å

$b = 20.1275(6)$ Å

$c = 11.4067(3)$ Å

$\alpha = 90^\circ$

$\beta = 109.1770(10)^\circ$

$\gamma = 90^\circ$

$V = 2105.77(11)$ Å³

$Z = 4$

$T = 120.0$ K

Radiation: $MoK\alpha$ ($\lambda = 0.71073$ Å)

$\mu(MoK\alpha) = 2.035$ mm⁻¹

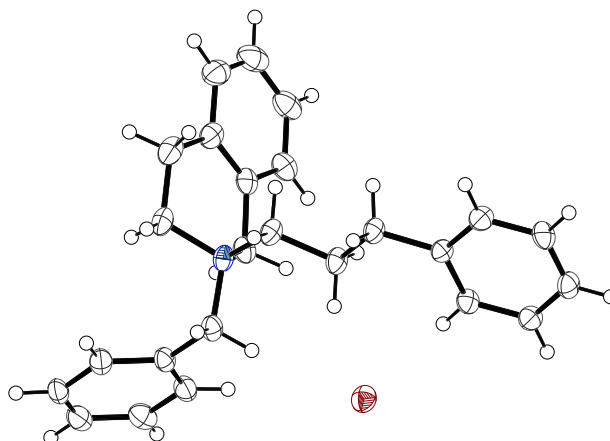
$D_{calc} = 1.367$ g cm⁻³

35585 reflections measured ($4.288 \leq 2\theta \leq 59.992^\circ$), 6113 unique ($R_{int} = 0.0309$,

$R_{sigma} = 0.0236$) which were used in all calculations.

The final $R1$ was 0.0296 ($I > 2\sigma(I)$) and $wR2$ was 0.1060 (all data)

Crystal Structure: 416



Crystal data for $C_{25}H_{28}BrN$ ($m = 422.39$ g/mol);

Monoclinic, space group $C2/c$ (no. 15)

$a = 21.6224(6)$ Å

$b = 10.3543(3)$ Å

$c = 18.3590(5)$ Å

$\alpha = 90^\circ$

$\beta = 100.9620(10)^\circ$

$\gamma = 90^\circ$

$V = 4035.3(2)$ Å³

$Z = 8$

$T = 120.0$ K

Radiation: $MoK\alpha$ ($\lambda = 0.71073$ Å)

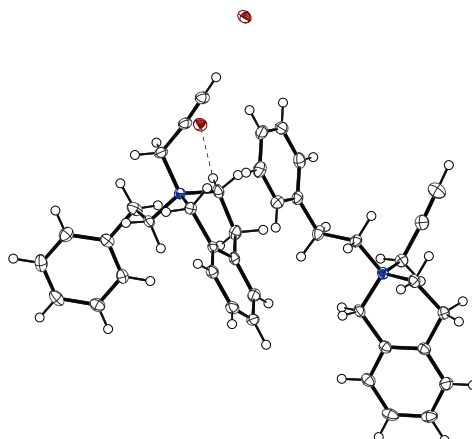
$\mu(MoK\alpha) = 2.047$ mm⁻¹

$D_{calc} = 1.391$ g cm⁻³

33924 reflections measured ($4.376 \leq 2\theta \leq 59.988^\circ$), 5884 unique ($R_{int} = 0.0430$, $R_{sigma} = 0.0361$) which were used in all calculations.

The final $R1$ was 0.0403 ($I > 2\sigma(I)$) and $wR2$ was 0.1243 (all data)

Crystal Structure: 417



Crystal data for $C_{20}H_{22}BrN$ ($m = 356.29$ g/mol);

Monoclinic, space group $P2_1/n$ (no. 14)

$a = 13.7653(3)$ Å

$b = 10.3248(3)$ Å

$c = 24.1287(6)$ Å

$\alpha = 90^\circ$

$\beta = 94.5530(10)^\circ$

$\gamma = 90^\circ$

$V = 3418.45(15)$ Å³

$Z = 8$

$T = 120.0$ K

Radiation: MoK α ($\lambda = 0.71073$ Å)

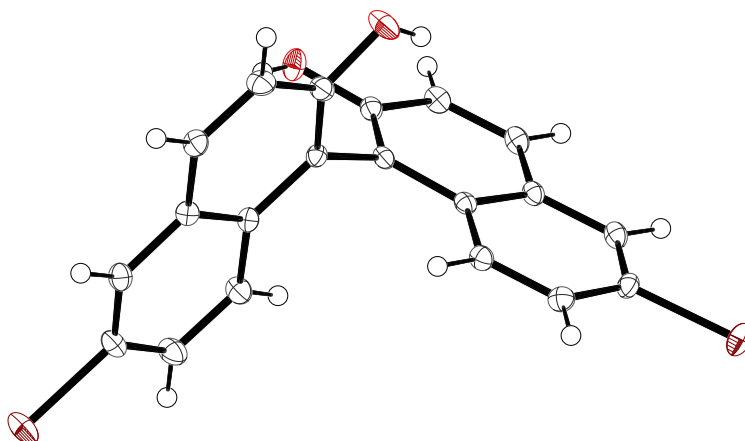
$\mu(\text{MoK}\alpha) = 2.402$ mm⁻¹

$D_{\text{calc}} = 1.385$ g cm⁻³

57923 reflections measured ($3.298 \leq 2\theta \leq 60^\circ$), 9954 unique ($R_{\text{int}} = 0.0389$, $R_{\text{sigma}} = 0.0316$) which were used in all calculations.

The final R_1 was 0.0279 ($I > 2\sigma(I)$) and wR_2 was 0.0545 (all data)

Crystal Structure: 246



Crystal data for $C_{20}H_{12}Br_2O_2$ ($m = 444.12$ g/mol);

Monoclinic, space group $P2_1/n$ (no. 14)

$a = 9.9396(3)$ Å

$b = 8.3061(3)$ Å

$c = 19.7919(7)$ Å

$\alpha = 90^\circ$

$\beta = 98.1820(10)^\circ$

$\gamma = 90^\circ$

$V = 1617.37(10)$ Å³

$Z = 4$

$T = 120.0$ K

Radiation: $MoK\alpha$ ($\lambda = 0.71073$ Å)

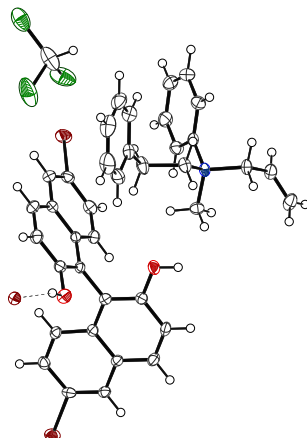
$\mu(MoK\alpha) = 5.021$ mm⁻¹

$D_{calc} = 1.824$ g cm⁻³

26795 reflections measured ($4.158 \leq 2\theta \leq 60^\circ$), 4702 unique ($R_{int} = 0.0305$, $R_{sigma} = 0.0238$) which were used in all calculations.

The final $R1$ was 0.0241 ($I > 2\sigma(I)$) and $wR2$ was 0.0608 (all data)

Crystal Structure: 247



Crystal data for $C_{39}H_{35}Br_3Cl_3NO_2$ ($m = 895.76$ g/mol);

Monoclinic, space group $P2_1$ (no. 4)

$a = 11.9980(4)$ Å

$b = 10.5662(4)$ Å

$c = 15.2000(5)$ Å

$\alpha = 90^\circ$

$\beta = 103.3610(10)^\circ$

$\gamma = 90^\circ$

$V = 1874.80(11)$ Å³

$Z = 2$

$T = 120.0$ K

Radiation: MoK α ($\lambda = 0.71073$ Å)

$\mu(\text{MoK}\alpha) = 3.477$ mm⁻¹

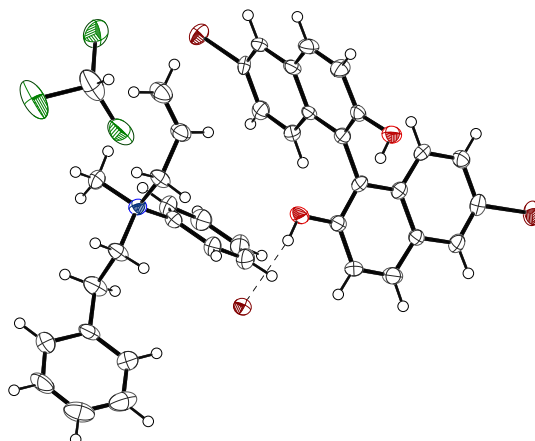
$D_{calc} = 1.587$ g cm⁻³

32779 reflections measured ($4.738 \leq 2\theta \leq 60^\circ$), 10900 unique ($R_{int} = 0.0386$, $R_{sigma} = 0.0550$) which were used in all calculations.

The final $R1$ was 0.0347 ($I > 2\sigma(I)$) and $wR2$ was 0.0614 (all data)

Flack parameter = $-0.004(3)$

Crystal Structure: 247a



Crystal data for $C_{39}H_{35}Br_3Cl_3NO_2$ ($m = 895.76$ g/mol);

Monoclinic, space group $P2_1$ (no. 4)

$a = 11.9898(15)$ Å

$b = 10.5630(13)$ Å

$c = 15.2229(19)$ Å

$\alpha = 90^\circ$

$\beta = 103.293(5)^\circ$

$\gamma = 90^\circ$

$V = 1876.3(4)$ Å³

$Z = 2$

$T = 120.0$ K

Radiation: MoK α ($\lambda = 0.71073$ Å)

$\mu(\text{MoK}\alpha) = 3.474$ mm⁻¹

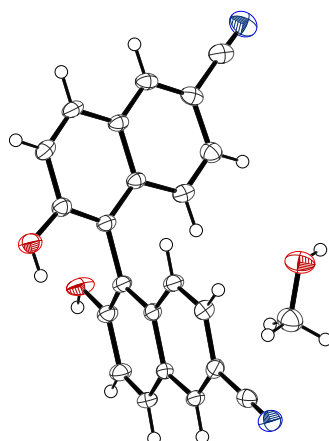
$D_{\text{calc}} = 1.586$ g cm⁻³

22803 reflections measured ($3.916 \leq 2\theta \leq 50.86^\circ$), 6837 unique ($R_{\text{int}} = 0.0758$, $R_{\text{sigma}} = 0.0812$) which were used in all calculations.

The final $R1$ was 0.0575 ($I > 2\sigma(I)$) and $wR2$ was 0.1396 (all data)

Flack parameter = 0.003(14)

Crystal Structure: 245



Crystal data for $C_{23}H_{16}N_2O_3$ ($m = 368.38$ g/mol);

Triclinic, space group $P\bar{1}$ (no. 2)

$a = 7.0913(3)$ Å

$b = 7.6326(3)$ Å

$c = 16.8236(7)$ Å

$\alpha = 100.143(2)^\circ$

$\beta = 96.212(2)^\circ$

$\gamma = 95.363(2)^\circ$

$V = 885.17(6)$ Å³

$Z = 2$

$T = 120.0$ K

Radiation: MoK α ($\lambda = 0.71073$ Å)

$\mu(\text{MoK}\alpha) = 0.093$ mm⁻¹

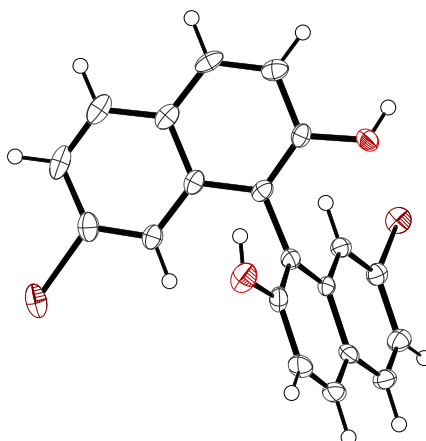
$D_{\text{calc}} = 1.382$ g cm⁻³

15497 reflections measured ($4.96 \leq 2\theta \leq 59.996^\circ$), 5125 unique ($R_{\text{int}} = 0.0432$,

$R_{\text{sigma}} = 0.0598$) which were used in all calculations.

The final R_1 was 0.0597 ($I > 2\sigma(I)$) and wR_2 was 0.1293 (all data)

Crystal Structure: 244



Crystal data for $C_{20}H_{12}Br_2O_2$ ($m = 444.12$ g/mol);

Tetragonal, space group $I4_1/a$ (no. 88)

$a = 25.2683(8)$ Å

$b = 25.2683(8)$ Å

$c = 10.6109(5)$ Å

$\alpha = 90^\circ$

$\beta = 90^\circ$

$\gamma = 90^\circ$

$V = 6774.9(5)$ Å³

$Z = 16$

$T = 120.0$ K

Radiation: MoK α ($\lambda = 0.71073$ Å)

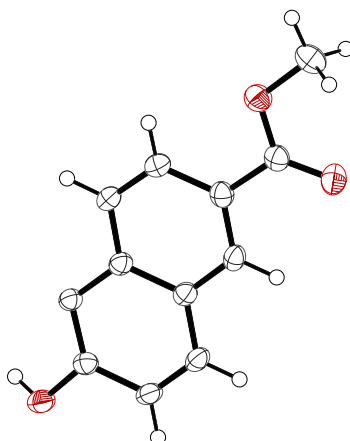
$\mu(\text{MoK}\alpha) = 4.795$ mm⁻¹

$D_{\text{calc}} = 1.742$ g cm⁻³

57855 reflections measured ($4.164 \leq 2\theta \leq 59.984^\circ$), 4942 unique ($R_{\text{int}} = 0.0765$, $R_{\text{sigma}} = 0.0454$) which were used in all calculations.

The final $R1$ was 0.0384 ($I > 2\sigma(I)$) and $wR2$ was 0.1064 (all data)

Crystal Structure: 243



Crystal data for $C_{24}H_{18}O_6$ ($m = 402.38$ g/mol);

Monoclinic, space group $C2/c$ (no. 15)

$a = 20.4448(12)$ Å

$b = 8.6649(5)$ Å

$c = 13.6602(8)$ Å

$\alpha = 90^\circ$

$\beta = 127.913(2)^\circ$

$\gamma = 90^\circ$

$V = 1909.2(2)$ Å³

$Z = 4$

$T = 120.0$ K

Radiation: $MoK\alpha$ ($\lambda = 0.71073$ Å)

$\mu(MoK\alpha) = 0.101$ mm⁻¹

$D_{calc} = 1.400$ g cm⁻³

15980 reflections measured ($5.05 \leq 2\theta \leq 59.996^\circ$), 2787 unique ($R_{int} = 0.0509$, $R_{sigma} = 0.0415$) which were used in all calculations.

The final $R1$ was 0.0556 ($I > 2\sigma(I)$) and $wR2$ was 0.1275 (all data)

Appendix B

CSD searches

B.1 Refcodes of conglomerates with $Z' > 1$

CCDC refiles of conglomerates with $Z' > 1$

ABAFAL	DAVGUE	FEBPUA	IVUPIZ	NERQUZ	PODGIZ	UQIYIF	WIZFET
AHUPID	DIDPAI	FEGZOH	IVURIB	NECAS	PUFPOW	UQOPIK	WOZWAL
AKAXIT	DIFLAF	FIZRUD01	IVUSEY	NOHTOT	PUYXUD	UTAZAT	WUHBOT
AQIPAU	DIYWOY	FUYKOB	JETLEA01	NONMUB	QOKDOL	VALRIL	WUTQOT
ARIVUS	DONZIQ	GASCEK	JIVWET	NONNOW	RARGOJ	VAVZUP	XEDKIC
ASOBER	DOQQOP	GAZPEE	JODQOJ	NOYKEU	ROCQOS	VAXFUY	XICDIW
ASOCOB	DUBQUN	GAZPII	JOPMIN	NOYKUK	RUJHUA	VEJLOM	XICQIM
ASUBOI	DUTWEX	GIJGUE	KAZVAL	NUFLUW	RUJMEP	VEWMIU	XISLET
BAZQIC	EFABIY	GIZKEI	KIGJUH	OBAYOF01	SACJIT	VIKLIL	XUQYEN
BEQGUB	EFIXIA	GOZKEO	KISYAO	OGOMUV	SECYII	VIXVEG	XURPUX
BUBTAU	EJEXOI	GUCMAT	LAMDUA	OKOXES	SOFKON	VIYQOL	XUVYAQ
BUKNIG	EPOLUT	GUDMOI	LEGZUT	ONONUC	SUBJUX	VURQAD	YACWOR
CEMBUT	EYIJAY	HAVYIP	LIDCUZ	OSUZUY	SUCKOS	WAHKOG	YEYFOY
CIHWAT	EZAKEY	HEYSUZ	LOLLIK	OTOGIP	TIJCUM	WAKWEM	YUKPEA
CIXHAV	FAGSIS	HEYSUZ10	LUDMON	OVIDUT	TIRVAT	WAPHIH	ZAQBEA
CONZUB	FAKSOC	IJUNUW	MAMHAM	PACCED	TUBDOJ	WAPVUF	ZETBEF
COSXAM	FALWUK	INAFUA	MOKPUX	PAGXAA	UFOCOH	WASHOP	
CUCJUH	FAQGOT	INAGAH	MUJWAQ	PEMWOU	UJUNAR	WEDJIB	
CUMDAR	FAXNAW	IVIMOQ	NABKIN	PIYFEI	ULAHUM	WIJZIY	

B.2 Refcodes of kryptoracemates

Refcodes of kryptoracemates							
ABIVIT	CAPFIL	DIXREI	FASQOF	HAJGEH	ISEBAL	LITCEW	NEDYEC
ABOBUR	CASXEB	DIXZAM	FAZSOR	HAJNOY	IVUNIX	LIWMOW	NEHPIZ01
ABUQOF	CAYWUX	DODPAP	FEJLOW	HAWPIG	IWIGON	LOPYEW	NEPHCL
ACICEU	CAYXAE	DOGQUN	FLDAZP	HEFGIL	IYEPAD	LOZZEF	NIBXEE
ADARII	CEHYEW	DOHVII	FODLAN	HEGSAP	JAGQUD	LULTEU	NIHFER
AFUCUC	CEVQIG	DOWFUT	FOHLIY	HEQRAY	JANYON	LUMJUZ	NIJGIW
AKIPIW	CEVQOM	DUSCOL	FURRIW	HEYROS	JAPDAG	LUQLUF	NIKTAD
ALEXAQ	CEZQOO	EBEWAM	FUVYIG	HIGGEL	JAXZIR	LUWHOC	NIMDEV
APOYAG	CILCAD	EBIMAG	GABGOF	HIJBIM	JAYWUE	LUYMAV	NINROU
AREZEE	CIXHOG	EBOHUY	GACWUE	HIKGEN	JECPEP	MALFEO	NISMUX02
AVOBAR	CIZGIC	EDEHIF	GAFJIH	HIKGEN01	JEKRIB	MALXOQ	NITSUH
AWIJAT	COCROD	EGOXEG	GAFWAL	HILXUW	JOHJIA	MANBOU	NOKRIP
AWURUH	COCXEA	EGURIH	GAGFAX	HISGOH	JOJCET	MAPXUX	NOLFUP
AWUYAT	COGNOC	ELIJAK	GAKLAJ	HISRIL01	JOLMUU	MEBCUT	NOLWAO
AXEGEQ	COQYOZ	EMEKOX	GANMUD	HOBMAO	KABTIT	MEKJIX	NOPMAH
AXIXUB	COVXOC	EMIXIH	GAPFIO	HOFNEY	KAQKOF	MEQMAZ	NOSPOD
BACTUX	CUKDAN10	EMOYIO	GEFNEM01	HONXEQ	KEHDOR	MEXXOF	NUBKEA
BAZGOZ	CUMYOZ	ENIVAZ	GEFQUE	HUYBIN	KEKJAO	MIBGIO	NUCLIG
BEGGAV	CUTGAZ	EPOJUR	GENLET01	IBOVEA	KETWAK	MIKTUY	NUFQAI
BERCIL	DAGTAH	EROXUH	GENLET02	IDILIQ	KIGKOD	MIVZAT	NUGVER
BIKCUV	DAGXUH	ETAFUA	GEWQAC	IFEJEL	KOMKII	MOHVEK	NULBIH
BINGOU	DAHSIR	EXIGID	GIBXAR	IFEJOV	KOVBIG	MORSAO	NUPQAR
BISFER	DAJKAC	EYONIS	GICSOA	IGAFIG	KUKFOM	MUBYIR	NUYTAC
BOGYUS	DAQKAI	EYUKAN	GIPLID	IGAKEI	KUSTOJ	MUDQIN	OBAVIZ
BOKSOL	DAQSUJ	EZAJAT	GIZSOZ	IGAREO	LABFAV	MUFZEV	OGOLUU
BONKEW	DASHAJ	EZAKAU	GOLXOU	IHEMEO	LACFEB	MUKCUS	OGOMAB
BULTUA	DEMNIV	FABDIZ	GUCJOE	IHULUU	LALKUF	MUMXAV	OHABIK
CABHUM	DIGMOX	FAHQUB	GULFID	ILOTUB	LAZTIQ	NACNAI	OHAKIT
CABXIM	DIGPEQ	FAHYUM	GUMCEY	IPAZUN	LIKDAM	NAJCUX	OHELIY
CACKOJ	DIPNIC	FARVEB	GUXCEJ	IQAYUW	LINJAW	NAMBIP	OLAJES

B.2. REFCODES OF KRYPTORACEMATES

Refcodes of kryptoracemates continued...

OLOHAY	PIWVUN	REVSOC	SINPEL	TUWCIX	VEHDEU	XEPHUX	YOGVAR
OLOKOR	PONVOE	REZZOM	SODTEM	TUYFOJ01	VETFIK	XERTUM	YOJZIH
ONALIB	POPQUH	RIGMAW	SOGSOW	UCIPIG	VIGHOL	XERWIC	YOSKAU
ONODAY	POXSIG	RISNIS	SUHYIG	UFAZUZ	VIGLEF	KEYWOQ	YOVLON
ONUBAC	PTHAZO10	ROBTUZ	SUKMIX	UGOTOA	VIWNOE	XIGGEB	YOXREI
ONUBEG	PUYXIS	ROKPUD	SUMMUK	UHACUE	VIWTIH	XIHWOB	YUBYIG
OQABAK	QAHSUQ	ROKTAM	SUPRIF	UJIWOC	VOBFOK	XIRZED	YUDGEK
OSARUX	QALCIQ	RUCXAQ	SUSVEK	UMISIT	VOBKEE	XOCWES	YUFVAX
OTOGOW	QAVBIB	RUDCUR	TABLUD	UMULOE	VOLDOQ	XOLDOS	YUGTOK
OVUTOQ	QEFJAP	RUMTOK	TADPIZ	UNUGEQ	VORHIW	XONWUS	ZADYEL
OXADAU	QEFJUJ	RURBIQ	TADRIZ	UPOXIH	VUFWEB	XOPVIK	
OXATAK02	QELQOQ	RUWHEX	TAQKAZ	USAGIF	VUKCEJ	XOZFIB	
OXOSEC	QERFAX	RUYJON	TARPEK	USARUC	VULTAZ	XUBPUG	
OYACUO	QESVOC	RUZVOA	TAWFAA	USESUJ	VUMKUK	XUBROC	
OYOGOAO	QETXAO	SABSIZ	TAYTEU	USODUE	WABFIS	XUBTEU	
OYUGAT	QEWTES	SAGFEN	TAZKUC	UTEYEZ	WABJIW	XUMQEC	
OYUQOQ	QIJMAX	SAGKAP	TEFDIT	UTIHEM	WAPKUW	XUPMEB	
OZIKAK	QIKSAG	SAGTUP	TICMEA	UTUNIH	WEDFIW	XUPMUR	
OZIRUN	QIJYIR	SAKFUF	TITYOM	UVOJUL	WEPWUJ	XUWLOT	
PAFSIC	QOWROM	SAPVAG	TITZED	UWUYUJ	WETGEK	XUYQIT	
PALPAW	QOWRUS	SAQSAE	TMENQU	UXAZOL	WINSAQ	YAHYIP	
PAMHAN	QOWSAZ	SARQOQ	TOFTAM	UXUGEB	WIYPAV	YAQVUK	
PEGKUJ	QOZQUS	SAXBIF	TOGYOG	UZEPIZ	WONMIY	YERGOR	
PELDOC	QUGPIR	SAXMIQ	TOPSOI	VAJZIQ	WONRAS	YIMBAZ	
PELDUF	QUTWAE	SEJTAC	TOQJAK	VATNEL	WOQQIE	YIPNUI	
PENFEV	RAMSED	SEPFOI	TOQRUP	VAXHOT	WOWXOV	YIRYAA	
PENLUS	RAQDOF	SEPXUI	TUGLIR	VEBTEE	WUFSUO	YISTOL	
PEXLOU	RARMEE	SIFMOK	TUHJEN	VEBZIL	WUMJEW	YIYPIH	
PIGBOX	RENRIO	SIHDEV	TUPQUS	VEFDES	XADZOS	YOBNEI	
PIHPUU	RETYUM	SIKCAR	TUQDER	VEFNIE	XEFNAX	YOFNOY	

B.3 Refcodes of solid solutions of enantiomers

Refcodes of solid solutions of enantiomers

ABONEM	CUXHUZ06	FULYUJ	IKUDOK	KUXHER	MIYGAC	QIKSIM	TOMTIB
AQEBUT	CUXLAJ	FUQJAF	INUBOK	LAHVUN	NILYIR	QIVPIX	UFEFEQ
AWUMUB	CUXLAJ01	GAGQOV	IYOGUZ	LAWWEN	NOQHUX	QUMZOO	VAQZUJ
BADJAT	CUXLAJ02	GLPCHO	JALVUQ	LAZLON	OLELUP	RAFVEC	VEQTUH
BADWOW	DABZOX	GOJPAZ	JIPPED	LIPYUE	OPIMAD	REBLIU	WODQAJ
BEDCUK	DAXQEB	HANBOP	JODMUN	LOHQIL	OPIMEH	REVMOU	WOVRUU
BEWFOZ	DEMMEQ	HAPTOK	JODNIC	LOSRIX	OVIGEG	RIGQIJ	WUTXOA
BEYSUU	DIZLOP	HITZAO	JOSHIL	LOYMER	PEQBEB	RIYKIT	XAYKEQ
BEZPUU	ENIPUO	HIVWUH	KAZTIR	MEFFAF	PEZNAK	ROBSUZ	YODQAM
BIWYIR	EQANAO	HUSJEK	KICDEH	MIHZOT	PUGZUP	ROBTAG	ZAWXAZ
CORKOM	FATGAL	IDIMUD	KICDOR	MIJBAJ	QADXAV	SEQGAX01	
CUXHUZ03	FONVOW	IFECOM	KITLUV	MIJBEN	QAQPED	SOQQOE	
